INŻYNIERIA MINERALNA
CZASOPISMO POLSKIEGO TOWARZYSTWA PRZERÓBKI KOPALIN

Szanowni Państwo,

mam przyjemność zaprosić Państwa do lektury najnowszego numeru Inżynierii Mineralnej (*Journal of the Polish Mineral Engineering Society*), który został przygotowany przez naukowców ukraińskich i polskich. Obszar zainteresowań i badań Kolegów zza naszej wschodniej granicy pokrywa się z naszymi badaniami, toteż współpraca zaowocowała kilkoma wspólnymi publikacjami. Mamy nadzieję, że kooperacja przyniesie korzyści ukraińskiej i polskiej nauce oraz przyczyni się do zacieśnienia kontaktów.

Od wielu lat trwa wymiana poglądów i doświadczeń z pracownikami naukowymi instytutów i uniwersytetów Ukrainy. Wspólnie przygotowaliśmy wieloautorskie monografie w latach 2018 i 2023. W tym roku dzielimy się doświadczeniami w dziedzinie inżynierii górniczej i środowiskowej z naukowcami reprezentującymi następujące jednostki:

- Central Ukrainian National Technical University,
- Cherkasy State Technological University,
- Dnipro University of Technology,
- Dniprovsk State Technical University,
- LLC “DTEK Energy”,
- Higher Institute of Mining and Geology of Boké, Republic of Guinea,
- Kryvyi Rih National University,
- National University of Water and Environmental Engineering, Rivne,
- National Academy of Sciences of Ukraine, Dnipro,
- National Technical University of Ukraine "Igor Sikorsky Kyiv Polytechnic Institute",
- Taras Shevchenko National University of Kyiv,
- Zhytomyr Polytechnic State University.

Слава Україні!

Z górniczym pozdrowieniem
Wiktoria Sobczyk

INŻYNIERIA MINERALNA
CZASOPISMO POLSKIEGO TOWARZYSTWA PRZERÓBKI KOPALIN

Dear colleagues, friends,

I have pleasure in presenting issue 1/2023 of the "Inzynieria Mineralna" journal.

This issue of the journal is not quite usual. Thanks to the support of the POLISH MINERAL ENGINEERING SOCIETY and the editorial board of the journal "Inzynieria Mineralna" in the person of Prof. Barbara Tora, Editor-in-Chief of the Journal who invited Ukrainian scientists to contribute their research findings in mining to the journal, we now have such a fine issue.

Miners of Ukraine have always been the vanguard of the scientific world regarding mineral extraction in difficult mining and geological conditions. And in this issue, they are happy to share their experience.

The articles of this issue consider the full cycle of mining operations, from exploration of mineral deposits, their surveying estimation, technological aspects of mineral extraction applying the latest technology and equipment to high quality processing and obtaining the final product.

Environmental issues have become an important area of scientific development. This is especially topical since Ukraine's mining is integrating into the European and world mining science which preaches the principles of environmental safety in mineral extraction and processing.

I would like to once again thank the Polish Mineral Processing Society and the editorial board of the "Inzynieria Mineralna" for supporting Ukrainian science, as well as the entire Polish people for supporting Ukraine in the struggle for independence from the Russian invaders.

Glory to Ukraine! Glory to heroes!

Sincerely yours,
Serhii Chukharev,

quest editor of the issue 1/2023 of "Inzynieria Mineralna",
PhD (Engineering), Associate Professor,
National University of Water and Environmental Engineering, Ukraine

Research of the Dehydration Process of Amber-Containing Mining Mass

Valerii KORNIIENKO[1)], Yevhenii MALANCHUK[2)], Vitalii ZAIETS[3)], Vasyl SEMENIUK[4)], Myroslava KUCHERUK[5)]

[1)] Doctor of Engineering, Professor, Department of Mineral Deposits Development and Mining Engineering, National University of Water and Environmental Engineering, Soborna str, 11, Rivne, Ukraine; ORCID https://orcid.org/0000-0002-7921-2473
[2)] Doctor of Engineering, Professor, Department of Automation, Electrical Engineering and Computer-Integrated Technologies, National University of Water and Environmental Engineering, Soborna str, 11, Rivne, Ukraine; ORCID https://orcid.org/0000-0001-9352-4548
[3)] PhD, Associate Professor, Department of Mineral Deposits Development and Mining Engineering, National University of Water and Environmental Engineering, Soborna str, 11, Rivne, Ukraine; ORCID https://orcid.org/0000-0003-0659-7402; email:v.v.zayets@nuwm.edu.ua
[4)] Senior Lecturer, Department of Development of Deposits and Mining,National University of Water and Environmental Engineering, Soborna str, 11, Rivne, Ukraine; ORCID https://orcid.org/0000-0002-2348-3143
[5)] Senior Lecturer, Department of Development of Deposits and Mining,National University of Water and Environmental Engineering, Soborna str, 11, Rivne, Ukraine; ORCID https://orcid.org/0000-0002-0443-9139

http://doi.org/10.29227/IM-2023-01-01

Submission date: 02-02-2023 | Review date: 13-03-2023

Abstract

The article highlights the results of research into the process of dehydration of amber-containing mining mass using a vibroclassifier. Features of the technological scheme of amber extraction are described, as it relates to water supply points. The state of equilibrium of the liquid in the cell of the vibroclassifier under different conditions of sieve wettability was studied: a liquid that does not wet the sieve fibers; liquid that wets the fibers of the sieve; a thin film of liquid that wets the sieve fibers.

As a result of the research, it was established that in the case when the liquid does not wet the fibers of the sieve, the height of the layer of liquid that is maximally retained in the cell is at least 3 times greater than in the case of the liquid that wets the fibers of the sieve. The reliability of the obtained results is confirmed by the use of proven research methods and a relative error between calculated and experimental values at the level of 20%.

Keywords: *amber, vibroclassifier, sieve cell, dehydration*

Introduction

The technology and equipment offered by us for the extraction of amber from the mining mass is carried out, to a large extent, to implement the requirements for increasing the extraction of amber due to the processing of off-balance reserves in man-made deposits and improving the ecological situation of the environment [1]. This technology of amber extraction has a number of advantages over the existing ones (hydraulic and well technologies), but for a full assessment of its economic efficiency, it is necessary to determine a number of influential factors that were considered in other works [2–5]. The paper [2] considered the technology of classification and calculation of the water-sludge scheme. With the use of computer modeling, a program for calculating the water-sludge operation scheme of the vibroclassifier was developed. It allows you to determine the indicators of the classification products under different modes of operation. According to this technology, the raw feed is mixed with water in a mixer and submitted for classification in a vibroclassifier of complex action, the discharge of which is sent to dewatering classification on a vibrating screen. The sands of the vibroclassifier and the over-sieve product of the vibroscreen are removed as waste. After screening, the sieved product is returned to the feeder of the vibroclassifier in the form of a circulating load.

Amber extraction technology has two main features. The first refers to the points of introduction of additional (fresh) water and the saving of total water consumption, and the second – to the volume of the circulating load.

The technological scheme uses two fresh water supply points.

First, in the mixer, where it is mixed with the mining mass, since it is not possible to introduce dry feed into the classifier.

Secondly, water is introduced directly into the bath of the classifier. At this point, the supply of fresh water is necessary, since it is the main factor that allows you to adjust the density of the pulp in the bath, the volume of the drain, the speed of the upward flow and the amount of circulating load.

The circulating load is the sublattice product of the dewatering screen. The magnitude of this load (further – circulation) can theoretically reach 100% of the power supply or more. However, in practice, it cannot be kept within high limits for two reasons: the first reason is that with high circulation, the density of the suspension in the classifier bath will decrease; the second – the volume of the downpour will increase and, accordingly, the speed of the upward flow. Due to this, larger fractions of the rock will be carried out in the drain and their number will increase. This is a negative factor – instead of removing the empty rock from the process, we organize its circulation in the scheme.

Note that the rational range of pulp density in the bath is 1400–1600 g/l. The calculation of technology parameters is performed for the upper limit of density, that is, for "hard" conditions, based on the need to reduce water consumption to ensure the amber extraction process.

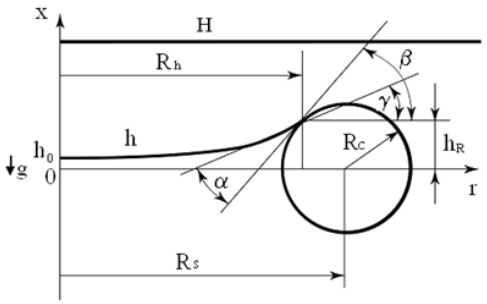

Fig. 1. Calculation diagram of the equilibrium of the liquid layer that does not wet the mesh fibers
Rys. 1. Schemat obliczeniowy równowagi warstwy cieczy, która nie zwilża włókien siatki

The study of the process of dehydration during the classification of the mining mass allows to evaluate the efficiency of the equipment in the extraction and processing of amber.

Study of liquid equilibrium in vibroclassifier cell

Various mineral processing technologies involve classification of the rock mass in the form of pulp and subsequent dehydration of the classification products on sieving surfaces in the form of nets. For this purpose, both stationary devices and a number of modifications of vibrating screens have been created and continue to be improved. At the same time, one of the most important engineering tasks is to increase the efficiency of classification and dewatering on sieving surfaces. The greatest difficulty is caused by the screening of the rock mass with a grain size in the range from 5.0 mm to 50 microns. This is due to the formation of a film of liquid in the cells of the sieve, which makes it difficult to screen the pulp, which significantly reduces the efficiency of the process. The practice of using various sieving surfaces during pulp classification indicates the need for intensive dynamic excitation of this surface.

Therefore, it is relevant to determine the dependence of the efficiency of dehydration in the classification of mining mass on the specified factors.

The study of the equilibrium of liquids with free surfaces has long attracted the attention of researchers and forms a separate section of hydromechanics, which considers the forms of equilibrium of liquid in capillaries, the forms of equilibrium of drops on surfaces, capillary surfaces without gravity, contact angles of the liquid with the walls of the container. Equilibrium changes in the capillary fluid are the subject of research by various authors. In it, mathematical models of equilibrium figures are built, and the stability of various changes is determined. In some fundamental works, a wide range of tasks related to weightlessness and the hydromechanics of a liquid rotating under weak gravity is considered. In the studies presented in this article, the problems related to the equilibrium of a liquid with known capillary properties are considered. These studies were conducted under the supervision of Doctor of Technical Engineering, Prof. V.P. Nadutiy (Institute of Geotechnical Mechanics named by N. Poljakov, Dnipro, Ukraine) jointly with scientists of the National University of Water and Environmental Engineering (Rivne, Ukraine) both in laboratories and in field conditions at facilities in the Rivne region (Ukraine). Without going into the nature of capillarity and using known provisions, we consider the equilibrium layers of liquid in a cell formed by a fiber that can be wetted or not wetted by a stationary liquid. The hydrostatics equation is the basis for the performance of the tasks on the equilibrium of immobile capillary liquids

$$dp/dx=\pm\rho g \tag{1}$$

where x is the coordinate, m;
ρ – liquid density, kg/m^3;
g – acceleration of the free fall of the body, m/s^2;
p – pressure, Pa.

Condition on the surface of phase separation

$$p_h - p_a = -\sigma\left[\frac{h''}{(1+(h')^2)^{3/2}} + \frac{h'}{r(1+(h')^2)^{1/2}}\right] \tag{2}$$

where r is the radius, m;
p_a – atmospheric pressure, Pa;
p_h – pressure on the free surface of the liquid, Pa;
σ – coefficient of surface tension, N/m;
h – the coordinate x surface points, m.

A liquid that does not wet the fibers of the sieve. In the case when the liquid does not wet the material from which the mesh is made (Fig. 1), after integrating equation (1) from the lower surface h to the upper surface H, which is also under atmospheric pressure, and taking into account the direction of the x axis and the acceleration of free fall g, the equation of statics of the liquid layer in the sieve cell has the form

$$\frac{h''}{(1+(h')^2)^{3/2}} + \frac{h'}{r(1+(h')^2)^{1/2}} + \frac{\rho g}{\sigma}(h-H) = 0 \tag{3}$$

where a dash and two dashes denote the first and second derivatives of r, respectively.

After transformations of expression (3), the equilibrium equation in the sieve cell is obtained

$$h = H - \frac{R_h\theta}{\kappa R_S J_1(\kappa)} J_0(\kappa n) \tag{4}$$

where $n=r/R_h$; $\bar{h}=h/R_S$; $\bar{H}=H/R_S$; - dimensionless quantities;
R_c – radius of the mesh fiber, m;
R_h – the radius of the circle along which the liquid contacts the surface of the fiber, m;
R_S – the sum of the radii of the mesh fiber and the cell opening, m;
h_0 – height of the surface at the point n = 0, m;
h_R – height of the surface at the point n = 1, m;

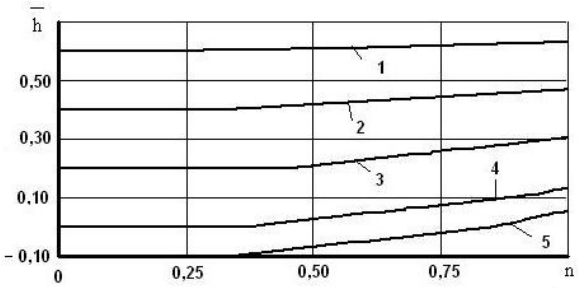

Fig. 2. Curves characterizing the shape of the lower free boundary of the liquid layers, which does not wet the mesh fibers: 1 – H=0.042 m; 2 – H=0.138 m; 3 – H=0.243 m; 4 – H=0.348 m; 5 – H=0.391 m

Rys. 2. Krzywe charakteryzujące kształt dolnej swobodnej granicy warstw cieczy, która nie zwilża włókien siatki: 1 – H=0.042 m; 2 – H=0.138 m; 3 – H=0.243 m; 4 – H=0.348 m; 5 – H=0.391 m

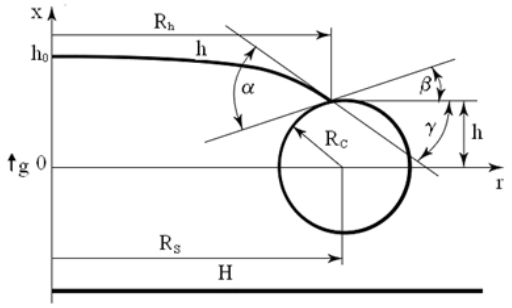

Fig. 3. Calculation diagram of the equilibrium of the liquid layer that wets the fiber in the grid cell

Rys. 3. Schemat obliczeniowy równowagi warstwy cieczy zwilżającej włókno w komórce siatki

θ=tgγ (γ is the angle between the liquid tangent to the surface at the point of engagement and the straight line parallel to the abscissa axis);

J_0– Bessel function of the first kind of zero order;

$\kappa=Bo^{1/2}$, $Bo=\rho g R h^2/\sigma$ – Bond number;

α – wetting angle;

β – the angle between the tangent to the fiber surface at the point of liquid engagement and the abscissa axis,

γ=β-α.

To determine the numerical values, it is necessary to set hR, then calculate R_h, tgβ and θ, after which H is determined. By performing such calculations, you can make sure that for some values $h_R^* \le h_R \le 1$ H≤0. Such a solution cannot exist physically, solutions of this problem begin at H≥1. If 0<H<1, we will get a problem about a drop "sitting" on a sieve cell. It requires a slightly different mathematical formulation and falls out of the class of tasks under consideration. Thus, the analytical approach determines what situations may arise during the numerical solution of this problem. In fig. 2. the results of the calculations are given in the form of curves characterizing the shape of the lower free boundary. Calculations were made for the following conditions: $R_C=50\cdot10^{-6}$ m, $R_S=75\cdot10^{-6}$ m, tgα=1, σ=0.072 N/m. The curves given in the figure correspond to different values of the height of the liquid layer H above the cell.

From fig. 2, it follows that with a decrease in h_0, the liquid layer retained by the grid cell increases, or more precisely, with an increase in the liquid layer above the cell, the liquid sinks deeper into the center of the cell, which is quite natural, but this becomes a limit at larger positive values of θ. With a further decrease in h_0, the solution ceases to exist, which means the loss of the static equilibrium state.

A liquid that wets the sieve fibers. For the liquid that wets the mesh fibers, the calculation scheme for determining the equilibrium of the layer has a slightly different form (Fig. 3). For ease of solution, the x-axis is pointing up, but in the same direction as g (the figure is upside down).

Integrating expression (1) within the appropriate limits, the following equation is obtained in a dimensionless form

$$\frac{h''}{\left[1+\left(h'/R_h/R_S\right)^2\right]^{3/2}}+\frac{h'}{n\left[1+\left(h'/R_h/R_S\right)^2\right]^{1/2}}+Bo(h+H)=0 \quad (5)$$

It differs from the equation of the already considered case only by a plus sign before the value H (for physically correct solutions, H must be greater than zero). Using an analytical solution that will look like this

$$h=-H-\frac{R_h\theta}{\kappa R_S J_1(\kappa)}J_0(\kappa n) \quad (6)$$

determine the values of h_R at which the solution of the problem exists. For this case, solutions exist for tgα<θ<0.

In fig. 4 shows the curves of the lower limit of the liquid characterizing the equilibrium of the layers. The given curves correspond to different values of the height of the liquid layer above cell H. The calculations were performed for the same values of R_C, R_S, and α as in the previous case. From fig. 4, it follows that with a decrease in h_0, the height of the H layer increases, or more precisely, with an increase in the liquid layer, the lower limit lowers, however, there is also a limitation due to the fact that the liquid reaches the radius R_S.

Curve 3 in fig. 4 approaches this limiting value. A circle of radius R_S separates liquids that are in equilibrium in neighboring cells. Upon contact, the equilibrium structure is disturbed and a film is formed that connects the cells of the sieve. This is a condition for the loss of stability of the structure un-

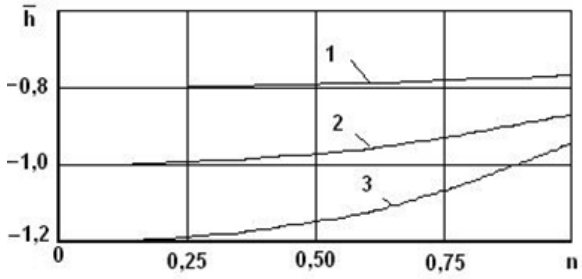

Fig. 4. Curves characterizing the shape of the lower free boundary of the liquid layers that wets the sieve fibers
1 – H = 0.031 m, 2 – H = 0.077 m, 3 – H = 0.109 m

Rys. 4. Krzywe charakteryzujące kształt dolnej swobodnej granicy warstw cieczy zwilżającej włókna sita
1 – H = 0.031 m, 2 – H = 0.077 m, 3 – H = 0.109 m

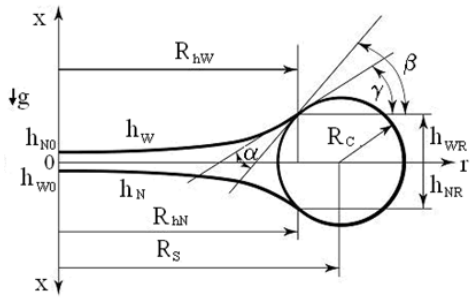

Fig. 5. Calculation diagram of the equilibrium in the cell of a thin film of liquid that wets the sieve fibers

Rys. 5. Schemat obliczeniowy równowagi w komórce cienkiej warstwy cieczy zwilżającej włókna sita

der consideration: the task undergoes qualitative changes in its formulation. Another case is possible when the value of H<1 is the presence of a thin film covering the cell.

A thin film of liquid that wets the fibers of the sieve. In fig. 5 schematically shows the specified case, which may be of practical interest, and fits into the formulated class of tasks. For ease of resolution, the x-axis in the upper and lower parts of the figure are directed in different directions (the lower part is viewed upside down). When integrating equation (1) over x, the equilibrium equation for the upper and lower surfaces is obtained in a dimensionless form

$$\frac{h''_W}{\left[1+\left(h'_W R_{hW}/R_S\right)^2\right]^{3/2}}+\frac{h'_W}{n\left[1+\left(h'_W R_{hW}/R_S\right)^2\right]^{1/2}}-Bo_W(h_W+H_W)=0 \quad (7)$$

$$\frac{h''_N}{\left[1+\left(h'_N R_{hN}/R_S\right)^2\right]^{3/2}}+\frac{h'_N}{n\left[1+\left(h'_N R_{hN}/R_S\right)^2\right]^{1/2}}+Bo_N(h_N-H_N)=0 \quad (8)$$

where the index W refers to the upper surface, and N – to the lower and $H_W=H_N=H=(p_a-p_0)/(\rho g R_S)$
p_0 – pressure at point x = 0, Pa.

When $B_o=0$, equations (7) and (8) become the same. This suggests that in weightlessness the boundaries of the surfaces are symmetrical. Discarding the quadratic terms in the denominators, the solution, using Bessel functions, will be written as

$$h_W=-H+\frac{R_{hW}\theta_W}{\kappa_W R_S J'_1(\kappa_W)}J'_0(\kappa_W n),\quad h_N=H-\frac{R_{hN}\theta_N}{\kappa_N R_S J_1(\kappa_N)}J_0(\kappa_N n) \quad (9)$$

Excluding H from these equations and assuming n=1, the relationship between the points of engagement of the lower and upper boundaries of the liquid with the fiber is obtained

$$h_{WR}+h_{NR}=\frac{R_{hW}\theta_W}{\kappa_W R_S J'_1(\kappa_W)}J'_0(\kappa_W)-\frac{R_{hN}\theta_N}{\kappa_N R_S J_1(\kappa_N)}J_0(\kappa_N) \quad (10)$$

In this equation, it is necessary to set the value of h_{NR}, then to calculate h_{WR} by selection, and to calculate the shape of the upper and lower boundaries of the film according to equations (9). After calculating the Bond number for the parameters of interest, it was determined that its maximum value is $B_o=0.000766$ at $R_h=R_S$. In this regard, the lower and upper boundaries of the film are similar in shape. Calculations show that the values of the corresponding points of the calculated lower and upper surfaces differ from each other in the third order. In fig. 6 shows the curves of the surfaces of films with different volumes. It is calculated using analytical solutions (9), according to the following formula:

$$\begin{aligned}V_P=\pi\Big\{&(h_{RW}+h_{RN})(R_C^2+R_S^2)-R_C R_S^2\left[\arcsin\left(\frac{h_{RW}}{R_S}\right)+\arcsin\left(\frac{h_{NW}}{R_S}\right)\right]-\\&-R_C R_S\left[h_{RW}\left(1-\frac{h_{RW}^2}{R_S^2}\right)^{1/2}+h_{RN}\left(1-\frac{h_{RN}^2}{R_S^2}\right)^{1/2}\right]-\frac{1}{3}(h_{RW}^3+h_{RN}^3)\Big\}+\\&+2\pi\left\{R_{hW}^3\frac{\theta_W}{\kappa_W^2}\left[1-\frac{\kappa_W J'_0(\kappa_W)}{2J'_1(\kappa_W)}\right]-R_{hN}^3\frac{\theta_N}{\kappa_N^2}\left[1-\frac{\kappa_N J_0(\kappa_N)}{2J_1(\kappa_N)}\right]\right\}\end{aligned} \quad (11)$$

In fig. 6 shows the curves corresponding to some values of the volume of the liquid in the sieve cell.

Analyzing the data shown in fig. 6, it can be concluded that thinner films are characterized by concave surfaces (curves 1, 2). Surface 3 is almost straight, and curve 4 is convex, which characterizes the shape of the upper surfaces of liquid films.

Conclusion

As a result of the research, the equilibrium conditions of the liquid in the sieve cell of the vibroclassifier for fine-grained classification and dehydration were determined depen-

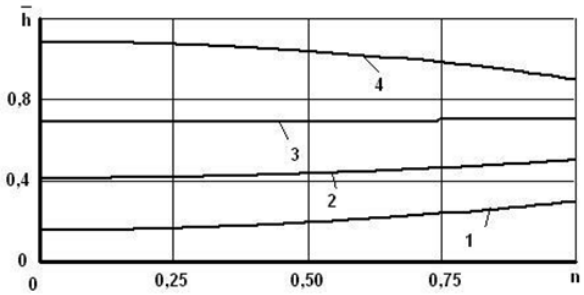

Fig. 6. Curves characterizing the shape of the upper surfaces of the films of the liquid that wets the mesh fibers: 1 – V=0.458·10^{-10}m^3; 2 – V=0.103·10-9m^3; 3 – V=0.193·10^{-9}m^3; 4 – V=0.407·10^{-9}m^3

Rys. 6. Krzywe charakteryzujące kształt górnych powierzchni warstw cieczy zwilżającej włókna siatki: 1 – V=0.458·10^{-10}m^3; 2 – V=0.103·10-9m^3; 3 – V=0.193·10^{-9}m^3; 4 – V=0.407·10^{-9}m^3

ding on the wetting conditions and the height of the liquid layer: in the case when the liquid does not wet the fibers of the sieve, the height of the liquid layer that is maximally retained in the cell is not less than 3 times the height of the layer held by the liquid wetting the sieve fibers.

The reliability and validity of scientific results are confirmed by the use of proven research methods, satisfactory convergence of calculated and experimental values with a relative error not exceeding 20%.

Literatura – References

1. Belichenko, O., & Ladzhun, J. (2016). Complex gemological research of new types of treated amber. Visnyk of Taras Shevchenko National University of Kyiv. Geology, 4(75), 30-34.https://doi.org/10.17721/1728-2713.75.04
2. Natkaniec-Nowak, L., Dumańska-Słowik, M., Naglik, B., Melnychuk, V., Krynickaya, M. B., Smoliński, W., & Ładoń, K. (2017). Depositional environment of Paleogen amber-bearing quartz-glauconite sands from Zdolbuniv (Rivne region, NW Ukraine): mineralogical and petrological evidences. Gospodarka Surowcami Mineralnymi, 33(4), 45-62.https://doi.org/10.1515/gospo-2017-0041
3. Alekseev, V.I. (2013). The beetles Baltic amber: The checklist of described species and preliminary analysis of biodiversity. Zoology and Ecology, 23(1), 5-12.https://doi.org/10.1080/21658005.2013.769717
4. Zakharenko, A.M., & Golokhvast, K.S. Using confocal laser scanning microscopy to study fossil inclusion in Baltic amber, a new approach. Key Engineering Materials, (806), 192-196. https://doi.org/10.4028/www.scientific.net/KEM.806.192
5. Zabyelina, Y., & Kalczynski, N. (2020). Shadowy deals with "sunny stone": Organized crime, informal mining, and the illicit trade of amber in Ukraine. Illegal Mining, 241-272.https://doi.org/10.1007/978-3-030-46327-4_9
6. Łazowski, L. (2007). The comments regarding usage and conservation of the amber resources. Przeglad Geologiczny, 55(8), 670-672.
7. Yakymchuk, N.A., Levashov, S.P., & Korchagin, I.N. (2019). New evidence of amber endogenous genesis. 18th International Conference on Geoinformatics – Theoretical and Applied Aspects.https://doi.org/10.3997/2214-4609.201902017
8. Krek, A., Ulyanova, M., & Koschavets, S. (2018). Influence of land-based Kaliningrad amber mining on coastal zone. Marine Pollution Bulletin, (131), 1-9.https://doi.org/10.1016/j.marpolbul.2018.03.042
9. Poulin, J., & Helwig, K. (2016). The characterization of amber from deposit sites in western and northern Canada. Journal of Archaeological Science: Reports, (7), 155-168.https://doi.org/10.1016/j.jasrep.2016.03.037
10. Xing, Q.Y., Yang, M., Yang, H.X., & Zu, E.D. (2013). Study on the gemological characteristics of amber from Myanmar and Chinese Fushun. Key Engineering Materials, (544), 172-177.https://doi.org/10.4028/www.scientific.net/KEM.544.172
11. Zhu, W.C., & Wei, C.H. (2010). Numerical simulation on mining-induced water inrushes related to geologic structures using a damage-based hydromechanical model. Environmental Earth Sciences, 62(1), 43-54.https://doi.org/10.1007/s12665-010-0494-6
12. Lemos, J.V., & Lorig, L.J. (2020). Hydromechanical modelling of jointed rock masses using the Distinct Element Method. Mechanics of Jointed and Faulted Rock, 605-612.https://doi.org/10.1201/9781003078975-85
13. Cappa, F., Guglielmi, Y., Fénart, P., Merrien-Soukatchoff, V., & Thoraval, A. (2005). Hydromechanical interactions in a fractured carbonate reservoir inferred from hydraulic and mechanical measurements. International Journal of Rock Mechanics and Mining Sciences, 42(2), 287-306.https://doi.org/10.1016/j.ijrmms.2004.11.006
14. Moshynsky, V. (2001). Modern water conditions in the northwest part of Ukraine: An analysis. Water Engineering and Management, 148(4), 22-26.
15. Burnashov, E., Chubarenko, B., & Stont, Z. (2010). Natural evolution of western shore of the sambian peninsula on completion of dumping from an amber mining plant. Archives of Hydroengineering and Environmental Mechanics, 57(2), 105-117.
16. Mikhlin, Y.V., & Zhupiev, A.L. (1997). An application of the ince algebraization to the stability of non-linear normal vibration modes. International Journal of Non-Linear Mechanics, 32(2), 393-409.https://doi.org/10.1016/s0020-7462(96)00047-9
17. Sorin, C. (2013). Research studyes on mining activity impact on the area focsanei scurtesti, case study vadu pasii, buzau county. SGEM Geoconference on Ecology, Economics, Education and Legislation.https://doi.org/10.5593/sgem2013/be5.v1/s20.112
18. Stupnik, M., Kolosov, V., Kalinichenko, V., & Pismennyi, S. (2014). Physical modeling of waste inclusions stability during mining of complex structured deposits. Progressive Technologies of Coal, Coalbed Methane, and Ores Mining, 25-30.https://doi.org/10.1201/b17547
19. Van der Werf, I.D., Fico, D., De Benedetto, G.E., Sabbatini, L. (2016). The molecular composition of Sicilian amber. Microchemical Journal, (125), 85-96.http://doi.org/10.1016/j.microc.2015.11.012
20. Korniyenko V.Ya., Vasylchuk O.Yu., Zaiets V.V., Semeniuk V.V., Khrystyuk A.O., Malanchuk Ye.Z. (2022). Research of amber extraction technology by vibroclassifier. IOP Conf. Ser.: Earth Environ. Sci. 1049 012027. https://doi.org/10.1088/1755-1315/1049/1/012027

21. Korniyenko V., Nadutyi V., Malanchuk Y., Yeluzakh M. (2020) Substantiating velocity of amber buoying to the surface of sludge-like rock mass. Mining of Mineral Deposits, 14(4), 90-96. DOI:https://doi.org/10.33271/mining14.04.090

22. Malanchuk Z., Korniyenko V., Malanchuk Ye., Khrystyuk A., Kozyar M. Identification of the process of hydromechanical extraction of amber. E3S Web of Conferences. Volume 166 (2020) 02008 DOI: https://doi.org/10.1051/e3sconf/202016602008

23. Malanchuk, Z., Korniienko, V., Malanchuk, Y., Moshynskyi, V. Analyzing vibration effect on amber buoying up velocity.E3S Web of Conferences 123, 01018 (2019). Ukrainian School of Mining Engineering - 2019. DOI: 10.1051/e3sconf/201912301018

24. Malanchuk, Y., Korniienko, V., Moshynskyi, V., Soroka V., Khrystyuk, A., Malanchuk, Z. Regularities of hydromechanical amber extraction from sandy deposits. Mining of mineral deposits. - 2019. DOI: 10.33271/mining13.01.049

25. Low-grawity Fluid Mechanics. Mathematical Theory of Capillary Phe-nomena / A.D. Myshkis, V.G. Babskii, N.D. Kopachevskii, L.A. Slobozhanin, A.D. Tyuptsov - Springer-Verlag Berlin, Heidelberg, New York, London, Paris, Tokyo, 1986. 602 pp.

26. Nadutyi, V., Korniyenko, V., Malanchuk, Z., Cholyshkina, O. Analytical presentation of the separation of dense suspensions for the extraction of amber. E3S Web of Conferences 109, 00059 (2019). Essays of Mining Science and Practice. DOI: 10.1051/e3sconf/20191090005

27. Malanchuk Z., Moshynskyi V., Martyniuk P., Stets S., Galiyev D. (2020) Modelling hydraulic mixture movement along the extraction chamber bottom in case of hydraulic washout of the tuff-stone. E3S Web of Conferences. Volume 211 (2020) 01011 DOI:https://doi.org/10.1051/e3sconf/202020101011

28. Sai, K., Malanchuk, Z., Petlovanyi, M., Saik, P., Lozynskyi, V. Research of thermodynamic conditions for gas hydrates formation from methane in the coal mines. Solid State Phenomena (2019). DOI: 10.4028/www.scientific.net/SSP.291.155.

Badanie procesu odwadniania mas wydobywczych zawierających bursztyn

W artykule przedstawiono wyniki badań procesu odwadniania masy wydobywczej zawierającej bursztyn, za pomocą wibroklasyfikatora. Opisano cechy schematu technologicznego wydobywania bursztynu w odniesieniu do punktów zaopatrzenia w wodę. Badano stan równowagi cieczy w komorze wibroklasyfikatora w różnych warunkach zwilżalności sita: ciecz niezwilżająca włókien sita; płyn zwilżający włókna sita; cienka warstwa cieczy zwilżającej włókna sita.

W wyniku przeprowadzonych badań ustalono, że w przypadku gdy ciecz nie zwilża włókien sita, wysokość maksymalnie zatrzymanej w komórce warstwy cieczy jest co najmniej 3 razy większa niż w przypadku cieczy zwilżającej włókna sita. Wiarygodność uzyskanych wyników potwierdza zastosowanie sprawdzonych metod badawczych oraz względny błąd pomiędzy wartościami obliczonymi a doświadczalnymi na poziomie 20%.

Słowa kluczowe: *bursztyn, wibroklasyfikator, komora sitowa, odwadnianie*

Dominant Determinants of Adaptation of the Mining Complex in the Conditions of a Dynamic Environment

Yulian HRYHORIEV[1)], Serhii LUTSENKO[2)], Serhii JOUKOV[3)]

[1)] Kryvyi Rih National University, Vitaly Matusevich str, 11, Kryvyi Rih, Ukraine; email: yulian.hryhoriev@knu.edu.ua; lutsenkoserhii@knu.edu.ua; joukov07@knu.edu.ua; ORCID https://orcid.org/0000-0002-1780-5759
[2)] Kryvyi Rih National University, Vitaly Matusevich str, 11, Kryvyi Rih, Ukraine; email: lutsenkoserhii@knu.edu.ua; ORCID https://orcid.org/0000-0002-5992-3622
[3)] Kryvyi Rih National University, Vitaly Matusevich str, 11, Kryvyi Rih, Ukraine; email: joukov07@knu.edu.ua; ORCID https://orcid.org/0000-0001-7933-6575

http://doi.org/10.29227/IM-2023-01-02

Submission date: 14-02-2023 | Review date: 20-03-2023

Abstract

Modern business conditions increasingly clearly demonstrate the dynamism of the surrounding world. Such changes in economic, technological, social and economic factors must be taken into account when planning and designing mining operations. In this article, it is proposed to consider the mining region as an anthropotechnical complex from the standpoint of a systemic approach. Management strategy of an open-pit group was developed and nomograms for practical use are given on its basis. Based on this decomposition approach, an adaptation mechanism is proposed. Its principle is that a set of adaptation tools is adopted for each rank of the anthropotechnical complex. The experience of using these tools in the conditions of the Kryvyi Rih mining region is given, in particular, the use of worked out space for the placement of overburden from other open-pits, the joint placement of enrichment tailings and waste rocks, etc. An approach to distinguishing stages and indicators of adaptation according to the proposed mechanism is proposed.

Keywords: *open-pit mining, adaptation mechanism, anthropotechnical complex, adaptation tools, dynamic environment*

INTRODUCTION

The dynamics of fluctuations in demand and prices for products of mining enterprises is characterized by high volatility. At the same time, significant inertia is inherent in the dynamics of fluctuations in the volume of consumption of mineral products, but almost never the graphs of the curves of these dependent indicators are consistent over time.

In economic theory, many thorough studies have been carried out, which particularly interested us, regarding price forecasting by distinguishing cycles of different durations: over a century, over several decades, normal economic cycles, small cycles, specific fluctuations within certain branches of the economy (for example, mining production), etc. Cycles of different durations were named after the names of their researchers: cycles with a duration of 45–60 years (long or large) are Kondratiev cycles; 15–20 are Kuznets cycles; 7–12 (average cycles) are Juglyar cycles; 3–4 years (short or small) are Kitchin cycles [1–2].

The graphs of the dynamics of the price of iron ore from 1980 to 2022 (Figure 1) [3] and world steel production (Figure 2) [4] can serve as confirmation of the above. The second graph is characterized by a constant growth for almost its entire history, while the price at Figure 1 fell by more than 60%.

A number of scientific studies were conducted for conditions of unpredictable price and demand for products of mining enterprises [5–7].

These studies fully explained the effect of the pricing mechanism, established the main interdependencies of cause and effect factors and clearly proved their corresponding regularities. But, at the same time, existing theories do not always allow comprehensively specifying the parameters of a particular manufacturing system, predicting its development, and reliably explaining some inconsistencies that experts constantly encounter, especially in mining [8–10].

This clearly leads to the conclusion about the presence of non-market factors in price formation, which makes it even more difficult to forecast the price of mineral products, without which it becomes impossible to effectively manage the mining complex, which, in fact, determined the direction of the research described below.

The essence of the considered problem is determined by the fact that large mining enterprises are extremely inert manufacturing systems, mostly unable to adequately and promptly change their productivity in accordance with the dynamics of real conjunctural evolutions of the raw material market. Therefore, having practically no levers of influence on this market, they have adaptive capabilities, environment and methods limited exclusively to the internal operational space, the implementation of which becomes possible mainly in the form of clearly targeted and comprehensively dosed adaptive variation of the parameters of the elements of their manufacturing systems.

FORMATION OF A DYNAMIC BUSINESS ENVIRONMENT

Under these conditions, controlling influences on the mining complex, according to the observations of the authors of this study, often lead to quite diverse reactions, both in time and in the network structures of production subsystems, including sometimes quite indirectly connected with the "main

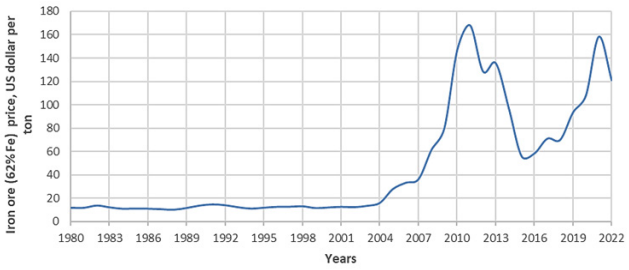

Fig. 1. Iron Ore (Fe 62%) spot price dynamic from 1980 to 2022
Rys. 1. Dynamika ceny spotowej rudy żelaza (Fe 62%) w latach 1980–2022

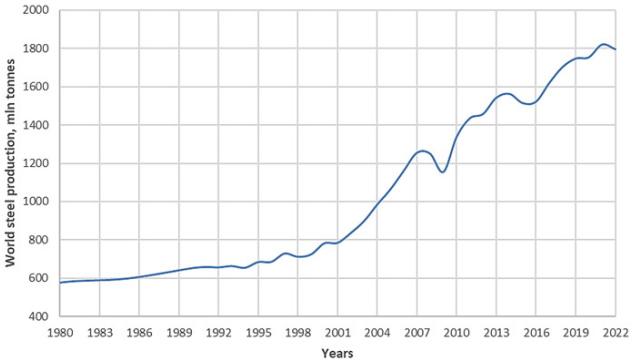

Fig. 2. World steel production from 1980 to 2022
Rys. 2. Światowa produkcja stali w latach 1980–2022

production chain". Not only that, the authors have repeatedly observed a rather unexpected new phenomenon, which by its nature of repetition with fading intensity is remotely reminiscent of the effect of reverberation. We are only developing the study of this phenomenon, as it is hypothetically a mediated manifestation of a certain cyclical nature of the permanent functioning of the mining complex under the influence of external factors, primarily of a strategic level, the scale and effects of which do not correspond to the scope of this article, except for a very brief directed only at them causal analysis.

The main indicators of open-pit mining, which we consider below as an example, at the level of strategic design decisions, are: the mining schedule, characterized by overburden ratio; step-by-step productivity of the open-pit for ore and secondary raw materials and perspective contours of the open-pit. Since it is they who determine the composition and structure of technological complexes (types and quantity of mining equipment with its distribution and grouping), the volume of mining capital works and the construction of industrial facilities, the number of workers, etc. That is, they determine the volume, structure and dynamics of investments, capital and operating costs, and income from the sale of goods. And here, in the conditions of modern post-Soviet Ukraine, two fundamentally opposite problems collide:

1. The total inertia of mining complexes due to the colossal scale and duration of development, as well as the size and productivity of mining machines, which are often unique.

2. Exceptionally dynamic evolution of the global and regional raw material markets as a result of rapid changes in economic and political situations, and most importantly – fundamental transformations in technique and technology caused by the transition of society to a fundamentally new system.

In mining, this duality of the problem is not only not compensated promptly, but even on the contrary it is even more intensified and complicated due to the deepening of mining operations. And all this under the condition that the "life cycle" of mining enterprises is 40 years or more on average.

The development of iron ore deposits of Ukraine at the current stage consists in the fact that mining enterprises work with constant production capacity, which, taking into account the above-mentioned inertness of mines, worked almost perfectly under the conditions of a planned socialist economy, but under current conditions they did not absolutely.

This shows that, in general, the existing mining development strategies are based on an outdated principle, when the final state of mining operations is determined as accurately as possible, which must be achieved after a long period of time. Next, it is recorded what needs to be done in order to reach this final state. After that, an action plan is drawn up with a breakdown by time intervals (five-year periods, years and quarters), the implementation of which should ensure the achievement of the final, clearly set goal. With this understanding, the mining development strategy is a classic long-term plan for achieving a specific final goal, namely a long-term mining plan, in which the volume of ore production is fixed in each specific time period and in the final period.

MANAGEMENT STRATEGY OF AN OPEN-PIT GROUP

This approach is based on the fact that all changes in the external environment are considered predictable, and therefore stable, while significant fluctuations in prices and demand for products are observed in the markets of mineral raw materials. It is almost impossible to predict these fluctuations in the long term due to the above-mentioned problems, therefore, during the operation of open-pits with a constant

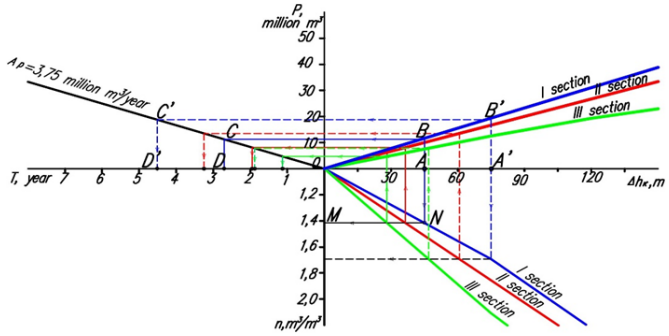

Fig. 3. Nomogram for determining the duration of working out of open-pit sections at different mining intensity

Rys. 3. Nomogram do wyznaczania czasu eksploatacji odkrywek przy różnej intensywności eksploatacji

production capacity, there are additional costs associated with the forced unplanned storage of unsold finished products in the warehouse – during the period of falling demand. And on the other hand, enterprises lose the opportunity to increase profits during the period of growth in demand due to the impossibility of operational intensification of production to cover market needs [11–13]. In this connection, the goals of mining enterprises are changing significantly. The issue of ensuring competitiveness, which depends on the adopted strategy for the development of mining operations, becomes of primary importance. Therefore, this strategy of any combine and Kryvbas as a whole will change.

In the conditions of the market environment, there is a need for adequate adaptation of mining productions to changing market conditions. Examples of such adaptation clearly show that the current mining development strategies (methods of mining development planning and pit design) do not foresee changes in the intensity of deposit development over long periods [14]. At the same time, we note the lack of a mechanism for a reasonable selection of the production capacity of the open-pits and the mining schedule, taking into account their interrelationship when the demand for iron ore raw materials changes. Thus, the increase in demand for minerals, in most cases, leads to an increase in the volume of its extraction, while the strip ratio do not change. A decrease in demand leads to a decrease in the volume of mineral extraction, simple equipment and other fixed assets, a reduction in the number of employees, etc. At the same time, the strip ratios are reduced to reduce the cost of commodity products. The consequence of which is the accumulation of overburden backlog at enterprises, the occurrence of unscheduled temporarily non-working sides at the expense of the violation of the principle of proportional conduct of work and the development of the open-pit space, as well as the formation of temporarily non-working sides in the mining zone, which is unacceptable. Periodically, but inevitably, there is a need to revise previous projects due to the deviation of the actual state of mining operations from the design solutions [15, 16]. Therefore, the mining development strategy should take into account the possibility and mechanisms of adaptive adjustment of the intensity of deposit development when the demand for commodity products changes, both at the level of an individual open-pit or a group of mine pits, and at the level of a group of mines that are part of the same company.

In connection with the above, we have developed a strategy for the development of mining works of open-pits in the conditions of changing demand for iron ore products, according to which this development should ensure the given intensity of working out the deposit, which is determined by the maximum efficiency of the development of the raw material base of the plant in the specified conditions (Fig. 3).

In any case, the volume of production of commodity products of mining and processing plants is adjusted when the need for it changes due to changes in the productivity of open-pits that are part of one plant [17]. Therefore, the optimization of the production capacity of the mining and processing plants that are part of one company can be achieved only under the condition of systematic optimization of the ore productivity of the open-pits that are part of each separate plant. Increasing the production capacity of the plants above the maximum possible values entails the commissioning of new processing factories or the reconstruction of existing ones with more advanced ore processing technology.

The efficiency of the mining and processing plant with different options for productivity and schedule of mining operations in each pit (Fig. 4) can be judged by the economic-mathematical model of the work of a group of pits in the plant system, that shown in Eqs. (1) below:

$$\sum_{t=1}^{T}\sum_{k=1}^{K}\sum_{i=1}^{I}\left(\left(\frac{\sum_{j=1}^{J}(A_{p\,tkij}\cdot\gamma_{k\,tkij}\frac{\beta_{(tkij)}}{\beta_{пл\,(ki)}}Ц_{tki})-c_{tki}\cdot\sum_{j=1}^{J}(A_{p\,tkij}\cdot\gamma_{k\,tkij})-BF_{tki}}{(1+E)^{t}}\right.\right.$$
$$-\left.\left.\frac{\sum_{j=1}^{J}((a_{o\,tkij}+n_{tij}\cdot b_{tij})\cdot A_{p\,tkij}+BK_{tkij})}{(1+E)^{t}}\right)\times(1-N)-\right.$$
$$\left.-\sum_{t=1}^{T}\frac{\sum_{j=1}^{J}\left(\left(\Delta V^{y}_{lag(tij)}+\Delta Q_{пл(tij)}\right)k_{in}+KF_{ti}\right)}{(1+E)^{t}}\right)\rightarrow max \qquad (1)$$

where $\Delta V^{y}_{lag(tij)}$ – increase in annual volumes of overburden lag liquidation at the j-th pit of the i-th plant in the t-th year, m³

$\Delta Q_{m(tij)}$ – the increase in production capacity of the open-pit by mining mass with an increase in productivity by ore at the j-th pit of the i-th plant in the t-th year, m³

k_{in} – specific capital costs for increasing open-pit productivity by mining mass, monetary units/m³;

KF_t – capital investments in the t-th year to increase the productivity of the enrichment factory, monetary units.

ADAPTATION MECHANISM OF THE MINING SYSTEM

Let's take a closer look at the mechanism of adaptation of the mining system to changes in external factors. Managed adaptation of the mining enterprise in this context is a set of

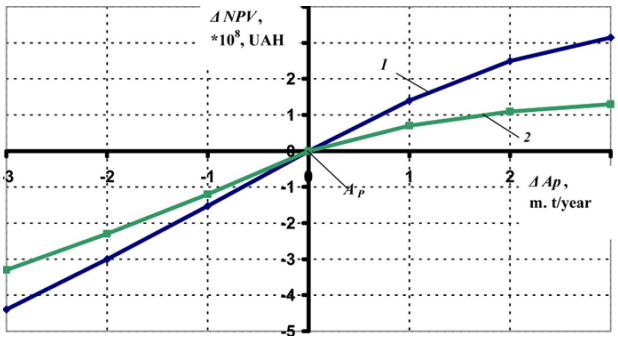

Fig. 4. Change in the annual net present value of cash flows (ΔNPV) depending on the change in productivity (Ap) of ore pits: 1 – Pershotravnevoho; 2 – Hannivskoho

Rys. 4. Zmiana rocznej wartości bieżącej netto przepływów pieniężnych (ΔNPV) w zależności od zmiany produktywności (Ap) wyrobisk rudnych: 1 – Perszotrawnewoho; 2 – Hanniwskoho

organizational, technical and technological measures to preserve or improve the technical and economic performance of the mining enterprise when external factors change [18, 19]. The mechanism of adaptation is a set of phenomena in the environment of its implementation.

To systematize the tools that can be used within the scope of these measures, a decomposition of the mining complex should be carried out from the standpoint of a systemic approach [20].

Mining production can be hierarchically considered as proposed by Prof. Sinchkovsky [21], it is an anthropotechnical system consisting of anthropotechnical complexes of various ranks. The anthropotechnical complex here is understood as a single technical and technological object, which is considered in conjunction with the personnel and ensures the execution of specified production operations.

Mining operations in open-pits are technologically constructed in such a way that each stage of changing the state of the massif or the properties of rocks in the process of their processing requires the functioning of a certain elementary anthropotechnical complex that has its own potential. In the production process, one or another sequence of the use of disparate elements of anthropotechnical complexes in joint work reveals in them the system-forming property of complementing each other, creating a collective potential. Based on this, we can hierarchically distinguish anthropotechnical complexes of three ranks, while the complex of a higher rank includes complexes of a lower rank.

Anthropotechnical complex of the 1st rank is a technological complex of equipment or a complex of mechanization in n open-pit, mine or man-made deposit. For example, an extraction and delivery complex, a drilling and blasting complex, a bulking complex, etc.

Anthropotechnical complex of the 2nd rank is a separate mining enterprise formed by a collection of mining facilities. In other words, it is an extractive production unit that includes anthropotechnical complexes of the 1st rank. For example, an open-pit, a mine, a dump, a separate warehouse, a tailings storage facility, a bulk man-made deposit, etc.

Anthropotechnical complex of the 3rd rank is mining complex. The complex refers to a set of mining enterprises located in the same region and having stable technological, logistical, economic and financial connections between them. Unification of enterprises into such structures becomes possible when mining enterprises belong to the same owner. Then the outlined connections between such enterprises strengthen, and market competition between them, on the contrary, disappears. Accordingly, the market position and technological potential of the entire complex are strengthened. The formation of such complexes begins with the simultaneous development of natural and man-made deposits of individual enterprises, and in the future it is reduced to the management of the schedule of mining operations and the productivity of the entire complex of enterprises.

From the point of view of a systemic approach, at every level the work of a mining enterprise is influenced by external and internal factors. However, depending on the order of the anthropotechnical complex, the same factor can be both internal and external. The change of external factors leads to failure of the rhythmic functioning of the system. However, when managing an anthropotechnical complex of the third rank – a mining complex – the set of internal, controlled factors increases, and therefore the possibilities of system adaptation increase.

Thus, we are talking about the second component of the system adaptation mechanism – adaptation tools. Adaptation tools mean internal factors that can change at the system level of the chosen order. Obviously, the set of these tools will differ for anthropotechnical complexes of each rank.

An example of the implementation of adaptation tools for an anthropotechnical complex of the first rank can be the results of industrial tests at the Petrivskyi quarry of PJSC "Central GZK" of the company "Metinvest" regarding the installation of buckets of increased capacity when working with excavators on overburden. As a result of the difficult economic situation in the country, the company does not have the opportunity to update the fleet of loading and unloading equipment in a timely manner. However, the need to carry out the planned volumes of mining works requires adaptation of the production system. Replacing an 8 m³ bucket with a 10 m³ bucket will significantly increase excavator productivity, reduce dump truck loading times and potentially reduce the fleet of primary mining equipment [22, 23].

An example of tools for adapting the second-rank complex can be the implementation of a system for dispatching and automating the operation of the main mining equipment at the open pit of "Inguletskii GZK". The introduction of a single software complex helps to reduce the waiting time of

dump trucks for loading by an average of 30–60 seconds. This leads to an increase in the rhythm of the entire quarry, reduces fuel costs and increases the efficiency of equipment use. Since the digitization of production processes by a single system concerns several complexes of the first order, the tool belongs to the complex of the second order.

The management of the developed space [24] within the entire enterprise or adjacent enterprises within the mining complex can be an example of a third-rank adaptation tool [25–27]. For example, for the placement of overburden extracted from the Gleyuvatskiy open-pit of PJSC "Central GZK", the worked-out space of the open-pit №2 of the same enterprise is used, the funnels formed as a result of the underground development of the deposit are filled, and the stop prisms of the tailings storage facility of the plant are formed [28–31].

The next component of the adaptation mechanism of the mining complex is the allocation of adaptation stages:

1) detection of changes in the external environment and assessment of the impact on the system. Depending on the nature of external changes, at this stage the technical-economic, technological and organizational indicators of the system are evaluated in two states: before the occurrence of external changes and after it;

2) selection of a complex rank, at which a decision should be made regarding changes in the internal environment. For this, the components and processes affected by the changes should be studied and determined;

3) calculation and modeling of changes in the internal environment in response to the dynamics of external factors;

4) application of the adaptation tool;

5) evaluation of the result of system adaptation and obtaining conclusions. At this stage, techno-economic, technological and organizational indicators are evaluated after the application of the adaptation tool and compared with the evaluations at the first stage.

A comparison of these indicators allows determining the adaptive potential of the anthropotechnical complex.

CONCLUSION

Thus, the management conditions of mining enterprises are characterized by high dynamics of external factors, and in view of the retrospective analysis, these dynamics will only increase in the future. Mining enterprises in Ukraine partially still offer planned economy approaches in the design of their activities. This problem can be corrected by following the management strategy of the mining complex, taking into account changes in the price of products of enterprises. In their work, mining enterprises must use the mechanism of adaptive management, taking into account the systematic decomposition of mining units.

Future scientific research will be aimed at a more in-depth study of the indicators of the adaptation mechanism of mining enterprises and their adaptive potential.

Literatura – References

1. Žižlavský, O. (2014). Net Present Value Approach: Method for Economic Assessment of Innovation Projects. Procedia - Social and Behavioral Sciences, 156, 506–512. https://doi.org/10.1016/j.sbspro.2014.11.230
2. Kirilenko, V. (2007). Istoria ekonomichnih vchen (p. 233). Ekonomichna dumka.
3. International Monetary Fund. (2022, October). World Economic Outlook Database, October 2022. IMF. https://www.imf.org/en/Publications/WEO/weo-database/2022/October
4. World Steel Association. (2022). World Steel in Figures 2022. Worldsteel.org; WSA. https://worldsteel.org/steel-topics/statistics/world-steel-in-figures-2022/
5. Lamghari, A., & Dimitrakopoulos, R. (2020). Hyper-heuristic approaches for strategic mine planning under uncertainty. Computers & Operations Research, 115, 104590. https://doi.org/10.1016/j.cor.2018.11.010
6. Xu, X., Gu, X., Wang, Q., Zhao, Y., Kong, W., Zhu, Z., & Wang, F. (2023). Enumeration optimization of open pit production scheduling based on mobile capacity search domain. Scientific Reports, 13(1), 91. https://doi.org/10.1038/s41598-022-27336-y
7. Lutsenko, S., Hryhoriev, Y., Peregudov, V., Kuttybayev, A., & Shampykova, A. (2021). Improving the methods for determining the promising boundaries of Iron Ore Open pits. E3S Web of Conferences, 280, 01005. https://doi.org/10.1051/e3sconf/202128001005
8. Lutsenko, S. (2017). Open pits productivity control along with iron ore products demand variation. Quality – Access to Success, 18(S1), 226-230
9. Hałasik, K., & Kulczycka, J. (2016). CSR, environment-friendly investments and innovations - the three elements necessary to build a modern and strong coal mining company? E3S Web of Conferences, 10, 00051. https://doi.org/10.1051/e3sconf/20161000051
10. Lamghari, A., & Dimitrakopoulos, R. (2016). Network-flow based algorithms for scheduling production in multi-processor open-pit mines accounting for metal uncertainty. European Journal of Operational Research, 250(1), 273–290. https://doi.org/10.1016/j.ejor.2015.08.051
11. Pysmennyi, S., Fedko, M., Shvaher, N., & Chukharev, S. (2020). Mining of rich iron ore deposits of complex structure under the conditions of rock pressure development. E3S Web of Conferences, 201, 01022. https://doi.org/10.1051/e3sconf/202020101022
12. Selyukov, A., Gerasimov, A., & Byrdin, K. (2019). Justification of the Relationship of Production Capacity and the Parameters of the Blocks at Surface Mining of Existing Kuzbass Quarry Fields. E3S Web of Conferences, 105, 01047. https://doi.org/10.1051/e3sconf/201910501047
13. Tyukov, P. O., & Loginov, E. V. (2021). Substantiation of development system parameters taking into account the main dimensions of working equipment used in the development of mineral deposits by open-pit method. E3S Web of Conferences, 266, 04014. https://doi.org/10.1051/e3sconf/202126604014
14. Bakhtizin, A., Loginov, E., Shkuta, A., & Abramov, V. (2018). Counter-Strategy to Emergencies in the Coal Mining Industry Based on the Use of Multi-Agent Systems and Fuzzy Logic. E3S Web of Conferences, 41, 04037. https://doi.org/10.1051/e3sconf/20184104037
15. Selyukov, A., & Rybár, R. (2019). Calculation of Boundary Stripping Ratio Errors at the Stage of Quarries Designing. E3S Web of Conferences, 105, 01043. https://doi.org/10.1051/e3sconf/201910501043
16. Shustov, O. O., Pavlychenko, A. V., Bielov, O. P., Adamchuk, A. A., & Borysovska, O. O. (2020). Calculation of the overburden ratio by the method of financial and mathematical averaged costs. Naukovyi Visnyk Natsionalnoho Hirnychoho Universytetu, 5, 30–36. https://doi.org/10.33271/nvngu/2021-5/030
17. Blizniukov, V.H., & Lutsenko, S.O. (2017). Improvement of technical criteria for comparative evaluation of mining operation options of iron ore open pits. Naukovyi Visnyk Natsionalnoho Hirnychoho Universytetu, 1, 44–49
18. Cehlár, M., Janočko, J., Demirel, N., Anyona, S., Vöth, S., Tyulenev, M., & Zhironkin, S. (2017). From Mining Innovations to Sustainable Development: Keynote Speakers of the First to the Second International Innovative Mining Symposium. E3S Web of Conferences, 21, 00002. https://doi.org/10.1051/e3sconf/20172100002
19. Kalenov, O., & Kukushkin, S. (2018). Techno-Park Assistance in Mining Regions' Integration into the Innovative Economy. E3S Web of Conferences, 41, 04025. https://doi.org/10.1051/e3sconf/20184104025
20. Koščová, M., Hellmer, M., Anyona, S., & Gvozdkova, T. (2018). Geo-Environmental Problems of Open Pit Mining: Classification and Solutions. E3S Web of Conferences, 41, 01034. https://doi.org/10.1051/e3sconf/20184101034
21. Sinchkovskiy, V., Vokin, V., & Sinchkovskaya, E. (2007). Tekhnologiya otkrytykh gornykh rabot (2nd ed., p. 528). SFU.

22. Strelnikov, A., Markov, S., Rattmann, L., & Weber, D. (2018). Theoretical Features of Rope Shovels and Hydraulic Backhoes Using at Open Pit Mines. E3S Web of Conferences, 41, 01003. https://doi.org/10.1051/e3sconf/20184101003

23. Voronov, Y., & Voronov, A. (2017). Functional Quality Criterion of Rock Handling Mechanization at Open-pit Mines. E3S Web of Conferences, 21, 03003. https://doi.org/10.1051/e3sconf/20172103003

24. Selyukov, A., Blištan, P., Jacko, S., & Bauer, V. (2018). Proportionality and Cyclicity of the Quarry Working Area Development. E3S Web of Conferences, 41, 01031. https://doi.org/10.1051/e3sconf/20184101031

25. Solovitskiy, A., Brel, O., Nikulin, N., Nastavko, E., & Meser, T. (2017). Land Resource Management as the Ground for Mining Area Sustainable Development. E3S Web of Conferences, 21, 02012. https://doi.org/10.1051/e3sconf/20172102012

26. Bolatova, A., & Kuttybayev, A. (2022). Use of mining and metallurgical waste as a backfill of worked-out spaces. Series of geology and technical sciences, 1(451), 33–38. https://doi.org/10.32014/2022.2518-170x.137

27. Joukov, S., Lutsenko, S., Hryhoriev, Y., Martyniuk, M., & Peregudov, V. (2020). Justification of the method of determination of the border overburden ratio. E3S Web of Conferences, 166, 02005. https://doi.org/10.1051/e3sconf/202016602005

28. Lutsenko, S., Hryhoriev, Y., Peregudov, V., Kuttybayev, A., & Shampykova, A. (2021). Improving the methods for determining the promising boundaries of iron ore open pits. E3S Web of Conferences, 280, 01005. https://doi.org/10.1051/e3sconf/202128001005

29. Belov, O., Shustov, O., Adamchuk, A., & Hladun, O. (2018). Complex Processing of Brown Coal in Ukraine: History, Experience, Practice, Prospects. Solid State Phenomena, 277, 251–268. https://doi.org/10.4028/www.scientific.net/ssp.277.251

30. Peregudov, V., Hryhoriev, I., Joukov, S., & Hryhoriev, Y. (2020). Determination of the transfer step of the ore chute while mining the technogenic deposit of the bulk type. E3S Web of Conferences, 166, 02004. https://doi.org/10.1051/e3sconf/202016602004

31. Grigoryev, Y. & Pyzhik, N. (2015). Dry raw material technogenic deposits formation and development technique. Metallurgical and Mining Industry, 3, 298–303. https://www.metaljournal.com.ua/assets/Journal/english-edition/MMI_2015_3/039%20Pyzhik.pdf

Dominujące uwarunkowania adaptacji kompleksu górniczego w warunkach środowiska dynamicznego

Współczesne uwarunkowania biznesowe coraz wyraźniej pokazują dynamikę otaczającego świata. Takie zmiany czynników ekonomicznych, technologicznych, społecznych i ekonomicznych muszą być brane pod uwagę przy planowaniu i projektowaniu działalności górniczej. W artykule proponuje się potraktowanie rejonu górniczego jako kompleksu antropotechnicznego z punktu widzenia podejścia systemowego. Opracowano strategię zarządzania kopalnią odkrywkową i na jej podstawie podano nomogramy do praktycznego wykorzystania. Na tej podstawie zaproponowano mechanizm adaptacyjny. Jego zasadą jest przyjmowanie zestawu narzędzi adaptacyjnych dla każdej rangi zespołu antropotechnicznego. Podano doświadczenia w stosowaniu tych narzędzi w warunkach górniczych Krzywego Rogu, w szczególności wykorzystanie zagospodarowanej przestrzeni do składowania nadkładu z innych odkrywek, wspólnego składowania odpadów poflotacyjnych i skał płonnych itp. Zaproponowano podejście do wyodrębnienia etapów i wskaźników adaptacji według proponowanego mechanizmu.

Słowa kluczowe: *górnictwo odkrywkowe, mechanizm adaptacyjny, kompleks antropotechniczny, narzędzia adaptacyjne, środowisko dynamiczne*

Substantiating the Patterns of Geomechanical Factors Influence on the Shear Parameters of the Coal-Overlaying Formation Requiring Degassing at High Advance Rates of Stoping Faces in the Western Donbas

Volodymyr BONDARENKO[1)], Ildar SALIEIEV[2)], Hennadii SYMANOVYCH[3)], Iryna KOVALEVSKA[4)], Maksym SHYSHOV[5)]

[1)] Dnipro University of Technology; 19 Yavornytskoho Ave., Dnipro, Ukraine; ORCID http://orcid.org/0000-0001-7552-0236; email: v_domna@yahoo.com
[2)] LLC "DTEK Energy"; 57 Lva Tolstoho St., Kyiv, Ukraine; ORCID https://orcid.org/0009-0004-5830-352X; email: donenkomi@dtek.com
[3)] Dnipro University of Technology; 19 Yavornytskoho Ave., Dnipro, Ukraine; ORCID http://orcid.org/0000-0002-2121-1742; email: symanovych.h.a@nmu.one
[4)] Dnipro University of Technology; 19 Yavornytskoho Ave., Dnipro, Ukraine; ORCID https://orcid.org/0000-0002-0841-7316; email: kovalevska_i@yahoo.com
[5)] LLC "DTEK Energy"; 57 Lva Tolstoho St., Kyiv, Ukraine; ORCID https://orcid.org/0000-0003-1627-0868; email: shyshovmv@dtek.com

http://doi.org/10.29227/IM-2023-01-03

Submission date: 03-02-2023 | Review date: 05-03-2023

Abstract

The issues of developing ideas about the mechanism of coal mining from gas fields and two components of providing the country with energy carriers are studied: coal mining and methane utilization from coal-bearing stratum. These issues are inextricably linked with the mining of deposits with high-velocity longwall faces. The actual problem of resolving the above contradictions is studied. The patterns of the geomechanical factors influence based on the finite element method (FEM) modeling of the coal-overlaying formation shear parameters are studied from the point of view of substantiating the location schemes for the site outgassing wells at high advance rates of stoping faces in the Western Donbas. The obtained results of computational experiments are compared with the corresponding studies of specialists. The conclusions about the degree of geomechanical factors influence and the need to take them into account are substantiated. Three calculation models have been developed and substantiated in terms of the shape and size of the calculation zone, the rock mass texture, the mechanical properties of its lithotype, the loading conditions at the model boundaries, the characteristics of the link between stresses and deformations in the model elements, and the criteria for determining the limiting state. The significant influence of the longwall face location depth and the mass texture on the shear parameters of the coal-overlaying formation has been proved. Based on the data of computational experiments, the corresponding dependences and regression equations have been obtained. The conducted research makes it possible to choose appropriate location schemes for outgassing wells.

Keywords: *coal seam, drift, longwall face, powered support, mine*

1. INTRODUCTION

The coal industry is the main sector in ensuring Ukraine's energy independence and remains so for the long term. The country has all the possibilities to minimize dependence on resource imports [1–3]. Despite the experts' statements, the dynamics of demand for coal in the world markets indicates an increase in its consumption [4]. For example, over the past two years, the global coal consumption volume has increased by 5.7% [5], and the thermal coal cost has risen to $430 per ton. Thus, the energy component will continue to play a key role in the country's energy independence. Currently, there are two components of energy supply: coal mining and methane utilization from the coal-bearing stratum. However, gas emission limits the coal mining rates during the operation of modern high-velocity longwall faces. Modern high-performance stoping equipment in the Western Donbas often fails to achieve its technical targets due to the emission of excess methane. Therefore, the parameters of the site outgassing technology are an influential factor in increasing the productivity of coal mining. The choice of expedient site outgassing parameters is related to the shear patterns of coal-overlaying formation and its main characteristics [6, 7]. In this sense, there is an opinion among experts that the process of the coal-overlaying formation shear is most adequately reflected by modern methods of modeling geomechanical objects, of which the finite element method is the most common [8–11]. As for the Western Donbas conditions, a lot of experience has been gained in the studies [12–16], which were used to determine the patterns of influence of mining-geological and mining-technical factors on the process of transforming the texture of a rock mass adjacent to the area of stope operations [17–19]; it is worth recalling here that, according to existing ideas, stratification, weakening, fracturing, etc. in the coal-overlaying formation lithotypes have a significant influence on the gas emission in the undermined mass [20, 21].

2. PROBLEM FORMULATION

Research is performed by conducting a series of computational experiments, which determine the distribution fields of the main stress components: vertical σy, horizontal σx,z and

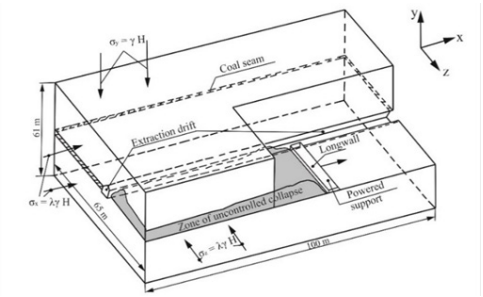

Fig. 1. Calculation scheme of the geomechanical model for mining the extraction site
Rys. 1. Schemat obliczeniowy geomechanicznego modelu eksploatacji miejsca wydobycia

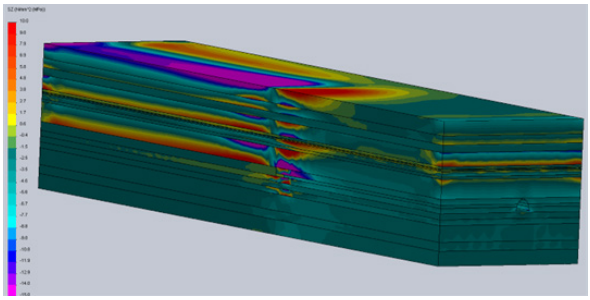

Fig. 2. The curve of horizontal stress σx distribution in a spatial model of predominantly thin- and medium-bedded textures
Rys. 2. Krzywa rozkładu naprężeń poziomych σx w przestrzennym modelu z przewagą cienko- i średniowarstwowych tekstur

the integral stress intensity index σ. Since we are particularly interested in the stratification and bending deformation of rock layers, close attention during the stress-strain state (SSS) analysis is paid to the horizontal stresses σx,z, which most clearly reflect these types of deformations. In this case, the research algorithm involves the identification (according to σx,z curves) of the distribution peculiarities of maximum bending zones of lithotypes in the rock mass under the influence of geomechanical and technological factors [22–24]. Among the experts, it is noted that a number of factors have a significant impact on the outgassing process, such as, for example, bearing pressure, physical-mechanical properties, the degree of stratification and disturbance of the coal-overlaying formation rocks, the depth of stope operations, the longwall face advance velocity, the dimensions of the mined-out area, etc [25–28]. Therefore, within the framework of the research, it is planned to study the patterns of influence of such geomechanical factors as the depth of stope operations, texture and mechanical properties of the coal-overlaying formation lithotypes, parameters of bearing pressure and de-stressing zones; the influence of the stoping face advance velocity and the parameters of outgassing wells location are also studied, but at the subsequent stages of this comprehensive research.

The own results of computational experiments are compared with the corresponding studies of other specialists, and then conclusions are drawn on the degree of influence of the listed factors and the need to take them into account at the subsequent stages of this complex program. The deformation mechanism of the coal-overlaying formation lithotypes has convincingly proved the spatial nature of this process, that is, the need to consider it simultaneously in terms of the rise – dip and along the strike of the coal seam [29]. Therefore, an objective situation requires the construction of spatial geomechanical models, which provide the opportunity to study these processes in any direction [30–33].

It is also necessary to study the influence of rock pressure anomalies in the form of frontal bearing pressure zones ahead of the longwall face, lateral bearing pressure in the non-working wall of the extraction working, and de-stressing zone behind the longwall face. To do this, appropriate sizes of geomechanical models are selected in order to fully represent the anomaly parameters.

The declared study of the texture and mechanical properties of the coal-overlaying formation lithotypes is implemented as follows. A basic texture model has been selected, which reflects the mining-geological conditions of 501 and 503 extraction sites at the Heroiv Kosmosu mine, PJSC "DTEK Pavlohradvuhillia". This model is necessary for further comparison with other textures. For this purpose, two more, typical for the Western Donbas conditions, textures of the coal-overlaying formation are modeled.

The mechanical properties of lithotypes are averaged, which is conditioned by the action of such factors. Firstly, among the mechanical properties are compressive strength and elasticity modulus (deformation). The tensile strength of lithotype samples is very low (on average 1–4 MPa), and given the impact of fracturing and moisture, it is practically absent. The same applies to adhesion along the surfaces of stratification of lithotypes, which is sometimes insignificant, and sometimes completely absent. Secondly, the data of geological survey and laboratory testing of samples provide a rather large variety in compressive strength indicators – usually, the range is 2–3 times. This relative uncertainty is enhanced by the action of weakening factors of fracturing and moisture saturation. Therefore, the error in assigning the compressive resistance index is quite large; the same relates to the index of elasticity modulus. Thirdly, weakly metamorphosed Western Donbas rocks are mainly characterized by fairly stable indicators of lithotype types. All these arguments give grounds to average the indicators of mechanical properties of lithotypes, and in order to increase

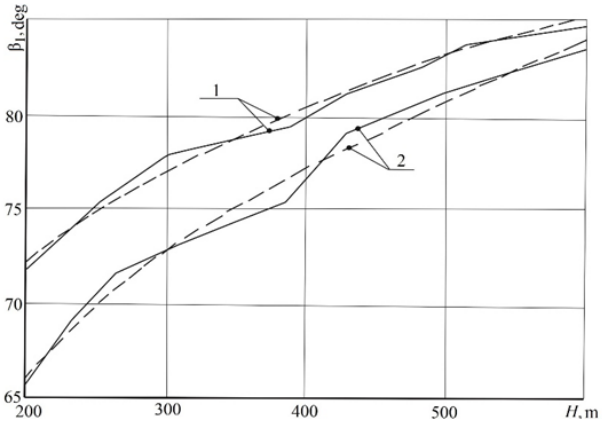

Fig. 3. The dependence of the angle β1 of the line of changing curvature sign of the coal-overlaying formation lithotypes on the depth H of stope operations: 1 – predominantly thin- and medium-bedded texture; 2 – predominantly thick- and medium-bedded texture; –––– FEM calculation results; ------regression equation

Rys. 3. Zależność kąta β1 linii zmieniającego się znaku krzywizny litotypów formacji nadwarstwowych węgla od głębokości H operacji stopowych: 1 – tekstura z przewagą cienko- i średnioławicową; 2 – tekstura z przewagą grubo- i średnioziarnistą; –––– wyniki obliczeń MES; ------ równanie regresji

the reliability of the modeling results, the lower limit of their variation has been chosen, which precisely corresponds to the mining-geological conditions of the Heroiiv Kosmosu mine.

The last paragraph of the general provisions should highlight the requirement for the selection of a physical model of the behavior of the rock mass lithotypes. In our opinion, the elastic-plastic model is the most appropriate for use, which is also substantiated in the following papers [30, 31]. This model allows, on the one hand, to take into account the plastic deformations of the Western Donbas weak rocks, and, on the other hand, it is not too complicated (in a bilinear formulation) and requires a moderate computational resource. In addition, the step-by-step calculation technology makes it possible to vary the depth of conducting stope operations within the framework of one computational experiment.

3. RESEARCH METHODS

The object of research – the processes of gas emission during the coal-overlaying formation shear – has a component related to the study of rock pressure anomalies in the area of stope operations, which for the Western Donbas conditions is described in detail in many scientific papers [12, 15, 20]. Therefore, when constructing a geomechanical model and substantiating its parameters, a number of proven recommendations from these studies are used.

Any geomechanical model is substantiated according to the generally defined FEM principles according to the following components: the shape of the calculation zone, its dimensions, the rock mass texture, the mechanical properties of its lithotypes, the conditions of their interaction along the contact planes, the loading conditions at the model boundaries, the characteristic of link between stresses and deformations in the model elements, and the criteria for determining the limiting state. Based on the above components, the parameters of three geomechanical models are substantiated. Such a quantity is caused by the need to determine the tendencies of the coal-overlaying formation texture influence on the parameters of its shear into the mined-out area.

According to the existing recommendations, the rectangular parallelepiped shape is chosen, which is the most appropriate for displaying the zone of a stratified rock mass, containing a mine working and part of the longwall face with a powered support. With regard to the objectivity and reliability of the calculation zone, it should reflect the following objects:

– a part of the virgin rock mass ahead of the longwall face, which completely encloses the propagating frontal bearing pressure (usually this distance is up to 20–30 m);

– a part of the undermined mass behind the longwall face, where rock pressure manifestations are gradually stabilizing (usually the distance is estimated to be 40–60 m);

– a part of the virgin rock mass from the non-working wall of the extraction working, where lateral bearing pressure is formed (usually this SSS anomaly propagates deep to a distance of 20–30 m);

– a part of the rock mass from the side of the longwall face; in this direction, the coal-overlaying formation SSS is stabilized at a distance of up to 20–30 m from the extraction working;

– in the coal seam roof rocks, the active coal-overlaying formation shear ceases in the zone of smooth bending of the rock layers without discontinuity; for the Western Donbas conditions, the lower zones of uncontrolled collapse and hinge-block shear occupy up to 12–15 m in height;

– in the coal seam bottom rocks, rock pressure anomalies propagate to a depth of 15–20 m.

Based on the data presented, the minimally sufficient dimensions of spatial geomechanical models characterizing three coordinates have been substantiated: Y – the height (depth) of the mass; X – the length to the dip (rise) of the seam, that is, the direction along the extraction working; Z – the width along the strike of the seam, that is, the direction along the longwall face. The geomechanical model itself and its dimensions are represented in Fig. 1 and with a certain reserve of the previously specified distances, the model has: length to the rise X = 100 m, the width along the strike Z = 65 м, height Y = 61 m, extraction working width – 5 m, extraction thickness of the seam – 1.0 m.

The coal-bearing mass texture variants are consistent with the mine's geological documentation. Special attention is paid

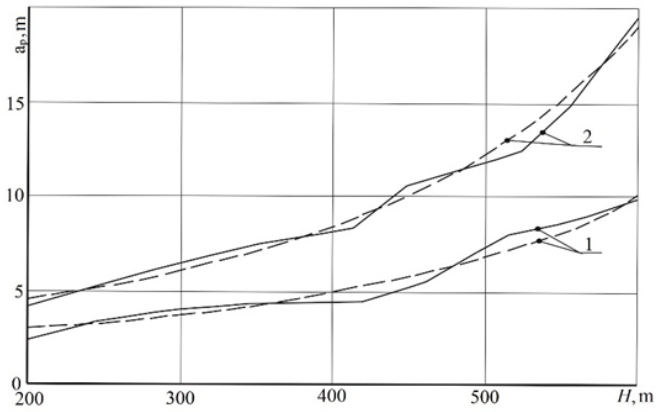

Fig. 4. An example of the dependence of the maximum bending distance ap of the most rigid lithotypes in the undermined mass bottom hole zone on the longwall face location depth H: 1 – lithotype is at a height of 14.6 m from the seam bottom; 2 – lithotype is at a height of 19.2 m; –––– FEM calculation results; ------ regression equation

Rys. 4. Przykład zależności maksymalnej odległości ugięcia ap najsztywniejszych warstw od głębokości usytuowania przodka w strefie poeksploatacyjnej H: 1 – litotyp znajduje się na wysokości 14,6 m od dna pokładu; 2 – litotyp znajduje się na wysokości 19,2 m; –––– wyniki obliczeń MES; ------ równanie regresji

to the modeling of two zones behind the longwall face: the uncontrolled collapse and hinge-block shear zones. Textural disturbances, thickness and mechanical properties of rocks in these zones are represented in accordance with the recommendations [12, 13, 15].

The mechanical properties of the roof and bottom lithotypes in the C5 seam are selected from the data of the relevant mining-geological sections, and other required mechanical characteristics are taken from the research data [34, 35] exclusively for the Western Donbas conditions. The calculated compressive resistance is determined according to the normative document [36] with supplements [13], taking into account the action of weakening factors, such as fracturing, moisture and rheology.

In accordance with the existing data of geological survey and numerous studies of the coal-bearing stratum texture in the Western Donbas, the condition of lack of adhesion between lithotypes along the planes of their bedding is accepted. This condition, while requiring additional computational resources, has a significant impact on the mass SSS [3, 13, 15] and its stability as a whole and creates a certain safety reserve for SSS calculations.

The boundary conditions on the model surfaces are selected according to proven recommendations [12]. A geostatic vertical pressure is applied to the upper horizontal surface

$$\sigma_y = \gamma H, \tag{1}$$

where γ – the weight-average unit specific gravity of rocks in the coal-overlaying formation;
H – the depth of conducting stope operations.

On the lower horizontal surface there is a rock bearing that balances the vertical pressure σy. To eliminate the local impact of a rigid bearing, a layer of damping material with the mechanical properties of argillite is placed on its surface.

On the lateral vertical surfaces of the model, according to the proven "symmetry" condition, a horizontal geostatic pressure is automatically applied

$$\sigma_{x,z} = \lambda \gamma H, \tag{2}$$

where $\lambda = \mu / 1 - \mu$ – the side thrust coefficient;
μ – the lateral deformation coefficient (in the elastic formulation – Poisson's ratio).

For the rock behavior physical model, the elastic-plastic formulation of the SSS calculation problem is chosen in the form of the so-called bilinear deformation diagram in the "stress-relative deformation" coordinates. The first linear section represents the elastic rock state with the appropriate deformation characteristics. The second linear section models the plastic (almost ideal) rock state with a very low proportionality modulus (Eel = 5 MPa) and Poisson's ratio μel = 0.5. The conjugation point of two linear sections is determined by the condition

$$\sigma = R, \tag{3}$$

where σ – the stress intensity according to the von Mises strength theory [37];
R – calculated compressive resistance of the rock, which is determined according to [13].

As for the operation of the longwall face powered support, according to the recommendations [12, 13], it is very convenient to model the real performance of hydraulic-resistant sections using a bilinear deformation diagram. The powered support is displayed as a rectangular parallelepiped, and the deformation-strength characteristics of its material completely model the section resistance. This approach is substantiated in the studies [12, 15], and for the maximum powered support resistance of up to 500–650 kPa, the elasticity modulus for the simulator material is chosen as E = 50 MPa, which takes into account the backlashes in the hinges of the hydraulic prop stays and the "lifting" of their rods at the initial stage of resistance.

Regarding the support and protection of the extraction working, it is decided not to model these structures, since their resistance affects the SSS of the adjacent rocks by no more than 1–3%.

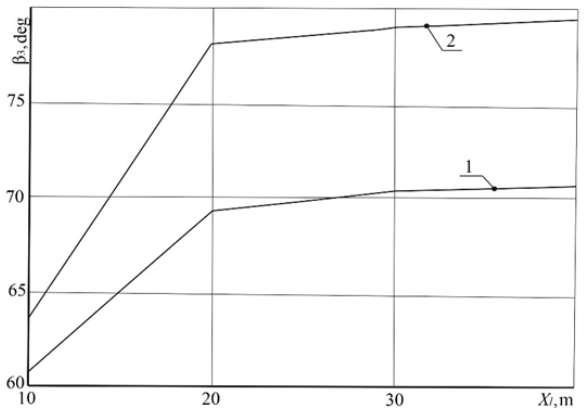

Fig. 5. Dependence of the inclination angle β3 of changing curvature line of bending the lithotypes as the distance Xl from the longwall face increases: 1 – H = 200 m; 2 – H = 600 m

Rys. 5. Zależność kąta nachylenia β3 zmieniającej się linii krzywizny zagięcia litotypów wraz ze wzrostem odległości Xl od przodka ściany: 1 – H = 200 m; 2 – H = 600 m

4. RESEARCH RESULTS

One of the main geomechanical factors is the depth H of the extraction site location, and the task arises to assess its influence on the coal-overlaying formation shear parameters, which primarily include: coordinates of lines of complete advances, areas of change in the curvature sign for bending the lithotypes (angle β_1 to the dip and angle β_3 along the strike of the coal seam), distance a_p of the maximum bending of the most rigid lithotypes in the bottom hole zone ahead of the longwall face.

The bending deformations of the rock layers are most clearly displayed on the horizontal stress $\sigma_{x,z}$ curves. For example, Fig. 2 shows a spatial curve σx in the geomechanical model of predominantly thin- and medium-bedded texture for H = 420 m elevation. The field σ_x parameters do not contradict the assumption about the frontal bearing pressure propagation ahead of the longwall face and the associated transformations of the coal-overlaying formation rock texture:

- weakening occurs in the immediate and adjacent main roof layers at a distance of up to 7–8 m;
- the tension cracks occur and develop over a distance of 12–20 m.

The bending of the rock layers in the direction of the coal seam continues above the longwall face, but immediately after the spread of powered support sections at a distance of up to 1–2 m, the bending first disappears, and then the bending curvature sign changes. It is well known that this zone of intense fracturing and stratification is recommended for crossing it by outgassing wells. Geometric characteristics of the area of change in the curvature sign of bending the lithotypes in the roof are as follows:

- it begins in the uncontrolled collapse zone at a distance of up to 2–3 m behind the section fence;
- the area extends into the main roof at an angle β1 = 75–80° to the bedding plane.

These peculiarities (for the Western Donbas) prove the approach to the longwall face of the area of change in the curvature sign of bending the roof lithotypes. It is therefore expedient that outgassing wells are also concentrated near longwall face: with the simplest geometric constructions, an outgassing well should be drilled at a distance of up to 8–10 m from the section fence.

With regard to the influence of increasing depth H, it is well known that there is an increase in stresses and deformations in the adjacent mass, as well as an expansion of the zones of weakening and stratification of roof rocks. This causes a more intense bending, the collapse of rock and an approach of the line of changing curvature sign to the longwall face, that is, an increase in the gradient angle β1.

The analysis results of the link between β1 and H are presented in the graphs of Fig. 3 for two opposite mass textures: regardless of the texture type, there is a pattern of increasing gradient angle β1 with increasing H – the essence of this tendency is increasing geostatic pressure. It has been determined that in the range 200 m ≤H≤ 600 m, there is an increase in β1 by 12.8° for predominantly thin- and medium-bedded textures (from 71.8 to 84.6°) and by 17.8° for predominantly thick- and medium-bedded textures (from 65.6 to 83.4°).

Based on the above results, it is necessary to pay attention to two peculiarities:

- firstly, the specified tendencies are observed for different texture types when conducting separate independent computational experiments, which, though implicit, confirms their reliability;
- secondly, the patterns for two quite opposite texture types approach each other at great depths (as for the Western Donbas conditions); this is explained by the significant geostatic pressure influence on the process of coal-overlaying formation advance into the mined-out area.

As a result of the above research, a conclusion can be drawn about the importance of taking into account the depth H of conducting stope operations when determining the angle β1. It is possible to use the revealed patterns from the graphs in Fig. 3 or regression equations obtained from the data of computational experiments using known methodologies:

- for thin- and medium-bedded textures

$$\beta_1 = 178 - 200H^{-0.12},\ \text{deg}; \tag{4}$$

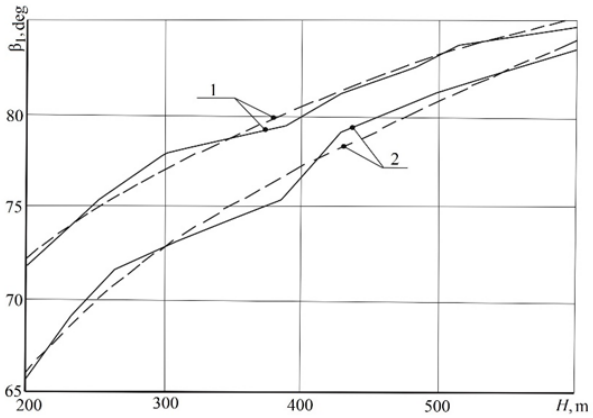

Fig. 6. Dependence of the inclination angle β_3 of the line of changing curvature sign for bending the lithotypes in the coal-overlaying formation on the depth H of conducting stope operations: 1 – predominantly thin- and medium-bedded textures; 2 – predominantly thick- and medium-bedded textures; –––– FEM calculation results; ------- regression equation

Rys. 6. Zależność kąta nachylenia β_3 linii zmieniającego się znaku krzywizny zagięcia litotypów w nadkładzie na głębokości H prowadzenia operacji postojowych: 1 – dominują tekstury cienko- i średnioławicowe; 2 – przeważają tekstury grubo- i średnioziarniste; –––– wyniki obliczeń MES; ------ równanie regresji

– for thick- and medium-bedded textures

$$\beta_1 = 236.7 - 290.3H^{-0.10},\ \text{deg.} \quad (5)$$

In expressions (4) and (5), the depth H is substituted in meters, while the parameter β_1 is determined in degrees.

Another important factor related to the fracture formation is the zone of the most active bending of the rock layers immediately ahead of the stoping face. From the point of view of gas emission, these zones are the primary link in the release and transfer of methane volumes into the longwall face working space. As can be seen from Fig. 2, the degree of bending of roof lithotypes is different and is mainly determined by three factors: the thickness of layers, their mechanical properties and the value of load on a particular lithotype.

Under the classical provisions of rock mechanics, a thicker layer with increased deformation characteristics experiences high rock pressure compared to other easily deformable lithotypes. For example, a thick sandstone experiences a higher load than the adjacent thin argillites and siltstones, which is quite clearly reflected on the curve σ_x (see Fig. 2); the same is also observed on the curve σz. At the same time, the sandstone is usually a gas-saturated lithotype, and, therefore, it is necessary for the outgassing well to cross this lithotype in the zone of maximum bending in the area ahead of the longwall face.

Thus, the second requirement has been formulated for the appropriate coordinates of the location of outgassing wells. To implement this requirement, it is necessary to determine the coordinates of the zone of formation of maximum bending deformations. Naturally, the formation of these zones depends on the texture and mechanical properties of the rocks in the coal-overlaying formation; however, the influence of the depth H of conducting stope operations is also predicted, since with its growth, the zones of plastic deformation of rocks expand, affecting both the value and the distance of propagation of a significant degree of lithotype bending.

The variation of longwall face location depth within the range of 200 m ≤H≤ 600 m provides the following results. First, at relatively small H values, the location of the maximum bending zones of the most rigid lithotypes remains almost unchanged, and mainly the bending deformations increase. However, with the expansion of the plastic state areas of the lithotypes, the bending deformations of the rock layers increase more rapidly (as H increases) than horizontal stresses σx. In this case, the second tendency occurs – the expansion of the zone of weakening bending deformations along the bedding planes of lithotypes. The indicated tendency has a predominant direction away from the stoping face into the still undermined rock mass.

Therefore, with an increase in the depth H of the longwall face location, two tendencies are noted regarding the coordinates of acting maximum bending deformations, which is identical to intense fracturing:

- at relatively shallow depths (H ≤ 300–350 m), the distance ap (from the face plane) of the maxima σx location increases rather slowly;
- when moving to deeper horizons (H >350 m), the distance ap begins to increase more intensively in proportion to H according to a non-linear dependence.

An example of the determined patter is given in Fig. 4 for a fixed height hp of gas-bearing sandstone occurrence relative to the coal seam, as well as its constant thickness m_p. Usually, h_p and m_p parameters influence on the link between ap and H, but the function $a_p(H)$ is very important from the point of view of substantiating an expedient route for outgassing wells.

An example of determining the function $a_p(H)$ for a predominantly thin- and medium-bedded textures is given, where several gas-bearing layers of increased rigidity can be located throughout the coal-overlaying formation height. This texture variant is shown on the σ_x curve (see Fig. 2), where two layers of increased rigidity are located in the main roof at once – at a height of 14.6 m and 19.2 m from the seam bottom to the upper layer surface. Note that concentrations of tensile σx stresses also occur higher in the roof, but they have a limited distribution and are located at a considerable distance.

For the selected two rigid layers, two patterns of the change in the a_p parameter have been obtained, which is calculated from the middle part of the width of acting maximum tensile

σ_x stresses. According to the two experimental dependences (for different hp), two regression functions have been obtained:

– with $h_{P_1} = 14.6$ m $\quad a_{P_1} = 1.9 + 1.1\exp\left(\frac{H}{200} - 1\right)$, m; (6)

– with $h_{P_2} = 19.2$ m $\quad a_p = 2.25\left[1 + \exp\left(\frac{H}{200} - 1\right)\right]$, m. (7)

As for the peculiarities, it should be additionally noted the more distant maxima σ_x location in the layers occurring above the coal seam bottom. The value a_p indicates the expediency of turning the outgassing well in such a way as to cross the gas--saturated lithotypes at some distance from the stoping face and thereby, in part, perform something like preliminary outgassing. Moreover, the distance a_p increases along the height of the mass and it is possible to cross both layers in the desired zone with one inclined well.

The constructed spatial model is used to monitor the influence of the longwall face location depth H on the process of coal-overlaying formation shear along the strike of the coal seam (along the longwall face) that provides the required number of sections in the vertical YZ planes along an arbitrary X coordinate of the location of these sections.

When considering the process of the roof rock deformation into the mined-out area, the most influential (in relation to gas emission) parameter has been substantiated – the coordinates of the zones of curvature change of lithotypes bending along the strike, which are characterized (throughout the coal-overlaying formation height) by the inclination angle β_3 of the line connecting the indicated zones with the extending coal seam. It is logical to predict that as the longwall face retreats, the angle β_3 will change at a certain distance simultaneously with a decrease in the intensity of rock pressure manifestations. To confirm this prediction, YZ sections are cut at a distance of 10 m, 20 m, 30 m and 40 m from the longwall face. These prosedures are taken for the spatial curve σz for the variant of predominantly thin- and medium-bedded textures at two extreme depth values: H = 200 m and H = 600 m. For each section, the inclination angle β_3 is specified relative to the coal seam bedding plane and, based on the obtained indicators, the graphs are plotted (Fig. 5). As can be seen, the tendencies in the β_3 parameter change from the Xl coordinate of the YZ section location behind the longwall face remain unchanged: an active increment in β_3 occurs in areas of Xl ≤ 20 m, and then the value of β_3 stabilizes at a certain level, and this occurs regardless of the depth H of conducting stope operations.

Based on the revealed tendencies, the question arises: at what distance behind the longwall face should the dependence $\beta_3(H)$ be determined? In our opinion, the value of β_3 should be determined in the zone of the most active disturbances of the coal-overlaying formation, that is, near the longwall face; here there is an intense stratification and destruction of rocks, many fractures and cavities with a corresponding increase in gas emission occur. Therefore, it is consider appropriate to determine the parameter β_3 on an area of 10 m ≤ Xl ≤ 20 m and choose its calculated value as an average.

According to this algorithm, the β_3 angle values are calculated over the entire range of 200 m ≤H≤ 600 m. As an example, Fig. 6 shows the corresponding graphs.

The $\beta_3(H)$ function is close to linear one with a gradual increase in the range of 65°≤ β_3 ≤ 71° for predominantly thin- and medium-bedded textures and in the range of 58°≤ β_3 ≤ 66° for predominantly thick- and medium-bedded textures. The influence of depth H is relatively small: in the range of 200 m ≤H≤ 600 m, the angle β_3 increases by only 6° and 8° for the corresponding textures of the coal-overlaying formation. However, on the length of the outgassing well lw = 40–50 m, these β_3 variations correspond to a change in the location of its deepened part up to 5–7 m, which can be an important factor in terms of the most appropriate coordinates for the location of wells with the maximum flow rate of methane gas. Based on the above results of computational experiments, the corresponding regression equations for calculating the angle β_3 have been obtained:

– for thin- and medium-bedded textures

$$\beta_3 = 62 + 0.015H, \text{ deg}; \quad (8)$$

– for thick- and medium-bedded textures

$$\beta_3 = 54 + 0.02H, \text{ deg}. \quad (9)$$

Thus, a number of dependences of the depth H and texture on the shear parameters of the coal-overlaying formation into the mined-out area has been obtained; they make it possible to choose appropriate parameters for the location of outgassing wells based on the influence of geomechanical factors. In this way, it has been proven that effective outgassing is associated with disturbances in the mass texture, when it experiences intense stratification and destruction in the process of subsidence of the coal-overlaying formation. An analysis of the peculiarities of deformation of weakly metamorphosed Western Donbas rocks, given the increased advance velocities of the stoping faces, makes it possible to formulate an idea of the mechanism of texture transformations of stratified weak rock mass in terms of the outgassing technology parameters for an extraction site of a coal mine.

5. CONCLUSION

1. Quantitative patterns of the coal-overlaying formation shear parameters under the influence of geomechanical factors have been determined using FEM. For this purpose, the parameters of a spatial geomechanical model have been substantiated, which contains zones of a stratified weakly metamorphosed mass ahead and behind the longwall face with a part of virgin coal-rock stratum from the side of the adjacent extraction site. They contain the end longwall face area with a powered support simulator, the extraction drift and their conjugation. In accordance with generally recognized requirements, the spatial model dimensions, the texture and mechanical properties of the lithotypes, the boundary conditions of loading along all model planes at its boundaries have been substantiated. The expediency of using an elastic--plastic physical model of the behavior of rock layers and the deformation-strength characteristic of a powered support has been proven.

2. Based on the results of computational experiments, a significant influence of the longwall face location depth H and the mass texture on the shear parameters of the coal-overlaying formation has been proven:

– there is an increase in the inclination angle β_1 of the line of changing curvature sign for bending the lithotypes to the rise of the seam – for predominantly thin- and me-

dium-bedded textures in the range of 71.8–84.6°; for predominantly thick- and medium-bedded textures in the range of 65.6–83.4°;

– with an increase in H, two tendencies have been noted relative to the coordinates of acting maximum bending deformations of lithotypes (ahead of the longwall face), which is identical to intense fracturing: at relatively shallow depths (H≤ 300–350m), the distance a_p of the location (from the face plane) of maximum horizontal stresses increases rather slowly – up to 30–50%; when moving to deeper horizons (H> 350 m), the distance ap begins to increase intensively (up to 3.3–4.2 times) according to a non-linear dependence;

– along the strike of the coal seam, there is a tendency of increasing inclination angle β_3 of the line of changing curvature sign for bending the lithotypes when moving away from the stoping face, and an almost linear influence of H adds an increase in the value of β_3: up to 6° for predominantly thin- and medium-bedded textures and up to 8° for predominantly thick- and medium-bedded textures.

3. It is possible to use revealed patterns with the help of a number of graphs of the corresponding dependences or regression equations obtained from the data of computational experiments. Thus, a quantitative relationship between the coal-overlaying formation shear parameters and geomechanical factors has been determined, which makes it possible to choose appropriate schemes for the location of outgassing wells.

6. ACKNOWLEDGEMENTS

The authors express their gratitude to the management of the Administration of PJSC "DTEK Pavlohradvuhillia" for the provided technical information, organization of mining surveys and active participation in the discussion of the research results.

Literatura – References

1. Moellerherm, S., Kretschmann, J., Tiganj, J., & Poplawski, M. (2022). Post-mining Challenges and Knowledge Transfer for the Ukrainian coal industry. IOP Conference Series: Earth and Environmental Science, 970(1), 012034). https://doi.org/10.1088/1755-1315/970/1/012034
2. Bazaluk, O., Ashcheulova, O., Mamaikin, O., Khorolskyi, A., Lozynskyi, V., & Saik, P. (2022). Innovative activities in the sphere of mining process management. Frontiers in Environmental Science, (10), 878977. https://doi.org/10.3389/fenvs.2022.878977
3. Pivnyak, G., Bondarenko, V., & Kovalevska, I. (2015). New developments in mining engineering 2015: Theoretical and practical solutions of mineral resources mining, 607. https://doi.org/10.1201/b19901
4. Miletenko, N.A. (2022). Improvement and systematization of principles and process flows in mineral mining. Eurasian Mining, (1), 41-45. https://doi.org/10.17580/em.2022.01.08
5. Tong, M., Dong, J., Luo, X., Yin, D., & Duan, H. (2022). Coal consumption forecasting using an optimized grey model: The case of the world's top three coal consumers. Energy, 242, 122786. https://doi.org/10.1016/j.energy.2021.122786
6. Serdaliyev, Y., Iskakov, Y., Bakhramov, B., & Amanzholov, D. (2022). Research into the influence of the thin ore body occurrence elements and stope parameters on loss and dilution values. Mining of Mineral Deposits, 16(4), 56-64. https://doi.org/10.33271/mining16.04.056
7. Amralinova, B.B., Frolova, O.V., Mataibaeva, I.E., Agaliyeva, B.B., & Khromykh, S.V. (2021). Mineralization of rare metals in the lakes. Naukovyi Visnyk Natsionalnoho Hirnychoho Universytetu, (5), 16-21. https://doi.org/10.33271/nvngu/2021-5/016
8. Sepehri, M., Apel, D. B., Adeeb, S., Leveille, P., & Hall, R. A. (2020). Evaluation of mining-induced energy and rockburst prediction at a diamond mine in Canada using a full 3D elastoplastic finite element model. Engineering Geology, 266, 105457. https://doi.org/10.1016/j.enggeo.2019.105457
9. Dudek, M., Tajduś, K., Misa, R., & Sroka, A. (2020). Predicting of land surface uplift caused by the flooding of underground coal mines - A case study. International Journal of Rock Mechanics and Mining Sciences, 132, 104377. https://doi.org/10.1016/j.ijrmms.2020.104377
10. Utemaganbetov, Z.S. (2021). Boundary condition transfer method (Thomas algorithm) numerical solution of a mixed boundary value problem for second-order linear differential equations. Engineering Journal of Satbayev University, 143(6), 162-173. https://doi.org/10.51301/vest.su.2021.i6.21
11. Wu, N., Liang, Z., Zhang, Z., Li, S., & Lang, Y. (2022). Development and verification of three-dimensional equivalent discrete fracture network modelling based on the finite element method. Engineering Geology, 306, 106759. https://doi.org/10.1016/j.enggeo.2022.106759
12. Snihur, V., Bondarenko, V., Kovalevska, I., Husiev, O., & Shaikhlislamova, I. (2022). Optimization solution substantiation for resource-saving maintenance of workings. Mining of Mineral Deposits, 16(1), 9-18. https://doi.org/10.33271/mining16.01.009

13. Bondarenko, V., Kovalevska, I., Symanovych, G., Sotskov, V., Barabash, M. (2018). Geomechanics of interference between the operation modes of mine working support elements at their loading. Mining Science, (25), 219-235. https://doi.org/10.5277/msc182515

14. Zhulay Y., Zberovskiy V., Angelovskiy A., & Chugunkov I. (2012). Hydrodynamic cavitation in energy-saving technological processes of mining sector. Geomechanical Processes During Underground Miming – Proceedings of the School of Underground Mining, 51-56. https://doi.org/10.1201/b13157

15. Bondarenko. V., Kovalevs'ka, I., Svystun, R., & Cherednichenko, Yu. (2013). Optimal parameters of wall bolts computation in the united bearing system of extraction workings frame-bolt support. Annual Scientific-Technical Collection – Mining of Mineral Deposits, 5-9. https://doi.org/10.1201/b16354-2

16. Krykovskyi, O., Krykovska, V., & Skipochka, S. (2021). Interaction of rock-bolt supports while weak rock reinforcing by means of injection rock bolts. Mining of Mineral Deposits, 15(4), 8-14. https://doi.org/10.33271/mining15.04.008

17. Kovalevs'ka I., Vivcharenko, V., & Snigur, V. (2013). Specifics of percarbonic rock mass displacement in longwalls end areas and extraction workings. Annual Scientific-Technical Collection – Mining of Mineral Deposits, 29-33. https://doi.org/10.1201/b16354-2

18. Bondarenko, V., Kovalevska, I., Cawood, F., Husiev, O., Snihur, V. & Jimu, D. (2021). Development and testing of an algorithm for calculating the load on support of mine workings. Mining of Mineral Deposits, 15(1), 1-10. https://doi.org/10.33271/mining15.01.001

19. Skipochka, S. (2019). Conceptual basis of mining intensification by the geomechanical factor. E3S Web of Conferences, (109), 00089. https://doi.org/10.1051/e3sconf/201910900089

20. Prusek, S., Rajwa, S., Wrana, A., & Krzemień, A. (2017). Assessment of roof fall risk in longwall coal mines. International Journal of Mining, Reclamation and Environment, 31(8), 558-574. https://doi.org/10.1080/17480930.2016.1200897

21. Małkowski, P., Niedbalski, Z., & Balarabe, T. (2021). A statistical analysis of geomechanical data and its effect on rock mass numerical modeling: a case study. International Journal of Coal Science & Technology, (8), 312-323. https://doi.org/10.1007/s40789-020-00369-2

22. Sedina, S., Altayeva, A., Shamganova, L., & Abdykarimova, G. (2022). Rock mass management to ensure safe deposit development based on comprehensive research within the framework of the geomechanical model development. Mining of Mineral Deposits, 16(2), 103-109. https://doi.org/10.33271/mining16.02.103

23. Malanchuk, Y., Moshynskyi, V., Khrystyuk, A., Malanchuk, Z., Korniienko, V., & Abdiev, A. (2022). Analysis of the regularities of basalt open-pit fissility for energy efficiency of ore preparation. Mining of Mineral Deposits, 16(1), 68-76. https://doi.org/10.33271/mining16.01.068

24. Bitimbayev, M.Zh., Rysbekov, K.B., Akhmetkanov, D.K., Kunayev, M.S. & Elemesov, K.K. (2022). The role and importance of chemical elements clarks in the practical expanded reproduction of mineral resources. Engineering Journal of Satbayev University, 1(144), 47-54. https://doi.org/10.51301/ejsu.2022.i1.08

25. Lu, J., Jiang, C., Jin, Z., Wang, W., Zhuang, W. & Yu, H. (2021). Three-dimensional physical model experiment of mining-induced deformation and failure characteristics of roof and floor in deep underground coal seams. Process Safety and Environmental Protection, 150, 400-415. https://doi.org/10.1016/j.psep.2021.04.029

26. Sakhno, I., Liashok, Ia., Sakhno, S., & Isaienkov, O. (2022). Method for controlling the floor heave in mine roadways of underground coal mines. Mining of Mineral Deposits, 16(4), 1-10. https://doi.org/10.33271/mining16.04.001

27. Pysmennyi, S., Fedko, M., Chukharev, S., Rysbekov, K., Kyelgyenbai, K., & Anastasov, D. (2022). Technology for mining of complex-structured bodies of stable and unstable ores. IOP Conference Series: Earth and Environmental Science, 970(1), 012040. https://doi.org/10.1088/1755-1315/970/1/012040

28. Smoliński, A. (2022). Research into Impact of Leaving Waste Rocks in the Mined-Out Space on the Geomechanical State of the Rock Mass Surrounding the Longwall Face. Energies, 15(24), 9522. https://doi.org/10.3390/en15249522

29. Shashenko, A., Gapieiev, S., & Solodyankin, A. (2009). Numerical simulation of the elastic-plastic state of rock mass around horizontal workings. Archives of Mining Sciences, 54(2), 341-348.

30. Pivnyak, G., Bondarenko, V., Kovalevs'ka, I. & Illiashov, M. (2012). Geomechanical processes during underground mining. London, United Kingdom: CRC Press, Taylor & Francis Group. https://doi.org/10.1201/b13157

31. Bondarenko, V., Kovalevska, I., Symanovych, H., Barabash, M., & Snihur, V. (2018). Assessment of parting rocks weak zones under the joint and downward mining of coal seams. E3S Web of Conferences, (66), 03001. https://doi.org/10.1051/e3sconf/20186603001

32. Ishchenko, K.C., Krukovskyi O.P., Krukovska V.V., & Ishchenko, O.K. (2012). Fizychne i chyselne modeliuvannia napruzheno-deformovanoho stanu masyvu hirskykh porid u zaboi vyrobky. Viznyk Natsionalnoho Hirnychoho Universytetu, (2), 85-91.

33. Dyczko, A., Kamiński, P., Jarosz, J., Rak, Z., Jasiulek, D., & Sinka, T. (2021). Monitoring of roof bolting as an element of the project of the introduction of roof bolting in polish coal mines-case study. Energies, 15(1), 95. https://doi.org/10.3390/en15010095

34. Usachenko, B.M. (1979). Svoystva porod i ustoychivost gornykh vyrabotok. Kiïv: Naukova dumka, 136 p.

35. Usachenko, B.M., Cherednichenko, V.P., & Golovchanskiy, I.E. (1990). Geomekhanika okhrany vyrabotok v slabometamorfizovannykh porodakh. Kiïv: Naukova dumka, 144 p.

36. SOU 10.1.00185790.011:2007. (2008). Pidhotovchi vyrobky na polohykh plastakh. Vybir kriplennia, sposobiv i zasobiv okhorony. Standart Minvuhlepromu Ukrainy. Donetsk: Vydavnytstvo DonVUHI, 114 p.

37. Barsanescu, P. D. & Comanici, A. M. (2017). von Mises hypothesis revised. Acta Mechanica, 228, 433-446. https://doi.org/10.1007/s00707-016-1706-2

Uzasadnienie wzorców wpływu czynników geomechanicznych na parametry ścinania formacji nadkładu węgla, wymagającej odgazowania, z dużymi prędkościami posuwu ścian postojowych w Zachodnim Donbasie

W artykule rozważane są zagadnienia opracowania koncepcji mechanizmu wydobywania węgla ze złóż gazowych oraz dwóch składowych zaopatrzenia kraju w nośniki energii: wydobycie węgla i zagospodarowanie metanu z warstwy węglonośnej. Zagadnienia te są nierozerwalnie związane z eksploatacją złóż przodkami ścianowymi o dużych postępach. Badany jest rzeczywisty problem rozwiązania powyższych sprzeczności. Wzory wpływu czynników geomechanicznych na podstawie modelowania metodą elementów skończonych (MES) parametrów ścinania formacji nadkładkowych badane są pod kątem uzasadnienia schematów lokalizacyjnych dla otworów odgazowujących miejsca przy dużych prędkościach postępu przodków w Zachodnim Donbasie. Uzyskane wyniki eksperymentów obliczeniowych są porównywane z badaniami prowadzonymi przez specjalistów. Wnioski dotyczące stopnia oddziaływania czynników geomechanicznych i konieczności ich uwzględnienia są uzasadnione. Opracowano i uzasadniono trzy modele obliczeniowe pod względem kształtu i wielkości strefy obliczeniowej, tekstury górotworu, właściwości mechanicznych jego litotypu, warunków obciążenia na granicach modelu, charakterystyki związku naprężeń i odkształceń w elementy modelu oraz kryteria wyznaczania stanu granicznego. Wykazano istotny wpływ głębokości zalegania przodka oraz tekstury masy na parametry ścinania formacji nadkładu. Na podstawie danych z eksperymentów obliczeniowych otrzymano odpowiednie zależności i równania regresji. Przeprowadzone badania pozwalają na wybór odpowiednich schematów lokalizacji otworów odgazowujących.

Słowa kluczowe: *pokład węgla, sztolnia, przodek ścianowy, obudowa zmechanizowana, kopalnia*

Assessment of the Efficiency of Hematite Quartzite Enrichment Technologies

Tetiana OLIINYK[1)], Liudmila SKLYAR[2)], Natalia KUSHNIRUK[3)], Nadiya HOLIVER[4)], Barbara TORA[5)]

[1)] Kryvyi Rih National University, mining and metallurgical faculty, Ukraine; ORCID https://orcid.org/0000-0002-0315-7308; email: taoliynik@knu.edu.ua
[2)] Kryvyi Rih National University,mining and metallurgical faculty, Ukraine; ORCID https://orcid.org/0000-0002-2721-1436; email: lyuda.cuclina@knu.edu.ua
[3)] Kryvyi Rih National University, mining and metallurgical faculty, Ukraine; ORCID https://orcid.org/0009-0005-7900-4091; email: kushniruk-natalia@knu.edu.ua
[4)] Kryvyi Rih National University, mining and metallurgical faculty, Ukraine; ORCID https://orcid.org/0000-0002-9252-2839; email: nadiyaholiver@knu.edu.ua
[5)] AGH University of Science & Technology, Faculty of Civil Engineering and Resource Management, Dept. of Environmental Engineering, Poland; ORCID https://orcid.org/0000-0002-0850-3054; email: tora@agh.edu.pl

http://doi.org/10.29227/IM-2023-01-04

Submission date: 23-02-2023 | Review date: 15-03-2023

Abstract

The present paper deals with the problem of developing an efficient technology for the enrichment of hematite ores. The aim of the research is to investigate the process properties of thinly disseminated hematite ores of Ukraine, taking into account their mineralogical characteristics, to develop flowsheets for the enrichment of hematite ores and to assess the efficiency of mineral separation during enrichment by gravity, magnetic, and flotation methods.

The research was carried out on a sample of hematite ores from the Kryvyi Rih iron ore basin of Ukraine, which consisted of 9 mineralogical ore types, distinguished by the quantitative ratio of the main groups of ore and non-ore minerals. As a result of WLIMS magnetic separation with a magnetic field induction of 0.07 T, an iron-containing concentrate with a mass fraction of 63.5% iron was obtained from ore with a size of minus 0.074+0 mm, with a total iron recovery of 12.8%.

It was found that with an increase in the magnetic field induction from 0.2 to 0.8 T, the recovery of total iron in the WHIMS magnetic product increased from 78.8 to 86.9%. The mass fraction of total iron in the WHIMS magnetic product was 57.9–59.8%. Losses of total iron with the non-magnetic product ranged from 21.2 to 13.1% with a mass fraction of total iron of 32–27.8%. The mass fraction of SiO_2 in the magnetic product was 11–13.8%.

Flotation research resulted in a hematite concentrate with a mass fraction of total iron of 64.05–65.95%, with iron recovery in the concentrate of 60.3–70.68%. Based on the results of process tests, seven variants of flowcharts for the enrichment of hematite ores were developed. The schemes were evaluated by the Hancock efficiency criterion, which ranged from 42.49–64.7%. The magnetic flotation technology for the enrichment of hematite quartzite was recommended for implementation. This technology makes it possible to obtain a commercial concentrate with a mass fraction of total iron of 37.02% from hematite ore with a mass fraction of total iron of 65.41%.

Keywords: *hematite quartzite, technology, efficiency, magnetic separation, gravity, flotation*

Introduction

Hematite ores take a significant share in potential iron ore reserves and are the main iron ore raw material for the prospective development of ferrous metallurgy in many countries. They account for about 23% of the total volume of ores being processed. Ukraine's hematite ferruginous quartzite reserves are concentrated mainly in Kryvbas and amount to 12% of total iron ore reserves [1,2,3].

In today's mining environment, it is necessary to have detailed information about the process properties of ores to respond to the following questions: what kind of scheme and efficiency is required for ore enrichment, and what sort of commercial products will be obtained.

The key enrichment criterion for most industrial ore types is the granulamentric parameters of minerals. Their estimation makes it possible to determine the opening of minerals in the process of ore crushing and grinding and, based on the data obtained, to calculate the main indicators of enrichment and further determine the type of ore in terms of enrichment.

Hematite ores of different types differ in textural and structural features and mineral composition, which necessitates the use of different methods and technologies for their enrichment. At the same time, a competitive hematite concentrate should contain at least 64.0–66.0% iron, which is equivalent to magnetite concentrates with a mass fraction of iron of 67.0–68.0% in terms of silica content [4].

The mineral composition of hematite ores comprises martite, hematite-martite, limonite-martite, hematite, martite-limonite, and limonite varieties of hematite ores. The total iron content of these ores varies from 46 to 69 m.%. [5].

By textural features, they are broad-, medium-, thin-, and vaguely layered. The structure of hematite quartzites is divided into fine, very fine, and fine-grained kinds. According to physical properties, oxidized quartzites are classified as strong, very strong, weak, and very weak [6,7].

Based on the size of ore inclusions, hematite quartzites of the Kryvyi Rih iron ore basin are classified as thinly inclusions, very thinly inclusions and dispersed inclusions and are considered to be hard-to-dress raw materials [8]. The most

Tab. 1. Ratio of combined hematite-quartzite species in the process sample for research

Tab. 1. Stosunek połączonych gatunków hematytu i kwarcytu w próbce procesowej do badań

Combined Mineralogical Varieties of Hematite Quartzites		The Content in the Composition of the General Process Sample, mass %
Index	Name	
1o	Iron-iron-mica quartzites	2,18
2o	Iron-mica martite quartzites	11,40
3o	Marschlitic iron-mica martite quartzites	8,36
4o	Martite quartzites	27,45
5o	Martite quartzites marshallitized	24,60
6o	Hettitized martite quartzites	10,31
7o	Quartzites dispersedhematite-martite and martite-dispersedhematite (suric)	6,64
8o	Magnetite-bearing martite quartzites (weakly weathered)	4,50
9o	Shale and ore-free quartzites	4,56

frequently used quartzites are those with very thin inclusions of ore and non-ore minerals (0.01–0.07 mm), where the ore minerals are exposed at a size of -0.05 mm. Hematite quartzites of the Kryvyi Rih iron ore basin are divided into: "lean" ores containing less than 40% iron, ores with an average iron content of 40% to 50%, and "rich" ores with an iron content of 50% and above [9].

"Rich" ores and ores with medium iron content are enriched by selective screening or dry magnetic separation. The commercial product is sinter ore with a mass fraction of iron of 55–64%.

"Lean" ores are mainly mined together with magnetite quartzites. Their associated production reaches 15–30% of the total production of magnetite ores, which is about 22.5–45 million tons per year. These ores are characterized by a complex and variable mineral and chemical composition and a thinly disseminated structure from 0.001 to 0.1 mm. "Lean" hematite quartzites of the Kryvyi Rih iron ore basin are classified as hard-to-dress ores due to the presence of a significant amount of low-magnetic fine-grained and fine-grained iron oxides and hydroxides. Among them there are the following varieties: martite-iron-ore quartzites; iron-mica-martite quartzites; iron-ore-martite marshallitized quartzites; martite quartzites; martite marshallitized quartzites; martite goethite quartzites; dispersed-hematite-martite quartzites; martite magnetite-containing quartzites; shales and ore-free quartzites. [10,11,12].

The analysis of the world practice of hematite ore enrichment shows that various methods and technologies can be used for their processing. Hematite quartzite enrichment can be carried out by gravity [13,14,15], magnetic [13,16–22], flotation [23–27], combined; magnetic-gravity or magnetic-flotation methods [28–31].

The methods depend on the textural and structural features of the ore, dissemination of ore and non-ore minerals, and the composition of waste rock. The combination of methods ensures an increase in the efficiency of hematite quartzite enrichment. The magnetic method of hematite quartzite enrichment allows to obtain iron ore concentrate with a total iron content of 59.9–63.5 mass % with the recovery of total iron in the concentrate of 68–75%; flotation method – 62–65.6 mass % with the recovery of total iron in the concentrate of 70.2–77.8%; gravity method – 66.9–68.3 mass%. The combined magnetic and gravity method – up to 67–68 mass % with the recovery of total iron in a concentrate of 66–67%; the combined magnetic and flotation method – up to 67–68 mass %, with the recovery of total iron in a concentrate of 70.1–75.6% [3].

The choice of a particular method is determined by the efficiency of the process, material composition, capital and operating costs.

The research is aimed at studying the processing properties of thinly disseminated hematite ores of Ukraine, taking into account their mineralogical characteristics. Based on the results obtained, to develop flowsheets for the enrichment of "lean" hematite ores and to evaluate the efficiency of mineral separation during enrichment by gravity, magnetic, and flotation methods.

Materials

The study received 200 in-line samples of 9 mineralogical varieties of hematite quartzites of the Kryvyi Rih iron ore basin, which in certain proportions made up the technological sample for research (Table 1). The formed sample was then submitted for process research in order to develop a technology for the enrichment of hematite quartzite and to determine the effectiveness of various methods and their combinations.

The quantitative ratio of the main groups of ore and non-ore minerals in the composition of the studied samples of hematite ores of the Kryvyi Rih iron ore basin has allowed us to focus on the main groups of minerals:

Martite, iron mica, goethite, lepidocrocite, and magnetite are granular ore minerals.

Aggregates of dispersed hematite and dispersed goethite are fine ore minerals.

Quartz, chalcedony, opal are minerals of the quartz group [10, 12, 15].

Individuals and aggregates of weathered ferruginous silicates and carbonates, newly formed iron-free silicates and carbonates make up the fourth type.

Martite is the main ore mineral in hematite ores. In the process of weathering, the structure of ore layers is kept. [32–33]. Figure 1 shows the nature of the change in the internal structure of martite aggregates depending on the intensity of primary magnetite replacement.

The martitization process gradually captured magnetite crystals and aggregates in the direction from the peripheral to their central zones. Figure 2 shows the direction of martite replacement of magnetite from the initial stages (Figure 2, a) to the formation of almost monomineral pseudomorphoses of hematite on magnetite (Figure 2, c). The average size of martite in the ores of the fifth ferrous horizon is 0.072 mm, and the sixth ferrous horizon is 0.064 mm.

Iron mica is represented by small flaky inclusions in the quartz matrix of non-metallic layers – the so-called

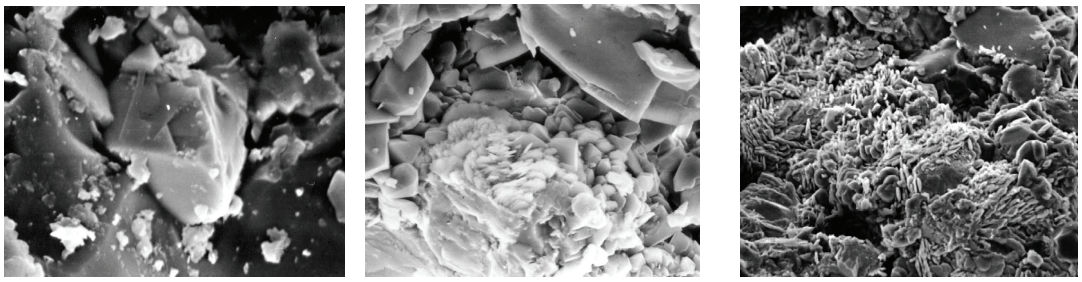

a b c

Fig. 1. Changes in the internal structure of individuals and aggregates of magnetite (well-faceted octahedral and cubo-octahedral crystals) in the process of its increasing (a → b) replacement by martite (aggregates of thin flaky crystals of ferrous mica). Scanning electron microscope MREM-100. Magnification: a – 1500x; b – 2000x; c – 1000x; d – 800x

Rys. 1. Zmiany struktury wewnętrznej osobników i agregatów magnetytu (dobrze fasetowanych kryształów ośmiościennych i sześcienno-ośmiościennych) w procesie jego narastającej (a → b) wymiany przez martyt (agregaty cienkich płatkowatych kryształów miki żelazistej). Skaningowy mikroskop elektronowy MREM-100. Powiększenie: a – 1500x; b – 2000x; c – 1000x; d – 800x

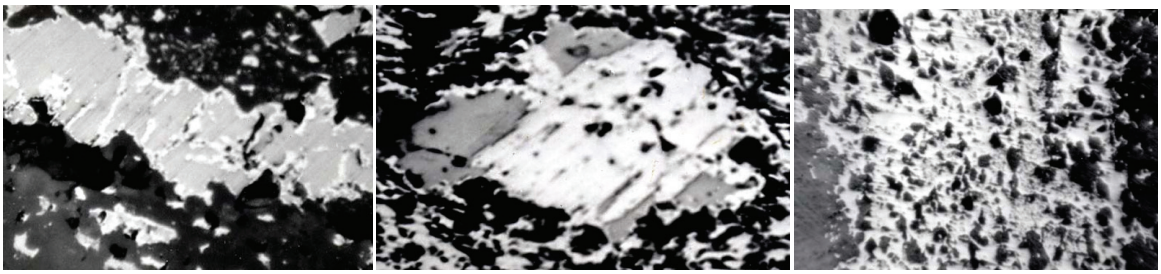

a b c

Fig. 2. Structure of ore layers of hematite quartzite with different degrees of magnetite martitization: a – the initial stage of magnetite martitization in a ribbon-like ore layer of magnetite quartzite; b – idiomorphic crystal of magnetite with the manifestation of its replacement by martite along the cracks of octahedral separation; c – monomineral banded aggregate of martite in the ore layer of martite quartzite.White – martite; light gray – magnetite; dark gray – quartz; black – voids. Reflected light; never parallel; magnification: a – 32x; b, c – 42x; d – 25x

Rys. 2. Struktura warstw rudnych kwarcytu hematytowego o różnym stopniu martyzacji magnetytu: a – początkowy etap martyzacji magnetytu we wstęgowej warstwie rudy kwarcytu magnetytu; b – idiomorficzny kryształ magnetytu z zastąpieniem go martytem wzdłuż pęknięć separacji oktaedrycznej; c – monomineralne pasmowane kruszywo martytu w warstwie rudy kwarcytu martytowego. Biały – martyt; jasnoszary – magnetyt; ciemnoszary – kwarc; czarny – puste przestrzenie. Odbite światło; nierównolegle; powiększenie: a – 32x; b, c – 42x; d – 25x

"Emulsion iron mica" [32,33]. The size of its crystals ranges from 0.001 to 0.05 mm in maximum dimension (Figure 3, a, b).

In the composition of ferruginous-martite and martite--ferruginous quartzites, tabular, lamellar and flaky crystals of iron mica are present not only in the non-ore but also in the ore layers. They are characterized by a much larger size – from 0.02 to 1.0 and more mm (Figure 3, d).

Dispersed hematite is represented by very small flaky crystals ranging in size from 0.001 to 0.01 mm [32–36]. Dispersed hematite and kaolinite-dispersed hematite aggregates form in hematite quartzites as smears, and rarely as independent layers up to 10 mm thick.

Goethite is most abundant in the upper crustal horizons of the weathered fifth-sixth ferruginous horizons. It develops by metasomatic replacement and ore minerals or fills cracks and voids, forming intersecting or harmonious veins with rock layering, containing veins up to a hundredth of 5–6 cm or more (Figure 4).

Magnetite in goethite-hematite quartzites is present in small volumes (no more than 1–2 vol%) (Figure 5). The average size of relict magnetite formations in hematite quartzites of the fifth ferruginous horizon is 0.024 mm, and of the sixth ferruginous horizon – 0.021 mm.

Quartz is the main non-ore mineral of hematite quartzites. It is the basic component of non-ore layers and is present in ore layers in the amount of up to 30–40 vol.% with grain size from 0.01 to 0.1 mm, sometimes up to 0.3 mm (Fig. 6). Often, in non-ore layers of hematite quartzite, a subparallel orientation of elongated quartz individuals is noted (Fig. 6, b).

In the non-metallic layers, quartz individuals often contain thin (up to 0.01 mm) inclusions of iron mica, rarely martite, and dispersed hematite.

The weathering crust of the studied deposit often contains products of marshallitization of ferruginous quartzite formed under the influence of alkaline hypergenic solutions (Fig. 7).

The role of minor and accessory minerals is played by about 20 other minerals and mineral types that are part of the studied hematite ores.

Methods

Processing tests included studies by gravity, magnetic and flotation methods. The studies were conducted in laboratory conditions.

Gravity enrichment was carried out at a screw sluice at a feed material size of 0.5–0.074 mm.

Magnetic separation of hematite ore was carried out in two stages. First, WLIMS separation was performed on a drum magnetic separator with a magnetic field induction of 0.07 T. The purpose of the WLIMS separation is to remove strongly magnetic minerals from the hematite ore to protect

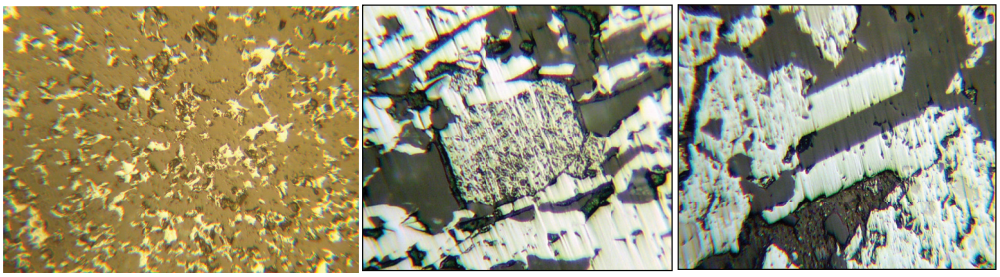

a b c

Fig. 3. Composition and structure of non-metallic (a) and ore (b, c,) layers of iron-mica-martite quartzite; a – small flaky inclusions of iron mica in quartz aggregates from non-metallic layers of ferruginous martite quartzite; b – large iron mica leists in the ore layer of martite-ferruginous quartzite; porous oval crystal in the center is martite; c – large tabular crystals of iron mica in an alpine iron-mica quartz vein from the ferruginous martite-iron-mica quartzite ore bed; relict magnetite inclusions (light gray) are present in the martite aggregates surrounding the veins. White: porous – martite, smoothly polished – iron mica; light gray – magnetite; dark gray – quartz; black – voids. Reflected light; never parallel; magnification: a, b – 20x, c, d – 35x

Rys. 3. Skład i struktura warstw niemetalicznych (a) i rudnych (b, c,) kwarcytu żelazowo-mikowo-martytowego; a – drobne płatkowate wtrącenia miki żelazowej w agregatach kwarcowych z niemetalicznych warstw żelazistego kwarcytu martytowego; b – duże miki żelazowe w warstwie rudy kwarcytu martytowo-żelazistego; porowaty owalny kryształ w środku to martyt; c – duże tabelaryczne kryształy miki żelazowej w alpejskiej żyle kwarcowo-żelazowo-mikowej ze złoża żelazistego martytowo-żelazowo-mikowego kwarcytu; w skupiskach martytu otaczających żyły obecne są reliktowe inkluzje magnetytu (jasnoszare). Biały: porowaty – martytowy, gładko wypolerowany – mika żelazowa; jasnoszary – magnetyt; ciemnoszary – kwarc; czarny – puste przestrzenie. Odbite światło; nierównolegle; powiększenie: a, b – 20x, c, d – 35x

the magnetic system of the WLIMS separator from blockage. Subsequently, the non-magnetic WLIMS product was fed to the WHIMS separation, which was carried out in a 259-CE rotary type separator. The magnetic field induction at the WHIMS separation varied from 0.2 to 0.8 T.

In order to obtain high-quality hematite concentrates, reverse cation flotation was studied in the current work. The following reagents were used in the experiments: amines Lilaflot-811M, Lilaflot-D817M and Lilaflot-D819MI as collectors, dextrin as a selective flocculant and depressor of iron ore minerals, caustic soda as a medium regulator.

Research on the cationic flotation of quartz from a magnetic hematite product was carried out on a laboratory flotation machine 237 Fl with removable chambers of 0.5, 1 and 3 liters. To determine the optimal flotation mode, the "Latin square" design method was used during the studies. After determining the optimal conditions and flotation scheme, studies were conducted on the principle of a continuous process to specify the developed process mode, to find out the effect of circulation of industrial products on the enrichment indicators and to determine the points of their feeding into the process.

Hancock's efficiency criterion was chosen as the efficiency criterion for the hematite quartzite enrichment technology:

$$E = \frac{\varepsilon_к - \gamma_k}{100 - \frac{\alpha}{\alpha_m}} * 100\% \quad (1)$$

where

ε – the concentrate recovery, %;

$\gamma_к$ – concentrate yield, %;

α – iron content in the final product, %;

α_m – iron content in the final product, %;

The estimates of the enrichment results were monitored by chemical analysis and mineralogical studies. Quality control of separation products is performed by measuring the mass fraction of iron by chemical methods. The process experiments were carried out in accordance with the State Standards of Ukraine DSTU 3195-95, 3196-95, 3198-95, 3207-95, 3210-95; DSTU ISO 3082: 200, MOD; DSTU ISO 10836: 200, MOD).

Results and discussion

The issue of ore preparation is critical for hematite quartzites of the Kryvyi Rih iron ore basin due to the mineral composition.

The main direction of further advancement of hematite quartzite enrichment is the development of ore preparation schemes that ensure the separation of mineral grains with minimal formation of fine grains of 0.01–0.016 mm using new grinding processes. In our previous studies, we recommended the use of HPGR crushers – high-pressure roll presses. In these crushers, material crushing occurs in a layer of ore lumps that crush each other. Such crushing allows the grains to be opened without re-grinding and produces material with a particle size of 1.2 mm. This makes it possible, in the first stage of magnetic separation, to dump waste rock in the amount of 49.22% [37–38].

The use of dry magnetic pretreatment in hematite ore enrichment schemes solves an important issue of stabilizing the quality of crushed ore, reducing the ore grinding front by at least 40% of the initial one, and, as a result, reducing operating and capital costs by more than 30% [4,39–40].

This paper considers a different problem. Namely, the development of an effective technology for enrichment of "lean (poor)" thinly fractured hematite ores of the Kryvyi Rih iron ore basin of Ukraine.

Due to the fact that the hematite ores under study contain jaspillites, chlorite, dispersed hematite-chlorite schists and low-ore quartz layers, which are very challenging to process, the feasibility of using gravity enrichment, namely screw separation, in the processing technology of hematite quartzites was studied.

Ore with a size of -0.5+0.07 mm was sent to the screw separation. As a result, three products were obtained: concentrate, industrial product and light fraction (Table 2).

As can be seen from Table 2, the enrichment of the feed ore with a particle size of -0.5+0.07 mm at the screw sluice produced a high quality concentrate: The mass fraction of total iron in the hematite concentrate was 63.7%. However, the concentrate yield is low and amounts to 6.22%. The recovery of total iron in the concentrate was 8.57%.

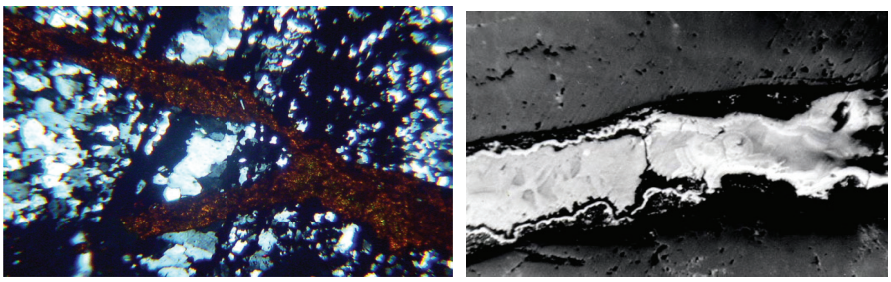

a b

Fig. 4. Dissecting veins of goethite in non-ore layers of iron mica-martite (a) and martite (b) quartzites; a – transmitted light; never intersecting; magnification 35x; light – quartz, dark gray – goethite; black – iron mica; b – reflected light; never parallel; magnification 22x; light gray – goethite; dark gray – quartz; black – voids

Rys. 4. Preparowanie żył getytu w nierudnych warstwach kwarcytów mikowo-martytowych (a) i martytowych (b) a – światło przechodzące; nierównoległe; powiększenie 35x; jasny – kwarc, ciemnoszary – getyt; czarny – mika żelazna; b – światło odbite; nierównolegle; powiększenie 22x; jasnoszary – getyt; ciemnoszary – kwarc; czarny – puste przestrzenie

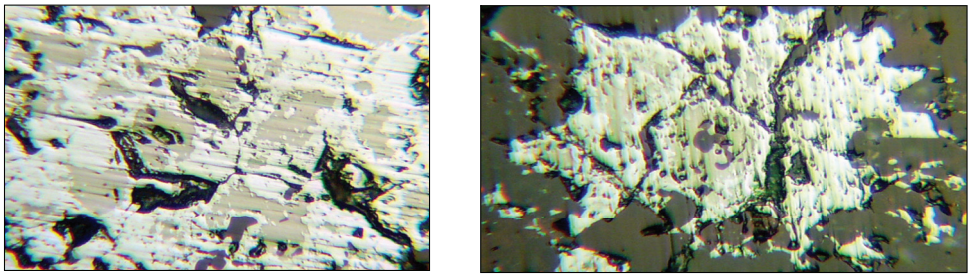

a b

Fig. 5. Relict inclusions of magnetite (light gray) in aggregates of newly formed martite (white) from ore layers of magnetite-martite quartzite. Reflected light; never parallel; magnification 37x. Dark gray – quartz; black – voids

Rys. 5. Reliktowe wtrącenia magnetytu (jasnoszare) w agregatach nowo powstałego martytu (białego) z warstw rudnych kwarcytu magnetytowo-martytowego. Odbite światło; nierównolegle; powiększenie 37x. Ciemnoszary – kwarc; czarny – puste przestrzenie

The industrial product and the light fraction of gravity concentration, which were formed during the separation of material with a particle size of -0.5+0.07 mm, were further sent for grinding to a particle size of 80% of the class minus 0.05 mm and then for flotation.

At the next stage of research, magnetic beneficiation of ore and its products was performed in a magnetic field with an induction of 0.07 T and 0.2–0.8 T.

Before magnetic beneficiation, the ore was crushed to different sizes; 0.25–0 mm, 0.2–0 mm, 0.15–0 mm, 0.074–0 mm, followed by beneficiation in a magnetic separator with a magnetic field induction of 0.07 T and 0.2–0.8 T. Magnetic separation of the crushed ore in a magnetic separator with a magnetic field induction of 0.07 T (WLIMS) was performed to protect the magnetic system of separators with a magnetic field induction of 0.2–0.8 T (WHIMS) from strongly magnetic minerals. As a result of WLIMS separation, two products were obtained: magnetic (concentrate) and non-magnetic industrial product – the starting product for WHIMS separation. The results of the experiments are shown in Fig. 8.

The analysis of the separation parameters of the WLIMS separation products revealed the possibility of extracting iron-containing concentrate with a mass fraction of 63.5% from ore with a particle size of minus 0.074+0 mm. The recovery of total iron in the concentrate amounted to 12.8%. Compared to gravity concentration, this figure is 4.23% higher.

Thus, in the technological scheme, WLIMS magnetic separation performs not only the protective function of the WNIMS separator magnetic system, but also allows to obtain commercial products. Unfortunately, the products are characterized by low quality. The mass fraction of SiO_2 in this concentrate is 23.7%. This product is mainly represented by magnetite and maghemite, their growths with quartz and flocs.

WHIMS magnetic enrichment of samples of non-magnetic material of the WLIMS separator was performed on a rotary separator of the type 259-CE in one step with a magnetic field induction of 0.2–0.8 T. The grinding size of the samples was 90% class minus 0.05 mm (maximum grain size 0.074 mm). The results of the experiments are shown in Table 3.

The analysis of the results shows that with an increase in magnetic field induction from 0.2 to 0.8 T, the recovery of total iron in the magnetic product increases from 78.8 to 86.9%. At the same time, the mass fraction of total iron in the concentrate (magnetic product) is 57.9–59.8 %. Losses of total iron with the non-magnetic product ranged from 21.2 to 13.1% with a mass fraction of total iron of 32–27.8%. The mass fraction of SiO_2 in the magnetic product was 11–13.8%. Such a product cannot be considered a concentrate and therefore was further sent for flotation processing.

Flotation enrichment

To obtain high-quality hematite concentrates, we studied reverse cation flotation. The following reagents were used in the experiments: Lilaflot-811M, Lilaflot-D817M and Lilaflot-D819MI amines as collectors, dextrin as a selective flocculant and depressor of iron ore minerals, caustic soda as a medium regulator and calcium chloride as a silica activator.

The results of the tests on the selection of the collector reagent are shown in Fig. 9. Further studies were carried out

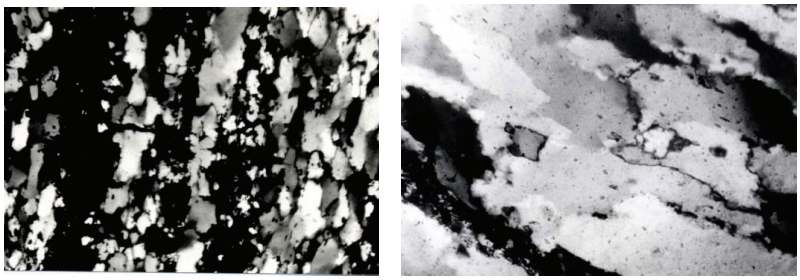

a b

Fig. 6. Morphology of quartz individuals and aggregates from non-ore layers of iron mica-martite (a) and martite (b) quartzites. White and gray – quartz; black – martite and iron mica. Transmitted light; never intersected; 30x magnification

Rys. 6. Morfologia pojedynczych ziaren i agregatów kwarcu z nierudnych warstw kwarcytu miki-martytu żelaza (a) i martytu (b). Biały i szary – kwarc; czarny – mika martytowa i żelazowa. Światło przechodzące; nieprzecinające się; 30-krotne powiększenie

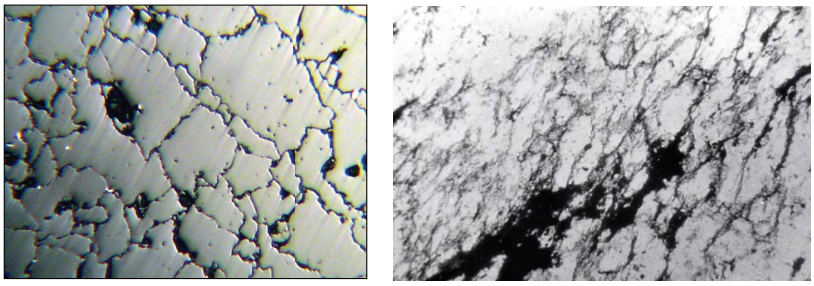

a b

Fig. 7. Structure of marshalized quartz aggregates from non-ore layers of martite (a) and goethite-martite (b) quartzite. Along the weakened contact zones of quartz individuals, it was partially replaced by a near-crystalline goethite aggregate (b). Reflected (a) and transmitted (b) light; never parallel; magnification: a – 40x; b – 30x.a: white – iron mica; dark gray – quartz; black – voids; b: white – quartz; dark gray – dispersed goethite; black – goethite

Rys. 7. Struktura zorganizowanych agregatów kwarcowych z nierudnych warstw martytu (a) i getytu-martytu (b) kwarcytu. Wzdłuż osłabionych stref kontaktowych jednostek kwarcu został on częściowo zastąpiony przez prawie krystaliczne kruszywo getytu (b). Światło odbite (a) i przechodzące (b); nierównolegle; powiększenie: a – 40x; b – 30x. a: biała – mika żelazowa; ciemnoszary – kwarc; czarny – puste przestrzenie; b: biały – kwarc; ciemnoszary – getyt rozproszony; czarny – getyt

using Lilaflot-D817M 260 g/t, which has a higher selectivity for SiO_2 and iron-containing particles.

The optimal consumption of the depressant reagent Dextrine was tested at two dosages of 1250 g/t of dextrin and 250 g/t with the same amount of Lilaflot-D819MI. The results of the two tests are presented in the form of an iron recovery graph in Fig.10.-11.

It was determined that the recovery of total iron in the concentrate is lower when tested with a depressor flow rate of 250 g/t compared to the flow rate of dextrin 1250 g/t (Fig. 10). Thus, with a mass fraction of total iron in the concentrate of 65.8%, the iron recovery into the concentrate at a dextrin flow rate of 1250 g/t was 78%, and at a flow rate of 250 g/t – 73%.

Evaluation and analysis of the results of the kinetics of flotation separation of iron-containing minerals and quartz (Fig. 11) showed that an increase in the mass fraction of total iron in the concentrate from 55 to 65% is possible only with an increase in flotation time from 8 minutes to 20 minutes and above. At the same time, with a decrease in dextrin consumption from 1250 g/t to 250 g/t, the mass fraction of total iron in the concentrate increases by an average of 3–4%.

In flotation with cationic collectors, the pH of the medium is of great importance. Therefore, we conducted studies to determine the optimal pH of the suspension during flotation. The studies were carried out at two values of pH 11 and pH 9.5 (Figs. 12, 13).

As can be seen from the results shown in Fig. 12, the efficiency of separation of iron-containing minerals and quartz improves with increasing pH. Thus, when the mass fraction of total iron in the concentrate is above 65%, the iron recovery in the concentrate is higher by 5% at pH 11 compared to pH 9.5.

The analysis of the results of reverse flotation kinetics (Fig. 13) allowed us to establish that the effect of pH on the quality of the concentrate is not eliminated when the flotation time is increased from 10 minutes to 20 minutes and above

As a result of the analysis of the flotation study results, the optimal reagent mode for reverse cationic flotation of quartz to produce hematite concentrate was determined: caustic soda – 1000 g/t, Dextrine – 250 g/t, Lilaflot D817 M – 260 g/t. This mode was used as the basis for a control test for flotation study of the hematite ore sample.

The study resulted in a hematite concentrate with a mass fraction of total iron of 64.05–65.95%, with iron recovery in the concentrate of 60.3–70.68%. The maximum achieved value of iron recovery was 70.68% with a mass fraction of total iron of 65.95%.

It has been established that depending on the feed material for flotation, the flowsheet for obtaining hematite concentrate changes.

Based on the data of the process experiments carried out in the laboratory, we have developed 7 variants of schemes (Table 4) using combined magnetic-gravity-flotation technologies.

According to the developed technologies, it is possible to obtain a hematite concentrate with a mass fraction of total iron of 64.14–65.95%, with a yield of 27.13–40.27%. Total

Tab. 2. Results of hematite ore enrichment using a screw separator

Tab. 2. Wyniki wzbogacania rudy hematytu za pomocą separatora ślimakowego

Name of the sample	Name	Yield %	Mass fraction of total iron, %	Recovery of total iron, %
Hemitite ore, size of -0,5+0,07 mm	concentrate	6,22	63,7	8,57
	inductrial product	31,76	58,33	40,07
	light fraction	62,02	38,3	51,37
	feed	100,00	46,24	100,00

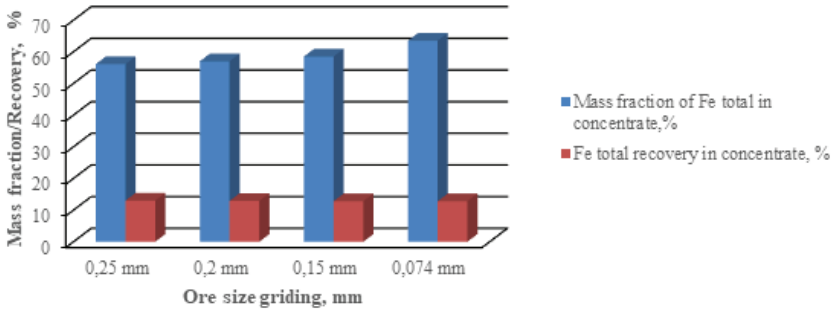

Fig. 8. Results of enrichment of hematite ore of different sizes

Rys. 8. Wyniki wzbogacania rudy hematytu o różnej wielkości

Tab. 3. Results of WHIMS magnetic separation of non-magnetic product WLIMS of hematite ore

Tab. 3. Wyniki separacji magnetycznej WHIMS produktu niemagnetycznego WLIMS rudy hematytu

Magnetic field induction, T	Product name	Yield, %	Mass fraction, %		Recovery, %	
			Fe	SiO_2	Fe	SiO_2
0,2	Feed	100	49,8	24,5	100	100
	Magnetic product	67,0	58,6	11,0	78,8	30,1
	Non-magnetic product	33,0	32,0	51,9	21,2	69,9
0,3	Feed	100	50,3	24,5	100	100
	Magnetic product	68,5	59,7	11,4	81,3	31,9
	Non-magnetic product	31,5	29,9	53,0	18,7	68,1
0,5	Feed	100	50,8	24,5	100	100
	Magnetic product	72,9	59,8	11,0	85,8	32,7
	Non-magnetic product	27,1	26,6	60,8	14,2	67,3
0,8	Feed	100	50,7	24,5	100	100
	Magnetic product	76,1	57,9	13,8	86,9	42,9
	Non-magnetic product	23,9	27,8	58,5	13,1	57,1

iron recovery of the concentrate ranges from 47.15 to 70.68%, depending on the combination of enrichment methods and grinding conditions of industrial products

The main criterion for the efficiency of hematite quartzite enrichment technology was the Hennock efficiency criterion, which ranged from 42.49–64.7%. According to the efficiency criterion, all scheme variants can be divided into three groups: efficient, inefficient, and ineffective.

Group I – schemes of variants 2.4, which obtained the highest concentrate values in terms of mass fraction of iron 63.77–64.7% and recovery 70.23–70.3%;

Group II – schemes of variants 1,6,7, which produce a concentrate with a mass fraction of iron in the range of 64.14–65.06% and recovery of 64.09–65.11%; efficiency criterion 55.9–58.49%.

Group III – schemes of variants 3.5, which produce a concentrate with a mass fraction of iron in the range of 64.34–65.95% and recovery of 47.15–58.30%. The efficiency criterion is 42.49–54.27 %.

Conclusions

1. The study was carried out on a sample of hematite ores from the Kryvyi Rih iron ore basin of Ukraine, which consisted of 9 mineralogical ore varieties, distinguished by the quantitative ratio of the basic groups of ore and non-ore minerals.

2. As a result of enrichment of the feed ore with a grain size of -0.5+0.07 mm, a high quality concentrate was obtained at the screw sluices. The mass fraction of total iron in the hematite concentrate was 63.7%. The concentrate yield was 6.22%. The recovery of total iron in the concentrate was 8.57%.

3. As a result of WLIMS and WHIMS magnetic separation with a magnetic field induction of 0.07 T, an iron-containing concentrate with a mass fraction of 63.5% iron was obtained from ore with a size of minus 0.074+0 mm, with a total iron recovery of 12.8%.

4. It was determined that with an increase in the magnetic field induction from 0.2 to 0.8 T, the recovery of total iron in the magnetic product of WHIMS increases from 78.8 to 86.9 %. The mass fraction of total iron in the WHIMS magnetic product was 57.9–59.8%. Losses of total iron with the non-magnetic product ranged from 21.2 to 13.1% with a mass fraction of total iron of 32–27.8%. The mass fraction of SiO_2 in the magnetic product was 11–13.8%.

5. Based on the results of flotation studies, the optimal reagent mode of reverse cationic flotation of quartz to obtain a hematite concentrate was determined: caustic soda – 1000

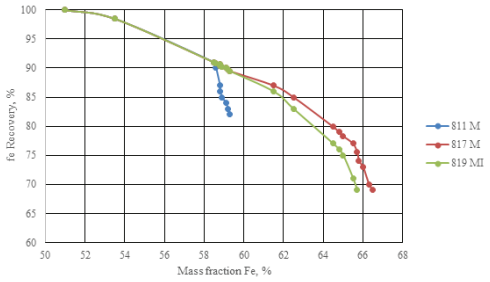

Fig. 9. Selectivity indicators of Lilaflot reagent

Rys. 9. Wskaźniki selektywności odczynnika Lilaflot

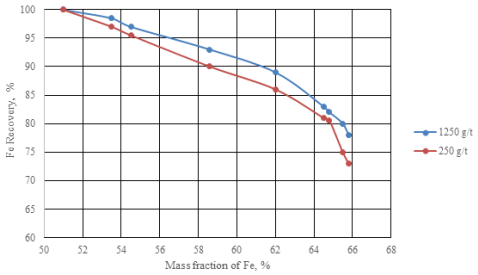

Fig. 10. Dependence of total iron recovery on the mass fraction of total iron in the chamber flotation product at different depressor flow rates

Rys. 10. Zależność całkowitego odzysku żelaza od udziału masowego żelaza ogólnego w produkcie flotacji komorowej przy różnych prędkościach przepływu w depresorze

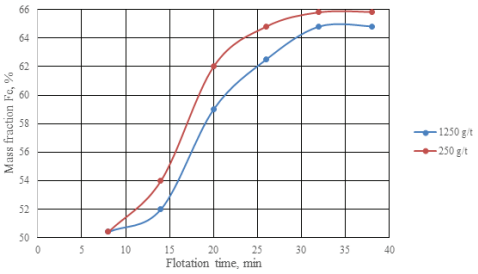

Fig. 11. Dependence of the mass fraction of total iron in the concentrate on the flotation time at different depressor flow rates

Rys. 11. Zależność udziału masowego żelaza ogólnego w koncentracie od czasu flotacji przy różnych prędkościach przepływu przez depresor

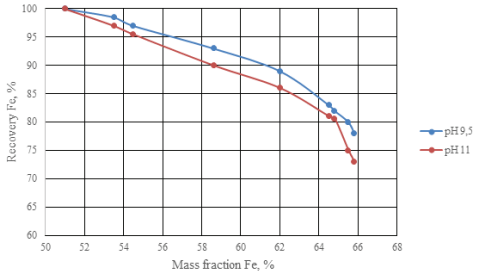

Fig. 12. Dependence of total iron recovery on the mass fraction of total iron in the flotation chamber product at different pH values

Rys. 12. Zależność całkowitego odzysku żelaza od udziału masowego żelaza ogólnego w produkcie komory flotacyjnej przy różnych wartościach pH

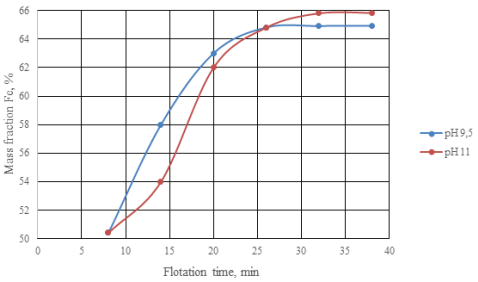

Fig. 13. Dependence of the mass fraction of total iron in the concentrate on the flotation time at different pH values

Rys. 13. Zależność udziału masowego żelaza ogólnego w koncentracie od czasu flotacji przy różnych wartościach pH

Tab. 4. Indicators of hematite ore enrichment by different flowsheets

Tab. 4. Wskaźniki wzbogacania rudy hematytu według różnych schematów

Variant	Product name	Yield, %	Mass fraction of total iron, %	Total iron recovery, %	Hancock efficiency criterion
1*	concentrate	34,77	65,06	61,11	55,90
	waste	65,23	22,07	38,89	
	feed	100	37,02	100,0	
2*	concentrate	40,27	64,64	70,3	63,77
	waste	59,73	18,4	29,7	
	feed	100	37,02	100	
3*	concentrate	32,72	65,95	58,3	54,27
	waste	67,28	22,95	41,7	
	feed	100	37,02	100	
4*	concentrate	39,75	65,41	70,23	64,70
	waste	60,25	18,29	29,77	
	feed	100	37,02	100,00	
5*	concentrate	27,13	64,34	47,15	42,49
	waste	72,87	26,85	52,85	
	feed	100	37,02	100	
6*	concentrate	37,55	64,19	65,11	58,49
	waste	62,45	20,68	34,89	
	feed	100	37,02	100,0	
7*	concentrate	36,99	64,14	64,09	57,52
	waste	63,01	21,1	35,91	
	feed	100	37,02	100,00	

Note: *1–7 variants of flowcharts and their description

1 – 100% feed ore is crushed in 2 stages and sent to WLIMS and WHIMS magnetic separation, reverse cation flotation of hematite in one stage

2 – 100% feed ore is crushed in stage 2 and sent to WLIMS and WHIMS magnetic separation, reverse cationic flotation of hematite in two stages with additional grinding of the froth product

3 – ore is preliminarily enriched by dry magnetic separation (DMS), magnetic industrial product of DMS is crushed in two stages to 0.5 and 0.074 mm and sent to WLIMS and WHIMS magnetic separation, reverse cation flotation of hematite in one stage

4 – ore is preliminarily enriched by dry magnetic separation (SMS), magnetic industrial product of SMS is crushed in two stages to 0.5 and 0.074 mm and sent to WLIMS and WHIMS magnetic separation, reverse cation flotation of hematite in two stages with additional grinding of the froth product

5 – ore is preliminarily enriched by dry magnetic separation (DMS), the magnetic product of DMS is crushed to 0.5 mm and fed for classification by grain size of 0.074 mm The -0.5+0.074 mm fraction is fed to gravity, and the -0.074 mm fraction is fed to WLIMS and WHIMS magnetic separation. Gravity and magnetic separation products are sent to hematite flotation in one stage

6 – ore is preliminarily enriched by dry magnetic separation (DM), the magnetic product of DM is crushed to 0.5 mm and fed to the classification by grain size of 0.074 mm The -0.5+0.074 mm fraction is fed to gravity, and the -0.074 mm fraction is fed to WLIMS and WHIMS magnetic separation. Gravity and magnetic separation products are sent to hematite flotation in two stages with froth grinding

7 – 100% feed ore is crushed in stage 2 and sent to hematite flotation. The scheme consists of the main and control flotations, grinding of the froth product and its re-cleaning.

g/t, calcium chloride (5%) – 200 g/t, Dextrine – 1250 g/t, Lilaflot D817 M – 260 g/t. During flotation studies, a hematite concentrate was obtained with a mass fraction of total iron of 64.05–65.95%, with an iron recovery of 60.3–70.68%.

6. On the basis of the results of process tests, seven variants of flowsharts for hematite ore enrichment were developed. The main criterion for the efficiency of hematite quartzite enrichment technology was the Hancock efficiency criterion, which ranged from 42.49–64.7%.

7. According to the efficiency criterion, all flowshart scenarios can be divided into three groups: efficient, inefficient and ineffective. Effective technologies for the enrichment of hematite quartzite (process efficiency criterion 63.77–64.7%) include technologies using a combination of magnetic flotation separation of ore and products of different sizes.

8. It is recommended to implement the enrichment technology using dry magnetic separation, grinding of preliminary enrichment products in two stages to 0.5 and 0.074 mm, magnetic separation WLIMS and WHIMS with magnetic field induction of 0.07 T and 0.8 T, cationic flotation of quartz from magnetic products. This technology makes it possible to obtain a commercial concentrate with a mass fraction of iron of 37.02% from hematite ore with a total mass fraction of iron of 65.41%. The concentrate yield was 39.75%, with a total iron recovery of 70.23%.

Literatura – References

1. Stupnik, M.,I., Peregudov, V.,V., Morkun, V.,S., Oliinyk, T.,A.. & Korolenko, M.,K. (2021). Development of concentration technology for medium-impregnated hematite quartzite of kryvyi rih Iron ore basin. Science and Innovation, 16 (6). 56–71. SOURCE-WORK-ID: PR1YE.
2. Pysmennyi, S., Peremetchyk, A., Chukharev, S., Anastasov, D.,& Tomiczek, K. (2022). The mining and geometrical methodology for estimating of mineral deposits. IOP Conference Series: Earth and Environmental Science, 1049 (1), 012029 https://doi.org/10.1088/1755-1315/1049/1/012029
3. Oliinyk, T., A. (2018). Perspektyvy rozvytku tekhnolohii zbahachennia zaliznykh rud.Zbahachennia korysnykh kopalyn: Nauk.-tekhn. zb. Vyp. 69 (110). 32-44. [Oliinyk, T., A. Prospects for the development of iron ore beneficiation technologies Mineral processing: Scientific and technical journal 69 (110). 32-44] (in Ukrainian)
4. Oleynik, T., A. (2013). Sovremennyie tendentsii razvitiya tehnologiy obogascheniya gematitovyih rud v Ukraine. Zbagachennya korisnih kopalin: Nauk.-tehn. zb., 56(97), 18–28 [Oleinik, T., A. (2013) Modern trends in the development of hematite ore enrichment technologies in Ukraine. Beneficiation of useful minerals: Scientific and Technical Journal, 56(97), 18-28.] (in Russian)
5. Belevtsev, Ya., (1952). Geneticheskaya klassifikatsiya zheleznikh rud Krivogo Roga. Mineralogicheskii sbornik, 6, 125-130 [Belevtsev Ya.,N. Genetic classification of iron ores of Krivoy Rog .Mineralogical journal,6. 125-130].(in Russian)
6. Akhkozov, Yu.,L., Kupovets, V.,A., & Kopertekhin, I.,A. (1982). Nekotorie geologo-mineralogicheskie faktori, opredelyayushchie svoistva rud Inguletskogo mestorozhdeniya. Gornii zhurnal, 2, 9-10 [Akhkozov Y., L., Kupovets V.,A., & Kopertekhin I.,A. Some geological and mineralogical factors determining the properties of Ingulets ore deposit. Mining journal,2, 9-10]. (in Russian)
7. Bespoiasko, E.,O., (2004). Vplyv mineralnoho skladu na fizychni ta tekhnichni vlastyvosti vyvitrenykh zalizystykh porid Inhuletskoho rodovyshcha (Kryvorizkyi basein). Heoloho-mineralohichnyi visnyk Kryvorizkoho tekhnichnoho universytetu,1,40-47 [Bespoyasko E.,O. Influence of mineral composition on physical and technical properties of weathered ferruginous rocks of Ingulets deposit (Kryvyi Rih basin) . Geological and Mineralogical Journal of Kryvyi Rih Technical University,1, 40-47]. (in Ukrainain)
8. Dokuchaeva, I.,N., (1966). K voprosu otsenki effektivnosti obogashcheniya zhelezistikh porod Krivogo Roga i tekhnologicheskaya klassifikatsiya ikh. Sb. nauch. tr. in-ta Mekhanobrchermet. 5, [Dokuchaeva I.,N. To the evaluation of efficiency of enrichment of ferruginous rocks of Krivoy Rog and their technological classification. Collection of scientific works of the institute Mekhanobrchermet, 5]. (in Russian)
9. Pysmennyi, S., Fedko, M., Shvaher, N., & Chukharev, S. Mining of rich iron ore deposits of complex structure under the conditions of rock pressure development. E3S Web of Conferences, 2020, 201, 01022 https://doi.org/10.1051/e3sconf/202020101022
10. Bespoiasko, E., O. (2014). Mineralohichni osoblyvosti zaliznykh rud Kryvorizkoho baseinu u svitli zbilshennia yikh kondytsiinykh zapasiv. Mineralohichnyi zhurnal, 36 (3), 86–91 [Bespoiasko, E., O. (2014). Mineralogical properties of iron ores of the Kryvyi Rih basin in the light of the increase in their conditioned reserves. Mineralogical Journal, 36 (3), 86-91]. (in Ukrainian)
11. Morkun, V., S.; Semerikov, S., O., & Hryshchenko, S., M. (2017). Content and teaching technology of course "ecological geoinformatics" in training of future mining engineers. Information technologies and learning тools., 57 (1), 115-125.
12. Bespoiasko, E., A., Evtekhov, V., D., & Bespoiasko, T., V. (2014). Lokalizatsiia i mineralnyi sklad pokladiv bahatykh hematytovykh rud Inhuletskoho rodovyshcha Kryvbasu. Mineralohichnyi zhurnal, 36 (4), 122–127 [Bespoiasko, E.,A., Evtekhov, V.,D., & Bespoiasko, T.,V. (2014). Localization and mineral composition of rich hematite ore deposits of the Ingulets deposit of Kryvbas. Mineralogical Journal, 36 (4), 122-127] (in Ukrainian)
13. Seifelnassr, A.A., S., Eltahir M., M. & Abdel-Zaher M., A. (2012). Effective processing of low-grade iron ore through gravity and magnetic separation techniques. Physicochem. Probl. Miner. Process., 48(2), 567–578.
14. Das, B., Prakash, S., Das S.. K., & Redd, P., S., R. (2007). Effective beneficiation of low grade iron ore through jigging operation. Journal of Minerals & Materials Characterization & Engineering, 7 (1), 27–37.
15. Evtekhov, V.,D., Peregudov, V.,V., Yevtekhov, Ye..V., Dudar, L.,T., Filenko, V.,V., Smirnov, A.,Ya., Bilenko, A.,E., & Nikolenko, Ye.,M. (2013). Geologicheskaya otsenka rezultatov poiska optimalnoi skhemi obogashcheniya gematitovikh kvartsitov zhelezistokremnistoi formatsii dokembriya. Geologo-mineralogichnii visnik Krivorizkogo natsionalnogo universitetu,1-2, (29-30), 87-94.[Evtekhov V.,D., Peregudov V.,V., Evtekhov E.,V., Dudar L.,T., Filenko V.,V., Smirnov A.,Y., Bilenko A.,E., & Nikolenko E.M. Geological assessment of the results of searching for the optimal scheme of hematite quartzite enrichment of the iron-silica formation of the Precambrian. Geological and Mineralogical Bulletin of Kryvyi Rih National University, 1-2 (29-30), 87-94.] (in Russian).
16. Gubin, G.,V., Bogdanova, I.,P., & Lukyanchikov, I.,N. (1976). O ratsionalnoi tekhnologii obogashcheniya okislennikh zhelezistikh kvartsitov. Obogashchenie rud chernikh metallov: Sb. nauch. Tr., 5, 81-88 [Gubin G.,V., Bogdanova I.,P., & Luk'yanchikov I.,N. On efficient technology of oxidized ferruginous quartzite enrichment. Enrichment of ferrous metal ores: Collection of scientific papers, 5, 81-88]. (in Russian)

17. Malii, V.,M., Ganzenko, T.,B., & Titlyanov, Ye.,A.(1984). Razrabotka tekhnologii magnitnogo obogashcheniya okislennikh zheleznikh rud. Obogashchenie slabomagnitnikh rud chernikh metallov, Nedra, 12-16. [Malyi V.,M., Ganzenko T.,B., & Titlyanov E.,A. Development of magnetic enrichment technology of oxidized iron ores. Enrichment of low-magnetic ores of ferrous metals,12-16] (in Russian)

18. Suslikov, G.,F., Malii, V.,M., Ganzenko, T.,B. & i dr. (1984). Promishlennie ispitaniya tekhnologii magnitnogo obogashcheniya okislennikh kvartsitov Krivbassa. Obogashchenie slabomagnitnikh rud chernikh metallov: Sb. nauch. tr. in-ta Mekhanobrchermet, Nedra, 16-22. [Practical tests of magnetic enrichment technology of oxidized quartzites of Krivbass. Suslikov, G.,F., Maly, V.,M., Ganzenko T.,B. & et al. Enrichment of weakly magnetic ores of ferrous metals: Collection of scientific papers of Mekhanobrchermet Institute, 16-22] (in Russian)

19. Shiryaev, A., A., Velichko, Yu.,V., & Botvinnikov, V.,V. (2005). Osobennosti tekhnologii podgotovki i obogashcheniya okislennikh zhelezistikh kvartsitov so stadialnim videleniem kontsentrata. Metallurgicheskaya i gornorudnaya promishlennost,4, 86-88 [Shiryaev A.,A., Velichko Yu.,V., & Botvinnikov V.,V. Specific features of technology of preparation and enrichment of oxidized ferruginous quartzite with staged concentrate separation. Metallurgical and ore-mining industry,4, 86-88] (in Russian)

20. Umadevi, Tekkalakote., Amit, Pratap., Singh, Kumar., Abhishek, Basavareddy., & Suresh, Rameshwar Sah (2013). Recovery of iron bearing minerals from beneficiation plant 2 thickener underflow of JSW Steel limited. Journal of Minerals and Materials Characterization and Engineering, 1, 55–60.

21. Karmazin, V., V., Pak, S., G., & Maslov, D., S. (2012). Magnitnoe obogashchenie okislennikh zhelezistikh kvartsitov Mikhailovskogo mestorozhdeniya. Gornii informatsionno-analiticheskii byulleten. Nauchno-tekhnicheskii zhurnal, 12, 212–219. [Karmazin, V., V., Pak, S., G., & Maslov, D., S. (2012). Magnetic enrichment of oxidized ferruginous quartzites of Mikhailovskoe deposit. Mining Information and Analytical Bulletin. Scientific and Technical Journal, 12, p.212-219.] (in Russian)

22. Karmazin, V.,I., Mostepan, L.,F., & Levchenko K.,A. (1994). O povishenii effektivnosti visokogradientnogo obogashcheniya ilistikh fraktsii okislennikh zhelezistikh kvartsitov TsGOKa pri ispolzovanii setchatoi matritsi s vertikalnim namagnichivaniem. Sovremennoe sostoyanie i perspektivi razvitiya tekhniki i tekhnologii magnitnogo obogashcheniya rud i materialov, Krivoi Rog, 29-30 [Karmazin V.,I., Mostepan L.,F., & Levchenko K.,A. On increasing efficiency of high-gradient enrichment of silt fractions of oxidized ferruginous quartzites of CGOK using mesh matrix with vertical magnetization. Modern state and prospects of technology of magnetic enrichment of ores and materials, Krivoy Rog, 29-30] (in Russian)

23. Oleinik, T.,A., Sklyar, L.,V., Kushniruk, N.,V., Oleinik, M.,O., &Tatarinov F.,G. (2014). Razrabotka tekhnologii flotatsionnoi dovodki nekonditsionnikh gematitovikh kontsentratov. Zbagachennya korisnikh kopalin, 56 (97), 129-138 [Oleinik, T.,A., Sklyar, L.,V., Kushniruk, N.,V., Oleinik, M.,O., & Tatarinov F.,G. Development of technology of flotation finishing of substandard hematite concentrates. Enrichment of useful minerals, 56 (97), 129 -138].(in Russian)

24. Sokolova, V., P. (2003). Ispolzovanie apolyarnikh sobiratelei pri flotatsii tonkovkraplennikh okislennikh zheleznikh rud. Novoe v tekhnologii, tekhnike i pererabotke mineralnogo sirya: Sb. nauch. tr. in-ta Mekhanobrchermet, Krivoi rog,. 17-22. [Sokolova V.,P. Use of apolar collectors in flotation of thinly disseminated oxidized iron ores. New in technology, technique and processing of mineral raw materials: Collection of scientific works of the Institute of Mechanobrchermet, Krivoy Rog, 17-22] (in Russian)

25. Villar, J., W., & Dawe G., A. (1975). Obogashchenie zheleznikh rud novim sposobom na kombinate Tilden. The Tilden mine. A new processing techique for iron ore. "Mining Congr. J.", 61,10, 40-48.

26. Osobennosti protsessa selektivnoi flokulyatsii i obesshlamlivaniya pri flotatsionnom obogashchenii okislennikh zheleznikh rud (1981). Ekspress-informatsiya TsNIITEI ChM. Ser. Obogashchenie rud, Vip. 2, 7. [Features of selective flocculation and desliming process in flotation enrichment of oxidized iron ores. Express-information of CNIITEI CHM. Ser. Ore Enrichment, Issue. 2, 7] (in Russian)

27. Gornorudnoe predpriyatie Tilden otmechaet 25-letie proizvodstva okatishei. Tilden Mine Marks 25 years of pellet production (1999). Skill. Mining Rev. – 1999. – 88, № 50. – P. 9-10 [Tilden mining company celebrates 25 years of pellet production. Skill. Mining Rev.88, (50), 9-10] (in Russian)

28. Ma, X., Marques, M., & Gontijo, C. (2011). Comparative studies of reverse cationic/anionic flotation of Vale iron ore. International Journal of Mineral Processing, 100, 179–183.

29. Filippov, L., O., Severov, V., V., & Filippova, I.,V. (2014). An overview of the beneficiation of iron ores via reverse cationic flotation. International Journal of Mineral Processing, 127, 62–69.

30. Braga, A., Junior, M., M., & Peres, E., C. (2011). Effect of coarse quartz scalping on the reverse cationic flotation of iron ore. Revista de la Facultad de Ingenieria, 25, 1–9.

31. Ganzenko, T.,B., Malii, V.,M., & Skorodumova, L.P. (1983). Otrabotka tekhnologii obogashcheniya okislennikh zhelezistikh kvartsitov Krivbassa. Razvitie tekhniki i tekhnologii rudopodgotovki v chyornoi metallurgii: Sb. nauch. tr. in-ta Mekhanobrchermet, 22-25. [Ganzenko T.,B., Maly V.,M., & Skorodumova L.,P. Development of enrichment technology of oxidized ferruginous quartzites of Krivbass.Development of equipment and technology of ore dressing in ferrous metallurgy: Collection of scientific papers of the Institute of Mechanobrchermet, 22-25] (in Russian)

32. Belevtsev, Ya.,N., Tokhtuev, G.,V., Strigin A.,I. & et al. (1962). Geologiya Krivorozhskikh zhelezorudnikh mestorozhdenii. Kiev: Naukova dumka, T. 1,484 [Belevtsev Y.,N., Tokhtuev G.,V., Strygin A.,I. & and others. Geology of Krivoy Rog iron-ore deposits. Kiev: Naukova Dumka, T. 1,484] (in Russian)
33. Lazarenko, Ye.K., Gershoig, Yu.,G., Buchinskaya, N.I. & all (1977). Mineralogiya Krivorozhskogo basseina. Kiev: Naukova dumka, 543. [Lazarenko E.,K., Gershoig Y.,G., Buchinskaya N.,I. & and others. Mineralogy of Krivoy Rog Basin. Kiev: Naukova Dumka, 1977. 543] (in Russian)
34. Bielievtsev, Ya. M. (1951) Mineral hidrohematyt i yoho rol v rudoutvorenni Kryvoho Rohu. Heolohichnyi zhurnal,3, 3-16.[Belevtsev Y.,M. Mineral hydrohematite and its role in ore formation in Kryvyi Rih. Geological Journal, 3, 3-16] (in Ukrainian)
35. Bespoyasko, E.,A., Yevtekhov, Ye.,V., Machado, O.,T., & Smirnova, A.Ya. (2001). Mineralogicheskie i geokhimicheskie osobennosti vivetrennikh zheleznikh rud verkhnei chasti razreza saksaganskoi sviti Inguletskogo mestorozhdeniya. Geologo-mineralogichnii visnik Krivorizkogo tekhnichnogo universitetu,2, 46-54. [Bespoyasko E.,A., Evtekhov E.,V., Machado O.,T., & Smirnova A.,Y. Mineralogical and geochemical features of weathered iron ores of upper part of section of Saksaganskaya Formation of Ingulets deposit. Geology and Mineralogy Newsletter of Krevyi Rih Technical University, 2, 46-54] (in Russian)
36. Malykh V.M. (1983). Mineralogo-geokhimicheskie osobennosti zhelezistikh kvartsitov v glubinnikh zonakh okisleniya Saksaganskoi polosi (raion Krivogo Roga). Izvestiya vuzov. Geologiya i razvedka,2, 48-52. [Malykh V.,M. Mineralogical and geochemical properties of ferruginous quartzites in the deep oxidation zones of the Saksagan band (Krivoy Rog area). Izvestiya vuzov. Geology and Exploration, 2, 48-52] (in Russian)
37. Oliinyk,T.,A., Nikolaienko, K.,V. & Nikolaienko, P.K. (2019). Vplyv droblennia hematytovykh rud v valkovii drobartsi z valkamy vysokoho tysku na kintsevi pokaznyky yikh zbahachennia. Zbahachennia korysnykh kopalyn, 73(114), 85 – 92 [Oliinyk T.,A., Nikolayenko K.,V., & Nikolayenko P.,K. Influence of crushing hematite ores in a roller crusher with high-pressure rolls on the final indicators of their enrichment. Mineral Processing, 73(114), 85 - 92] (in Ukrainian)
38. Oliinyk, T., Nikolaienko, P., Nikolaienko K. & Oliinyk M. (2021). Optimization of the crushing process of oxidized iron quartzites in HPGR. Eastern-European Journal of Enterprise Technologies, 6, 1(109), 41–51. DOI: 10.15587/1729-4061.2021.224939
39. Huifen Zhang, Luzheng Chen, Jianwu Zeng, Li Ding & Jian Liu (2015). Processing of lean iron ores by dry high intensity magnetic separation. Separation Science and Technology, 50: 1689-1694.
40. Oliinyk, T., Sklyar, L. & Kushniruk, N. (2015). Development of pre-processing technology for hematite quartzite of Kryvyi Rih iron ore basin. Proceedings from the International conference "X Congeress of ore enrichment specialists of CIS contries", 344-346.

Ocena skuteczności technologii wzbogacania kwarcytu hematytowego

W artykule podjęto problem opracowania wydajnej technologii wzbogacania rud hematytu. Celem badań jest zbadanie właściwości procesowych słabo rozsianych rud hematytu Ukrainy, z uwzględnieniem ich właściwości mineralogicznych, opracowanie schematów wzbogacania rud hematytu oraz ocena skuteczności separacji minerałów podczas wzbogacania grawitacyjnego, magnetycznego i metody flotacji.

Badania przeprowadzono na próbce rud hematytu z krzyworoskiego zagłębia rud żelaza na Ukrainie, która składała się z 9 mineralogicznych typów rud, wyróżniających się stosunkiem ilościowym głównych grup minerałów kruszcowych i nierudnych.

W wyniku separacji magnetycznej WLIMS przy indukcji pola magnetycznego 0,07 T otrzymano koncentrat zawierający żelazo o udziale masowym żelaza 63,5% z rudy o wielkości minus 0,074+0 mm, przy całkowitym uzysku żelaza 12,8%.

Stwierdzono, że wraz ze wzrostem indukcji pola magnetycznego od 0,2 T do 0,8 T, uzysk żelaza ogólnego w produkcie magnetycznym WNIMS wzrósł z 78,8% do 86,9%. Udział masowy całkowitego żelaza w produkcie magnetycznym WIMS wynosił 57,9–59,8%. Straty żelaza ogólnego z produktem niemagnetycznym wahały się od 21,2% do 13,1% przy udziale masowym żelaza całkowitego 32–27,8%. Udział masowy SiO2 w produkcie magnetycznym wynosił 11–13,8%.

W wyniku badań flotacyjnych otrzymano koncentrat hematytu o udziale masowym żelaza ogólnego 64,05–65,95%, z odzyskiem żelaza w koncentracie 60,3–70,68%. Na podstawie wyników badań procesowych opracowano siedem wariantów schematów wzbogacania rud hematytu. Schematy oceniono według kryterium sprawności Hancocka, które mieściło się w przedziale 42,49–64,7%. Zarekomendowano do wdrożenia technologię flotacji magnetycznej do wzbogacania kwarcytu hematytowego. Technologia ta umożliwia otrzymanie koncentratu handlowego o udziale masowym żelaza ogólnego 37,02% z rudy hematytu o udziale masowym żelaza ogólnego 65,41%.

Słowa kluczowe: *kwarcyt hematytowy, technologia, wydajność, separacja magnetyczna, grawitacja, flotacja*

Supporting a Mine Working with a Shelter in Various Mining and Geological Conditions

Oleksandr KRUKOVSKYI[1)], *Viktoriia KRUKOVSKA*[2)]

[1)] Corresponding Member of NAS of Ukraine, Doctor of Technical Sciences (D. Sc), Deputy Director of the institute, Institute of Geotechnical Mechanics named by N. Poljakov of National Academy of Sciences of Ukraine, Dnipro, Ukraine;
ORCID https://orcid.org/0000-0002-2659-5095; email: igtm@ukr.net
[2)] Doctor of Technical Sciences (D. Sc), Senior Researcher, Institute of Geotechnical Mechanics named by N. Poljakov of Na-tional Academy of Sciences of Ukraine, Dnipro, Ukraine; ORCID https://orcid.org/0000-0002-7817-4022; email: vikakrukk@gmail.com

http://doi.org/10.29227/IM-2023-01-05

Submission date: 22-02-2023 | Review date: 20-03-2023

Abstract

Shelters are used to protect miners from exposure to harmful gases and for the work of rescuers. Such shelters are built in a niche adjacent to the mine working. The purpose of this work is a numerical study of the stress state of a coal-rock massif with a mine working and a shelter, their stability in various mining and geological conditions and with various supporting schemes.
Numerical simulation of the stress state of a coal-rock massif with a mine working and a shelter was performed; their stability was studied in various mining and geological conditions and with various supporting schemes. It is shown that, over time, near-contour rocks are unloaded from rock pressure, and an area of increased difference of the stress tensor compo-nents expands around the mine working and the shelter. This leads to cracks formation of varying degrees of intensity. When the mine working with the shelter is driven at a shallow depth in hard rocks, the basic scheme, which consists mainly of metal frames and a reinforced concrete barrier, is sufficient for their supporting. If the host rocks are weaker, the stability of the mine working and the shelter is broken and it is necessary to strengthen their supporting with rock bolts. In the bolted area, the rocks are in triaxial compression conditions, a rock-bolts arch is formed above the mine working and the shelter, which pre-vents the displacement of the roof rocks into the mine working and increases its stability. With an increase in the depth of min-ing operations, the stability of the mine working decreases; the inelastic deformation zone in the mine walls grows; the load on the support increases. For the rock-bolts arch formed in the mine roof, supports are required in the walls of the mine working and the shelter. For this purpose, side rock bolts are installed. The use of an appropriate supporting scheme leads to a de-crease of the area of inelastic deformation zone by 2.5 times and the area of the zone unloaded from rock pressure by 2.6 times. Thus, such schemes for supporting the mine working and the shelter are selected, which ensure their stability in the considered mining and geological conditions.

Keywords: *mine workings stability, mining safety, numerical simulation, rock deformation, shelters, supporting of mine workings*

1. Introduction

Coal mining is of paramount importance during the conduct of warfare, when the demand for energy carriers is increased and there is a constant threat to the country's energy infrastructure. Most mines in Ukraine develop gas--bearing coal seams, and host rocks also contain methane. In order to meet air sanitary standards in the mine workings, their ventilation and degassing of the coal-rock massif are used. Emergency power cuts lead to the shutdown of many technological processes, in particular, ventilation, degassing, mine hoisting. Under such conditions, methane accumulations and explosions of the methane-air mixture represent a significant danger to miners. Shelters are used to protect miners from lack of oxygen and exposure to harmful gases [1, 2]. Shelters are also necessary for the work of rescuers who must explore and take the victims out of the emergency area. Such shelters are built in a niche adjacent to the mine working [3, 4].

To ensure non-repair operation of the mine working and the shelter for a long time, as well as the tightness of the shelter, it is necessary to choose their supporting correctly [5, 6]. Therefore, the purpose of this work is a numerical study of the stress state of a coal-rock massif with a mine working and a shelter, their stability in various mining and geological conditions and with various supporting schemes.

2. Problem definition

Fig. 1 shows a typical design of a shelter adjacent to a mine working that is driven through a coal seam. Both the mine working and the shelter are supported with frames, the astel of the walls and the roof is reinforced concrete, the shelter is separated from the mine working by a concrete barrier 200 mm thick. The floor of the shelter is located 700 mm above the floor of the mine working.

Several variants for mining and geological conditions were considered in this work: the depth of the mine working construction is 400 m and 800 m, the host rock is hard sandstone and weak argillite. For these conditions, the effectiveness of the use of three supporting schemes was investigated:

- the 1st supporting scheme, basic (fig. 1);
- the 2nd supporting scheme, basic scheme + 7 steel rock bolts 2.4 m long with polymer fastening in the borehole in the mine roof + 2 of the same rock bolts in the shelter roof;
- the 3rd supporting scheme, basic scheme + 7 steel rock bolts 2.4 m long with polymer fastening in the borehole in the mine roof + 2 of the same rock bolts in the shelter roof + 2 plastic bolts 1.5 m long in the coal seam in the right wall of the mine working and in the left wall of the shelter.

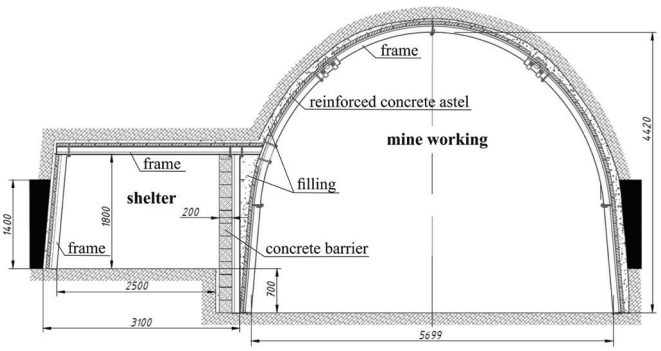

Fig. 1. The typical design of the shelter

Rys. 1. Typowy projekt schronu

Tab. 1. The properties of rocks and materials

Tab. 1. Właściwości skał i materiałów

Rocks and materials	Ultimate strength σ_{ci}, MPa	Modulus of elasticity, E, GPa	Poisson's ratio, ν	Cohesion, C, MPa	Friction angle, φ, deg
Sandstone	42	13	0.36	11.2	34.0
Argillite	20	11	0.32	5.8	30.0
Coal	15	5	0.26	4.5	28.5
Steel	650	200	0.25	-	-
Concrete	40	20	0.2	11.5	30.0
Reinforced concrete	50	24	0.2	13.9	32.0
Backfilling	2	1.2	0.18	0.7	20.0

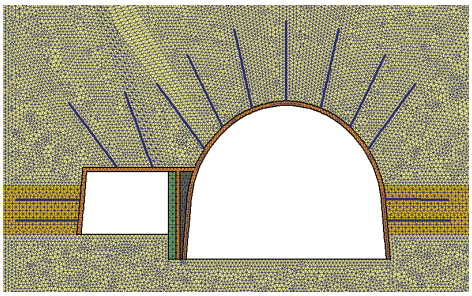

Fig. 2. The central fragment of the finite element mesh

Rys. 2. Centralny fragment siatki elementów skończonych

The properties of rocks and materials support that were used in the calculation are given in Tab. 1.

3. Methods

The process of rocks deformation is described by such equations [7, 8]:

$$c_g \frac{\partial u_i}{\partial t} = \sigma_{ij,j} + X_i(t) + P_i(t),$$

where c_g – the damping coefficient, kg/(m³·s); u_i – displacements, m; t – time, s; $\sigma_{ij,j}$ – derivatives of the stress tensor components along x, y, Pa/m; $X_i(t)$ – projections of the external forces acting on the volume unit of a solid body, N/m³.

The initial and boundary conditions for this task set are:

$$\sigma_{yy}\big|_{t=0} = \gamma H; \quad \sigma_{xx}\big|_{t=0} = \lambda\gamma H; \quad u_x\big|_{t=0} = 0; \quad u_y\big|_{t=0} = 0;$$

$$u_x\big|_{\Omega_1} = 0; \quad u_y\big|_{\Omega_2} = 0,$$

where λ – the side thrust coefficient; H – the mining depth, m; Ω_1 – vertical boundaries of the outer contour; Ω_2 – horizontal boundaries of the outer contour.

The problem is solved in an elastic-plastic formulation by the finite element method [9–11]. For the mathematical description of the process of rocks changeover into a disturbed state, the Mohr-Coulomb failure theory is applied [12, 13]. The rock bolts are simulated by the rod finite elements [14–16]. The central fragment of the finite element mesh with the mine working and the shelter, which are supported according to the 3rd scheme, is shown in Fig. 2.

Such geomechanical parameters as Q* characterizing the difference of the stress tensor components and P* characterizing a probable rock failure mode are applied to evaluate the stress state of rock [17]:

$$Q^* = \frac{\sigma_1 - \sigma_3}{\gamma H}; \quad P^* = \frac{\sigma_3}{\gamma H},$$

where σ_1, σ_3 – maximum and minimum components of the principal stress tensor, Pa; γ – averaged weight of the overlying rocks, N/m³.

4. Study of the stability of a mine working and a shelter, and their supporting in various mining and geological conditions

First, it was investigated whether the basic support shown in Fig. 1 ensures the stability of the mine working and the shelter at a relatively shallow depth of 400 m, if the host rock is sandstone or argillite. Figure 3 demonstrates the results of calculating of Q* parameter values and zones of inelastic de-

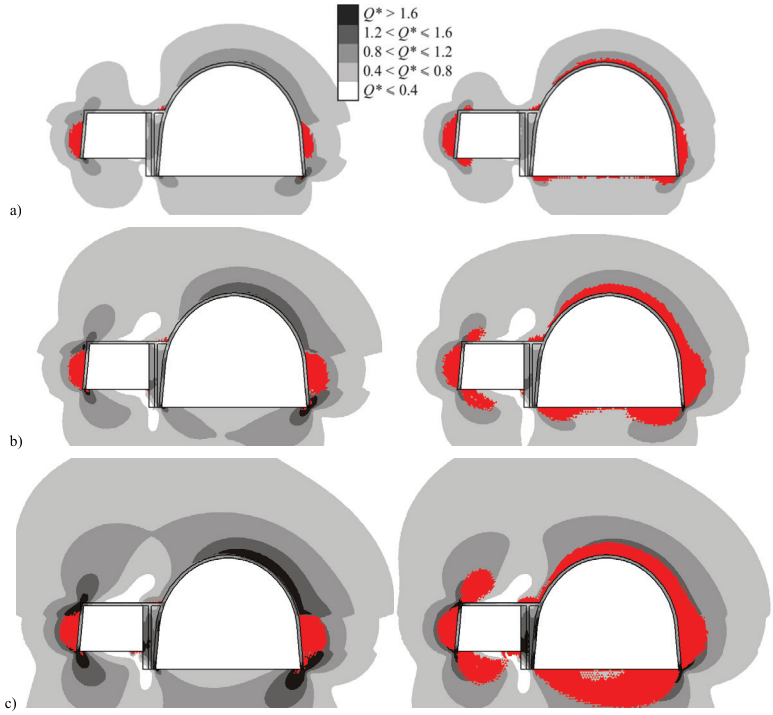

Fig. 3. Distributions of Q* parameter values and inelastic deformation zones (red color) in the rocks around the mine working and the shelter with the 1st supporting scheme, H = 400 m, host rock is sandstone (on the left side) and mudstone (on the right side) at the time points: a) t = 1 day; b) t = 3 days; c) t = 20 days

Rys. 3. Rozkłady wartości parametrów Q* i stref odkształceń niesprężystych (kolor czerwony) w skałach wokół wyrobiska i schronu przy pierwszym schemacie obudowy, H = 400 m, skałą macierzystą jest piaskowiec (po lewej stronie) oraz mułowiec (po prawej stronie) w punktach czasowych: a) t = 1 dzień; b) t = 3 dni; c) t = 20 dni

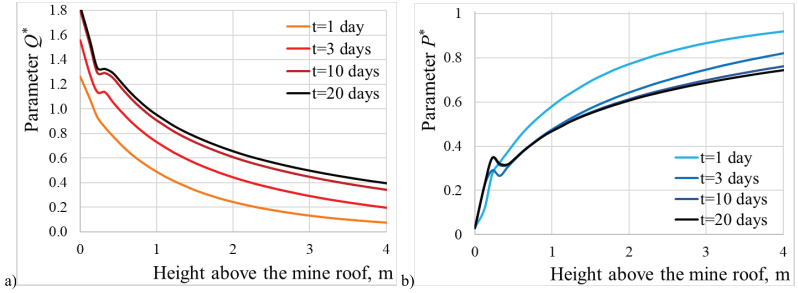

Fig. 4. Changes in the values of geomechanical parameters in the mine roof along the vertical axis passing through the center of the mine working at different points in time; the host rock is argillite; the 1st supporting scheme: a) Q* parameter; b) P* parameter

Rys. 4. Zmiany wartości parametrów geomechanicznych stropu kopalni wzdłuż pionowej osi przechodzącej przez środek kopalni pracującej w różnych punktach czasowych; skałą macierzystą jest argilit; pierwszy schemat wspomagający: a) parametr Q*; b) parametr P*

formations, which are shown in red, in the rocks and support at various points in time.

Mine working drivage leads to a redistribution of the stress field in the host rock (Fig. 3). Over time, the zone of increased difference of the stress tensor components (Q* parameter) expands around the mine working and the shelter. During one day, the zone, where Q* > 0.4, extends deep into the mine roof by 1.3 m and in 20 days it reaches 4.0 m (Fig. 4a). An increase of Q* parameter values leads to cracks formation with different degrees of intensity. If the values of this parameter decrease, the mine working becomes more stable. Q* parameter takes on large values in the mine roof, in the coal seam near the exposed surface and in the roof of the shelter, above its left wall (Fig. 3). P* parameter values, on the contrary, decrease with time because the near-contour rocks are gradually unloaded from rock pressure (Fig. 4b). On the mine working contour P* parameter values are equal to zero.

Zones of inelastic deformations arise if the ultimate strength of rock is exceeded and its destruction is possible [18]. In this case, we will assume that the mine working is unstable. It can be seen how the zone of inelastic deformations grows with time in the mine roof, composed of argillite, and the mine working loses its stability. In both cases, the weaker coal seam is fractured in the walls of the mine working and the shelter. However, it can be seen that the zone of inelastic deformations does not occur in the mine roof if it is composed of sandstone. Durable sandstone withstands such a load without fracture; the mine roof does not lose stability. The concrete barrier, which is part of the support structure located between the mine working and the shelter, deforms elastically under these conditions and performs its function of supporting the rock arch.

Therefore, in the case when the mine working with the shelter is driven at a shallow depth, in hard rocks, the basic

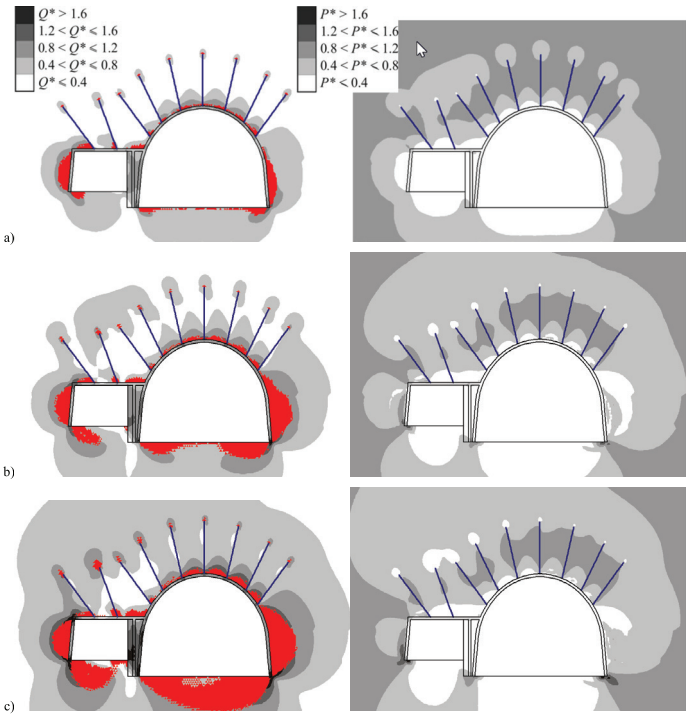

Fig. 5. Inelastic deformation zones (red color) and distributions of Q* parameter values (on the left side) and P* parameter values (on the right side); the 2nd supporting scheme; H = 400 m; host rock is argillite; at the time points: a) t = 1 day; b) t = 3 days; c) t = 20 days

Rys. 5. Strefy odkształceń niesprężystych (kolor czerwony) oraz rozkłady wartości parametrów Q* (po lewej stronie) i wartości parametrów P* (po prawej stronie); drugi program wsparcia; H = 400 m; skałą macierzystą jest argilit; w punktach czasowych: a) t = 1 dzień; b) t = 3 dni; c) t = 20 dni

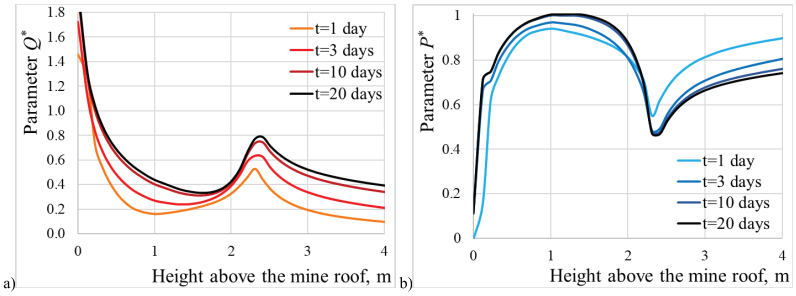

Fig. 6. Changes in the values of geomechanical parameters in the mine roof along the vertical axis passing through the center of the mine working at different points in time; the host rock is argillite; the 2nd supporting scheme: a) Q* parameter; b) P* parame-ter

Rys. 6. Zmiany wartości parametrów geomechanicznych stropu kopalni wzdłuż pionowej osi, przechodzącej przez środek kopalni pracującej w różnych punktach czasowych; skałą macierzystą jest argilit; drugi schemat wspomagający: a) parametr Q*; b) parametr P*

scheme is sufficient for their supporting. If the host rocks are weaker, it is necessary to strengthen the supporting of the mine working and the shelter.

Next, calculations are performed for the following conditions: H = 400 m; host rock is argillite; the 2nd supporting scheme is used. Figure 5 shows the calculation results.

If rock bolts are installed in the roof of the mine working and the shelter, the distribution of Q* parameter values changes. The difference of the stress tensor components is significantly reduced, the area of undisturbed rock zones where Q* < 0.4 increases. Areas where Q* > 0.8 are closely adjacent to the surface of the mine roof. The zone of inelastic deformations in the near-contour rocks of the mine roof practically disappears (Fig. 5, on the left side).

When the free surface is exposed during the mining excavation, the minimum component of the principal stress tensor decreases, which is shown by the P* parameter. An increase of the P* parameter value in a certain area of the rock massif will bring the state of this area closer to equal-component compression, and the probability of its fracture will decrease. Figure 5 (on the right side) shows that the rocks of the floor and walls of the mine working and the shelter are unloaded from rock pressure, here P* < 0.4. While above the working, in the bolted area, a zone was formed, where P* > 0.8.

Let us compare the graphs of geomechanical parameters in the cases of basic supporting and basic supporting with the addition of roof bolting, Fig. 4 and Fig. 6.

The length of the rock bolt is 2.4 m and the depth of its influence in the mine roof corresponds to this value. At a distance of 0–2.4 m, when installing rock bolts, Q* parameter values decrease by an average of 1.8 times, maximum by 3.1 times in the initial period of time at a depth of 1 m from the mine working contour (Fig. 6a). P* parameter values increase by an average of 1.9 times, with a maximum of 4.0 times in the near-contour zone.

Thus, in the bolted area, the rocks are in triaxial compression conditions with increased values of the minimum principal stress component [19]. Consequently, a rockbolts arch

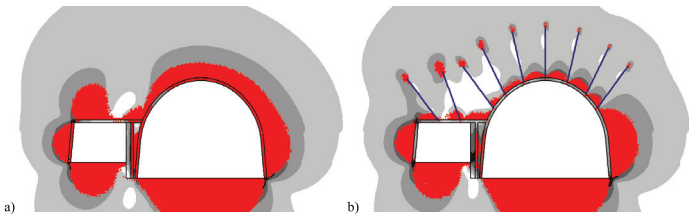

Fig. 7. Inelastic deformation zones (red color) and distributions of Q* parameter values; H = 800 m; host rock is argillite; t = 20 days: a) the 1st supporting scheme; b) the 2nd supporting scheme

Rys. 7. Strefy odkształceń niesprężystych (kolor czerwony) i rozkłady wartości parametrów Q*; H = 800 m; skałą macierzystą jest argilit; t = 20 dni: a) pierwszy schemat wsparcia; b) drugi schemat wsparcia

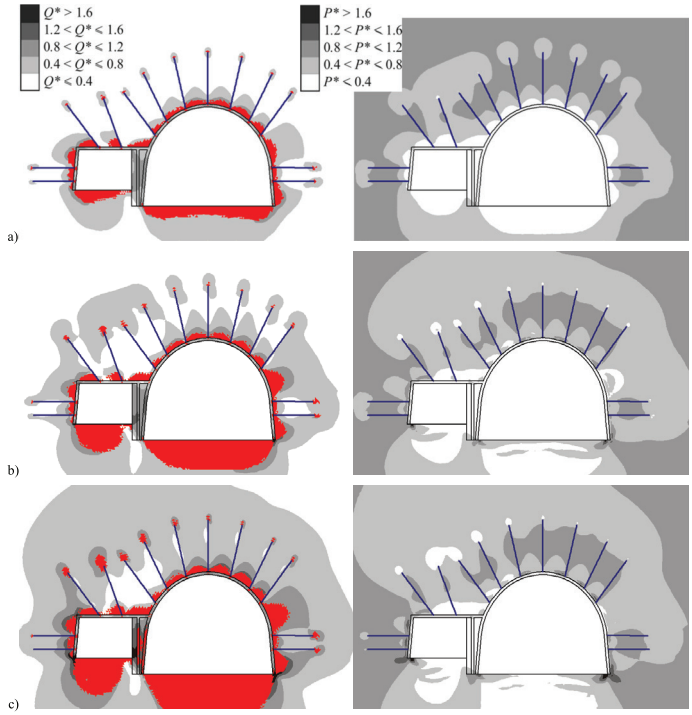

Fig. 8. Inelastic deformation zones (red color) and distributions of Q* parameter values (on the left side) and P* parameter values (on the right side); the 3rd supporting scheme; H = 800 m; host rock is argillite; at the time points: a) t = 1 day; b) t = 3 days; c) t = 20 days

Rys. 8. Strefy odkształceń niesprężystych (kolor czerwony) oraz rozkłady wartości parametrów Q* (po lewej stronie) i P* (po prawej stronie); trzeci program wspierający; wys. = 800 m; skałą macierzystą jest argilit; w punktach czasowych: a) t = 1 dzień; b) t = 3 dni; c) t = 20 dni

is formed above the mine working and the shelter, where the rocks are preserved in a natural, undisturbed state, and the rock bolts effectively interact with each other, preventing the displacement of the near-contour rocks into the mine working and increasing its stability [20].

With an increase in the depth of mining operations from 400 m to 800 m, the initial stress state of the rocks deteriorates and the mine working stability decreases, Fig. 7. It can be seen that distributions of the Q* parameter values for the same conditions at a depth of 400 m (Fig. 5c) and 800 m (Fig. 7b) are the same, since the Q* parameter is a relative value and does not depend on the depth H.

The area of the inelastic deformation zone increases by 68% around the mine working with basic supporting scheme and by 58% around the mine working with supporting according to the 2nd scheme. With increasing depth, the support structure located between the mine working and the shelter begins to experience limiting stresses. However, the durable reinforced concrete barrier, which is the main element of this structure, withstands high stresses and does not fracture. With the transition to a greater depth, the load on the anchor lining also increases. With increasing depth, the load on the roof bolting also increases. For the rock-bolts arch formed in the mine roof, supports are required in the walls of the mine working and the shelter. For this purpose, in the 3rd supporting scheme, it is provided to install side rock bolts in the coal seam.

Fig. 8 shows that with the installation of side rock bolts, the zone of inelastic deformations in the coal seam is significantly reduced; Q* parameter values decrease; P* parameter values in the bolted area in the walls of the mine working and the shelter increase to a value characterizing undisturbed rocks not unloaded from rock pressure. The coal seam is not fractured in the near-contour zone when using the 3rd supporting scheme. Thus, rockbolts supports for the rock-bolts arch, which is located in the mine roof, are formed in the walls of the mine working and the shelter.

It is possible to evaluate the change in the zone of inelastic deformations and the zone unloaded from rock pressure, the growth of which negatively affects the stability of mine workings, using the graphs shown in Fig. 9.

The inelastic deformation zone increases in size with time (Fig. 9a) and its growth is much slower if the 2nd or 3rd sup-

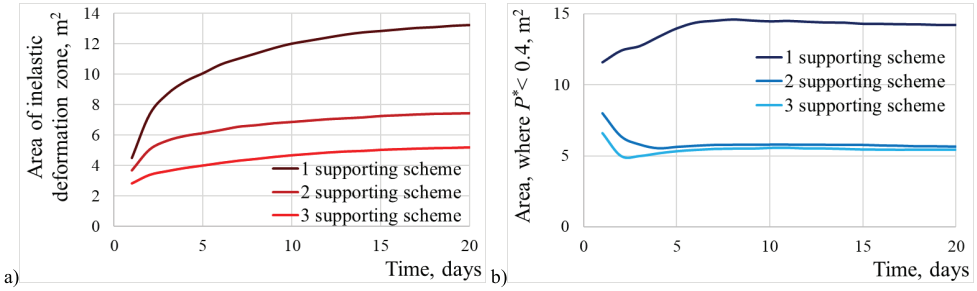

Fig. 9. Time change of the area of: a) the zone of inelastic deformations; b) the zone where P* < 0.4 in the roof and walls of the mine working and shelter, depending on the applied supporting scheme; the host rock is argillite; H = 800 m

Rys. 9. Zmiana czasowa obszaru: a) strefy odkształceń niesprężystych; b) strefa, w której P* < 0,4 w stropie i ścianach wyrobiska i schronu w zależności od zastosowanego systemu wsparcia; skałą macierzystą jest argilit; H = 800 m

porting scheme is used [21, 22]. Installation of rockbolts in the roof and walls of the mine working and the shelter reduces the area of the non-elastic deformation zone by 2.5 times.

The zone unloaded from rock pressure in the roof and walls practically does not change in size starting from the 6th day after the installation of the supporting, Fig. 9b. If the 3rd supporting scheme is applied, then the area of the zone where P* < 0.4 is reduced by 2.6 times.

5. Conclusions

Numerical simulation of the stress state of a coal-rock massif with a mine working and a shelter was performed; their stability was studied in various mining and geological conditions and with various supporting schemes.

It is shown that, over time, near-contour rocks are unloaded from rock pressure, and an area of increased difference of the stress tensor components expands around the mine working and the shelter. This leads to cracks formation with different degrees of intensity. When the mine working with the shelter is driven at a shallow depth in hard rocks, the basic scheme, which consists mainly of metal frames and a reinforced concrete barrier, is sufficient for their supporting. If the host rocks are weaker, the stability of the mine working and the shelter is broken and it is necessary to strengthen their supporting with rock bolts. In the bolted area, the rocks are in triaxial compression conditions, a rock-bolts arch is formed above the mine working and the shelter, which prevents the displacement of the roof rocks into the mine working and increases its stability.

With an increase in the depth of mining operations, the stability of the mine working decreases; the inelastic deformation zone in the mine walls grows; the load on the support increases. For the rock-bolts arch formed in the mine roof, supports are required in the walls of the mine working and the shelter. For this purpose, side rock bolts are installed. The use of an appropriate supporting scheme leads to a decrease in the area of the inelastic deformation zone by 2.5 times and the area of the zone unloaded from rock pressure by 2.6 times.

Thus, such schemes for supporting the mine working and the shelter are selected, which ensure their stability in the considered mining and geological conditions.

Literatura – References

1. Mineev, S.P., Belikov, I.B., Mogilchenko, A.N., Chekmezov, V.M., Sergeev, Y.N., 2019. Ground of parameters of res-cue chamber for underground workers in the Dobropolskaya mine. Geo-Technical Mechanics, 149. 150–159 (in Rus-sian). https://doi.org/10.15407/geotm2019.149.150.
2. Minieiev, S.P., Belikov, I.B., 2019. Methodology for estimating the parameters of the deposition of the rescue camera in coal mine. Geo-Technical Mechanics, 144, 126–136 (in Russian). https://doi.org/10.15407/geotm2019.144.126.
3. Ministry of Coal Industry of Ukraine, 2004. System of self-defense of miners. General requirements. JUU 10.1.00174102-002-2004 (in Ukrainian).
4. Ministry of Coal Industry of Ukraine, 2007. Stationary rescue mines shelters. General technical requirements. JUU 10.1.202020852.002:2006 (in Ukrainian).
5. Shen, B., 2014. Coal Mine Roadway Stability in Soft Rock: A Case Study. Rock Mechanics and Rock Engineering, 47, 2225–2238, https://doi.org/10.1007/s00603-013-0528-y.
6. Tan, X., Chen, W.Z., Liu, H.Y., Andrew, H.C., Tian, H.M., Meng, X.J., Wang, F.Q., Deng, X.L., 2017. A combined supporting system based on foamed concrete and U-shaped steel for underground coal mine roadways undergoing large deformations. Tunnelling and Underground Space Technology, 68, 196–210. https://doi.org/10.1016/j.tust.2017.05.023.
7. Krukovskyi, O.P., 2011. Modelling changes of stress-strain state of solid edge during the distance of working face of mine workings. Problems of computational mechanics and strength of structures, 17, 175–181 (in Russian).
8. Krukovskyi, O., Krukovska, V., Vynohradov, Y., Dyomin, V., 2021. Application of roof bolting to reduce water inflow into mine workings during the crossing of tectonic faults. E3S Web of Conferences 280, 01006. https://doi.org/10.1051/e3sconf/202128001006.
9. Zienkiewicz, O.C., Taylor, R.L., Zhu, J.Z., 2013. The Finite Element Method: Its Basis and Fundamentals, Butterworth-Heinemann.
10. de Borst, R., Crisfield, M.A., Remmers, J.J.C., Verhoosel, C.V., 2012. Non-linear finite element analysis of solids and structures, John Wiley & Sons.
11. Tan, C.H., 2016. Difference solution of passive bolts reinforcement around a circular opening in elastoplastic rock mass. International Journal of Rock Mechanics and Mining Sciences, 81, 28–38. https://doi.org/10.1016/j.ijrmms.2015.11.001.
12. Labuz, J.F., Zang, A., 2012. Mohr-Coulomb Failure Criterion. Rock Mechanics and Rock Engineering, 45, 975–979. https://doi.org/10.1007/s00603-012-0281-7.
13. Wang, H.-C., Zhao, W.-H., Sun, D.-S., Guo, B.-B., 2012. Mohr-Coulomb yield criterion in rock plastic mechanics. Chi-nese Journal of Geophysics, 55, 733–741. https://doi.org/10.1002/cjg2.1767.
14. Ho, D.-A., Bost, M., Rajot, J.-P., 2019. Numerical study of the bolt-grout interface for fully grouted rockbolt under different confining conditions. International Journal of Rock Mechanics and Mining Sciences, 119, 168–179. https://doi.org/10.1016/j.ijrmms.2019.04.017.
15. Krykovskyi, O., Krykovska, V., Skipochka, S., 2021. Interaction of Rock-Bolt Supports While Weak Rock Reinforcing by Means of Injection Rock Bolts. Mining of Mineral Deposits, 15, 8–14. https://doi.org/10.33271/mining15.04.008.
16. Chen, J., Li, D., 2022. Numerical simulation of fully encapsulated rock bolts with a tri-linear constitutive relation. Tunnel-ling and Underground Space Technology, 120, 104265. https://doi.org/10.1016/j.tust.2021.104265.
17. Krukovskyi, O., Krukovska, V., 2019. Numerical simulation of the stress state of the layered gas-bearing rocks in the bottom of mine working. E3S Web of Conferences 109, 00043. https://doi.org/10.1051/e3sconf/201910900043.
18. Moussaei, N., Sharifzadeh, M., Sahriar, K., Khosravi, M.H., 2019. A new classification of failure mechanisms at tunnels in stratified rock masses through physical and numerical modeling. Tunnelling and Underground Space Technology, 91, 103017. https://doi.org/10.1016/j.tust.2019.103017.
19. Li, C.C., 2017. Numerical study of the bolt-grout interface for fully grouted rockbolt under different confining conditions. Journal of Rock Mechanics and Geotechnical Engineering, 9, 396–414. https://doi.org/10.1016/j.jrmge.2017.04.002.
20. Tran, T.M., Do, N.T., Dang, T.T., Nguyen, D.P., Vo, T.H., 2021. Stabilization of Deep Roadways in Weak Rocks Using the System of Two-level Rock Bolts. Inżynieria Mineralna, 2, 157–166. https://doi.org/10.29227/IM-2021-02-13.
21. Skipochka, S., Krukovskyi, O., Serhiienko, S., Krasovskyi, I., 2019. Non-destructive testing of rock bolt fastening as an element of monitoring the state of mine workings. Mining of Mineral Deposits, 13(1), 16–23. https://doi.org/10.33271/mining13.01.016.
22. Małkowski, P., Niedbalski, Z., Bednarek, Ł., 2021. Automatic Monitoring System Designed for Controlling the Stability of Underground Excavation. Inżynieria Mineralna, 2, 15–29. https://doi.org/10.29227/IM-2021-02-02.

Wspomaganie kopalni pracującej ze schronem w różnych warunkach górniczych i geologicznych

Schrony służą do ochrony górników przed narażeniem na szkodliwe gazy oraz do pracy ratowników. Schrony takie budowane są w niszy przylegającej do wyrobiska kopalnianego. Celem pracy jest numeryczne badanie stanu naprężeń masywu węglowo-skalnego z wyrobiskiem i osłoną, jego stateczności w różnych warunkach górniczo-geologicznych i przy różnych układach obudowy.

Wykonano symulację numeryczną stanu naprężeń masywu węglowo-skalnego z wyrobiskiem i schronem. Badano ich stabilność w różnych warunkach górniczych i geologicznych oraz przy różnych schematach podparcia. Pokazano, że w miarę upływu czasu skały przykonturowe odciążają się od naporu skał, a wokół wyrobiska i schronu rozszerza się obszar zwiększonej różnicy składowych tensora naprężeń. Prowadzi to do powstawania pęknięć o różnym stopniu intensywności. Gdy kopalnia współpracująca ze schronem jest prowadzona na płytkiej głębokości w twardych skałach, do ich podparcia wystarcza podstawowy schemat, składający się głównie z metalowych ram i bariery żelbetowej. Jeżeli skały macierzyste są słabsze, stabilność wyrobiska kopalnianego i osłony jest zerwana i konieczne jest wzmocnienie ich podparcia kotwami skalnymi. W rejonie kotwionym skały znajdują się w stanie trójosiowego ściskania, nad wyrobiskiem i schronem tworzy się łuk kotwowy, co zapobiega przemieszczaniu się skał stropowych do wyrobiska i zwiększa jego stateczność. Wraz ze wzrostem głębokości eksploatacji zmniejsza się stabilność wyrobiska górniczego, powiększa się strefa odkształceń niesprężystych w ścianach kopalni, obciążenie podpory wzrasta. Dla łuku kotwiowego formowanego w stropie kopalni wymagane są podpory w ścianach wyrobiska i schronu. W tym celu montowane są boczne kotwy skalne. Zastosowanie odpowiedniego schematu podparcia prowadzi do 2,5-krotnego zmniejszenia powierzchni strefy odkształceń niesprężystych oraz 2,6-krotnej powierzchni strefy odciążonej od parcia skał. W związku z tym dobierane są takie schematy obudowy wyrobiska i osłony, które zapewniają ich stabilność w rozważanych warunkach górniczo-geologicznych.

Słowa kluczowe: *stateczność wyrobisk górniczych, bezpieczeństwo górnicze, symulacje numeryczne, deformacje skał, osłony, obudowy wyrobisk górniczych*

Management of the Parameters of the Explosive Impact on the Soil Mass Due to the Use of Low-Density Explosives

Natalya REMEZ[1)], Alina DYCHKO[2)], Oksana VOVK[3)], Tamara KHLEVNIUK[4)], Denys KHLEVNIUK[5)]

[1)] DSc, Eng., Prof., Institute of Energy Saving and Energy Management, National Technical University of Ukraine "Igor Sikorsky Kyiv Polytechnic Institute", Peremohy Ave. 37, 03056 Kyiv, Ukraine; ORCID https://orcid.org/0000-0002-8646-6527; email: nataly.remez@gmail.com
[2)] DSc, Eng., Prof., Institute of Energy Saving and Energy Management, National Technical University of Ukraine "Igor Sikorsky Kyiv Polytechnic Institute", Peremohy Ave. 37, 03056 Kyiv, Ukraine; ORCID https://orcid.org/0000-0003-4632-3203; email: aodi@ukr.net
[3)] DSc, PhD, Eng., Prof., Had of the Dep.; Institute of Energy Saving and Energy Management, National Technical University of Ukraine "Igor Sikorsky Kyiv Polytechnic Institute", Peremohy Ave. 37, 03056 Kyiv, Ukraine; 0000-0002-7531-9847; email: oksanavovk@ gmail.com
[4)] Senior Researcher, Institute of Hydromechanics of the National Academy of Sciences of Ukraine, Marii Kapnist st. 8/4, 03057 Kyiv, Ukraine; ORCID https://orcid.org/0009-0007-8825-568X; email: levnyk@ukr.net
[5)] PhD, Researcher, Institute of Hydromechanics of the National Academy of Sciences of Ukraine, Marii Kapnist st. 8/4, 03057 Kyiv, Ukraine; ORCID https://orcid.org/0009-0001-1754-3170; email: levnyk@ukr.net

http://doi.org/10.29227/IM-2023-01-06

Submission date: 16-01-2023 | Review date: 22-02-2023

Abstract

On the basis of numerical calculations of the problem of the explosion of cylindrical charges of explosive substances in soils, the dependences of maximum pressure, maximum and residual deformations for various types of explosive substances on time and distance are obtained. It is established that the lowest peak pressure with the longest duration of the explosive pulse is observed for charges based on foamed types of explosives, both conventional and treated with ultrasonic radiation. The maximum pressure of these types of explosives is 20–49% less, and the duration of the explosive impulse is in 3–3.5 times longer than compared to the standard low-density explosive – igdanite. The low value of the peak detonation pressure, achieved by reducing the density of explosives, reduces the volume concentration of the energy of the charges, which, in turn, increases the efficiency of the explosive transformation energy in the far zone. The growth time of the explosive impulse of charges based on foamed explosives, both conventional and treated with ultrasonic radiation, is in 2.47 times greater than for igdanite. It is found that in the near zone during the explosion of an igdanite charge, significantly higher values of hydrostatic pressure and maximum volumetric deformation are achieved than in the case of a foamed explosive explosion, which is a consequence of higher detonation characteristics of igdanite: density, pressure at the Jouget point, detonation rate. The time to reach the maximum pressure and deformation during an igdanite explosion is much shorter, because the detonation rate of igdanite is higher than that of foamed explosives. The parameters of shock waves during explosions of charges of new mixed explosives in the middle zone can be compared with the same parameters from traditional industrial explosives, such as igdanite, and in the far zone of the explosion, they exceed them. The difference in the maximum volumetric deformations in igdanite explosions is 7–15% compared to the explosions of foamed explosive and foamed explosive treated with ultrasound, respectively. When detonating a sonicated foamed explosive, the residual deformation is 9–10% greater than when detonating a non-sonicated foamed explosive charge.

Keywords: *mixed explosives, subsidence soils, mathematical simulation*

1. Introduction

The main methods of management of the parameters of the explosive impulse are to control the contact impact of explosive charges on the surrounding array, the order of detonation of the charges. The nature of such influence is defined by: a) properties of explosives materials, chemical composition, concentration; b) density, dispersion and geometric parameters of the charge; c) nature of initiation; d) other structural features of the charge; e) mechanical properties of the array in the contact zone; e) the order of detonation.

The variety of practical applications of explosives, explosive structures and properties of massifs disturbed by an explosion objectively create prerequisites for the most rational use of explosion energy for various purposes in construction and mining in general under certain conditions.

One of the unsolved problems is the stabilization of detonation in non-cartridge charges of considerable length. There is a number of reasons for non-stationary explosive disturbance and attenuation of the detonation process, among which the most significant are: a) non-uniformity of the components of explosive substances and the properties of heterogeneous (multiphase) mediums; b) discharge action of the charge boundary; c) non-water resistance (soaking), due to the hydrophobicity of the main component, saltpeter; e) changing the parameters of the explosive transformation at the contact of different explosive substances.

There are other problems associated with the action of the explosion in the external environment. If a full explosive decomposition of the charge occurs, then the necessary amplitude of the explosive pulse, emitted into the medium, is at

Tab. 1. The main physical and mechanical characteristics of loess soil

Tab. 1. Główne właściwości fizyczne i mechaniczne gleby lessowej

№	Soil density	Natural moisture	Density of the soil skeleton	Moisture at the yield point	Moisture on the verge of rolling	Plasticity number	Flow rate	Density of mineral particles	Porosity coefficient
	ρ_0,g/sm^3	W_e,p. units	ρ_d g/sm^3	W_l, p. units	W_p, p. units	I_p	I_l	ρ_s g/sm^3	e
1	1,55	0,137	1,36	0,24	0,20	0,04	≤0	2,63	0,934
2	1,77	0,143	1,55	0,26	0,22	0,04	≤ 0	2,68	0,729

Tab. 2. The component composition of low-density explosives and igdanite [2]

Tab. 2. Skład materiałów wybuchowych małej gęstości i igdanitu [2]

№	Explosives component	Igdanite	Low-density explosives
1	Ammonium nitrate	94,5	90
2	Diesel fuel	5,5	–
3	Sulfonal - powder	–	6
4	Aluminum powder	–	4

a distance of up to 10 radii of the charge or more. At the same time, the sharp nature of the pulse leads to an extremely fast dissipation of the wave energy, while the impact of the charge in space is rather uneven. This is characteristic of most industrial explosives with a stationary detonation rate of more than 3.5–4 km/s.

Therefore, the urgent problem is to change the parameters of the pulse to reduce unnecessary energy losses in the explosive zone as much as possible and increasing the radius of propagation by the action of one charge.

No less important is the problem of the optimal location of the wells in the massif, which allows choosing the deceleration parameters that provide the necessary blasting mode to achieve the maximum effect of using the energy of the explosion.

In addition, an important factor under the conditions of real soil massifs is the heterogeneity of their geological structure and physical and mechanical characteristics. This heterogeneity is especially evident in the upper layers of soil sediments, where the original layered structure of the massif, related to its geological origin, is often observed. However, if the object of engineering activity is a loess subsidence massif, its composition is more uniform in depth with a uniform increase in density or a decrease in porosity in the natural setting. The situation changes in connection with the application of any technology of compaction of such an array. It involves pre-soaking it to destroy sufficiently strong natural bonds between blocks and aggregates composed of grant particles and interconnected by salt films that can dissolve under the influence of excessive moisture. Since this moisture is practically incompressible, it is forced to move relative to the soil skeleton under the action of stresses on and outside the force front. The rate of movement of soil particles and moisture is directly proportional to the rate of first shock and then blast waves. In turn, the rate of the shock wave is directly proportional to the rate of the detonation front in the charge, that is, to the energy of the explosive substance in the charge. Thus, the known inertia of the medium in the dynamic process of the development of deformations is strengthened due to the mutual movement of the components that makes up the soil, since the influence of the viscous component on the process of the development of volumetric deformations increases.

2. Mathematical simulation of the explosive impact on the soil mass with the use of low-density explosives

It is known from soil dynamics [1] that an inertial multicomponent soil medium with relatively weak structural connections requires a slower increase and decrease of the load during the passage of the stress wave for the full development of the deformation process in the dynamic mode. This places appropriate requirements on the parameters of the explosive impulse, which provides a sufficient load that lasts longer in time. The problem can be solved only by using explosives with the lowest possible detonation rate.

The solution to this issue can be implemented in the following ways:

1. Improvement of the chemical composition of explosives. Since almost all the main components of low-explosive explosives are currently known, the improvement of the component composition, depending on the specific goals, is carried out by introducing hydrophobic, catalytic, inert, quasi-inert (low-calorie) and other additives.

2. Treatment of the structure of explosives or the main component (saltpeter) in order to increase chemical activity, which is complicated by the small area of chemical contact in coarsely dispersed explosives. The aim is to increase the surface area and partial ionization. It can be achieved due to mechanical (including ultrasonic) processing, by irradiation with electromagnetic waves and charged particles.

At the current stage of development of means of mechanization of charging works, two ways of improving the characteristics of the pulse are of practical interest, namely: using thin outer shells made of inert material; with the use of intermediate fighters in long wells, which well perceive the impulse from the main weak explosives.

Tab. 3. Dynamic characteristics of mixed explosives [2]

Tab. 3. Charakterystyki dynamiczne mieszanek wybuchowych [2]

№	Characteristics	Unit of measurement	Explosive		
			Igdanite	Foam explosive	Ultrasonically processed foamed explosive
1	Density of explosives, ρ_0	g/sm^3	0,85	0,6	0,5
2	Detonation rate: *D*, open charge	10^3m/s	3450	1500	1500
3	Heat of explosion *Q*	kcal/kg	870	1500	1500
2	Brisance of explosives	10^{-3}m	15-20	9-11	9-11
4	Time of pressure rise in the pulse	10^{-6}s	30	43	48
5	Pressure on the wave front	10^9Pa	2,0	0.95	0,85
6	Rate of pressure increase	10^{14}Pa/s	0,5-0,8	0.22	0,18
7	Polytropy index, *N*		4.41	2.24	2.12
8	Isentrope indicator, γ		0,264	0,235	0,212

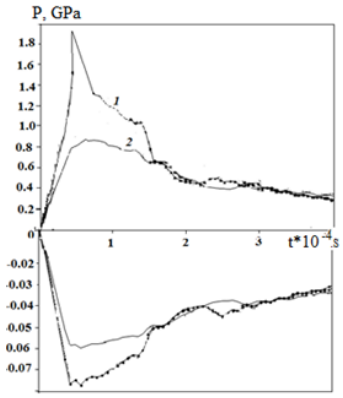

Fig. 1. Dependencies of average hydrostatic pressure and volume deformation of loess soil on time at the boundary with the explosive cavity during the explosion: 1 – igdanite, 2 – foamed explosives; 3 – foamed explosives, processed by ultrasound

Rys. 1. Zależności średniego ciśnienia hydrostatycznego i deformacji objętości gleby lessowej na granicy z wnęką wybuchową w czasie wybuchu: 1 – igdanit, 2 – spienione materiały wybuchowe; 3 – spienione materiały wybuchowe przetwarzane ultradźwiękami

In solving other problems, the determining factor is the mechanical properties of the surrounding mass: impedance, compressive strength, dilatancy, conditions of fragility, anisotropy, and heterogeneity.

In order to control the explosive impulse process, it is necessary to establish the following interrelationships: charging parameters, properties of the soil mass in the contact zone, and the initial parameters of the explosive impulse acting on the medium; mechanical properties of the array and wave parameters in the external medium; parameters of the external load on the soil massif.

On the basis of numerical experiments and theoretical research conducted in the last decade, it is established that in a number of typical conditions of detonation of explosive charges, the flow regime of the explosive transformation reaction is close to stationary, that is, the rate of propagation of the shock wave is close to constant.

The simplest quasi-stationary mode of detonation of a cylindrical charge is detonation with axial initiation, which generates a cylindrical wave.

An increase in the volume concentration of the energy charge due to an increase in the density of explosives leads to an increase in the peak pressure of detonation, which in some cases reduces the efficiency of the energy of the explosive transformation due to a greater loss in the near zone of the explosion.

At research of the parameters of the explosive impulse for compaction of the territory of subsidence soils due to surface or horizontal cylindrical charges of explosives the limitation of explosive action of charges of explosives is required. This can be achieved by using low-density foamed explosive mixtures [2–3].

The analysis of previous studies when solving the problem of finding the radius zone of the base sealing around the well [4–6] with low-density foamed compositions demonstrates that it is necessary to determine the pressure at their contact "detonation products – medium". Based on numerous experimental data, the researchers believe that the efficiency of compaction of subsiding foundations when using an explosion is defined not only by the maximum pressure at the front of the detonation wave, but also by the duration of the explosive pulse. This occurs in the increase of the general form of the explosion at large distances from the charge, and, accordingly, in the improvement of the compaction of the grounded array at a considerable distance.

In this regard, it is necessary to study the relationship between the effectiveness of explosives (igdanite) and the foamed explosive composition, both conventionally and after treatment with ultrasonic irradiation, for the compaction of subsiding water-saturated soils with the maximum pressure, duration and shape of the explosive impulse that occurs at the boundary "products of detonation – medium".

Let's perform a numerical simulation of the camouflage effect of explosions of cylindrical charges of standard and new mixed explosives. Let a cylindrical explosive charge of infinite length and radius is placed in the soil space at a distance from the surface . Let the charge detonates instantly and the same average pressure is established throughout its volume , and the density of the explosion products is equal to the initial density of the explosive substance. The movement of soil explosion products is described by the laws of conservation of momentum, mass and internal energy, which for the explosion of a cylindrical charge have the form [7–8]:

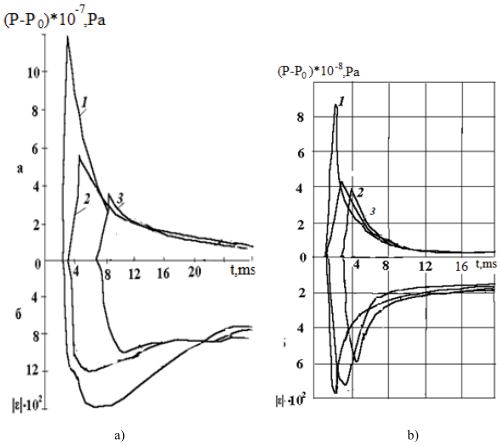

Fig. 2. Dependences of the average hydrostatic pressure (a) and volumetric deformation (b) of the medium on time in loam No. 1 and No. 2 at a relative distance r =5,5 r₀ at explosions of charges of various explosive substances: 1 – igdanite, 2 – foamed explosive; 3 – foamed explosive processed by ultrasound

Rys. 2. Zależności średniego ciśnienia hydrostatycznego (a) i odkształcenia objętościowego (b) w czasie w ośrodku ilastym nr 1 i nr 2 przy względnej odległości r =5,5 r₀ przy wybuchach ładunków różnych substancji wybuchowych: 1 – igdanit, 2 – spieniony materiał wybuchowy; 3 – spieniony materiał wybuchowy przetwarzany ultradźwiękami

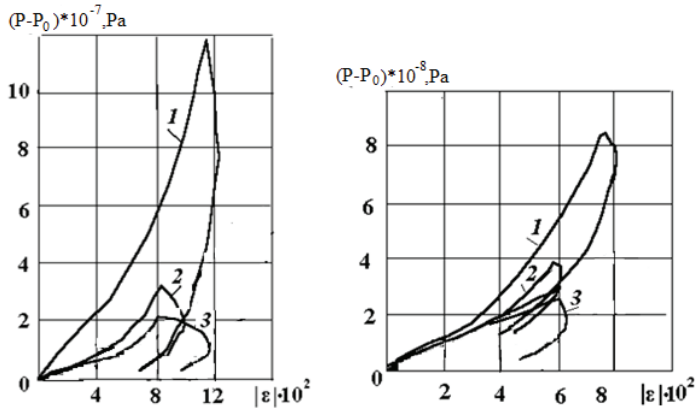

Fig. 3. Compression diagrams at loading and unloading in loam No. 1 and No. 2 at a relative distance r =5,5 r0 at explosions of charges of various explosive substances: 1 – igdanite, 2 – foamed explosive; 3 – foamed explosive processed by ultrasound

Rys. 3. Wykresy ściskania przy załadunku i rozładunku w iłach nr 1 i nr 2 na odległość względną r = 5,5 r0 przy wybuchach ładunków różnych substancji wybuchowych: 1 – igdanit, 2 – spieniony materiał wybuchowy; 3 – spieniony materiał wybuchowy przetwarzany ultradźwiękami

$$\frac{\partial \sigma_{rr}}{\partial z}+\frac{\partial \tau_{rz}}{\partial r}+\frac{\tau_{rz}}{r}=\rho\ \frac{du}{dt}, \tag{1}$$

$$\frac{\partial \tau_{rz}}{\partial z}+\frac{\partial \sigma_{zz}}{\partial r}+\frac{\sigma_{zz}-\sigma_{\theta\theta}}{r}=\rho\ \frac{dw}{dt}, \tag{2}$$

$$\frac{1}{V}\frac{dV}{dt}=\frac{\partial u}{\partial z}+\frac{\partial w}{\partial r}+\frac{w}{r},\ V=\frac{\rho_0}{\rho}, \tag{3}$$

$$u=\frac{dz}{dt},\ w=\frac{dr}{dt}, \tag{4}$$

$$\sigma_{zz}=S_{zz}-P,\ \sigma_{rr}=S_{rr}-P,\quad \sigma_{rr}=S_{rr}-P, \tag{5}$$

$$P=\frac{1}{3}\left(\sigma_{rr}+\sigma_{\theta\theta}+\sigma_{zz}\right), \tag{6}$$

Where ρ₀, ρ – initial and current density; u, w – rate tensor components; t – time; P –average hydrostatic pressure; r, θ, z – cylindrical coordinates; σ_i, S_i,(rr, θθ, zz) – tensor and deviator components of the stress tensor; $\overline{V}$ = V/V₀, V, V₀ – relative, current and initial specific volumes. For detonation products S_i=0. The relations are performed for the components of the strain rate tensor:

$$\dot{\varepsilon}_r=\frac{\partial U}{\partial r},\qquad \dot{\varepsilon}_\theta=\frac{U}{r},\qquad \dot{\varepsilon}_z=0. \tag{7}$$

The expansion of the explosion products occurs according to the binomial is entropy, i.e

$$P=A\rho^{n_0}+B\rho^{\gamma_0+1} \tag{8}$$

The constant values A, B, n₀, γ₀in ratio (8) are calculated unambiguously based on the known characteristics of explosives [9].

The soil is simulated as a solid porous multicomponent medium with a variable coefficient of bulk viscosity η(ε) . The equations of loading and unloading of this medium have the form [10]:

$$\varepsilon=\varphi(P,\varepsilon)\dot{P}-\frac{\alpha_1\lambda(P,\varepsilon)}{\eta(P,\varepsilon)}\psi(P,\varepsilon). \tag{9}$$

The functions included in equation (9) for loading and unloading are determined according to [12], where ε – volumetric deformation.

The condition of soil plasticity is the Mises-Botkin condition.

The initial conditions for this task are:

$$U=0,P=P_{cp},\ \rho=\rho_{BP}\ \text{at}\ 0\le r\le r_0,$$

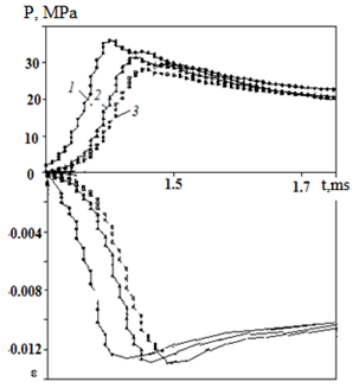

Fig. 4. Dependences of the average hydrostatic pressure (a) and volume deformation (b) on time in loam No.1 at a relative distance = 25.3: 1 – igdanite, 2 – foamed explosives; 3 – foamed explosive processed by ultrasound

Rys. 4. Zależności średniego ciśnienia hydrostatycznego (a) i odkształcenia objętościowego (b) od czasu w glinie nr 1 w odległości względnej = 25,3: 1 – igdanit, 2 – spienione materiały wybuchowe; 3 – spieniony materiał wybuchowy przetwarzany ultradźwiękami

$$P = \sigma_r = \sigma_\theta = \sigma_z = 0, \quad \rho = \rho_0 \text{ at } r > r_0 \tag{10}$$

where ρ_{BP}– initial density of the explosive.

The limiting conditions are:

1) the condition of continuity of rate and stresses at the boundary between the explosion product and the soil;

2) the condition of "no flow", i.e., the rate on the axis of the charge is zero.

To approximate the system of differential equations (1)–(10), the finite difference method applying the finite difference scheme of the "cross" type [10, 11] of the second order accuracy in spatial and temporal coordinates is used. A moving grid that automatically expands as the shock wave propagates is used at the solution. As an additional term to the average hydrostatic pressure in the differential equation of motion, a linear-quadratic artificial viscosity qis introduced, which allows conducting through-flow calculations, both on smooth and discontinuous flows.

Calculations are made for loess loams with the following physical and mechanical characteristics (Table 1).

Angle of internal friction (φ, degrees) – 19, specific adhesion (c, MPa) – 0.043, modulus of deformation (E, MPa) – 6.48 in the natural state and 2.41 in the water-saturated state, Poisson's ratio (μ) – 0,35.

An explosion of a charge with a radius r0= 0,09m is considered.

The component composition of low-density explosives and igdaniteis presented in Table 2, and their dynamic characteristics are in Table 3 (calculated according to the method [2–3].

Figure 1 presents the dependences of the average hydrostatic pressure and volumetric deformation of loam at the boundary with an explosive cavity during the explosion of igdanite (1) and foamed explosive (2).

It is demonstrated at the figure that at the border with the cavity during the explosion of the igdanite charge, significantly higher values of hydrostatic pressure and maximum volume deformation are achieved than during the explosion of the foamed explosives. It can be explained by the higher detonation characteristics of igdanite: density, pressure at the Juguet point. The time to reach the maximum pressure and deformation during an igdanite explosion is much shorter, because the detonation rate of igdanite is higher than that of foamed explosives.

Figure 2 demonstrates the dependences of the average hydrostatic pressure (a) and volume strain (b) in loams No. 1 and No. 2 at a relative distance r =5,5 r_0.

Analysis of these figures demonstrates that the nature of the dependence of pressure and maximum volumetric strain at the corresponding distance from time is the same as at the boundary with the explosive cavity: the greater the values of the detonation characteristics of explosives, the higher the values of pressure and volumetric strain.

From the comparison of the dependences for soils No. 1 and No. 2, it can be concluded that at the same distance from the explosive cavity in the first loam, lower pressures are achieved, but larger volume deformations. It is explained by the fact that the first soil has a lower density and higher volumetric porosity, therefore it is more contactable, and this in turn leads to larger deformations even at lower values of hydrostatic pressure. An increase in the porosity of the soil mass leads to a faster transformation of the shock wave into a continuous compression wave.

The same regularities are presented in Figure 3, which demonstrates compression diagrams during loading and unloading in loams No. 1 and No. 2. The explosion of the igdanite charge achieves significantly higher values of hydrostatic pressure and maximum volumetric strain than the explosion of foamed explosive and foamed explosive processed by ultrasound.

However it should be noted that the largest residual deformation is achieved in the case of explosions of foamed explosives compared to the explosion of igdanite. In addition, in the case of the explosion of the foamed explosive processed by ultrasound, the residual deformation is 9–10% greater than in the case of the explosion of the charge of the foamed explosives, not processed by ultrasound. This is due to the fact that the time of rise and fall of the pressure pulse of foamed explosives is on 13...18 mks longer than that of igdanite, which leads to a more complete transfer of energy from the explosion products to the soil.

Figure 4 shows the dependence of the average hydrostatic pressure and volume strain on time in loam No. 1 at a relative distance of 25.3. From the analysis of the figure, it is demonstrated that with distance from the center of the explosion,

the difference in pressure maxima decreases and amounts to 16...21%, and the difference in initial pressures is 110...120%. This is because although igdanite has a higher density and initial pressure, foamed explosives have a higher heat of explosion.

In addition, the index of polytropy in igdanite is also higher, and this leads to a faster attenuation of the shock wave.

It can be noted that at this distance, not only the residual, but also the maximum volumetric deformations are greater in the case of foamed explosive explosions than in the case of an igdanite explosion. The difference in the maximum volume deformations during explosions of igdanite is 7...15% compared to explosions of ultrasonically foamed and ultrasonically processed, respectively.

It is interesting to note the result obtained by numerical calculations, which consists in the fact that at distances greater than 40, the greatest pressure and volume deformations are achieved during explosions of foamed explosives.

This allows us to make a conclusion about the advantages of using foamed explosives for the compaction of subsiding soils in comparison with traditional ones, because when they are used, thanks to a more complete transfer of the energy of the explosion to the soil mass, more uniform deformations are achieved over the entire interval from the source of the explosion to significant distances from it.

3. Conclusion

1. An inertial multicomponent soil medium with relatively weak structural connections requires a slower increase and decrease of the load during the passage of the stress wave for the full development of the deformation process in the dynamic mode. This leads to the appropriate requirements to the parameters of the explosive impulse, which provides a sufficient load that lasts longer in time. The greatest efficiency in the compaction of subsiding soils can be achieved when using a foamed explosive due to the action of the explosion at a considerable distance from the charge, and accordingly, uniform and better compaction to the required depth.

2. A mathematical formulation of the problem is made and an algorithm for calculating shock wave parameters in detonation products and soils during explosions of cylindrical charges of various industrial explosives is developed.

3. The dependences of the maximum pressure on the front of the detonation wave for different types of explosives on time and distance are obtained, which indicates that the lowest peak pressure at the longest duration of the explosive pulse is observed for charges based on foamed types of explosives, both conventional and processed ultrasonic radiation. The maximum pressure of these types of explosives is 20–49% less, and the duration of the explosive impulse is in 3–3.5 times longer compared to the standard low-density explosive – igdanite. The low value of the peak detonation pressure, achieved by reducing the density of explosives, reduces the volume concentration of the energy of the charges, which, in turn, increases the efficiency of the explosive transformation energy in the far zone.

4. The growth time of the explosive impulse of charges based on foamed explosives, both conventional and processed by ultrasonic radiation, is in 2.47 times greater than for igdanite.

5. It is established that in the near zone during the explosion of an igdanite charge, significantly higher values of hydrostatic pressure and maximum volume deformation are achieved than during the explosion of a foamed explosive. This is explained by the higher detonation characteristics of igdanite: density, pressure at the Juguet point. The time to reach the maximum pressure and deformation during an igdanite explosion is much shorter, because the detonation rate of igdanite is higher than that of foamed explosives.

6. Parameters of shock waves during explosions of charges of new mixed explosives in the middle zone can be compared with the same parameters from traditional industrial explosives, such as igdanite, and in the far zone of the explosion, they exceed them. The difference in the maximum volumetric deformations in igdanite explosions is 7–15% compared to the explosions of foamed explosive and foamed explosive processed by ultrasound, respectively. When detonating a sonicated foamed explosive, the residual deformation is 9–10% greater than when detonating a non-sonicated foamed explosive charge.

Literatura – References

1. Shvets, V.B., Boyko, I.P., Vynnykov, Y.L., Zotsenko, M.L., Petrakov, O.O., Bida, S.V. (2014) Soil mechanics. Basics and foundations. (Textbook), Dnipropetrovsk: Porohy.
2. Han, O., Boiko, V., Kravets, V. &Han, A. (2020). Formation of parameters of foamed explosive mixtures fo rsealing soils. ScienceRise, 5, pp. 6–12. doi: 10.21303/2313-8416.2020.001430.
3. Han, O.V., Boyko, V.V., Han, A.L., Kravets, V.G., Vapnichna, V.V. (2019). Changes in the porosity and retention capacity of ammonium nitrate under the influence of ultrasonic irradiation. Problems of Geoengineering and Underground Urbanism (May).
4. Litvin, L.N. (1981). NEW DESTRUCTION METHODS AND ROCK MECHANICS. KYIV: NAUKOVADUMKA.
5. Vovk, A.A. (1979). Control of the action of an explosion in soils and rocks. Kyiv: Naukovadumka.
6. Vovk, A.A., Kravets, V.H., Demeshchuk, L.Y. et. al. (1976) The method of compaction of subsidence loess soils. Patent 572094 (USSR). SKTB Institute of geophysics AS USSR. MKY E02D 3/10, UDK 624.5.
7. Luchko, I.A., Remez, N.S. and Luchko, A.I. (2006) Wave processes in soil massifs during explosions of new mixed explosives. Bulletin of scientific works of the National Technical University of Ukraine "Kyiv Polytechnic Institute", "Mining" series: Collection of scientific works, 14, pp.24-30.
8. Remez, N., Dychko, A., Besarabets, Y. et al.(2019) Impact Modelling of Explosion of Mixture Explosive Charges on the Environment. Latvian Journal of Physics and Technical Sciences, 3, pp.37-49. doi: 10.2478/lpts-2019-0018.
9. Remez, N.S. (2000). Peculiarities of deformation of a solidrich-componen viscoplastic medium with a minimum coefficientin viscosity with dynamic stresses. Herald of science practices of NTU of Ukraine "Kyiv Polytechnic Institute". Series "Mining": Collection of science practices, 3, pp.34-39.
10. George, W., Collins, I.I. (2003) Fundamental Numerical Methods and Data Analysis.
11. Richtmyer R., Morton K. (1972) Difference methods for solving boundary value problems.

Zarządzanie parametrami oddziaływania materiału wybuchowego na masę gleby w wyniku użycia materiałów wybuchowych małej gęstości

Na podstawie obliczeń numerycznych problemu wybuchu cylindrycznych ładunków substancji wybuchowych w glebach uzyskuje się zależności maksymalnego ciśnienia, odkształceń maksymalnych i szczątkowych dla różnych rodzajów substancji wybuchowych w czasie i odległości. Stwierdzono, że najniższe ciśnienie szczytowe przy najdłuższym czasie trwania impulsu wybuchowego obserwuje się dla ładunków opartych na materiałach wybuchowych spienionych, zarówno konwencjonalnych, jak i poddanych działaniu promieniowania ultradźwiękowego. Maksymalne ciśnienie tego typu materiałów wybuchowych jest o 20–49% mniejsze, a czas trwania impulsu wybuchowego jest 3–3,5 razy dłuższy niż w przypadku standardowego materiału wybuchowego małej gęstości – igdanitu. Niska wartość szczytowego ciśnienia detonacji, osiągnięta poprzez zmniejszenie gęstości MW, zmniejsza koncentrację objętościową energii ładunków, co z kolei zwiększa efektywność energii przemiany MW w strefie dalekiej. Czas narastania impulsu wybuchowego ładunków na bazie spienionych materiałów wybuchowych, zarówno konwencjonalnych, jak i poddanych działaniu promieniowania ultradźwiękowego, jest 2,47 razy większy niż dla igdanitu. Stwierdzono, że w strefie bliskiej podczas wybuchu ładunku igdanitu osiągane są znacznie wyższe wartości ciśnienia hydrostatycznego i maksymalnego odkształcenia objętościowego niż w przypadku wybuchu spienionego materiału wybuchowego, co jest konsekwencją wyższych charakterystyk detonacyjnych igdanitu: gęstości, ciśnienia w punkcie Jougeta, szybkości detonacji. Czas do osiągnięcia maksymalnego ciśnienia i odkształcenia podczas wybuchu igdanitu jest znacznie krótszy, ponieważ szybkość detonacji igdanitu jest większa niż w przypadku spienionych materiałów wybuchowych. Parametry fal uderzeniowych podczas wybuchów ładunków nowych mieszanek MW w środkowej strefie można porównać z parametrami tradycyjnych przemysłowych MW, takich jak igdanit, a w dalszej strefie wybuchu przewyższają je. Różnica w maksymalnych odkształceniach objętościowych w wybuchach igdanitu wynosi 7–15% w porównaniu odpowiednio do wybuchów spienionego materiału wybuchowego i spienionego materiału wybuchowego poddanego działaniu ultradźwięków. Podczas detonacji spienionego ładunku wybuchowego poddanego działaniu dźwięku, deformacja szczątkowa jest o 9–10% większa niż podczas detonacji spienionego ładunku wybuchowego nie poddanego działaniu dźwięku

Słowa kluczowe: *mieszanki wybuchowe, gleby osiadające, symulacje matematyczne*

Technological Solutions for Increasing the Efficiency of Beneficiation Processes at the Mining of Titanium-Zirconium Deposits

Oleksii LOZHNIKOV[1)], Borys SOBKO[2)], Artem PAVLYCHENKO[3)]

[1)] DUT Dnipro University of Technology, Institute of Nature Management, Department of Surface Mining, Dmytro Yavornytsky ave. 19, Dnipro, Ukraine; ORCID http://orcid.org/0000-0003-1231-0295; email: oleksii.lozhnikov@gmail.com
[2)] DUT Dnipro University of Technology, Institute of Nature Management, Department of Surface Mining, Dmytro Yavornytsky ave. 19, Dnipro, Ukraine; ORCID http://orcid.org/0000-0001-9533-5126
[3)] DUT Dnipro University of Technology, Institute of Nature Management, Department of Ecology and Technology of Environmental Protection, Dmytro Yavornytsky ave. 19, Dnipro, Ukraine; ORCID https://orcid.org/0000-0003-4652-9180

http://doi.org/10.29227/IM-2023-01-07

Submission date: 08-02-2023 | Review date: 29-02-2023

Abstract

The article is devoted to the issue of effective use of associated minerals at the development of titanium-zirconium ore deposits. Since deposits of sedimentary titanium-zirconium ores have large areas, hundreds of million tons of mining mass are transformed into man-caused formations during their exploitation. Of the entire volume of mining mass, only 1% after beneficiation is used for the production of metal titanium, the rest of the mining rocks are stored in dumps and tailings. The use of resource-saving technological solutions at the development of these deposits allows obtaining loam, clay and sand as accompanying minerals. They can be used for the manufacture of brick products, molding and construction sand, sub-base layers in construction works and cosmetic materials. A significant part of sand and clay rocks in titanium-zirconium deposits is in a mixed state and cannot be effectively used without additional a technological solution, that is why it is placed in bulk tailings storage facilities. The article provides the rationale solutions for resource-saving technological that allow during the process of titanium-zirconium ores beneficiation to separate clay rocks from sand within the pit, which allows to obtain additional volumes of titanium-zirconium components and associated minerals for the building industry and reduce the land area required for the location of tailings storage facilities.

Keywords: *surface mining, titanium and zirconium deposits, mining technology, ore beneficiation, accompany minerals*

1. Introduction

The development of new and existing titanium-zirconium deposits of Ukraine is of strategic importance for the development of the economy, as it allows providing the needs of many sectors of the economy with scarce raw materials. Up to 10% of the world's reserves of titanium-zirconium ores are concentrated in the depths of Ukraine, which makes it an influential player on the world market. The importance of titanium-zirconium ores is extremely important for high-precision branches of the economy, since they have a wide range of applications in aircraft construction, in the production of rockets, electronics, high-precision devices, medical equipment, etc. Every year, the extraction of titanium-zirconium ores provides Ukraine with revenues to the economy in the amount of 3–4 billion Euros, which allows for high tax revenues and ensures the sustainable development of the economic and social sphere [1].

In addition to the significant economic effect of the development of placer titanium-zirconium mineral deposits, there is a certain list of problematic issues. First of all, this is the need to set aside significant land areas for the exploitation of pits, as well as the location of dumps and tailings storage facilities [2]. The main feature of the development of this type deposits is the insignificant content of useful minerals in the ore layer (an average of 8% by mass), which requires significant costs for the movement of ore pulp and the storage of beneficiation waste in external tailings. Since the productivity of this group pits is 3–5 million cubic meters per year, the accumulation of landfill waste occurs on a significant scale. This leads to the fact that the volumes of their accumulation lead to a critical level of filling of tailings storage facilities. For example, the total area of Vilnohirsky MMP tailings is 770 hectares, in which more than 250 million m³ of solid waste from beneficiation production was placed during the years of enterprise operation [3].

The second problem that has emerged acutely for the titanium industry of Ukraine today is the depletion of large deposits of minerals with relatively simple hydrogeological conditions of occurrence, which requires involvement in the development of new deposits with complex mining and geological problems. For the organization of sustainable extraction, technological and organizational tasks related to significant volumes of water inflow must be solved. The development of new deposits is also accompanied by the formation of a significant amount of production waste, which requires large areas for the location of tailings storage facilities. For example, during the operation of the new pit of the Motronivsky MPP, the share of useful minerals in the ore is 5%, and in the volume of the mining mass – about 1%. During the operation of this pit using the old technology, the total volume of production waste will be 830 million m³ with the volume of titanium-zirconium minerals – 7.5 million m³.

2. Analyzes of conducted researches

Increasing the level of resource conservation at the development of titanium deposits is possible due to the separation

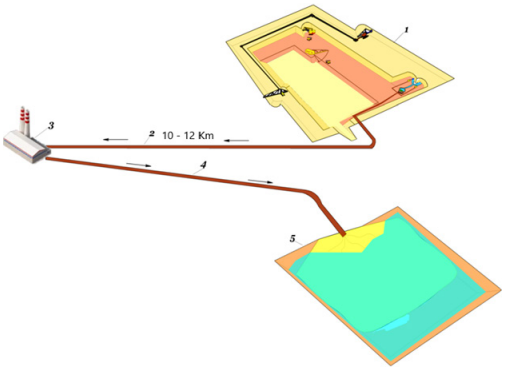

Fig. 1. The existing technological scheme for the development and beneficiation of titanium-zirconium ores at the Vilnohirsky MMP: 1 – pit, 2 – ore (mineral fraction content 8%); 3 – beneficiation plant; 4 – processing waste (tails 92%: clay 20%, quartz sand 70%, mineral fraction 2.55%); 5 – tailings storage

Rys. 1. Istniejący schemat technologiczny zagospodarowania i wzbogacania rud tytanowo-cyrkonowych w Vilnohirskim MMP: 1 – odkrywka, 2 – ruda (zawartość frakcji mineralnej 8%); 3 – zakład wzbogacania; 4 – odpady przeróbcze (odpady 92%: glina 20%, piasek kwarcowy 70%, frakcja mineralna 2,55%); 5 – zbiornik odpadów poflotacyjnych

of contained in ore sand and clay rocks with their subsequent separate storage in order to prevent the need to create a tailings repository. The research carried out in the work [4] is devoted to the issue of formation of hydraulic dumps from contained sand-clay rocks of the ore layer with low filtration properties. In order to solve the problem of low filtration properties of rocks an additional process of cleaning containing rocks from clay using a hydromechanical method of separation is proposed. The authors of [5], who studied the separation of sand-clay rocks using a special sand washing device, also studied the process of separation of the containing rocks of the ore layer. The developed method allows separating particles of quartz sand from clay rocks within the limits of the pit field due to the compact dimensions of the installation. To optimize the separation process it can be installed on a concentrator which is located inside of the pit [6].

Part of the scientific and research work is devoted to the formation of the internal dump pit from sand containing rocks by the hydromechanization method [7]. The formation of the internal hydraulic dump from quartz sand occurs in tiers using a hydro-mechanized method. Thus, after washing the lower dump layer the rocks of the upper dump layers are deposited on its surface by a mechanized method. The results of research [8] made it possible to establish the order of separation of sand from clay, followed by sending the clay to the gravity thickener. This process allows for thickening, after which the clay is safely stored in the rock dump, thereby forming a man-made resource for the future [9].

A significant shortcoming of these works is the field of application of research results, because there are no specific studies on establishing effective parameters for the storage of associated raw materials in man-made formations on the surface of internal dumps during pit development [10]. The reason is that the accompanying raw materials, which are represented by clays, as a rule, are not considered as a resource that is promising for future use. Because of this, clays are stored in bulk in dumps or tailings, which leads to their loss from the point of reuse.

3. Establishing unresolved problems

Solving the existing problems of the development of titanium-zirconium deposits in complicated hydrogeological conditions can be achieved by improving the processes of extracting and enriching the mineral with the aim of creating a closed cycle of obtaining titanium-zirconium raw materials at the mining enterprise. At the same time, it should be taken into account that the placement of the sandy mixture in the lower level of the internal dump and the clay mixture in the man-made deposit on the side of the pit will allow to reduce the volume of haulage work in the pit due to the reduction of the volume of haulage of the containing rocks of the ore layer to the stationary concentration plant, as well as speed up the process of reclamation of disturbed lands, since there is no need to wait for the end of the term for the formation of the tailings storage facility.

4. Tasks Settings

The aim of conducted researches is creation of a closed cycle of obtaining titanium-zirconium raw materials at a mining enterprise by establishing technological parameters for the development placer deposits with the separation of containing rocks at a concentration plant of collective concentrate. To achieve the aim, the following tasks were solved: research of the existing technology parameters at the development of titanium-zirconium deposits; conduct an analysis of the resources of titanium ore beneficiation technology with the existing field development technology; determine the characteristics of the man-made deposit formed in the tailings; to study the possibility of involving mineral resources of tailings in the closed cycle of the enterprise; to develop technological solutions for the creation of a waste-free technology for the development of titanium-zirconium deposits with the repeated involvement of beneficiation waste in the production process.

5. Improvement of existing mining technology of titanium-zirconium raw materials

The existing development and beneficiation technology at the Vilnohirsky MMP is implemented by means of hydraulic washing and supplying the mineral to the beneficiation plant. Sustainable operation of the enterprise using this technology requires the use of significant water resources. On average, in one year of operation, about 10 million tons of ore is supplied to the beneficiation plant, which requires the use of more than 30 million m^3 of water. The total cost of hydrohaulage of ore

Fig. 2. Concentrated release of tails from the pulp duct
Rys. 2. Skoncentrowane uwalnianie odpadów

Fig. 3. Release of tailings from hydrocyclones
Rys. 3. Zrzut odpadów poflotacyjnych z hydrocyklonów

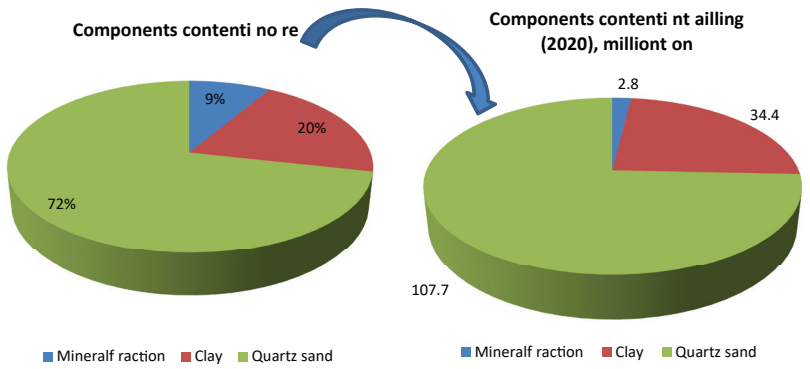

Fig. 4. Comparison of the useful components content in ore and tailings during the development of the Vilnohirsky MMP pit
Rys. 4. Porównanie zawartości składników użytecznych w rudzie i odpadach poflotacyjnych podczas robot przygotowawczych w Vilnohirsky MMP

sands for a length of more than 10 km from the pit to the beneficiation plant amounts to more than 5.1 million Euros per year.

In addition, about 100 million m³ of water per year is supplied to the beneficiation plant at all stages of ore separation and gravity haulage of tailings. The costs of providing such technology with water amount to more than 3.8 million Euros per year. The need to use such large volumes of water to haulage ore sands to the beneficiation plant is due to outdated technology. The main consumption of water is explained by the lack of division of tailings into clay and sandy components with further thickening (Fig. 1). This process is accompanied by the pumping of more than 80 million m³ of beneficiation tailings into tailings storage facilities, which consumes about 43 million kW per year, or 2.9 million Euros.

With the average cost of haulage 1 m³ of tailings – 0.05 Euro the total costs for this process are about 4.0 million Euro per year. The amount of floating tailings is about 30 million m³. Thus, on average, the volume of waste from the beneficiation plant at the Vilnohirsky MPP is about 110 million m³ per year. Due to the imperfection of the beneficiation process, a certain part of the mineral fraction falls into the tailings reservoir, which is formed by a hydromechanical method (Figs. 2, 3).

The necessity of forming a tailings storage facility (Fig. 2) is related to the physical and mechanical properties of the containing rocks. These rocks are represented by a sand-clay mixture and have low filtration properties, which do not allow them to form a stable slope of the inner dump layer by hydromechanical method with the existing technology.

The process of forming tailings in Ukraine is regulated by the "State Waste Classifier DK 005-96", and tailings are solid, fine-grained particles belonging to the IV hazard class (low-hazard waste).

Under the conditions of the Vilnohirsky MMP, due to the imperfect beneficiation technology, up to 3% of the mineral fraction from the ore is lost and together with the sand-clay mixture, enters the tailings repository (Fig. 4). Thus, the process of stacking the beneficiation tailings in the tailings storage is a process of forming a man-made deposit that is prospect of further processing.

After the tailings deposit has already been formed, the mineral fraction contained in it must be accounted for. The composition of man-made formations of beneficiation tailings is recorded annually in accordance with the "Instructions on the Procedure for Maintaining the State Balance of Solid Minerals Stocks". Together with this procedure the characteristics of the man-made deposit formed in the bowl of the tailings storage facility are determined (Table 1).

In order to perform the tasks related to the protection of the subsoil and the complex use of minerals in the formation of man-made formations, the geological surveying service of enterprises must provide:

- control of storage and saving of sand-clay beneficiation waste in tailings in accordance with the requirements of the Code of Ukraine "On Subsoil";
- accounting for the movement of waste tailings from beneficiation production, which are sent to tailings storage facilities for the formation of a man-made deposit, which contains useful components that are temporarily not used, in accordance with the current regulatory documents;
- execution of geological and geological-exploration works at the sites of tailings storage facilities according to approved projects.

Tab. 1. Characteristics of the man-made deposit formed in the tailings basin

Tab. 1. Charakterystyka złoża antropogenicznego utworzonego w osadniku

Factors	Indexes
1. Method of formation	Hydraulic method of formation
2. Morphological feature	Bulk, which is formed when filling low ground of the day surface
3. Composition	Rock, consisting of natural rocks and represented by sand-clay material
4. Possibility of use	Extraction of ilmenite, rutile and zircon, as well as extraction of disten, sillimanite and staurolite
5. Environmental impact	Safe, represented by sand and clay fractions that are weakly destroyed during storage

Fig. 7. Development of man-made deposit of titanium-zirconium ores by hydromechanized method

Rys. 7. Rozwój antropogenicznego złoża rud tytanowo-cyrkonowych metodą hydromechanizowaną

Fig. 8. Beneficiation plant of titanium-zirconium ores from man-made deposits

Rys. 8. Zakład wzbogacania rud tytanowo-cyrkonowych ze złóż antropogenicznych

A detailed study of the mineral composition of the Vilnohirsky MMP tailings made it possible to determine that with the existing technology of titanium-zirconium ores beneficiation, the tails contain from 1 to 3% of the final amount of the main components: zircon, rutile, ilmenite and related ones: disten, sillimanite, staurolite (Fig. 5).

According to the conducted studies, it was established that during the titanium-zirconium deposits development up to 25% of valuable minerals fall into the tailings. Thus, a new man-made resource with a rich content of mineral raw materials is created. According to a preliminary estimate, there may be mineral resources worth up to 1 billion Euros within the Vilnohirsky MMP tailings storage facility (Fig. 6).

The tailings deposits, formed as a result of Vilnohirsky MMP activities, were transferred to the status of man-made deposits, which allows another company to extract titanium-zirconium raw materials from them. The development of these deposits is carried out by a hydromechanized method with the subsequent extraction of valuable components at the beneficiation plant (Figs. 7, 8). Thus, the imperfection of the beneficiation technology organization leads to financial losses. According to preliminary estimates, the involvement of auxiliary resources of the raw material base of a mining enterprise (on the example of Vilnohirsky MMP) at the expense of the mineral components of the tailings repository (which was formed over 50 years) would increase the value of the raw material base of the enterprise by $1.0 billion.

The scheme of mining mass beneficiation from the tailings depository involves the use and placement of a collective concentrate beneficiation plant near the tailings depository (Fig. 8). The collective concentrate obtained after preliminary beneficiation is sent to the main beneficiation plant.

The processing of titanium-zirconium components from tailings is a more efficient process compared to the development of a natural deposit. Since during the development of the latter, along with the formation of large volumes of waste placed in the tailings repository, an additional disadvantage is the need to haulage the entire volume of useful mineral to a stationary beneficiation plant (10–12 km), which, provided that 90–95% of the containing rocks in ore causes a significant volume of excess haulage work.

The cost of obtaining a collective concentrate during the development of a man-made titanium-zirconium deposit at a wet beneficiation plant located near the tailings storage facility is 48.5 Euros/t, which is more than 4 times less (due to the reduction in the use of energy carriers, volumes of hydropulp and tailings haulage, amount of water) than when receiving a collective concentrate at the main concentration plant (231 Euro/t), which is located on the industrial site of the plant at a distance of up to 10 km.

It is worth noting that today, in connection with the improvement of beneficiation technologies, reprocessing of tailings is possible within the scope of the existing main enterprise. Therefore, according to the Laws of Ukraine, beneficiation tailings are not classified as waste. In this regard, the easiest solution to implement is proposed, which will allow to attract mineral resources of tailings storage facilities into the closed work cycle of the enterprise (Fig. 9).

6. Development of the closed cycle concept of titanium-zirconium raw materials mining

The presented technological scheme (Fig. 9) is the most effective for titanium-zirconium pits that have been in operation for a long time and have managed to accumulate significant mineral resources in the tailings repository, and the involvement of mineral raw materials from the tailings repository in the closed work cycle of the mining and beneficiation complex allows to reduce the cost obtaining a collective concentrate of titanium minerals up to 40%. However, the use of this technology in the operation of existing and new pits has a number of significant disadvantages. First of all, it requires large areas of free land for the location of the tailings storage facility, secondly, its operation requires the construction of a system of enormous length pipelines, and thirdly, the need to supply the plant with the entire volume of useful mineral remains. As already noted earlier, on average only 5% of the total volume of ore consists of titanium-zirconium minerals, the delivery of which is necessary to a stationary beneficiation

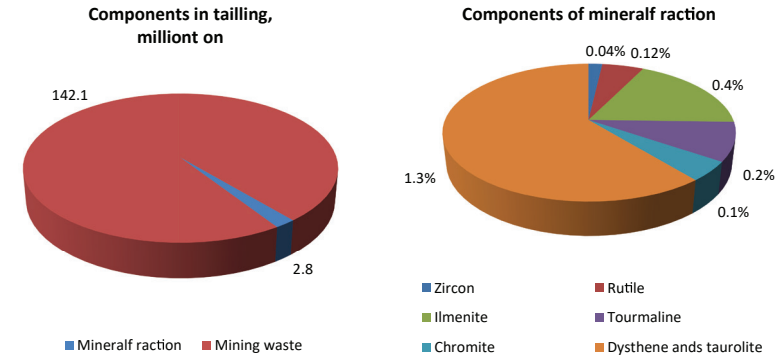

Fig. 5. The content of valuable useful components in the man-made deposit

Rys. 5. Zawartość cennych składników użytkowych w złożu antropogenicznym

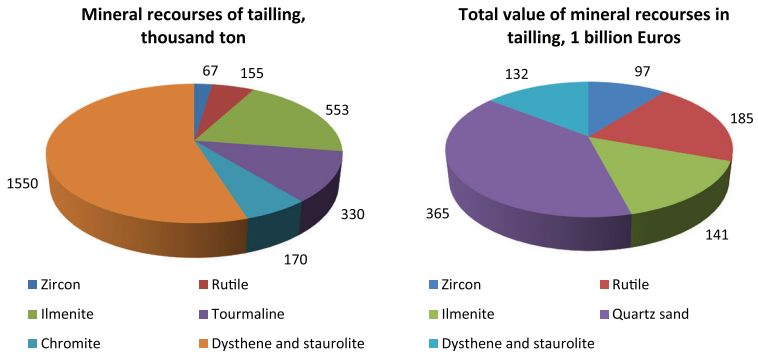

Fig. 6. Projected value of mineral resources in the Vilnohirsky MMP tailings

Rys. 6. Prognozowana wartość zasobów mineralnych w odpadach poflotacyjnych w Wilnohirskim MMP

plant. The above-mentioned problems also lead to a low level of integrated use of associated minerals in the enterprise's production activities, which prompts the search for new technological solutions [11]. In this regard, when developing new titanium-zirconium deposits, there is a critical need to develop a technological scheme that will allow reducing the area of tailings storage facilities and reducing the volume of haulage work during the operation of the mining and beneficiation plant.

The proposed technological scheme is primarily aimed at creating a waste-free technology for the development of new titanium-zirconium deposits with the possibility of re-involving beneficiation waste into the production process (Fig. 10).

The implementation of the technological scheme (Fig. 10) is carried out by building a beneficiation plant of collective concentrate on board the pit, which receives 100% of titanium-zirconium ore from the pit. Mined ore in the form of pulp enters the collective concentrate plant, where ore beneficiation and distribution of ore pulp into rough concentrate (up to 7%), clay fraction beneficiation tails (up to 20%), and sand beneficiation tails (up to 72%) take place in parallel. The crude concentrate is transported to a stationary concentrator through a pulp pipeline [12]. The tailings of clay fraction beneficiation are carried through the pulp pipeline to the thickener, which is located in the immediate vicinity of the pit, where the clay is thickened with the subsequent placement of accompanying raw materials in the man-made deposit. Sand beneficiation tailings are pumped through the slurry pipeline to the second part of the internal hydro dump from the non-working slope of the pit. Due to the separation of clay from sand, the resistance of the dump layers to landslides is ensured and it is possible to place new dump layers on their surface mechanically [13].

The main feature of the proposed technology is the separation of sand-clay containing rocks for the purpose of their further separate storage in the residual space of the pit. However, the most difficult task is the handling of clay, which after beneficiation is in a watered form and dries for a long time in natural condition. To solve this problem, it is worth turning to world experience, because today there are effective technologies for thickening waste from beneficiation factories. They are widely used in the Timmins, Langmuir Mine in Canada [14], in the USA – in the Blue mine Hills, at the mining in South Africa (Fig. 11).

The application of the tailings separation technology into clay and sand components with their subsequent thickening (Fig. 11) allows to significantly reducing the amount of mining waste. For example, when 10 million tons of ore are fed to the beneficiation plant of Vilnohirsky MMP, only 0.6 million tons (6–7%) of useful minerals are extracted and the remaining waste (9.4 million tons) is a sand-clay mixture in a liquid state. During the separation of the sandy and clay mixture, 70% of the water (16.5 million m^3) is found in the sandy tailings and 50% (1.77 million m^3) in the clay tailings when they are thickened. Thus, according to the proposed technology, the amount of tailings of the beneficiation plant will be reduced to 22.7 million m^3, which is more than four times less than with the existing technology. At the same time, the savings in electricity costs only due to the pumping of waste to the tailings storage facility will amount to about $1 million/

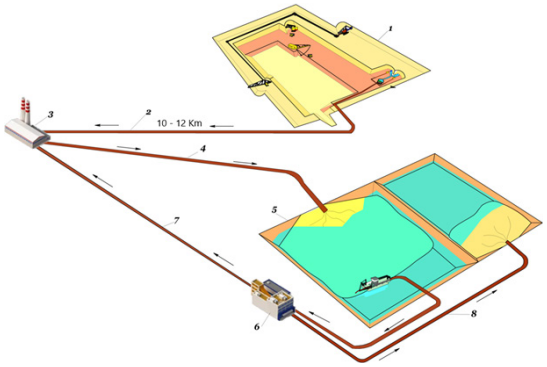

Fig. 9. Technological scheme for the development of a titanium-zirconium deposit with the involvement of mineral resources of the tailings repository: 1 – pit; 2 – ore (mineral fraction content 8%); 3 – beneficiation plant; 4 – processing waste (tails 92%: clay 20%, quartz sand 70%, mineral fraction 2.55%); 5 – tailings storage facility; 6 – concentration plant of collective concentrate; 7 – collective proofing concentrate (2.3%); 8 – tailings (sand-clay mixture)

Rys. 9. Schemat technologiczny zagospodarowania złoża tytanowo-cyrkonowego z udziałem surowców mineralnych składowiska odpadów: 1 – odkrywka; 2 – ruda (zawartość frakcji mineralnej 8%); 3 – zakład wzbogacania; 4 – odpady przetwórcze (odpady 92%: glina 20%, piasek kwarcowy 70%, frakcja mineralna 2,55%); 5 – obiekt składowania odpadów poflotacyjnych; 6 – zakład zagęszczania koncentratu zbiorowego; 7 – zbiorczy koncentrat wzmacniający (2,3%); 8 – odpady przeróbcze (mieszanka piasku i gliny)

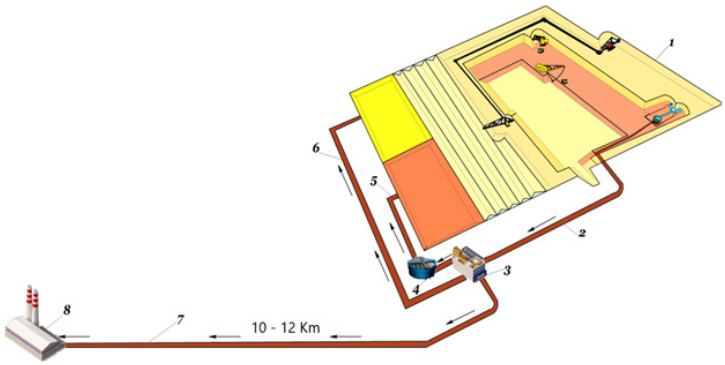

Fig. 10. Technological scheme for the closed cycle mining of a titanium-zirconium deposit: 1 – pit; 2 – ore (8% mineral fraction); 3 – concentration plant of collective concentrate; 4 – clay thickener; 5, 6 – processing waste (clay 20% of the volume of ore, quartz sand – 72%, respectively); 7 – mineral fraction 7%; 8 – beneficiation plant

Rys. 10. Schemat technologiczny eksploatacji złoża tytanowo-cyrkonowego w obiegu zamkniętym: 1 – odkrywka; 2 – ruda (8% frakcji mineralnej); 3 – zakład zagęszczania koncentratu zbiorczego; 4 – zagęszczacz gliny; 5, 6 – odpady przetwórcze (glina 20% objętości rudy, piasek kwarcowy – odpowiednio 72%); 7 – frakcja mineralna 7%; 8 – zakład wzbogacania

year. A comparison of the main technical and economic indicators of the existing and proposed technological schemes is given in the table. 2.

In addition to the economic effect of reducing operational costs, the use of modern equipment allows for additional extraction of conditioned zircon, rutile and ilmenite concentrates and aluminosilicates (dysthene, staurolite) from the ore layer. The rates of beneficiation according to modern schemes are quite high and the extraction of commercial concentrates from the original ore reaches 95–98%.

Thus, the implementation of the proposed technological scheme for the development of titanium-zirconium deposits allows obtaining three significant advantages. First, there is the possibility of selective separation of sand from clay, after which separate man-made deposits are formed from the clay; secondly, due to the separation of clay from sand, there is an opportunity to stack sand in the internal dump of the pit with the subsequent placement of dump layers on its surface by a mechanical method. And as a result, due to the mechanical formation of the upper dump layers, it is possible to significantly reduce the area of external tailings storage facilities. Thus, compared to other technological solutions, up to 20% of clay and 72% of quartz sand will be selectively extracted from 92% of the sand-clay mass. All the sand is placed in the internal dump of the pit and the man-made deposit of building raw materials is formed from the clay, which will be involved in further use.

7. Conclusions

The carry out researches confirm the effectiveness of the proposed technology for the development of a titanium-zirconium deposit with a closed cycle. Its implementation makes it possible to ensure cost-effective and practically ecologically clean and waste-free production with a significantly lower cost of the main products of existing mining and beneficiation enterprises. In this way, the task of the circular economy of mining production is implemented, which consists in expanding the possibilities of using renewable resources (waste from beneficiation production) and creating cycled technological schemes with multiple use of water at the development of a titanium-zirconium deposit.

It has been proven that the repeated extraction of mineral raw materials from man-made deposits (tailings) of already existing mining and beneficiation plants will help to minimize economic damage to the environment. It was established that for the operating conditions of the Vilnohirsky MMP, the ap-

Fig. 11. Installation for thickening beneficiation waste

Rys. 11. Instalacja do zagęszczania odpadów

Tab. 2. Comparison of technological schemes for the development of titanium-zirconium deposits

Tab. 2. Porównanie schematów technologicznych udostępnienia złóż tytanowo-cyrkonowych

Indicator	Existing technological scheme	The proposed technological scheme
Hydrohaulage of ore to the beneficiation plant:		
- share of the total mass of ore, %	100	7
- volume, million tons	10	0.7
- costs, million Euros	5.15	0.36
Hydrohaulage of beneficiation tailings:		
- distance, km	6	0.5
- costs, million Euros	4.0	0.33
Annual economic effect, EUR million	-	8.5

plication of the proposed technological solutions will reduce the area for the location of tailings storage facilities by 4 times.

It was proved that the proposed solutions allow reducing the cost of the main products of the mining and beneficiation plant due to additional volumes of mineral raw materials extraction from man-made resources by 30–40% and additional creation of man-made deposits of building raw materials. The implementation of such an approach is connected with the use of the most important principle of creating environmentally safe technologies of mining production – the organization of a closed technological cycle of the mining enterprise.

Literatura – References

1. Lozhnikov, O., Shustov, O., Chebanov, M., & Perkova, T, (2022). Methodological principles of the selection of a resource-saving technology while developing water-bearing placer deposits. Mining of Mineral Deposits, 16(3), 115-122. https://doi.org/10.33271/mining16.03.115.
2. Perks, C., & Mudd, G. (2019). Titanium, zirconium resources and production: A state of the art literature review. Ore Geology Reviews, 107, 629-646.
3. Sobko B., Lozhnikov O. "Determination of cut-off wall cost efficiency at Motronivskyi pit mining." Natsional'nyi Hirnychyi Universytet. Naukovyi Visnyk. 3 (2018): 44-49.
4. Sobko B.Yu., Gaydin A.M., Laznikov O.M. (2016) Mining flooded titanium ores deposits. Dnepr: Lithograph. - 216 s.
5. Padmalal, D. & Maya, K. (2014). Sand mining: environmental impacts and selected case studies. Springer
6. Sobko B.Yu., Denyschenko O.V., Lozhnikov O.V., Kardash V.A. "The belt conveyor effectiveness at the rock haulage under flooded pit excavations" Natsional'nyi Hirnychyi Universytet. Naukovyi Visnyk 6 (2018): 26-32.
7. Lawrence, S., & Davies, P. (2014). The sludge question: the regulation of mine tailings in nineteenth-century Victoria. Environment and History, 20(3), 385-410.
8. Panchang, R. (2014). Sand Mining and Industrial Effluents Threaten Mangroves Along Central West Coast of India. Open journal of ocean and coastal sciences, 1.Zhai, J., Wang, H., Chen, P., Hu, Y., & Sun, W. (2020). Recycling of iron and titanium resources from early tailings: From fundamental work to industrial application. Chemosphere, 242, 125178.
9. Sdvyzhkova, O., Babets, D., Moldabayev, S., Rysbekov, K., Sarybayev, M. (2020). Mathematical modeling a stochastic variation of rock properties at an excavation design. International Multidisciplinary Scientific GeoConference Surveying Geology and Mining. Ecology Management, SGEMthis, 2020-August (1.2), pp. 165–172. https://DOI:10.5593/sgem2020/1.2/s03.021
10. Hein, J. R., Koschinsky, A., & Kuhn, T. (2020). Deep-ocean polymetallic nodules as a resource for critical materials. Nature Reviews Earth & Environment, 1(3), 158-169.
11. Issagulov, A. Matayev (2022). Substantiation and development of innovative container technology for rock mass lifting from deep open pits. Mining of Mineral Deposits. 2022, 16(4):87-95. https://doi.org/10.33271/mining16.04.087
12. Buzylo V., Pavlychenko A., Borysovska O., Saveliev D. Investigation of processes of rocks deformation and the earth's surface subsidence during underground coal mining. E3S Web of Conferences. 2019, vol. 123, article 01050. DOI: 10.1051/e3sconf /201912301050.
13. Demir, F., & Derun, E. M. (2019). Modelling and optimization of gold mine tailings based geopolymer by using response surface method and its application in Pb2+ removal. Journal of Cleaner Production, 237, 117766.

Rozwiązania technologiczne zwiększające efektywność procesów wzbogacania w eksploatacji złóż tytanowo-cyrkonowych

Artykuł poświęcony jest zagadnieniu efektywnego wykorzystania minerałów towarzyszących przy zagospodarowaniu złóż rud tytanowo-cyrkonowych. Ponieważ złoża osadowych rud tytanowo-cyrkonowych mają duże powierzchnie, setki milionów ton masy wydobywczej podczas ich eksploatacji przekształcane są w formacje antropogeniczne. Z całej masy wydobywczej zaledwie 1% po wzbogacaniu jest wykorzystywane do produkcji tytanu metalicznego, reszta skał wydobywczych składowana jest na hałdach jako odpady poflotacyjne. Wykorzystanie zasobooszczędnych rozwiązań technologicznych przy zagospodarowaniu tych złóż pozwala na uzyskanie iłów, glin i piasku jako kopalin towarzyszących. Mogą być one stosowane do produkcji wyrobów z cegły, piasku formierskiego i budowlanego, warstw podkładowych w budownictwie oraz materiałów kosmetycznych. Znaczna część skał piaskowych i ilastych w złożach tytanowo-cyrkonowych jest w stanie wymieszanym i nie może być efektywnie wykorzystana bez dodatkowego rozwiązania technologicznego, dlatego jest umieszczana na składowiskach odpadów poflotacyjnych. W artykule przedstawiono przesłanki rozwiązań technologicznych oszczędzających zasoby, które w procesie wzbogacania rud tytanowo-cyrkonowych pozwalają na oddzielenie skał ilastych od piasku w obrębie wyrobiska, co pozwala na uzyskanie dodatkowych ilości komponentów tytanowo-cyrkonowych i minerałów towarzyszących dla budownictwa oraz na zmniejszenie powierzchni gruntów, wymaganej pod lokalizację składowisk odpadów poflotacyjnych.

Słowa kluczowe: *górnictwo odkrywkowe, złoża tytanu i cyrkonu, technologia górnicza, wzbogacanie rudy, minerały towarzyszące*

Study of Stress Concentration on the Contour of Underground Mine Workings

Serhii PYSMENNYI[1)], Serhii CHUKHAREV[2)], Andrii PEREMETCHYK[3)], Serhii FEDORENKO[4)], Anatolii MATSUI[5)]*

[1)] Kryvyi Rih National University, Faculty of Mining and Metallurgy,11 Vitalii Matusevych Str., Kryvyi Rih, 50027, Ukraine; ORCID https://orcid.org/0000-0001-5384-6972; email: psvknu@gmail.com
[2)] National University of Water and Environmental Engineering, 11 Soborna Str., Rivne, 33028, Ukraine; ORCID https://orcid.org/0000-0002-4623-1598
[3)] Kryvyi Rih National University, Faculty of Mining and Metallurgy,11 Vitalii Matusevych Str., Kryvyi Rih, 50027, Ukraine; ORCID https://orcid.org/0000-0001-6274-146X
[4)] Kryvyi Rih National University, Faculty of Mining and Metallurgy,11 Vitalii Matusevych Str., Kryvyi Rih, 50027, Ukraine; ORCID https://orcid.org/0000-0001-5753-9603
[5)] Central Ukrainian National Technical University, 8, Prospekt Universytetskyi, Kropyvnytskyi, 25006, Ukraine; ORCID https://orcid.org/0000-0001-5544-0175

http://doi.org/10.29227/IM-2023-01-08

Submission date: 06-02-2023 | Review date: 17-03-2023

Abstract

Kryvyi Rih iron ore basin consists of complex structured ore deposits and is developed by the underground method at depths of over 1000 m. The underground method is used to mine reserves of rich iron ores with a useful component content of more than 59% applying bulk ore and rock caving systems. This leads to significant changes in the stress state of the rock massif. During underground operations, mine workings are strained and in some cases destructed. As a result, enterprises are constantly increasing operating costs for maintaining mine workings, which adversely impacts the cost of production. Industrial research results demonstrate that in most cases workings fail in their upper part which is vaulted in shape. Available methods for determining the state of rocks around mine workings do not fully take into account physical and mechanical properties of the rocks in which the working is located. The developed technique allows determining not only the destructive pressure impacting the workings, but also the angle at which the destructive force acts. This technique differs from the available ones in taking into account not only mining and geological characteristics of the deposit, but also most factors of physical and mechanical properties of rocks. This technique helps to choose a rational place for driving mine workings at the stage of design, thus avoiding significant additional cost for their maintenance.

Keywords: *stress, working, vault of stable equilibrium, pressure, stability, ultimate strength, rocks*

1. INTRODUCTION

Underground mining of mineral deposits leads to significant changes in the primary stress state of the rock massif that cause man-made disasters of a geomechanical nature [1–3]. In solving this problem, experimental research methods are used the results of which are the basis for determining the positive and negative nature of the change in the stress state of the rock massif [4–6]. The change in stresses occurs due to changes in the forces of mutual attraction and mutual repulsion between ions in the crystal lattice of rocks resulting in internal forces that counteract external ones [7–9].

According to [10–13], various measures to change the stress state of the rock massif lead to an increase in stability of mine workings through reducing concentration of stresses or cutting the cost of drilling and blasting due to increased concentration of stresses in the rock massif.

It is proved that if an elementary cube is separated from a stressed rock massif, three stress vectors can generally be detected on each of its faces: two tangential (mutually perpendicular) and one normal, Fig. 1, [14–16].

The internal stress state of the rock volume under consideration is a stress tensor and looks as follows

$$s_{ij} = \begin{vmatrix} \sigma_x & \tau_{xy} & \tau_{xz} \\ \tau_{yx} & \sigma_y & \tau_{yz} \\ \tau_{zx} & \tau_{zy} & \sigma_z \end{vmatrix} = p_{ik} \cdot n_i , \quad (1)$$

where σ_z is the internal stress arising in the rock MPa; τ_{ik} is tangential stresses arising in rocks, MPa; p_{ik} is a set of stresses relative to three mutually perpendicular areas at one point; n_i is a single normal vector to the corresponding plane under consideration; i, k are indices of the axes of coordinates x, y, z.

Stress concentration on the contour of workings can be reduced by changing their cross-sectional shape depending on the ratio of stresses acting in the cross-sectional plane of the workings. At that, the shape of the workings can be elliptical, arched, vaulted, round, tent-shaped, rectangular, rectangular-vaulted, etc. [17–19].

However, to ensure technological processes (drilling of the massif, ore drawing and haulage, ventilation, etc.), it is necessary to create workings of a large cross-sectional area which significantly reduces stability of the workings regardless of their shape.

The required area of underground mine workings depending on application of the relevant type of equipment is given in Table 1 [20, 21].

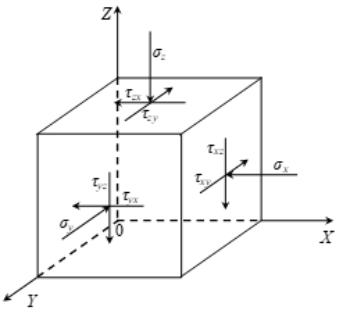

Fig. 1. Distribution of stress vectors in an elementary volume located in the rock massif

Rys. 1. Rozkład wektorów naprężeń w jednostkowej objętości znajdującej się w masywie skalnym

Tab. 1. Area of mine workings in underground mining at mineral deposits of Kryvyi Rih iron ore basin (Ukraine)

Tab. 1. Powierzchnia wyrobisk górniczych w górnictwie podziemnym na złożach kopalin Krzywego Rogu (Ukraina)

Mine workings	Mine workings area, when applying:	
	traditional equipment	self-propelled equipment
Capital workings (crosscut), m^2	12-18	18-24
Preparatory workings (haulage drift, haulage ort), m^2	8-16	16-20
Subsidiary workings, m^2:		
- drilling	8-12	14-18
- undercut	4-8	8-12
- raise	2-4	4-6
- transport	4-7	10-14
- reloading rooms	6-14	22-25
Compensation rooms, m^3	3750-45000	3750-45000

Thus, according to data of mining enterprises of Kryvyi Rih iron ore basin, retimbering of capital, preparatory and subsidiary underground workings averages 3–10%, 5–15% and 10–25% respectively.

2. PURPOSE

The present study aims to determine stress concentration on the contour of underground mine workings to reduce operating costs for their maintainance. For this, it is necessary to solve the following tasks:

1. To study the impact of the field of primary stresses of a multi-module massif on formation of a destructive force arising on the contour of the vaulted mine working.

2. To improve the method for determining the active zone that leads to destruction of the mine working.

3. ANALYSIS OF RESEARCHES AND PUBLICATIONS

The rock massif of Kryvyi Rih iron ore basin is comprised of a complex of rocks with their own mining, geological, physical and mechanical properties. In terms of geomechanics, rocks of the rock massif should be considered in relation to adjacent rocks as an elastic or plastic inclusion. If an external load is applied to such a complex of rocks, a complex field of stresses is formed in it depending on geometrical and physical-mechanical parameters of the rock massif area under study. Therefore, the larger the volume of the massif where the field of stresses is being determined, the greater the number of geological and tectonic factors impacting the final result is.

Ideally, the gravitational forces formed in an undisturbed massif are composed of vertical and horizontal stresses, which can be determined by the expressions [22–24]

$$\sigma_z = \gamma H, \quad \sigma_x = \sigma_y = \frac{\mu\sigma_z}{(1-\mu)}, \tag{2}$$

where σz is vertical stresses, MPa; σ_x, σ_y are horizontal components of the vertical stress, MPa; γ is the volumetric weight of rocks, H/m^3; H is the depth of mining, m; μ is Poisson ratio.

Changes in the stress field on the contour of the working as well as determination of places of maximum stress concentration with respect to the exposure surface are treated in works by a great number of scientists including M.M. Protodyakonov, I.A Turchaninov, Z.M. Galaev, G.N. Kuznetsov, M.I. Stupnik, V.M. Tarasyutin, V.O. Kalinichenko, V.I. Bondarenko, A.M. Zorin etc. The results of many years of studies of the stress state of the rock massif enable arguing that the structure of the primary stress field is impacted by the following factors: gravitational forces, tectonic forces and residual stresses [22–27]. Every particle located at a depth is pressed by the weight of overlying rocks, it transfers this pressure in all directions, and due to the impossibility of displacement, horizontal stresses arise [22–24]. When determining stresses in the rock massif, the scope of studies must be limited to a structural block, then the obtained fields of primary gravitational-tectonic stresses will be characteristic of this structural block [25–27].

Due to the fact that a real rock massif is not an ideal environment, the earth's crust can be divided into geoblocks represented by more than 20 ranks according to its disturbances. According to [23], dimensions of geoblocks are on average: 1 m, 10 m, 100 m, 1 km, 10 km, 100 km, 1000 km and over. Disturbances of each rank have their own strains and their own field of the gravitational-tectonic stress.

According to [22, 24, 27], tectonic stresses in the vertical direction should equal zero, and in the horizontal direction they should have the maximum and the minimum value with the azimuth of their action: σ_{1t}, σ_{2t}, σ_{1g}, and σ_{2g}. Thus, in the ideal case, the total of gravitational-tectonic stresses is determined by the formulas

Tab. 2. Classification of rocks and ores of Kryvyi Rih iron ore basin

Tab. 2. Klasyfikacja skał i rud Krzyworoskiego zagłębia rud żelaza

Compressive strength, MPa	Rocks	Degree of fracturing		
		weak < 5; $K_{s.w.}$ = 0.9-1.0	medium 6-15; $K_{s.w}$ = 0.5-0.8	great > 15; $K_{s.w}$ <0.5
> 140	Jaspilite, hematite quartzites	*I*	*II*	*III*
120-140	Oxidized, magnetite quartzites	*II*	*III*	*IV*
70-120	Quartz-chlorite, aspid schists, colour hornfels	*III*	*IV*	*V*
40-60	Colour and chlorite schists, martite ores	*IV*	*V*	*VI*
< 40	Colour ores	*VI*	*VI*	*VI*

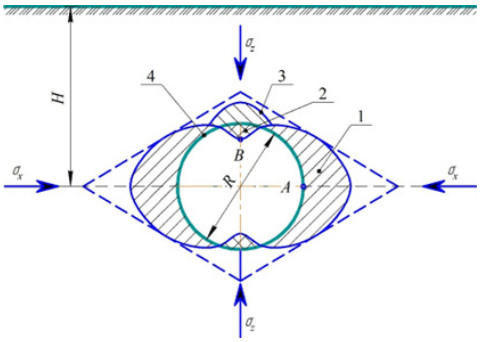

Fig. 2. Formation of stresses on the contour of the round working: 1 – the area of compressive stresses; 2 – the area of tensile stresses; 3 – the beginning of vault formation; 4 – the contour of the mine working

Rys. 2. Powstawanie naprężeń na obrysie wyrobiska okrągłego: 1 – obszar naprężeń ściskających; 2 – obszar naprężeń rozciągających; 3 – początek formowania się sklepień; 4 – zarys wyrobiska kopalnianego

$$\sigma_{1g} = \sigma_{1t} + \frac{\mu_1 \gamma H}{1-\mu_1}, \quad \sigma_{2g} = \sigma_{2t} + \frac{\mu_2 \gamma H}{1-\mu_2}, \tag{3}$$

where σ_{1t}, σ_{2t} are tectonic stresses, MPa, σ_{1g}, σ_{2g} are gravitational stresses, MPa.

Under the impact of external forces, rocks are subjected to linear strains ε which are determined by the expression

$$\varepsilon = \frac{(l' - l)}{l} = \frac{\Delta l}{l}, \tag{4}$$

where l′ is the length of the edge of the separated elementary cube l after straining, mm; Δl is the change in the length of the edge of the elementary cube after straining, mm.

By separating linear and shear strains into their constituent vectors along the coordinate axes, the strain tensor, which determines the nature of the strain of any point in the body, has the form

$$\varepsilon_{ki} = \begin{vmatrix} \varepsilon_x & \frac{1}{2}\tau_{xy} & \frac{1}{2}\tau_{xz} \\ \frac{1}{2}\tau_{yx} & \varepsilon_y & \frac{1}{2}\tau_{yz} \\ \frac{1}{2}\tau_{zx} & \frac{1}{2}\tau_{zy} & \varepsilon_z \end{vmatrix} = \frac{1}{2}\left(\frac{\partial u_i}{\partial x_k} + \frac{\partial u_k}{\partial x_i}\right), \tag{5}$$

where u is the general designation of any strain.

In this tensor (5), two of any tangential stresses τ lying in the same plane and directed oppositely, must be equal, since the body is in equilibrium, and therefore, the total moment of forces relative to the center of the elementary cube equals zero [22, 25].

Given that the opposite shear strains are equal to each other, the strain tensor is symmetrical. The nature and value of the strain depend on the type and value of applied stresses. An increase in load leads to an increase in strains, and when ultimate strength is exceeded, the rock is destructed [28–30].

Depending on the ratio of values of these strains, rocks can be divided into elastic-fragile (the plastic zone is practically not observed until destruction), elastic-plastic (destructive strain is preceded by a zone of plastic strain) and plastic (elastic strain is practically not available) [24, 31–33]. The rock massif of Kryvyi Rih basin is heterogeneous, therefore, at the same depth, different stresses act on the mine working and cause different strains [24–36].

Thus, on the contour of the working with a large radius of curvature, there appear angular points that are foci of high concentration of stresses resulting in partial destruction of the contour of the working with changed stresses on it. The working is being destructed until it acquires stable outlines [37–40]. The contour of the working is under destruction throughout its entire life. To maintain the mine workings throughout this period, various types of timbering are used according to the developed classification given in Table 2.

Rocks of Kryvyi Rih iron ore basin are divided into six classes: I – very stable; II – stable; III – medium stability; IV – low stability; V – very low stability and VI – unstable.

Depending on the compressive strength and the class of rock stability, the following types of timbering are used to maintain mine workings: class I – timberless, sprayed-concrete, anchor; class II – sprayed-concrete, anchor with mesh; class III – anchor with sprayed-concrete concrete, metal; class IV – metal, anchor with reinforced sprayed-concrete; class V – yieldable steel arch, anchor with elongated anchors with reinforced sprayed concrete; class VI – paired steel arch yieldable, round tubbing.

4. METHODS

According to [17–21], tensile and compressive stresses occur around workings, Fig. 2, while at points A and B there are maximum compressive and tensile stresses respectively.

The maximum stress-strain state around the round working in the gravitational-tectonic field of primary stresses is described by the following expressions for the elastic medium [13, 19, 41–43]

a) b)

Fig. 3. Condition of underground mine workings under pressure at the depth of 1350 m (u/m "POKROVSKA", the JSC "KRYVBASZALIZRUDKOM"): a – without destruction of mine workings; b – destruction of the working in its upper part

Rys. 3. Stan podziemnych wyrobisk górniczych pod ciśnieniem na głębokości 1350 m („POKROVSKA", „KRYVBASZALIZRUDKOM"): a – bez niszczenia wyrobisk górniczych; b – zniszczenie wyrobiska w jego górnej części

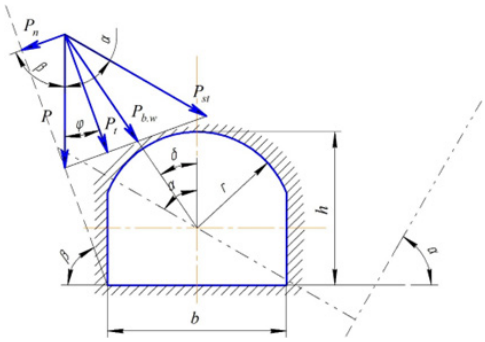

Fig. 4. Computational scheme for determining the destructive load on the contour of the working

Rys. 4. Schemat obliczeniowy wyznaczania obciążenia niszczącego na kontur wyrobiska

$$\begin{cases} \sigma_r = \left(1-\frac{a^2}{r^2}\right)\left(\frac{\sigma_z+\sigma_x}{2}-\left(1-\frac{3a^2}{r^2}\right)\frac{\sigma_z-\sigma_x}{2}\cos 2\theta\right), \\ \sigma_\theta = \left(1+\frac{a^2}{r^2}\right)\left(\frac{\sigma_z+\sigma_x}{2}+\left(1+\frac{3a^2}{r^2}\right)\frac{\sigma_z-\sigma_x}{2}\cos 2\theta\right), \end{cases} \quad (6)$$

where σr, σθ are normal and tangential stresses respectively, MPa; a is the radius of the working, m; r is the distance from the center of the working to the elementary volume, m; θ is the calculated angle at which normal and tangential stresses act on the contour of the mine working, degrees.

If compressive stresses on the contour of the working exceed ultimate compressive strength of the rocks, the working is destrructed 1, at that there is an increase in the span and a decrease in the contour of the vaulted part, which in turn leads to occurence of tensile stresses 2 in the roof with subsequent formation of the caving vault 3.

The main condition for stability of the boundary equilibrium at any site is described by Coulomb law and looks as follows [44–46]

$$\tau_{zx} \geq \tau_0 + \sigma_n tg\rho, \quad (7)$$

where τ_{xy} is shear forces, MPa; τ_o is initial shear resistance, MPa; σп is the normal stress at a given site, MPa; ρ is the angle of internal friction of rocks, degrees.

The normal and tangent stresses included in (7) are determined by the system of equations

$$\begin{cases} \sigma_n = \sigma_z \cos\theta, \\ \tau_{zx} = \sigma_z \sin\theta, \end{cases} \quad (8)$$

If there are no compacting stresses, the initial shear resistance is equal to adhesion of rocks. According to [13, 24, 47], the initial shear resistance is determined depending on the characteristics of the rock massif:

- for a homogeneous massif

$$\tau_0 = \tilde{n}$$

- for a microlayer massif

$$\tau_0 = (0.6\ldots0.7)c;$$

- for individual layers and contacts

$$\tau_0 = (0.2\ldots0.5)c;$$

where c is adhesion of rocks for the main thickness of the massif, H/m².

In layered rocks on the contour of the working, a local fall is observed, manifestation of which occurs due to a decrease in ultimate strength of rocks and the coefficient of adhesion between the layers. The value of the strength characteristics on contacts between the layers is considerably less, so destruction in the massif occurs on contact between the rocks.

Stresses arising on the contour of the working lead to its destruction, which in turn adversely impacts heterogeneous properties of the multi-module massif.

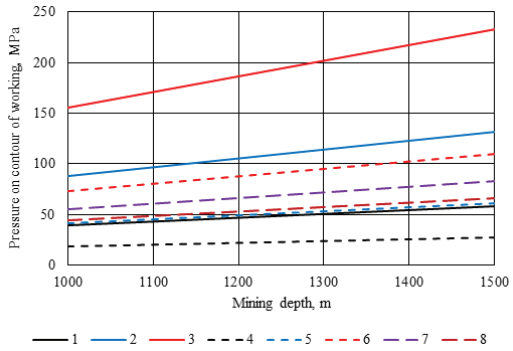

Fig. 5. Dependencies of the value of the active load on the contour of the working beyond the zone of the stoping operations impact on the depth of mining, the radius of the vaulted part of the mine working and rocks: 1–3 – the working is in magnetite ores with the radius of 2, 3 and 4 m respectively; 4–6 – the working is in schistous rocks with the radius of 2, 3 and 4 m respectively; 7, 8 – calculations according to (9) for magnetite ores and schistous rocks respectively

Rys. 5. Zależności wartości obciążenia czynnego od obrysu wyrobiska poza strefą oddziaływania postoju na głębokość urabiania, promień sklepienia wyrobiska i skały: 1–3 – eksploatacja odbywa się w rudach magnetytu o promieniu odpowiednio 2, 3 i 4 m; 4–6 – wyrobisko w skałach łupkowych o promieniu odpowiednio 2, 3 i 4 m; 7, 8 – obliczenia wg (9) odpowiednio dla rud magnetytu i skał łupkowych

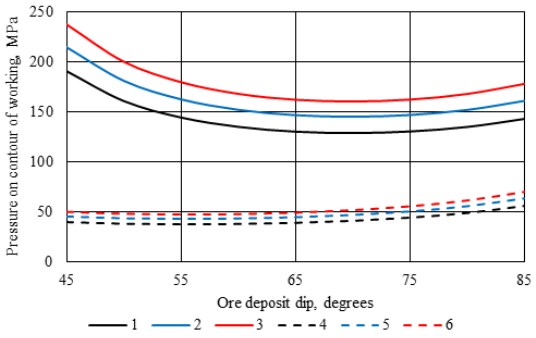

Fig. 6. Dependencies of the value of the actual load on the contour of the workins beyond the zone of stoping operations impact on the angle of the ore deposit dip, the depth of mining and rocks: 1–3 – the working is in magnetite ores at the depth of 1200, 1350 and 1500 m respectively; 4–6 – the working is in schistous rocks at the depth of 1200, 1350 and 1500 m respectively

Rys. 6. Zależności wartości rzeczywistego obciążenia od konturu wyrobisk poza strefą zatrzymania eksploatacji, od kąta upadu złoża, głębokości eksploatacji i skał: 1–3 – wyrobisko w magnetycie rudy na głębokości odpowiednio 1200, 1350 i 1500 m; 4–6 – wyrobisko w skałach łupkowych na głębokości odpowiednio 1200, 1350 i 1500 m

5. RESULTS

In Kryvyi Rih iron ore basin, ore bodies are represented by complex structured deposits [32–34]. Mine workings driven are destructed over time. In most workings, the roof is destroyed with formation of a vault of various configurations and sizes, Fig. 3.

Rock caving is caused by a significant span of exposure or results from the action of destructive compressive or tensile stresses.

As the radius of the vault curvature decreases, compressive stresses increase and tensile stresses decrease, and vice versa, when the radius of the vault curvature increases in the areas of the working contour, compressive stresses decrease, and tensile stresses increase.

For an arbitrary elementary site oriented at the angle β_{zx} in the ore massif adjacent to the open pit contour, normal σn and tangential τ stresses arise, which are determined by the formulas

$$\begin{cases} \sigma_{n_i} = \sigma_{z_i} \cos^2 \beta_{zx} + \sigma_{x_i} \sin^2 \beta_{zx} + \tau_{z_i x_i} \sin 2\beta_{zx}, \\ \tau_{zx} = 0{,}5\left(\sigma_{z_i} - \sigma_{x_i}\right) \sin 2\beta_{zx} - \tau_{z_i x_i} \cos 2\beta_{zx}. \end{cases} \quad (9)$$

Thus, the destructive pressure (weight of rocks) arising and acting on the contour of the working is determined by the expression

$$P_{b.w} = \pm \frac{P_t \sin\left(\alpha + \beta - 90\right)}{l}, \quad (10)$$

where $P_{b.w}$ is the destructive force acting on the contour of the working, MPa; P_t is the weight of the overlying rocks, H/m³; l is the arc length of the working vault contour, m.

On performing relevant transformations of (9) and after transition from the polar coordinate system to the rectangular one, and substituting the obtained values into (7), the formula of the boundary equilibrium on the contour of the workings is obtained, Fig. 4

$$\frac{P_t \sin 2\left(\alpha + \beta - 90\right)}{r^2} = \tau_0 + \gamma H \cos \beta tg\, \rho, \quad (11)$$

where β is the angle of displacement of rocks, degrees.

On multiplying the right and left parts of (11) by the square of the radius of the working and performing relevant transformations, the value of the maximum destructive force on the contour of the working is obtained which provides the boundary equilibrium

$$P_t = \frac{r^2 \tau_0 + r^2 \gamma H \cos \beta tg\, \rho}{\sin 2\left(\alpha + \beta - 90\right)}. \quad (12)$$

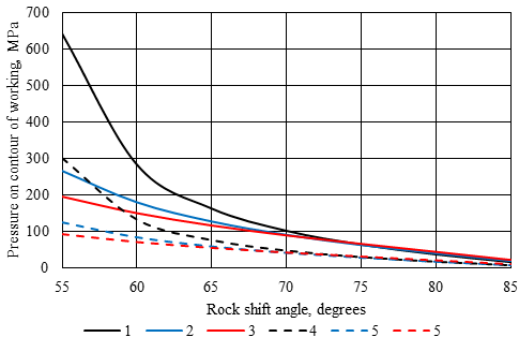

Fig. 7. Dependencies of the active load value on the contour of the working beyond the zone of the stoping operations impact on the angle of rock shift, the angle of the dip of the ore deposit and rocks: 1–3 – the working is in magnetite ores with the deposit dip of 40, 50 and 60 degrees respectively; 4–6 – the working is in schistous rocks with the deposit dip of 40, 50 and 60 degrees respectively

Rys. 7. Zależności wartości obciążenia czynnego od konturu wyrobiska poza strefą zatrzymania eksploatacji na kąt przesunięcia skały, kąt upadu złoża rudy i skał: 1–3 – wyrobisko jest w rudach magnetytu o spadku złoża odpowiednio 40, 50 i 60 stopni; 4–6 – wyrobisko w skałach łupkowych o nachyleniu złoża odpowiednio 40, 50 i 60 stopni

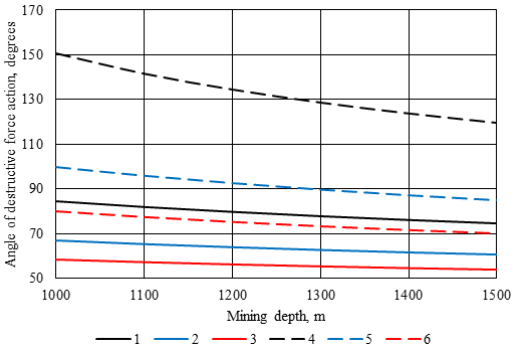

Fig. 8. Dependencies of the change in the angle of active pressure on the contour of the working on the mining depth, the radius of the vaulted part of the working and rocks: 1–3 – the working is in magnetite ores with the radius of the vaulted part 2, 3 and 4 m respectively; 4–6 – the working is in schstous rocks with the radius of the vaulted part 2, 3 and 4 m respectively

Rys. 8. Zależności zmiany kąta parcia czynnego od konturu wyrobiska na głębokości urabiania, promienia sklepionej części wyrobiska i skał: 1–3 – wyrobisko występuje w rudach magnetytu o promieniu części sklepionej odpowiednio 2, 3 i 4 m; 4–6 – wyrobisko w skałach łupkowych o promieniu części sklepionej odpowiednio 2, 3 i 4 m

On performing relevant transformations, the final equation of the destructive force acting on the contour of the working is obtained

$$P_{b.w} = \frac{r^2\tau_0 \sin\alpha + r^2\gamma H \sin\alpha \cos\beta tg\rho}{\sin 2(\alpha+\beta-90)}. \quad (13)$$

Based on (13), the dependencies of distribution of the destructive pressure on the contour of the working on the depth of mining, the angle of the ore deposit dip and the angle of shift of the hanging wall rocks are built, Fig. 5–7.

Fig. 5 shows that with an increase in the depth of mining operations, the pressure on the contour of the working increases. Thus, with an increase in the depth of mining from 1000 to 1500 m and a change in the radius of the vaulted part from 2 to 4 m, the pressure on the contour of the working increases from 39.8 to 233.3 MPa if the working is driven in magnetite ores. If the mine working is driven in schistous rocks, the pressure on its contour increases from 18.2 to 109.4 MPa. Comparing the obtained values enables the conclusion that if workings are located in schistous rocks, the pressure on their contour is almost 2 times smaller than in magnetite ores.

Thus, for conditions of Kryvyi Rih iron ore basin, it is reasonable to locate mine workings in waste rocks to reduce the cost of their maintenance and re-timbering.

Comparing the results of our study with those in [48] enables the conclusion that the pressure acting on the contour of the working does not depend on the radius of the vaulted part (curves 7 and 8). However, the nature of the pressure change calculated by (9) and proposed (13) is almost the same, which indicates reliability of the results.

It should be noted that the angle of the ore deposit dip significantly impacts the rock pressure around the mine working. Thus, the minimum magnetite ores pressure on the working acts at the angle of the ore deposit dip from 65 to 75 degrees, and if the working is located in schistous rocks – from 50 to 60 degrees.

Thus, depending on physical and mechanical properties of rocks at the same depth and angle of the ore deposit dip, the pressure on the mine working differs significantly for magnetite ores and schistous rocks.

As is seen from Fig. 7, with an increase in the angle of rock shift, the pressure on the contour of the mine working decreases significantly. Analysis of the graphs given reveals that if the shift of rocks exceeds 65–70 degrees, the pressure on the mine working contour stabilizes regardless of the ore deposit dip.

Thus, when designing a mining system or a scheme of opening, it is necessary to have a complete geological char-

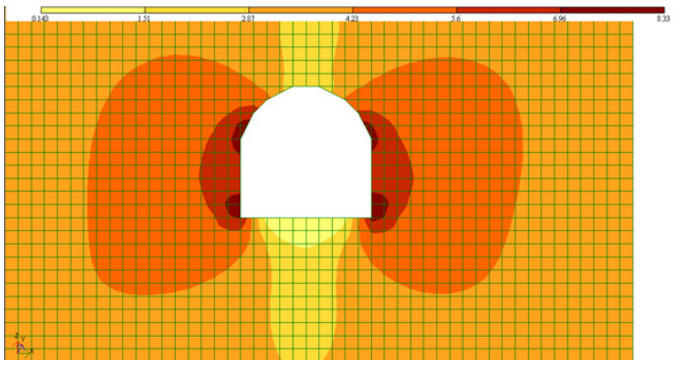

Fig. 9. Epures of equivalent stresses acting around the mine working

Rys. 9. Diagram naprężeń równoważnych działających wokół wyrobiska górniczego

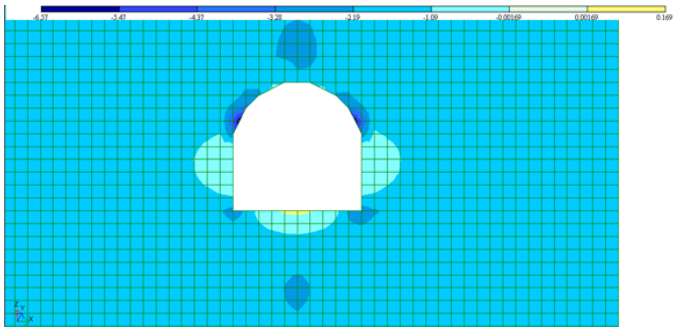

Fig. 10. Epures of vertical stresses according to Mohr theory acting around the mine working

Rys. 10. Diagram naprężeń pionowych według teorii Mohra, działające wokół wyrobiska górniczego

acteristic and physical and mechanical properties of rocks. Therefore, creation of underground mine workings in certain rocks enables reduction of costs for maintaining the workings during their life period.

If the destructive pressure determined by (13) is greater than the rock ultimate compressive strength (Table 2), the working is stable and subject to strains at the angle δ, Fig. 4.

Depending on physical and mechanical properties of rocks, the angle of action of the maximum stresses on the contour of the working is determined by the formula

$$\delta = \alpha r \cdot \cos \frac{r^2 \tau_0 + r^2 \gamma H \cos \beta tg\rho}{2[\sigma_{st}]}, \qquad (14)$$

where $[\sigma_{st}]$ is the rock ultimate compressive strength, MPa.

Based on (14), dependencies of the change in the angle of the destructive force action on the depth of mining, the radius of the working and physicomechanical properties of rocks are built.

Fig. 8 shows that with an increase in the depth of mining from 1000 to 1500 m, the angle of action of the destructive force that occurs on the contour of the working decreases from 150 to 54 degrees. With an increase in the radius of the working from 2 to 4 m for magnetite ores at the depth of 1300 m, the angle of destructive force action decreases from 78 to 55 degrees.

Thus, the angle at which the destructive force acts on the contour of the working depends on physical and mechanical properties of rocks, the radius of the vaulted part and the depth of mining.

The LIRA 9.4 software package is applied to confirm reliability of the proposed methods and determine the field of actual stresses around the vaulted mine working. To determine the stress-strain state of the rock massif, the finite element method is used which allows solving systems of equations with a large number of unknowns.

The above complex is also used to solve the issues of the stress-strain state: in a linear-elastic medium; within the framework of the nonlinear theory of elasticity and in the elastic-plastic formulation by step-by-step and step iteration methods with automatic selection of a load step. The results of calculating equivalent and vertical stresses at a mine working height of 5 m and the radius of the vaulted part of 3 m in the homogeneous rock massif of magnetite ores at the depth of 1350 m are shown in Fig. 9, 10.

The epures of equivalent and vertical stresses in Fig. 8, 9 show that the greatest stresses arise on the contour of the mine working in its vaulted part, and the angle of the destructive pressure action is 60 degrees.

Thus, modeling by the finite element method confirms reliability of the methods for determining the active zone of the destructive force on the working contour when mining iron ore deposits of Kryvyi Rih iron ore basin (see Fig. 8, curve 2).

The results of the present study prove that stability of mine workings depends on the acting stresses that occur in a multi-modular rock massif on the contour of the workings in their vaulted part. The angle of the maximum destructive force action act is determined. When designing, this will allow determining measures to increase stability of mine workings, as well as extend their life without additional operating costs.

CONCLUSIONS

As a result of the study conducted, it is established:

1. The contour of the horizontal working in a homogeneous and heterogeneous massif is impacted by a destructive

field of stresses around which a vault of stable equilibrium is formed. The contour of the working is affected by a destructive pressure at the angle of over 50 degrees.

2. When mining and geological conditions change, stability of mine workings can be provided if they are located in strong rocks, or in rocks with increased angles of their shift. This will reduce the destructive pressure on the contour of the mine working.

ACKNOWLEDGMENTS

The work was supported by the Ministry of Education and Science of Ukraine within the framework of the state scientific themes "Investigation and scientific and practical substantiation of technological means for raw material control in mining ores on deep levels" (State registration 0122U000843).

Literatura – References

1. Pysmennyi, S., Fedko, M., Chukharev, S., Rysbekov, K., Kyelgyenbai, K., & Anastasov, D. (2022). Technology for mining of complex-structured bodies of stable and unstable ores. IOP Conference Series: Earth and Environmental Science, 970(1), 012040. https://doi.org/10.1088/1755-1315/970/1/012040.
2. Pysmennyi, S., Chukharev, S., Khavalbolot, K., Bondar, I., & Ijilmaa, J. (2021). Enhancement of the technology of mining steep ore bodies applying the "floating" crown. E3S Web of Conferences, 280, 08013. https://doi.org/10.1051/e3sconf/202128008013.
3. Pysmennyi, S., Chukharev, S., Kyelgyenbai, K., Mutambo, V., & Matsui, A. (2022). Iron ore underground mining under the internal overburden dump at the PJSC "Northern GZK". IOP Conference Series: Earth and Environmental Science, 1049(1), 012008. https://doi.org/10.1088/1755-1315/1049/1/012008.
4. Sobczyk, W., Perny, K.C.I., Sobczyk, E.J. (2021). Assessing the Real Risk of Mining Industry Environmental Impact. Case Study. Inzynieria Mineralnathis, 1 (1), 33–41. https://doi.org/10.29227/IM-2021-01-05.
5. Radwanek-Bąk, B., Sobczyk, W., Sobczyk, E.J. (2020). Support for multiple criteria decisions for mineral deposits valorization and protection. Resources Policy, 68. 101795. https://doi.org/10.1016/j.resourpol.2020.101795.
6. Sobczyk, W. (2015). Sustainable development of Middle East region. Problemy Ekorozwoju – problems of sustainable Development, 10 (2), 51–62.
7. Stupnik, N.I., Kalinichenko, V.A., Fedko, M.B., & Mirchenko, Ye.G. (2013). Influence of rock massif stress-strain state on uranium ore breaking technology. Naukovyi Visnyk Natsionalnoho Hirnychoho Universytetu, 2, 11–16.
8. Stupnik, N., & Kalinichenko, V. (2012). Parameters of shear zone and methods of their conditions control at underground mining of steep-dipping iron ore deposits in Kryvyi Rig basin. Geomechanical Processes During Underground Mining - Proceedings of the School of Underground Mining, 15–17.
9. Stupnik, N.I., Kalinichenko, V.A., Fedko, M.B., & Mirchenko, Ye.G. 2013. Prospects of application of TNT-free explosives in ore deposites developed by udergound mining. Naukovyi Visnyk Natsionalnoho Hirnychoho Universytetu, 1, 44–48.
10. Petlovanyi, M., Lozynskyi, V., Zubko, S., Saik, P., & Sai, K. (2019). The infuence of geology and ore deposit occurrence conditions on dilution indicators of extracted reserves. Rudarsko Geolosko Naftni Zbornik, 34(1), 83-91. https://doi.org/10.17794/rgn.2019.1.8.
11. Bazaluk, O., Petlovanyi, M., Lozynskyi, V., Zubko, S., Sai, K., & Saik, P. (2021). Sustainable Underground Iron Ore Mining in Ukraine with Backfilling Worked-Out Area. Sustainability, 13(2), 834. https://doi.org/10.3390/su13020834.
12. Bazaluk, O., Petlovanyi, M., Zubko, S., Lozynskyi, V., & Sai, K. (2021). Instability Assessment of Hanging Wall Rocks during Underground Mining of Iron Ores. Minerals, 11(8), 858. https://doi.org10.3390/min11080858.
13. Galayev, N.Z. (1990). Upravleniye sostoyaniyem massiva gornykh porod pri podzemnoy razrabotke rudnykh mestorozhdeniy [Management of the state of the rock mass in the underground mining of ore deposits]. (Moscow: Nedra).
14. Stupnik, M.I., Kalinichenko, V.O., Fedko, M.B., & Kalinichenko, O.V. (2018). Investigation into crown stability at underground leaching of uranium ores. Naukovyi Visnyk Natsionalnoho Hirnychoho Universytetu, 6, 20–25.
15. Bazaluk, O., Rysbekov, K., Nurpeisova, M., Lozynskyi, V., Kyrgizbayeva, G., & Turumbetov, T. (2022). Integrated monitoring for the rock mass state during large-scale subsoil development. Frontiers in Environmental Science, 10, 852591. https://doi.org/10.3389/fenvs.2022.852591.
16. Stupnik, M., Kalinichenko, V., Fedko, M., Pysmennyi, S., Kalinichenko, O., & Pochtarev, A. (2022). Methodology enhancement for determining parameters of room systems when mining uranium ore in the SE "SkhidGZK" underground mines, Ukraine. Mining of Mineral Deposits, 16(2). 33–41. https://doi.org/10.33271/mining16.02.033.

17. Stupnik, M., & Kalinichenko, V. (2013). Magnetite quartzite mining is the future of Kryvyi Rig iron ore basin. Annual Scientific-Technical Colletion - Mining of Mineral Deposits 2013, 49–52

18. Lozynskyi, V., Medianyk, V., Saik, P., Rysbekov, K., & Demydov, M. (2020). Multivariance solutions for designing new levels of coal mines. Rudarsko Geolosko Naftni Zbornik, 35(2), 23-32. https://doi.org/10.17794/rgn.2020.2.3.

19. Stupnik, N.I., Fedko, M.B., Pismennyi, S.V., & Kolosov, V.A. (2014). Development of recommendations for choosing excavation support types and junctions for uranium mines of state-owned enterprise skhidhzk. Naukovyi Visnyk Natsionalnoho Hirnychoho Universytetu, 5, 21–25.

20. Lyashenko, V., Andreev, B., & Dudar, T. (2022). Substantiation of mining-technical and environmental safety of underground mining of complex-structure ore deposits. Mining of Mineral Deposits, 16(1), 43-51. https://doi.org/10.33271/mining16.01.043.

21. Issayeva, L., Togizov, K., Duczmal-Czernikiewicz, A., Kurmangazhina, M., & Muratkhanov, D. (2022). Ore-controlling factors as the basis for singling out the prospective areas within the Syrymbet rare-metal deposit, Northern Kazakhstan. Mining of Mineral Deposits, 16(2), 14-21. https://doi.org/10.33271/mining16.02.014.

22. Takhanov, D., Muratuly, B., Rashid, Z., & Kydrashov, A. (2021). Geomechanics substantiation of pillars development parameters in case of combined mining the contiguous steep ore bodies. Mining of Mineral Deposits, 15(1), 50-58. https://doi.org/10.33271/mining15.01.050.

23. Stupnik, M.I., Kalinichenko, O.V., & Kalinichenko, V.O. (2012). Economic evaluation of risks of possible geomechanical violations of original ground in the fields of mines of Kryvyi rih basin. Naukovyi Visnyk Natsionalnoho Hirnychoho Universytetu, 6, 126–130.

24. Malakhov, G.M. (1990). Upravleniye gornym davleniyem pri razrabotke rudnykh mestorozhdeniy Krivorozhskogo basseyna [Management of rock pressure in the development of ore deposits of the Krivoy Rog basin]. (Kyiv: Naukova dumka).

25. Pysmenniy, S., Shvager, N., Shepel, O. Kovbyk, K., & Dolgikh O. (2020). Development of resource-saving technology when mining ore bodies by blocks under rock pressure. E3S Web of Conferences, 166, 02006. https://doi.org/10.1051/e3sconf/202016602006.

26. Turchaninov, I.A., Iofis, M.A., & Kaspar'yan, Z.Z. (1989). Osnovy mekhaniki gornykh porod [Fundamentals of rock mechanics]. (Leningrad: Nedra).

27. Zorin, A.N., Kolesnikov, V.G., & Minayev, S.P. (1986). Upravleniye sostoyaniyem gornogo massiva. [Managing the state of the mountain range]. (Kyiv: Naukova dumka).

28. Morkun, V., & Morkun, N. (2018). Estimation of the crushed ore particles density in the pulp flow based on the dynamic effects of high-energy ultrasound. Archives of Acoustics, 43(1), 61–67.

29. Golik, V., Komashchenko, V., Morkun, V., & Zaalishvili, V. (2015). Enhancement of lost ore production efficiency by usage of canopies. Metallurgical and Mining Industry, 7(4), 325–329.

30. Morkun, V., Morkun, N., & Tron, V. (2015). Distributed control of ore beneficiation interrelated processes under parametric uncertainty. Metallurgical and Mining Industry, 8(7), 18–21.

31. Fedko, M.B., Muzyka, I.O., Pysmennyi, S.V. & Kalinichenko, O.V. (2019). Determination of drilling and blasting parameters considering the stress-strain state of rock ores. Naukovyi Visnyk Natsionalnoho Hirnychoho Universytetu, 1, 37–41. https://doi.org/10.29202/nvngu/2019-1/20.

32. Stupnik, M., Kalinichenko, V., Fedko, M., Kalinichenko, O., Pukhalskyi, V., & Kryvokhin, B. (2019). Investigation of the dust formation process when hoisting the uranium ores with a bucket. Mining of Mineral Deposits, 13(3), 96–103. https://doi.org/10.33271/mining13.03.096.

33. Golik, V., Komashchenko, V., Morkun, V., & Irina, G. (2015). Improving the effectiveness of explosive breaking on the bade of new methods of borehole charges initiation in quarries. Metallurgical and Mining Industry, 7(7), 383–387.

34. Kyelgyenbai K., Pysmennyi S., Chukharev S., Purev B., & Jambaa I. (2021). Modelling for degreasing the mining equipment downtime by optimizing blasting period at Erdenet surface mine. E3S Web of Conferences, (280), 08001. https://doi.org/10.1051/e3sconf/202128008001.

35. Stupnik, N.I., Fedko, M.B., Kolosov, V.A., & Pismennyy S.V. (2014). Razrabotka rekomendatsiy po vyboru tipa krepleniya gornykh vyrabotok i sopryazheniy v uslovii uranovykh shakht GP "VOSTGOK". Naukovyi Visnyk Natsionalnoho Hirnychoho Universytetu, 5, 21–25.

36. Kalinichenko, V., Dolgikh, O., Dolgikh, L., & Pysmennyi, S. (2020). Choosing a camera for mine surveying of mining enterprise facilities using unmanned aerial vehicles. Mining of Mineral Deposits, 14(4), 31-39. https://doi.org/10.33271/mining14.04.031.

37. Pysmennyi, S., Peremetchyk, A., Chukharev, S., Fedorenko, S., Anastasov, D., & Tomiczek, K. (2022). The mining and geometrical methodology for estimating of mineral deposits. IOP Conference Series: Earth and Environmental Science, 1049(1), 012029. https://doi.org/10.1088/1755-1315/1049/1/012029.

38. Kalinichenko, V., Dolgikh, O., & Dolgikh, L. (2019). Digital survey in studying open pit wall deformations. E3S Web of Conferences, 123, 01047.

39. Kalinichenko, O., Fedko, M., Kushnerov, I., & Hryshchenko, M. (2019). Muck drawing by inclined two-dimensional flow. E3S Web of Conferences, 123, 01015.

40. Stupnik, M.I., Kalinichenko, O.V., Kalinichenko, V.O. 2012. Technical and economic study of self-propelled machinery application expediency in mines of krivorozhsky bassin. Naukovyi Visnyk Natsionalnoho Hirnychoho Universytetu, 5, 39–42.

41. Panchenko, V., Sobko, B., Lotous, V., Vinivitin, D., & Shabatura, V. (2021). Openwork scheduling for steep-grade iron-ore deposits with the help of near-vertical layers. Mining of Mineral Deposits, 15(1), 87-95. https://doi.org/10.33271/mining15.01.087.

42. Zeylik, B., Arshamov, Y., Baratov, R., & Bekbotayeva, A. (2021). New technology for mineral deposits prediction to identify prospective areas in the Zhezkazgan ore region. Mining of Mineral Deposits, 15(2), 134-142. https://doi.org/10.33271/mining15.02.134.

43. Morkun, V., Morkun, N., & Tron, V. (2015). Distributed closed-loop control formation for technological line of iron ore raw materials beneficiation. Metallurgical and Mining Industry, 7(7), 16–19.

44. Stupnik, M., Kalinichenko, O., Kalinichenko, V., Pysmennyi, S. & Morhun, O. (2018). Choice and substantiation of stable crown shapes in deep-level iron ore mining. Mining of Mineral Deposits, 12(4), 56–62. https://doi.org/10.15407/mining12.04.056.

45. Stupnik, N., Kalinichenko, V., Pismennij, S. & Kalinichenko, E. (2015). Features of underlying levels opening at "ArsellorMittal Kryvyic Rih" underground mine. New Developments in Mining Engineering 2015: Theoretical and Practical Solutions of Mineral Resources Mining, 39–44.

46. Rysbekov, K., Bitimbayev, M., Akhmetkanov, D., Yelemessov, K., Barmenshinova, M., Toktarov, A., & Baskanbayeva, D. (2022). Substantiation of mining systems for steeply dipping low-thickness ore bodies with controlled continuous stope extraction. Mining of Mineral Deposits, 16(2), 64-72. https://doi.org/10.33271/mining16.02.064.

47. Stupnik, N.I., Fedko, M.B., Kolosov, V.A., & Pismennyy S.V. (2014). Development of recommendations for choosing excavation support types and junctions for uranium mines of state-owned enterprise skhidhzk. Naukovyi Visnyk Natsionalnoho Hirnychoho Universytetu, 5, 21–25.

48. Stupnik, M., Kalinichenko, V., Fedko, M., Pysmennyi, S., Kalinichenko, O., & Pochtarev, A. (2022). Methodology enhancement for determining parameters of room systems when mining uranium ore in the SE "SkhidGZK" underground mines, Ukraine. Mining of Mineral Deposits, 16(2). 33–41. https://doi.org/10.33271/mining16.02.033.

Badanie koncentracji naprężeń na konturze wyrobisk kopalni podziemnych

W kopalni Krzywy Róg występują złoża rudy o złożonej strukturze, wydobywane metodą podziemną z głębokości ponad 1000 m. Stosując systemy zawałowe eksploatuje się złoża bogatych rud żelaza o zawartości składników użytecznych powyżej 59%. Prowadzi to do znacznych zmian stanu naprężeń masywu skalnego. Podczas prac podziemnych wyrobiska kopalniane podlegają naprężeniom, a w niektórych przypadkach ulegają zniszczeniu. W efekcie przedsiębiorstwa stale podwyższają koszty eksploatacji wyrobisk górniczych, co niekorzystnie wpływa na koszty produkcji. Wyniki badań przemysłowych wskazują, że w większości przypadków wyrobiska zawodzą w swojej górnej części. Dostępne metody określania stanu skał wokół wyrobisk górniczych nie uwzględniają w pełni właściwości fizycznych i mechanicznych skał, w których znajduje się wyrobisko. Opracowana technika pozwala na określenie nie tylko ciśnienia destrukcyjnego działającego na wyrobiska, ale również kąta działania siły destrukcyjnej. Technika ta różni się od dostępnych tym, że uwzględnia nie tylko cechy górniczo-geologiczne złoża, ale także większość czynników właściwości fizykomechanicznych skał. Technika ta pozwala już na etapie projektowania na dobór racjonalnych miejsc prowadzenia wyrobisk górniczych, unikając w ten sposób znacznych dodatkowych kosztów ich utrzymania.

Słowa kluczowe: *naprężenie, praca, sklepienie równowagi stabilnej, ciśnienie, stabilność, wytrzymałość graniczna, skały*

Substantiating and Assessing the Stability of the Underground System Parameters for the Sawn Limestone Mining: Case Study of the Nova Odesa Deposit, Ukraine

Mykhailo PETLOVANYI[1], Pavlo SAIK[2], Vasyl LOZYNSKYI[3], Kateryna SAI[4], Oleksii CHERNIAIEV[5]

[1] Dnipro University of Technology; 19 Yavornytskoho Ave., Dnipro, Ukraine; https://orcid.org/0000-0002-8911-4973; email: petlyovanyi1986@gmail.com
[2] Dnipro University of Technology; 19 Yavornytskoho Ave., Dnipro, Ukraine; https://orcid.org/0000-0001-7758-1083; email: saik.nmu@gmail.com
[3] Dnipro University of Technology; 19 Yavornytskoho Ave., Dnipro, Ukraine; https://orcid.org/0000-0002-9657-0635; email: lvg.nmu@gmail.com
[4] Dnipro University of Technology; 19 Yavornytskoho Ave., Dnipro, Ukraine; https://orcid.org/0000-0003-1488-3230; email: kateryna.sai@gmail.com
[5] Dnipro University of Technology; 19 Yavornytskoho Ave., Dnipro, Ukraine; https://orcid.org/0000-0001-8288-4011; email: chernyaev.aleksey82@ukr.net

http://doi.org/10.29227/IM-2023-01-10

Submission date: 24-02-2023 | Review date: 23-03-2023

Abstract

Due to the russian federation aggression against Ukraine, the infrastructure of many settlements has undergone significant destruction, so in the post-war period, limestone can become a reliable and useful resource for its reconstruction. A significant number of limestone deposits in southern Ukraine are suitable for the production of wall (block) stone, but the geotechnical conditions of many mining sites require the use of an underground mining method. To study the mining system parameters of the Nova Odesa sawn limestone deposit, analytical and calculation methods are used based on known and proven hypotheses of stable spans and pillars, as well as verification by numerical modeling based on the finite element method in the SolidWorks software package. It has been determined that with a change in the ceiling thickness by 50% (from 0.8 to 1.2 m), the safe width of the chamber in the absence tensile stresses in the sawn limestone roof, under given mining-geological and mining-technical conditions of mining operations, increases by 22%. It has been revealed that the area of 25.0 m² corresponds to the required safety factor of the square-shaped supporting pillar. It has been shown by numerical modeling that under the conditions of the Nova Odesa deposit, the load on a 5×5 m supporting pillar will reach 26% of its load-bearing capacity, and the extraction chamber ceiling is in a stable state without the formation of tensile stresses. The research results are useful for substantiating and assessing the stability of the room-and-pillar mining system elements with supporting pillars in the underground mining of sawn limestone or other mineral deposits.

Keywords: *mine, sawn limestone, extraction chamber, supporting pillar, ceiling*

1. Introduction

The rapid growth of the world's population has led to a natural increase in resource consumption, where an important role is played by mining of various types of minerals. A wide range of minerals is used in metallurgy, electronics, information technology, medicine, military and space technology, agriculture, and in the construction industry, since intensive population growth requires the civil infrastructure development [1, 2]. Important types of building materials are wall blocks made of natural stone – limestones, volcanic tuff, chalk, marl, gaize and tripoli [3]. They are characterized by uniform composition, low hardness and are easily sprayed onto blocks for wall materials [4-6]. The use of limestone has become the most widespread in the world. It can be used in the form of lump limestone, crushed stone, artificial (sawn, wall) and crushed stone, facing slabs, mineral chips, crushed sand, mineral powder, mineral wool, and limestone powder [7].

Due to the russian federation aggression against Ukraine, the infrastructure of many settlements has undergone significant destruction, which will require reconstruction in the post-war period [8]. The strategic direction is to intensify the mining of building material deposits for the construction of new and reconstruction of destroyed industrial and civil infrastructure facilities [9]. An important building material will be limestone, which is a valuable in many countries around the world [10-12].

As of 2021, the balance limestone reserves in Ukraine, mined at 31 deposits, are estimated at 1.0 billion m³. Natural sawn limestones are widely distributed within the Black Sea Depression, the Volyn-Podilsky Plate, the Pre-Carpathian Depression, the Trans-Carpathian Trough, the Crimean Fold-Thrust Belt, the Donetsk Folded Structure, and the southwestern slope of the Ukrainian Shield [13]. Most of the limestone deposits in Ukraine are suitable for the production of wall stone. The sawn limestone is mostly mined by a surface method, but underground mining is also used. Mining processes are mechanized, and the rock is cut into large wall blocks and standard wall stone [14, 15]. The geotechnical conditions in

Fig. 1. Overview map of the Nova Odesa sawn limestone deposit location

Rys. 1. Mapa poglądowa lokalizacji złoża wapienia Nowa Odesa

Fig. 1. Overview map of the Nova Odesa sawn limestone deposit location

Rys. 1. Mapa poglądowa lokalizacji złoża wapienia Nowa Odesa

Depth of occurrence		Thickness, m	Lithology description
from	to		
0.0	0.3	0.3	Soil and vegetation layer
0.3	13.5	13.2	Clay is motley – yellowish-gray, greenish-gray, brownish-gray, viscous, sometimes sandy. In the range of 9.0-13.5 m, there is a clay-limestone stratum, in which limestone debris are bound by limestone-clay material.
13.5	14.5	1.0	Limestone is yellow, shell-detrital, sometimes detrital, lighter, yellowish-gray, destroyed, fractured.
14.5	24.0	9.5	Sawn limestone is of layered color: yellow-gray, light gray, sometimes brownish-yellow. The limestone composition is predominantly shell-detrital, slightly cavernous.
24.0	24.8	0.8	Limestone is gray, yellowish-gray, recrystallized, shell-detrital, strong.

which many deposits are mined require the use of an underground mining method, the accumulated experience of which is not enough today [16, 17].

The uniqueness of underground mining of sawn limestone deposits is in the fact that it is possible to achieve waste-free production cycle. Mined full-sized, non-full-sized wall stone and crushed stone will always be used in construction, and relatively cheap production waste, which sometimes reaches 50% of the mined rock mass, is a valuable carbonate raw material. This raw material is suitable for additives in a range of building materials, concrete, as a component of the solid backfill for the mined-out areas, feeding for animals and poultry, for soil deoxidation, etc. [18-21].

To date, various scientists in the world have conducted enough research to substantiate the rational and stable parameters for the chamber system and room-and-pillar system for mining various types of mineral deposits [22-26], that it becomes efficient and geometrically expedient to prepare the reserves of the mine field [27]. However, the issues of research into the optimal parameters of underground mining of sawn limestone deposits, which can ensure the rock mass stability for a long time of mining operations at the mine field, as well as create safe working conditions for underground workers, are not sufficiently covered.

The presented research is aimed at substantiating the rational and sustainable parameters of the underground mining of Nova Odesa sawn limestone deposit, which will additionally provide Ukraine with valuable mineral raw materials for the infrastructure reconstruction in the post-war period.

2. Study area

The sawn limestone deposit at the Nova Odesa site with an area of 27.8 ha is located on the southeastern outskirts of the city of Nova Odesa, Novoodeskyi administrative center, Mykolaiv Oblast. The minefield has the shape of a parallelogram, which is adjacent to (Fig. 1):

- in the west – at a distance of 1.0 km from the deposit, the Highway Ulyanivka-Mykolaiv was laid, and closer to the mine field, there is a depleted Novoodeske limestone deposit;
- in the north – the outskirts of the city of Nova Odesa;
- in the east – agricultural lands;
- in the southwest of the deposit, there is an old closed sawn limestone quarry;
- in the southeast – the Kashperivske limestone deposit (TOV Kashperivske Rodovische), which was mined by a quarrying method and is currently mothballed.

Geologically, the Nova Odesa deposit is located on the northern flank of the Black Sea Depression, and its structure involves Quaternary and Neogene sedimentary rocks. The sawn limestone minerals are confined to the coarse-layered stratum of the Upper Sarmatian. They constitute a continuous sheet-like deposit of nonuniform internal composition. Sawn limestones are confined, as a rule, to the middle and lower part of the deposit, with a thickness of 4.5 to 10.2 m, averaging 7.5 m. The deposit is not water-flooded. The piezometric level of the main aquifer lies below the Upper Sarmatian limestone stratum or is confined to its lower part. The thickness of the rocks that overlie the mineral varies from 14.2 to 35.0 m, averaging 20.0 m.

A preliminary geological and economic assessment of the limestone reserves at the Nova Odesa deposit became a prerequisite for choosing a method for its mining. This is conditioned by the significant thickness of overburden rocks from 14.5 m to 25.3 m. The absence of groundwater is also a favorable prerequisite for underground mining. They occur below the level of deposit mining.

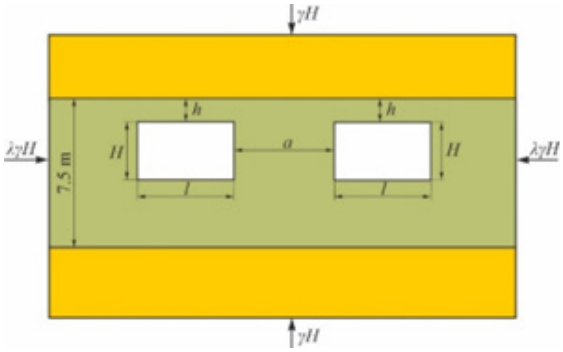

Fig. 2. Calculation schemes for modeling the stability of the chamber width and ceiling (a), as well as the supporting pillar (b): h – the ceiling height; l – the chamber width; H – the chamber height, a – the supporting pillar width

Rys. 2. Schematy obliczeniowe modelowania stateczności szerokości i stropu komory (a) oraz filaru nośnego (b): h – wysokość stropu; l – szerokość komory; H – wysokość komory, a – szerokość filaru nośnego

Tab. 2. Physical-mechanical rock mass properties

Tabela 2. Fizyczno-mechaniczne właściwości górotworu

Factor name	Limestone thickness
Elasticity modulus E, MPa	6000
Poisson's ratio, μ	0.3
Density γ, kg/m^3	1760
Compressive strength, σ_c, MPa	3.1
Tensile strength, σ_t, MPa	0.43

When conducting preliminary geological and economic assessment, 11 geological exploration wells have been drilled to a depth from 24.3 to 34.7 m. And during the initial experimental-industrial mining of the deposit, 184 meters of underground mine workings have been conducted. The stratigraphic section for one of the wells is presented in Table 1.

In the process of experimental-industrial mining, when tunnelling and conducting drifts in the sawn limestone body, the following fracture systems are noted: vertical and steep-dipping slightly inclined (90-70°) fractures, usually uneven, wavy with a strike azimuth of 330-350° with frequent small feathering fissures that penetrate the entire thickness of the limestone deposit. Perpendicular to these fractures, the fractures with a strike of 40-60° (vertical and inclined – 90-70°), uneven, wavy, are noted. The width of fractures varies from a few millimeters to 1.0-2.0 cm, rarely up to 7-8 cm (open fissure). In places of intersection of these fracture systems, there were also inrushes both along the walls of the mine workings and in the roof. However, the inrushes were of a local nature and did not affect the stability of the mine working ceiling. The output of marketable products – full-sized and non-full-sized wall stone is 31.75%, and together with crushed stone it is 50.95%, which indicates the influence of fracturing. The waste is 49.05%.

The technical and economic feasibility of the quality requirements has determined that, based on current limestone underground mining technologies, the maximum limestone thickness that can be mined in the first place is 3.0 m. The balance reserves of the deposit in B+C1 category, calculated and approved by the State Committee on Reserves for a mineral thickness of 3.0 m, within the limits of a special permit is 777.1 thousand m^3, and with an undetermined industrial value of C1 category – 1295.0 thousand m^3 (calculated for a thickness from 3.0 to 7.5 m).

The sawn limestones of the deposit are suitable for the wall stone production in accordance with the requirements of DSTU B V.2.7-246:2010 "Curbstones and wall stones from rocks". Based on the results of conducted physical-mechanical studies, the sawn limestones of the Nova Odesa deposit meet the requirements of the normative document in all parameters. To date, the development of geomechanically stable parameters of the sawn limestone underground mining system for this promising deposit remains a relevant issue, which is directly studied further.

3. Research methods

The experience of underground mining of sawn limestone deposits indicates the spread of the most optimal mining method – a chamber system with leaving square pillars, intended to support the overlying roof rocks [28, 29]. With this mining method, it is important to determine rational parameters, such as the chamber height, the chamber width, the ceiling thickness, and the size of the pillars [30-32]. The rock mass stability and the safety of mining operations depend on the determination of these rational parameters [33, 34].

3.1. Analytical Calculation Methods for Determining the Sawn Limestone Mining System Parameters

The extraction chamber height depends on the technological parameters of stone-cutting mining machines [35]. Therefore, to substantiate it, the existing mining equipment for the sawn limestone underground mining and the experience of its use, especially for deposits with similar mining-geological conditions, is studied. Analytical and calculation methods are used to determine the parameters of the sawn limestone underground mining:

- stable span (width) of the drift or chamber, which ensures the absence of tensile stresses in the roof, is determined based on the V.D. Slesarev calculation method [36, 37];
- stable parameters of inter-chamber supporting pillars in sawn limestone mines are determined based on the Turner – Shevyakov methods [38].

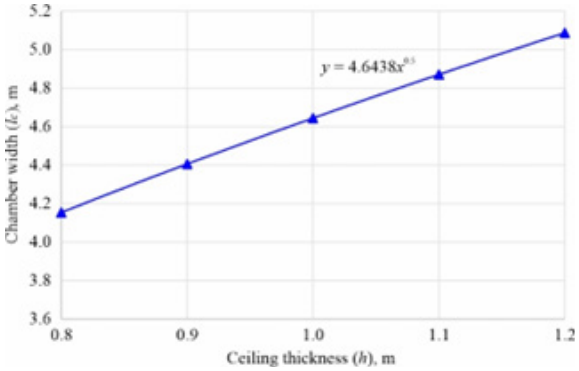

Fig. 3. The influence of the extraction chamber ceiling thickness on its width

Rys. 3. Wpływ grubości stropu komory na jej szerokość

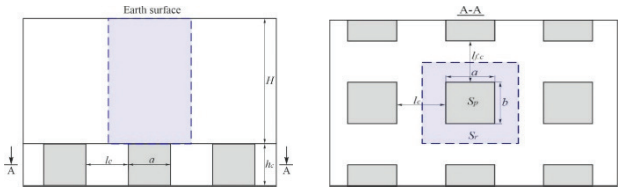

(a) (b)

Fig. 4. The scheme for determining the sizes of the supporting pillars: (a) – view in section; (b) – top view

Rys. 4. Schemat wyznaczania wymiarów podpór: (a) – widok w przekroju; (b) – widok z góry

The main parameters for determining the above-mentioned mining system elements are the density of overlying rocks from the earth's surface (t/m³), the sawn limestone material density (t/m³), the mining depth (m), the compressive strength of limestone (MPa), the tensile strength of limestone (MPa), and safety factor. Further, when performing analytical research, the actual and calculated mining-geological and mining-technical mining system parameters are substituted into the mathematical expressions of the system parameters for deposit mining in order to determine the stable mining system elements.

3.2. Numerical Modeling of the Stability of the Sawn Limestone Mining System Elements

It is intended to test the sawn limestone mining system parameters determined by analytical and calculation methods using numerical modeling based on the finite element method. Numerical modeling has been widely used for studying the state of geotechnical systems, adequately reflecting the development of geomechanical processes operating in the rock mass during mining operations [39-41]. The SolidWorks software package is used to assess the stability of the predetermined thickness of the ceiling and supporting pillars in the chamber system for the sawn limestone seam mining, which provides safe conditions for mining operations. The software product is designed to study the physical processes characterizing the stress-strain state of solid bodies [42, 43].

A rock mass area of 25x15 m is modelled, containing a sawn limestone layer, as well as laminated limestones in the roof and bottom. The geomechanical problem is solved in an elastic formulation, the obtained stress values are compared with the maximum permissible rock strength values. The maximum normal stress criterion, also known as the Mohr-Coulomb criterion, based on the maximum normal stress theory, is chosen as the failure criterion [44]. According to this theory, failures occur when the maximum principal load reaches the material's strength level. The criterion is used for brittle materials, which are limestones. It is believed that if the resulting stresses exceed the maximum permissible, the material is destroyed.

The calculation schemes for modeling the stability of the mining system parameters according to their analytical and calculation values are shown in Fig. 2.

Initial data for modeling: the average rock mass structure containing minerals according to geological sections in wells (a mineral of an average thickness 7.5 m – sawn limestone, the roof and bottom are laminated limestone); average mining depth is 27 m; the extraction chamber width is determined from analytical calculations (m); the supporting pillar width and length are determined from analytical calculations (m); the ceiling thickness is conditioned by the mining experience and analytical calculations (m); the value of the load applied to the model is 0.38 MPa (with an average overlying rock density of 1.8 t/m³). Physical-mechanical rock properties are presented in Table 2.

The main attention is paid to the stresses arising precisely in the sawn limestone mass when driving the extraction chambers, because the main mining system elements (the chamber width and height, the ceiling thickness, the supporting pillar parameters) are laid directly in the sawn limestone layer. Using the Simulation probing function in SolidWorks, it is possible to measure stresses at any point of a model. Particular attention is paid to the stressed state of the ceiling and the vertical wall of the supporting pillar.

4. Results and discussion

4.1. Substantiating the extraction chamber height

The sawn limestone deposit balance reserves in the amount of 770.0 thousand m³ have been calculated and approved for a mineral thickness of 3.0 m (with an average seam thickness of 7.5 m). Therefore, the sawn limestone mining

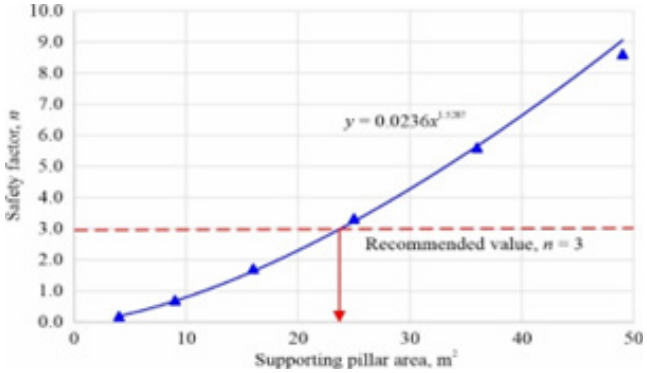

Fig. 5. Dependence of the change in the calculated safety factor of a square-shaped supporting pillar on its area

Rys. 5. Zależność zmiany obliczonego współczynnika bezpieczeństwa kwadratowego filara nośnego od jego powierzchni

is primarily assumed in one layer. According to the normative document NPAOP 0.00-1.77-16, from the condition of single-layer sawn stone mining, the face height should not exceed 3 m and should not be less than 2.2 m [45]. The extraction chamber height during single-layer mining is determined by the parameters of stone-cutting machines.

For cutting wall stone from a sawn limestone seam in the conditions of deposits within the former Soviet Union countries, stone-cutting machines of MKD-1, MKD-2 and KMAZ-188 types have been widely used [46]. When using a MKD-type stone-cutting machine, according to the technical specifications, the chamber height is no more than 2.6 m, with KMAZ-188 – 2.54-2.7 m.

In addition, the face height must be combined with an integer number of wall stone rows cut along the height of the chamber and, together with the thickness of the cuttings, must be a constant value, which will make it possible to cut a certain integer number of rows of stone with a standard height. The size of the wall stone from the sawn limestone seam, cut by the mentioned stone-cutting machines according to [47] is 390 mm×190 mm×188 mm, and the average cutting width of the working body is 27 mm. Thus, given the height of the cut wall stone, as well as the cutting width, 12 units of wall stone are cut along the extraction chamber height. In this case, the extraction chamber height will be 2.6 m. For the rational conducting of mining operations in the extraction chambers and face cuts, driven perpendicular to them with leaving the square-shaped supporting pillars, the same height of mine workings of 2.6 m is recommended for the operation with MKD-1 and KMAZ-188.

Further, with a detailed additional exploration of the deposit reserves with an uncertain commercial value of the C1 category, which is 1295.0 thousand m³, it is expedient to consider mining of the lower layer of the sawn limestone seam. In this case, when planning the mining of the lower layer, it is necessary to take into account the extraction chamber height of the upper layer, the height of ceiling left, and also the inter-horizon pillar. The total value of these parameters will make it possible to select the deposit areas where it is possible to use multilayer mining over the mine field area, because the seam thickness of the sawn limestone material ranges from 4.5 to 10.0 m.

4.2. Determining the width and thickness of the extraction chamber ceiling

The specificity of sawn stone underground mining, unlike other minerals, is in the fact that mining operations are planned in such a way as to obtain as many block products as possible from the mined rock mass. This is complicated by the increased sizes of the extraction chamber width, as a result of which the intensity of the rock pressure manifestation increases, and the rock mass is broken by fractures, both in the roof of the drift and on the surface of the mining face. Therefore, determining the rational size of the extraction chamber width by the geomechanical factor is of great importance.

The size of the extraction chamber width is significantly influenced by the strength properties and thickness of the ceiling left to ensure the chamber stability. If a strong and dense recrystallized limestone occurs above the sawn limestone seam, then the ceiling cannot be left, since a strong roof is a reliable ceiling. The presence of a strong roof reduces the loss of mineral resources.

Under the conditions of the Nova Odesa sawn limestone deposit, the roof of the sawn limestone seam is represented by slab limestone, shell-detrital, densely destroyed, fragmental, fractured, clayey, layered limestone with a thickness of 0.6-5.4 m. Given the slab limestone structure and its fracturing in the conditions of the deposit, it is recommended to leave the ceiling in the sawn limestone seam. The stable span (width) of the drift or extraction chamber of rectangular section, which ensures the absence of tensile stresses in the roof, is determined based on the V.D. Slesarev calculation method:

$$l_k = A\sqrt{\frac{R_t \cdot h}{\gamma_c \cdot n_s}}, \text{ m} \quad (1)$$

where A – a coefficient taking into account the manner in which the roof is clamped on the bearings (for an elastic beam);

h – the accepted ceiling thickness, m. The thickness of the ceiling left in the mine workings (h), given the operational experience of sawn limestone mines, ranges within 0.75-1.0 m, and in some cases 1. m – when conducting long-term capital workings.

R_p – the ultimate tensile strength of ceiling rocks parallel to bedding, t/m². The ultimate tensile strength of ceiling rocks is correlated with the ultimate compressive strength of limestone and is determined by the expression:

$$R_t = 0.1R_c + 0.12 = 0.42\ MPa \quad (2)$$

γ_c – unit specific gravity of ceiling rocks, t/m³. According to the data of laboratory tests, the average unit specific gravity value of the sawn limestone deposit is 1.76 t/m³.
R_c – the ultimate compressive strength of rocks, MPa. According to the data of laboratory tests, the average compressive strength value of the sawn limestone deposit is 3.1 MPa.
n_s – safety factor;

The safety factor is determined as follows:

$$n_s = n_1 \cdot n_2 \cdot n_3 \quad (3)$$

n_1 – a coefficient taking into account the range of variation when determining the average sample strength, is accepted within 1.3-1.6. According to the results of laboratory tests of 10 samples taken from the well core, the limestone compressive strength ranges within 2.2-4.1 MPa with an average value of 3.1 MPa. According to the analysis of the variation in the limestone strength indicators in the sample, $n_1 = 1.4$ is taken.
n_2 – a coefficient taking into account the structural mass weakening due to the presence of macro- and microfracturing, as well as the impact of the time factor, is accepted within 1.4-1.9. The coefficient value n_2 is mostly determined by the mining depth H. When H is up to 60-70 m, the n_2 value in the conditions of a fractured mass can be taken within 1.0-1.5, but with H more than 70 m, it is 1.5-2.0. Given the average mining depth of 30 m and limestone fracturing, $n_2 = 1.5$ is taken.
n_3 – a coefficient taking into account the decrease or increase in the chamber deflection compared to the design ones, as well as the presence of technological cuttings, is accepted within 1.0-1.1. It is taken $n_3 = 1.05$.

The calculated safety factor for the chamber makes 2.2 (according to formula 3).

In sawn limestone mines, the safety factor is in the range of 1.5-2.5. Typically, the safety factor is chosen in the range of 1.5-2.0, and in difficult mining-geological and mining-technical conditions – 2.5. Given the insignificant mining depth, water-free state of the deposit, a safety factor of 2.0 is finally accepted. In the analytical calculation according to expression (1), to determine the degree of influence of the ceiling thickness on the extraction chamber width, its value is varied with an increment of 0.8; 0.9; 1.0; 1.1 and 1.2 m, which is presented in Fig. 3.

Analysis of Fig. 3 shows that when the value of ceiling thickness is changed by 50% (from 0.8 to 1.2 m), the safe chamber width, at which there are no tensile stresses in the sawn limestone roof under given mining-geological and mining-technical conditions, increases by 22% according to the power-law dependence by the expression (1). The extraction chamber width, determined analytically in the range of 4.15-5.1 m, is a safe range and can be accepted for mining the Nova Odesa sawn limestone deposit with a single-layer mining of sawn limestone reserves.

Depending on the options for mining all the Nova Odesa deposit reserves, some peculiarities in determining the ceiling thickness are possible:

a) with an approved single-layer mining of the sawn limestone deposit reserves up to a certain seam mining height of 2.6 m (p. 4.1) and, taking into account variations in the sawn limestone seam thickness within 4.5-10 m, any ceiling thickness in the range of 0.8-1.2 m can be accepted, thus assuming a safe chamber width in the range of 4.15-4.5 m.

b) when considering in perspective multilayer mining of sawn limestone deposit reserves, the ceiling thickness (interlayer pillar) and, accordingly, the width of the chambers can vary within each mining layer, while observing safety in order to achieve the maximum mining of its reserves through its entire thickness, which varies in the range of 4.5-10 m.

Since the balance Nova Odesa deposit reserves are approved for a thickness of 3.0 m, their actual mining will be conducted with a single-layer mining. According to Fig. 3, it is recommended to take a width of 4.4 m with a ceiling thickness of 0.9 m. Similar to the extraction chamber height, its width should also be combined with an integer number of cut rows of wall stone and, together with the thickness of the cuttings, make a constant value that will allow cutting a certain integer number of stone rows of a standard height. With the wall stone size of 390 mm×190 mm×188 mm, which is cut by an average cutting width of the working body of 27 mm, the extraction chamber width of 4.4 m, determined by the analytical and calculation method, allows cutting 21 rows from the stoping face. Finally, the extraction chamber is selected and corrected in the mine in such a way as to ensure safe conditions for mining operations without the use of mine working support or its use should be minimal.

4.3. Determining the size of supporting pillars to support the overlying rock stratum

In underground limestone mining, in order to prevent collapse and rapid overlying roof subsidence, the issue of determining the rational sizes of the supporting pillars is especially relevant. In the case of a chamber system for mining the saw limestone, the use of square-shaped supporting pillars left to support roof rocks has become widespread.

To prevent collapses and rapid roof rock subsidence, the rational choice of the sizes of inter-chamber supporting pillars is of current importance. The supporting pillars must provide sufficient resistance to the overlying rock stratum pressure and must not be excessively strong, which usually leads to significant losses of the mineral in the subsoil. The sufficient size of supporting pillars depends on the physical-mechanical properties of sawn limestone and rock stratum, as well as the mining depth. The square shape of a supporting pillar is formed when, after the advance of extraction chambers, face cuts are driven perpendicular to them for mining inter-pillar sawn limestone reserves. It is recommended to take the face cut width (lf.c) and the ceiling thickness, similar to the extraction chamber, 4.4 m and, respectively, not less than 0.9 m.

To determine the parameters of the supporting pillars in sawn limestone mines, the Turner – Shevyakov method is the most optimal. The calculation scheme for determining the size of supporting pillars in the conditions of the Nova Odesa sawn limestone deposit is shown in Fig. 4.

The basic calculation equation, under the condition of stable rock equilibrium for a deposit with a flat occurrence of a sawn limestone seam, should have the following form:

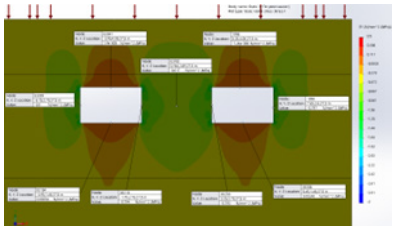

Fig. 6. Curve of vertical (SY) stress distribution in a rock mass
Rys. 6. Krzywa rozkładu naprężeń pionowych (SY) w górotworze

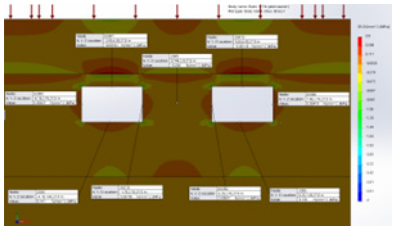

Fig. 7. Curve of horizontal (SX) stress distribution in a rock mass
Rys. 7. Krzywa rozkładu naprężeń poziomych (SX) w górotworze

$$\frac{k_e \cdot \gamma_l \cdot H \cdot S_r}{S_p} + \gamma_o \cdot h = \frac{R_c \cdot k_s}{n_s} \quad (4)$$

Where k_e – a coefficient taking into account the influence of the size of the extraction site and the mining depth on the average load value applied to the inter-chamber pillars. It has been statistically determined that at L/H ≥ 1, a load is formed on the supporting pillars from the full mass of the overlying rock to the earth's surface. At L/H > 1, ke = 1.
γ_l – unit specific gravity of sawn limestone, t/m³ (p. 4.3);
H – distance from the daylight surface to the chamber roof (mining depth), m (p. 4.3);
S_r – the area of the roof rocks per a pillar, m²;
γ_o – unit specific gravity of overlying rocks, t/m³. The arithmetic mean value of the overlying stratum rocks is γ_o = 1.8 t/m³;
R_c – the ultimate compressive strength of rocks, MPa (p. 4.3).

Due to the fact that the output of wall stone during experimental-industrial mining is less than 60%, it is necessary to take into account the mass fracturing, which is average. The mass structural weakening factor of 0.5 is taken.
k_s – shape factor taking into account the change in the strength of the rocks that constitute a pillar at different values of the ratio of the pillar height to its width. It is determined from the expression $k_s = \sqrt{a/h}$, where a – a pillar width, m; h – a pillar height, m.
S_p – horizontal sectional area of a pillar, m²;

If, according to the calculation scheme (Fig. 4), the chamber width is taken as l (equal to 4.4 m), the pillar width is – a, and the length is b, then for square pillars the Turner – Shevyakov equation takes the form:

$$\frac{k_e \cdot \gamma \cdot H \cdot (l+a) \cdot (l+b)}{ab} + \gamma_1 \cdot h \le \frac{R_c \cdot k_s}{n_s} \quad (5)$$

Analytical research on determining the size of the supporting pillar is performed as follows. Based on expression (5), the calculated value of the safety factor (ns) is determined:

$$n_s = \frac{R_c \cdot (a/h)^2}{\frac{\gamma \cdot H \cdot (l+a) \cdot (l+b)}{ab} + \gamma_1 \cdot h} \quad (6)$$

Further, in expression (6), the sizes of the square-shaped supporting pillar (a×b) are varied with the following increments: 2×2; 3×3; 4×4; 5×5; 6×6; and 7×7 m. Based on the result of the analytical research (6), the dependence of the safety factor on the supporting pillar area is determined. The rational area and the supporting pillar size are selected from the conditions of its compliance with the safety factor. The safety factor of the pillar is taken equal to 3-5 if the chamber is maintained for an indefinite time and 2-3 if the chamber is maintained only for the duration of mining operations. Under the conditions of the Nova Odesa deposit, long-term maintenance of pillars is supposed to support the overlying rock stratum as mining operations develop within the area of the deposit's mining field. The results of analytical calculations are presented in Fig. 5.

Analysis of Fig. 5 indicates that the safety factor of the supporting pillar for mining-geological and mining-technical conditions of the Nova Odesa sawn limestone deposit development has a power-law dependence on its area. Due to the fact that mining operations will be developed deep into the deposit over the area of the mine field and with a long time of mining the reserves, the safety factor of the supporting pillars should be at least 3.0. According to the dependence, a safety factor of 3.0 corresponds to the supporting pillar area of 24.0 m². With a square shape of the supporting pillar, its width and length are 4.9 m². It is recommended to take an integer value of the width and length of the supporting pillar 5×5.

4.4. The numerical modeling results of stability of mining system elements

Numerical modeling based on the finite element method is used to verify the results of analytical research on the stability of the chamber system elements for mining with square-shaped supporting pillars. The model consists of a sawn limestone layer of 7.5 m, laminated limestone of 4.0 m thick in the roof and bottom. The model includes chambers 4.4 m wide

and 2.6 m high, as well as 5 m wide square-shaped supporting pillar with a ceiling thickness of 0.9 m. The results of modeling with obtaining curves of vertical SY and horizontal SX stresses are shown in Figs. 6 and 7.

An analysis of the vertical stress distribution curve (Fig. 6) shows that the vertical stress component forms areas of too weak stresses in the chamber ceiling that are almost equal to 0. A similar situation is in the extraction chamber bottom, where too weak tensile stresses reach 0.002 MPa. A de-stressing zone is formed in the roof and bottom of the chamber. In the extraction chamber corners, regular compressive stress concentrations up to 1.0 MPa are observed. Given the sawn limestone ultimate tensile strength of 0.42 MPa, the accepted extraction chamber ceiling thickness (0.9 m) will be in a stable state when exposed to the vertical component of rock pressure.

In the extraction chamber sides (supporting pillar mass), zones of compressive stresses are formed with values of 0.8 MPa, which does not exceed the limestone ultimate compressive strength, the value of which is 3.1 MPa. The supporting pillar is in a stable state and its loading is 26%. In the supporting pillar center, the loads are up to 0.6 MPa.

An analysis of the horizontal stress distribution curve (Fig. 7) shows that in the chambers ceiling the stress areas are close to 0 MPa. Stresses of 0.14 MPa are formed in the extraction chamber bottom. Given the sawn limestone ultimate tensile strength of 0.43 MPa, the accepted ceiling thickness (0.9 m) and the bottom of the extraction chamber will be in a stable state under the action of horizontal stresses. In the extraction chamber sides (supporting pillar mass), zones of superweak tensile stresses are formed with values close to 0. It should be noted that in the roof, in the laminated limestone layer, at the contact with the sawn limestone seam, zones of tensile stresses of 0.45 MPa appear, and in sawn limestone, compressive stresses of 0.7 MPa occur. The tensile stresses in laminated limestone reach the ultimate tensile strength of limestone, which over time will lead to fracturing and destruction. However, this phenomenon does not pose a threat, because the limestone mass is destroyed in the mass depth behind the ceiling. Analysis of curves (Figs. 6, 7) indicates that the most stressed element of the mining system due to the action of vertical stresses is the supporting pillar. If the resulting stresses do not exceed the rock ultimate strength, then there will be almost no displacements and deformations, and the chamber contour destruction will not be observed.

It should be noted that there is a sufficient convergence of analytical research and numerical modeling, because their results indicate the absence of tensile stresses in the chamber ceiling and a sufficient safety factor of the supporting pillar. Based on this, the adopted mining system parameters, namely, the extraction chamber width is 4.4 m, the extraction chamber height is 2.6 m, the ceiling thickness is 0.9 m, and the supporting pillar size is 5x5 m will ensure the rock mass stability and the safety of mining operations. Determining the mining system rational parameters makes it possible to further develop a scheme for mining and preparing the Nova Odesa deposit mine field.

5. Conclusion

As a result of research on the substantiation and assessment of the stability of the elements of the sawn limestone underground mining system, the following results have been determined using the example of a specific promising deposit:

1. The peculiarities of mining-geological and mining-technical conditions for mining a promising Nova Odesa sawn limestone deposit have been generalized and analyzed. It is noted that the balance reserves have been approved for the primary mining of a limestone layer of 3.0 m with a thickness variation of 4.5-10 m through the deposit, which indicates the prospects of multilayer mining in the future. A deposit is of flat occurence, water-free, with a developed mineral fracturing system, which is suitable for wall stone production.
2. It is proposed to use a combined scientific and methodological approach together with analytical and calculation research to substantiate and assess the stability of the sawn limestone mining system elements on the basis of known and proven hypotheses for the stability of spans and pillars with substantiation of all constituent elements and verification by numerical modeling based on the finite element method.
3. The rational value of the extraction chamber height (2.6 m) is substantiated, influenced by the permissible parameters of single-layer limestone seam mining, the technological parameters of stone-cutting machines and the need to observe the integer number of wall stone rows cut along the height of the chamber.
4. It has been analytically determined that when the ceiling thickness value is changed by 50% (from 0.8 to 1.2 m), the safe chamber width, at which there are no tensile stresses in the sawn limestone roof under given mining-geological conditions, increases by 22%. The rational value of the chamber width and ceiling (4.4 and 0.9 m respectively) has been substantiated.
5. It has been analytically determined that the safety factor of the supporting pillar for mining-geological and mining-technical conditions of the Nova Odesa sawn limestone deposit development has a power-law dependence on its area. It has been determined that the required safety factor of a square-shaped supporting pillar corresponds to an area of about 25.0 m², and the value of the width and length of the pillar will be 5×5 m.
6. It has been found by numerical modeling that under the conditions of the Nova Odesa deposit, the load on a 5×5 m supporting pillar will reach 26% of its load-bearing capacity, and the extraction chamber ceiling is in a stable state without the formation of tensile stresses.

Acknowledgements

The work was done within the framework of General State Program Development of the Mineral and Raw Material Base of Ukraine for the Period Until 2030 (approved by the Verkhovna Rada of Ukraine, dated 21 April 2011 No. 3268-VI) to provide the leading sectors of the economy with their own building materials.

Literatura – References

1. Henckens, T. (2021). Scarce mineral resources: Extraction, consumption and limits of sustainability. Resources, Conservation and Recycling, 169, 105511. https://doi.org/10.1016/j.resconrec.2021.105511
2. Nassani, A.A., Aldakhil, A.M., & Zaman, K. (2021). Ecological footprints jeopardy for mineral resource extraction: Efficient use of energy, financial development and insurance services to conserve natural resources. Resources Policy, 74, 102271. https://doi.org/10.1016/j.resourpol.2021.102271
3. Bitimbayev, M.Zh., Rysbekov, K.B., Akhmetkanov, D.K., Kunayev, M.S., & Elemesov, K.K. (2022). The role and importance of chemical elements clarks in the practical expanded reproduction of mineral resources. Engineering Journal of Satbayev University, 1(144), 47-54. https://doi.org/10.51301/ejsu.2022.i1.08
4. Christmann, P. (2017). Towards a More Equitable Use of Mineral Resources. Natural Resources Research, 27(2), 159-177. https://doi.org/10.1007/s11053-017-9343-6
5. Mineral resource governance for sustainable development. (2020). Mineral Resource Governance in the 21st Century. https://doi.org/10.18356/5db747b4-en
6. Markevych, K., Maistro, S., Koval, V., & Paliukh, V. (2022). Mining sustainability and circular economy in the context of economic security in Ukraine. Mining of Mineral Deposits, 16(1), 101-113. https://doi.org/10.33271/mining16.01.101
7. Carran, D., Hughes, J., Leslie, A., & Kennedy, C. (2012). A short history of the use of lime as a building material beyond Europe and North America. International Journal of Architectural Heritage, 6(2), 117-146. https://doi.org/10.1080/15583058.2010.511694
8. Brenner, J. (2022). Some ideas for a post-war recovery of Ukrainian cities. Urban Research & Practice, 1-7. https://doi.org/10.1080/17535069.2022.2097646
9. Bergmann, J., & Romanyshyn, I. (2022). Rebuilding Ukraine: How the EU should support Ukraine's reconstruction and recovery (No. 6/2022). IDOS Policy Brief, -1-12. https://doi.org/10.23661/ipb6.2022
10. Gul, E. (2022). Mineral extraction and processing industries: Do they have socioeconomic benefits in a developing country scenario?. Mining of Mineral Deposits, 16(1), 32-42. https://doi.org/10.33271/mining16.01.032
11. Nurlybayev, R.E., Zhuginisov, M.T., Zhumadilova, Z.O., Orynbekov , Y.S., Khamza, E.E., & Sangulova, I.B. (2021). Investigation of the effect of diatomite and bentonite clays on the properties of local loam-based products. Engineering Journal of Satbayev University, 143(4), 180-195. https://doi.org/10.51301/vest.su.2021.i4.23
12. Chang, Z., Long, G., Xie, Y., & Zhou, J. L. (2022). Recycling sewage sludge ash and limestone for sustainable cementitious material production. Journal of Building Engineering, 49, 104035. https://doi.org/10.1016/j.jobe.2022.104035
13. Mineralni resursy Ukrainy. (2020). Shchorichnyk, Derzhavne naukovo-vyrobnyche pidpryiemstvo «Derzhavnyi informatsiinyi heolohichnyi fond Ukrainy», Kyiv, 270.
14. Peryt, T.M., Durakiewicz, T., Peryt, D., & Poberezhsky, A. (2012). Carbon and oxygen isotopic composition of the Middle Miocene Badenian gypsum-associated limestones of West Ukraine. Geologica Acta, 10(4), 319-332. https://doi.org/10.1344/105.000001753.
15. Trach, Y., Trach, R., Kalenik, M., Koda, E., & Podlasek, A. (2021). A Study of Dispersed, Thermally Activated Limestone from Ukraine for the Safe Liming of Water Using ANN Models. Energies, 14(24), 8377. https://doi.org/10.3390/en14248377
16. Rysbekov, K., Bitimbayev, M., Akhmetkanov, D., Yelemessov, K., Barmenshinova, M., Toktarov, A., & Baskanbayeva, D. (2022). Substantiation of mining systems for steeply dipping low-thickness ore bodies with controlled continuous stope extraction. Mining of Mineral Deposits, 16(2), 64-72. https://doi.org/10.33271/mining16.02.064
17. Rahimi, B., Sharifzadeh, M., & Feng, X. T. (2021). A comprehensive underground excavation design (CUED) methodology for geotechnical engineering design of deep underground mining and tunneling. International Journal of Rock Mechanics and Mining Sciences, 143, 104684. https://doi.org/10.1016/j.ijrmms.2021.104684
18. Rana, A., Kalla, P., & Csetenyi, L.J. (2016). Recycling of dimension limestone industry waste in concrete. International Journal of Mining, Reclamation and Environment, 31(4), 231-250. https://doi.org/10.1080/17480930.2016.1138571
19. Petlovanyi, M.V, Zubko, S.A, Popovych, V.V, & Sai, K.S. (2020). Physicochemical mechanism of structure formation and strengthening in the backfill massif when filling underground cavities Voprosy Khimii Khimicheskoi Tekhnologii, 6, 142-150 https://doi.org/10.32434/0321-4095-2020-133-6-142-150
20. Panesar, D.K., & Zhang, R. (2020). Performance comparison of cement replacing materials in concrete: Limestone fillers and supplementary cementing materials – A review. Construction and Building Materials, 251, 118866. https://doi.org/10.1016/j.conbuildmat.2020.118866

21. Doina-Cezara, A. (2021). Use of Limestone Blocks in Constructions in the Republic of Moldova. Bulletin of the Polytechnic Institute of Iași. Construction. Architecture Section, 67(1), 47–56. https://doi.org/10.2478/bipca-2021-0004

22. Pysmennyi, S., Fedko, M., Chukharev, S., Rysbekov, K., Kyelgyenbai, K., & Anastasov, D. (2022). Technology for mining of complex-structured bodies of stable and unstable ores. IOP Conference Series: Earth and Environmental Science, 970(1), 012040. https://doi.org/10.1088/1755-1315/970/1/012040

23. Bazaluk, O., Petlovanyi, M., Zubko, S., Lozynskyi, V., & Sai, K. (2021). Instability Assessment of Hanging Wall Rocks during Underground Mining of Iron Ores. Minerals, 11(8), 858. https://doi.org/10.3390/min11080858

24. Ghazdali, O., Moustadraf, J., Tagma, T., Alabjah, B., & Amraoui, F. (2021). Study and evaluation of the stability of underground mining method used in shallow-dip vein deposits hosted in poor quality rock. Mining of Mineral Deposits, 15(3), 31-38. https://doi.org/10.33271/mining15.03.031

25. Iannacchione, A., Miller, T., Esterhuizen, G., Slaker, B., Murphy, M., Cope, N., & Thayer, S. (2020). Evaluation of stress-control layout at the Subtropolis Mine, Petersburg, Ohio. International Journal of Mining Science and Technology, 30(1), 77-83. https://doi.org/10.1016/j.ijmst.2019.12.009

26. Petlovanyi, M, Medianyk, V., Sai, K., Malashkevych, D., & Popovych, V. (2021). Geomechanical substantiation of the parameters for coal auger mining in the protecting pillars of mine workings during thin seams development. ARPN Journal of Engineering and Applied Sciences, 16(15), 1572-1582

27. Pysmennyi, S., Peremetchyk, A., Chukharev, S., Fedorenko, S., Anastasov, D., & Tomiczek, K. (2022). The mining and geometrical methodology for estimating of mineral deposits. IOP Conference Series: Earth and Environmental Science, 1049(1), 012029. https://doi.org/10.1088/1755-1315/1049/1/012029

28. Kun, M. (2014). Evaluation and applications of empirical approaches and numerical modeling of an underground limestone quarry with room and pillar design. Journal of Mining Science, 50(1), 126-136. https://doi.org/10.1134/s1062739114010189

29. Esterhuizen, G. S., Dolinar, D. R., & Ellenberger, J. L. (2008). Assessment of Stable and Failed Pillars in Underground Limestone Mines. Mining Engineering, 61(11), 43-48.

30. Uteshov, Y., Galiyev, D., Galiyev, S., Rysbekov, K., & Nauryzbayeva, D. (2021). Potential for increasing the efficiency of design processes for mining the solid mineral deposits based on digitalization and advanced analytics. Rozrobka Rodovyshch, 15(2), 102-110. https://doi.org/10.33271/mining15.02.102

31. Ulanova, N., Sdvyzhkova, O., & Prikhodko, V. (2014). Optimization of room-and-pillar method parameters under conditions of limestone rocks. Progressive Technologies of Coal, Coalbed Methane, and Ores Mining, 511-516. https://doi.org/10.1201/b17547-86

32. El-Latif, A., Mohamed, Y., Awad, T., & Aly, R. (2022). Influence of Swelling on Shear Strength of Shale-Limestone Interface. Rudarsko Geolosko Naftni Zbornik, 37(5), 75-82. https://doi.org/10.17794/rgn.2022.5.7

33. Sakhno, I., Liashok, Ia., Sakhno, S., & Isaienkov, O. (2022). Method for controlling the floor heave in mine roadways of underground coal mines. Mining of Mineral Deposits, 16(4), 1-10. https://doi.org/10.33271/mining16.04.001

34. Pysmenniy, S., Shvager, N., Shepel, O. Kovbyk, K., & Dolgikh O. (2020). Development of resource-saving technology when mining ore bodies by blocks under rock pressure. E3S Web of Conferences, (166), 02006. https://doi.org/10.1051/e3sconf/202016602006

35. Shaffiee Haghshenas, S., Mikaeil, R., Esmaeilzadeh, A., Careddu, N., & Ataei, M. (2022). Statistical Study to Evaluate Performance of Cutting Machine in Dimension Stone Cutting Process. Journal of Mining and Environment, 13(1), 53-67. https://doi.org/10.22044/jme.2022.11362.2118

36. Demchenko, I.I., & Spivakov, F.P. (1982). Povyshenie effektivnosti i bezopasnosti podzemnoy razrabotki pilnykh izvestnyakov. Moldovenyaske, 192.

37. Mikhaylov, Yu.I., Spivakov, F.P., & Yakubets, A.A. (1986). Tekhnologiya i mekhanizatsiya dobychi pilnogo kamnya podzemnym sposobom. Nedra, 167.

38. Ulanova, N., Sdvyzhkova & V. Prikhodko. Optimization of room-and-pillar method parameters under conditions of limestone rocks. (2014). Progressive Technologies of Coal, Coalbed Methane, and Ores Mining, 523-528. https://doi.org/10.1201/b17547-86

39. Kumar, A., Kumar, R., Singh, A.K., Ram, S., Singh, P.K., & Singh, R. (2017). Numerical modelling-based pillar strength estimation for an increased height of extraction. Arabian Journal of Geosciences, 10(18), 411. https://doi.org/10.1007/s12517-017-3179-6

40. Smoliński, A., Malashkevych, D., Petlovanyi, M., Rysbekov, K., Lozynskyi, V., & Sai, K. (2022). Research into Impact of Leaving Waste Rocks in the Mined-Out Space on the Geomechanical State of the Rock Mass Surrounding the Longwall Face. Energies, 15(24), 9522. https://doi.org/10.3390/en15249522

41. Takhanov, D., Muratuly, B., Rashid, Z., & Kydrashov, A. (2021). Geomechanics substantiation of pillars development parameters in case of combined mining the contiguous steep ore bodies. Mining of Mineral Deposits, 15(1), 50-58. https://doi.org/10.33271/mining15.01.050

42. Pivnyak, G., Bondarenko, V., & Kovalevska, I. (2015). New developments in mining engineering 2015: Theoretical and practical solutions of mineral resources mining, 607. https://doi.org/10.1201/b19901

43. Dychkovskyi, R., Shavarskyi, Ia., Saik, P., Lozynskyi, V., Falshtynskyi, V., & Cabana, E. (2020). Research into stress-strain state of the rock mass condition in the process of the operation of double-unit longwalls. Mining of Mineral Deposits, 14(2), 85-94. https://doi.org/10.33271/mining14.02.085

44. Labuz, J.F., & Zang, A. (2012). Mohr-Coulomb failure criterion. Rock mechanics and rock engineering, 45, 975-979. https://doi.org/10.1007/s00603-012-0281-7

45. NPAOP 0.00-1.01-85. (1985). Iedyni pravyla okhorony nadr pry rozrobtsi rodovyshch tverdykh korysnykh kopalyn.

46. Spyvakov, F.P. (1980). Mekhanyzatsyia rabot na yzvestniakovykh shakhtakh. Kyshynev: Kartia Moldoveniaske, 91.

47. DSTU B V.2.7-246:2010. (2010). Budivelni materialy. Kameni bortovi i stinovi z hirskykh porid. Tekhnichni umovy.

Uzasadnianie i ocena stabilności parametrów systemu podziemnego dla wydobycia wapienia: studium przypadku złoża Nowa Odesa, Ukraina

W wyniku agresji federacji rosyjskiej na Ukrainę infrastruktura wielu osiedli uległa znacznemu zniszczeniu, dlatego w okresie powojennym wapień może stać się niezawodnym i użytecznym surowcem do jej odbudowy. Znaczna liczba złóż wapienia na południowej Ukrainie nadaje się do produkcji kamienia ściennego (blokowego), jednak warunki geotechniczne wielu miejsc wydobywczych wymagają zastosowania metody urabiania podziemnego. Do badania parametrów systemu wydobywczego złoża wapienia Nowa Odessa stosowane są metody analityczne i obliczeniowe oparte na znanych i sprawdzonych hipotezach stabilnych przęseł i filarów oraz weryfikacja poprzez modelowanie numeryczne w oparciu o metodę elementów skończonych w pakiecie oprogramowania SolidWorks. Stwierdzono, że przy zmianie grubości stropu o 50% (z 0,8 na 1,2 m) bezpieczna szerokość komory przy braku naprężeń rozciągających w stropie, w danych warunkach górniczo-geologicznych i górniczo-technicznych działalności wydobywczej wzrasta o 22%. Stwierdzono, że powierzchnia 25,0 m² odpowiada wymaganemu współczynnikowi bezpieczeństwa kwadratowego słupa nośnego. Modelowanie numeryczne wykazało, że w warunkach złoża Nova Odesa obciążenie filaru nośnego o wymiarach 5m×5m osiągnie 26% jego nośności, a strop komory wydobywczej jest w stanie stabilnym bez powstawanie naprężeń rozciągających. Wyniki badań są przydatne do uzasadnienia i oceny stateczności elementów systemu urabiania komorowo-filarowego wraz z filarami oporowymi w podziemnym wydobyciu wapienia lub innych złóż kopalin.

Słowa kluczowe: *kopalnia, wapień, komora wydobywcza, filar nośny, strop*

Control of Dump Stability Loading Rock on its Edge

Andrii ADAMCHUK[1)], Oleksandr SHUSTOV[2)]

[1)] The Department of Surface Mining; Dnipro University of Technology, 19, Dmytro Yavornytskyi Ave., Dnipro, Ukraine; ORCID https://orcid.org/0000-0002-8143-3697; email: adamchuk.a.a@nmu.one
[2)] The Department of Surface Mining; Dnipro University of Technology, 19, Dmytro Yavornytskyi Ave., Dnipro, Ukraine; ORCID https://orcid.org/0000-0002-2738-9891

http://doi.org/10.29227/IM-2023-01-11

Submission date: 14-02-2023 | Review date: 23-03-2023

Abstract

The question of the overburden rock dump formation during the development of iron ore deposits of Ukraine was considered. An analysis of the technology of forming a high single-tier dump in an abandoned deep pit was carried out. Two technology options are considered: loading rock on the slope of high single-tier dump and on its edge. The influence of the dependence of the loading rock on the edge of high single-tier dump on its stability of a has been established. The nature of the change in the width of the possible landslide prism, the safe distance of the dragline location has been established. The prospects for the formation of a high single-tier dump in the regime of controlled deformations are substantiated. For high single-tier dump the ordinary method of slices was justified and used to calculate the safety factor. Recommendations on the use of draglines available in Ukraine for forming the high single-tier dumps of overburden rock have been issued.

Keywords: *slope stability, single-tier dump, safety factor, method of slices*

1. Introduction

The demand for steel has always been big [1–4]. Iron ore mining is a highly developed and important part of the Ukrainian economy [5–8]. Ukraine is one of the leaders in the export of iron ore products [9–12]. Unfortunately, the Russian invasion of 2022, in particular the shelling of Kryvyi Rih and other industrial cities, seriously complicated the extraction of iron ore and the production of products from it. After the victory, Ukraine will need to rebuild its destroyed infrastructure. This will significantly increase domestic demand for construction materials, including steel.

Despite the relatively small overburden ratio, the total volume of overburden stockpiling in external dumps is colossal [13–18]. Even though during the development of coal deposits [19–22], the overburden ratio is an order of magnitude higher, there is a possibility of stockpiling rocks during their extraction in the spent space of an active mine. During the development of iron ore deposits, such stacking of rocks is significantly limited. This is due to the conditions of occurrence of iron ore deposits. Therefore, during their development, external piles of overburden rocks are formed until they are fully developed. In addition, with an increase in the depth of development of an iron ore deposit, the volume of extraction and storage of overburden rocks also increases. Accordingly, an increase in the volume of iron ore mining will increase the necessary volume of stockpiling of overburden. At the same time, even more lands are wasted.

An effective solution is the storage of overburden rocks and the construction of dumps in used-up abandoned open pit mines [23–25]. PJSC "ArcelorMittal Kryvyi Rih" has such an experience, which puts overburden rocks from its mine No. 2-bis into the abandoned open-pit mine No. 1 of former mining and processing plant "Novokryvorizkyi Mining and Processing Plant (MPP)". Storage takes place with the help of draglines. Unloading takes place directly from the earth's surface, without vehicles entering the pit. Thanks to this, minimal costs are achieved. But over time, the backfill massif of a high single-tier dump begins to deform, which creates a danger for personnel and equipment.

2. Forming the single-tier internal dump

External dumps of overburden rocks are formed with the formation of safety berms in several tiers [26–28]. The height of such dumps rarely exceeds 100–120 m. The horizontal berms and slopes of the tiers of the external dump form a resulting angle of 13–15 degrees to the earth's surface. The berms of internal dumps during the development of horizontal deposits are formed according to the horizons of the installation of mining equipment.

The formation of a dump of overburden rocks in an abandoned deep pit is possible with the formation of berms. Then the transport delivers the rock through ramps built in the pit. However, they don't do that. Usually, transport delivers the rock to a reloading point on the surface near the pit. After that, the mining mass is unloaded into the produced space directly from the surface. A single-tier dump is formed in the abandoned open pit mine. This method allows you to reduce the transportation distance by 1.5 km. The practice of forming a single-tier dump is successfully applied at the abandoned mine No. 1 of former mining and processing plant "Novokryvorizkyi MPP" by employees of PJSC "ArcelorMittal Kryvyi Rih" [24].

2.1. Loading Rock on the Slope

Usually, the process of formation of overburden rock dump in an abandoned deep pit is as follows. Along the side of the mine, the dragline excavator forms a pit on the surface. Transport unloads overburden rock into this pit. Rocks from

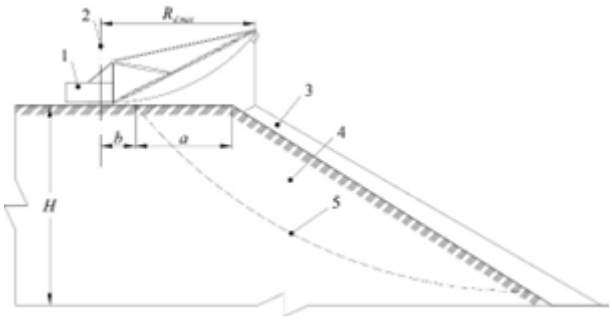

Fig. 1. Scheme of loading rock on the slope: 1 – dragline; 2 – dragline movement axis; 3 – rock loaded on the slope; 4 – possible landslide prism; 5 – curved sliding surface for the safety factor of 1.2; a – width of the possible landslide prism, m; b – safe distance of the dragline installation, m; H – height of the single-tier dump, m; $R_{d.max}$ – maximum dumping radius, m

Rys. 1. Schemat załadunku skały na zboczu: 1 – koparka; 2 – oś ruchu koparki; 3 – skała załadowana na zboczu; 4 – możliwy pryzmat osuwiska; 5 – zakrzywiona powierzchnia ślizgowa dla współczynnika bezpieczeństwa 1,2; a – szerokość możliwego graniastosłupa osuwiskowego, m; b – bezpieczna odległość instalacji koparki, m; H – wysokość składowiska jednopoziomowego, m; $R_{d.max}$ – maksymalny promień zrzutu, m

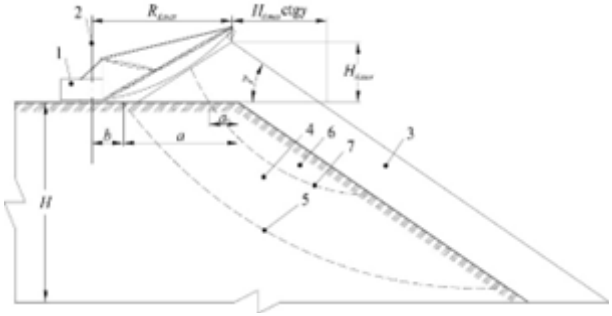

Fig. 2. Scheme of loading rock on the edge: 1 – dragline; 2 – dragline movement axis; 3 – rock loaded on the slope; 4 – possible landslide prism; 5 – curved sliding surface for the safety factor of 1.2; 6 – guaranteed landslide prism; 7 – curved sliding surface for the safety factor of 1.0; a – width of the possible landslide prism, m; a1 – width of the guaranteed landslide prism, m; b – safe distance of the dragline installation, m; H – height of the single-tier dump, m; $R_{d.max}$ – maximum dumping radius, m; Rd.max – maximum dumping height, m; γ – dump slope angle, degrees

Rys. 2. Schemat załadunku skały na krawędzi: 1 – koparka; 2 – oś ruchu koparki; 3 – skała załadowana na zboczu; 4 – możliwy pryzmat osuwiska; 5 – zakrzywiona powierzchnia ślizgowa dla współczynnika bezpieczeństwa 1,2; 6 – gwarantowany pryzmat osuwiska; 7 – zakrzywiona powierzchnia ślizgowa dla współczynnika bezpieczeństwa 1,0; a – szerokość możliwego graniastosłupa osuwiskowego, m; a1 – szerokość graniastosłupa gwarantowanego osuwiska, m; b – bezpieczna odległość instalacji koparki, m; H – wysokość składowiska jednopoziomowego, m; Rd.max – maksymalny promień zrzutu, m; $R_{d.max}$ – maksymalna wysokość zrzutu, m; γ – kąt nachylenia wysypiska w stopniach

the pit are unloaded by the dragline into the created space of the abandoned mine on the slope of the formed overburden rock dump, as shown in Fig. 1.

The formation of an internal dump according to the scheme with the dumping of overburden rocks on a slope is effective and is used under the following condition:

$$R_{d.max} = a + b, \; m \tag{1}$$

In Ukraine, the regulations on design require compliance with the distance (a, m), at which the safety factor SF = 1.2. The safe distance of the dragline installation (b, m) is calculated based on its overall dimensions (b = 10…15 m).

2.2. Loading Rock on the Edge

If condition (1) is not fulfilled, effective use of the selected excavator model with the maximum dumping radius $R_{d.max}$ is not possible. Then there are two ways out of the situation. The first is to change the equipment to one in which the maximum dumping radius $R_{d.max}$ meets the condition (1). The second is to operate the available equipment in the mode of controlled deformations of the overburden rock dump by loading rock on its edge. This dump formation scheme allows to increase the dumping radius of the dragline by $H_{d.max}ctg\gamma$, as shown in Fig. 2.

The guaranteed landslide prism is a part of the dump, limited by its slope on one side and the farthest curved sliding surface for the safety factor of 1.0 on the other.

Using the scheme of loading rock on the dump edge is possible to increase dumping radius only on the following conditions:

$$R_{d.max} = a + b - H_{d.max}ctg\gamma, \; m \tag{2}$$

To work in the mode of controlled deformations of the overburden rock dump, it is necessary to create the following conditions:

$$R_{d.max} = a + b - a_1, \; m \tag{3}$$

If conditions (2) and (3) are not fulfilled, then further development of the overburden rock dump is not possible using the available equipment.

2.3. Draglines Manufactured in Ukraine

In Ukraine, draglines are manufactured at Novokramatorsk Machine-Building Plant (NKMZ). All draglines manufactured by NKMZ are equipped with a stepping eccentric stroke, which ensures high dragline maneuverability. Specifications of draglines listed in Table 1.

Tab. 1. Draglines produced by the Novokramatorsk Machine-Building Plant (NKMZ) and their specifications

Tab. 1. Koparki produkowane przez Nowokramatorski Zakład Budowy Maszyn (NKMZ) i ich specyfikacje

Specifications	Dragline model					
	6.5/45	11/70	14/50	15/80	15/90	10/100
Bucket volume, m^3	6,5	11	14	15	15	10
Boom length, m	45	70	50	80	90	100
Maximum dumping radius, m	43,5	66,5	46,5	76,5	83	93,5
Maximum dumping height, m	19,5	27,5	20,5	32	37	42
Theoretical productivity, m^3/h	557	754	1292	931	900	600

PJSC "ArcelorMittal Kryvyi Rih" has experience in the use of NKMZ draglines to form the single-tier overburden rock dump in the abandoned mine No. 1 of former mining and processing plant "Novokryvorizkyi MPP". Dragline models they use are 6.5/45 and 11/70 with a maximum dumping radius of 43.5 m and 66.5 m respectively.

3. Methodology

Calculations of the stability of the slopes of the dumps were made by algebraic summation of forces using the method of slices in Rocscience Slide software. The calculation of the width of the prism of the possible landslide (a, m) and the guaranteed landslide (a_1, m) of the formed one-tier dump relates to finding the curved sliding surface.

For this, a cross-section of a one-tier dump with the necessary parameters is constructed. The location of the square is determined, in which the centers of the radii of the curved sliding surfaces are located. Next, the program finds the safety factor on curved surfaces according to all center points and radii. After that, it is necessary to determine the distance from the crest of the dump to the farthest point of intersection of the curved surface SF = 1.2 and SF = 1 with the surface.

For the simulation of single-tier dumps of overburden rocks, their height (H, m) was taken from 100 m to 500 m with a step of 50 m, dumping height (H_d, m) from 0 m to 40 m with a step of 50 m, the following physical and mechanical properties of the material: unit weight – 18,83 kN/m^3, cohesion – 20 kN/m^2, internal friction angle – 30 degrees.

4. Discussion

The practice of calculating the stability parameters of high single-tier dumps has shown that when calculating by the method of slices, it is advisable to use its ordinary variant, known as the Swedish circle method or Fellenius method. This method makes it possible to build a model the single-tier dump that is the closest to real conditions. The value of distance calculated by this method is the most 'pessimistic' compared with the other methods, which guarantee the safest dragline use conditions.

The results of modeling the slopes of a single-tier dump and the values of the width of the of possible landslide prism and the guaranteed landslide prism are presented in Fig. 3-6. Graphs have the form of a broken line. The analysis of the obtained data showed that loading rock on the edge of single-tier dump does not affect on its slope stability if loaded on 4…5% of dump height in conditions of the material with the given physical and mechanical properties. Guaranteed landslides possible only in conditions of 400 m, 450 m and 500 m high single-tier dump.

In Fig. 3 shown the dependence of the width of the possible landslide prism on the dragline dumping height for single-tier dumps of 100 m, 150 m and 200 m high. 100 m high dump starts with possible landslide prism 31 m wide, which does not change until achieve a critical point, then increases up to 70 m. 150 m high dump – 52 m wide possible landslide prism, loaded on 40 m height – 88 m. 200 m high single-tier dump not loaded has possible landslide prism 78 m wide, loaded on 40 m height – 107 m. Curved sliding surface for the safety factor less than 1.0 are not observed.

Forming of 100 m, 150 m and 200 m height single-tier dump in the mode of controlled deformations is impossible. Using the scheme of loading rock on the edge is unnecessary. 100 m height dump can be formed by any model of NKMZ dragline. 150 m height single-tier dump – by any model of NKMZ dragline but 6.5/45 and 14/50. 200 m height single-tier dump – by 10/100 using the scheme of loading rock on the slope and 15/90 using the scheme of loading rock on the edge.

Graphs in Fig. 4 have the similar form as it shown in Fig. 3. There are no guaranteed landslides on 250 m, 300 m and 350 m height single-tier dumps. Width of the possible prism have value of 107 m 130 m, 151 m for not loaded edge and 130 m 155 m 176 m maximally loaded for 250 m, 300 m and 350 m height single-tier dump respectively. There are no model of dragline in Ukraine capable to form single-tier dumps of such height, neither loading rock on the slope, nor on the edge.

The same situation is on the 400 m, 450 m and 500 m height single-tier dumps (Fig. 5). But there are guaranteed landslides shown in Fig. 6. Graphs of dependence of the width of the guaranteed landslide prism on the dragline dumping height have different shape. 400 m height dump graph exists between value of dumping height from 25 m to 40 m. It has concave up shape. 450 m height dump graph has increasing linear form. 450 m height dump graph has the similar broken line form as it shown in Fig. 3-5.

Despite the theoretical possibility of forming the single-tier dump in the mode of controlled deformations, can only be done by dragline with maximum dumping radius more than 150 m. There are no such dragline models. Moreover, calculations of width of the guaranteed landslide prism have been carried out using ordinary method of slices, which gets the biggest value comparing to another methods. Brief analysis of slope stability using Spencer method shows no sliding surfaces with safety factor less than 1. It means that that loading rock on the edge of single-tier dump does not guarantee to collapse it.

3. Conclusion

Forming the high single-tier dump of overburden rock in abandoned open-pit mines using available in Ukraine equipment is possible only up to 200 m. Analysis of single-tier dumping technology and its two schemes: loading rock on the slope and on the edge showed that the first variant is more

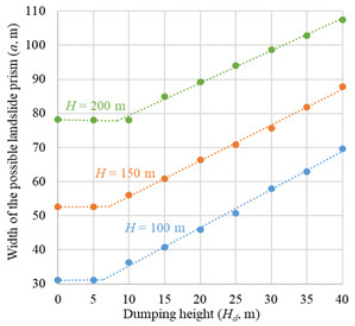

Fig. 3. Dependence of the width of the possible landslide prism (a, m) of 100…200 m height dump on the dragline dumping height (H_d, m)
Rys. 3. Zależność szerokości możliwego graniastosłupa osuwiskowego (a, m) wysokości zwału 100…200 m od wysokości zwału koparki (H_d m)

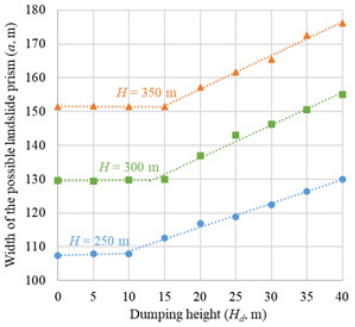

Fig. 4. Dependence of the width of the possible landslide prism (a, m) of 150…350 m height dump on the dragline dumping height (H_d, m)
Rys. 4. Zależność szerokości możliwego graniastosłupa osuwiskowego (a, m) o wysokości zwału 150…350 m od wysokości zwału koparki (H_d, m)

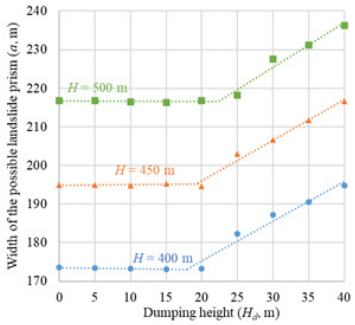

Fig. 5. Dependence of the width of the possible landslide prism (a, m) of 400…500 m height dump on the dragline dumping height (H_d, m)
Rys. 5. Zależność szerokości możliwego graniastosłupa osuwiskowego (a, m) zwału o wysokości 400…500 m od wysokości zwału koparki (H_d, m)

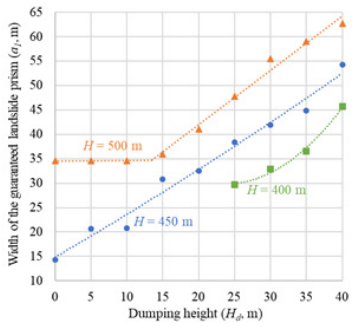

Fig. 6. Dependence of the width of the guaranteed landslide prism (a1, m) of 400…500 m height dump on the dragline dumping height (H_d, m)
Rys. 6. Zależność szerokości graniastosłupa gwarantowanego osuwiska (a1, m) zrzutu o wysokości 400…500 m od wysokości zwału koparki (H_d, m)

effective than the second one. Forming a pile of rock on the edge closes further access for dragline to work. Moreover, controlled deformations is not guaranteed. Loading the edge of the high single-tier dump on the 4–5% of its height does not affect on its stability. Loading rock on the edge may only be applied in conditions of 200 m height dump of overburden rock using 15/90 NKMZ dragline to increase its dumping radius from 83 m up to 97 m forming 10 m height pile of rock on the edge.

Literatura – References

1. Sobczyk, W., Perny, K. C. I., & Sobczyk, E. (2021). Assessing the Real Risk of Mining Industry Environmental Impact. Case Study. Inżynieria Mineralna, 1(1). https://doi.org/10.29227/IM-2021-01-05
2. Radwanek-Bąk, B., Sobczyk, W., & Sobczyk, E. J. (2020). Support for multiple criteria decisions for mineral deposits valorization and protection. Resources Policy, 68, 101795. https://doi.org/10.1016/j.resourpol.2020.101795
3. Sobczyk, W. (2015). Sustainable development of Middle East Region. Problemy ekorozwoju–problems of sustainable development, 10(2), 51–62.
4. Sobczyk, E. J., Kicki, J., Sobczyk, W., & Szuwarzyński, M. (2017). Support of mining investment choice decisions with the use of multi-criteria method. Resources Policy, 51, 94–99. https://doi.org/10.1016/j.resourpol.2016.11.012
5. Pysmennyi, S., Fedko, M., Shvaher, N., & Chukharev, S. (2020). Mining of rich iron ore deposits of complex structure under the conditions of rock pressure development. E3S Web of Conferences, 201, 01022. https://doi.org/10.1051/e3sconf/202020101022
6. Shvaher, N., Komisarenko, T., Chukharev, S., & Panova, S. (2019). Annual production enhancement at deep mining. E3S Web of Conferences, 123, 01043. https://doi.org/10.1051/e3sconf/201912301043
7. Pysmennyi, S., Fedko, M., Chukharev, S., Rysbekov, K., Kyelgyenbai, K., & Anastasov, D. (2022). Technology for mining of complex-structured bodies of stable and unstable ores. IOP Conference Series: Earth and Environmental Science, 970(1), 012040. https://doi.org/10.1088/1755-1315/970/1/012040
8. Peremetchyk, A., Kulikovska, O., Shvaher, N., Chukharev, S., Fedorenko, S., Moraru, R., & Panayotov, V. (2022). Predictive geometrization of grade indices of an iron-ore deposit. Mining of Mineral Deposits, 16(3), 67–77. https://doi.org/10.33271/mining16.03.067
9. Pysmennyi, S., Chukharev, S., Khavalbolot, K., Bondar, I., & Ijilmaa, J. (2021). Enhancement of the technology of mining steep ore bodies applying the "floating" crown. E3S Web of Conferences, 280, 08013. https://doi.org/10.1051/e3sconf/202128008013
10. Kyelgyenbai, K., Pysmennyi, S., Chukharev, S., Purev, B., & Jambaa, I. (2021). Modelling for degreasing the mining equipment downtime by optimizing blasting period at Erdenet surface mine. E3S Web of Conferences, 280, 08001. https://doi.org/10.1051/e3sconf/202128008001
11. Pysmennyi, S., Chukharev, S., Kyelgyenbai, K., Mutambo, V., & Matsui, A. (2022). Iron ore underground mining under the internal overburden dump at the PJSC "Northern GZK." IOP Conference Series: Earth and Environmental Science, 1049(1), 012008. https://doi.org/10.1088/1755-1315/1049/1/012008
12. Pysmennyi, S., Peremetchyk, A., Chukharev, S., Fedorenko, S., Anastasov, D., & Tomiczek, K. (2022). The mining and geometrical methodology for estimating of mineral deposits. IOP Conference Series: Earth and Environmental Science, 1049(1), 012029. https://doi.org/10.1088/1755-1315/1049/1/012029
13. Sdvyzhkova, O., Moldabayev, S., Bascetin, A., Babets, D., Kuldeyev, E., Sultanbekova, Z., Amankulov, M., & Issakov, B. (2022). Probabilistic assessment of slope stability at ore mining with steep layers in deep open pits. Mining of Mineral Deposits, 16(4), 11–18. https://doi.org/10.33271/mining16.04.011
14. Shcherbakov, P., Tymchenko, S., Bitimbayev, M., Sarybayev, N., & Moldabayev, S. (2021). Mathematical model to optimize drilling-and-blasting operations in the process of open-pit hard rock mining. Mining of Mineral Deposits, 15(2), 25–34. https://doi.org/10.33271/mining15.02.025
15. Moldabayev, S., Adamchuk, A., Sarybayev, N., & Shustov, A. (2019). Improvement of open cleaning-up schemes of border Mineral reserves. International Multidisciplinary Scientific GeoConference Surveying Geology and Mining Ecology Management, SGEM, 19(1.3), 331–338. https://doi.org/10.5593/sgem2019/1.3/S03.042
16. Moldabayev, S., Rysbaiuly, B., Sultanbekova, Z., & Sarybayev, N. (2019). Methodological approach to creation of the 3D model of an oval-shaped open pit mine. E3S Web of Conferences. https://doi.org/10.1051/e3sconf/201912301049
17. Moldabayev, S., Sultanbekova, Z., Adamchuk, A., & Sarybayev, N. (2019). Method of optimizing cyclic and continuous technology complexes location during finalization of mining deep ore open pit mines. International Multidisciplinary Scientific GeoConference Surveying Geology and Mining Ecology Management, SGEM, 19(1.3), 407–414. https://doi.org/10.5593/sgem2019/1.3/S03.052
18. Moldabayev, S. K., Adamchuk, A. A., Toktarov, A. A., Aben, Y., & Shustov, O. O. (2020). Approbation of the technology of efficient application of excavator-automobile complexes in the deep open mines. Naukovyi Visnyk Natsionalnoho Hirnychoho Universytetu, 4, 30–38. https://doi.org/10.33271/nvngu/2020-4/030
19. Shustov, O. O., Bielov, O. P., Perkova, T. I., & Adamchuk, A. A. (2018). Substantiation of the ways to use lignite concerning the integrated development of lignite deposits of Ukraine. Naukovyi Visnyk Natsionalnoho Hirnychoho Universytetu, 3, 5–13. https://doi.org/10.29202/nvngu/2018-3/6

20. Shustov, O. O., Pavlychenko, A. V, Bielov, O. P., Adamchuk, A. A., & Borysovska, O. O. (2021). Calculation of the overburden ratio by the method of financial and mathematical averaged costs. Naukovyi Visnyk Natsionalnoho Hirnychoho Universytetu, 5, 30–36. https://doi.org/10.33271/nvngu/2021-5/030

21. Khorolskyi, A., Mamaikin, O., Fomychova, L., Pochepov, V., & Lapko, V. (2022). Developing and implementation a new model optimizing the parameters of coal mines under diversification. ARPN Journal of Engineering and Applied Sciences, 17(16), 1544-1553.

22. Khorolskyi, A., Mamaikin, O., Medianyk, V., Lapko, V., & Sushko, V. (2021). Development and implementation of technical and economic model of the potential of operation schedules of coal mines. ARPN Journal of Engineering and Applied Sciences, 16(18), 1890-1899.

23. Moldabayev, S. K., Sultanbekova, Z. Z., Adamchuk, A. A., Sarybaev, N. O., & Nurmanova, A. N. (2022). Technology of an open pit refinement under limit stability of sides. Naukovyi Visnyk Natsionalnoho Hirnychoho Universytetu, 6, 5–10. https://doi.org/10.33271/nvngu/2022-6/005

24. Babets, Y. K., Adamchuk, A. A., Shustov, O. O., Anisimov, O. O., & Dmytruk, O. O. (2020). Determining conditions of using draglines in single-tier internal dump formation. Naukovyi Visnyk Natsionalnoho Hirnychoho Universytetu, 6, 5–14. https://doi.org/10.33271/nvngu/2020-6/005

25. Fomychov, V., Fomychova, L., Khorolskyi, A., Mamaikin, O., & Pochepov, V. (2020). Determining optimal border parameters to design a reused mine working. ARPN Journal of Engineering and Applied Sciences, 15(24), 3039–3049.

26. Buzylo, V., Pavlychenko, A., Borysovska, O., & Saveliev, D. (2019). Investigation of processes of rocks deformation and the earth's surface subsidence during underground coal mining. E3S Web of Conferences, 123. https://doi.org/10.1051/e3sconf/201912301050

27. Kolesnik, V. Y., Pavlichenko, A. V., & Buchavy, Y. V. (2016). Determination of dynamic parameters of dust emission from a coal mine fang. Naukovyi Visnyk Natsionalnoho Hirnychoho Universytetu, (2), 81-87.

28. Gorova, A., Pavlychenko, A., Kulyna, S., & Shkremetko, O. (2013). The investigation of coal mines influence on ecological state of surface water bodies. Paper presented at the Annual Scientific-Technical Colletion - Mining of Mineral Deposits 2013, 303-305.

Kontrola stabilności zrzutu załadunku skały na krawędzi wyrobiska

W artykule rozważono kwestię powstawania nadkładu skalnego podczas eksploatacji złóż rudy żelaza na Ukrainie. Przeprowadzono analizę technologii formowania zwałowiska wysokiego jednopoziomowego w nieczynnym wykopie głębokim. Rozważane są dwa warianty technologiczne: załadunek skały na zboczu wysokiego zwałowiska jednopoziomowego oraz na jego krawędzi. Określono wpływ zależności skały obciążającej od krawędzi zwałowiska wysokiego jednopoziomowego na jego stateczność. Ustalono charakter zmiany szerokości ewentualnego graniastosłupa osuwiskowego oraz bezpieczną odległość położenia liny zgarniającej. Możliwości powstania wysokiego zwałowiska jednopoziomowego w reżimie kontrolowanych deformacji są uzasadnione. Dla wysokiego zrzutu jednopoziomowego zasadna była zwykła metoda przekrojów, wykorzystana do obliczenia współczynnika bezpieczeństwa. Wydano zalecenia dotyczące wykorzystania dostępnych na Ukrainie koparek do formowania wysokich jednopoziomowych zwałów nadkładu.

Słowa kluczowe: *stateczność zbocza, zwałowisko jednopoziomowe, współczynnik bezpieczeństwa, metoda przekrojów*

Simulating Filtration to Evaluate Hydrodynamic Indices of the Underground Gas Storage Operation

Ivan SADOVENKO[1)], Olexander INKIN[2)], Nataliia DEREVIAHINA[3)]

[1)] Dnipro University of Technology, 19 Dmytra Yavornytskoho ave., 49005, Dnipro, Ukraine; ORCID https://orcid.org/0000-0001-5324-9836
[2)] Dnipro University of Technology, 19 Dmytra Yavornytskoho ave., 49005, Dnipro, Ukraine; ORCID https://orcid.org/0000-0003-3401-9386
[3)] Dnipro University of Technology, 19 Dmytra Yavornytskoho ave., 49005, Dnipro, Ukraine; ORCID https://orcid.org/0000-0001-5584-8592; email: natali.derev@gmail.com

http://doi.org/10.29227/IM-2023-01-12

Submission date: 12-02-2023 | Review date: 20-03-2023

Abstract

The research objective is to develop and test mathematical model of gas storage in the layered aquifer with poorly permeable interlayer if plane-parallel and axisymmetric filtration takes place. The paper evaluates the gas-hydrodynamic operational indices of the underground gas storages within aquifers in the South East Ukraine. Comprehensive approach has been applied involving collection, systematization, and analysis of actual data on filtration and physicomechanical properties of enclosing rocks impacting formation of natural and technogenic deposits as well as analytical and numerical methods to solve equations of the gas-water contact shift under different conditions. A gas-hydrodynamic model of underground gas storage within the nonuniform aquifer has been substantiated to calculate its cyclic operation in the three-layered seam taking into consideration crossflows through a poorly permeable stopping. The calculation results show significant impact of characteristics of the layered porous environment on the gas water contact transfer through certain seams. The derived new technique linearizing a system of differential equations to identify pressure within a reservoir is generalization of the earlier applied procedures with introduction of 'boundary schemes'. The calculation results demonstrate significant impact of the layered porous environment on the gas water contact transfer through certain seams. The findings may be applied while making evaluations at the stage of gas storage design within aquifers.

Keywords: *aquifer, gas storage, filtration, gas water contact, nonuniformity*

Introduction

Along with the necessity to develop alternative energy sources, stable operation of fuel and energy complex of Ukraine depends heavily upon the reliable functioning of the unified gas supply system involving production facilities to mine, transport, store, and distribute gaseous hydrocarbons. A significant feature of the system is complete interconnection of its components expressed by changes in operation conditions of the system if working conditions of its certain object varies. In such a way, nonuniform gas consumption may result in its interrupted recovery while demanding the development of underground gas storages (UGSs) within the deposits of aqueous rock as well as mathematical models able to calculate hydrodynamic indices of their operations under different geological and technological conditions [1–5].

The earlier considered [5–6] hydrodynamic models of UGSs were obtained while assuming piston nature of water displacement with gas. Such a schematization of the process is popular and completely justified in many cases [7–8]. Nevertheless, optimum ratio between buffer gas volume and active one, and determination of coefficients of gas saturation and average weighed pressure for different aquifer zones cannot be identified in terms of a piston problem formulation.

The problem has been solved partially under Backley-Leverett theory; numerous papers concern it (for example, [9–10]). The essential point is as follows: in this context, gas saturation distribution has been determined under constant initial conditions irrespective of solution for gas which makes it it possible to simplify drastically the calculation procedure. However, the abovementioned complicates interpretation of the calculation results since the undefined pressure prevents from recalculation of gas amount within the seam to the normal conditions. In this connection, the paper objective is to substantiate the methods determining the basic hydrodynamic UGS indices in terms of its cyclic operation based upon a two-phase filtration model, and determination of the average weighed pressure and gas saturation within different storage zones.

Research material and methods

Dynamics of cyclic water displacement with gas is analyzed within a uniform infinite reservoir. A radial displacement case is considered. It is anticipated that in terms of degassing, mass discharge of gas $\rho_{at}G(t)$ is known and gas saturation at the well is constant. Gas is extracted until R(t) front, having a high water saturation value, approaches the well.

It is also anticipated that the displacement process forms three typical zones (Fig. 1): 1st being a zone with high average gas saturation σ_1 limited by a circle with R(t) radius; 2nd being a zone with low average gas saturation $\sigma_2<\sigma_1$; and 3rd being a zone inflated with pure water $\sigma(x,y)=0$. Since pressure within a high average gas saturation zone is almost equal to pressure within R(t) front, we assume that pressure in the 1st zone depends only upon time. We also assume that within the 2nd and 3rd zones, pressure follows the equation of elastic liquid filtration.

Pressure distribution within the 2nd and 3rd zones is identified using a method of 'fictive' sources and drainages [11]. Thus, we have

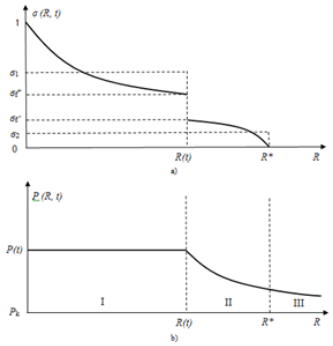

Fig. 1. Diagrams to calculate gas saturation (a) and pressure (b) within a horizontal aquifer

Rys. 1. Diagramy do obliczania nasycenia gazem (a) i ciśnienia (b) w poziomej warstwie wodonośnej

$$P_{at}\int_0^t G(t)dt = \tilde{P}(t)\int_0^t Q(t)dt - \frac{Q(t)\bar{\sigma}_2\mu_v}{K}\left(\frac{R^2}{2}ln\left(\frac{R^{*2}}{R(t)^2}\right) - \frac{1}{4}(R^{*2} - R^2(t))\right), \quad (1)$$

where P_k is pressure at infinity; μ_v is water viscosity; k, h, and a are permeability, thickness, and piezoconductivity of a seam; and $Q_0(\tau)$`is specific rate of a 'fictive' source located in the central share of a seam.

Within the 1st boundary, $P_f(R(t),t)$ pressure and hence average weighed P(t) pressure is determined relying upon equation (1)

$$\bar{P}(r,t) = P_k + \frac{\mu_v}{4\pi kh}\int_0^t \frac{Q_0(\tau)}{(t-\tau)} exp(-R^2(t)/(4a(t-\tau)))\, d\tau, \quad (2)$$

The specific rate of a 'fictive' source $Q_0(\tau)$ is selected in such a way to equalize at the r = R(t) front consumption on the left and right of the boundary. Within the 1st zone, the total Q(t) consumption is constant along the whole area (under the assumption on incompressibility of phases being filtered) inclusive of R(t) boundary. From the 2nd zone, Q(t) consumption may be derived using equation (1). Hence, to identify specific rate of the 'fictive' source, we have following integral equation

$$Q(t) = 2\pi R(t)h\left(-\frac{k}{\mu_v}\frac{\partial P}{\partial r}\right)_{r=R(t)} = \frac{R^2(t)}{4a}\int_0^t \frac{Q_0(\tau)e^{-\frac{R^2(t)}{4a(t-\tau)}}}{(t-\tau)^2}d\tau \quad (3)$$

A law of R(t) front advance is known from saturation solution [11]

$$R^2(t) = \frac{f'(\sigma^+)}{\pi mh}\int_0^t Q(t)dt, \quad (4)$$

where f'(σ+) is the derived Backley-Leverett function applied for gas saturation within the front; and m is a seam porosity.

Equation of gas balance is used to close (1)-(4) system.

$$P_{at}\int_0^t G(t)dt = \bar{P}(t)\pi R^2(t)mh\bar{\sigma}_1 + \int_{R(t)}^{R^*} P(r,t)2\pi hrm\bar{\sigma}_2 dr \quad (5)$$

P(r,t) function, located under integral in expression (5), is determined from ratio (1). However, in view of the 2nd limitedness, it is possible to apply simpler logarithmic pressure distribution corresponding to uncompressible liquid filtration

$$P(r,t) = \tilde{P}(t) - \frac{Q(t)\mu_v}{2\pi kh}ln\frac{r}{R(t)}, \quad (r > R(t)). \quad (6)$$

Having inserted ratio (6) into equation (5) and calculated the integral in the right side, we will obtain

$$P(r,t) = P_k + \frac{\mu_v}{4\pi kh}\int_0^t \frac{Q_0(\tau)}{(t-\tau)} exp(-r^2/(4a(t-\tau)))\, d\tau, \quad (7)$$

where G(t) is consumption of gas injected into the seam under the standard conditions.

It should be mentioned that the simplification, connected with substitution of expression for P(r,t), is not of principal nature; thus, ratio (1) can be used for equation (5) during numerical implementation.

Introduce dimensionless variables

$$x = \frac{t}{T};\ \tilde{p} = \frac{\bar{p}}{P_k};\ \zeta = \frac{\tau}{T};\ q = \frac{Q\mu_v}{P_k hk};\ q_0 = \frac{Q_0\mu_v}{P_k hk};\ \alpha = \frac{R^2}{4aT}, \quad (8)$$

where T is typical process life; as a rule, it is equal to a year.

Owing to the use of the introduced variables, (2)-(4), and (7) expression will look like

$$\tilde{p}(x) = 1 + \frac{1}{4\pi}\int_0^x \frac{q_0(\zeta)e^{-\frac{\alpha(x)}{x-\zeta}}}{x-\zeta}d\zeta, \quad (9)$$

$$q(x) = \alpha(x)\int_0^x \frac{q_0(\zeta)e^{-\frac{\alpha(x)}{x-\zeta}}}{(x-\zeta)^2}d\zeta, \quad (10)$$

$$\alpha(x) = \beta f'(\bar{\sigma^+})\int_0^x q(x)dx, \quad (11)$$

$$\gamma W = \tilde{p}(x)\int_0^x q(x)dx - \frac{q(x)}{4\pi\beta}\left(\alpha^* ln\frac{\alpha^*}{\alpha} - (\alpha^* - \alpha)\right), \quad (12)$$

Assume that injection and withdrawal follow a harmonic law.

(9)-(12) ratios are the closed system of integral equations to identify p(x), q(x),q_0(x),and α(x). In this context, σ₁, σ₂, and σ+ values are determined along with solving a problem for saturation [11].

Then single out and consider separately three specific stages of UGS operation: initial gas injection into the undisturbed aquifer; extraction; and gas injection into the seam during a random cycle of UGS operation.

Initial gas injection into the undisturbed aquifer. If gas is injected into the undisturbed aquifer then gas saturation distribution is represented by means of the known Backley-Leverett solution [12]; zone 2 (Fig.1) is not available, R*=R(t). In this regard, the saturation jump R(t) is defined using the ratio

$$R^2(t) = \frac{f'(\sigma^+)}{2\pi kh}\int_o^t Q(\tau)d\tau. \quad (12)$$

Gas saturation σ+ within R(t) front is determined by means of the transcendental equation solution

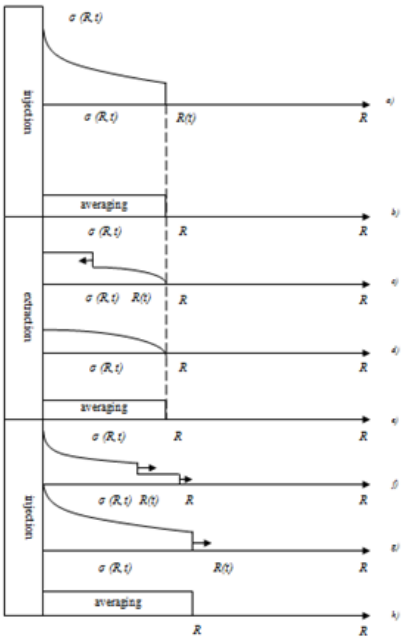

Fig. 2. On the calculation of gas saturation under cyclic UGS operation

Rys. 2. Obliczenia nasycenia gazem przy cyklicznej pracy PMG

$$\frac{f(\sigma^+)}{\sigma^+} = f'(\sigma^+) \tag{13}$$

Average gas saturation is identified from the ratio

$$\bar{\sigma}_1 = \frac{1}{f'(\sigma^+)} \tag{14}$$

Assume for the numerical (9)-(12) system that within $X_{j-1} \le X \le X_{j-1} + \Delta X_j$ moment, q(x) and q0(x) functions are constant. Subsequently, (9)-(12) equations for the specified time interval may be represented as follows

$$q_j(X) = \frac{\gamma w(X) - \acute{p}_j(x) \sum_{i=1}^{j-1} q_i \Delta x_i}{\acute{p}_j(x) \Delta X_j}; \tag{15}$$

$$\alpha_j(x) = \beta f'(\sigma^+) \sum_{i=1}^{j} q_i \Delta x_i; \tag{16}$$

$$q_{oj}(x) = (q_j - \sum_{i=1}^{j-1} q_{0i} \left(e^{-\frac{\alpha_j}{x-x_{i-1}}} - e^{-\frac{\alpha_j}{x-x_i}}\right) e^{\frac{\alpha_j}{\Delta x_j}} \tag{17}$$

$$\acute{p}_j(x) = 1 + \frac{1}{4\pi} \sum_{i=1}^{j-1} q_{0i} \left(-E_i\left(-\frac{\alpha_j}{x-x_{i-1}}\right) + E_i\left(-\frac{\alpha_j}{x-x_i}\right)\right). \tag{18}$$

W(x) function is given by the expression

$$W(x) = 0.5(1 + \cos(2\pi x)). \tag{19}$$

Analytical model for the case looks like: W(x) is the initial value to solve (15)-(18) system. The value is determined through ratio (19). While inserting W(x) into (15) and setting p'j*(x) value, to a first approximation, it may be specified as that one being equal to p'_{j-1}. Identify $q_j(x)$ value. (16)-(18) ratios help define successively α_j, q_{oj}, and p'_j values. In general, the latter does not coincide with p'j*. New approximation of p'j* is selected; the iteration process continues until p'j* matches p'j with the specified E accuracy. The final p'j(x) value, calculated for the time interval, also defines $q_j(x)$ and $\alpha_j(x)$ values corresponding to it.

Gas extraction during a random cycle. As it has been mentioned above, according to the accepted planning, gas is extracted until saturation jump with a coordinate nears a well placed in the central share of the seam. In this context, volume of the gas, extracted from Q_k^* seam, may be defined as well as normalized to the reservoir conditions. Then, relying upon the specified harmonic selection law, it becomes possible to identify gas consumption normalized to the reservoir conditions

$$q(x) = -\frac{\pi Q_H^*}{T} \sin(2\pi(x - x_N)) \tag{20}$$

In this case, the equation takes the form

$$\alpha_j(x) = \alpha^* - \beta f'(1 - \sigma_f) \sum_{i=N}^{j} q_i \Delta x_i \tag{21}$$

where α* is the maximum α(x) value achieved during gas injection; N is number of x_N time moment corresponding to the extraction start; and σ_f is front value of gas saturation in terms of k^{th} extraction.

Since q(x)value is entered by means of (20) then $\alpha_j(x)$, $\sigma_{oj}(x)$, and p'j(x) values may also be identified through direct computation using formulas (16), (18), and (21); $W_j(x)$value is defined using the formula

$$W_{j(x)} = \frac{1}{\gamma} (\bar{p}_j(x) \sum_{i=1}^{j} q_i \Delta x_i - \frac{q_i}{4\pi\beta} (\alpha^* \ln\frac{\alpha^*}{\alpha} - \alpha^* + \alpha). \tag{22}$$

In such a way, while extracting, W_j is not the initial (specified) value. It is determined during the problem solving. The abovementioned depends upon the selected operational schedule of UGS. In the context of the schedule, gas extraction is maximum possible and volume of gas, remained in the seam, is minimal.

Under reservoir conditions $Q_к^*$, front saturation value σf as well as the extracted gas volume is determined through the solution analysis for saturation [13].

If the extraction takes place within a random k^{th} cycle, then solution for saturation is divided into two cases:

1. In terms of $0 < \sigma'_2 < \sigma_n$ (where σ_n is gas saturation corresponding to Backley-Leverett bending point function) case,

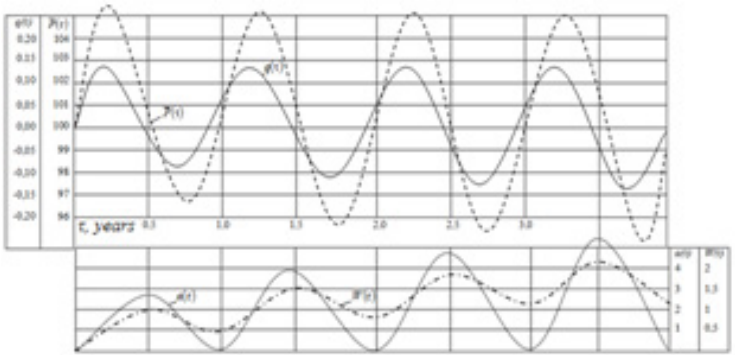

Fig. 3. Calculation example of hydrodynamic indices of UGS operation in terms of a cyclic mode
Rys. 3. Przykład obliczeń wskaźników hydrodynamicznych pracy PMG w trybie cyklicznym

volume of gas $Q_к^*$, extracted from a seam during k^{th} cycle, is identified using the expression

$$Q_3 = \int_{x_{N+1}}^{x_{N+2}} q(x)dx. \tag{23}$$

2. If $\sigma_n<\sigma_2'<1$ then $Q_к^*$ determination should involve gas saturation assessment within σf front by means of the transcendental equation solving

$$\frac{f(\overline{\sigma_2'})-f(\sigma_f)}{\overline{\sigma_2'}-\sigma_f} = f'(\sigma_f) \tag{24}$$

While applying the determined σf value, the following is đefined

$$Q_к^* = \beta \sum_{i=1}^{N} q_i \Delta xi - \alpha^*(\sigma_f - \frac{f(\sigma_f)}{f'(\sigma_f)}) \tag{25}$$

At the end of the extraction, average gas saturation value σ_2 is defined with the help of the formula

$$\overline{\sigma_2} = \overline{\sigma} - \frac{Q_к^*}{\alpha^*} \tag{26}$$

Moreover, it is taken up as the initial distribution at the start of following injection (Fig. 2 c, d, and e).

Gas injection within a random k+1st cycle. Within a random cycle, gas injection into UGS differs from its initial injection in the fact that there is some gas saturation distribution in the seam; for the case, it is substituted for a constant σ_2 value. During injection, the seam demonstrates two gas saturation jumps with R(t) and R* coordinates as well as corresponding dimensionless variables α(x) and α* (Fig. 2, f).

In this case, expression (15), determining mass balance in the UGS, will take the form

$$q_j(x) = \frac{\gamma W_j(x) - \overline{p}_j(x)\sum_{i=1}^{j-1} q_i \Delta x_i}{\overline{p}_j \Delta x_j - (\frac{\overline{\sigma}_2}{4\pi\beta})(\alpha^* ln(\frac{\alpha*}{\alpha_j}) - \alpha* + \alpha_j)}. \tag{27}$$

The unknowns q_{0j}, α_j, and p_j are identified from (16)-(18) ratios. (1)-(18), and (27) system is solved similarly to the initial injection case. Law of $W_j(x)$ variation is taken up as follows

$$W_j(x) = W_0 + 0.5W_{к+1}(1-cos(2\pi(x-x_N))) \tag{28}$$

where W_0 is amount of gas in the seam before previous extraction is over; $W_{к+1}$ is amount of gas injected in the seam during active injecting; and x_{N+1} is starting point of the active injective.

If gas is injected within a random cycle, the saturation solution depends upon the injected gas volume (under the reservoir conditions)

$$Q_к^* = \beta \sum_{i=1}^{N} q_i \Delta xi - \alpha^*(\overline{\sigma_2'} - \frac{f(\overline{\sigma_2'})}{f'(\overline{\sigma_2'})}) \tag{29}$$

Having determined the value of front gas saturation σ_f from the ratio

$$\frac{f(\sigma_f)-f(\overline{\sigma_2})}{\sigma_f-\overline{\sigma_1}} = f'(\sigma_f), \tag{30}$$

and having identified 'critical' value of the injected gas volume

$$Q_{cr} = \frac{\alpha^*}{\beta}\frac{\overline{\sigma_2}}{(\overline{\sigma_2}f(\sigma_f)-f(\overline{\sigma_2}))}, \tag{31}$$

consider two probable solution alternatives:

1. Assume that Q_3 value is less than critical volume Q_{cr}; then motion of two saturation jumps takes place within the seam. In this context, before injection is over, maximum zone the maximum zone with gas α^*_{N+2}, is (Fig. 2, f)

$$\alpha^*_{N+2} = \alpha^*_{N+1} + \beta Q_3 f'(\overline{\sigma_2})/\overline{\sigma_2}. \tag{32}$$

Amount of gas within the seam as well as average gas saturation until injection is over will be defined as follows

$$Q_{N+2} = Q_{N+1} + Q_3, \tag{33}$$

$$\sigma_1 = \beta Q_{N+2} / a^*_{N+2} \tag{34}$$

σf value, being a part of equation (17), is defined from (30) ratio.

2. If $Q_3 > Q_{cr}$ then frontal gas saturation value is identified by solving the equation

$$\beta(\sigma_f f'(\sigma_f) - f(\sigma_f) + 1)Q_3 - \overline{\sigma_2}\alpha^*_{N+1} = \beta Q_3 \tag{35}$$

In addition, geometry of zone with gas before injection is over α^*_{N+2} is defined from the ratio

$$\alpha^*_{N+2} = \beta Q_3 f'(\sigma_f) \tag{36}$$

Q_{N+2} and σ_1 values are determined from (33) and (34) expressions.

Case two solving for injection arises if one saturation jump is in the seam (Fig. 2, g). It should be mentioned that the initial injecting stage will always involve case one; consequently, if a back edge α(x) nears and passes α* ($Q_з > Q_{cr}$) front case two may happen (Fig. 2, f, g).

The considered algorithm to solve the formulated problem has been represented based upon approximate solution for saturation [9]. It is possible to examine similar solution algorithm for the case when saturation is solved relying upon accurate statement [16]. Comparative analysis of two solutions, performed on the basis the processed calculation results, has shown their good agreement for the first six operational UGS cycles. Computation for more prolonged period, based upon a model with averaging, results in significant errors. However, simple implementation and short period, required to make the calculations, help recommend the methods while making multivariant computations of a gas storage transfer to cyclic operation.

Results and their analysis

The represented algorithm has been implemented in the software environment Mapple for a hypothetic case. The seam parameters were specified as follows: $\kappa = 10^{-12}$ m² being permeability; m = 0.2 being porosity; a = 1 m²/s being piezoconductivity coefficient; h = 10 m being seam thickness; $\mu v = 10^{-3}$ Pa·s being formation water viscosity; Pк = 9.8 MPa being pressure within the undisturbed seam boundary; and period of the complete operational UGS cycle being T = 1 year = $3.15 \cdot 10^7$ s (four three month periods: injection – idle time –extraction – idle time). The calculations involved the idea that one and the same gas mass $G_з$ is injected into the seam during any period. Mass of the extracted Gext gas was defined during the solution.

Phase penetrations for gas $k_g(\sigma)$ and water $k_w(\sigma)$, involved by Backley-Leverett functions , i.e. f(σ)

$$f(\sigma) = \frac{k_g \mu_g}{k_g \mu_g + k_w \mu}$$

were assumed as follows according to paper [10]

$$\begin{cases} k_g(\sigma) = \left(\frac{\sigma - 0.1}{0.9}\right)^{3.5} (4 - 3\sigma), (0.1 \le \sigma \le 1) \\ k_w(\sigma) = \left(\frac{0.8 - \sigma}{0.8}\right)^{3.5}, \quad (0 \le \sigma \le 0.8) \end{cases}$$

where σ is gas saturation.

Fig. 3 shows the calculation results. Curve I is dimensionless gas consumption under the formation conditions q(τ); II is change in average weighed pressure in the seam P(τ); III is change in space of pores with gas having high average gas saturation α(τ); and IV is volume of gas in the seam normalized to the standard conditions. Analysis of the data explains that pressure in UGS during the operation transfers to a cyclic mode rather rapidly; moreover, amplitude changes in terms of pressure variations during different cycles are not higher than several percent. In this context, formation pressure excess over a reservoir boundary while gas injecting is 5% (P = 10.3 MPa). Subsequently, when following idle period is over the pressure equalizes (P = Pк); in the period of gas extraction, formation pressure is 3–5% less than its boundary pressure (P = 9.5-9.3 MPa) depending upon the operational UGS cycle.

Dimensionless gas consumption under the formation conditions, being the ratio between product of its viscosity consumption and boundary pressure product per seam thickness and permeability, also increases up to 0.13 while injecting. It is almost matches 1100 m³/day gas consumption. During following idle time, gas consumption decreases vanishing to the period end. By the end of extraction stage, gas flow rate increases annually. It was 0.08 (-678 m³/day) in the first year; 0.11 (-932 m³/day) in the second year; 0.13 (-1100 m³/day); and 0.14 (-1185 m³/day). It should be mentioned that after gas extraction and following idle time, its consumption was equal to zero again.

By the end of injection period, dimensionless space of pores with gas as well as during following idle time increased cycle by cycle. It was 2.5 in the first year; 4 in the second year; 4.8 in the third year; and 5.2 in the fourth year. The values correspond to a radius of a reservoir zone differing in high gas saturation, i.e. 17.7; 22.4; 24.5; and 25.6 km. In this regard, values of gas volume within the seam normalized to the standard conditions correspond to 1; 1.5; 1.8; and 2.1, respectively. It is also possible to mention a phase shift between W(τ) and q(τ) arising owing to the availability of elastic zone III (Fig. 1) with the formation liquid being contracted.

Conclusion

Numerical hydrodynamic model of underground gas storage within a horizontal aquifer has been developed; the model takes into consideration two-phase nature of liquid and gas filtration. Processing of the obtained results has made it possible to substantiate the approximate method calculating formation gas volume, consumption, and pressure at different stages of storage development as well as during its operational cycles. According to the calculation results in the software environment Maple for a hypothetic case, it has been identified that gas pressure in the storage transfers to a cyclic mode rather quickly under a minor (i.e. several percent) amplitude change during different cycles. In this context, formation pressure excess over a reservoir boundary while gas injecting is 5%; in the period of gas extraction, formation pressure is 3–5% less than its boundary pressure. In the injection period, gas consumption is almost constant; in turn, its flow rate during extraction increases year by year. In addition, space of pores with high average gas saturation also increases annually.

The proposed methods calculating the basic hydrodynamic UGS parameters in aquifers make it possible to identify the optimum ratio between buffer gas volume and active one in the storage as well as determine the fundamental technical and economic indicators of its operation at the design stage. The abovementioned may be applied to make business plans and investment proposals concerning seasonal accumulation of gaseous hydrocarbons in the natural environment. Further research is expedient to test adequacy of the developed methods while comparing the obtained calculation results with actual operational data of the operating UGSs.

Literatura – References

1. Sobczyk, W., Ishimi Perny, K.C., Sobczyk, E.J. (2021). Assessing the real risk of mining industry environmental impact - case study. Journal of the Polish Mineral Engineering Society; ISSN 1640-4920, 1, 33-41. http://www.potopk.com.pl/Full_text/2021_v1_full/IM%201-2021-a5.pdf}
2. Sobczyk, W., Sobczyk, E.J. (2021). Varying the energy mix in the EU-28 and in Poland as a step towards sustainable development.. Energies; 14 (5/1502), 1–19. https://www.mdpi.com/1996-1073/14/5/1502
3. Pysmennyi, S., Fedko, M., Chukharev, S., ...Kyelgyenbai, K., Anastasov, D. (2022). Technology for mining of complex-structured bodies of stable and unstable ores. IOP Conference Series: Earth and Environmental Science, 970(1), 012040. https://doi.org/10.1088/1755-1315/970/1/012040.
4. Pysmennyi, S., Peremetchyk, A., Chukharev, S., ...Anastasov, D., Tomiczek, K. (2022). The mining and geometrical methodology for estimating of mineral deposits. IOP Conference Series: Earth and Environmental Science, 1049(1), 012029. https://doi.org/10.1088/1755-1315/1049/1/012029.
5. Inkin, O., Derevyagina, N., & Khryplyvets, Y. (2020). Modeling of gas storage performance in massive aquifers. Physical and technical problems of mining. Institute of Physics of Mining Processes of the National Academy of Sciences of Ukraine, 22, 31-45. (In Ukrainian).
6. Inkin O., Tishkov V, Dereviahina N. and Sotskov V. (2018). Integrated analysis of geofiltrational parameters in the context of underground coal gasification relying upon calculations and modelling. Ukrainian School of Mining Engineering, 60, 1-9 https://doi.org/10.1051/e3sconf/20186000035.
7. Voitenko Yu., Vapnichna V. & Voitenko O. (2022). ON THE DESTRUCTION AND PREFRACTURING OF SOLID ROCKS UNDER BLASTING IN FORMATION CONDITIONS. GEOENGINEERING, 7, 7–16. https://doi.org/10.20535/2707-2096.7.2022.267555 (In Ukrainian).
8. Zheltov, Yu. (1975). Mechanics of the oil and gas reservoir. Nedra. (In Russian).
9. Biletskyi, V.S. (2004). Mining encyclopedia. Donetsk: Donbas, 640. (In Ukrainian).
10. Arkhipova, L. (2012). The concept of ecological safety of basin systems of oil and gas production areas. Ecological security and balanced resource use, 2 (6), 67-71. (In Ukrainian).
11. Collins, R.E. (1976). Flow of fluids through porous materials. United States.
12. Bugay, Yu., Globa, V., Nagorny, V., & Vengertsev, Yu. (2000). Construction of oil depots and gas storage facilities. Kyiv: VIPOL. (In Ukrainian).
13. Sukhin, E. (2004). Elements of creation, formation and operation of underground gas storage facilities. E.I. Sukhin, B.I. Navrotskyi. K.: PNNV, 528. (In Ukrainian).
14. Boyko, V.S. (1995). Underground hydromechanics: A textbook. Kyiv: ISDO. (In Ukrainian).

Symulacja filtracji w celu oceny wskaźników hydrodynamicznych podziemnego magazynowania gazu

Celem badań jest opracowanie i przetestowanie modelu matematycznego magazynowania gazu w warstwie wodonośnej ze słabo przepuszczalną międzywarstwą, przy założeniu filtracji płasko-równoległej i osiowo-symetrycznej. W artykule dokonano oceny gazowo-hydrodynamicznych wskaźników eksploatacyjnych podziemnych magazynów gazu w warstwach wodonośnych południowo-wschodniej Ukrainy. Zastosowano kompleksowe podejście polegające na zebraniu, usystematyzowaniu i analizie rzeczywistych danych, dotyczących właściwości filtracyjnych i fizykomechanicznych skał otaczających, wpływających na powstawanie osadów naturalnych i technogenicznych, a także analityczne i numeryczne metody rozwiązywania równań przesunięcia kontaktu gaz-woda w różnych warunkach. Model gazowo-hydrodynamiczny podziemnego magazynowania gazu w niejednorodnej warstwie wodonośnej został uzasadniony w celu obliczenia jego cyklicznej pracy w pokładzie trójwarstwowym z uwzględnieniem przepływów krzyżowych przez słabo przepuszczalną zaporę. Wyniki obliczeń wskazują na istotny wpływ charakterystyk warstwowego środowiska porowatego na kontakt gazu z wodą przez określone pokłady. Nową techniką linearyzującą układ równań różniczkowych do identyfikacji ciśnienia w zbiorniku jest uogólnienie wcześniej stosowanych procedur poprzez wprowadzenie „schematów brzegowych". Wyniki obliczeń wskazują na istotny wpływ warstwowego środowiska porowatego na kontakt gazu z wodą przez określone pokłady. Uzyskane wyniki mogą być wykorzystane przy dokonywaniu ocen na etapie projektowania magazynów gazu w warstwach wodonośnych.

Słowa kluczowe: *warstwa wodonośna, magazynowanie gazu, filtracja, kontakt gazu z wodą, niejednorodność*

Development of Technologies for Mining Ores with Instable Hanging Wall Rocks

Serhii PYSMENNYI[1)], Serhii CHUKHAREV[2)], Ibrahima Kalil KOUROUMA[3)], Vsevolod KALINICHENKO[4)], Anatolii MATSUI[5)]

[1)] Kryvyi Rih National University, Faculty of Mining and Metallurgy, 11 Vitalii Matusevych Str., Kryvyi Rih, 50027, Ukraine; ORCID https://orcid.org/0000-0001-5384-6972; email: psvknu@gmail.com
[2)] National University of Water and Environmental Engineering, 11 Soborna Str., Rivne, 33028, Ukraine; ORCID https://orcid.org/0000-0002-4623-1598; Central Ukrainian National Technical University, 8, Prospekt Universytetskyi, Kropyvnytskyi, 25006, Ukraine
[3)] Higher Institute of Mining and Geology of Boké, BP:84, Republic of Guinea; https://orcid.org/0000-0002-8387-1420
[4)] Kryvyi Rih National University, Faculty of Mining and Metallurgy, 11 Vitalii Matusevych Str., Kryvyi Rih, 50027, Ukraine; ORCID https://orcid.org/0000-0002-1938-2286
[5)] National University of Water and Environmental Engineering, 11 Soborna Str., Rivne, 33028, Ukraine; ORCID https://orcid.org/0000-0001-5544-0175

http://doi.org/10.29227/IM-2023-01-13

Submission date: 10-01-2023 | Review date: 12-02-2023

Abstract

Underground mines of Kryvyi Rih iron ore deposit apply room mining systems or systems with bulk caving of ore and overlying rocks in a ratio of 35% to 65%. Most mines prefer room mining systems with pillar caving due to high, technical and economic indicators. However, when mining certain areas, the problem arises of hanging wall rocks stability. Under the same mining and geological conditions of the deposit, stopes are stable in some areas, but in others waste rocks get in the stope from the side of the hanging wall when a slight exposure is created. Thus, in conditions of instable rocks of the hanging wall, development and improvement of the technology involving room mining is an urgent issue. Analysis of researchers reveals factors that significantly indluence stability of the hanging wall rocks and ore. The developed methods enable determining stability parameters and applying an improved option of room mining system in conditions of the instable hanging wall with the help of a protective ore pillar located at the instable hanging wall. Calculations performed demonstrate that application of the proposed mining system enables an increase in the iron content in the mined ore mass by 0.94%, the increased amount of the ore mass extracted and a profit of 18.73 thousand euros for the whole of a block.

Keywords: *mining system, stress, methods, pillar width, rock strength, losses, dilution*

1. INTRODUCTION

Kryvyi Rih iron ore deposit (Ukraine) is represented by narrow strips of metamorphic rocks stretching for about 100 km from south to north. In terms of stratigraphy, Kryvyi Rih series of rocks is divided into four formations: schist-amphibolite (K_0), lower arkose-phyllite (K_1), middle iron ore (K_2) and upper schist (K_3) ones [1–5]. The main productive thickness is the iron ore formation (K_2) which consists of seven pairs (ferruginous and schistous horizon) of rocks alternating with each other. The main ferruginous layers of the iron ore formation (K_2) mined by the underground method are: the fourth (PR_1Sx^{4f}), the fifth (PR_1Sx^{5f}) and the sixth (PR_1Sx^{6f}). Within these layers, deposits of rich ores are located, which are represented by a wide variety of shapes (seam-, lens-, pillar- and nest-like) and their combinations, [6–8].

Almost all rich iron ore deposits are composed of hematite and differ in physical and mechanical properties and the ratio of mineral varieties. Martite ores are characteristic of the northern group of mines. The ore is 2–3 points stronger than in the southern district. Stability of rocks depends on their physical and mechanical properties, the most important of which are: strength, mineral composition, fissuring, porosity, etc. Physical and mechanical properties and elements of occurrence can change dramatically within one mine block [9–11].

In Kryvyi Rih iron ore basin, iron ore is mined by room mining systems and systems with bulk caving of ore and country rocks [12–14].

The system with bulk ore caving is the most widely applied in mining the deposits. However, this system is characterized by significant ore dilution. [15–17]. In most cases, these mining systems are improved by optimizing structural elements of the block or by changing parameters of ore breaking and drawing [18–20]. Availability of a great number of options of the system with bulk caving enable their classification according to methods of breaking, transportation and location of the compensation room in the block [1, 8, 16]. It should be noted that the specific volume of subsidiary development systems with bulk caving is 4–7 m/1000 t, however, due to more intensive extraction, the cost of maintaining the workings is reduced by 15–20% as compared with room mining systems. However, this option of the mining system is characterized by the following disadvantages: the volume of pure ore mined does not exceed 35–55%; sharp fluctuations in the iron content in the mined ore mass lead to its sorting on the surface; significant ore losses on the footwall of the deposit; depression craters are formed on the surface [18–20].

When applying room mining systems, the iron content in the mined ore mass increases, but so do ore losses in pillars (up to 35–50%) and the volume of subsidiary workings (6–7 m/1000 t).

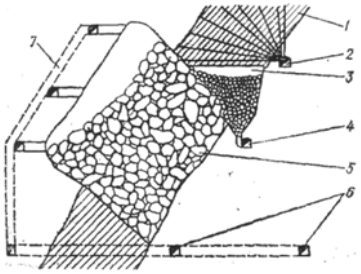

Fig. 1. Mining the deposit with the hanging wall rocks blasting: 1 – crown; 2 – drilling drift; 3 – undercutting space; 4 – collecting sublevel drift; 5 – caved hanging wall rocks filling the mined out room; 6 – workings of the transportation level; 7 – block raise from which special workings are created for vertical concentrated charges placement

Rys. 1. Eksploatacja złoża z odstrzałem skał wiszących: 1 – korona; 2 – sztolnia wiertnicza; 3 – przestrzeń podcięcia; 4 – zbieranie dryfu podpoziomowego; 5 – zawalone wiszące skały wypełniające wyrobisko; 6 – wyrobiska transportu poziomego; 7 – podwyższenie bloku, z którego tworzone są specjalne wyrobiska do pionowego umieszczania ładunków skoncentrowanych

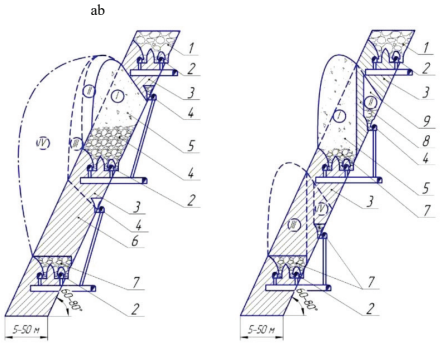

Fig. 2. Mining ore deposits in contact with clay rocks: a – with bulk blasting of the hanging wall; b – with local blasting of waste rocks of the hanging wall; I, II, III, IV – stages of mining; 1 – caved rocks; 2 – workings of the draw level; 3 – crown; 4 – auxiliary draw workings; 5 – sand-clay rocks; 6 – ore massif; 7 – caved ore; 8 – inter-room pillar; 9 – undercutting room for mining the "triangle" of the footwall and the crown

Rys. 2. Eksploatacja złóż rudy w kontakcie ze skałami ilastymi: a – z masowym wysadzaniem wiszącej ściany; b – z miejscowym wysadzeniem skał płonnych wiszącej ściany; I, II, III, IV – etapy wydobycia; 1 –skały zawału; 2 – wyrobiska wydobywcze; 3 – korona; 4 – wyrobiska pomocnicze; 5 – skały piaskowo-gliniaste; 6 – masyw rudy; 7 –urobiona ruda; 8 – filar międzykomorowy; 9 – pomieszczenie podrębowe do urabiania „trójkąta" spągu i korony

This mining system can only be applied in deposits represented by stable rocks of the hanging wall or with no less than medium ore stability and strength. While designing a block, optimal structural elements for this mining system are determined by the industry methodology developed by the Research Mining Institute (Kryvyi Rih, Ukraine).

According to practical data, mining of room reserves is 45–65%, which enables obtaining the maximum iron content in the mined ore mass. However, during mining of pillars, ore losses increase to 50%, and the iron content in the mined ore mass decreases by 3–15%.

Room mining systems have the following disadvantages: the two-stage extraction of ore, availability of a large volume of voids, significant ore losses and dilution during mining of pillars, high costs for maintaining mine workings, restricted conditions of application [12, 14].

It should be noted that in order to ensure stability, in practice, the volume of reserves in stopes with the instable hanging wall is reduced to 40–42%.

To increase efficiency of mining deposits with instable ores and rocks of the hanging wall, an option of combined mining is used, which involves simultaneous application of the room system and a system with bulk ore caving.

This option enables extraction of about 50–70% of pure ore from a block, but losses and maintenance costs for mine workings increase significantly [21–23].

2. ANALYSIS OF RESEARCHES AND PUBLICATIONS

The rock massif of Kryvyi Rih iron ore basin is not homogeneous. Application of room systems to mining rich ores causes, among others, a problem of providing conditions that exclude emergence of uncontrolled and randomly created areas of rock massif displacements.

To ensure stability of the rock massif, artificial structures are created, ore pillars are left unmined [12], or various methods of additional strengthening of instable local areas of the deposit are applied [24–26]. At the same time, a complex of mining operations is provided for that require significant labor and material costs, ultimately influencing economic efficiency and expediency of stoping.

One of possible options for stoping is application of the technology involving partial destruction of the hanging wall rocks to ensure replacement of the volume of ore mass with rocks, Fig. 1. However, in this case, extraction indicators deteriorate sharply, especially at deposit dips of 45–55 degrees, [27–29].

This is due to the fact that the ore mass is replaced with a relatively limited layer of rocks near the plane of the hanging wall, which results in a significant part of the caved ore left on the footwall. Creation of auxiliary sublevel transportation workings dramatically increases the costs for preparatory and subsidiary workings, complexity of their maintenance, especially in instable fissured rocks, which results in increased ore mining costs.

The monograph [30] describes the technology of creating a rock "pillow", proposed by B.I. Rymarchuk, as one of

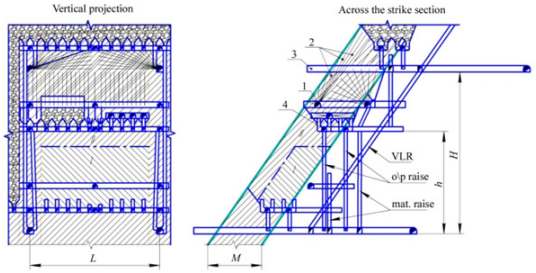

Fig. 3. System of sublevel bulk caving with transportation in drifts and a compacted layer of caved ore: 1 – drilling drift; 2 – long blasthole rings for creating an overcompacted ore layer; 3 – access ort of the upper level; 4 – scraper level

Rys. 3. System podpoziomowego zawału z transportem w sztolniach i zagęszczoną warstwą zawału rudy: 1 – sztolnia wiertnicza; 2 – długie pierścienie otworów strzałowych do tworzenia zagęszczonej warstwy rudy; 3 – wejście na górny poziom; 4 – poziom zgarniacza

the ways to combat clay rushes or uncontrolled destruction of rocks from the hanging wall side.

Fundamental flowsheets for mining the ore deposit, which allow reduction of the amount of additional mining of overlying rocks, are given in Fig. 2. These flowsheets differ in conditions of their application that depend primarily on the ore deposit dip, the ore deposit thickness, as well as location of instable rocks in the hanging wall.

The idea behind the technology presented in Fig. 2,a consists in the following: at the first stage, the ore reserve is mined out near the hanging wall I. During caved ore drawing 7, rocks of the hanging wall move simultaneously with the caved ore creating a caving zone.

After the upper sublevel is mined out, a crown 3 is drilled and blasted. With the help of the auxiliary draw working 4, the reserve of the crown is removed, while a displacement zone III is created. The disadvantage of this technology includes significant ore losses and dilution ranging from 16 to 25–45%.

The main feature of the flowsheet b, (see Fig. 2) is the local blasting of waste rocks of the hanging wall and their moving into the mined out stoping space. At the same time, between the caved rocks 5 and the "triangle" of the footwall 9, the ore massif (pillar) 8 is left.

Bulk ore caving and the use of a compacted layer, Fig. 3, is also a commonly used option. This technology enables reduction of caved ore losses and dilution in the instable area from the hanging wall side.

The idea behind this mining system is as follows. The mined block is divided into two technological areas; I – for bulk caving of the ore massif; II – for mining using a compacted ore layer.

On the contact of the caved ore with rocks, an additional drilling drift 1 is driven which is necessary for creating a compacted layer, by drilling the ore area of the hanging wall with long blasthole rings 2. To create a protective layer above the main reserve of the ore massif in the upper part of the block, previously driven workings of the above lying levels 3, 4 are used.

The ore massif of the main reserve is caved first. To do this, a drilled ore massif is broken on the previously created compensation room. Then, the long blasthole rings from the hanging wall and above the main block are exploded with delay. Consideration should be given to the fact that when breaking the massif onto a compressed medium, the optimal thickness of the broken ore layer is the main parameter.

According to V.R. Imenitov, displacement of broken ore (rock) after explosion of the first set of blasholes in the compressed medium is 2.0–2.5 m and reaches 3.0 m when blasting 4–5 sets of blastholes [31–33]. With average ore strength and thick deposits, compaction of the massif is 25–30 m.

To create a compacted layer, parameters of drilling and blasting (the line of least resistance and the distance between hole toes) must be reduced by 15–20% compared to the mass breaking of the main massif. Excessive amount of explosives in the ore massif in the peripheral zone of the block inevitably leads to an additional compaction of the broken ore mass by 3–5 m. The broken ore layer thickness in the hanging wall and in the upper part of the caved massif depends on the ratio of primary loosening of the main massif and its compaction factor [34–36].

However, it should be noted that the ore layer II from the side of the hanging wall is caved last. Therefore, at a considerable pressure of hanging wall rocks, when the main massif I is destructed, its additional destruction occurs. Ill-timed destruction of the ore layer from the hanging wall side can result in significant losses and dilution during ore drawing from the main massif.

3. PURPOSE

The presented study aims to determine the minimum permissible thickness of rocks of the hanging wall, which ensures stability of the rocks depending on rock pressure. For this, the following tasks should be solved:

1. To investigate the influence of the initial field of massif stresses on stability parameters of the rock massif.
2. To develop methods for determining the minimum permissible thickness of rocks of the hanging wall at which it is advisable to apply a system with bulk ore caving and a compacted layer in conditions of instable rocks of the hanging wall.

4. METHODS

To determine stability parameters of structural elements in Kryvyi Rih iron ore basin, the method of calculated functional characteristics is used, numerical values of which depend on basic factors associated with dimensions of structural elements and their stress-strain state [37]. Geometrical parameters are determined by using two types of functional characteristics: equivalent exposure spans; dimensionless characteristics for determining the width of the inter-room and the thickness of the inter-floor pillars.

Actual values between the equivalent spans of exposures in the room and their dimensions are described by the formulas:

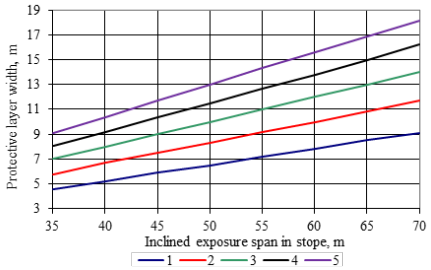

Fig. 4. Dependencies of the width of the protective layer on the exposure span in the stope and the ultimate compression strength of rocks: 1–5 – the ultimate strength of rocks of 140, 120, 100, 80 and 60 MPa respectively

Rys. 4. Zależności szerokości warstwy ochronnej od rozpiętości ekspozycji w przodku wybierkowym i ostateczna wytrzymałość skał na ściskanie: 1–5 – wytrzymałość skał odpowiednio 140, 120, 100, 80 i 60 MPa

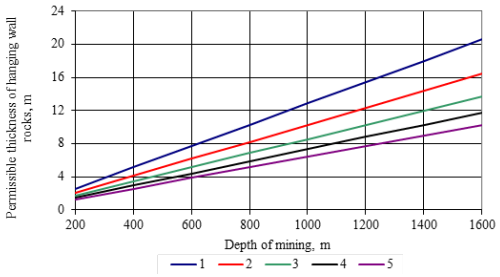

Fig. 5. Dependencies of the permissible thickness of the hanging wall rocks on the depth of mining operations and the ultimate strength of rocks at the stope width of 15 m and the deposit dip of 60 degrees: 1, 2, 3, 4 and 5 – the ultimate compression strength of 80, 100, 120, 140 and 160 MPa respectively

Rys.5. Zależności dopuszczalnej miąższości skał wiszących od głębokości eksploatacji i wytrzymałości skał przy szerokości przodka 15 m i upadzie złoża 60 stopni: 1, 2, 3, 4 i 5 – ściskanie graniczne odpowiednio 80, 100, 120, 140 i 160 MPa

- for horizontal exposures

$$m_h = \frac{aM_h}{\sqrt{a^2 + M_h^2}}, \text{m}; \quad (1)$$

- for vertical exposures

$$m_v = \frac{bM_n}{\sqrt{b^2 + M_n^2}}, \text{m}; \quad (2)$$

- for inclined exposures

$$l_n = \frac{ab}{\sqrt{a^2 + b^2}}, \text{m}, \quad (3)$$

where a, b are the dimensions of rooms along the strike and downdip respectively; M_h, M_n are the horizontal and normal thickness of the deposit respectively.

The influence of the stress-strain state of the massif on parameters of rooms and pillars is taken into account in the classification of deposits according to the proposed methodology, [37].

As a rule, permissible spans of exposures are established on the basis of experiments conducted according to a special method [38–40]. The use of calculation methods is limited by certain conditions, e.g. heterogeneity of roof rocks. However, the results obtained should be considered as preliminary, requiring further experimental clarification. The most likely are the results obtained by the methods of calculating roofs represented by undisturbed or weakly layered rocks. In this system, the mined-out space is supported by ore pillars.

Based on the analysis results, it is established that the advantage of the methods developed by S.G. Borisenko, in comparison with the NDGRI (Research Mining Institute of Kryvyi Rih National University) methods, consists in considering the weight of not only overlying rocks but also those of the hanging wall [41–43].

5. RESULTS

To obtain high indicators of ore mass extraction during mining reserves by room mining systems, it is necessary to ensure stability of exposures and pillars within the entire period of mining the stoping block. Therefore, when mining ore deposits by room systems, structural elements of the stoping block should be refined and the thickness of rocks in the hanging wall should be taken into account.

When applying a room mining system, various stresses (tensile or compressive) act on pillars.

From the strength of materials theory, it is known that if a sample is evenly loaded over time, normal stresses increase in it to the ultimate compression strength. As soon as normal stresses exceed the ultimate compression strength, either linear strains occur or the room pillar is destructed. Thus, in order to preserve integrity of the rocks of the inter-room pillar, the following condition must be met.

$$\begin{cases} \sigma \le \sigma_{kr} \equiv [\sigma_{st}], \\ \varepsilon = 0, \end{cases} \quad (4)$$

where σ is normal stresses, MPa; σkr is critical stresses, MPa; [σst] is the ultimate compression strength of rocks, MPa; ε is linear strains.

If the pillar is under action of compressive and tensile stresses throughout its lifetime, normal stresses in it first increase and then decrease. Repeated stresses cause linear strains in the pillar that significantly reduce the ultimate compressive strength of rocks.

If the pillar undergoes increasing stresses, normal stresses increase, according to (4); if stresses decrease, normal stresses do not reach the ultimate strength of rocks, the pillar is not destructed and the following condition is met

$$\begin{cases} \sigma \le \sigma_{kr} \equiv \sigma_v << [\sigma_{st}], \\ \varepsilon \ne 0. \end{cases} \quad (5)$$

where σv is the destructive pressure, MPa.

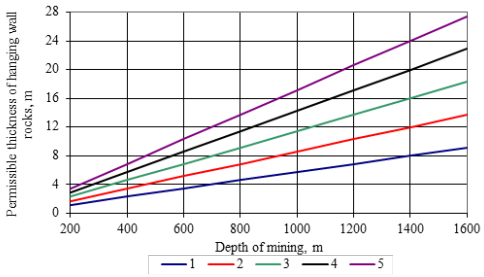

Fig. 6. Dependencies of the permissible thickness of the hanging wall rocks on the depth of mining operations and the stope width at the rock strength of 12 and the deposit dip of 60 degrees: 1, 2, 3, 4 and 5 – widths of the stope of 10, 15, 20, 25 and 30 m respectively

Rys. 6. Zależności dopuszczalnej miąższości skał wiszących od głębokości eksploatacji i szerokości przodka przy sile 12 i upadzie złoża 60 stopni: 1, 2, 3, 4 i 5 – szerokości przodka odpowiednio 10, 15, 20, 25 i 30 m

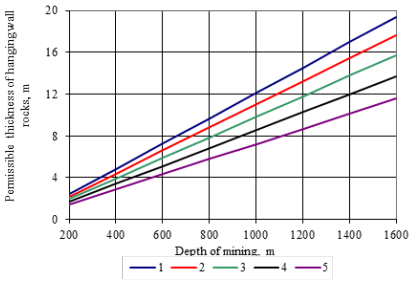

Fig. 7. Dependencies of the permissible thickness at the rock strength of 12 and the width of the stope of 15 m: 1, 2, 3, 4 and 5 – ore deposit dips of 45, 50, 55, 60 and 65 degrees respectively.

Rys. 7. Zależności dopuszczalnej miąższości przy wytrzymałości skały 12 i szerokości przodka 15 m: 1, 2, 3, 4 i 5 – upały złoża rudy odpowiednio 45, 50, 55, 60 i 65 stopni

Taking into account the above, parameters of structural elements at different stages of block mining can be determined for the first option (the stoping block is mined from the foot- to the hanging wall).

At the first stage of block mining, parameters of the stope (the width of the stope along the strike, the height and width of the pillar, the length of the inclined exposure span, the height of the level (sublevel) are determined by the NDGRI methods [17].

Then, in the conventional way, certain technological operations are performed in the stoping block: preparation, drilling and blasting, selection of the mode of caved ore mass drawing and transportation. It should be noted that after caved ore drawing from the first stope, inter-room ore pillars and the crown are not caved at this stage. Therefore, when determining exposure and pillars lifetime, it is necessary to take into account the total time needed for mining the stoping block (taking into account the second stage).

Maximum permissible thickness of the protective ore layer is obtained by the formula

$$m = \frac{la\gamma K_z}{4[\sigma_{st}]K_{str.o}}, \quad (6)$$

where l is the maximum permissible exposure span, m; a is the width of the stope, m; γ is the volumetric weight of ore, N/m³; Kz is the factor of safety (accepted 1.5–2.0); Kstr.o is the factor of rock structural weakening by fissures (accepted from 0.65 to 0.95).

Based on (6), the dependencies of the width of the compacted layer on the exposure span in the stope and the ultimate compressive strength of rocks are built (Fig. 4).

Fig. 4 demonstrates that an increase in the exposure span from 35 to 70 m requires the increase in the width of the protective layer from 9 to 18 m at the rock compression strength of 140 MPa.

If longitudinal compressive forces acting along the inclined exposure plane of the pillar are withstood without its integrity failure, lateral stresses and strains in the direction of previously mined out stopes, the thickness of the inter-room pillar is determined by the formula

$$m_\sigma = \frac{H\gamma aK_dK_z\cos\alpha}{n[\sigma_{st}]K_{str.o}}. \quad (7)$$

where H is the depth of mining, m; α is the ore deposit dip, degrees; n is the number of pillars per stope.

The dependencies of the permissible thickness of waste rocks from the hanging wall side when applying room mining systems on the depth of mining, the width of the stope and the ore deposit dip are shown in Fig. 5–7.

The above dependencies demonstrate that the permissible thickness of waste rocks from the hanging wall side increases directly proportional to the increase in the mining depth, the width of the stope and inversely proportional to the increase in the ultimate compressive strength of rocks and the ore deposit dip.

Fig. 5 demonstrates that with an increase in the depth of mining from 200 to 1600 m, the permissible thickness of the hanging wall rocks, which enables maintaining their stability for the period of mining out the stope, must be at least 1.3–20.5 m at the decreased ultimate compressive strength of rocks from 160 to 80 MPa and the width of the stope of 15 m.

At an increase in the width of the stope from 10 to 30 m and the depth of mining from 200 to 1600 m, the thickness of the hanging wall rocks at the rock ultimate compressive strength of 120 MPa and the deposit dip of 60 degrees must be at least 1.1–27.4 m, Fig. 6. Thus, at the increased mining depth

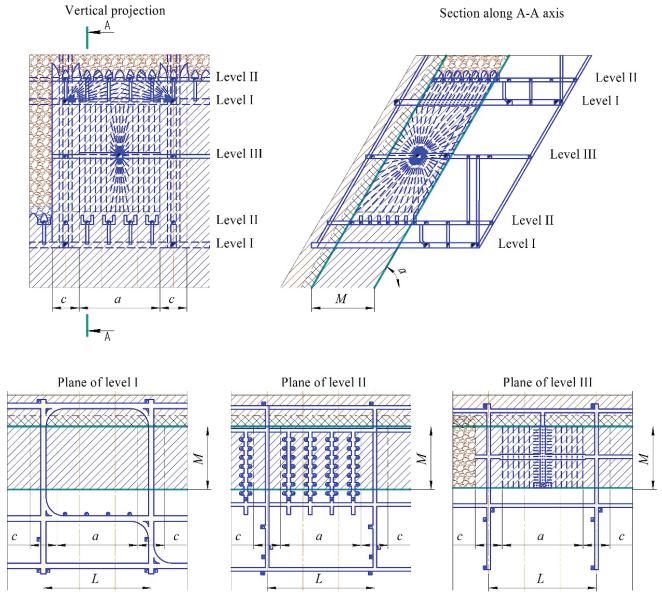

Fig. 8. The proposed option of the room system with a protective layer and subsequent pillar caving

Rys. 8. Proponowany wariant układu pomieszczeń z warstwą ochronną i późniejszym zawałem filarów

and the ultimate compression strength of 120 MPa, to ensure its stability, the width of the stope should be: at the depth of 700 m – ak = 30 m; at the depth of 850 m – ak = 25 m; at the depth of 1050 m – ak = 20 m; at the depth is 1400 m – ak = 15 and at the depth of 1600 m – ak = 10 m.

The dependencies shown in Fig. 7 demonstrate that with an increase in the deposit dip from 45 to 65 degrees, the permissible thickness of the hanging wall rocks must be at least 15–8 m at the depth of stoping works of 1200 m.

Thus, application of room mining systems is limited by the ultimate compressive strength of rocks, the thickness of the hanging wall rocks, as well as the height of the caved layer, the deposit dip and the rock stability factor.

Based on the results of the presented study, it is established that application of the room system to mining ore deposits is reasonable if the thickness of the hanging rocks exceeds 6 m.

According to the study conducted, an option of the room mining system is developed, Fig. 8.

The idea behind the proposed mining system consists in a certain order of mining operations depending on mining and geological conditions of the deposit.

At the first stage, a stope of the reduced by 10–15 m width is created across the strike leaving the ore thickness in the hanging wall. The parameters of the stope at the first stage are determined by the NDGRI methods [17].

The thickness of the protective layer from the hanging wall side is determined by the above described methods. Calculations by (6) and (7) for the conditions of the HVARDIISKA underground mine of the JSC KRYVBASZALIZRUDKOM enable obtaining the minimum width of the ore pillar based on the rock thickness in the hanging wall:

$$m = \frac{90 \times 50 \times 3.6 \times 2.0}{4 \times 100 \times 12 \times 0.65} \approx 11 \text{ m};$$

$$m_\sigma = \frac{1260 \times 3.6 \times 50 \times 1.8 \times 2 \times cos\,60}{1000 \times 2 \times 14 \times 0.65} \approx 23 \text{ m}.$$

Thus, if the thickness of the rocks of the hanging wall does not exceed 23 m, an 11 m thick ore pillar is left. Therefore, dimensions of the stope are as follows: the length along the strike is 50 m, the width is M–m=35-11=24 m.

The mine block is drilled by circular long blasthole rings from the drilling drift to the full height of the level. The vertical compensation room is created in the middle part of the block, and it should be noted that the slot raise is located at the footwall.

After caving the stope reserve, the crown and the inclined pillar at the hanging wall are drilled. The crown is caved first, and then the pillar is caved on the compressed medium.

Caved pillars are drawn in direction from the hanging to the footwall. According to G.M. Malakhov theory of drawing, ore moves in a 8–12 m wide stream parallel to the angle of the hanging wall to the drawpoint. The inter-room pillar is mined out after the caved ore is drawn.

Advantages: a smaller volume of drilling workings; fewer redeployments of the drilling rig, as all holes in the ring are drilled from the same drilling level; additional fragmentation of ore due to collision of ore pieces caused by exploding opposite long blasthole rings; a significant amount of pure ore extracted.

Disadvantages: uneven fragmentation of the massif (excessive fragmentation of ore at the start of long blastholes and increased oversized yield at the toes); increased costs for drilling long holes; application in strong and stable ores and rocks of the hanging wall.

General technical and economic indicators are given in Tab. 1.

Analysi of the calculation results show that application of room mining systems with a protective layer on the side of the instable hanging wall enables reduction of ore losses from 16.3 to 12.4%, an increase in the iron content in the mined ore mass from 58.44 to 59.38% and an increase in profits from 105.27 to 111.54 euros/t.

6. CONCLUSIONS

As a result of the study, the following conclusions can be drawn:

1. Based on the study conducted, it is established that

Tab. 1. Technical and economic indicators

Tab. 1. Wskaźniki techniczne i ekonomiczne

No.	Indicators	u/m data	proposed option
1	Balance reserve of ore in block, kt	604.80	604.80
2	Ore reserve by elements, kt		
	- in stope	264.60	181.44
	- in inter-room pillars	151.20	151.20
	- in crown	113.40	113.40
	- in pillar of protective layer of hanging wall	0	106.92
	- in compensation room	75.60	51.84
3	Useful component content, %		
	- in massif	63	63
	- in rocks	38	38
4	Average useful component content in mined ore, %	58.44	59.38
5	Losses, %	16.30	12.40
6	Dilution, %	18.25	14.50
7	Ore mass extracted, kt	619.23	619.65
8	Mining cost, euro/t	150	170
9	Income, thousand euros	198.15	216.88
10	Profit, euro/t	105.27	111.54

the method for determining structural elements does not take into account the thickness of rocks that significantly influences stability.

2. The methods are proposed for determining the stability parameters of the structural elements of the mining system that enable the use of a room mining system.
3. The technology of the room mining system with the use of a protective layer of the ore massif from the side of the instable hanging wall is developed that ensures stability of the stope and an increase in the iron content in the mined ore mass by 0.94%, resulting in an estimated profit growth by 6.27 euros/t.

7. ACKNOWLEDGMENTS

The work was supported by the Ministry of Education and Science of Ukraine within the framework of the state scientific theme «Investigation and scientific and practical substantiation of technological means for raw material control in mining ores on deep levels» (State registration 0122U000843).

Literatura – References

1. Pysmennyi, S., Chukharev, S., Kyelgyenbai, K., Mutambo, V., & Matsui, A. (2022). Iron ore underground mining under the internal overburden dump at the PJSC "Northern GZK". IOP Conference Series: Earth and Environmental Science, 1049(1), 012008. https://doi.org/10.1088/1755-1315/1049/1/012008.
2. Stupnik, M., Kalinichenko, V., Fedko, M., Pysmennyi, S., Kalinichenko, O., & Pochtarev, A. (2022). Methodology enhancement for determining parameters of room systems when mining uranium ore in the SE "SkhidGZK" underground mines, Ukraine. Mining of Mineral Deposits, 16(2). 33–41. https://doi.org/10.33271/mining16.02.033.
3. Fedko, M.B., Muzyka, I.O., Pysmennyi, S.V. & Kalinichenko, O.V. (2019). Determination of drilling and blasting parameters considering the stress-strain state of rock ores. Naukovyi Visnyk Natsionalnoho Hirnychoho Universytetu, 1, 37–41. https://doi.org/10.29202/nvngu/2019-1/20.
4. Morkun, V., Morkun, N., & Tron, V. (2015). Distributed control of ore beneficiation interrelated processes under parametric uncertainty. Metallurgical and Mining Industry, 8(7), 18–21.
5. Golik, V., Komashchenko, V., Morkun, V., & Irina, G. (2015). Improving the effectiveness of explosive breaking on the bade of new methods of borehole charges initiation in quarries. Metallurgical and Mining Industry, 7(7), 383–387.
6. Bazaluk, O., Rysbekov, K., Nurpeisova, M., Lozynskyi, V., Kyrgizbayeva, G., & Turumbetov, T. (2022). Integrated monitoring for the rock mass state during large-scale subsoil development. Frontiers in Environmental Science, 10, 852591. https://doi.org/10.3389/fenvs.2022.852591.
7. Lozynskyi, V., Medianyk, V., Saik, P., Rysbekov, K., & Demydov, M. (2020). Multivariance solutions for designing new levels of coal mines. Rudarsko Geolosko Naftni Zbornik, 35(2), 23-32. https://doi.org/10.17794/rgn.2020.2.3.
8. Pysmennyi, S., Fedko, M., Chukharev, S., Rysbekov, K., Kyelgyenbai, K., & Anastasov, D. (2022). Technology for mining of complex-structured bodies of stable and unstable ores. IOP Conference Series: Earth and Environmental Science, 970(1), 012040. https://doi.org/10.1088/1755-1315/970/1/012040.
9. Morkun, V., & Morkun, N. (2018). Estimation of the crushed ore particles density in the pulp flow based on the dynamic effects of high-energy ultrasound. Archives of Acoustics, 43(1), 61–67.
10. Golik, V., Komashchenko, V., Morkun, V., & Zaalishvili, V. (2015). Enhancement of lost ore production efficiency by usage of canopies. Metallurgical and Mining Industry, 7(4), 325–329.
11. Morkun, V., Morkun, N., & Tron, V. (2015). Distributed closed-loop control formation for technological line of iron ore raw materials beneficiation. Metallurgical and Mining Industry, 7(7), 16–19.
12. Pysmennyi, S., Peremetchyk, A., Chukharev, S., Fedorenko, S., Anastasov, D., & Tomiczek, K. (2022). The mining and geometrical methodology for estimating of mineral deposits. IOP Conference Series: Earth and Environmental Science, 1049(1), 012029. https://doi.org/10.1088/1755-1315/1049/1/012029.
13. Kyelgyenbai K., Pysmennyi S., Chukharev S., Purev B., & Jambaa I. (2021). Modelling for degreasing the mining equipment downtime by optimizing blasting period at Erdenet surface mine. E3S Web of Conferences, (280), 08001. https://doi.org/10.1051/e3sconf/202128008001.
14. Stupnik, M., Kalinichenko, V., Fedko, M., Pysmennyi, S., Kalinichenko, O., & Pochtarev, A. (2022). Methodology enhancement for determining parameters of room systems when mining uranium ore in the SE "SkhidGZK" underground mines, Ukraine. Mining of Mineral Deposits, 16(2). 33–41. https://doi.org/10.33271/mining16.02.033.
15. Bazaluk, O., Petlovanyi, M., Zubko, S., Lozynskyi, V., & Sai, K. (2021). Instability Assessment of Hanging Wall Rocks during Underground Mining of Iron Ores. Minerals, 11(8), 858. https://doi.org10.3390/min11080858.
16. Petlovanyi, M., Lozynskyi, V., Zubko, S., Saik, P., & Sai, K. (2019). The infuence of geology and ore deposit occurrence conditions on dilution indicators of extracted reserves. Rudarsko Geolosko Naftni Zbornik, 34(1), 83-91. https://doi.org/10.17794/rgn.2019.1.8.
17. Bazaluk, O., Petlovanyi, M., Lozynskyi, V., Zubko, S., Sai, K., & Saik, P. (2021). Sustainable Underground Iron Ore Mining in Ukraine with Backfilling Worked-Out Area. Sustainability, 13(2), 834. https://doi.org/10.3390/su13020834.
18. Sobczyk, W., Perny, K.C.I., Sobczyk, E.J. (2021). Assessing the Real Risk of Mining Industry Environmental Impact. Case Study. Inzynieria Mineralnathis, 1 (1), 33–41. https://doi.org/10.29227/IM-2021-01-05.
19. Malakhov, G.M. (1990). Upravleniye gornym davleniyem pri razrabotke rudnykh mestorozhdeniy Krivorozhskogo basseyna [Management of rock pressure in the development of ore deposits of the Krivoy Rog basin]. (Kyiv: Naukova dumka).
20. Issayeva, L., Togizov, K., Duczmal-Czernikiewicz, A., Kurmangazhina, M., & Muratkhanov, D. (2022). Ore-controlling factors as the basis for singling out the prospective areas within the Syrymbet rare-metal deposit, Northern Kazakhstan. Mining of Mineral Deposits, 16(2), 14-21. https://doi.org/10.33271/mining16.02.014.

21. Zeylik, B., Arshamov, Y., Baratov, R., & Bekbotayeva, A. (2021). New technology for mineral deposits prediction to identify prospective areas in the Zhezkazgan ore region. Mining of Mineral Deposits, 15(2), 134-142. https://doi.org/10.33271/mining15.02.134.

22. Lyashenko, V., Andreev, B., & Dudar, T. (2022). Substantiation of mining-technical and environmental safety of underground mining of complex-structure ore deposits. Mining of Mineral Deposits, 16(1), 43-51. https://doi.org/10.33271/mining16.01.043.

23. Takhanov, D., Muratuly, B., Rashid, Z., & Kydrashov, A. (2021). Geomechanics substantiation of pillars development parameters in case of combined mining the contiguous steep ore bodies. Mining of Mineral Deposits, 15(1), 50-58. https://doi.org/10.33271/mining15.01.050.

24. Panchenko, V., Sobko, B., Lotous, V., Vinivitin, D., & Shabatura, V. (2021). Openwork scheduling for steep-grade iron-ore deposits with the help of near-vertical layers. Mining of Mineral Deposits, 15(1), 87-95. https://doi.org/10.33271/mining15.01.087.

25. Rysbekov, K., Bitimbayev, M., Akhmetkanov, D., Yelemessov, K., Barmenshinova, M., Toktarov, A., & Baskanbayeva, D. (2022). Substantiation of mining systems for steeply dipping low-thickness ore bodies with controlled continuous stope extraction. Mining of Mineral Deposits, 16(2), 64-72. https://doi.org/10.33271/mining16.02.064.

26. Radwanek-Bąk, B., Sobczyk, W. & Sobczyk, E.J. (2020). Support for multiple criteria decisions for mineral deposits valorization and protection. Resources Policy, 68. 101795. https://doi.org/10.1016/j.resourpol.2020.101795.

27. Byzov, V.F., & Korzh, V.A. (2003). Osnovy tekhnolohiyi hirnychoho vyrobnytstva [Basics of mining technology]. (Kryvyy Rih: Mineral).

28. Kalinichenko, V., Dolgikh, O., Dolgikh, L., & Pysmennyi, S. (2020). Choosing a camera for mine surveying of mining enterprise facilities using unmanned aerial vehicles. Mining of Mineral Deposits, 14(4), 31-39. https://doi.org/10.33271/mining14.04.031.

29. Turchaninov, I.A., Iofis, M.A., & Kaspar'yan, Z.Z. (1989). Osnovy mekhaniki gornykh porod [Fundamentals of rock mechanics]. (Leningrad: Nedra).

30. Rymarchuk, B. I. (2007). Rozrobka resursozberihayuchoyi tekhnolohiyi pidzemnoyi vidbiyky zaliznykh rud [Development of resource-saving technology for underground iron ore]. (Kryvyy Rih: KTU).

31. Pysmennyi, S., Chukharev, S., Khavalbolot, K., Bondar, I., & Ijilmaa, J. (2021). Enhancement of the technology of mining steep ore bodies applying the "floating" crown. E3S Web of Conferences, 280, 08013. https://doi.org/10.1051/e3sconf/202128008013.

32. Sobczyk, W. (2015). Sustainable development of Middle East region. Problemy Ekorozwoju – problems of sustainable Development, 10 (2), 51–62.

33. Stupnik, N., Kalinichenko, V., Pismennij, S. & Kalinichenko, E. (2015). Features of underlying levels opening at "ArsellorMittal Kryvyic Rih" underground mine. New Developments in Mining Engineering 2015: Theoretical and Practical Solutions of Mineral Resources Mining, 39–44.

34. Khomenko, O., Kononenko, M., & Danylchenko, M. (2016). Modeling of bearing massif condition during chamber mining of ore deposits. Mining Of Mineral Deposits, 10(2), 40-47. https://doi.org/10.15407/mining10.02.040.

35. Myronova, I. (2016). Prediction of contamination level of the atmosphere at influence zone of iron-ore mine. Mining of Mineral Deposits, 10(2), 64–71. https://doi.org/10.15407/mining10.02.064.

36. Kononenko, M., Khomenko, O., Kovalenko, I., & Savchenko, M. (2021). Control of density and velocity of emulsion explosives detonation for ore breaking. Naukovyi Visnyk Natsionalnoho Hirnychoho Universytetu, 2, 69-75. https://doi.org/10.33271/nvngu/2021-2/069.

37. Tsarikovskiy, V.V. (1987). Opredeleniye i kontrol' dopustimykh razmerov konstruktivnykh elementov sistem razrabotki na rudnikakh Krivbassa [Determination and control of the allowable dimensions of structural elements of development systems at the mines of Krivbass]. (Krivoy Rog: NIGRI).

38. Khomenko, O., & Kononenko, M. (2019). Geo-energetics of Ukrainian crystalline shield. Naukovyi Visnyk Natsionalnoho Hirnychoho Universytetu, 3, 12-21. https://doi.org/10.29202/nvngu/2019-3/3.

39. Mironova, I., Borysovs'ka, O. (2014). Defining the parameters of the atmospheric air for iron ore mines. Progressive Technologies of Coal, Coalbed Methane, and Ores Mining, 333-340. https://doi.org/10.1201/b17547-57.

40. Galayev, N.Z. (1990). Upravleniye sostoyaniyem massiva gornykh porod pri podzemnoy razrabotke rudnykh mestorozhdeniy [Management of the state of the rock mass in the underground mining of ore deposits] (Moscow: Nedra).

41. Zorin, A.N., Kolesnikov, V.G., & Minayev, S.P. (1986). Upravleniye sostoyaniyem gornogo massiva. [Managing the state of the mountain range] (Kyiv: Naukova dumka).

Rozwój technologii wydobywania rudy z niestabilnymi wiszącymi skałami

Kopalnie podziemne złoża rudy żelaza w Krzywym Rogu stosują systemy urabiania komorowego lub systemy z zawałem rudy i nadległych skał w stosunku 35% do 65%. Większość kopalń preferuje systemy eksploracji komorowej z zawałem filarowym ze względu na wysokie wskaźniki techniczne i ekonomiczne. Jednak podczas eksploatacji niektórych obszarów pojawia się problem ze stabilnością wiszących skał. W takich samych warunkach górniczo-geologicznych złoża stopnie na niektórych obszarach są stabilne, ale na innych skały płonne dostają się do stopu od strony wiszącej ściany, gdy powstaje niewielkie odsłonięcie. Dlatego też w warunkach niestabilnych skał wiszącej ściany pilnym zagadnieniem jest rozwój i doskonalenie technologii eksploatacji komorowej. Analiza badań ujawnia czynniki, które znacząco wpływają na stabilność wiszących skał i rudy. Opracowane metody umożliwiają wyznaczenie parametrów statecznościowych oraz zastosowanie udoskonalonego wariantu systemu eksploracji pomieszczenia w warunkach niestabilnej ściany wiszącej za pomocą filaru ochronnego rudy, znajdującego się przy niestabilnej ścianie wiszącej. Z przeprowadzonych obliczeń wynika, że zastosowanie proponowanego systemu urabiania umożliwia zwiększenie zawartości żelaza w wydobywanej masie rudy o 0,94%, zwiększenie ilości wydobywanej masy rudy oraz zysk w wysokości 18,73 tys. euro za cały blok.

Słowa kluczowe: *system wydobywczy, naprężenia, metody, szerokość filaru, wytrzymałość skały, straty, rozcieńczenie*

Express-Method for Determination of Rock Heaving Parameters

Oleksandr SHASHENKO[1)], Eugeniusz Jacek SOBCZYK[2)], Volodymyr SHAPOVAL[3)], Volodymyr KONOVAL[4)], Sofiia BARSUKOVA[5)]

[1)] Doctor of Technical Sciences, Professor of the Department of Construction, Geotechnics and Geomechanics; Dnipro University of Technology, ave. D. Yavornytskoho 19, Dnipro, Ukraine; ORCID https://orcid.org/0000-0002-7012-6157; email: shashenko.o.m@nmu.one
[2)] Professor of the Department of Mineral Resource Management Mineral and Energy Economy; Research Institute of the Polish Academy of Sciences, ul. Wybickiego 7A, Krakow, Poland, ORCID https://orcid.org/ 0000-0003-3968-2312; email: jsobczyk@meeri.eu
[3)] Doctor of Technical Sciences, Professor of the Department of Construction, Geotechnics and Geomechanics; Dnipro University of Technology, ave. D. Yavornytskoho 19, Dnipro, Ukraine; ORCID https://orcid.org/0000-0003-2993-1311; email: shapvv27@gmail.com
[4)] Candidate of Technical Sciences, Docent of the Department of industrial and civil construction; Cherkasy State Technological University, boulevard. Shevchenko, 460, Cherkasy, Ukraine; ORCID https://orcid.org/0000-0002-6740-6617; email: konovalvolodymyr2019@gmail.com
[5)] PhD student of the Department of Construction, Geotechnics and Geomechanics; Dnipro University of Technology, ave. D. Yavornytskoho 19, Dnipro, Ukraine; ORCID https://orcid.org/0000-0003-0821-1091; email: barsukova.s.o@nmu.one

http://doi.org/10.29227/IM-2023-01-14

Submission date: 24-02-2023 | Review date: 20-03-2023

Abstract

Purpose. The problem of determining the contours of the area in which rock heaving occurs is important in the design of underground excavations. The solution of such problems is usually performed either in an elastic-plastic formulation using numerical methods, or using semi-empirical methods, which, as a rule, form the basis of regulatory documents. When writing this article, an attempt was made to use the approach described in work Determining the parameters of a natural arch while forming support load of a horizontal roadways to find answers to such questions: is it possible under these conditions to heave rock at all; what are the outlines of the heaving area.

Theoretical studies of geomechanical processes occurring in the vicinity of horizontal excavations using analytical and numerical mathematical methods. Analysis and generalization of the results of theoretical studies. Simple analytical dependencies are obtained that allow calculating the boundary of the base area in which rock heaving occurs and the stability coefficient of this area. As a stability coefficient, it is proposed to use the ratio of the projection onto the vertical axis of the forces holding the heaving rock mass to the projection of the forces that shift this mass. It has been established for the first time that the maximum depth under the excavation, where the heaving of the rock occurs, is directly proportional to its strength, calculated using the strength criterion of O. Shashenko, multiplied by half the width of the excavation and inversely proportional to the specific adhesion of the rock. It was also established for the first time that the coefficient of rock stability in the area of its heaving is directly proportional to its strength, calculated using the strength criterion of O. Shashenko, and back - to rock pressure at the calculated depth. The results obtained in the course of this work make it possible, using mathematical methods, to perform: forecast of the stability of horizontal excavations in the area of rock heaving, taking into account the depth of the excavation, its geometric dimensions, specific gravity and strength properties of the rock; the boundaries of the rock heaving area, taking into account the depth of the excavation, its geometric dimensions, specific gravity and strength properties of the rock.

Keywords: *excavation, Mohr-Coulomb strength criterion, strength criterion O. Shashenko, rock heaving, arched effect, rock pressure*

1. ANALYSIS OF ACHIEVEMENTS IN THIS AREA

From the practice of operating underground mine excavations, it is known that in their lower part, rock heaving occurs.

A large amount of research in this direction was carried out by M. Protodyakonov, P. Tsimbarevich, M. Pokrovsky, M. Evdokimov-Rokotovsky, V. Orlov, D. Rostovtsev, A. Labas, O. Gurdus, I. Chernyak, O. Shashenko and representatives of his school (O. Solodiankin, S. Hapieiev, O. Sdvyzhkova), as well as other scientists [1, 2, 3, 4, 5, 6, 7].

These studies differ in approaches to assessing the causes of the heaving process, the acting forces, etc. and as a result – results that contradict each other.

In our opinion, when studying the process of rock heaving, the answers to such questions are very important:

1. Does the heaving process take place under given specific conditions (i.e. at the calculated depth, with given excava-tions sizes, given rock properties, etc.).
2. If so, what area of the base is subject to heaving.

In our opinion, answers to these questions can be obtained using the arch effect hypothesis (it was proposed by M. Pro-todyakonov) and the interpretation of this hypothesis set out in [10].

2. MATERIALS AND RESEARCH METHODS

The research task was formulated as follows.:

1. A horizontal excavation is arranged inside the base (fig. 1).
2. The rock pressure in the upper part of the excavation and the lateral pressure are taken by the support, which is able to move vertically. At the same time,

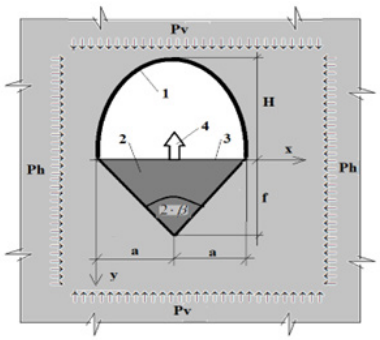

Fig. 1. To determine the area of destruction of rock under a horizontal excavation. Note. The following designations are adopted in the figure: 1 – holding structure; 2 – heaving area; 3 – load-free from loads adit surface; 4 – heaving deformation direction; – vertical pressure; – horizontal pressure; – arch lifting boom; – half the width of the excavation span; – coordinates

Rys. 1. Określenie obszaru zniszczenia skały pod wykopem poziomym. Na rysunku przyjęto następujące oznaczenia: 1 – struktura podtrzymująca; 2 – obszar wypiętrzania; 3 – wolna od obciążeń powierzchnia wyrobiska; 4 – kierunek wypiętrzania; – nacisk pionowy; – ciśnienie poziome; – wysięgnik do podnoszenia łuku; – połowa szerokości przęsła wykopu; – współrzędne

movements of the support and its elements in the horizontal direction are excluded. This is achieved by embedding foundations into the rock and (or) horizontal spacers (fig. 1).

3. There is no support at the bottom of the excavation (fig. 1).
4. The shape of the contour of the area of the rock fall above the excavation is known (more precisely, its equation Y(x). At the same time, the parameters of this are unknown and they should be determined in the course of solving the problem.
5. The rock destruction mechanism is shear. Therefore, its behavior during destruction obeys the Coulomb-Mohr strength condition.
6. The strength characteristics of the rock are known (specific cohesion c and the angle of internal friction φ or the strength of the rock for uniaxial compression R_c and uniaxial tension R_p)
7. The specific gravity of the soil (rock) is known γ.
8. The horizontal and vertical pressures at the estimated depth are known (fig. 1).
9. We need:
   9.1. Find out if rock heaving takes place in this particular case.
   9.2. Determine the boundary separating the destroyed and undestroyed rocks in the roof of the excavation (fig. 1).

In order to determine the zone in which rock heaving takes place, we will take the following assumptions:

1. Rock strength obeys the Coulomb-Mohr law [8]:

$$\tau = \sigma \cdot tg(\varphi) + c = \frac{\sigma}{2} \cdot \frac{R_c - R_p}{\sqrt{R_c \cdot R_p}} + \frac{1}{2} \cdot \sqrt{R_c \cdot R_p}, \quad (1)$$

Here: τ – breaking stress;
σ – normal stress;

$\varphi = \arcsin\left(\frac{R_c - R_p}{R_c + R_p}\right)$ – rock internal friction angle;

$c = \frac{1}{2} \cdot \sqrt{R_c \cdot R_p}$ – specific cohesion;
R_c – soil compressive strength;
R_p – the same, in tension.

2. Equation of the boundary for the heaving region using the Heaviside step function in the first approximation can be represented as a lancet arch:

$$Y(x) = \frac{f}{a} \cdot x \cdot \left[1 - U(a-x)\right] + f \cdot \left(2 - \frac{x}{a}\right) \cdot \left[U(a-x) - U(2 \cdot a - x)\right]. \quad (2)$$

Next, consider the holding and shearing forces acting at some point M (fig. 3).

Since the reason for the destruction of the rock is shear, the forces holding and shifting the rock are directed tangentially to the curve Y(x) at point M (fig. 2).

We also take into account that

$$\beta = \pi/2 - \alpha, \quad (3)$$

(this follows from the scheme in figure 2).

In view of symmetry, in the future we will consider the left side of the arch.

First, we find the differentials of the forces acting at the point M. To do this, consider infinitely small increments of the abscissa dx , ordinate dy и arcs ds (fig. 2 and fig. 3). We have:

$$\left.\begin{aligned} tg(\alpha) = \frac{dY(x)}{dx} = \frac{f}{a};\ \ \alpha = arctg\left[\frac{dY(x)}{dx}\right] = arctg\left(\frac{f}{a}\right); \\ dy = dx \cdot tg(\alpha) = dx \cdot \frac{f}{a};\ \ ds = \sqrt{d^2x + d^2y} = \frac{dx}{a} \cdot \sqrt{a^2 + f^2}. \end{aligned}\right\} \quad (4)$$

Next, we find the differential of the shearing and holding forces. The shear force differential dT_{sd} is equal to:

$$dT_{sd} = P_v \cdot \cos(\beta) \cdot dx = P_v \cdot \sin(\alpha) \cdot dx = P_v \cdot \frac{f}{\sqrt{f^2 + a^2}} \cdot dx. \quad (5)$$

The normal force differential dN is equal to:

$$dN = P_v \cdot dx \cdot \cos(\alpha) = P_v \cdot \frac{a}{\sqrt{f^2 + a^2}} \cdot dx. \quad (6)$$

Driving force differential dT_{ud} is equal to:

$$dT_{ud} = dN \cdot tg(\varphi) + c \cdot ds = P_v \cdot tg(\varphi) \cdot \cos(\alpha) + \frac{c}{\cos(\alpha)} = P_v \cdot tg(\varphi) \cdot \frac{a}{\sqrt{f^2 + a^2}} \cdot dx + c \cdot \frac{\sqrt{f^2 + a^2}}{a} \cdot dx \quad (7)$$

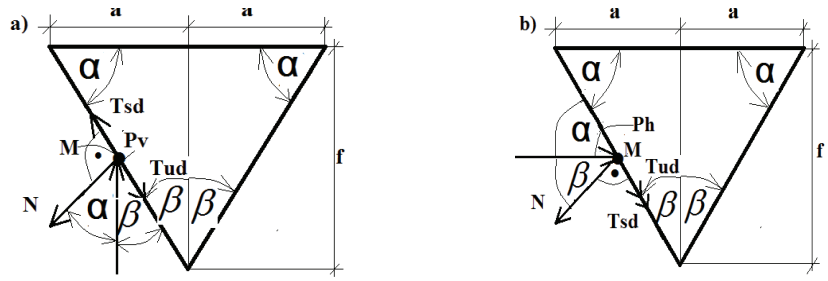

Note: The following designations are adopted in the figure: α – angle of inclination of the generatrix of the wedge to the abscissa axis; $\beta = \pi/2 - \alpha$; $\alpha = \frac{\pi}{2} - \beta$; P_V and P_h – vertical and horizontal components of rock pressure, respectively, acting within one meter of the excavation length (they are measured in $\frac{kN}{m^2} \cdot m$); T_{sd} and T_{ud} – shearing and holding wedge loads, respectively, at a certain point on the wedge surface.

Fig. 2. To the definition of shearing and holding forces (scheme). a) scheme for determining the holding and shear forces from a vertical load P_v; b) the same, from the horizontal

Rys. 2. Do definicji sił ścinających i trzymających (schemat). a) schemat wyznaczania sił trzymania i ścinania od obciążenia pionowego P_v; b) jak w a), od obciążenia poziomego.

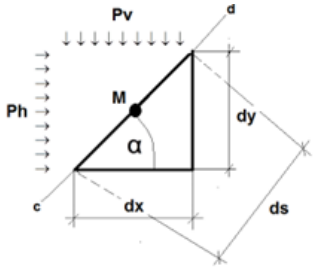

Fig. 3. To the definition of differentials of shearing and holding forces (scheme). Note: this figure should be read together with figure 2

Rys. 3. Do definicji różniczek sił ścinających i trzymających (schemat). Uwaga: ten rysunek należy czytać razem z rysunkiem 2

After that, we find the projections of the holding and shear forces on the vertical axis.

Projection of shear forces on the vertical axis $T_{sd,y}$ is equal to:

$$T_{sd,y} = 2 \cdot \int_0^a dT_{sd} \cdot \cos(\beta) = 2 \cdot \int_0^a P_V \cdot \frac{f}{\sqrt{f^2 + a^2}} \cdot dx \cdot \cos(\beta) = 2 \cdot P_V \cdot \frac{a \cdot f^2}{f^2 + a^2} \tag{8}$$

Projection of holding forces on the vertical axis $T_{ud,y}$ is equal to:

$$T_{ud,y} = 2 \cdot \int_0^a dT_{ud} \cdot \cos(\beta) + Q_{op} = 2 \cdot f \cdot c + 2 \cdot f \cdot P_V \cdot tg(\varphi) \cdot \frac{a^2}{a^2 + f^2} + \gamma \cdot a \cdot f \tag{9}$$

Here $Q_{op} = \gamma \cdot a \cdot f$ – the weight of the rock enclosed within the heaving zone, and γ – specific gravity. In order to simplify (9) and provide some margin of safety, we set $Q_{op} = 0$.

Equalities (8) and (9) make it possible to estimate the strength of the rock subjected to heaving by introducing the stability coefficient in the form of the ratio of the projection onto the vertical axis of the holding forces to the projection onto this axis of the shearing forces:

$$k_u = \frac{T_{ud,y}}{T_{sd,y}} = \frac{c \cdot \left(a^2 + f^2\right) + P_V \cdot a^2 \cdot tg(\varphi)}{f \cdot P_V \cdot a}. \tag{10}$$

This approach allows you to quite simply establish in what state (stable, indifferent or unstable) the base area under the excavation is located.

So, if the rock in the heaving zone is in a stable state, $k_u = (T_{ud,y})/(T_{sd,y}) > 1$. If the rock in the heaving zone is in an indif-ferent state, then $k_u = (T_{ud,y})/(T_{sd,y}) = 1$. Finally, if the rock in the heaving zone is in an unstable state, then $k_u = (T_{ud,y})/(T_{sd,y}) < 1$.

From equalities (8)–(10) it follows that, given different values of the height of the arch lifting boom f we obtain dif-ferent values of the stability coefficient k_u.

However, of interest are such values of the arch lifting boom f at which the value of the stability coefficient will be minimal.

From a mathematical point of view, the above statements are the formulation of the problem of finding the minimum of a certain functional [9].

To find the function $k_u = (T_{ud,y})/(T_{sd,y}) < 1$ take from the functional (10) the first partial derivative with respect to the variable and equate the function thus obtained to zero. We have:

$$\frac{\partial k_u}{\partial f} = -\frac{c \cdot a^2 + P_V \cdot a^2 \cdot tg(\varphi) - c \cdot f^2}{f^2 \cdot P_V \cdot a} = 0, \tag{11}$$

where:

$$f_{1,2} = \pm(a/c) \cdot \sqrt{P_V \cdot c \cdot tg(\varphi) + c^2}. \tag{12}$$

Next, we find out which of the values (12) corresponds to the minimum or maximum of the functional (10).

To do this, we find from (10) the second partial derivative with respect to the variable f and substitute the values of the arch lifting arrow (18) into the expression obtained in this way. We have:

$$\frac{\partial^2 k_u}{\partial^2 f} = 2 \cdot a \cdot \frac{c + P_V \cdot tg(\varphi)}{P_V \cdot f^3}. \tag{13}$$

Tab. 1. The results of determining the stability coefficient of the rock and the depth of the heaving area (see the scheme in fig. 1)

Tab. 1. Wyniki wyznaczenia współczynnika stateczności skały i głębokości strefy wypiętrzania (patrz schemat na rys. 1)

№	Depth of the roof of the excavation, m	Excavation width $2 \cdot a$, m	Depth of heaving deformation area f, .m	Minimum stability factor k_u, fractions of a unit
1	10	6	3,26	11,53
2	100	6	5,04	1,78
3	200	6	6,47	1,14
4	250	6	7,07	1,00
5	300	6	7,63	0,90

Next we find:

$$\lim_{f \to f_{1,2}} \left(\frac{\partial^2 k_u}{\partial^2 f} \right) = \pm \frac{2 \cdot c^2}{P_v \cdot a^2 \cdot \sqrt{P_v \cdot tg(\varphi) \cdot c + c^2}} \quad (14)$$

According to [9], functional (10) has a minimum at the value of the lifting arrow equal to:

$$f = (a/c) \cdot \sqrt{P_v \cdot c \cdot tg(\varphi) + c^2}. \quad (15)$$

Next, we find the minimum value of the stability coefficient of the excavation during heaving of the rock. To do this, we substitute into formula (10) the value of the depth of the heaving region (15). We have:

$$k_{u,\min} = \lim_{f \to f_1} \left(\frac{T_{ud,y}}{T_{sd,y}} \right) = \lim_{f \to f_1} \left\{ \frac{c \cdot \left(a^2 + f^2 \right) + P_v \cdot a^2 \cdot tg(\varphi)}{f \cdot P_v \cdot a} \right\} = 2/P_v \cdot \sqrt{P_v \cdot c \cdot tg(\varphi) + c^2} \quad (16)$$

It is also appropriate to note that despite the fact that the above results were based on the Coulomb-Mohr criterion, the stability coefficient is numerically equal to its double strength, calculated in accordance with the strength criterion of O. Shashenko [1, 2, 3, 4, 5, 6, 7], divided by the vertical component of rock pressure at the estimated depth.

In rock mechanics, it is customary to operate with such strength characteristics as the strength of the rock in uniaxial compression R_c and its strength in uniaxial tension R_p. Therefore, it is advisable to consider the results obtained above using strength characteristics c and φ the results with strength characteristics R_c and R_p.

To pass to new characteristics, we use relations (1). We have:

- for the maximum depth of the base in which heaving takes place:

$$f = a \cdot \sqrt{1 + P_v \cdot \left(1/R_r - 1/R_c \right)}; \quad (17)$$

- for the minimum value of the stability coefficient:

$$k_{u,\min} = \sqrt{R_c \cdot R_r + P_v \cdot \left(R_c - R_r \right)} \Big/ P_v. \quad (18)$$

To illustrate our results, consider the problem of determining the size of the heaving area at the base of horizontal exca-vation with a span of 6 meters located at various depths equal to 10, 100, 200, 250 and 500 meters using the following initial data: specific gravity of the rock γ = 20 kN/m^3; rock compressive strength – Rc = 5000 kPa; compressive strength – Rr = 900 kPa. These strength values are typical for sedimentary rocks such as siltstone, mudstone, marl, chalk, and weak limestone in a fully water-saturated state [11].

The results of calculations by formulas (17) and (18) are summarized in Tab. 1. Analysis of the data presented in Table 1 allowed us to draw the following conclusions:

1. When the bottom of the excavation is located at depths of up to 250 meters, the rock is in a stable state (because Ku>1).

2. When the bottom of the excavation is located at a depth of 250 meters, the rock is in an indifferent state (because Ku=1).

3. When the bottom of the excavation is located at a depth of more than 250 meters, the rock is in an unstable state (because Ku<1). In this case, for example, when the bottom of the excavation is at a depth of 300 meters, the lower boundary of the heaving area is at a depth equal to 300+7,63=307,63 meters.

In our opinion, this information is very important in the design of underground excavations. In particular, from the data presented in the table 1, it follows that there will be no rock heaving up to a depth of 250 meters.

At the same time, if the bottom of the excavation is at a depth of 300 meters, in order to avoid heaving, the rock should be fixed at a depth interval of 300...307,63 meters.

3. CONCLUSIONS

In general, the research materials presented in this paper made it possible to draw the following conclusions.:

1. It is shown that the modification of the theory of the arch effect by M. Protodyakonov proposed by the authors of [10] can be used to determine the geometric dimensions of the heaving zone of rocks in underground excavations.

2. To solve this problem, it is proposed to introduce the so-called stability coefficient k_u, numerically equal to the ratio of the forces holding the rock in the zone of its heaving to the shearing forces. In this case, if the k_u>1 rock in the heaving zone is in a stable state, k_u=1 – in an indifferent state, and if k_u<1 – in an unstable.

3. It has been established that the maximum depth of the soil heaving area is numerically equal to the strength criterion of O. Shashenko [1, 2, 3, 4, 5, 6, 7], divided by the specific cohesion of the soil and multiplied by the excavation span width. This result is obtained for the first time.

4. It is shown that the rock stability coefficient in the area of its heaving is numerically equal to the strength calculated in accordance with the strength criterion of O. Shashenko [1, 2, 3, 4, 5, 6, 7], divided on the vertical component of the rock depth and multiplied by two.

5. Application area of the obtained results: Forecast of the state in which the rock is located in the lower part of the excavation (i.e. is heaving or not). Approximate determination of the boundaries of the base area in the vicinity of an excavation, in which rock heaving takes place. Initial data for the first approximation when solving problems of determining the parameters of the heaving area of the soil by numerical methods using the iteration process.

Literatura – References

1. Shashenko O.M., Sdvyzhkova O.O., & Hapieiev S.M. (2008). Deformovanist ta mitsnist masyviv hirskykh porid: Monohrafiia. [Deformability and strength of rock massifs. Monograph]. Natsionalnyi hirnychyi universytet – National Mining University, 224 [in Russian].
2. Bondarenko V.I., Kovalevska I.A., Symanovych H.A., & Snihur V.H. (2014). Eksperymentalni doslidzhennia zdy-mannia porid pidoshvy pidhotovchykh vyrobok na polohykh plastakh Donbasu: Monohrafiia. [Experimental studies of heaving of the rocks of the sole of the preparatory excavations on the gentle layers of the Donbass: Monograph]. TOV «LizunovPres» - Ltd «LizunovPres», 224 [in Russian].
3. Shashenko O.M., Solodiankin O.V., & Martovytskyi O.V. (2012). Upravlinnia stiikistiu protiazhnykh vyrobok hlybokykh shakht: Monohrafiia. [Management of stability of long workings of deep excavations: Monograph]. Lyzunov Pres - Lyzunov Press, 384 [in Russian].
4. Shashenko O.M., Hapieiev S.M., & Martovytskyi O.V. (2005). Kompleksne doslidzhennia sposobu zabezpechennia stiikosti protiazhnoho vyroblennia z gruntom, shcho vytikaie, roztashovanoi v zoni vplyvu lavy. [Comprehensive study of the method for ensuring the stability of an extended excavation with heaving soil located in the zone of lava influ-ence]. Naukovyi visnyk NHU - Scientific Bulletin of NMU, 52-55 [in Russian].
5. Hapieiev S.M., Lozovskyi S.P., & Riazantsev A.P. (2003). Kompiuterne modeliuvannia protsesu puchennia gruntu v pidhotovchykh vyrobkakh. [Computer modeling of the process of soil heaving in development excavations]. MHHU, 99-101 [in Russian].
6. Soloviov H.I., Nehrii S.H. (1999). Pro osoblyvosti puchennia gruntu vyimkovykh vyrobok v umovakh shakhty «Pivdenno-Donbaska №3» [On the features of heaving of the soil of excavation s in the conditions of the mine "South Donbass No. 3"]. Visti Donetskoho hirnychoho instytutu - News of the Donetsk Mining Institute, 38-45 [in Russian].
7. Shashenko O.M., Khoziaikina N.V., Dubovyk O.I., & Sosna D.O. (2017). Metodyka chyselnoi imitatsii protsesu puchennia porid gruntu u mahistralnykh vyrobkakh. [Method of numerical simulation of soil heaving processes in trunk excavations]. Visti Donetskoho hirnychoho instytutu - News of the Donetsk Mining Institute, 2, 33-42 [in Russian].
8. Shapoval, V., Shashenko, O., Hapieiev, S., Khalymendyk, O., & Andrieiev, V. (2020). Stability assessment of the slopes and side-hills with account of the excess pressure in the pore liquid. Mining of Mineral Deposits, 14(1), 91-99. https://doi.org/10.33271/mining14.01.091
9. Hidrotekhnichni, enerhetychni ta melioratyvni systemy ta sporudy, pidzemni hirnychi vyrobky. Hidrotekhnichni sporudy. Osnovni polozhennia. [Hydrotechnical, energy and reclamation systems and structures, underground mine excavations. Hydraulic structures. Key points]. (2010). DBN V.2.4-3:2010 from 1th January 2011. Kyiv: Minrehionbud Ukrainy [in Ukrainian].
10. Shapoval, V., Solodyankin, A., Hryhoriev, O. & Dubovyk, O. Determining the parameters of a natural arch while forming support load of a horizontal roadways. Naukovyi Visnyk Natsionalnoho Hirnychoho Universytetu. 2021. №2. p. 69-80.
11. Melnykov M. V., Rzhevskyi V. V., Protodiakonov M. M. (Eds.). (1975). Dovidnyk (kadastr) fizychnykh vlastyvostei hirskykh porid. Moskva: «Nedra».

Ekspresowa metoda wyznaczania parametrów wypiętrzania skał

Problem określenia konturów obszaru, w którym występuje wypiętrzanie skał, jest istotny w projektowaniu wyrobisk podziemnych. Rozwiązanie takich problemów jest zwykle wykonywane albo w preparacie sprężysto-plastycznym metodami numerycznymi, albo metodami półempirycznymi, które z reguły stanowią podstawę dokumentów regulacyjnych. Pisząc niniejszy artykuł, podjęto próbę wykorzystania podejścia opisanego w pracy: Determining the parameters of a natural arch while forming support load of a horizontal roadways do znalezienia odpowiedzi na następujące pytania: czy w tych warunkach w ogóle możliwe jest wypiętrzanie skał; jakie są kontury wypiętrzania obszaru.

Zastosowano następujące metody: teoretyczne badania procesów geomechanicznych zachodzących w sąsiedztwie wyrobisk poziomych z wykorzystaniem analitycznych i numerycznych metod matematycznych; analiza i uogólnienie wyników badań teoretycznych. Otrzymano proste zależności analityczne pozwalające na obliczenie granicy obszaru bazowego, w którym występuje wypiętrzanie skały, oraz współczynnika stateczności tego obszaru.

Jako współczynnik stateczności proponuje się przyjąć stosunek rzutu na oś pionową sił utrzymujących falujący górotwór do rzutu sił przesuwających ten masyw. Po raz pierwszy ustalono, że maksymalna głębokość pod wyrobiskiem, na której występuje wypiętrzanie skał, jest wprost proporcjonalna do jej wytrzymałości, obliczonej według kryterium wytrzymałościowego O. Szaszenki, pomnożonej przez połowę szerokości wyrobiska, i odwrotnie proporcjonalna do przyczepności właściwej skały.

Po raz pierwszy ustalono również, że współczynnik stateczności skały w obszarze jej wypiętrzania jest wprost proporcjonalny do jej wytrzymałości, obliczonej za pomocą kryterium wytrzymałościowego O. Szaszenki, i odwrotnie – do ciśnienia na obliczonej głębokości. Uzyskane w toku pracy wyniki pozwalają, metodami matematycznymi, na wykonanie: prognozy stateczności wyrobisk poziomych w rejonie wypiętrzenia skał z uwzględnieniem głębokości wyrobiska, jego wymiarów geometrycznych, ciężaru właściwego i właściwości wytrzymałościowych skały; granic obszaru falowania skał z uwzględnieniem głębokości wyrobiska, jego wymiarów geometrycznych, ciężaru właściwego i właściwości wytrzymałościowych skały.

Słowa kluczowe: *wyrobisko, kryterium wytrzymałościowe Mohra-Coulomba, kryterium wytrzymałościowe O. Shashenki, wypiętrzanie skał, efekt łukowy, ciśnienie skał*

Modeling and Prediction of Iron Ore Quality Indicators

Andrii PEREMETCHYK[1], Serhii PYSMENNYI[2], Nataliia SHVAHER[3], Serhii FEDORENKO[4], Tatyana PODOYNITSYNA[5]

[1] Kryvyi Rih National University, Ukraine; ORCID https://orcid.org/0000-0001-6274-146X; email: a.v.peremetchyk@gmail.com
[2] Kryvyi Rih National University, Ukraine; ORCID https://orcid.org/0000-0001-5384-6972
[3] Kryvyi Rih National University, Ukraine; ORCID https://orcid.org/0000-0002-9986-8605
[4] Kryvyi Rih National University, Ukraine; ORCID https://orcid.org/0000-0001-5753-9603
[5] Kryvyi Rih National University, Ukraine; ORCID https://orcid.org/0009--0000-9905-8912

http://doi.org/10.29227/IM-2023-01-15

Submission date: 16-02-2023 | Review date: 24-03-2023

Abstract

The paper proposes solution of the topical scientific problem that consists in developing a geometrical method of predicting quality indicators of iron ore deposits, applying a mathematical model of a multidimensional random geochemical field which is realized on the basis of self-organizing prediction methods. The authors develop a multidimensional heuristic prediction algorithm that uses a polynomial of arbitrary power and enables description of any functional dependency. It is demonstrated that a system of equations of a multidimensional random geochemical field should be used to mathematically describe elements of the rock massif. The grapho-analytical model of the deposit is built using geostatistical methods. It is determined that at Kryvbas deposits the kriging method is the most suitable for assessing and improving reliability of the input geological data since detailed geological exploration is carried out by means of an irregular grid of boreholes. An important aspect of geometrization of iron ore deposits is geometrical prediction of their quality indicators for solving tasks of long-term and current planning in order to provide the most efficient performance of the mining enterprise to improve rationalization of deposit development.

Keywords: *geometrization, mining geometrical methods of prediction, geostatistical methods, kriging, heuristic algorithms of prediction, multidimensional random geochemical field*

1. Introduction

Sustainable economic development based on scientific and technological achievements is impossible without further development of the mining industry which requires expansion of the raw material base of mining enterprises [1], improvement of mining technologies [2–5], substantiation of mining methods [6, 7], selection of rational technical means of mining [8, 9]. This, in turn, requires improving the scientific basis of predictions and geological assessment of mineral deposits, increasing completeness of mineral use and applying an integrated approach [10–12]. To solve these problems, it is necessary to create deposit models that provide reliable mining and geological data obtained by geometrical methods.

Geometrical graphs depicting the quality of deposits enable establishing a certain relationship between components of the useful mineral, thus determining these components' location. This is of great importance for the deposit design and operation [13–15]. Such graphs make it possible to plan extraction of minerals with a certain composition necessary for their mining and processing.

Sustainable safe economic development dependent on the use of subsoils [16–18] requires deepening of mining operations as well as industrial processing of ores with the low iron content and complex mineral composition. Application of flowsheets and equipment of large unit capacity results in increased quantitative and qualitative losses of the useful component [19] that affect processing, and decreased concentrate quality due to inefficient processing caused by uneven ore quality. The quality composition of ore most greatly influences the cost of the final product of metallurgical treatment. At the same time, it should be borne in mind that technical and economic indicators of metallurgical treatment can be improved by not only the increased iron content but also achievement of a high degree of ore blending on the basis of geometrical assessment of the massif.

Increased depth of mining results in a stress-strai state of the rock massif [20–22], as well as the need to find reliable materials for timbering mine workings [23]. The problem of stability and geometric monitoring of the rock massif is gaining topicality [24–26].

A particularly important aspect of appying geometrization of iron ore deposits is geometrical prediction of their quality indicators for solving tasks of current and long-term planning in order to provide the most efficient performance of the mining enterprise in terms of ore blending and to improve rationalization of deposit development. It is also of great importance to carry out mining operations with the minimal impact on the environment and the rock massif [27-30]. This can be achieved based on a clear understanding of rock properties and geological indicator distribution in the massif.

Mining and geometrical graphs of location of the deposit parameters are widely used in solving a wide range of practical problems of exploration, design and operation of the deposit, but in some cases they do not meet practical requirements in terms of both their accuracy and efficiency of geological-surveying data use. Poor quality of assessment of geological data in the subsoil plays a major role here. Reliability of geological data assessement in conditions of high variability of distribution of the indicators in the massif can be increased through geostatistical methods of assessment [31–33].

Tab. 1. Comparison of methods of assessing subsoil ore quality

Tab. 1. Porównanie metod oceny jakości rud podglebia

Distribution of components in the massif	Assessment error (%) obtained by methods of				
	weighted arithmetic average	weighing inversely as square of distances	weighing and accounting anisotropy	discrete kriging	universal kriging
Fe_{mag}	12.1	11.8	11.5	9.6	8.3
Fe_{tot}	18.1	18.2	18.1	16.4	16.4
Si	8.5	8.6	8.4	8.5	–

Many methods of geometrization are based on a simplified representation of a mathematical model of geological location in the form of a geochemical field and a random geochemical field. In this case, methods of geometrization of deposits based on principles of self-organization can most completely describe models of location of mining and geological parameters in the subsoil [34–36]. Such models enable description of complex patterns of location of indicators which makes it possible to predict location of geological indicators in the subsoil with great accuracy and, on this basis, plan the rational performance of the mining enterprise. Development of such methods are dealt with in the present paper.

2. Methods

The authors develop a methodology of geometricization of the iron ore deposit and prediction of quality indicators of its reserves on the basis of self-organizing algorithms [37].

Depending on the coordinates of space x, y, z and time t, regularity of location of the parameter P can be described by the general type function (P.K. Sobolevsky geochemical field):

$$P = f(x, y, z, t) \tag{1}$$

If location of the parameter φ(P) is random, the mathematical model of its location can be written as a random geochemical field:

$$P = f(x, y, z, t) + \bar{\phi}(p) \tag{2}$$

where $\bar{\phi}(p)\{\delta_x(p); \delta_y(p); \delta_z(p); \delta_i(p)\}$; $\delta_x(p)$, $\delta_y(p)$, $\delta_z(p)$, $\delta_i(p)$ are dispersions of the parameter by the space and time i coordinates.

These models, with the help of which a number of major theoretical and practical problems have been solved, can no longer be considered adequate in terms of complexity to the objects under study. Existing geometrization methods have therefore a number of serious limitations which either cannot be overcome in principle within the framework of the applied mathematical models or cause great theoretical and practical difficulties.

In addition, the predominantly linear interpolation used in mining plotting can lead to significant parameter errors in the inter-borehole space. Application of other types of interpolation (square, cubic, etc.) for this purpose does not always yield good results, as there are no reliable techniques for determining the type of interpolation corresponding to the complexity of the surface under consideration. Besides, plotting models with nonlinear interpolation is very laborious.

The above leads to the search for a more perfect and complex model of parameter location and new methods based on it to solve a wide range of mining and geometrical problems. A multidimensional random geochemical field is the model of this type. This model is successive and logically develops and refines available mathematical models of location.

Kryvbas iron ore deposits have a very heterogeneous geological structure. The patterns of indicator location are multifaceted. Therefore, for their description, a multidimensional random geochemical field is accepted as a mathematical model:

$$P = f(\bar{p}) + \bar{\phi}(p) \tag{3}$$

where $\bar{p}\{x, y, z, t, p_1, p_2, ..., p_m$

and $\bar{\phi}(p)\{\delta_x(p); \delta_y(p); \delta_z(p); \delta_i(p); \delta_{p1}; \delta_{p2}; ..., \delta_{pm}\}$

From equation (3) it follows that the value of the geological parameter P consists of the multidimensional vector $f(\bar{p})$ that describes the pattern of the parameter location depending on the space-time coordinates x, y, z, t and other geological parameters p_1; p_2; p_3; ...; pm, as well as multidimensional dispersion of location $\bar{\phi}(p)$.

Practically, building model (3) is possible using principles of heuristic self-organization of mathematical models of complex systems. Given the limited amount of data in individual areas, the Group Method of Data Handling (GMDH) is the most preferred procedure for predicting the indicator within their boundaries.

The idea behind the GMDH is that a mathematical model of a complex system is built gradually, in the process of so-called multi-layer selection. Before building a model, a list of possible equation arguments and elements of the future equation (base function) is specified. According to the algorithm based on the suggested selection criteria by means of multiple searches, equations (their variables and coefficients are selected) are built that optimally correspond to complexity (variability) and degree of study of the modeled object.

In the GMDH procedure, all the input data

$$\{P_i\}_{i=1}^{n}; \{\bar{x}_j\}_{i=1}^{n},$$

where P is the predicted indicator; x ={x_1, x_2, ..., x_m} are possible arguments of prediction equations; i = 1, 2,..., n are of indicators P and x observation points, are divided into two sets: learning $\{P_i\}_{i=1}^{r}$; $\{\bar{x}_j\}_{i=1}^{r}$ and control $\{P_i\}_{i=1}^{k}$; $\{\bar{x}_j\}_{i=1}^{k}$, at that r + k = n.

On the first set of points, the equation is built (the model is learning), on the second one, which is an external complement, the quality of the obtained equation, its predictive properties are controlled.

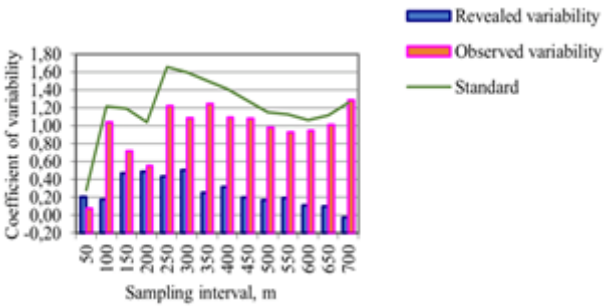

Fig. 1. Variability of the Femag content at different sampling intervals
Rys. 1. Zmienność zawartości Femag w różnych odstępach czasu pobierania próbek

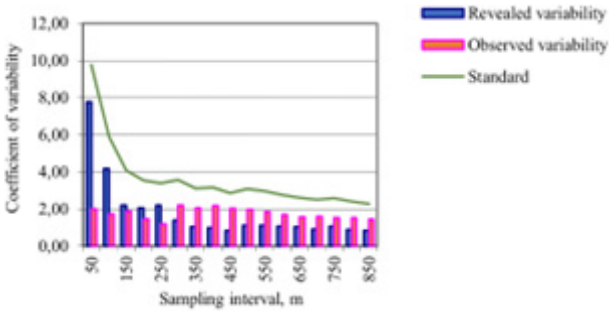

Fig. 2. Variability of the Fetot content at different sampling intervals
Rys. 2. Zmienność zawartości Fetot w różnych interwałach próbkowania

An important feature of the GMDH is that complete multidimensional description of a natural object is replaced by several layers of specially selected individual descriptions (base functions) compiled for pairs of input arguments:

$$P=a_o+a_1x_g+a_2x_c;$$
$$P=a_o+a_1x_g+a_2x_c+a_3x_gx_c; \quad (4)$$
$$P=a_o+a_1x_g+a_2x_c+a_3x_gx_c+a_5x^2_c$$

The building of a mathematical model starts with the least squares calculation of coefficients of any of the individual descriptions at the points of the learning set:

$$P_1 = f_1^{(1)}(x_1,x_2);\ P_2 = f_2^{(1)}(x_1,x_2),\ P_s = f_s^{(1)}(x_{m-1},x_m), \quad (5)$$

where s = c_2m; (1) is the selection layer number

At control points, which do not participate in calculating the coefficients of these models, their quality is checked by the criterion of the mean square deviation of the measured Pi from Pci calculated by the equations (5) of the values of the predicted indicator:

$$\overline{\delta}_k^{(1)} = \sqrt{\frac{1}{k}\sum_{i=1}^{k}\delta_i^2}\ ;\ \delta_i = P_i - P_i^c. \quad (6)$$

Next, all the equations (5) are ranked by criterion (6) and the best of them (by minimum values $\overline{\delta}_k$) are accepted as arguments in equations (4) on the second layer of model selection, after which coefficients of new dependencies are calculated at the points of the learning set:

$$y_1 = f_1^{(2)}(P_1,P_2);\ y_2 = f_2^{(2)}(P_1,P_3),\ y_V = f_V^{(2)}(P_{T-1},P_T). \quad (7)$$

At the points of the control set, criterion $\overline{\delta}_k^{(2)}$ (6) is calculated again for each equation of (7) and T of the best equations are ranked and selected according to it. If $\overline{\delta}_{k_{\min}}^{(1)} > \overline{\delta}_{k_{\min}}^{(2)}$, it is necessary to proceed to the third layer of the selection, where all the described procedures are repeated. The model is built until the inequality $\overline{\delta}_{k_{\min}}^{(j-1)} > \overline{\delta}_{k_{\min}}^{(j)}$ is met.

Complexity of the built equation increases from layer to layer of selection due to the increasing number of input variables and their power. When applying the first description from equations (4), only the number of accountable arguments increases, when applying the second and third ones the power is additionally taken into account.

Each individual description (4) is a function of two variables, this allowing reliable dependencies to be built on a small number of experimental points (7–10 points). The mathematical models of type (3) obtained in the described way are optimal both in terms of complexity and in the degree of study of the indicator to be predicted and arguments related to it. From a great number of arguments of the system "deposit", the method allows selecting only those ones that are actually related to the indicator to be predicted and establishing the type and strength of this relationship. The found equation describes the pattern of location of the indicator to be predicted. The value (6) evaluates the prediction error of this equation and is the multidimensional dispersion of the model.

Further modeling of the deposit is performed with the help of a multidimensional heuristic prediction algorithm (MHPA) developed by the authors. This algorithm realizes equations of a mathematical model of a multidimensional random geochemical field with maximum efficiency.

The idea behind the algorithm consists in finding the optimal type of function of indicator location, which gives the minimum deviation of the total of the absolute values of the calculated values from the actual ones.

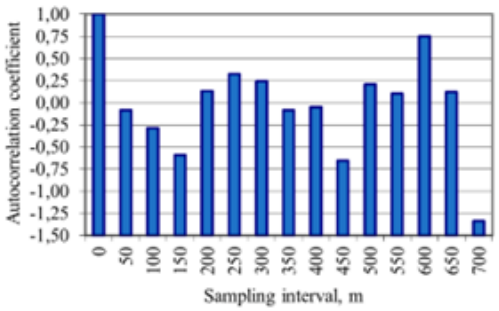

Fig. 3. Autocorrelation coefficient of the Femag content at different sampling intervals
Rys. 3. Współczynnik autokorelacji zawartości Femag w różnych interwałach próbkowania

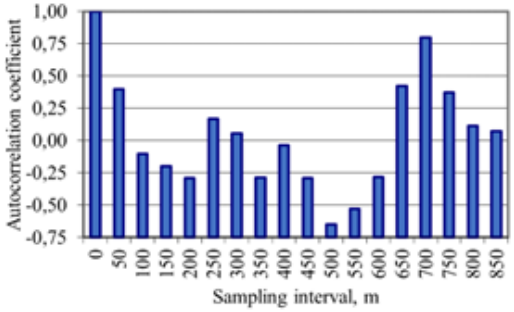

Fig. 4. Autocorrelation coefficient of the Fetot content at different sampling intervals
Rys. 4. Współczynnik autokorelacji zawartości Fetot w różnych przedziałach próbkowania

$$f_i = [c_i^p (a_{11}^p x_1^p + b_{11}^p x_1^p)^p \cdot (a_{12}^p x_2^p + b_{12}^p x_2^p)^p \cdot ... (a_{1n}^p x_2^p + b_{1n}^p x_2^p)^p \cdot (a_{21}^p x_1^p + b_{21}^p x_1^p)^p \cdot (a_{22}^p x_2^p + b_{22}^p x_2^p)^p \cdot ... (a_{mn}^p x_n^p + b_{mn}^p x_n^p)^p], \quad (8)$$

$$F_i(x_1, x_2, ..., x_n) = d_i^p [f_1(x_1, x_2, ..., x_n) + f_2(x_1, x_2, ..., x_n) + ... + f_n(x_1, x_2, ..., x_n)]^p + k^p, \quad (9)$$

$$P(x_1, x_2, ..., x_n) = g^p [F_1(x_1, x_2, ..., x_n) + F_2(x_1, x_2, ..., x_n) + ... + F_n(x_1, x_2, ..., x_n)]^p + h^p, \quad (10)$$

where a, b, c, d, k, h are numerical coefficients.

Functions (8)–(10) are a polynomial powers and coefficients of which can have both integer and fractional or negative values. Degrees, in turn, may be functions of the same kind as the whole polynomial. The increase in the order of powers or the number of variables that are added to the polynomial is not limited.

The procedure of the algorithm application is as follows. There is a grid of detailed exploration boreholes at the deposit. It is necessary to find a functional relationship between the quality indicators that are determined by the boreholes and the magnetic iron content in the blasted mass and then to extend it to the untreated areas of the deposit. In the inter-borehole space, the values obtained from the detailed exploration boreholes are interpolated to points with known magnetic iron values in the blasted mass and are accepted as arguments. It is reasonable to accept indicators with the distribution law similar to that of the one to be predicted as polynomial arguments. In this case, this is the total and magnetic iron content in detailed exploration boreholes. Distances from the point to the nearest detailed exploration borehole must be taken as arguments, since accuracy of interpolation decreases with the increased distance from the borehole. Introduction of these distances enables improvement of regularity of change in accuracy and determination of corrections.

The total of deviations of calculated absolute values from actual ones at all points of the deposit with known quality indicators is accepted as the criterion of the algorithm efficiency. Individual deviations are introduced into the total with the weight inversely proportional to the distance from a given point to the nearest borehole. Thus, more accurate results of the function building have a higher priority when assessing the quality of the predictive function built.

The algorithm consists of several basic algorithms, such as the algorithm of double increase (decrease) of a numerical coefficient based on increasing the absolute value of the coefficient at the argument until the optimum condition of functions (8)–(10) is met, and a modified half-interval algorithm improving results of the previous algorithm. Performance of both algorithms, as well as the sequence of their use, is regulated by the system of conditional transitions, which makes it possible, when the results of finding numerical coefficients of the predictive function decrease, to proceed to addition of new coefficients, or to another method of searching for the optimal type of already available coefficients. In this algorithm, numerical coefficients are changed and values of the predictive function are fixed by a special method. With the help of the above algorithms, numerical coefficients are searched for again, starting with the one that gives the largest change in the predictive function and shows the greatest sensitivity. Then, the coefficient that gives the least change and sensitivity etc. is considered. If this search method does not produce positive results, consideration begins with the coefficient that gives the least change when it is excluded. Thus, the optimal method and direction of the search for the type of the predictive function are determined. Then transition to the algorithm of data grouping by values of deviations and building local predictive functions for individual areas of the deposit is made according to the above-described methods.

Tab. 2. Dependency of Femag on Fetot content based on blasted rock mass sampling data
Tab. 2. Zależność zawartości Femag od Fetot na podstawie danych z prób wysadzonych górotworu

Ferruginous horizon PR_1sx^{4f}	Predictive function
PR_1sx^{4f6}	Fe_{mag}=0.98 Fe_{tot} – 6,24
PR_1sx^{4f5}	Fe_{mag}=0.87 Fe_{tot} – 0.14
PR_1sx^{4f4}	Fe_{mag}=0.70 Fe_{tot} + 4,10
PR_1sx^{4f3}	Fe_{mag}=0.85 Fe_{tot} + 0.68
PR_1sx^{4f2}	Fe_{mag}=1.34 Fe_{tot} – 18.48

Tab. 3. Dependency of concentrate yield ( ) on Femag content based on blasted rock mass sampling
Tab. 3. Zależność plonu koncentratu ( ) od Femag na podstawie danych z prób wysadzonych górotworu

Ferruginous horizon PR_1sx^{4f}	Predictive function
PR_1sx^{4f6}	γ=1.37 Fe_{mag} + 3.84
PR_1sx^{4f5}	γ=1.38 Fe_{mag} + 4.16
PR_1sx^{4f4}	γ=1.20 Fe_{mag} + 10.72
PR_1sx^{4f3}	γ=1.65 Fe_{mag} + 3.74
PR_1sx^{4f2}	γ=1.58 Fe_{mag} – 0.32

When dividing by zero or finding an even power root of a negative value, which may occur at individual points of the deposit, any constant value that best satisfies the efficiency criterion is conditionally accepted in the algorithm. This makes it possible to describe a discontinuous functional dependency. Based on the nature of the polynomial, any functional dependency can be described.

Geometrization and modeling of mineral deposit quality indicators are based on geological data assessment. Table 1 presents comparison of the most frequently used methods of geological data assessment.

As is seen from Table 1, geostatistical methods of assessment, including kriging, are the most efficient for assessing geological data.

Advantages of geostatistical methods include a clear mathematical statement; possibility of analytical formulation of calculations and high degree of their unification; when calculating reserves, the average values of indicators are compared with the geometrical shape of blocks and their spatial location, and anisotropy of mineralization is considered as well.

Kriging solves two main tasks: assessment of ore reserves and determination of this assessment accuracy.

The average content in a block is determined by the formula:

$$z^* = \sum_{i=1}^{n} a_i \cdot z(x_i) \tag{11}$$

where $z(x_i)$ is the useful component content in samples, %; a_i is the weighting coefficient (kriging).

The coefficient a is determined by solving the system of kriging equations. The value a depends on qualitative characteristics of variability of the content within the ore body under study and to which the block belongs. In this case, the main goal consists in finding such weighting coefficients that enable the best assessment of the content and the least assessment error.

There are several types of kriging, its selection depends on geological exploration and sampling data, mining systems, dimensions of blocks under assessment and their geometrical location.

Thus, it is reasonable to apply geostatistical methods to processing the input data and the modeling results.

3. Results and their discussion

The developed methodology was applied to assess Skelevatske deposit in Kryvbas.

At Skelevatske deposit of ferruginous quartzites, the ferruginous horizon PR_1sx^4f is being mined. It comprises seven geological subhorizons, the productive thickness includes five of them – $PR_1sx^4f^2$, $PR_1sx^4f^3$, $PR_1sx^4f^4$, $PR_1sx^4f^5$, $PR_1sx^4f^6$. Two subhorizons $PR_1sx^4f^1$ and $PR_1sx^4f^7$ are not mined due to high rock heterogeneity.

At the deposit of ferruginous quartzites, there is a close relationship between the magnetic iron content in the ore and the yield of concentrate from the ore and, in turn, between the total iron content and that of magnetic iron. In most cases, samples are taken for the content of total and magnetic iron. Therefore, it is necessary to find the relationship between the content of these components and the technological parameters of ores mined. During the detailed exploration of the deposit, the content of Fe_{mag} in ores was not determined, so the dependency of Fe_{mag} on Fe_{tot} was analyzed.

Areas with the regular character of variability of average useful component contents are singled out. Each of the selected areas is assigned the general value of the indicator to be predicted in it. This indicator is taken as the relationship between the magnetic iron and the concentrate yield from the ore. On this basis, predictive mining and geometrical modeling is performed.

Variability of the geological data on which prediction is based depends largely on location of the deposit parameters. Variability of the indicator can be detected and is considered standard. Different methods of assessing variability may produce ambiguous results. If the distance between the sampling points exceeds the critical geological exploration interval, the geological exploration grid is considered unusable because it does not reveal the nature of location of indicators in the subsoil. This requires so-called exploration grid thickening, i.e. addition of extra sampling points, which is expensive and not always feasible. However, it is possible that the method of assessing the geological exploration grid is not suitable for as-

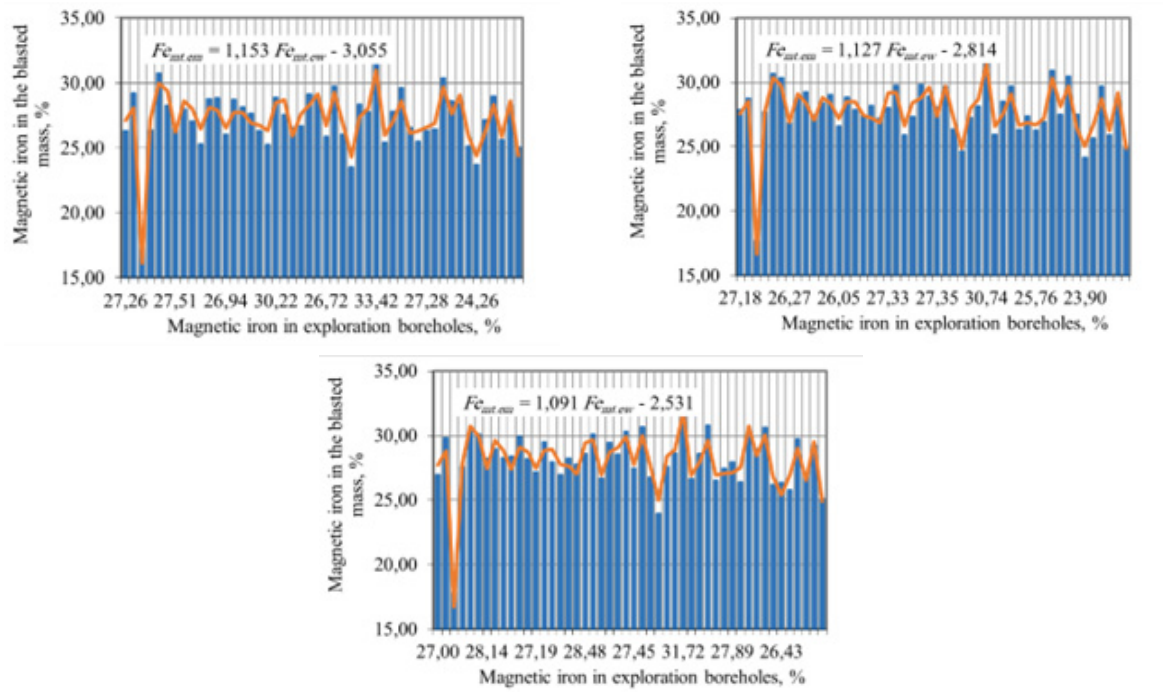

Fig. 5. Predictive functions of the dependency of the Femag content in the blasted mass on the Femag content based on geological exploration borehole sampling

Rys. 5. Funkcje predykcyjne zależności zawartości Femag w masie po odstrzale od zawartości Femag z próby geologicznych otworów wiertniczych

sessing the current grid, since the regularity of the geological indicators location is not consistent with assessment capabilities of this method. This raises the problem of selecting the method of exploration grid assessment.

The share of random and regular variability at a given exploration interval can be derived from the relation:

$$\sigma^2_{зак} = \sigma^2 - \sigma^2_u \tag{12}$$

where σ^2 is the standard; σ^2_u is the observed variability.

The dependency of assessment of the observed variability on the sampling interval, and the standard can be determined from the expressions:

$$\sigma^2_u = \frac{1}{2(n-1)} \sum^{n-1} (u_{i+1} - u_i)^2 \tag{13}$$

$$\sigma^2 = \frac{1}{n-1} \sum^{n} (u_i - \bar{u})^2 \tag{14}$$

where $\bar{u} = \frac{1}{n} \sum u_i$ is the arithmetic average of series of observations of the parameter; n is the sampling interval.

To determine the radius of auto-correlation, the auto-correlation function is applied, its individual values are calculated by the formula

$$\rho_x(l) = k(l) = \frac{1}{\sigma^2(N-k)} \sum_{i=1}^{N-k} (u_i - \bar{u})(u_{i+k} - \bar{u}) \tag{15}$$

where $\bar{u} = \frac{1}{n} \sum u_i$ is the arithmetic average of a series of observations of the parameter; σ^2 is the dispersion of this series; k = 1,… N – 1 is the exploration interval; N is the total number of exploration grid pitches along the section.

Assessment based on successive differences of the indicator slightly dependent on the nature of the pattern of quality indicators location is given in Figures 1, 2. As is seen from Figures 1, 2, the minimum critical geological exploration interval for magnetic iron at Skelevatske deposit is 600 m, which corresponds to the exploration grid parameters.

Figures 3, 4 demonstrate that the autocorrelation coefficient states the sinusoidal character of variability of the regular component of spatial location of indicators. This testifies to the non-linear nature of the existing pattern of component location. This enables the conclusion that the autocorrelation coefficient based on deviation from the sample average does not provide reliable assessment of geological data in Kryvbas conditions.

According to the GMDH procedure, the main regularities of distribution of geological indicators in the ferruginous subhorizons of the deposit are determined.

Preparatory operations include allotment of geologically homogeneous areas for prediction, selection of the variable scope needed for the prediction equation, and selection of points of the learning and control sets.

The stage of homogeneous geological areas allotment is necessary to improve accuracy of prediction equations. The areas should be allotted considering degrees of exploration, major tectonic disturbances, wedging-out, geological types of ore, etc. It should be noted that as the area and number of exploration boreholes decrease, the equation more accurately describes the local pattern in the predicted area, but it is unsuitable for identifying more general regularities throughout the minefield. The reverse is true for the increased prediction area (the number of exploration boreholes). The method enables finding coefficients of the equation even by 8 – 10 indicator measurement points. However, practice shows that the optimum number of exploration points in a homogeneous area is between 20 and 40 boreholes.

The variable scope needed for a prediction equation is chosen based on possible genetic relationships with the pre-

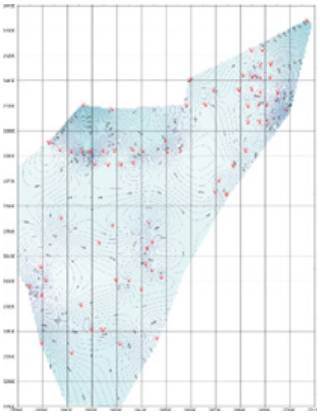

Fig. 6. Grapho-analytical model of isolines of the predictive content of Femag in the blasted rock mass in the PivdGZK open pit
Rys. 6. Grafo-analityczny model izolinii predykcyjnej zawartości Femag w odstrzelonym górotworze w odkrywce PivdGZK

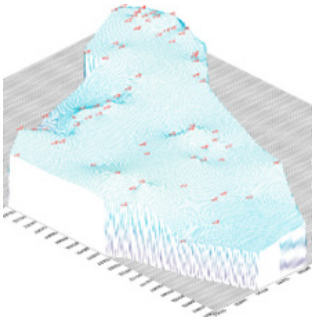

Fig. 7. Graphical visual model of the predictive Femag content in the blasted rock mass in the PivdGZK open pit
Rys. 7. Graficzny model wizualny predykcyjnej zawartości Femag w odstrzelonym górotworze w odkrywce PivdGZK

dicted indicator. In the case under study, in accordance with the geological concepts of genetic unity of the rocks forming Skelevatske deposit of ferruginous quartzites, as well as the need to predicrt technological parameters of the mined ores, such indicators as the total (Fe_{tot}) and magnetic iron (Fe_{mag}) content in the ores and concentrate yield (γ) are accepted as possible arguments for prediction equations. This is explained by the fact that the indicators have a regular character of location confirmed by the results of substitution of the obtained equations into the areas with known values of the indicators (Tables 2, 3).

Further modeling of the deposit was performed with the help of a multidimensional heuristic prediction algorithm (MHPA), developed by the authors. The magnetic iron content in the blasted rock mass was modeled. The contents of magnetic iron by exploration grid boreholes were taken as arguments of the predictive function. As a result of the algorithm performance, data grouping was made and three functional dependencies were found on the deposit, (Figure 5 (a), (b), (c)).

Kriging methods were used to create a grapho-analytical model of the deposit using the found predictive functions. The prediction results were interpolated to nodes of the 50×50 m square grid, then graphical models of the deposit were built (Figures 6, 7).

As a result of the study, prediction of spatial lcation of magnetic iron in the blasted rock mass is obtained. This is the most important technological indicator on which sustainable performance of the mining enterprise depends. Knowledge of spatial location of this indicator enables current and long-term planning of the enterprise, selection of optimal parameters of mining operations and improvement of mineral mining efficiency.

The developed prediction methodology has been implemented at the PivdGZK open pit and is used to estimate current and predictive reserves of the deposit and to plan mining operations in the open pit.

4. Conclusions

The article shows solution of the actual scientific and technical problem of geometrization of qualitaty indicators of iron ore deposits. As a result, a geometrical model of the deposit is built, which makes it possible to describe patterns of spatial location of the most important quality indicators and to predict their change in the process of mining development.

The article shows that equations of random geochemical field are the most suitable for describing the character of location of quality indicators of deposits with high anisotropy of geological characteristics. These equations can be solved using self-organizing analytical methods of prediction.

A mining and geometrical method of predicting quality indicators of iron ore deposits is developed based on a mathematical model of a multidimensional random geochemical field which is implemented using self-organizing analytical prediction methods. A new multi-dimensional heuristic prediction algorithm is develop that uses a polynomial of arbitrary power and enables description of any functional dependency. It is determined that geostatistical methods are the most suitable for assessing and improving reliability of the input geological data, since detailed geological exploration is carried out by means of an irregular borehole grid.

As a result of the deposit geometrzation, a grapho-analytical model of the deposit is built. It enables geometrical prediction of quality indicators of the deposit to solve the tasks of long-term and current planning to provide the most efficient performance of the mining enterprise in terms of ore blending and to improve rationalization of deposit development.

The most promising directions of geometrization of qualitative indicators of deposits include self-organizing methods of predicting spatial location of mining and geological indicators of deposits combined with geostatistical methods of assessment. These techniques require further development and extension of its application area.

Acknowledgments

The work was supported by the Ministry of Education and Science of Ukraine within the framework of the state scientific themes "Investigation and scientific and practical substantiation of technological means for raw material control in mining ores on deep levels" (State registration 0122U000843).

Literatura – References

1. Stupnik, M., Kalinichenko, V. (2013). Magnetite quartzite mining is the future of Kryvyi Rig iron ore basin. Annual Scientific-Technical Colletion - Mining of Mineral Deposits 2013, 49–52.
2. Stupnik, N., Kalinichenko, V., Pismennij, S. & Kalinichenko, E. (2015). Features of underlying levels opening at "ArsellorMittal Kryvyic Rih" underground mine. New Developments in Mining Engineering 2015: Theoretical and Practical Solutions of Mineral Resources Mining, 39–44.
3. Stupnik, N.I., Fedko, M.B., Kolosov, V.A., & Pismennyy S.V. (2014). Development of recommendations for choosing excavation support types and junctions for uranium mines of state-owned enterprise skhidhzk. Naukovyi Visnyk Natsionalnoho Hirnychoho Universytetu, (5), 21–25.
4. Stupnik, M., Kalinichenko, V., Fedko, M., Pysmennyi, S., Kalinichenko, O., & Pochtarev, A. (2022). Methodology enhancement for determining parameters of room systems when mining uranium ore in the SE "SkhidGZK" underground mines, Ukraine. Mining of Mineral Deposits, 16(2). 33–41. https://doi.org/10.33271/mining16.02.033
5. Stupnik, N.I., Kalinichenko, V.A., Fedko, M.B. & Mirchenko, Ye.G. (2013). Prospects of application of TNT-free explosives in ore deposites developed by udergrounds mining. Naukovyi Visnyk Natsionalnoho Hirnychoho Universytetu, 1, 44–48.
6. Kalinichenko, O., Fedko, M., Kushnerov, I. & Hryshchenko, M. (2019). Muck drawing by inclined two-dimensional flow. E3S Web of Conferences, 123, 01015.
7. Stupnik, M.I., Kalinichenko, O.V. & Kalinichenko, V.O. (2012). Technical and economic study of self-propelled machinery application expediency in mines of krivorozhsky bassin. Naukovyi Visnyk Natsionalnoho Hirnychoho Universytetu, 5, 39–42.
8. Stupnik, N.I., Fedko, M.B., Pismennyi, S.V. & Kolosov, V.A. (2014). Development of recommendations for choosing excavation support types and junctions for uranium mines of state-owned enterprise skhidhzk. Naukovyi Visnyk Natsionalnoho Hirnychoho Universytetu, 5, 21–25.
9. Stupnik, M., Kalinichenko, O., Kalinichenko, V., Pysmennyi, S. & Morhun, O. (2018). Choice and substantiation of stable crown shapes in deep-level iron ore mining. Mining of Mineral Deposits, 12(4), 56–62. https://doi.org/10.15407/mining12.04.056
10. Stupnik, N., Kalinichenko, V. (2012). Parameters of shear zone and methods of their conditions control at underground mining of steep-dipping iron ore deposits in Kryvyi Rig basin. Geomechanical Processes During Underground Mining - Proceedings of the School of Underground Mining, 15–17.
11. Bazaluk, O., Petlovanyi, M., Lozynskyi, V., Zubko, S., Sai, K., & Saik, P. (2021). Sustainable Underground Iron Ore Mining in Ukraine with Backfilling Worked-Out Area. Sustainability, 13(2), 834. https://doi.org/10.3390/su13020834
12. Panayotov, V., Panayotova, M., & Chukharev, S. (2020). Recent studies on germanium-nanomaterials for LIBs anodes. In E3S Web of Conferences (Vol. 166, p. 06012). EDP Sciences. https://doi.org/10.1051/e3sconf/202016606012
13. Lozynskyi, V., Medianyk, V., Saik, P., Rysbekov, K., & Demydov, M. (2020). Multivariance solutions for designing new levels of coal mines. Rudarsko Geolosko Naftni Zbornik, 35(2), 23-32. https://doi.org/10.17794/rgn.2020.2.3
14. Sobczyk, E., Kicki, J., Sobczyk, W. & Szuwarzyński, M. (2017). Support of mining investment choice decisions with the use of multi-criteria method. Resources Policy, 51. 94-99. https://doi.org/10.1016/j.resourpol.2016.11.012
15. Sobczyk, E.J., Galica, D., Kopacz, M. & Sobczyk, W. (2022). Selecting the optimal exploitation option using a digital deposit model and the AHP. Resources Policy, 78, 102952. https://doi.org/10.1016/j.resourpol.2022.102952
16. Sobczyk,W. (2015). Sustainable development of middle east region. Problems of Sustainable Development, 10 (2), 51–62. https://ssrn.com/abstract=2660718

17. Radwanek-Bąk, B., Sobczyk, W. & Sobczyk E. (2020). Support for multiple criteria decisions for mineral deposits valorization and protection. Resources Policy, 68. 101795. https://doi.org/10.1016/j.resourpol.2020.101795

18. Sobczyk, W., Sobczyk, E.J. (2021). Varying the energy mix in the eu-28 and in Poland as a step towards sustainable development. Energies, 14 (5), 1502. https://doi.org/10.3390/en14051502

19. Petlovanyi, M., Lozynskyi, V., Zubko, S., Saik, P., & Sai, K. (2019). The infuence of geology and ore deposit occurrence conditions on dilution indicators of extracted reserves. Rudarsko Geolosko Naftni Zbornik, 34(1), 83-91. https://doi.org/10.17794/rgn.2019.1.8

20. Stupnik, N.I., Kalinichenko, V.A., Fedko, M.B. & Mirchenko, Ye.G. (2013). Influence of rock massif stress-strain state on uranium ore breaking technology. Naukovyi Visnyk Natsionalnoho Hirnychoho Universytetu, 2, 11–16.

21. Kalinichenko, V., Dolgikh, O. & Dolgikh, L. (2019). Digital survey in studying open pit wall deformations. E3S Web of Conferences, 123, 01047.

22. Stupnik, M.I., Kalinichenko, V.O., Fedko, M.B. & Kalinichenko, O.V. (2018). Investigation into crown stability at underground leaching of uranium ores. Naukovyi Visnyk Natsionalnoho Hirnychoho Universytetu, 6, 20–25.

23. Sakhno, S., Yanova, L., Pischikova, O., & Chukharev, S. (2020). Study of the influence of properties of dusty ferromagnetic additives on the increase of cement activity. In E3S Web of Conferences (Vol. 166, p. 06012). EDP Sciences. https://doi.org/10.1051/e3sconf/202016606002

24. Stupnik, M.I., Kalinichenko, O.V. & Kalinichenko, V.O. (2012). Economic evaluation of risks of possible geomechanical violations of original ground in the fields of mines of Kryvyi rih basin. Naukovyi Visnyk Natsionalnoho Hirnychoho Universytetu, 6, 126–130.

25. Bazaluk, O., Petlovanyi, M., Zubko, S., Lozynskyi, V., & Sai, K. (2021). Instability Assessment of Hanging Wall Rocks during Underground Mining of Iron Ores. Minerals, 11(8), 858. https://doi.org10.3390/min11080858

26. Bazaluk, O., Rysbekov, K., Nurpeisova, M., Lozynskyi, V., Kyrgizbayeva, G., & Turumbetov, T. (2022). Integrated monitoring for the rock mass state during large-scale subsoil development. Frontiers in Environmental Science, (10), 852591. https://doi.org/10.3389/fenvs.2022.852591

27. Ciepiela, M., Sobczyk, W. (2021). A Study of PM 10, PM 2.5 Concentrations in the Atmospheric Air in Kraków, Poland. Inzynieria Mineralna, 1 (1), 129-135. https://doi.org/10.29227/IM-2021-01-17

28. Sobczyk, W., Kowalska, A. & Sobczyk, E.J. (2020). Analysis of the Causes of Conflict between the Miners and Naturalists. Inzynieria Mineralna 1 (1), 119–124. https://doi.org/10.29227/IM-2020-01-19

29. Sobczyk, W., Perny, K.C.I. & Sobczyk, E.J. (2021). Assessing the Real Risk of Mining Industry Environmental Impact. Case Study. Inzynieria Mineralna, 1 (1), 33–41. https://doi.org/10.29227/IM-2021-01-05

30. Stupnik, M., Kalinichenko, V., Fedko, M., Kalinichenko, O., Pukhalskyi, V. & Kryvokhin, B. (2019). Investigation of the dust formation process when hoisting the uranium ores with a bucket. Mining of Mineral Deposits, 13(3), 96–103. https://doi.org/10.33271/mining13.03.096

31. Matheron, G. (1963). Principles of Geostatistics. Economic Geology, 58(8), 1246-1266. http://dx.doi.org/10.2113/gsecongeo.58.8

32. David, M. (1980). Geostatisticheskiye metody pri otsenke zapasov rud. Advanced Geostatistics in the Mining Industry. Leningrad: Nedra

33. Huang, S. & Huaming, A. (2016). Application of geostatistics in the estimation of Sujishan graphite deposits, Mongolia Stavebn´ı obzor - Civil Engineering Journal, 27, 487-499. https://doi.org/10.14311/CEJ.2018.04.0039

34. Ivahnenko, A.G. (1982). Induktivnyj metod samoorganizacii modelej slozhnyh sistem. Kiev: Naukova dumka.

35. Muravina, O.M., Ponomarenko, I.A. (2016). Programmnaya realizatsiya metoda gruppovogo ucheta argumentov pri funktsional'nom modelirovanii geologo-geofizicheskikh dannykh. Vestnik Voronezhskogo gosudarstvennogo universiteta. Ser. Geologiya, 2, 107-110. http://www.vestnik.vsu.ru/pdf/heologia/2016/02/2016-02-15.pdf

36. Pysmennyi, S., Peremetchyk, A., Chukharev, S., Fedorenko, S., Anastasov, D., & Tomiczek, K. (2022). The mining and geometrical methodology for estimating of mineral deposits. Paper presented at the IOP Conference Series: Earth and Environmental Science, 1049(1). https://doi.org/10.1088/1755-1315/1049/1/012029

37. Peremetchyk, A., Kulikovska, O., Shvaher, N., Chukharev, S., Fedorenko, S., Moraru, R., & Panayotov, V. (2022). Predictive geometrization of grade indices of an iron-ore deposit. Mining of Mineral Deposits, 16(3), 67-77. https://doi.org/10.33271/mining16.03.067

Modelowanie i predykcja wskaźników jakości rudy żelaza

W artykule zaproponowano rozwiązanie aktualnego problemu naukowego polegającego na opracowaniu geometrycznej metody prognozowania wskaźników jakości złóż rud żelaza, z zastosowaniem modelu matematycznego wielowymiarowego losowego pola geochemicznego, realizowanego z wykorzystaniem samoorganizujących metod predykcyjnych. Autorzy opracowują wielowymiarowy algorytm predykcji heurystycznej, wykorzystujący wielomian o dowolnej potędze i umożliwiający opis dowolnej zależności funkcjonalnej. Wykazano, że do matematycznego opisu elementów masywu skalnego należy zastosować układ równań wielowymiarowego losowego pola geochemicznego. Model grafoanalityczny złoża jest budowany metodami geostatystycznymi. Stwierdzono, że w przypadku złóż Kryvbas metoda krigingu jest najbardziej odpowiednia do oceny i poprawy wiarygodności wejściowych danych geologicznych, ponieważ szczegółowe badania geologiczne prowadzone są za pomocą nieregularnej siatki otworów wiertniczych. Ważnym aspektem geometryzacji złóż rud żelaza jest geometryczne przewidywanie ich wskaźników jakościowych dla rozwiązywania zadań planowania długoterminowego i bieżącego w celu zapewnienia jak najbardziej efektywnego funkcjonowania przedsiębiorstwa górniczego dla poprawy racjonalizacji zagospodarowania złoża.

Słowa kluczowe: *geometryzacja, górnicze metody predykcji geometrycznej, metody geostatystyczne, kriging, wielowymiarowe losowe pole geochemiczne, heurystyczne algorytmy predykcji*

Study of Compensation Room Impacts on the Massif Stability and Mined Ore Mass Quality

Mykola STUPNIK[1)], Mykhaylo FEDKO[2)], Mykhaylo HRYSHCHENKO[3)], Olena KALINICHENKO[4)], Vsevolod KALINICHENKO[5)]

[1)] Kryvyi Rih National University, Faculty of Mining and Metallurgy,11 Vitalii Matusevych Str., Kryvyi Rih, 50027, Ukraine; ORCID https://orcid.org/0000-0003-3318-3889
[2)] Kryvyi Rih National University, Faculty of Mining and Metallurgy,11 Vitalii Matusevych Str., Kryvyi Rih, 50027, Ukraine; ORCID https://orcid.org/0000-0002-8437-3175
[3)] Kryvyi Rih National University, Faculty of Mining and Metallurgy,11 Vitalii Matusevych Str., Kryvyi Rih, 50027, Ukraine; ORCID https://orcid.org/0000-0002-9365-1886
[4)] Kryvyi Rih National University, Faculty of Mining and Metallurgy,11 Vitalii Matusevych Str., Kryvyi Rih, 50027, Ukraine; ORCID https://orcid.org/0000-0002-9138-9271
[5)] Kryvyi Rih National University, Faculty of Mining and Metallurgy,11 Vitalii Matusevych Str., Kryvyi Rih, 50027, Ukraine; ORCID https://orcid.org/0000-0002-1938-2286; email: kalinichenko@knu.edu.ua

http://doi.org/10.29227/IM-2023-01-16

Submission date: 24-01-2023 | Review date: 19-03-2023

Abstract

The paper presents the study and a functional analysis of requirements of the world metallurgical industry to the quality of underground iron ores at underground mines of Ukraine. There are found dependencies of the impact of the shape and parameters of compensation spaces on their stability and broken ore quality indicators. It is proved that a vertical trapezoidal compensation room possesses the highest stability and is stable within the range of all the considered depths, even in ores with hardness of 3–5 points. Less atabiity is demonstrated by a vertical compensation room of a vaulted shape with minor falls in the abutment of the room vault in ores with hardness of 3–5 points at the depth of 2000 m, and a tent-shaped one where falls of varying intensity occur in the lower part of inclined exposures of the tent in ores with hardness of 3–5 points at the depth of 1750 m or more. The horizontal compensation room is of the lowest stability; falls occur in ores with hardness of 3–5 points at the depth of 1400 m, and at the depths of 1750–2000 m it remains stable only in harder ores. It is established that the use of compensation rooms of high stability makes it possible to achieve their maximum volume, increase the amount of pure ore extracted, reduce its dilution, enhance the quality of the mined ore mass and concequently increase its price and competitiveness of marketable products.

Keywords: *underground mining, iron ore, compensation rooms, stress-strain state, stability, quality*

1. INTRODUCTION

Today, Ukraine posesses significant reserves of rich iron ores which are mined by the underground method. The main problem of underground mining is a decrease in the quality of the extracted raw materials due to deepening of mining operations.

In addition, completeness of extraction of broken ore and its deteriorated quality are factors that significantly ipmact economic results of underground mining. Currently, in Ukraine underground mining of iron ore is accompanied with ore losses and dilution at the level of 14–20% and 12–18% respectively. As a result, up to 20% of underground iron ore is lost.

Such rather low extraction degrees are largely due to obsolete mining equipment and technology. This causes losses of part of broken ore underground and dilution of a certain part of the reserve with waste rocks. Mining technologies that allow minimizing or even eliminating broken ore losses and dilutiion are expensive and used only in particularly difficult mining conditions.

Thus, achievement of maximum mining efficiency can be provided by establishing the optimal ratio between values of ore extraction indicators and the amount of allowable costs for ore production.

In our opinion, the mined ore quality can be enhanced by increasing the volume of compensation rooms, which will increase the amount of pure ore extracted from them, reduce ore dilution and enhance the mined ore mass quality. This results in the increased price and competitiveness of marketable products.

2. PURPOSE

The presented paper aims to theoretically and experimentally substantiate and develop efficient technological means of controlling the quality of raw materials through the study and selection of optimal shapes and sizes of compensation rooms.

For this, the following tasks are solved in the paper:

- analysis of relevant researches and publications;
- substantiation of the research methods;
- presentation of the study results and corresponding conclusions.

3. ANALYSIS OF RESEARCHES AND PUBLICATIONS.

Compensation rooms are known to be used when applying mining systems with breaking ore and country rocks to compensate for the increased volume of ore during its bulk caving [1–4,11].

Such systems are used in our underground mines in conditions of insufficient hardness and stability of both ore and country rocks. Iron ore deposits are mined mainly within the depths of 1200–1400 m with further deepening to 1800–2000

Tab. 1. Physical and mechanical properties of ore and caved rocks

Tab. 1. Właściwości fizyczne i mechaniczne rudy i skał zawałowych

Parameters	Units of measurement	Ore			Caved rocks
		1P (*f*=3-5)	2P (*f*=4-6)	3P (*f*=5-7)	
Young modulus	MPa	22000	25000	28000	5000
Specific weight	kg/m^3	3700	3650	3600	2300
Compressive strength	MPa	30	40	50	4
Tensile strength	MPa	3	4	5	0.2
Poisson ratio		0.30	0.28	0.26	0.24

Tab. 2. Pressure of caved rocks on the rock massif (computer-aided modeling)

Tab. 2. Nacisk skał zawałowych na masyw skalny (modelowanie komputerowe)

Parameter	Unit of measurement	P1	P2	P3
Pressure of caved rocks on massif, vertical/lateral	MPa	8.2/29	9.7/3.4	11.5/4

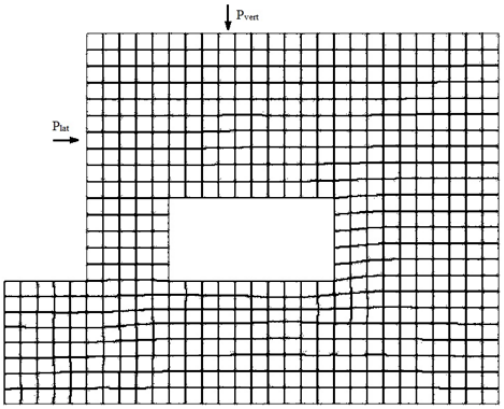

Fig. 1. Finite-element model with the horizontal compensation room

Rys. 1. Model elementów skończonych z pomieszczeniem kompensacji poziomej

m. Considering the above facts as well as negative effects of rock pressure at deep levels, the problem arises of choosing the most rational shape of compensation rooms [5–8,16].

It is established that the shape of the compensation room significantly impacts the stress-strain state (SSS) of the rock massif around it, which in turn impacts its stability [9–12]. Therefore, data on such disturbances is crucial both at the stage of designing and in the process of mining the deposit [11,13–15,17].

So, in practice, there is applied operational assessment of values of actual stresses in the massif, prediction of the nature of their change in creating compensation rooms [18–22]. This information allows assessing the input data on enhancement and development of new shapes of compensation spaces, selecting the optimal parameters of compensation rooms and determining the rational technology of their creation [23–27,29,30].

4. METHODS.

The main idea of the presented paper consists in finding a shape that would make it possible to avoid formation of areas of high compressive stresses which, as a rule, are concentrated around the corner areas of the rooms. It is also necessary to avoid emergence of areas of tensile stresses that are the most dangerous due to the fact that the tensile strength of rocks is an order of magnitude less than the their ultimate compressive strength [28,31–36].

The finite element method (FEM) and the specialized Ansis 2021-P2 software package are used for modeling [11,37–42].

In the course of the study, models of the following shapes of compensation rooms are processed: horizontal, vertical (rectangular, trapezoidal and vaulted), inclined (with different angles of inclination of the roof of these rooms – 20, 35 and 50 degrees), tent, trench, elliptical (parabolic) and spherical. For correct comparison, sizes of compensation rooms of different shapes are the same.

For each shape of the compensation room, finite-element models are developed that simulate mining of the extraction panel. The size of the finite elements is 2 m. Fig. 1 exemplifies the finite-element model with a horizontal compensation room.

To study the impact of ore hardness on the stress-strain state of the massif and stability of rooms, 3 types of ores are put in the model: with hardness of 3–5 (average 4), 4–6 (average 5) and 5–7 (average 6) points (Protodyakonov scale of hardness).

The main physical and mechanical properties of ore are given in Table 1.

The values of the caved rocks pressure on the ore massif P_1, P_2 and P_3 correspond to the mining conditions of Krivbas deposits at the depth of 1400, 1750 and 2000 m respectively and are given in Table 2.

5. RESULTS

The volume of each compensation room directly depends on the coefficient of loosening and the volume of ore to be caved during bulk blasting. Given that the compensation room is located in the ore massif and does not come into con-

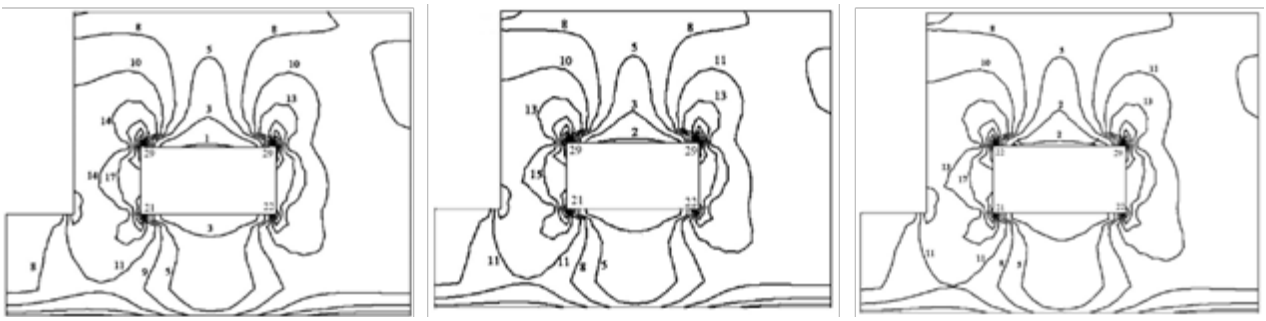

Fig. 2. Isolines of the principal stresses σ1 of the rock massif during creation of a horizontal compensation room in the panel: the pressure of caved rocks P1, ores with hardness a) 3–5, b) 4–6, c) 5–7 points respectively

Rys. 2. Izolinie naprężeń głównych σ1 masywu skalnego podczas tworzenia poziomego pomieszczenia kompensacyjnego w panelu: ciśnienie skał zawałowych P1, rudy o twardości a) 3–5, b) 4–6, c) 5–7 punktów

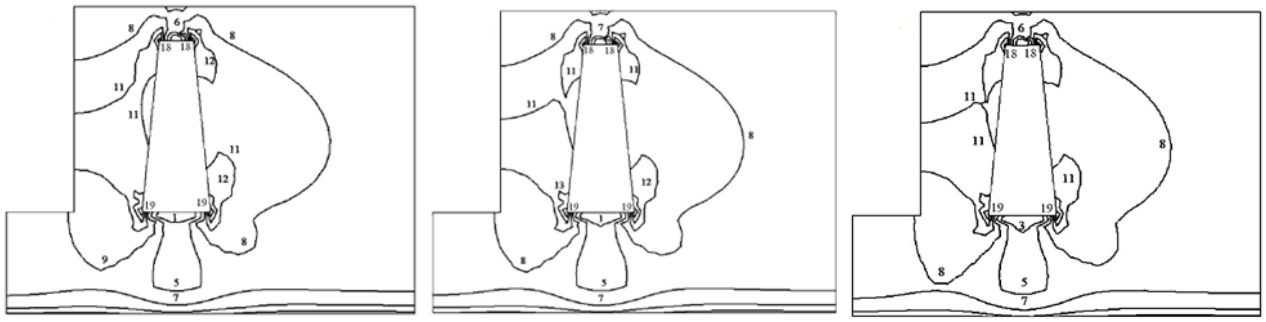

Fig. 3. Isolines of the principal stresses σ1 of the rock massif when creating a vertical trapezoidal compensation room in the panel: pressure of caved rocks P1, ores with hardness a) 3–5, b) 4–6, c) 5–7 points respectively

Rys. 3. Izolinie naprężeń głównych σ1 masywu skalnego przy tworzeniu w panelu pionowego trapezoidalnego pomieszczenia kompensacyjnego: ciśnienie skał zawałowych P1, rudy o twardości a) 3–5, b) 4–6, c) 5–7 pkt.

tact with waste rocks, it is resonable to increase the volume of compensation to increase the amount of pure ore extracted. By increasing the proportion of high-quality pure ore to be extracted from the compensation room during its creation, we enhance the quality of the mined ore mass on the whole.

Nowadays, in underground mines of Kryvyi Rih basin, the most common shapes of compensation rooms are classic ones: horizontal, vertical and inclined. Many scientific and technical developments are devoted to the search for other, more efficient shapes. The latter include trapezoidal, which is a kind of vertical room, tent, trench, parabolic (vaulted) and other shapes. The main idea behind such studies is to find a shape that would make it possible to avoid creation of areas of very high compressive stresses which, as a rule, are concentrated around the corner areas of the rooms. The shape of the rooms should reduce the possibility of emergence of areas of tensile stresses that are the most dangerous as the tensile strength of most iron ores is almost an order of magnitude less than their ultimate compressive strength.

Fig. 2 shows the results of modeling and isolines of the principal stresses σ1 of the rock massif when creating a horizontal compensation room in a panel in ores with hardness 1P, 2P and 3P respectively.

The figures demonstrate that the nature of distribution of the stress field around the compensation room is fully consistent with the classical ideas: areas of increased compressive stresses are concentrated around the corner areas of the room, and in the central part of the horizontal exposure there is an area of reduced compressive stresses. This confirms adequacy of the developed models and the modeling results obtained.

As is seen from the figures, at the same depth, with such a slight difference in ore hardness, absolute values of stresses do not practically differ from each other. Regarding the impact of the depth of operations, a very significant increase in the level of compressive stresses is observed in the corners of the room, which is also a natural phenomenon since this is a consequence of an increase in rock pressure.

Analysis of stability of the horizontal compensation room in different conditions reveals that in ores with hardness of 3–5 points at the depth of 1400 m, the maximum values of compressive stresses in the upper corners of the room practically reach the ultimate strength for these ores, i.e, in general, the room remains stable, but small local ore falls are possible in these areas. In harder ores at this depth, the room is stable.

With an increase in the depth of operations to 1750 m in ores with hardness of 3–5 points, the compensation room of this size loses its stability and fails, and in harder ores it remains stable.

At the depth of 2000 m, stability problems may occur in the form of small local ore falls in these areas. In harder ores at this depth, the room remains stable.

At the depth of 2000 m, stability problems may occur in such rooms when they are created in ores with hardness of 4–6 points, especially at increased fracturing degrees of the ore massif.

The value of the maximum principal stresses in the rock massif during creation of a horizontal compensation room is determined by the formula:

$$\sigma_1 = 24.678e^{0,1608H_p};$$

$$R^2 = 0.9987.$$

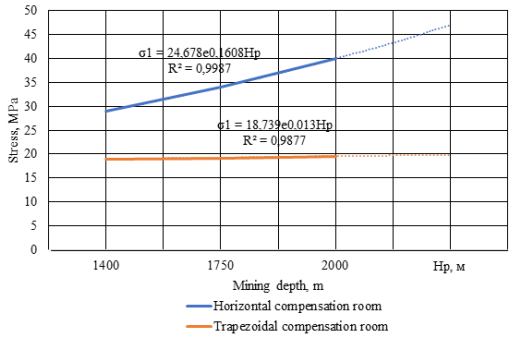

Fig. 4. Dependency of the value of the maximum principal stresses on the shape of compensation rooms and the depth of mining operations

Rys. 4. Zależność wartości maksymalnych naprężeń głównych od kształtu komór kompensacyjnych i głębokości eksploatacji

where σ_1 is the value of the maximum principal stresses
H_p is the depth of mining operations, m;
R^2 is the value of approximation reliability.

The results of modeling and isolines of the principal stresses σ1 of the rock massif during creation of the most common vertical rectangular compensation room in the panel in ores of different hardness (P1, P2 and P3) enable establishing the following.

Distribution of the stress field is characteristic of rooms of this shape: areas of concentration of high compressive stresses occur at the corners of the room, and areas of reduced compressive stresses are located in the central part of the roof and vertical exposures of the room.

At the same depth, at different ore hardness, values of stresses do not practically differ from each other. As in the previous option, there is a significant impact of the depth of operations on the stress-strain state of the massif. But the level of maximum compressive stresses is by15–20% smaller than for similar conditions (equal ore hardness and depth of operations) in the horizontal compensation room. A decrease in compressive stress values is not so significant either, which indicates higher stability of the vertical compensation room. Only at the depth of 1750 m with the ore hardness of 3–5 points in the upper corners of the room there may occur small falls, and at the depth of 2000 m volumes of falls will lead to failure of the crown of the room and its filling with overlying caved rocks. In harder ores, rooms remain stable throughout the range of the depths under consideration.

In addition to other shapes of compensation spaces, the authors propose an option of a vertical trapezoidal compensation room, Fig. 3.

The studies conducted enable asserting that in the proposed option, the nature of the stress field distribution is close to the previous ones. At the same time, compared to the previous option of the vertical rectangular compensation room, the level of maximum compressive stresses is much lower (by 25–30%) than in the most problematic upper corners of vertical rooms. This can be explained by a much smaller span of the roof of the room. As a result, compensation rooms of vertical trapezoidal shape remain stable at all the considered depths, even in ores of minimum (3–5 points) hardness.

The value of the maximum principal stresses in the rock massif during creation of a trapezoidal compensation room is determined by the formula:

$$\sigma_1 = 18.739e^{0.013H_p};$$

$$R^2 = 0.9877.$$

where σ_1 is the value of the maximum principal stresses
H_p is the depth of mining operations, m;
R^2 is the value of approximation reliability.

The graph of the dependency of the maximum principal stresses value on the shape of compensation rooms and the depth of mining operations is presented in Fig. 4.

6. CONCLUSIONS

Based on the modeling of the stress-strain state of the rock massif around compensation rooms of various shapes and its impact on their stability, the following conclusions can be drawn:

1. The level of the stress-strain state of the ore massif around compensation rooms with a small difference in ore hardness mainly depends on the depth of operations, and their stability is impacted by the value of stresses in particular conditions and physical and mechanical properties of ore which directly depend on its hardness.

2. The highest stability, as compared to all the others, is demonstrated by a vertical compensation room of a trapezoidal shape which remains stable within the range of all the considered depths, even in ores with hardness of 3–5 points.

3. Less stabiity is demonstrated by a vertical compensation room of a vaulted shape with minor falls in the abutment of the room vault in ores with hardness of 3–5 points at the depth of 2000 m, and a tent-shaped one, where falls of varying intensity occur in the lower part of inclined exposures of the tent in ores with hardness of 3–5 points at the depth of 1750 m or more but do not significantly impact its stability.

4. The inclined compensation room (roof inclination of 35–50°; minor falls occur primarily in ores of small (3–5 and 4–6 points) hardness but they do not impact significantly its stability at all the depths), the vertical rectangular compensation room (stability problems only occur in ores with hardness of 3–5 points at the depth of 2000 m) and the inclined compensation room (with the roof inclination angle of 20°) are somewhat inferior to the above mentioned ones. Regardless of falls, trench, elliptical and spherical compensation rooms only fail in ores with hardness of 3–5 points at the depth of 2000 m.

5. The horizontal compensation room demonstrates the lowest stability, falls occur in ores with hardness of 3–5 points

at the depth of 1400 m, and at greater depths (1750 and 2000 m) it remains stable only in harder ores.

6. The study conducted and practices of Kryvbas underground mines that extract rich iron ores enable the conclusion that so-called "unconventional" shapes of compensation rooms, in particular vertical trapezoidal ones, should find wider application.

7. Compensation rooms of higher stability enable their volume increase in ores of low stability, which will lead to a possible increase in the amount of pure ore extracted, reduced ore dilution and, accordingly, enhanced quality of the mined ore mass. This will result in the increased price and competitiveness of marketable products of our underground mines.

ACKNOWLEDGMENTS

The work was supported by the Ministry of Education and Science of Ukraine within the framework of the state scientific theme "Investigation and scientific and practical substantiation of technological means for raw material control in mining ores on deep levels" (State registration 0122U000843).

Literatura – References

1. Stupnik, N.I., Kalinichenko, V.A., Fedko, M.B., & Mirchenko, Ye.G. (2013). Influence of rock massif stress-strain state on uranium ore breaking technology. Naukovyi Visnyk Natsionalnoho Hirnychoho Universytetu, 2, 11–16.
2. Stupnik, N., Kalinichenko, V., Kalinichenko, E., Muzika, I., Fed'ko, M., & Pis'menniy, S. (2015). The research of strain-stress state of magnetite quartzite deposit massif in the condition of mine "Gigant-Gliboka" of central iron ore enrichment works (CGOK). Metallurgical and mining industry, 7. 377-382.
3. Sashurin, A.D., & Belikov, V.Ye. (2003). Problemy ustoychivosti podzemnykh i nazemnykh cooruzheniy v zone tektonicheskikh narusheniy [Problems of stability of underground and surface structures in the zone of tectonic disturbances]. Voprosy osusheniya, gornopromyshlennoy geologii i okhrany nedr: Materialy mezhdunarodnogo simpoziuma, 206-216.
4. Baluta, A.M., & Borisenko, V.G. (1972). Prognoznaya otsenka fiziko-mekhanicheskikh svoystv gornykh porod Krivbassa [Predictive assessment of the physical and mechanical properties of rocks of Kryvbas]. (Kyiv: Naukova dumka).
5. Nasonov, I.D. (1978). Modelirovaniye gornykh protsessov [Modeling of mining processes]. (Moscow: Nedra).
6. Kuznetsov, G.N., Bud'ko, M.N., & Filippova, A.A. (1959). Izucheniye proyavleniy gornogo davleniya na modelyakh [Study of manifestations of rock pressure on models]. (Moscow: Ugletekhizdat).
7. Kirpichev, M.V. (1953). Teoriya podobiya [Similarity theory]. (Moscow: Akademiya Nauk SSSR).
8. Glushikhin, F.P. (1991). Modelirovaniye v geomekhanike [Modeling in geomechanics]. (Moscow: Nedra).
9. Stupnik, N., & Kalinichenko, V. (2012). Parameters of shear zone and methods of their conditions control at underground mining of steep-dipping iron ore deposits in Kryvyi Rig basin. Geomechanical Processes During Underground Mining - Proceedings of the School of Underground Mining, 15–17.
10. Stupnik, N.I., Kalinichenko, V.A., Fedko, M.B., & Mirchenko, Ye.G. 2013. Prospects of application of TNT-free explosives in ore deposites developed by udergrounds mining. Naukovyi Visnyk Natsionalnoho Hirnychoho Universytetu, 1, 44–48.
11. Stupnik, M.I., Kalinichenko, V.O., Fedko, M.B., & Kalinichenko, O.V. (2018). Investigation into crown stability at underground leaching of uranium ores. Naukovyi Visnyk Natsionalnoho Hirnychoho Universytetu, 6, 20–25.
12. Stupnik, M., & Kalinichenko, V. (2013). Magnetite quartzite mining is the future of Kryvyi Rig iron ore basin. Annual Scientific-Technical Colletion - Mining of Mineral Deposits 2013, 49–52
13. Stupnik, M.I., Kalinichenko, O.V., & Kalinichenko, V.O. (2012). Economic evaluation of risks of possible geomechanical violations of original ground in the fields of mines of Kryvyi rih basin. Naukovyi Visnyk Natsionalnoho Hirnychoho Universytetu, 6, 126–130.
14. Stupnik, M., Kalinichenko, V., Fedko, M., Kalinichenko, O., Pukhalskyi, V., & Kryvokhin, B. (2019). Investigation of the dust formation process when hoisting the uranium ores with a bucket. Mining of Mineral Deposits, 13(3), 96–103. https://doi.org/10.33271/mining13.03.096.
15. Kalinichenko, V., Dolgikh, O., Dolgikh, L., & Pysmennyi, S. (2020). Choosing a camera for mine surveying of mining enterprise facilities using unmanned aerial vehicles. Mining of Mineral Deposits, 14(4), 31-39. https://doi.org/10.33271/mining14.04.031.
16. Stupnik, M.I., Kalinichenko, O.V., Kalinichenko, V.O. 2012. Technical and economic study of self-propelled machinery application expediency in mines of krivorozhsky bassin. Naukovyi Visnyk Natsionalnoho Hirnychoho Universytetu, 5, 39–42.
17. Pysmennyi, S., Chukharev, S., Khavalbolot, K., Bondar, I., & Ijilmaa, J. (2021). Enhancement of the technology of mining steep ore bodies applying the "floating" crown. E3S Web of Conferences, 280, 08013. https://doi.org/10.1051/e3sconf/202128008013.

18. Pysmennyi, S., Chukharev, S., Kyelgyenbai, K., Mutambo, V., & Matsui, A. (2022). Iron ore underground mining under the internal overburden dump at the PJSC "Northern GZK". IOP Conference Series: Earth and Environmental Science, 1049(1), 012008. https://doi.org/10.1088/1755-1315/1049/1/012008.

19. Petlovanyi, M., Lozynskyi, V., Zubko, S., Saik, P., & Sai, K. (2019). The infuence of geology and ore deposit occurrence conditions on dilution indicators of extracted reserves. Rudarsko Geolosko Naftni Zbornik, 34(1), 83-91. https://doi.org/10.17794/rgn.2019.1.8.

20. Bazaluk, O., Petlovanyi, M., Lozynskyi, V., Zubko, S., Sai, K., & Saik, P. (2021). Sustainable Underground Iron Ore Mining in Ukraine with Backfilling Worked-Out Area. Sustainability, 13(2), 834. https://doi.org/10.3390/su13020834.

21. Bazaluk, O., Petlovanyi, M., Zubko, S., Lozynskyi, V., & Sai, K. (2021). Instability Assessment of Hanging Wall Rocks during Underground Mining of Iron Ores. Minerals, 11(8), 858. https://doi.org10.3390/min11080858.

22. Bazaluk, O., Rysbekov, K., Nurpeisova, M., Lozynskyi, V., Kyrgizbayeva, G., & Turumbetov, T. (2022). Integrated monitoring for the rock mass state during large-scale subsoil development. Frontiers in Environmental Science, 10, 852591. https://doi.org/10.3389/fenvs.2022.852591.

23. Lozynskyi, V., Medianyk, V., Saik, P., Rysbekov, K., & Demydov, M. (2020). Multivariance solutions for designing new levels of coal mines. Rudarsko Geolosko Naftni Zbornik, 35(2), 23-32. https://doi.org/10.17794/rgn.2020.2.3.

24. Lyashenko, V., Andreev, B., & Dudar, T. (2022). Substantiation of mining-technical and environmental safety of underground mining of complex-structure ore deposits. Mining of Mineral Deposits, 16(1), 43-51. https://doi.org/10.33271/mining16.01.043.

25. Issayeva, L., Togizov, K., Duczmal-Czernikiewicz, A., Kurmangazhina, M., & Muratkhanov, D. (2022). Ore-controlling factors as the basis for singling out the prospective areas within the Syrymbet rare-metal deposit, Northern Kazakhstan. Mining of Mineral Deposits, 16(2), 14-21. https://doi.org/10.33271/mining16.02.014.

26. Takhanov, D., Muratuly, B., Rashid, Z., & Kydrashov, A. (2021). Geomechanics substantiation of pillars development parameters in case of combined mining the contiguous steep ore bodies. Mining of Mineral Deposits, 15(1), 50-58. https://doi.org/10.33271/mining15.01.050.

27. Pysmenniy, S., Shvager, N., Shepel, O. Kovbyk, K., & Dolgikh O. (2020). Development of resource-saving technology when mining ore bodies by blocks under rock pressure. E3S Web of Conferences, 166, 02006. https://doi.org/10.1051/e3sconf/202016602006.

28. Kyelgyenbai K., Pysmennyi S., Chukharev S., Purev B., & Jambaa I. (2021). Modelling for degreasing the mining equipment downtime by optimizing blasting period at Erdenet surface mine. E3S Web of Conferences, (280), 08001. https://doi.org/10.1051/e3sconf/202128008001.

29. Pysmennyi, S., Peremetchyk, A., Chukharev, S., Fedorenko, S., Anastasov, D., & Tomiczek, K. (2022). The mining and geometrical methodology for estimating of mineral deposits. IOP Conference Series: Earth and Environmental Science, 1049(1), 012029. https://doi.org/10.1088/1755-1315/1049/1/012029.

30. Panchenko, V., Sobko, B., Lotous, V., Vinivitin, D., & Shabatura, V. (2021). Openwork scheduling for steep-grade iron-ore deposits with the help of near-vertical layers. Mining of Mineral Deposits, 15(1), 87-95. https://doi.org/10.33271/mining15.01.087.

31. Zeylik, B., Arshamov, Y., Baratov, R., & Bekbotayeva, A. (2021). New technology for mineral deposits prediction to identify prospective areas in the Zhezkazgan ore region. Mining of Mineral Deposits, 15(2), 134-142. https://doi.org/10.33271/mining15.02.134.

32. Rysbekov, K., Bitimbayev, M., Akhmetkanov, D., Yelemessov, K., Barmenshinova, M., Toktarov, A., & Baskanbayeva, D. (2022). Substantiation of mining systems for steeply dipping low-thickness ore bodies with controlled continuous stope extraction. Mining of Mineral Deposits, 16(2), 64-72. https://doi.org/10.33271/mining16.02.064.

33. Shvaher N., Komisarenko, T., Chukharev, S., & Panova, S. (2019). E3S Web of Conferences, 123, 01043. https://doi.org/10.1051/e3sconf/201912301043.

34. Panayotov, V., Panayotova, M., & Chukharev, S. (2020). Recent studies on germanium-nanomaterials for LIBs anodes. E3S Web of Conferences, 166, 06012. https://doi.org/10.1051/e3sconf/202016606012.

35. Peremetchyk, A., Kulikovska, O., Shvaher, N., Chukharev, S., Fedorenko, S., Moraru, R., & Panayotov, V. (2022). Predictive geometrization of grade indices of an iron-ore deposit. Mining of Mineral Deposits, 16(3), 67-77. https://doi.org/10.33271/mining16.03.067.

36. Sakhno, S., Yanova, L., Pischikova, O.,& Chukharev, S. (2020). Study of the influence of properties of dusty ferromagnetic additives on the increase of cement activity. E3S Web of Conferences, 166, 06002. https://doi.org/10.1051/e3sconf/202016606002.

37. Khomenko, O., Kononenko, M., Kovalenko, I., & Astafiev, D. (2018). Self-regulating roof-bolting with the rock pressure energy use. E3S Web Of Conferences, 60, 00009. http://doi.org/10.1051/e3sconf/20186000009.

38. Kononenko, M., & Khomenko, O. (2010). Technology of support of workings near to extraction chambers. New Techniques and Technologies in Mining - Proceedings of the School of Underground Mining, 193-197. http://doi.org/10.1201/b11329-32.

39. Khomenko, O., Tsendjav, L., Kononenko, M., & Janchiv, B. (2017). Nuclear-and-fuel pow-er industry of Ukraine: production, science, education. Mining Of Mineral Deposits, 11(4), 86-95. http://doi.org/10.15407/mining11.04.086.

40. Khomenko, O., Kononenko, M., & Lyashenko, V. (2018). Safety Improving of Mine Preparation Works at the Ore Mines. Occupational Safety In Industry, 5, 53-59. http://doi.org/10.24000/0409-2961-2018-5-53-59.

41. Kononenko M., Khomenko O., Kovalenko I., & Savchenko M. (2021). Control of density and velocity of emulsion explosives detonation for ore breaking. Naukovyi Visnyk Natsionalnoho Hirnychoho Universytetu, 2, 69-75. https://doi.org/10.33271/nvngu/2021-2/069.

42. Kononenko M., & Khomenko O. (2021). New theory for the rock mass destruction by blasting. Mining of Mineral Deposits, 15(2), 111-123. https://doi.org/10.33271/mining15.02.111.

Badanie wpływu kompensacji na stabilność górotworu oraz jakość wydobywanej rudy

Artykuł przedstawia studium i analizę funkcjonalną wymagań światowego przemysłu metalurgicznego co do jakości rud żelaza w podziemnych kopalniach Ukrainy. Stwierdzono zależności wpływu kształtu i parametrów przestrzeni kompensacyjnych na ich stateczność i wskaźniki jakości rudy. Udowodniono, że komora wyrównawcza w kształcie trapezu pionowego charakteryzuje się największą stabilnością i jest stabilna w zakresie wszystkich rozważanych głębokości, nawet w rudach o twardości 3–5 punktów. Mniejszą stateczność wykazuje komora kompensacji pionowej o kształcie sklepionym z niewielkimi spadkami w przyczółku sklepienia komory w rudach o twardości 3–5 punktów na głębokości 2000 m. Komora z opadami o różnym natężeniu występuje w dolnej części nachylonych odsłonięć namiotu w rudach o twardości 3–5 punktów na głębokości 1750 m lub większej. Pomieszczenie kompensacji poziomej ma najmniejszą stateczność; spadki występują w rudach o twardości 3–5 punktów na głębokości 1400 m, a na głębokościach 1750–2000 m pozostają stabilne tylko w rudach twardszych. Stwierdzono, że zastosowanie komór kompensacyjnych o dużej stabilności umożliwia osiągnięcie ich maksymalnej objętości, zwiększenie ilości wydobywanej czystej rudy, zmniejszenie jej rozrzedzenia, poprawę jakości wydobywanej masy rudy, a co za tym idzie, wzrost jej ceny i konkurencyjności rynkowej.

Słowa kluczowe: *górnictwo podziemne, ruda żelaza, pomieszczenia kompensacyjne, stan naprężenie-odkształcenie, stateczność, jakość*

Augmented and Virtual Reality Tools in Training Mining Engineers

Viktoriia TKACHUK[1], Yuliia YECHKALO[2], Dmytro BROVKO[3], Wiktoria SOBCZYK[4]

[1] PhD; Kryvyi Rih National University, Kryvyi Rih, Ukrane; ORCID https://orcid.org/0000-0002-5879-5147; email: viktoriya.tkachuk@knu.edu.ua
[2] PhD; Kryvyi Rih National University, Kryvyi Rih, Ukrane; ORCID https://orcid.org/0000-0002-0164-8365; email: yechkalo_yuliia@knu.edu.ua
[3] DSc; Kryvyi Rih National University, Kryvyi Rih, Ukrane; ORCID https://orcid.org/0000-0001-9108-3857; email: brovko@knu.edu.ua
[4] Prof. DSc, PhD, Eng. Faculty of Energy and Fuels, AGH University of Science & Technology, Krakow, Poland; ORCID https://orcid.org/0000-0003-2082-9644

http://doi.org/10.29227/IM-2023-01-17

Submission date: 08-02-2023 | Review date: 22-03-2023

Abstract

The transition to smart mining has significantly increased the requirements for training modern mining engineers, this necessitating digitalization of this process. Based on scientific research, virtual and augmented reality technology are the most effective and safe. The article presents methods for using virtual and augmented reality technology in training mining engineers. The methods are successfully implemented in laboratories of Kryvyi Rih National University (Ukraine) and have been proven effective during distance learning in the context of the COVID-19 pandemic and the russian military aggression against Ukraine. Nevertheless, further scientific research is needed to introduce modern digital technologies into mining engineers' training at universities in order to form a competitive and competent specialist.

Keywords: *mining engineer training, Augmented Reality (AR), Virtual Reality (VR), digital transformation, distance education, COVID-19 pandemic, russian military aggression against Ukraine*

1. Introduction

Recently, there has been an increase in the number of projects for the introduction of augmented (AR) and virtual reality (VR) technology, which is actively used in many different areas of human life, from industry to education.

Since both AR and VR are key components of the Industry 4.0 concept (Fig. 1), companies around the world are investing heavily in their development. For example, Google and Microsoft, which initially focused their products on the consumer market, have now provided for both industrial and educational use of their technology. Industry 4.0, which is made up of cyberphysical systems, the Internet of Things and complex networks that combine industrial production with the latest information and communication technologies, involves creation of smart factories, such as network and automated ones [16].

In recent years, there has been a transition from traditional to smart mining, which has greatly improved mining engineers' capabilities to identify hazards and make further decisions to ensure industrial safety [7; 24; 25; 26; 30; 32; 39].

The latest technologies in mining are expanding the boundaries of practical training of future mining engineers. Thanks to these technologies, the learning process can provide an advanced simulation of the production environment that humans perceive almost as real.

AR and VR technology is being used to solve a variety of problems in training mining engineers, from designing new industrial lines and final products to supporting personnel training in repairs. The technology applied to training can change the role of the human factor by reducing the risks associated with improper operation of equipment while working at hazardous facilities.

Collaboration between universities and VR/AR manufacturers contributes to solving problems of forming competences of future mining engineers (Fig. 2).

The main advantage of using AR/VR in training mining engineers is the fact that the technology allow teaching in AR/VR environments close to the real one, through simulating virtual scenarios [1]. Clearly, the introduction of AR/VR as training technology requires new teaching methods that take into account future engineers' level of training and the changing role of educators [9].

2. Literature review

AR/VR technology is being actively introduced into the mining industry. Many enterprises are already applying it to increasing productivity and improving occupational safety. Therefore, the introduction of the technology into the process of training mining engineers is the need of the hour.

Australia, the United Kingdom and the United States are leaders in using the VR learning environment for mining simulation, reconstruction and accident investigation, and industrial safety. The UK has a long history of developing and using virtual reality technology for mine safety training. VR products such as SafeVR and Vroom are well known for training truck drivers at open pits [28].

Universities in Australia are actively introducing VR technology into the training of mining engineers:

– the University of Queensland is involved in research to develop VR training applications with rig models, Instron UCS rock testing models and ventilation models [18];

– the University of New South Wales is implementing iCinema, a VR environment with 18 modules, to improve teach-

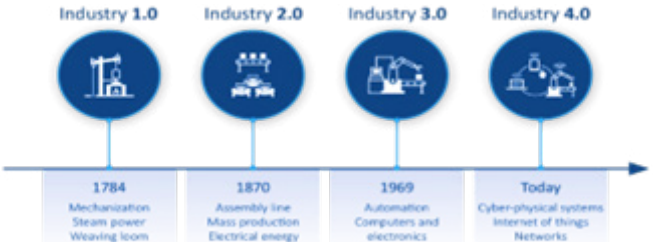

Fig. 1. The Four Industrial Revolutions [16]

Rys. 1. Cztery rewolucje przemysłowe [16]

Fig. 2. Advantages of collaboration between universities and VR/AR manufacturers

Rys. 2. Korzyści ze współpracy uczelni z producentami VR/AR

ing and learning activities in mining [12]. iCinema-based training allows students to recognize difficult work situations and receive training in a safe environment. The technology enables students to interact with the VR program that responds to movements in space and incorporates production situations (Fig. 3).

Scientists at the U.S. National Institute for Occupational Safety and Health have investigated how the mining industry can effectively use gamification and VR to learn how to escape fires. The Spokane Research Laboratory has developed fire evacuation training software for a mine safety training course (Fig. 4). The study notes that VR-based training significantly improves students' skills in determining proper evacuation routes in a possible emergency [23].

The expertise of educational institutions and mining companies in China includes VR technology applied to teaching safety regulations in rescue operations. Scientists [19; 20] have developed a cloud-based VR system for training mining engineers. This system includes VR hardware, a projected panoramic display system, a VR headset, a monitor, a tablet and other devices (Fig. 5).

In the context of the COVID-19 pandemic and the russian aggression against Ukraine, lecturers from the Physics Department of Kryvyi Rih National University have developed an AR-based manual for laboratory work in order to provide distance learning for future mining engineers [3; 29; 37; 40]. Future engineers use their smartphones to recognize AR markers, and the actual laboratory installation and its use are displayed on the screen (Fig. 6).

To summarize the national and international experience, we can say that in the process of training mining engineers, many courses, training laboratories, and research centers for mining research using AR/VR technology have been created at universities to improve mining engineers' training, prepare them for employment, and reduce training costs.

3. AR/VR apps analysis

The latest AR/VR technologies for simulating mining production processes expand the boundaries of practical mining training. In the educational process, it is important to ensure an advanced simulation of the production environment, perceived by students as reality. Professional AR/VR-based training of future engineers allows students to participate in production processes of a mining enterprise and be engaged in their future professional activities.

The VR/AR development in mining is based on automation of technological processes in the context of digital transformation of modern society. A significant effect of VR/AR technology applied to practical training of engineers is achieved through forming professional competencies in handling mining equipment.

3.1. Experience of using VR in the training process of mining engineers

Mobile communications, the Internet of Things, artificial intelligence, and cloud computing provide the information infrastructure needed for smart mining. Thanks to these modern technologies, next-generation VR systems for under-

Fig. 3. iCinema at the University of New South Wales [12]
Rys. 3. iCinema na Uniwersytecie Nowej Południowej Walii [12]

Fig. 4. The VR application for trainees to view a simulated underground mine [23]
Rys. 4. Aplikacja VR dla stażystów do oglądania symulowanej kopalni podziemnej [23]

Fig. 5. The VR Learning and Experiment Laboratory of the University of Mining and Technology in China [20]
Rys. 5. Laboratorium uczenia się i eksperymentowania VR Uniwersytetu Górniczo-Technologicznego w Chinach [20]

Fig. 6. Visualization for the laboratory work instruction
Rys. 6. Wizualizacja instrukcji pracy laboratorium

ground mining are being created to improve professional adaptation and occupational safety processes of future mining engineers [5; 10; 14; 22; 33; 36].

Scientist [6] studies the application of training with VR tools and concludes that students using VR applications learn four times faster than those learning in a classroom. The training was carried out using VR simulators (Fig. 7) to train operators and simulators for maintenance, which are key virtual reality training programs for the mining industry. These systems can monitor the training process and provide feedback to students. Gamification is a feature of VR training, which allows learning activities to be repeated until the desired level of competence and productivity is achieved.

Maptek, in collaboration with LlamaZOO MineLife, has developed VR digital tools to visualize production processes at mining companies in Canada, Australia, and South Africa. With the help of LlamaZOO MineLife, a digital model of an underground mine has been created, which can be used with a VR headset or a computer to explore the site (Fig. 8). This technology can be used for educational purposes for professional training and retraining of mining engineers. The use of digital models of mines makes the process of training mining engineers closer to real-life working conditions and safer [34].

First Quantum Minerals has installed Cybermine 5 Full-Mission simulators from ThoroughTec at its underground mine to train mining equipment operators. Simulation booths (Fig. 9) are copies of real mining equipment, with tools operating as they would in real mine transport. Simulators allow operators to test and practice the skills needed in an emergency (brake failure, fire, etc.). Notably, the two simulators can interact with each other to train teamwork in real production situations [8].

Thus, VR is an important component of smart mining, but there are a number of problems with introducing these technologies into the process of training mining engineers. They are expensive and there are no methods to assess their effectiveness. The technologies also require prior training for instructors and are complicated to adapt to different production conditions in different regions.

3.2. Experience of using AR in the training process of mining engineers

In the mining industry, AR technology is fast to develop, thus contributing to the evolution of training methods and tools for future professionals. When using AR, digital content is superimposed on the real-life production environment,

Fig. 7. Virtual Reality is a Game Changer for the Mining Industry [6]
Rys. 7. Rzeczywistość wirtualna zmienia zasady gry w przemyśle wydobywczym [6]

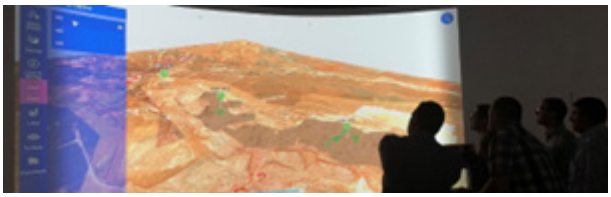

Fig. 8. Using VR to monitor the performance of mining machines in real-time [34]
Rys. 8. Wykorzystanie VR do monitorowania pracy maszyn górniczych w czasie rzeczywistym [34]

Fig. 9. The simulated mining cab [8]
Rys. 9. Symulowana kabina górnicza [8]

Fig. 10. Hands-Free AR with Visual Instructions [27]
Rys. 10. Hands-Free AR z instrukcjami wizualnymi [27]

bringing the training process as close to production conditions as possible. The advantage of the technology is that it is not expensive. A smartphone is all that is needed.

AR simulators enable preparing future mining engineers to work on the production floor without having to leave for the industrial facility. AR can be used to create conditions for the front-line mining experts to participate in remote consulting of future mining engineers.

Developer [13] create an AR platform to simulate unmanned mining in underground mines, revealing good results and stable operation. It has been noted that such production has a number of advantages, namely high efficiency, safety and low cost.

RealWear has developed an ergonomic device (Fig. 10) that fits under a helmet and does not interfere with the use of goggles in an industrial environment. The device helps workers to access documents (instructions, drawings, etc.), speeds up interactions with other employees, and facilitates navigation on the production floor [27].

DAQRI has developed an AR headset (fig. 11) for engineers and technicians, that can be used to repair, maintain and inspect industrial equipment. While working at the enterprise, instructions are displayed on the screen to direct the employee. In addition, the worker can remotely connect to a mentor or an expert to perform the task [38].

Plutomen designs and develops the innovative AR technology (Fig. 12) aimed at improving production processes, training mining engineers, and eliminating space and time constraints for communication between employees and experts. This technology allows experts who are located far from technical equipment to observe a production situation by means of employees' AR glasses and remotely give them advice on equipment diagnosis, repair, and control [17].

VSight develops applications based on AR technology (Fig. 13) to provide real-time remote assistance to operators in equipment maintenance and repair, drilling, as well as in training future specialists [21].

SensPlus Buddy AR tools (Fig. 14) provide smartphone communication for remote support of technicians at industrial facilities. Information is exchanged by sending images and text, this greatly improving efficiency of equipment maintenance and reducing the number of errors [29].

The TOMRA Visual Assist AR technology (Fig. 15) has three types of support: telephone and email support, real-time monitoring features, and remote login to the customer system by a TOMRA service engineer [11].

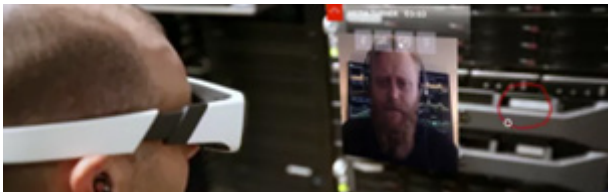

Fig. 11. The hard AR helmet of DAQRI [38]
Rys. 11. Twardy hełm AR firmy DAQRI [38]

Fig. 12. AR and VR in Mining Industry [17]
Rys. 12. AR i VR w górnictwie [17]

Fig. 13. Industrial Remote Service Platform Powered by AR [21]
Rys. 13. Przemysłowa Platforma Usług Zdalnych obsługiwana przez AR [21]

Fig. 14. Communication support service SensPlus Buddy [29]
Rys. 14. Usługa wsparcia komunikacji SensPlus Buddy [29]

Consequently, the use of AR technology allows for advanced operational readiness and improves the overall efficiency of the mining engineers training process. However, further research is needed to spur more innovative applications of virtual and augmented reality-based learning. It is effective because AR-based training can fully immerse future mining engineers in the production environment, allowing them to perform production tasks on simulators and receive advice from remote experts. Practice-oriented training has a significant impact on the formation of professional competences needed to work in production.

4. Methods of using AR/VR technologies in training mining engineers

Formation of professional competences, aimed at closing the gap between university education and real-life production, are key factors in training mining engineers.

Lecturers of Kryvyi Rih National University developed training materials using AR technology when training master's degree students in Specialty 184 Mining (Shaft Sinking and Drifting). The use of such materials is effective for independent work of students during distance learning, especially in the context of the COVID-19 pandemic and the russian aggression against Ukraine.

We offer several methods for making AR-based training materials for training mining engineers that contribute to modernization and digitalization of mining education.

1. The videos with digital training materials relevant to the topic of your class are freely available online, such as the following resources:

- https://www.imaker.ca/portfolio;
- https://www.herrenknecht.com/en/products/productdetail/gripper-tbm/;
- https://www.youtube.com/@HerrenknechtAG.

We offer as an example a video from Herrenknecht AG (Fig. 16).

2. Various AR applications can be used to visualize training material, such as:

- applications for creating AR (https://arize.io; https://www.augment.com);
- free applications for creating QR code for (https://goqr.me; https://www.qrstuff.com) (fig. 17).

3. Using the selected applications, you can create a QR code or and AR object.

Fig. 15. AR tool for remote assistance TOMRA Visual Assist [11]
Rys. 15. Narzędzie AR do zdalnej pomocy TOMRA Visual Assist [11]

Fig. 16. Shaft Boring Machine for Shaft Enlargement
Rys. 16. Wytaczarka wałkowa do powiększania wału

Fig. 17. Application for creating QR code (https://goqr.me)
Rys. 17. Aplikacja do tworzenia kodu QR (https://goqr.me)

Fig. 18. The QR code with a link to the video https://www.youtube.com/watch?v=hF6veu3zMbA
Rys. 18. Kod QR z linkiem do filmu https://www.youtube.com/watch?v=hF6veu3zMbA

When preparing training materials, we use applications for creating a QR code (https://goqr.me) and receive it with a link to our video (Fig. 18).

4. A QR code is added to the instruction for a laboratory work on mining with a link to training.

While performing a laboratory work, students must perform the following sequence of actions: 1) open the Camera application on the smartphone; 2) point the camera at the AR marker or the QR code and scan it; 3) a training video appears on the screen (Fig. 19).

This method of presenting the material has proven to be very effective in distance learning in the context of the COVID-19 pandemic and the russian aggression against Ukraine [40]. Thus, when teaching the subject Blasting Safety, lecturers use QR codes to visualize training materials. Students simply scan the QR code (Fig. 20) and view different types of explosions. It is essential to note that students remain in a safe place and receive all the information.

It should be noted that the use of AR for performing laboratory works by future mining engineers is an effective tool to motivate students to study and develop their research competences. Students can better understand abstract theoretical models of production processes through AR visualization.

Thus, after analyzing the available materials, we can conclude that the introduction of AR/VR technology into the training of Ukrainian mining engineers is a promising direction for further research. Prospects for further research include (Fig. 21):

5. Conclusions

Analysis of the data on the problem of training mining engineers reveals that the international experience with the use of AR/VR technology in mining is positive and shows a developing trend.

AR/VR technology, as a smart mining tool, is an innovative method of training mining engineers to control production processes. The technology is particularly effective for visualization of employee locations, safety monitoring, and handling of mining equipment. It should be noted that AR/VR technology is appropriate for building health-saving competences at safety training courses of mining enterprises aimed at preventing emergencies. An advantage of the AR/VR technology in the process of training mining engineers is the ability to visually present future production processes.

Fig. 19. Visualization of training videos to perform laboratory works
Rys. 19. Wizualizacja filmów szkoleniowych do wykonywania prac laboratoryjnych

Fig. 20. Types of explosions
Rys. 20. Rodzaje wybuchów

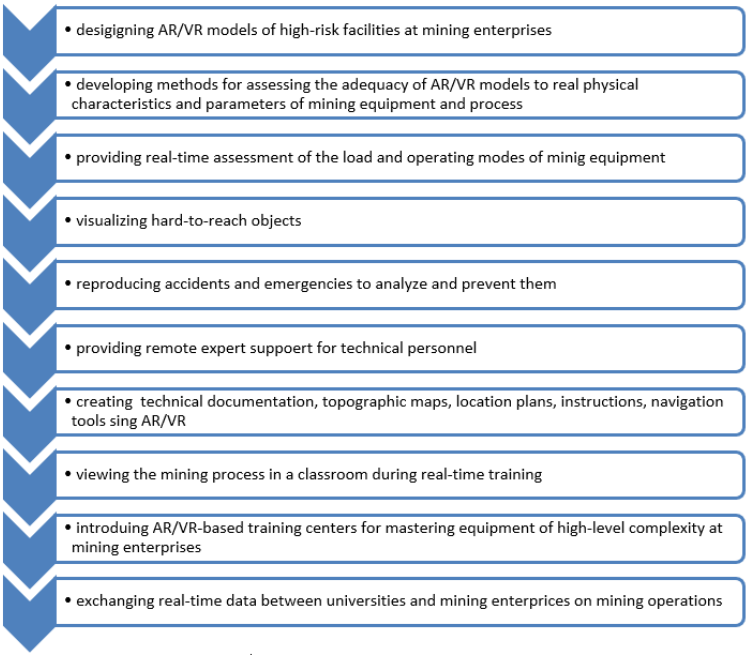

Fig. 21. Promising research areas of the implementation of the AR/VR technology in training mining engineers in Ukraine
Rys. 21. Perspektywiczne obszary badawcze zastosowania technologii AR/VR w szkoleniu inżynierów górnictwa na Ukrainie

The methods of using AR/VR technology in the training of mining engineers described in this paper have allowed University teachers to easily and effectively implement the technology in the educational process during distance learning in the context of the COVID-19 pandemic and the russian aggression in Ukraine. AR/VR-based teaching materials contribute to modernization of the process of training competitive specialists in the mining industry.

Literatura – References

1. Abdelrazeq, A., Daling, L., Suppes, R., Feldmann, Y. & Hees, F. (2019, March 11–13). A virtual reality educational tool in the context of mining engineering : the virtual reality mine [Conferense session]. 13th International Technology, Education and Development Conference, Valencia, Spain. https://doi.org/10.21125/inted.2019.2002
2. Augmented reality set to change the future of mine safety. (2020, August 4). Australasian Mine Safety Journal. https://www.amsj.com.au/augmented-reality-mine-safety/
3. Bakum, Z., Tkachuk, V. (2014). Mining engineers training in context of innovative system of Ukraine. Metallurgical and Mining Industry, 6(5), 29–34. https://www.metaljournal.com.ua/assets/Journal/7-Tkachuk.pdf
4. Barker, T. (2012). Images and eventfulness: expanded cinema and experimental research at the University of New South Wales. Studies in Australasian Cinema, 6(2), 111–123. http://dx.doi.org/10.1386/sac.6.2.111_1
5. Bastug, E., Bennis, M., Medard, M., & Debbah, M. (2017). Toward interconnected virtual reality: opportunities, challenges, and enablers. IEEE Communications Magazine, 55(6), 110–117. https://doi.org/10.1109/MCOM.2017.1601089
6. Bharathy, C. (2021, July 26). Virtual Reality is a Game Changer for the Mining Industry. Fusion VR. https://www.fusionvr.in/blog/2021/07/26/virtual-reality-is-a-game-changer-for-the-mining-industry/
7. Ciepiela, M., Sobczyk, W. (2021). A study of PM 10, PM 2.5 concentrations in the atmospheric air in Kraków, Poland. Journal of the Polish Mineral Engineering Society, 1, 129–135. http://www.potopk.com.pl/Full_text/2021_v1_full/IM%201-2021-a17.pdf
8. Cybermine Full Mission Mining Simulators. (2022). ThoroughTec Simulation. https://www.thoroughtec.com/cybermine-full-mission-mining-simulators/?gclid=Cj0KCQiA8aOeBhCWARIsANRFrQHl8DOib0VikhOtAbrAaEr4W-1GqVwPflrlddO_HVa8P6JzGj14VpM8aArmzEALw_wcB
9. Daling, L. M., Khodaei, S., Thurner S. (2021). A decision matrix for implementing AR, 360° and VR experiences into mining engineering education. In C. Stephanidis, M. Antona, S. Ntoa (Eds.), Communications in Computer and Information Science, (pp. 225–232). Springer Science and Business Media. https://doi.org/10.1007/978-3-030-78642-7_30
10. Daling, L., Kommetter, C., Abdelrazeq, A., Ebner, M. & Ebner, M. (2020). Mixed Reality Books: Applying Augmented and Virtual Reality in Mining Engineering Education. In: V .Geroimenko (Ed.), Augmented Reality in Education (pp. 185–195). Springer. https://doi.org/10.1007/978-3-030-42156-4
11. De Paoli, C. (2021, May 14). Tomra Expands Its Mining Services With a New Augmented Reality Tool: Tomra Visual Assist. Heavy Quip Magazine. https://www.heavyquipmag.com/2021/05/14/tomra-expands-its-mining-services-with-a-new-augmented-reality-tool-tomra-visual-assist/
12. Del Favero, D., Hardjorno, F. (2012). Building VR: Project Overview. iCinema. http://www.icinema.unsw.edu.au/projects/building-vr/project-overview/
13. Fang, J., Fan, C., Wang, F. et al. (2022). Augmented Reality Platform for the Unmanned Mining Process in Underground Mines. Mining, Metallurgy & Exploration, 39, 385–395. https://doi.org/10.1007/s42461-021-00537-1
14. Grabowski, A., Jankowski, J. (2015). Virtual reality-based pilot training for underground coal miners. Safety Science, 72, 310–314. https://doi.org/10.1016/j.ssci.2014.09.017
15. Ignite EDD [Video]. (2022). YouTube. https://www.youtube.com/@igniteEDD
16. IoT & Industry 4.0. (2020). b.telligent. https://www.btelligent.com/en/portfolio/industry-40/
17. Kanani, H. (2019, October 1). AR and VR in Mining Industry : Transforming the Future. Plutomen. https://pluto-men.com/ar-and-vr-in-mining-industry-transforming-the-future/#
18. Kizil, M. S., Kerridge, A. P., Hancock, M. G. (2004, June 15–16). Use of virtual reality in mining education and training [Conferense session]. CRC Mining Research and Effective Technology Transfer Conference, Noosa Heads, Australia. https://espace.library.uq.edu.au/view/UQ:100045
19. Li, M., Sun, Z. M.,. Lyu, P. Y, Chen, J., & Mao, S. (2018). Study on key technology of multiplayer virtual reality training platform for fully-mechanized coal mining face. Coal Science and Technology, 46(1), 156–161. https://doi.org/10.1155/2020/6243085
20. Li, M., Sun, Zh., Jiang, Zh., Tan, Zh., Chen, J. (2020). A Virtual Reality Platform for Safety Training in Coal Mines with AI and Cloud Computing. Multi-Goal Decision Making for Applications in Nature and Society, 2020. https://doi.org/10.1155/2020/6243085
21. Malecaj, L. (2021, August 9). Augmented Reality Revolutionizing Mining Industry. VSight. https://vsight.io/blog/augmented-reality-revolutionizing-mining-industry/

22. Mitra, R., Saydam, S. (2014). Can artificial intelligence and fuzzy logic be integrated into virtual reality applications in mining? Journal of the Southern African Institute of Mining and Metallurgy, 114(12), 1009–1016. https://www.researchgate.net/publication/279325623_Can_artificial_intelligence_and_fuzzy_logic_be_integrated_into_virtual_reality_applications_in_mining

23. Orr, T. J., Mallet, L. G., Margolis, K. A. (2009). Enhanced fire escape training for mine workers using virtual reality simulation. Mining Engineering, 61(11), 41–44. https://www.cdc.gov/niosh/mining%5C/UserFiles/works/pdfs/efet-fm.pdf

24. Pysmennyi, S., Fedko, M., Shvaher, N., Chukharev, S. (2020). Mining of rich iron ore deposits of complex structure under the conditions of rock pressure development. E3S Web of Conferences, 201. https://doi.org/10.1051/e3sconf/202020101022

25. Pysmennyi, S., Peremetchyk, A., Chukharev, S., Anastasov, D. & Tomiczek, K. (2022). The mining and geometrical methodology for estimating of mineral deposits. IOP Conference Series: Earth and Environmental Science, 1049(1). https://doi.org/10.1088/1755-1315/1049/1/012029

26. Radwanek-Bąk, B., Sobczyk, W., Sobczyk, E. J. (2020). Support for multiple criteria decisions for mineral deposits valorization and protection. Resources Policy, 68, 1–11. https://doi.org/10.1016/j.resourpol.2020.101795

27. Reality First, Digital Second. (2020). RealWear. https://www.realwear.com/hmt-1/

28. Schofield, D., Denby, B., Hollands, R. (2001). Mine safety in the twenty-first century: the application of computer graphics and virtual reality. In M. Karmis (Ed.), Mine Health and Safety Management (pp. 153–174). Society of Mining, Metallurgy, and Exploration, Inc.

29. SensPlus Buddy Communication. (2019). Yokogawa Electric Corporation. https://www.yokogawa.com/solutions/products-and-services/lifecycle-services/operation-and-maintenance-improvement/sensplus-buddy-communication/#Details

30. Shchokin, V., Tkachuk, V. (2014). Automatization of agglomerative production on the base of application of Neuro-Fuzzy controlling systems of the bottom level. Metallurgical and Mining Industry, 6(6), 32–39. https://www.metaljournal.com.ua/assets/MMI_2014_6/7-Shchokin.pdf

31. Shepiliev, D. S., Modlo, Y. O., Yechkalo, Y. V., Osadchyi, V. V. & Semerikov, S. O. (2020). WebAR development tools: An overview. CEUR Workshop Proceedings, 2832, 84–93. https://ceur-ws.org/Vol-2832/paper12.pdf

32. Sobczyk, W., Sobczyk, E. J. (2021). Varying the energy mix in the EU-28 and in Poland as a step towards sustainable development. Energies, 14(1502), 1–19. https://www.mdpi.com/1996-1073/14/5/1502

33. Someswar, M., Bhattacharya, A. (2018, January 11). MineAr: using crowd knowledge for mining association rules in the health domain [Conference session]. ACM India Joint International Conference on Data Science and Management of Data, New York, NY, USA. https://doi.org/10.1145/3152494.3152504

34. Sykes, J. (2019, March 21). How data visualisation is revolutionising mining. Maptek Pty Limited. https://www.maptek.com/blogs/how-data-visualisation-is-revolutionising-mining/

35. Takahashi, D. (2017, October 10). Founder Brian Mullins steps down as CEO of augmented reality firm Daqri. VentureBeat. https://venturebeat.com/business/founder-brian-mullins-steps-down-as-ceo-of-augmented-reality-firm-daqri/

36. Tichon, J., Burgess-Limerick, R. (2011). A review of virtual reality as a medium for safety related training in the minerals industry. Journal of Health & Safety Research & Practice, l(3), 33–40. https://eprints.qut.edu.au/123479/

37. Tkachuk, V. V., Yechkalo, Y. V., Markova, O. M. (2017). Augmented reality in education of students with special educational needs. CEUR Workshop Proceedings, 2168, 66–71. https://doi.org/10.55056/cte.136

38. Wheeler, A. (2019, October 9). DAQRI is Closing Up Shop: Another very promising industrial AR startup is biting the proverbial dust. engineering.com. https://www.engineering.com/story/daqri-is-closing-up-shop

39. Wu, Y., Chen, M., Wang, K., & Fu, G. (2019). A dynamic information platform for underground coal mine safety based on internet of things. Safety Science, 113, 9–18. https://doi.org/10.1016/j.ssci.2018.11.003

40. Yechkalo, Y., Tkachuk, V., Hruntova, T., Brovko, D. & Tron, V. (2019). Augmented reality in training engineering students: Teaching methods. CEUR Workshop Proceedings, 2393, 952–959. http://ceur-ws.org/Vol-2393/

Narzędzia rozszerzonej i wirtualnej rzeczywistości w szkoleniu inżynierów górnictway

Przejście na inteligentne wydobycie znacznie zwiększyło wymagania dotyczące szkolenia nowoczesnych inżynierów górnictwa, co wymaga cyfryzacji tego procesu. Bazując na badaniach naukowych, technologia wirtualnej i rozszerzonej rzeczywistości jest najskuteczniejsza i najbezpieczniejsza. W artykule przedstawiono metody wykorzystania technologii wirtualnej i rozszerzonej rzeczywistości w szkoleniu inżynierów górnictwa. Metody są z powodzeniem wdrażane w laboratoriach Krzyworoskiego Uniwersytetu Narodowego (Ukraina) i okazały się skuteczne podczas nauczania na odległość w kontekście pandemii COVID-19 i rosyjskiej agresji militarnej na Ukrainę. Niemniej jednak potrzebne są dalsze badania naukowe, aby wprowadzić nowoczesne technologie cyfrowe do kształcenia inżynierów górnictwa na uczelniach w celu ukształtowania konkurencyjnego i kompetentnego specjalisty

Słowa kluczowe: *szkolenie inżynierów górnictwa, rzeczywistość rozszerzona (AR), Rzeczywistość wirtualna (VR), transformacja cyfrowa, edukacja na odległość, pandemia COVID-19, rosyjska agresja militarna przeciwko Ukrainie*

Influence of Nonlinear Shear Modulus Change of Elastomeric Shell of a Composite Tractive Element with a Damaged Structure on its Stress State

Ivan BELMAS[1)], Dmytro KOLOSOV[2)], Serhii ONYSHCHENKO[3)], Olena BILOUS[4)], Hanna TANTSURA[5)]

[1)] Dniprovsk State Technical University, 2 Dniprobudivska str., 51900, Kamianske, Ukraine; ORCID https://orcid.org/0000-0003-2112-0303; evolyuta@gmail.com
[2)] Dnipro University of Technology, 19 Dmytra Yavornytskoho ave., 49005, Dnipro, Ukraine; ORCID https://orcid.org/0000-0003-0585-5908
[3)] Dnipro University of Technology, 19 Dmytra Yavornytskoho ave., 49005, Dnipro, Ukraine; ORCID https://orcid.org/0000-0002-5709-7021
[4)] Dniprovsk State Technical University, 2 Dniprobudivska str., 51900, Kamianske, Ukraine; ORCID https://orcid.org/0000-0001-6398-8843
[5)] Dniprovsk State Technical University, 2 Dniprobudivska str., 51900, Kamianske, Ukraine; ORCID https://orcid.org/0000-0002-8672-1153

http://doi.org/10.29227/IM-2023-01-18

Submission date: 08-02-2023 | Review date: 27-03-2023

Abstract

Purpose. Determination of a dependency of a stress state for composite elastomer-cable tractive element with a broken structure on a nonlinear dependency of shear modulus on deformations in the elastomeric shell.
Methods. Analytical solution of a model of a composite tractive element with disturbed structure and a deformation-dependent shear modulus of an elastomeric shell.
Findings. Algorithm for determining a stress state of a composite tractive element with broken structure and a deformation-dependent shear modulus.
Scientific novelty. Character of dependency for a stress state of a composite tractive element on a nonlinear dependency of shear modulus on deformations.
Practical significance. A possibility to determine the dependency of a stress state of a composite elastomer-cable tractive element on a nonlinear shear modulus allows considering the effect of this phenomenon on the tractive element strength and ensures an increase of its operational safety.

Keywords: *mineral resources, mining, lifting and transporting complexes, composite tractive element, damaged structure, elastomeric shell, stress state, analytical solution*

1. Introduction

Continuous improvement of technical systems in the fields of mining technologies [1–9], transportation and hoisting [10–12], deep-sea mining [13, 14], and dynamics of technical systems [15–19] facilitate wider and more thorough development of analytical and computational simulation methods of processes and phenomena occurring within the systems. Currently, researchers in many countries are conducting complex scientific studies aimed at developing methods and means of modernizing lifting and transporting complexes with the aim of increasing operational efficiency and safety of mining transport equipment. Composite elastomer-cable tractive elements, in particular rubber-cable ropes (also known as steel cord belts), are widely used in hoisting and transporting machines [20–24]. At the same time, these tractive elements have significant lengths. Conveyor belts of a closed shape are created by connecting ends of belts. Cables at belt ends in such connections are not mechanically connected and interact through rubber layers. Damage accumulates in ropes during use. One type of damage is rupture of one of reinforcing elements (cables). Rupture of continuity of cables and presence of non-continuing cables, in accordance with the Saint-Venant's principle, are sources of disturbance of a stress-strain state in a rope (belt).

2. State of question and statement of research problem

Rope strength in the cross-section of cable breakage is much lower [25–27], it is also lower in butt joints [28]. In paper [29], it is suggested to determine a stress-strain state of spatial structures reinforced with parallel elements by means of electrical modelling. A method of determining characteristics of materials with a system of regularly arranged parallel reinforcing elements is suggested in the article [30]. The papers [31–40] are devoted to investigation of features of a rope (belt) stress state, considering its interaction with structural elements of a machine. Experience indicates that there is a nonlinear dependency of stresses in elastic materials on their deformations, and rubber is no exception to this. Rubber layers in rubber-cable ropes ensure the connection of cables, determine a mechanism of redistribution of forces between the cables, which affects the operational characteristics of the entire rope. In these papers, the issue of a nonlinear law of rubber deformation is not considered. At the same time, it constitutes an actual scientific and technical problem of considering the specified feature during the design and continuous control of the condition of hoisting and transporting machines with a rubber-cable tractive element. The solution allows considering the influence of deformation character in rubber on rope strength and provides a possibility of increasing operational safety of rubber-cable ropes (belts).

Generally, the dependency graph of stresses on deformations has a shape of a curved line. The main factor in the occurrence of shear stresses in rubber layers of a rope or belt is breakage of continuity of cables. Discontinuity of cables occurs in the event of cable breakage and in butt joints of rub-

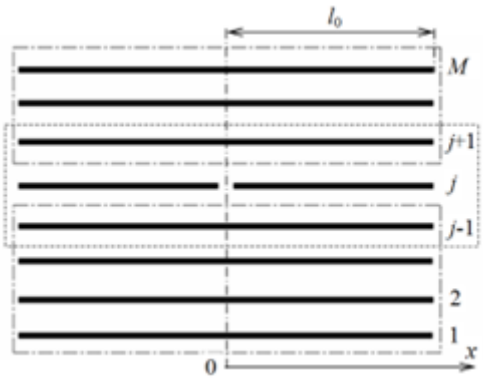

Fig. 1. Rope part with a broken cable

Rys. 1. Część liny z pękniętym kablem

ber-cable ropes and belts. In butt-joint connections, no cables at both ends of the connected belts continue. A cable break or a cable end is a source of stress-strain state disturbance in a rope (belt). Well-known studies [26] indicate that deformations of rubber take place practically only in the layers adjacent to the broken cable. Deformation values are maximum in the cross-section of cable continuity breakage and decrease exponentially with increasing distance from the specified cross-section.

3. Presentation of main research

Determining a stress-strain state considering the specified character of deformation changes and considering the nonlinear dependency of shear displacements on rubber shear stresses is a complex mathematical problem. Let's simplify it. Assume that the dependency of rubber shear stresses on its deformations is piecewise linear and consists of two parts. As in the studies mentioned above, we assume that the cables deform like rods. Rubber is subjected only to shear stress. The rope is infinitely long. It has M cables and is loaded with a tensile force P. The cable numbered j has a continuity breakage. The cross-section with the breakage is at a considerable distance from the rope edges. Rubber shear modulus of layers adjacent to the damaged cable at lengths l0 is different from the corresponding rubber shear modulus of the remaining layers. The linear size l0 is much smaller than the rope length, on which the stress state is changed because of a cable breaking. Direct the coordinate axis along the rope. Its beginning (x = 0) is located at the point where the cable breaks. Since the cross-section (x = 0) is a cross-section of symmetry, the displacements of cables are symmetrical. At the same time, the cross-sections of all cables except the ends of the broken cable do not move. A gap is formed between the ends of the damaged cable. Let's denote the displacement of the end of the damaged cable U_0.

Let's single out a part of length $l_0 (0 \le x \le l_0)$. Consider it the first one. Consider the part for which $x > l_0$ the second part. The first part of the rope is divided into three stripes with an unchanged number of cables in each. Include stripes that do not have a broken cable into the structure of the two extreme stripes. Give them numbers one and three. The rope part with the broken cable and the cables adjacent to it will be included in the structure of the second stripe (Fig.1).

Consider the specified stripes as separate belts. A characteristic feature of such rope stripes is that the properties of elastic material between the rope stripes do not change. Shear modulus of rubber in layers between cables is not variable in our case. This allows using the conditions of their equilibrium and the form of solutions for stripes [26], considering the number of cables in stripes and properties of elastic shell. Let's make expressions that allow determining the internal forces in cables and their displacements. Write down the expressions for the extreme stripes in similar forms. In the expressions, we will use additional indices to assign the parameters to one or another rope stripe. Take into account that cross-sections of cables of the extreme stripes do not move when (x = 0).

For a rope stripe with cable numbers

$$p_{1,i} = EF\sum_{m=1}^{j-2} A_m\left(e^{\beta_{1,m}x} + e^{-\beta_{1,m}x}\right)\beta_{1,m}\cos\left(\mu_{1,m}(i-0.5)\right) + P, \quad (1)$$

$$u_{1,i} = \sum_{m=1}^{j-2} A_m\left(e^{\beta_{1,m}x} - e^{-\beta_{1,m}x}\right)\cos\left(\mu_{1,m}(i-0.5)\right) + \frac{Px}{EF}, \quad (2)$$

where i is cable number in the first stripe ($1 \le i \le j-2$); A_m, B_m are integration constants; E, F are, respectively, reduced tensile modulus of elasticity and cross-sectional area of a cable in a rope (belt); $\beta_{1,m} = \sqrt{\frac{2G_0 b}{(h-d)EF}[1-\cos(\mu_{1,m})]}$; h is distance between the cables; b is rope thickness; d is cable diameter; G is shear modulus of elastic (rubber) layer connecting the cables.

For the second rope stripe with cable numbers ($j-1 \le i \le j+1$)

$$p_{2,i} = EF\sum_{m=1}^{2}\left[\left(A_{m+j-2}e^{\beta_{2,m}x} - B_{m+j-2}e^{-\beta_{2,m}x}\right)\beta_{2,m}\cos\left(\mu_{2,m}(i-j-1.5)\right)\right] + P, \quad (3)$$

$$u_{2,i} = \sum_{m=1}^{2}\left(A_{m+j-2}e^{\beta_{2,m}x} + B_{m+j-2}e^{-\beta_{2,m}x}\right)\cos\left(\mu_{2,m}(i-j-1.5)\right) + \frac{Px}{EF}, \quad (4)$$

where $\mu_{2,m} = \frac{\pi m}{3}$; $\beta_{2,m} = \sqrt{\frac{2G_0 bk}{(h-d)EF}[1-\cos(\mu_{2,m})]}$;

k is coefficient, which considers the difference in shear modulus of rubber for the second stripe.

For a rope stripe with cable numbers ($j+1 \le i \le M$)

$$p_{3,i} = EF\sum_{m=1}^{M-j-1} A_{m+j}\left(e^{\beta_{3,m}x} + e^{-\beta_{3,m}x}\right)\beta_{3,m}\cos\left(\mu_{3,m}(i-j-1.5)\right) + P, \quad (5)$$

$$u_{3,i} = \sum_{m=1}^{M-j-1} A_{m+j}\left(e^{\beta_{3,m}x} - e^{-\beta_{3,m}x}\right)\cos\left(\mu_{3,m}(i-j-1.5)\right) + \frac{Px}{EF}, \quad (6)$$

where $\mu_{3,m} = \frac{\pi m}{M-j}$; $\beta_{3,m} = \sqrt{\frac{2G_0 f(t) bk_G}{(h-d)EF}[1-\cos(\mu_{3,m})]}$.

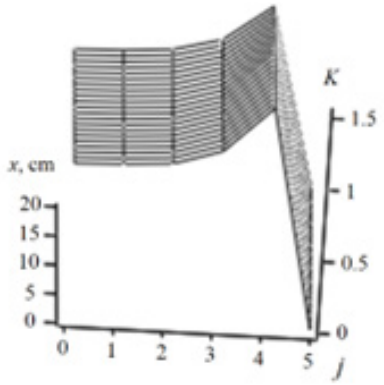

Fig. 2. Dependency of coefficients of uneven distribution of forces among cables with numbers i along the x-axis
Rys. 2. Zależność współczynników nierównomiernego rozkładu sił między kablami o liczbach i wzdłuż osi x

These solutions correspond to the conditions of influence absence of external factors on extreme cables in stripes on the interval ($0 \le x \le l_0$). The cables adjacent to the broken one are included in two stripes – the extreme one and non-extreme one. In the extreme stripes, there are no disturbances in cables adjacent to the broken one, in accordance with solutions of (1), (2) and (5), (6). They are loaded with only evenly distributed forces. Cables in the cross-section x = 0 are immovably fixed. In a general solution, based on the principle of superposition, we add their displacements as cables, which are part of the middle stripe, to displacements of these cables without considering the force of their external load.

The end of the middle cable in the middle stripe is displaced by an unknown amount U_0 under the action of an external force. Let's write the above in a form of a boundary condition for the cross-section x = 0

$$u_{2,i} = U_0 \begin{cases} 0 & i \neq j \\ 1 & i = j \end{cases} \tag{7}$$

According to (7), the law of cable displacements corresponds to the product of displacement of a middle cable and the Dirac function δ. Let's take the Dirac function in a form of a Fourier series on a given segment of cable numbers. From expression (4), we have the following

$$\sum_{m=1}^{2}\left(A_{m+j-2}+B_{m+j-2}\right)\cos\left(\mu_{2,m}(i-0.5)\right)=\frac{2}{3}U_0\sum_{m=1}^{2}\cos\left(\frac{3}{2}\mu_{2,m}\right)\cos\left(\mu_{2,m}(i-0.5)\right), \quad (i=1,2,3). \tag{8}$$

From where

$$B_{m+j-2}=\frac{2}{3}U_0\cos\left(1.5\mu_{2,m}\right)-A_{m+j-2}, \quad (m=1,2). \tag{9}$$

From the condition that a load on the broken cable in the cross-section of breakage is equal to zero from expression (3) we have

$$U_0=\frac{3P}{2\beta_{2,m}EF\cos^2\left(1.5\mu_{2,m}\right)}+3\frac{A_{m+j-2}}{\cos\left(1.5\mu_{2,m}\right)}. \tag{10}$$

Accordingly, expression (9) takes the form

$$B_{m+j-2}=\frac{P}{\beta_{2,m}EF\cos\left(1.5\mu_{2,m}\right)}+2A_{m+j-2}. \tag{11}$$

Expressions of forces (3) and displacements (4) considering the general numeration of cables in the cross-section of a rope take the following forms

$$p_{2,i}=EF\sum_{m=1}^{2}\left[\left(A_{m+j-2}\left(e^{\beta_{2,m}x}-2e^{-\beta_{2,m}x}\right)\beta_{2,m}-\frac{Pe^{-\beta_{2,m}x}}{\cos\left(1.5\mu_{2,m}\right)}\right)\times\cos\left(\mu_{2,m}(i-j-1.5)\right)\right]+P, \tag{12}$$

$$u_{2,i}=\sum_{m=1}^{2}\left[\left(A_{m+j-2}\left(e^{\beta_{2,m}x}+e^{-\beta_{2,m}x}+0.5\right)+\frac{P\left(e^{-\beta_{2,m}x}+0.5\right)}{\beta_{2,m}EF\cos\left(1.5\mu_{2,m}\right)}\right)\times\cos\left(\mu_{2,m}(i-j-1.5)\right)\right]+\frac{Px}{EF}. \tag{13}$$

Using (1), (2), (5), (6), (12), (13), we write down the values of forces and displacements as single functions on the finite axis of cable numbers

$$p_i=\frac{2EF}{M}\sum_{n=1}^{M-1}\rho_n(x)\cos\left(\mu_n(i-0.5)\right)+P, \tag{14}$$

where $\mu_n=\frac{\pi n}{M-1}$;

$$\begin{aligned}\rho_n(x)=&\sum_{\chi=1}^{j-1}\sum_{m=1}^{j-2}\left[A_m\left(e^{\beta_{1,m}x}+e^{-\beta_{1,m}x}\right)\beta_{1,m}\cos\left(\mu_{1,m}(\chi-0.5)\right)\cos\left(\mu_n(\chi-0.5)\right)\right]+\\&+\sum_{\chi=1}^{3}\sum_{m=1}^{2}\left[\left(A_{m+j-2}\left(e^{\beta_{2,m}x}-2e^{-\beta_{2,m}x}\right)\beta_{2,m}-\frac{Pe^{-\beta_{2,m}x}}{EF\cos\left(1.5\mu_{2,m}\right)}\right)\times\cos\left(\mu_{2,m}(\chi-0.5)\right)\cos\left(\mu_n(\chi+j-2.5)\right)\right]+\\&+\sum_{\chi=1}^{M-j-1}\sum_{m=1}^{M-j-1}\left[A_{m+2}\left(e^{\beta_{3,m}x}+e^{-\beta_{3,m}x}\right)\beta_{3,m}\times\cos\left(\mu_{3,m}(\chi-0.5)\right)\cos\left(\mu_n(\chi+j-0.5)\right)\right],\end{aligned} \tag{15}$$

$$u_i=\frac{2}{M}\sum_{n=1}^{M}\upsilon_n(x)\cos\left(\mu_n(i-0.5)\right)+\frac{Px}{EF},$$

where

$$\begin{aligned}\upsilon_n(x)=&\sum_{\chi=1}^{j-1}\sum_{m=1}^{j-2}\left(A_m\left(e^{\beta_{1,m}x}-e^{-\beta_{1,m}x}\right)\cos\left(\mu_{1,m}(\chi-0.5)\right)\cos\left(\mu_n(\chi-0.5)\right)\right)+\\&+\sum_{\chi=1}^{3}\sum_{m=1}^{2}\left[\left(A_{m+j-2}\left(e^{\beta_{2,m}x}+e^{-\beta_{2,m}x}\right)+\frac{Pe^{-\beta_{2,m}x}}{\beta_{2,m}EF\cos\left(1.5\mu_{2,m}\right)}\right)\times\cos\left(\mu_{2,m}(\chi-0.5)\right)\cos\left(\mu_n(\chi+j-2.5)\right)\right]+\\&+\sum_{\chi=1}^{M-j-1}\sum_{m=1}^{M-j-1}\left(A_{m+2}\left(e^{\beta_{3,m}x}-e^{-\beta_{3,m}x}\right)\cos\left(\mu_{3,m}(\chi-0.5)\right)\cos\left(\mu_n(\chi+j-0.5)\right)\right).\end{aligned}$$

Expressions (14), (15) are obtained for the first part of the rope for ($0 \le x \le l_0$). In cross-section $x = l_0$ the considered part of the rope interacts with its second part. Write expressions of forces ($p_{0,i}$) and displacements ($u_{0,i}$) for the second part in the forms [26]. At the same time, we consider that an infinite increase in the value of the x-coordinate cannot lead to an infinite increase in the loading forces of cables and their displacements

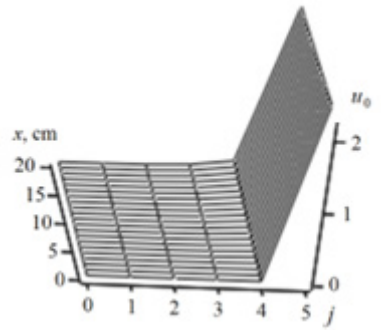

Fig. 3. Dependency of a product of rigidity and displacements of cables with numbers i along the x-axis

Rys. 3. Zależność iloczynu sztywności i przemieszczeń lin o liczbach i wzdłuż osi x

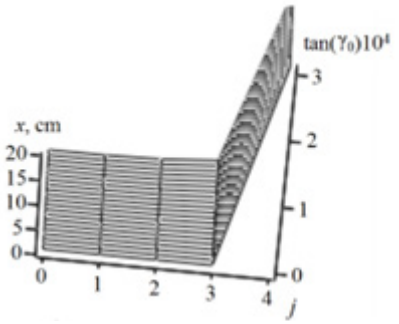

Fig. 4. Dependency of tangents of shear angles of elastic shell between cables with numbers j along the x-axis relative to its average value

Rys. 4. Zależność tangensów kątów ścinania powłoki sprężystej między kablami o numerach j wzdłuż osi x względem jej wartości średniej

$$p_{0,i} = -EF\sum_{n=1}^{M-1} B_{0,n}e^{-\beta_n^* x}\beta_n^*\cos\left(\mu_n(i-0.5)\right) + P, \tag{16}$$

$$u_{0,i} = \sum_{n=1}^{M-1} B_{0,n}e^{-\beta_n^* x}\cos\left(\mu_n(i-0.5)\right) + \frac{Px}{EF}, \qquad (1 \le i \le M), \tag{17}$$

where

$$\beta_n = \sqrt{\frac{2G_0 b}{(h-d)EF}[1-\cos(\mu_n)]}.$$

At the same time, in cross-section x=l0 the conditions of joint deformation of rope parts must be fulfilled

$$p_{0,i} = p_i, \tag{18}$$

$$u_{0,i} = u_i \tag{19}$$

From expressions (14), (15) and conditions (18), (19), we have equalities

$$B_{0,n}e^{-\beta_n^* l_0} = -\frac{2}{M\beta_n^*}\rho_n \qquad (x = l_0), \tag{20}$$

$$B_{0,n}e^{-\beta_n^* l_0} = \frac{2}{M}\upsilon_n \qquad (x = l_0). \tag{21}$$

Subtract (21) from (20). We get a system of N – 1 equations

$$\begin{aligned}
&\sum_{\chi=1}^{j-1}\sum_{m=1}^{j-2}\left(\begin{array}{c} A_m\left(e^{\beta_{1,m}l_0}\left(1+\frac{\beta_{1,m}}{\beta_n^*}\right)-e^{-\beta_{1,m}l_0}\left(1-\frac{\beta_{1,m}}{\beta_n^*}\right)\right)\times \\ \times\cos\left(\mu_{1,m}(\chi-0.5)\right)\cos\left(\mu_n(\chi-0.5)\right)\end{array}\right)+ \\
&+\sum_{\chi=1}^{3}\sum_{m=1}^{2}\left(\begin{array}{c}\left(\begin{array}{c} A_{m+j-2}\left(e^{\beta_{2,m}l_0}\left(1+\frac{\beta_{2,m}}{\beta_n^*}\right)+e^{-\beta_{2,m}l_0}\left(1-2\frac{\beta_{2,m}}{\beta_n^*}\right)\right)+ \\ +\frac{Pe^{-\beta_{2,m}l_0}}{EF\cos\left(1.5\mu_{2,m}\right)}\left(\frac{1}{\beta_{2,m}}-\frac{1}{\beta_n^*}\right)\end{array}\right)\times \\ \times\cos\left(\mu_{2,m}(\chi-0.5)\right)\cos\left(\mu_n(\chi+j-2.5)\right)\end{array}\right)+ \\
&+\sum_{\chi=1}^{M-j-1}\sum_{m=1}^{M-j-1}\left[\begin{array}{c} A_{m+2}\left(e^{\beta_{3,m}l_0}\left(1+\frac{\beta_{3,m}}{\beta_n^*}\right)-e^{-\beta_{3,m}l_0}\left(1-\frac{\beta_{3,m}}{\beta_n^*}\right)\right)\times \\ \times\cos\left(\mu_{3,m}(\chi-0.5)\right)\cos\left(\mu_n(\chi+j-0.5)\right)\end{array}\right].
\end{aligned} \tag{22}$$

The solution of obtained system of equations (22) allows determining the unknown constants and internal loading forces of cables, and their displacements. The known displacements make it possible to determine tangential stresses in material of the elastic shell located between the cables, which are directly proportional to the tangent of its shear angle

$$\tan(\gamma_i) = \frac{u_i - u_{i+1}}{h}, \qquad (1 \le i < M). \tag{23}$$

With the use of obtained dependencies, stress-strain state indicators are determined for a rope type RCB-3150 consisting of six cables. The sixth of them is broken. The area length l0 is assumed equal to 0.1 m. Coefficient of change of shear modulus is 0.5. The results of calculations are given below. Figure 2 shows the dependency of a ratio of internal loads in cables to the average load (coefficients of uneven distribution of forces among the cables) along the x-axis.

Let's pay attention to the fact that x = 10 cm corresponds to the boundary of rope parts. Presence of a boundary that divides the rope into parts with different values of shear modulus practically does not affect distribution of forces among the cables. The loads on the broken cable increase as the x-coordinate increases from zero. Cable adjacent to the broken one is loaded more than the other cables. Its maximum internal load – the coefficient of uneven distribution of forces occurs in the cross-section of cable breakage. This value reaches 1.53. The value of coefficients of unevenness decreases with a cable distance from the one adjacent to the broken one and with distance from the cross-section of breakage. We compare the values of force concentration coefficients for cases of linear and assumed nonlinear dependency of shear modulus on deformations. The analysis of results shows that an increase in

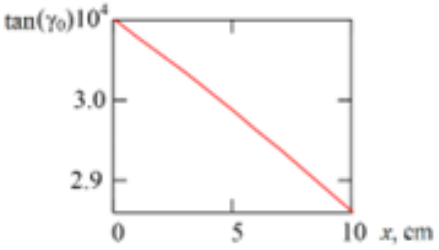

Fig. 2. Dependency of coefficients of uneven distribution of forces among cables with numbers i along the x-axis
Rys. 2. Zależność współczynników nierównomiernego rozkładu sił między kablami o liczbach i wzdłuż osi x

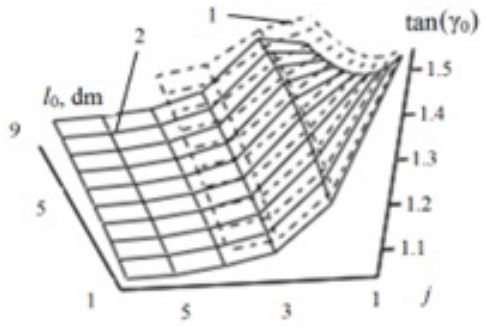

Fig. 6. Coefficients of force distribution among cables in ropes with a different number of cables
Rys. 6. Współczynniki rozkładu sił między kablami w linach o różnej liczbie kabli

the area of action of the reduced shear modulus leads to an increase in the maximum value of coefficient of uneven distribution of forces among cables. Therefore, when rope part length is 100 mm, the excess of the force concentration coefficient reaches 15%. For a rope part length of 500 mm it reaches 5%. For the infinite growth of the area of lower rigidity of rubber layers connecting the damaged cable with its adjacent cables, the coefficient of uneven distribution of forces infinitely approaches the corresponding coefficient obtained without considering the nonlinear law of dependency of shear modulus on the mutual shear of cables.

Butt joints have cross-sections, in which the number of cables changes, just as it changes in a rope with a broken cable. Such a change in the number of cables leads to a mutual displacement of cables in a rope cross-section. The cable with a breakage moves the most relatively to the adjacent ones. This is observed both in butt joints and in a rope with a broken cable. Accordingly, the obtained results can be extended to butt joints. Considering the nonlinearity of rubber shear deformations is expedient because the lengths of butt joint steps are smaller than the sizes of areas of stress disturbance from local change in the butt joint design.

The ratio between displacements of cables numbered i and a displacement of the broken cable in the cross-section of its breakage are shown in the Figure 3.

The displacements of cables shown in Figure 3 in the cross-section x = 0 correspond to the assumed form of displacements. As the distance from the cross-section of cable breakage increases, the character of curvature of the rope cross-sections changes – the amount of curvature decreases. The established distribution of displacements made it possible to find distributions of the tangents of shear angles of elastic material between cables. Figure 4 shows the tangents of shear angles of elastic shell between cables with numbers i along the x-axis, relative to its average value.

The shear of cables occurred practically only between the broken cable and the one adjacent to it. At the same time, rigidity of rubber between the specified cables in a rope part ($0 \le x \le 10$mm) is lower than the rigidity of other layers. The maximum mutual shear does not change significantly on the area ($0 \le x \le l_0$) (Fig. 5).

Figure 5 shows a slight deviation of tangents of shear angles of elastic shell from the average value.

In practice, ropes of various designs are used, including with a different number of cables. Figure 6 shows the dependency of distribution of force distribution coefficients among cables in ropes with different numbers of cables.

The figure shows that an increase in a number of cables in a rope does not significantly affect the maximum values of internal loading forces of cables. The analysis of expressions (19), (20) shows that the increase in the number of cables in a rope over ten practically does not affect the value of maximum stresses in a case of breakage of the extreme cable. In case of breakage of the middle cable, the maximum force in adjacent cables practically does not depend on their number when there are more than sixteen of them.

4. Conclusions

By analytically solving a model of a rubber-cable tractive element with a broken structure and nonlinear deformation-dependent rubber shear modulus, the dependencies of changes in a stress state of a rubber-cable tractive element with a broken structure in a form of a cable breakage are established.

In a process of solving the model, an algorithm for determining a stress state of a rubber-cable tractive element with a broken structure is formulated. A mechanism for changing a stress state of a rubber-cable rope is established, considering the nonlinear deformation-dependent shear modulus of rubber.

It is established that an increase in area of action of the reduced shear modulus leads to an increase in the maximum value of a coefficient of uneven distribution of forces between the cables. With infinite growth of area of lower rigidity of rubber layers connecting the broken cable with the adjacent cables, the coefficient of uneven distribution of forces infinitely approaches the corresponding coefficient determined without considering the nonlinear law of the dependency of shear modulus on deformations.

The obtained results can be extended to butt joints. Considering the non-linearity of rubber shear deformations is expedient because lengths of butt joint steps are smaller than sizes of areas of stress disturbance from a local change in butt joint design.

Considering the nonlinear deformation-dependent shear modulus of rubber provides an opportunity to specify the prediction of a rope stress state with a continuity breakage of cables, increase safety and operational reliability of rubber-cable tractive elements.

The results are obtained using well-known methods of theory of composite materials of a rubber-cable rope model and its solution using analytical methods. The model considers the nonlinear law of rubber deformation. This allows considering the obtained results as sufficiently reliable and as such that they clarify the idea of a mechanism of deformation of rubber-cable ropes and belts.

Literatura – References

1. Moldabayev, S.K., Adamchuk, A.A., Toktarov, A.A., Aben, Y. & Shustov, O.O. (2020). Approbation of the technology of efficient application of excavator-automobile complexes in the deep open mines. Naukovyi Visnyk Natsionalnoho Hirnychoho Universytetu, (4), pp. 30-38. DOI: 10.33271/nvngu/2020-4/030
2. Pysmennyi, S., Fedko, M., Shvaher, N. & Chukharev, S. (2020). Mining of rich iron ore deposits of complex structure under the conditions of rock pressure development. E3S Web of Conferences, 2020, 201, 01022. DOI: 10.1051/e3sconf/202020101022
3. Tytov, O., Haddad, J. & Sukhariev, V. (2019). Modelling of mined rock thin layer disintegration taking into consideration its properties changing during compaction. E3S Web of Conferences, 109, 00105. DOI:10.1051/e3sconf/201910900105
4. Shustov, O.O., Haddad, J.S., Adamchuk, A.A., Rastsvietaiev, V.O. & Cherniaiev, O.V. (2019). Improving the Construction of Mechanized Complexes for Reloading Points while Developing Deep Open Pits. Journal of Mining Science, 2019, 55(6), pp. 946-953. DOI: 10.1134/S1062739119066332
5. Bondarenko, A.O., Haddad, J.S., Tytov, O.O. & Alfaqs, F. (2021). Complex for processing of rubble wastes of stone dressing. International Review of Mechanical Engineering, 15(1), pp. 44-50. DOI: 10.15866/ireme.v15i1.20205
6. Peremetchyk, A., Kulikovska, O., Shvaher, N., Chukharev, S., Fedorenko, S., Moraru, R. & Panayotov, V. (2022). Predictive geometrization of grade indices of an iron-ore deposit. Mining of Mineral Deposits, 16(3), pp. 67-77. DOI: 10.33271/mining16.03.067
7. Kovalevska, I., Samusia, V., Kolosov, D., Snihur V. & Pysmenkova , T. (2020). Stability of the overworked slightly metamorphosed massif around mine working. Mining of Mineral Deposits, 14(2), 43-52. DOI: 10.33271/mining14.02.043
8. Sotskov, V., Dereviahina, N., & Malanchuk, L. (2019). Analysis of operation parameters of partial backfilling in the context of selective coal mining. Mining of Mineral Deposits, 13(4), 129-138. DOI: 10.33271/mining13.04.129
9. Shvaher, N., Komisarenko, T., Chukharev, S. & Panova, S. (2019). Annual production enhancement at deep mining. E3S Web of Conferences, 123, art. no. 01043. DOI: 10.1051/e3sconf/201912301043
10. Naumov, V., Zhamanbayev, B., Agabekova, D., Zhanbirov, Z. & Taran, I. (2021). Fuzzy-logic approach to estimate the passengers' preference when choosing a bus line within the public transport system. Communications - Scientific Letters of the University of Žilina, 23(3), pp. A150-A157. DOI:10.26552/com.C.2021.3.A150-A157
11. Kravets, V., Samusia, V., Kolosov, D., Bas, K. & Onyshchenko, S. (2020). Discrete mathematical model of travelling wave of conveyor transport. II International Conference Essays of Mining Science and Practic, Vol. 168. DOI: 10.1051/e3sconf/202016800030
12. Shpachuk, V., Chuprynin, A., Daleka, V. & Suprun, T. (2020). Simulation of impact interaction of rail transport carriage in a Butt Roughness Zone. Scientific Journal of Silesian University of Technology. Series Transport, 106, pp. 141-152. DOI:10.20858/sjsutst.2020.106.12
13. Sladkowski, A.V., Kyrychenko, Y.O., Kogut, P.I., Samusya, V.I. & Kolosov, D.L. (2019). Innovative designs of pumping deep-water hydrolifts based on progressive multiphase non-equilibrium models. Naukovyi Visnyk Natsionalnoho Hirnychoho Universytetu, (2), pp. 51-57. DOI: 10.29202/nvngu/2019-2/6
14. Bondarenko, A.O., Maliarenko, P.O., Zapara, Ye. & Bliskun, S.P. (2020). Testing of the complex for gravitational washing of sand. Naukovyi Visnyk Natsionalnoho Hirnychoho Universytetu, (5), 26-32. DOI: 10.33271/nvngu/2020-5/026

15. Shpachuk, V.P., Zasiadko, M.A. & Dudko, V.V. (2018). Investigation of stress-strain state of packet node connection in spatial vibration shakers. Naukovyi Visnyk Natsionalnoho Hirnychoho Universytetu, (3), 74-79. DOI: 10.29202/nvngu/2018-3/12

16. Bazhenov, V.A., Gulyar, A.I., Piskunov, S.O. & Shkryl, A.A. (2006). Life assessment for a gas turbine blade under creep conditions based on continuum fracture mechanics. Strength of Materials, 38(4), pp. 392-397.

17. Bazhenov, V.A., Gulyar, A.I., Piskunov, S.O. & Shkryl, A.A. (2008). Gas turbine blade service life assessment with account of fracture stage. Strength of Materials, 2008, 40(5), pp. 518-524.

18. Vynohradov, B.V., Samusya, V.I. & Kolosov, D.L. (2019). Limitation of oscillations of vibrating machines during start-up and shutdown. Naukovyi Visnyk Natsionalnoho Hirnychoho Universytetu, (1), pp. 69-75. DOI: 10.29202/nvngu/2019-1/6

19. Chigirinsky, V., Naumenko, O. (2020). Invariant Differential Generalizations in Problems of the Elasticity Theory As Applied to Polar Coordinates. Eastern-European Journal of Enterprise Technologies, 5(7 (107)), 56-73. DOI: 10.15587/1729-4061.2020.213476

20. Marasová, D., Ambriško, Ľ., Andrejiová, M. & Grinčová, A. (2017). Examination of the process of damaging the top covering layer of a conveyor belt applying the FEM. Journal of the International Measurement Confederation, (112), 47-52. DOI:10.1016/j.measurement.2017.08.016

21. Belmas, I., Kogut, P., Kolosov, D., Samusia, V. & Onyshchenko, S. (2019). Rigidity of elastic shell of rubber-cable belt during displacement of cables relatively to drum. International Conference Essays of Mining Science and Practice, Vol. 109, 00005. DOI: 10.1051/e3sconf/201910900005

22. Blazej, R., Jurdziak, L., Kirjanow-Blazej, A. et al. (2021). Identification of damage development in the core of steel cord belts with the diagnostic system. Sci Rep 11, 12349. DOI: 10.1038/s41598-021-91538-z

23. Webb, C., Sikorska, J., Khan, R., & Hodkiewicz, M. (2020). Developing and evaluating predictive conveyor belt wear models. Data-Centric Engineering, 1, E3. DOI: 10.1017/dce.2020.1

24. Pang, Y., Lodewijks, G. (2006). A Novel Embedded Conductive Detection System for Intelligent Conveyor Belt Monitoring. 2006 IEEE International Conference on Service Operations and Logistics, and Informatics, SOLI 2006. 803-808. DOI: 10.1109/SOLI.2006.328958

25. Volohovskiy, V.Yu., Radin, V.P., & Rudyak, M.B. (2010). Concentration of loads in cables and a bearing ability of rubber-cable conveyor belts with breakages. MPEI Vestnik, (5), 5-12.

26. Bel'mas, I.V. (1993). Stress state of rubber-rope tapes during their random damages. Problemy Prochnosti i Nadezhnos'ti Mashin, 1993, (6), pp. 45-48.

27. Ropay V.A. (2016) Shakhtnyye uravnoveshivayushchiye kanaty : monograph [Mining balancing ropes]. Dnipropetrovsk : National Mining University. 263 p.

28. Levchenya, Zh.B. (2004). Increase of reliability of butt-joint connections of conveyor belts at mining enterprises: PhD dissertation: 05.05.06.

29. Kolosov, L.V., Bel'mas, I.V. (1981). Use of electrical models for investigating composites. Mechanics of Composite Materials, 1981, 17(1), pp. 115-119.

30. Zade, D.S. (2013). Numerical method of determining effective characteristics of unidirectional reinforced composites. Bulletin NTU "KhPI", (58), 71-77.

31. Song, W. Shang, W. and Li, X. (2009). Finite element analysis of steel cord conveyor belt splice. International Technology and Innovation Conference 2009 (ITIC 2009), Xi'an, China, pp. 1-6. DOI: 10.1049/cp.2009.1415

32. Li X., Long, X., Shen, Z. & Miao, Z.Ch. (2019). Analysis of Strength Factors of Steel Cord Conveyor Belt Splices Based on the FEM. Advances in Materials Science and Engineering, Volume 2019, ID 6926413. DOI: 10.1155/2019/6926413

33. Fedorko, G., Molnar, V., Michalik, P., Dovica, M., Kelemenová, T. & Toth, T. (2018). Failure analysis of conveyor belt samples under tensile load. Journal of Industrial Textiles. 48. 152808371876377. DOI: 10.1177/1528083718763776

34. Andrejiova, M., Grincova, A. & Marasova, D. (2019). Failure analysis of the rubber-textile conveyor belts using classification models. Engineering Failure Analysis. 101. 407-417. DOI: 10.1016/j.engfailanal.2019.04.001

35. Belmas I.V., Kolosov D.L., Kolosov A.L. & Onyshchenko S.V. (2018). Stress-strain state of rubber-cable tractive element of tubular shape. Naukovyi Visnyk Natsionalnoho Hirnychoho Universytetu, (2), pp. 60-69. DOI: 10.29202/nvngu/2018-2/5

36. Kirjanów-Błażej, A., Błażej, R. Jurdziak, L. & Kozłowski, T. (2017). Core damage increase assessment in the conveyor belt with steel cords. Diagnostyka. 18. 93-98.

37. Romek D., Ulbrich D., Selech J., Kowalczyk J. & Wlad R. (2021). Assessment of Padding Elements Wear of Belt Conveyors Working in Combination of Rubber-Quartz-Metal Condition. Materials (Basel). Aug 2;14(15):4323. DOI: 10.3390/ma14154323

38. Yao Y., Zhang B. (2020). Influence of the elastic modulus of a conveyor belt on the power allocation of multi-drive conveyors. PLoS One. Jul 7; 15(7):e0235768. DOI: 10.1371/journal.pone.0235768

39. Zabolotny, K.S., Panchenko, E.V. & Zhupiev, A.L. (2011). Teoriya mnogosloynoy namotki rezinotrosovogo kanata [Theory of multilayer rubber-cable rope winding]. Dnipropetrovsk: NGU.

40. Haddad, J.S., Denyshchenko, O., Kolosov, D., Bartashevskyi, S., Rastsvietaiev, V., & Cherniaiev, O. (2021). Reducing Wear of the Mine Ropeways Components Basing Upon the Studies of Their Contact Interaction. Archives of Mining Sciences, 66(4), 579-594. DOI: 10.24425/ams.2021.139598

Badanie wpływu kompensacji na stabilność górotworu oraz jakość wydobywanej rudy

Artykuł przedstawia studium i analizę funkcjonalną wymagań światowego przemysłu metalurgicznego co do jakości rud żelaza w podziemnych kopalniach Ukrainy. Stwierdzono zależności wpływu kształtu i parametrów przestrzeni kompensacyjnych na ich stateczność i wskaźniki jakości rudy. Udowodniono, że komora wyrównawcza w kształcie trapezu pionowego charakteryzuje się największą stabilnością i jest stabilna w zakresie wszystkich rozważanych głębokości, nawet w rudach o twardości 3–5 punktów. Mniejszą stateczność wykazuje komora kompensacji pionowej o kształcie sklepionym z niewielkimi spadkami w przyczółku sklepienia komory w rudach o twardości 3–5 punktów na głębokości 2000 m. Komora z opadami o różnym natężeniu występuje w dolnej części nachylonych odsłonięć namiotu w rudach o twardości 3–5 punktów na głębokości 1750 m lub większej. Pomieszczenie kompensacji poziomej ma najmniejszą stateczność; spadki występują w rudach o twardości 3–5 punktów na głębokości 1400 m, a na głębokościach 1750–2000 m pozostają stabilne tylko w rudach twardszych. Stwierdzono, że zastosowanie komór kompensacyjnych o dużej stabilności umożliwia osiągnięcie ich maksymalnej objętości, zwiększenie ilości wydobywanej czystej rudy, zmniejszenie jej rozrzedzenia, poprawę jakości wydobywanej masy rudy, a co za tym idzie, wzrost jej ceny i konkurencyjności rynkowej.

Słowa kluczowe: *surowce mineralne, kompleksy wydobywcze wyciągowe i transportowe, kompozytowy element trakcyjny, uszkodzona konstrukcja, powłoka elastomerowa, stan naprężeń, rozwiązanie analityczne*

Wpływ obiektu górniczego na środowisko na przykładzie Kopalni Węgla Kamiennego LW Bogdanka (Polska)

Monika PIECH[1)], Wiktoria SOBCZYK[2)]

[1)] M.Sc.Eng.; AGH University of Krakow, Faculty of Drilling, Oil and Gas, Krakow, Poland, piech@agh.edu.pl; ORCID 0000-0001-7742-6892
2)Professor PhD. D.Sc. Eng.; AGH University of Krakow, Faculty of Energy and Fuels, Dept. of Fuel Technology, Krakow, Poland; ORCID 0000-0003-2082-9644; email: sobczyk@agh.edu.pl

http://doi.org/10.29227/IM-2023-01-19

Submission date: 10-02-2023 | Review date: 16-03-2023

Abstrakt

Podstawowym kryterium właściwego funkcjonowania obiektów przemysłowych jest utrzymanie równowagi w środowisku przyrodniczym. Działalność górnicza zawsze oddziałuje negatywnie na elementy środowiska: na litosferę, hydrosferę, atmosferę i biosferę. Zdarza się, że obszary górnicze sąsiadują z terenami chronionymi i przyrodniczo cennymi. Wydobycie węgla kamiennego wywołuje długotrwałe i często nieodwracalne zmiany w przyrodzie. Dlatego tak ważne jest prowadzenie konsekwentnej rekultywacji terenów zdegradowanych. Podejmując działalność górniczą, przedsiębiorstwa zobowiązane są do zidentyfikowania i opisania przewidywanych wpływów na środowisko przyrodnicze. Ocena oddziaływania na środowisko powinna zawierać dane na temat wpływu na glebę, powietrze, wodę, krajobraz i na człowieka.

W artykule przeprowadzono ocenę wpływu oddziaływania eksploatacji złóż węgla kamiennego na środowisko przyrodnicze z wykorzystaniem wielokryterialnej metody AHP i macierzy Leopolda. Stwierdzono znaczące oddziaływanie analizowanych wpływów w przypadku zajęcia powierzchni, składowania odpadów i działań rekultywacyjnych. Natomiast nie odnotowano negatywnego wpływu kopalni węgla kamiennego na obszary chronione, co jest następstwem długofalowych działań proekologicznych zakładu.

Słowa kluczowe: *węgiel kamienny, LW „Bogdanka", oddziaływanie na środowisko, macierz Leopolda*

1. Wstęp

Środowisko przyrodnicze obejmuje zewnętrzną część skorupy ziemskiej, część atmosfery, hydrosferę, świat roślinny i zwierzęcy. Środowisko jest przekształcane przez człowieka poprzez działalność gospodarczą, przemysłową i bytową. Działalność górnicza powoduje przekształcenia w środowisku, które określane są mianem szkód górniczych. Na negatywne zmiany najbardziej narażone są litosfera i hydrosfera [Kozioł et al., 2011]. Górnictwo oddziałuje na elementy środowiska w sposób bezpośredni i pośredni. Wpływ bezpośredni to zajmowanie terenów rolnych, leśnych i rekreacyjnych pod zakłady górnicze i składowiska odpadów. Oddziaływanie pośrednie to szeroko rozumiane wpływy eksploatacji górniczej, w tym przekształcenia geomechaniczne, degradacja gleb, zanieczyszczenia wód i atmosfery. Ocena oddziaływania górnictwa na środowisko powinna zawierać dane na temat wpływu na człowieka, faunę i florę, powietrze, wodę, glebę i na krajobraz. Po zakończeniu procesu eksploatacji złóż na zakładach górniczych ciąży obowiązek rekultywacji terenów zdegradowanych [Sobczyk, 2007].

Kopalnia „Bogdanka" jest położona w Centralnym Rejonie Węglowym (CRW), w północno-wschodniej, najlepiej rozpoznanej części Lubelskiego Zagłębia Węglowego (fig. 1). Pod względem geograficznym Centralny Okręg Węglowy leży w granicach Polesia Lubelskiego, a tylko niewielkie jego fragmenty przechodzą na Wyżynę Lubelską. Lubelski Węgiel „Bogdanka" SA jest jedyną kopalnią eksploatującą węgiel kamienny w Lubelskim Zagłębiu Węglowym.

Lubelski Węgiel „Bogdanka" SA jest jednym z liderów rynku producentów węgla kamiennego w Polsce (fig. 2). Sprzedawany przez Spółkę węgiel kamienny energetyczny stosowany jest przede wszystkim do produkcji energii elektrycznej, cieplnej. Odbiorcami Spółki są w głównej mierze firmy przemysłowe, przede wszystkim podmioty prowadzące działalność w branży elektroenergetycznej, zlokalizowane we wschodniej i północno-wschodniej Polsce. Kopalnia Lubelski Węgiel „Bogdanka" SA prowadzi eksploatację w granicach obszaru górniczego „Puchaczów V" o powierzchni około 73 km². W obszarze tym spośród 18 bilansowych pokładów węgla kamiennego, znajdujących się pod nadkładem od 650 m do 730 m, do eksploatacji wytypowano 8 pokładów o zasobach przemysłowych. Kopalnia posiada koncesję na eksploatację czterech pokładów oznaczonych numerami: 382, 385/2, 389 i 391. Aktualnie eksploatacja prowadzona jest w pokładach 385/2, 389 i 391 [https://www.lw.com.pl].

Głównym celem pracy było dokonanie oceny wpływu wydobycia węgla kamiennego na przykładzie kopalni LW „Bogdanka" na środowisko przyrodnicze. W tym celu wykorzystano wielokryterialną metodę AHP i macierz Leopolda. Celem metody AHP było wyłonienie elementów środowiska, na które w największym stopniu oddziałuje górnictwo węgla kamiennego. Prawdą jest, iż eksploatacja węgla kamiennego w negatywny sposób wpływa na środowisko przyrodnicze, jednak nie należy zapominać o potencjalnych korzyściach jakie przynosi działalność górnicza, pod warunkiem że wydobycie prowadzone jest w sposób zoptymalizowany, a tereny zdegradowane poddawane są efektywnej rekultywacji.

2. Obiekty ochrony przyrody

Infrastruktura kopalni oraz obszary górnicze Puchaczów V i Stręczyn oraz obszar górniczy Cyców otoczone są tere-

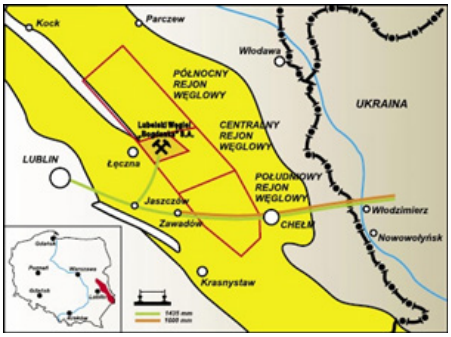

Fig. 1. Lokalizacja Lubelskiego Zagłębia Węglowego (fot. Lubelski Węgiel „Bogdanka" SA)
Fig. 1. Location of the Lublin Coal Basin (photo LW „Bogdanka" SA)

Fig. 2. Hałdy węglowe Kopalni LW Bogdanka (fot. Lubelski Węgiel „Bogdanka" SA)
Fig. 2. Coal heaps of the LW Bogdanka Mine (photo Lubelski Węgiel „Bogdanka" SA)

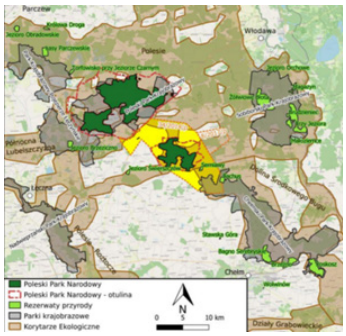

Fig. 3. Obiekty ochrony przyrody w regionie LW „Bogdanka" (opracowanie własne na podstawie Chibowski, Dzierża, Kozub, 2021)
Fig. 3. Nature protection facilities in the area of LW "Bogdanka" (based on Chibowski, Dzierża, Kozub, 2021)

nami chronionymi. W najbliższym sąsiedztwie zlokalizowane są: Poleski Park Narodowy, Park Krajobrazowy Pojezierze Łęczyńskie, Chełmski Obszar Chronionego Krajobrazu (fig. 3). Obszar górniczy Ludwin w części wschodniej obejmuje swoim zasięgiem znaczne połacie Parku Krajobrazowego Pojezierze Łęczyńskie. W jego też granicach znajduje się również rezerwat Brzeziczno wraz z wydzielonym Obszarem Natura 2000. Połączone obszary górnicze w części centralnej i wschodniej obejmują swoim zasięgiem niewielkie połacie otuliny wspomnianego parku krajobrazowego, która na tym obszarze została włączona do obszaru Natura 2000 – „Jeziora Uściwierskie" (KOD PLH 060009). Rejon ten wchodzi również w skład obszaru „Międzynarodowy Rezerwat Biosfery – Polesie Zachodnie". Od strony wschodniej zlokalizowany jest Poleski Obszar Chronionego Krajobrazu, a od południowego wschodu – Chełmski Obszar Chronionego Krajobrazu [Chibowski, Dzierża & Kozub, 2021]. Wpływ działalności kopalni LW Bogdanka na obiekty ochrony przyrody zostaną omówione w części badawczej.

3. Metodyka pracy

Ocenę oddziaływania eksploatacji kopalni węgla kamiennego na środowisko przeprowadzono w wykorzystaniem połączenia wielokryterialnej metody AHP i macierzy Leopolda. Stosując metodę AHP, uzyskano wielkości oznaczające wagi (priorytety) poszczególnych czynników w realizacji celu.

Do oceny oddziaływań kopalni wykorzystano metodę AHP oraz metodę macierzową Leopolda. Metoda AHP polega na porównaniu wpływu kopalni na elementy środowiska, które udało się zidentyfikować [Saaty, 2004; Biedrawa & Sobczyk W., 2010; Giang Huong, 2014] Tymi atrybutami są: litosfera, hydrosfera, atmosfera, antroposfera, biosfera, estetyka krajobrazu. Atrybuty są porównywane parami pod kątem wpływu, jaki wywiera na nie działalność kopalni węgla. Presja określana jest cyfrowo od 1 do 9. Na podstawie tej wartości obliczone zostały wagi, które zostaną użyte w macierzy Leopolda.

Macierz Leopolda jest ilościowym sposobem analizy wpływu na środowisko badanej KWK „Lubelski Węgiel". Jest to sposób na identyfikację i ilościowe określenie wielkości

Tab. 1. Macierz Leopolda dla LW Bogdanka

Tab. 1. Leopold matrix for LW Bogdanka

Działania/elementy środowiska	waga	Zajęcie powierzchni	Składowanie odpadów	Infrastruktura zakładu górniczego	Sczerpywanie zasobów	Deforestacja	Hałas	Wibracje
litosfera	**0,33**	5,00/1,65	5,00/1,65	4,00/1,32	5,00/1,65	4,00/1,32	0,00	0,00
hydrosfera	**0,31**	4,00/1,24	3,00/0,93	3,00/0,93	3,00/0,93	2,00/0,62	0,00	0,00
atmosfera	**0,13**	3,00/0,39	3,00/0,39	3,00/0,39	0,00	3,00/0,39	0,00	0,00
antroposfera	**0,04**	4,00/0,16	3,00/0,12	3,00/0,12	3,00/0,12	4,00/0,16	3,00/0,12	4,00/0,16
biosfera	**0,11**	4,00/0,44	4,00/0,44	4,00/0,44	3,00/0,33	4,00/0,44	3,00/0,33	2,00/0,22
estetyka krajobrazu	**0,08**	5,00/0,4	4,00/0,32	5,00/0,4	4,00/0,32	5,00/0,4	0,00	0,00
suma	**1,00**	**4,28**	**3,85**	**3,6**	**3,35**	**3,33**	**0,45**	**0,38**

Działania/elementy środowiska	waga	Odór odpadów górniczych	Wody w procesie przeróbczym	Działania rekultywacyjne	Transport kopaliny	Deformacja powierzchni ziemi	Emisja pyłów i gazów	**suma**
litosfera	**0,33**	0,00	3,00/0,99	5,001,65	4,00/1,32	5,00/1,65	1,00/0,33	**13,53**
hydrosfera	**0,31**	0,00	4,00/1,24	3,00/0,93	1,00/0,31	3,00/0,93	1,00/0,31	**8,06**
atmosfera	**0,13**	1,00/0,13	0,00	1,00/0,13	3,00/0,39	0,00	3,00/0,39	**2,21**
antroposfera	**0,04**	2,00/0,08	1,00/0,04	5,00/0,2	3,00/0,12	2,00/0,08	2,00/0,08	**1,48**
biosfera	**0,11**	1,00/0,11	2,00/0,22	4,00/0,44	4,00/0,44	3,00/0,33	2,000,22	**4,18**
estetyka krajobrazu	**0,08**	0,00	0,00	5,00/0,4	4,00/0,32	4,00/0,32	0,00	**2,88**
suma	**1,00**	**0,32**	**2,49**	**3,75**	**2,9**	**3,31**	**1,33**	**32,34**

presji wywieranej przez różne elementy środowiska (litosfera, hydrosfera, atmosfera, antroposfera, biosfera i estetyka krajobrazu), wynikające z różnych działań (lub czynników) związanych z działalnością kopalni węgla. Raport skupia się na 13 rodzajach presji, które są spowodowane działalnością kopalni węgla: zajęcie powierzchni, składowanie odpadów, infrastruktura zakładu górniczego, sczerpywanie zasobów, deforestacja, hałas, wibracje, odór odpadów górniczych, wody w procesie przeróbczym, działania rekultywacyjne, transport kopaliny, deformacja powierzchni ziemi, emisja pyłów i gazów. W uproszczonej formie macierzy Leopolda, tzn. macierzy oddziaływań, poddano analizie wyszczególnione elementy środowiska. Oceniono podatność elementów środowiska na wymienione wcześniej zagrożenia. Siłę wpływu wyceniono w skali od 0 do 5 punktów, gdzie 0 oznaczało brak oddziaływania, a 5 oddziaływanie bardzo silne [Sobczyk W., Kowalska & Sobczyk, E.J., 2014]. Zastosowana metoda umożliwiła identyfikację oddziaływań, które mają wpływ na komponenty środowiska, a jednocześnie pozwoliła kwantyfikować siłę tego wpływu. W wyniku pomnożenia sił oddziaływań przez wagi poszczególnych elementów środowiska oraz kolejno zsumowania wszystkich oddziaływań, uzyskano zagregowaną wartość siły oddziaływania obiektu na środowisko.

4. Wyniki przeprowadzonej analizy

Oddziaływanie analizowanych wpływów na elementy środowiska (fig. 4) jest znaczące w przypadku zajęcia powierzchni (4,28), składowania odpadów (3,85) i działań rekultywacyjnych (3,75). Najsłabsze oddziaływanie stwierdzono w przypadku hałasu (0,45), wibracji (0,38) oraz emisji pyłów i gazów. Składowisko skały płonnej jest źródłem zjawiska pylenia, ale wyłącznie podczas wietrznych dni. Pozostałe działania wykazywały średnie oddziaływanie.

Wpływ wydobycia węgla kamiennego na litosferę (13,53) odzwierciedla się w postaci sczerpywania zasobów, deforestację niezbędną do rozbudowy infrastruktury zakładu górniczego (zakład przeróbki węgla), a także składowiska skały płonnej oraz składowania odpadów górniczych (tab. 1). Wymienione wyżej czynniki znajdują odzwierciedlenie w zmianie formy terenu. Oddziaływanie hałasu (0,45), wibracji (0,38) oraz odoru z odpadów górniczych (0,32) na antroposferę (1,48) jest niewielkie. Nie stanowią one istotnego zagrożenia ze względu na lokalizację kopalni i składowiska odpadów na terenach o znikomym stopniu zabudowy mieszkalnej. Pozostałe rozważane wpływy, jak emisja pyłów i gazów (1,33) oraz transport kopaliny (2,9), oddziałują na atmosferę. Emitorem jest obiekt unieszkodliwiania odpadów wydobywczych w Bogdance, który może być źródłem pylenia w czasie suchych i wietrznych dni. Emisja do powietrza pochodzi również ze spalania paliw w silnikach spalinowych wykorzystywanych w kopalni, procesów spawania oraz wymiany czynnika chłodniczego w urządzeniach klimatyzacyjnych.

Z wyodrębnionych sześciu grup kryteriów najbardziej podatna na oddziaływanie eksploatacji węgla kamiennego w analizowanym obszarze okazała się litosfera (13,53), a następnie hydrosfera (8,06) (fig. 5). W przypadku Kopalni „Bogdanka" oddziaływanie na hydrosferę wiąże się z drenażem wód wgłębnych w ilości niezbędnej do prawidłowego funkcjonowania kopalni. Średnia roczna ilość wypompowanych wód z odwodnienia Kopalni Lubelski Węgiel „Bogdan-

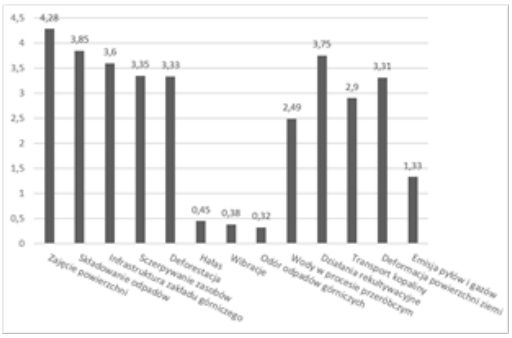

Fig. 4. Intensywność oddziaływania zdiagnozowanych rodzajów wpływów na elementy środowiska

Fig. 4. The intensity of the impact of the diagnosed types of impact on the elements of the environment

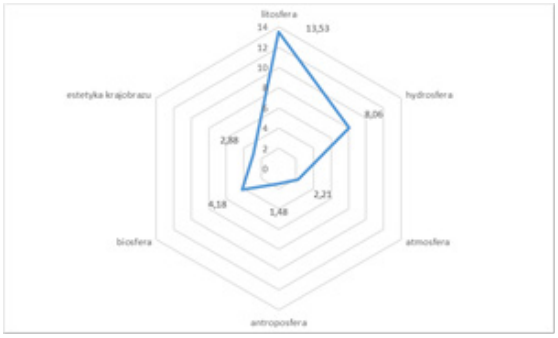

Fig. 5. Róża wiatrów. Ocena oddziaływania obiektu na poszczególne elementy środowiska

Fig. 5. Wind rose. Evaluation of the impact of the facility on individual elements of the environment

ka" SA wynosi około 24140 m³/dobę, mineralizacja łączna średnio ok. 1700 mg/dm³, przy zawartości jonów Cl- i SO_{4-}^{2} około 1000 mg/dm³. Zawartość jonów Cl- i SO_{4-}^{2} kwalifikuje wody dołowe do II grupy – wód przemysłowych (wg podziału GIG) [Mirkowski & Badera, 2015]. Poprzez m.in. deforestację i składowanie odpadów odnotowano znaczące oddziaływanie na biosferę (4,18) oraz estetykę krajobrazu (2,88). Zmiany związane z deformacją powierzchni i rozbudową infrastruktury górniczej również wpływają na estetykę krajobrazu. Niemniej prowadzone działania rekultywacyjne przyczyniają się do poprawy krajobrazu. Pozostałe rozważane elementy, jak emisja pyłów i gazów, spaliny pochodzące z transportu węgla kamiennego, wpływają negatywnie na atmosferę (2,21).

5. Conclusions

Ocena oddziaływania Kopalni Węgla Kamiennego LW „Bogdanka" wykazuje, że najbardziej podatnym na zmiany elementem środowiska jest litosfera. Silna presja obserwowana jest w hydrosferze, głównie w wodach wgłębnych. Powstawanie szkód górniczych wokół kopalni spowodowane jest wydobywaniem węgla metodą z zawałem. Szkody te uwidaczniają się w postaci osiadania terenu i podsiąkaniu wód gruntowych.

Zmiany w atmosferze związane są głównie z emisją pyłów i gazów oraz transportem węgla kamiennego. Źródłem emisji zanieczyszczeń do atmosfery jest zwałowisko odpadów (hałda), a także składy węgla, punkty załadunku węgla oraz zakład przeróbki węgla. Składowisko skały płonnej powoduje nieznaczne pylenie, które nasila się tylko w czasie suchych dni. Jest to zjawisko bardzo zmienne, zależne od warunków atmosferycznych (silne wiatry), a jego zasięg może sięgać do kilkudziesięciu metrów. Pylenie likwiduje się poprzez zraszanie hałdy i jej bieżącą rekultywację.

Odnotowano znaczące zmiany w biosferze i w estetyce krajobrazu, które spowodowane są deformacją powierzchni, składowiskami odpadów (hałda) i deforestacją terenu, niezbędną do rozbudowy infrastruktury górniczej, m.in. zakładu przeróbki mechanicznej węgla kamiennego. W działalności kopalni węgla kamiennego obserwuje się niewielkie zmiany w antroposferze, gdyż kopalnia ulokowana jest na terenach oddalonych od zabudowy mieszkalnej.

Wpływ kopalni węgla kamiennego na obszary chronione jest niewielki. Jest to efekt długofalowych działań proekologicznych zakładu, wdrożenia Zintegrowanego Systemu Zarządzania Jakością Środowiskiem i bhp, zgodnie z wymaganiami norm stanowiących fundament systemu ISO 9001:2015, ISO 14001:2015 oraz ISO 45001:2018, jak również bieżącej działalności operacyjnej, minimalizującej wpływ zakładu na środowisko [GIG, 2004]. Na Obszarze Górniczym „Puchaczów V" powstały dwa duże zalewiska poeksploatacyjne: na północ od szybów głównych Pola Bogdanka na powierzchni około 100 ha oraz w rejonie Pola Nadrybie około 30 ha. Zalewisko w rejonie Nadrybia zostało ujęte w sieć „Natura 2000" [Łyszczarz, 2005]. Podsumowując, należy stwierdzić, że wpływ działalności kopalni węgla kamiennego LW Bogdanka na środowisko przyrodnicza jest relatywnie niewielki.

Literatura – References

1. Kozioł, W. et al. (2011). Zastosowanie analitycznego procesu hierarchicznego (AHP) do wielokryterialnej oceny innowacyjności technologii zagospodarowania odpadów z górnictwa kamiennego. Rocznik Ochrona Środowiska, 13, 1619-1634.
2. Sobczyk, W. (2007). Badania opinii respondentów na temat uciążliwości środowiskowej górnictwa węgla kamiennego. Górnictwo i Geoinżynieria, 31 (3/1), 497-506.
3. https://www.lw.com.pl/pl,2,s17,ekologia.html; dostęp 29.01.2023.
4. Chibowski,. P., Dzierża, P. & Kozub, Ł. (2021). Ocena potencjalnych skutków przyrodniczych planowanej eksploatacji węgla kamiennego ze złoża Sawin w rejonie Poleskiego Parku Narodowego. Centrum Ochrony Mokradeł, 10.
5. Kubicz, J., Hämmerling, M. & Walczak, N. (2016). Porównanie oddziaływania na środowisko różnych metod technologii unieszkodliwiania odpadów wydobywczych z wykorzystaniem metody AHP. Inżynieria Ekologiczna, 47, 131-136.
6. Saaty, T.L. (2004). Decision making the analytic hierarchy and network processes (AHP/ANP). J. Syst. Sci. Syst. Eng. 13 (1).
7. Biedrawa, A. & Sobczyk, W. (2010). AHP - Komputerowe wspomaganie podejmowania złożonych decyzji. Rocznik Naukowy Edukacja - Technika – Informatyka, 1 (1), 285-291.
8. Giang Huong, N. (2014). The analytic hierarchy process: a mathematical model for decision making problems. Independent Study Thesis. The College of Wooster, 132.
9. Bascetin, A. (2009). The study of decision making tools for equipment selection in mining engineering operations. Gospodarka Surowcami Mineralnymi, 25 (3), 37-56.
10. Sobczyk, W., Kowalska, A. & Sobczyk, E.J. (2014). The use of AHP multi-criteria method and Leopold matrix to assess the impact of gravel and sand pits on the environment of the Jasiolka Valley. Mineral Resources Management 30 (2), 157-72.
11. Mirkowski, Z. & Badera, J. (2015). Odpady górnictwa węgla kamiennego, zagrożenia i ochrona środowiska w Raport z monitoringu zagospodarowania odpadów wydobywczych, Towarzystwo dla natury i człowieka, Lublin.
12. GIG Główny Instytut Górnictwa (2004). Monitoring własności fizykochemicznych odpadów - karbońskich skał płonnych z Kopalni Węgla Kamiennego „Bogdanka" SA w Bogdance. Dokumentacja, Pomiar. Lublin.
13. Łyszczarz, L. (2005). Działalność Lubelskiego Węgla „Bogdanka" SA w zakresie ochrony środowiska. Wiadomości Górnicze, 56 (3), 137-145.

Impact of a Mining Facility on the Environment, on the Example of the Hard Coal Mine LW Bogdanka (Poland)

The basic criterion for the proper functioning of industrial facilities is to maintain balance in the natural environment. Mining activity always has a negative impact on the elements of the environment: the lithosphere, hydrosphere, atmosphere and biosphere. It happens that mining areas are adjacent to protected and environmentally valuable areas. Hard coal mining causes long-term and often irreversible changes in nature. That is why it is so important to conduct consistent reclamation of degraded areas. When undertaking mining activities, companies are required to identify and describe the anticipated impacts on the natural environment. The environmental impact assessment should include data on the impact on soil, air, water, landscape and humans.

The article eyvaluates the impact of hard coal mining on the natural environment using the multi-criteria AHP method and the Leopold matrix. A significant impact of the analyzed impacts was found in the case of occupation, landfill and reclamation activities. On the other hand, no negative impact of the hard coal mine on protected areas was recorded, which is a consequence of the plant's long-term pro-ecological activities.

Keywords: *hard coal, LW "Bogdanka", impact on the environment, Leopold matrix*

Transboundary Air Pollution in the Krakow Agglomeration Using the HYSPLIT Model

Maciej CIEPIELA[1)], Wiktoria SOBCZYK[2)]

[1)] AGH University of Science and Technology, Faculty of Civil Engineering and Resource Management, Doctoral School, Krakow, Poland; ORCID.ORG/0000-0003-0362-8461; email: ciepiela@agh.edu.pl
[2)] AGH University of Science and Technology, Faculty of Energy and Fuels, Poland,; ORCID.ORG/0000-0003-2082-9644; email: sobczyk@agh.edu.pl

http://doi.org/10.29227/IM-2023-01-20

Submission date: 10-02-2023 | Review date: 16-03-2023

Abstract

The study aims to analyze the measurement data of PM10 particulate matter in the Krakow agglomeration. It develops a model of the backward trajectory of air masses to determine whether and to what extent natural phenomena, such as forest fires outside Poland, affect the level of air pollution.

The article describes the process of pollutant dispersion in the Earth's atmosphere and the principles of air monitoring in the Krakow agglomeration. The study uses 2022 measurement data from ten monitoring stations of the Chief Inspectorate of Environmental Protection in the Krakow agglomeration. Two periods of increased PM10 particulate matter were selected. On the basis of the HYSPLIT software, which uses backward air trajectories, the influx of transboundary pollution was simulated. Then, by analyzing the FIRMS fire information system, an attempt was made to document that the pollution sources considered were of natural origin and that human activity did not in any way determine the emissions and their magnitude.

Keywords: *particulate pollution, air pollution modeling, air quality assessment, environmental monitoring, forest fires*

1. Introduction

The Earth's atmosphere is the outer gaseous envelope whose function protects living beings from rapid changes in temperature, electromagnetic radiation, and the fall of meteoroids. The composition of the air depends on many factors and can change depending on the climate, season, and even time of day. Air is a homogeneous mixture of gases characterized by its lack of odor, color, and taste and poor solubility in water [5]. With the influx of various substances, both from natural and anthropogenic sources, there is a change in the natural composition of the atmosphere. The primary origin of anthropogenic sources includes electricity and heat production, domestic furnaces, industry, transportation, and agriculture. In contrast, sources of natural origin include volcanic eruptions, forests, savannahs, steppe fires, rock and soil erosion, and biological processes. Among the substances emitted into the ambient air are nitrogen oxides, sulfur oxides, carbon monoxide, tropospheric ozone, volatile organic compounds, PAHs, and, above all, PM10 (particles smaller than 10 μm in diameter) and PM2.5 (very fine particles less than 2.5 μm in diameter). These pollutants can directly affect the environment, such as by causing smog, and indirectly by accumulating toxic compounds in living organisms [1, 6].

Pollutants emitted into the environment are dispersed. Three factors that affect the dispersion of pollutants include meteorological, topographical, and technical factors. Undoubtedly, meteorological factors have a decisive influence, as climatic parameters are subject to the most significant changes due to atmospheric turbulence, vertical temperature gradient, wind action, mixing zone thickness, and precipitation [9].

The air quality measurement system plays a crucial role in identifying pollution. Poland's measurements are carried out as part of the State Environmental Monitoring program to provide reliable information on the state of the environment. Multi-year programs have been developed by the Chief Inspectorate of Environmental Protection and approved by the Climate Minister. Environmental monitoring is carried out in all voivodships. The number of permanent measuring stations depends on the number of inhabitants, the type and the sources of emissions, and exceedances of permissible concentrations. The measurement stations are located according to their purpose and the area of representativeness of the results obtained in terms of the type of station. A distinction is made between urban, suburban, traffic, industrial, non-urban, and regional background stations [4].

The selection of the location of the measurement points involves multistage planning and compliance with strict criteria described in the Environmental Ministry Regulation of September 13, 2012, on the assessment of the levels of substances in the air. The ordinance specifies location criteria on a micro- and macro-scale. First, in the case of PM10, special care is taken to ensure that the airflow within a few meters around the air intake is not impeded by other obstacles in the form of shrubs, trees, and buildings, and in the case of traffic stations at least 0.5 meters from buildings and 25 meters from the edge of the main intersections. Another crucial requirement is the elevation or height of the air intake station within the range between 1.5 and 4 meters above ground level. The design of the air intake station is also crucial for preventing the re-intake of the discharged air. For the latter scale regarding PM10, the station's location should be selected in terms of the study areas with the highest levels of substances to which the population is exposed during the averaging period of the results, as well as for those areas where the limit, tar-

Tab. 1. The minimum number of continuous measurement points required to assess the air quality of PM10 particulate matter [8]

Tab. 1. Minimalna liczba stałych punktów pomiarowych wymagana na potrzeby oceny jakości powietrza dla pyłu zawieszonego PM10 [8]

Zone Population (in Thousands)	Minimum Number of Continuous Measurement Points	
	The level of substances in the air exceeds the upper threshold estimate	The level of substances in the air between the upper and lower thresholds estimates
	PM10 Particulate Matter	PM10 Particulate Matter
0 – 249	2	1
250 – 499	3	2
500 – 749	3	2
750 – 999	4	2
1000 – 1499	6	3
1500 – 1999	7	3
2000 – 2749	8	4
2750 – 3749	10	4
3750 – 3749	11	6
4750 – 5999	13	6
> 6000	15	7

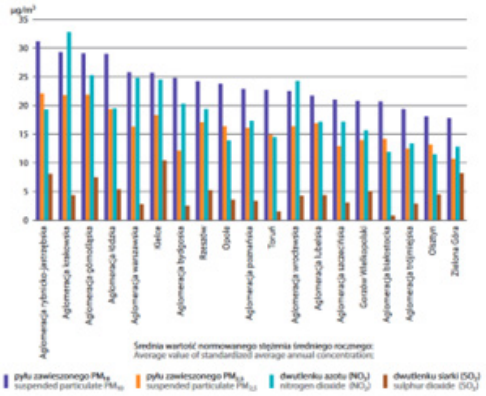

Fig. 1. PM2.5, PM10, NO_2, and SO_2 in selected regions of Poland in 2020 [2]

Fig. 1. PM2.5, PM10, NO_2 i SO_2 w wybranych regionach Polski w 2020 r. [2]

get and long-term goal levels of substances in the air are established. The minimum number of fixed measurement points to measure PM10 particulate matter depends on the number of residents (a directly proportional relationship) (Table 1). Additionally, the results must represent the place of the impact of transportation or industry. In the case of industrial impact, the location of at least one measurement point should be on the leeward side of the installation in the vicinity of a nearby residential area [8].

Particulate pollution is hazardous to the environment. Particulates adversely affect the health of humans and animals, disrupt the physiological functions of plants, and lead to the destruction of building materials. Under conditions of temperature inversion and high concentrations of sulfur dioxide, winter smog can form. This phenomenon irritates the respiratory tract and circulatory system of living organisms. During an outbreak of acid smog in London in 1952, more than 4,000 people died within a few days. The WHO confirms the negative impact of particulate matter that causes many diseases and disorders. The more urbanized and industrialized the area, the more significant the impact of pollution [3].

An example of an urbanized area is the Krakow agglomeration, which is struggling with many environmental problems [7]. Despite the ban on burning solid fuels, elevated and exceeded concentrations of particulate pollutants are observed in Krakow due to the lack of restrictions in the surrounding communities. Local industry and transport contribute a large share of dust emissions [1, 4]. According to the 2021 Regional Development of Poland Report by the Central Statistical Office, dust emissions from establishments particularly detrimental to clean air were observed in 37 large cities in 2020. Figure 1 presents the values of the average annual concentrations of air pollutants in Poland. The highest concentrations of PM10 particulate matter, right after the Rybnik-Jastrzębska agglomeration, were recorded in the Krakow agglomeration (29 μg/m³) [2].

2. Purpose and Methods

The study aimed to analyze the measurement data of PM10 particulate matter in the Krakow agglomeration and to build a model of the backward trajectories of air masses to determine the contribution of natural phenomena to air pollution.

The study used 2022 measurement data from ten Chief Inspectorate of Environmental Protection monitoring stations in the Krakow agglomeration. During data analysis, two periods lasting several days that exceeded limit levels or above-average concentrations of PM10 particulate matter outside the heating period were selected. The monitoring stations, both automatic and manual, are shown in Figure 2. If a station made measurements using both methods, measurements performed using the manual method were included in the analysis of daily averages due to their higher precision. Among the measurement stations were [11]:

1) Krakow urban background station, Bujaka Street (international station code: PL0501A), with the coordinates: 50.010575 N and 19.949189 E and an altitude of 223 m above sea level. The station measures PM10, PM2.5, benzo(a) pyrene, arsenic, benzo(anthracene), benzo(b)fluoranthene, benzo(j)fluoranthene, cadmium, dibenzo(a,h)anthracene, indeno(1, 2, 3-cd)pyrene, nickel, in PM10 with a 24-hour averaging time and PM10, nitric oxide, nitrogen dioxide, nitrogen oxides, ozone, sulfur dioxide, benzene with a 1-hour averaging time;

Fig. 2. Map of measuring stations in the Krakow agglomeration [11]
Fig. 2. Mapa stacji monitoringu w aglomeracji krakowskiej [11]

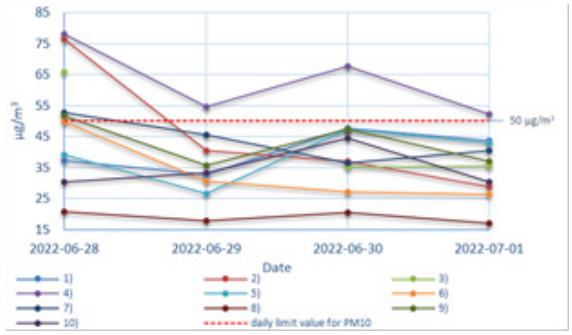

Fig. 3. Measurement data from PM10 particulate matter monitoring stations in period one at 12:00 pm [compiled from 11]
Fig. 3. Dane pomiarowe ze stacji monitoringu pyłów zawieszonych PM10 w epizodzie pierwszym dla godziny 12:00 [opracowanie na podstawie 11]

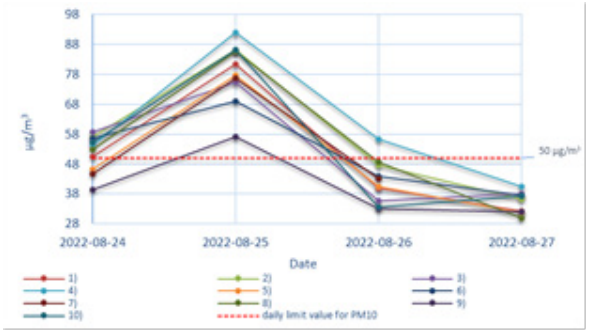

Fig. 4. Measurement data from PM10 particulate matter monitoring stations in period two at 12:00 pm [compiled from 11]
Fig. 4. Dane pomiarowe ze stacji monitoringu pyłów zawieszonych PM10 w epizodzie drugim dla godziny 12:00 [opracowanie na podstawie 11]

2) Krakow industrial station, Bulwarowa Street (international station code: PL0039A), with the coordinates 50.069308 N and 20.053492 E and an altitude of 195 m above sea level. The station measures PM10, benzo(a)pyrene, arsenic, cadmium, nickel, and lead in PM10 with a 24-hour averaging time and PM10, PM2.5, benzene, carbon monoxide, nitrogen oxide, sulfur dioxide with a 1-hour averaging time;

3) Krakow urban background station, Piastow Estate (international code of the station: PL0642A), with the coordinates 50.098508 N and 20.018269 E and an altitude of 239 m above sea level. The station measures PM10 particulate matter and benzo(a)pyrene in PM10 with a 24-hour averaging time and PM10 with a 1-hour averaging time;

4) Krakow transportation station, Dietla Street (international station code: PL0641A) with coordinates 50.057447 N and 19.946008 E and altitude 209 m above sea level. The station measures PM10 particulate matter, nitrogen oxide, nitrogen dioxide, nitrogen oxides with a 1-hour averaging time;

5) Krakow urban background station, Swoszowice District (international code of the station: PL0735A) with coordinates 49.991442 N and 19.936792 E and an altitude of 236 m above sea level. The station measures PM10 particulate matter and benzo(a)pyrene in PM10 with a 24-hour averaging time and PM10 with a 1-hour averaging time;

6) Krakow industrial station, Wadow Estate (international station code: PL0670A) with coordinates 50.100569 N and 20.122561 E and an altitude of 218 m above sea level. The station measures PM10, benzo(a)pyrene, arsenic, cadmium, nickel, lead in PM10 with a 24-hour averaging time and PM10 with a 1-hour averaging time;

7) Krakow urban background station, Zloty Rog Street (international code of the station: PL0643A) with coordinates 50.081197 N and 19.895358 E and an altitude of 218 m above sea level. The station measures PM10 particulate matter and benzo(a)pyrene in PM10 with a 24-hour averaging time and PM10 with a 1-hour averaging time;

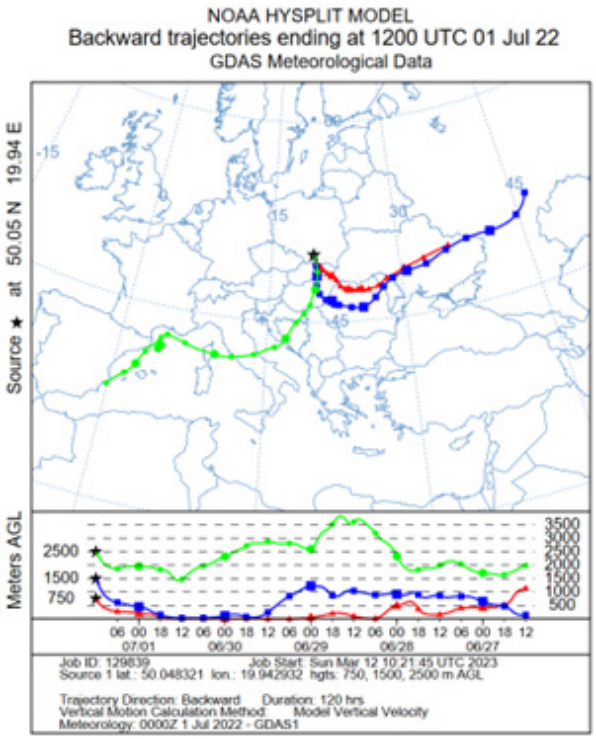

Fig. 5. HYSPLIT model of backward trajectories of air masses from June 27 to July 1, 2022 [compiled from 12]

Fig. 5. Model HYSPLIT wstecznych trajektorii mas powietrza w okresie od 27 czerwca 2022 r. do 1 lipca 2022 r. [opracowanie na podstawie 12]

Fig. 6. FIRMS data on fires during the first period of increased concentrations of PM10 particulate matter between August 16–20, 2022 [10]

Fig. 6. Dane FIRMS o pożarach w czasie pierwszego epizodu zwiększonego stężenia pyłów zawieszonych PM10 w okresie od 16 sierpnia 2022 r. do 20 sierpnia 2022 r. [10]

8) Niepolomice urban background station, 3 May Street (international station code: PM0125A) with coordinates 50.035117 N and 20.212689 E and altitude 201 m above sea level. The station measures PM10 particulate matter and benzo(a)pyrene in PM10 with a 24-hour averaging time and PM10 with 1-hour averaging time;

9) Skawina urban background station, Ogrody Estate (international station code: PL0273A) with coordinates: 49.971047 N and 19.830422 E and an altitude of 225 m above sea level. The station measures nitrogen oxide, carbon dioxide, oxides of nitrogen, PM10 particulate matter, sulfur dioxide, and benzene with a 1-hour averaging time.

10) Zabierzow urban background station, Wapienna Street (international station code: PL0728A) with coordinates: 50.116028 N and 19.800639 E and an altitude of 238 m above sea level. The station measures PM10 particulate matter and benzo(a)pyrene in PM10 with a 24-hour averaging time and PM10 with a 1-hour averaging time.

Daily average measurement data for the periods used for the analysis:

1. From June 28 to July 1, 2022, when daily values of PM10 particulate matter from 15.1 μg/m³ to 47.7 μg/m³ were recorded;
2. From August 24–27, 2022, when daily values of suspended particulate matter from 25.2 μg/m³ to 59.4 μg/m³ were recorded, and the 24-hour limit level of 50 μg/m³ was exceeded at the station numbers: 1), 2), 3), 4), 7), 10).

The measured values of the individual monitoring stations in period one at noon are shown in Figure 3. On June 28, 2022, notably increased PM10 values were observed at stations 2) and 4), reaching values of more than 75 μg/m³. Analyzing historical weather data on that day on the Weather Spark platform (https://pl.weatherspark.com), the following weather parameters were observed in Krakow: almost cloudless skies and a temperature of 30°C and at noon, an average wind speed of 7.49 km/h, measured at the height of 10 meters [13]. Such weather conditions and the lack of precipitation favored the occurrence of high concentrations of air pollution.

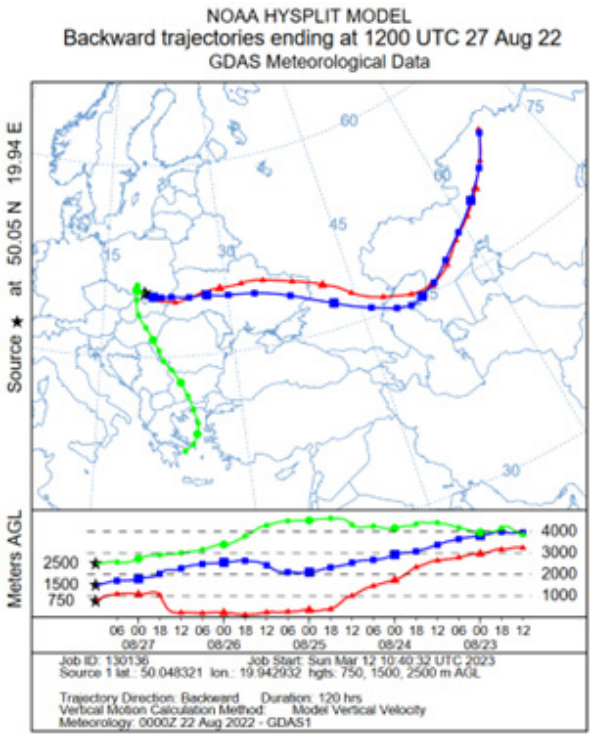

Fig. 7. HYSPLIT model of backward air trajectories from August 23–27, 2022 [compiled from 12]

Fig. 7. Model HYSPLIT wstecznych trajektorii powietrza w okresie od 23 sierpnia 2022 r. do 27 sierpnia 2022 r. [opracowanie na podstawie 12]

Fig. 8. Map of FIRMS data on fires during the second period of increased concentrations of PM10 particulate matter from August 24–28, 2022 [10]

Fig. 8. Mapa danych FIRMS o pożarach w czasie drugiego epizodu zwiększonego stężenia pyłów zawieszonych PM10 w okresie od 24 sierpnia 2022 r. do 28 sierpnia 2022 r. [10]

The highest concentrations of PM10 dust were recorded on August 25, 2022. Upon analyzing data from the mentioned weather platform, the day was characterized by partial cloud cover, an air temperature that reached 26°C, and an average wind speed of 7.41 km/h [13]. As in the first period, the weather conditions also contributed to the high PM10 values. In the case of period two, equally increased values were observed at all stations at noon, as confirmed by Figure 4.

Based on the HYSPLIT software (Hybrid Single-Particle Lagrangian Integrated Trajectories, https://www.ready.noaa.gov/hypub-bin/trajsrc.pl), using backward air trajectories, the influx of transboundary pollutants was simulated in selected periods of elevated PM10 concentrations. Based on European Commission guidelines, the simulation included: 5-day backward trajectories of air masses, measurement data for noon, a simulation of three elevations: 750 m above sea level, 1500 m above sea level, 2500 m above sea level, and a vertical wind speed profile.

The next step was to analyze NASA's Fire Information for Resource Management System (FIRMS) to identify whether the prevailing fires during the period affected the measurements. This type of analysis allows us to determine whether elevated concentrations of PM10 particulate matter in the Krakow metropolitan area were of natural or anthropogenic origin.

3. Results and Discussion

During the analysis of the first HYSPLIT model of backward trajectories of air masses from June 28 to July 1, 2022 (Fig. 5), an influx of masses was observed from the south of Poland. For preset heights of 750 m above sea level and 1500 m above sea level, trajectories could be observed coming from Ukraine via Romania and Slovakia. However, in the case of the highest altitude (2,500 meters above sea level), the masses were coming from Spain, through the French coast and Italy, to the Balkan Peninsula and Slovakia.

Observing the map of fires during the first period, shown in Figure 6, despite individual fires in most countries, special attention is drawn to the fact that there is a large outbreak of fires in Italy and Ukraine. A simulation of incoming air masses shows that natural phenomena in these areas indirectly affect the degree of air pollution in the Krakow metropolitan area.

Figure 7 presents the HYSPLIT model for August 23–27, 2022. In the second analyzed period, air masses were observed from the east and the south. For the simulation's preset altitude of 750 m above sea level and 1500 m above sea level, the masses came from Kazakhstan, Russia, and Ukraine. The air masses at 2500 m above sea level came from southeastern Europe. Therefore, it can be concluded with a high probability that dust from areas on Poland's eastern border may have entered the Krakow agglomeration along with the influx of air.

Considering the influx of air masses, let us note the large fire outbreak in Ukraine and southern Europe. In the example of the fire map shown in Figure 8, it is also possible to see the spread of fires in most countries between August 24–28, 2022. It is estimated that the influx of pollutants from the fires indirectly contributed to the increase in air pollution in the Krakow metropolitan area during this period. In the first and second periods, the sources were natural phenomena, and emissions and their magnitude were not determined by human factors.

4. Conclusions

The study made it possible to assess the daytime variability of meteorological conditions and document that in the analyzed periods of increased PM10 pollution in the Krakow agglomeration, i.e., from June 2 to July 1, 2022, and from August 24 to 27, 2022, the pollution sources considered were of natural origin, as a result of spreading fires in eastern Europe. Human activity in no way determined the fact of the emissions themselves and their magnitude.

In the first period, a simulation with the HYSPLIT software shows retrograde trajectories from Ukraine, through Romania and Slovakia, and from Spain, through the French coast, Italy, to the Balkan Peninsula, and Slovakia. However, the second period shows an influx of air masses from Kazakhstan, Russia, and Ukraine, as well as from the southern part of Europe. As mentioned above, the increase in air pollution in the Krakow agglomeration was correlated with the spread of fires in the regions.

Undoubtedly, air monitoring in Poland provides reliable information on the state of the environment, giving residents a sense of security and allowing them to respond to the presence of pollution, both from natural and anthropogenic sources. Measurements of monitoring stations in 2022 confirmed the problem of PM10 pollution above the daily limit value, so the developed models can be used in the future to predict the impact, even distant natural phenomena far from the surveyed area.

Literatura – References

1. Ciepiela M., Sobczyk W. (2021). The Role of the University in Environmental Education. The Problem of Particulate Pollution in Poland. Journal of Education, Technology and Computer Science, 204, 208.
2. Główny Urząd Statystyczny (2021). Departament Badań Przestrzennych i Środowiska: Rozwój regionalny Polski – raport analityczny 2021. Warszawa, 127.
3. Janka M. R. (2014). Zanieczyszczenia pyłowe i gazowe. Podstawy obliczania i sterowania poziomem emisji. PWN, Warszawa, 18-19.
4. Kleczkowski P. (2020). Smog w Polsce przyczyny | skutki | przeciwdziałanie. PWN, Warszawa, 263-265, 329.
5. Krystek J. (2018). Ochrona środowiska dla inżynierów. PWN, Warszawa, 17.
6. Mazurek H., Badyda A. (2018). Smog konsekwencje zdrowotne zanieczyszczeń powietrza. PZWL, Warszawa, 14-17.
7. Polski Klub Ekologiczny Fundacja Międzynarodowy Instytut Polityki i Strategii Ekologicznej: Problemy Ekologiczne Miasta Krakowa. (2018). Oficyna Wydawnicza Text, Kraków, 141.
8. Rozporządzenie Ministra Środowiska z dnia 13 września 2012 r. w sprawie dokonywania oceny poziomów substancji w powietrzu, Dz.U. 2012 poz. 1032.
9. Wielgosiński G., Zarzycki R. (2018). Technologie i procesy ochrony powietrza. PWN, Warszawa, 317-319.
10. https://firms.modaps.eosdis.nasa.gov (11.03.2023)
11. https://powietrze.gios.gov.pl (10.03.2023)
12. https://www.ready.noaa.gov/hypub-bin/trajsrc.pl (11.03.2023)
13. https://pl.weatherspark.com (12.03.2023)

Transgraniczne zanieczyszczenie powietrza w aglomeracji krakowskiej z zastosowaniem modelu HYSPLIT

Celem badań była analiza danych pomiarowych pyłów zawieszonych PM10 na terenie aglomeracji krakowskiej oraz wykonanie modelu trajektorii wstecznych mas powietrza w celu określenia, czy i w jakim stopniu zjawiska naturalne, takie jak pożary lasów poza granicami Polski, wpływają na stopień zanieczyszczenia powietrza.

W artykule opisano proces dyspersji zanieczyszczeń w atmosferze ziemskiej oraz zasady monitoringu powietrza w aglomeracji krakowskiej. Do opracowania posłużono się danymi pomiarowymi z 2022 r. z dziesięciu stacji monitoringu Głównego Inspektoratu Ochrony Środowiska, znajdujących się na terenie aglomeracji krakowskiej, gdzie wytypowano dwa epizody zwiększonego stopnia zanieczyszczenia pyłami zawieszonymi PM10. Bazując na oprogramowaniu HYSPLIT, który wykorzystuje wsteczne trajektorie powietrza, przeprowadzono symulację napływu zanieczyszczeń transgranicznych. Następnie analizując system informacji o pożarach FIRMS, podjęto się próby udokumentowania, iż uwzględnione źródła zanieczyszczeń miały pochodzenie naturalne, a działalność człowieka w żaden sposób nie decydowała o emisji i jej wielkości.

Słowa kluczowe: *zanieczyszczenie pyłowe, modelowanie zanieczyszczeń powietrza, ocena jakości powietrza, monitoring środowiska, pożary lasów*

The Use of Geomatics Tools in Critical Infrastructure Management

Anna BLUSZCZ[1)], Katarzyna TOBÓR-OSADNIK[2)], Krzysztof TOMICZEK[3)], Nur Suhaili MANSOR[4)], Hapini AWANG[5)]

[1)] dr hab. inż. prof. PŚ, Silesian University of Technology, Faculty of Mining, Safety Engineering and Industrial Automation, Gliwice, Poland; email: anna.bluszcz@polsl.pl
[2)] dr hab. inż. prof. PŚ, Silesian University of Technology, Faculty of Mining, Safety Engineering and Industrial Automation, Gliwice, Poland; email: katarzyna.tobor-osadnik@pols.pl
[3)] dr inż., Silesian University of Technology, Faculty of Mining, Safety Engineering and Industrial Automation, Gliwice, Poland; email: Krzysztof.tomiczek@pols.pl
[4)] dr, University Utara Malaysia, School of Computing, Malaysia; email: nursuhaili@uum.edu.my
[5)] dr, University Utara Malaysia, School of Computing, Malaysia; email: hapini.awang@uum.edu.my

http://doi.org/10.29227/IM-2023-01-21

Submission date: 10-03-2023 | Review date: 29-03-2023

Abstract

The purpose of the article is to characterize crisis management, including the main stages of the activities of anti-crisis headquarters. The paper presents extensive examples of critical infrastructure and develops sample maps in QGIS software, which can be important tools in conducting the activities of crisis management services. It presents A Free and OpenSource Geographic Information System QGIS software for identifying selected critical infrastructure objects based on available GIS Open data from the Malaysian region and Poland. The analysis presents selected geoprocessing tools for generating areas with a set distance from identified critical infrastructure objects called buffers. Buffer layers are areas, visible on the generated maps, that can be used as a tool to visualize potential actions for emergency management services. Identifying these buffer zones makes it possible to build strategies for implementing adequate prevention or rescue actions during an emergency. Risk classification in specific buffer zones is presented, which can be used to optimize the actions taken by crisis management services. A wide range of functionality of geographic spatial information systems is demonstrated, which increases the efficiency of operations and optimization of decision-making in crisis management. The publication can provide a valuable example of the use of available information systems in crisis management.

Keywords: *geomatics, crisis management, critical infrastructure*

1. INTRODUCTION

The dynamic development of civilization brings with it many changes and megatrends, which at the same time have a positive impact on the quality of life of society, but on the other hand, bring dynamic changes for ecology on a global scale[1,2].

Progressive digitization and dynamic development of new technologies is associated with a new era in the so-called Industry 4.0 and 5.0., however, it is still employees in the organization that are the main foundations for further development [3–6].

Every human activity is associated with risk, therefore there is a great need to reduce and prevent this risk, so as to effectively limit potential material and moral losses. Therefore, the subject of crisis management and the role of IT systems in the effectiveness of these activities has been addressed in this article.

The dynamic development of information systems is widely used in the practice of emergency management. Geographic information systems are tools that allow the collection, management and analysis of data on the spatial location of objects and phenomena, which involves working with layers containing the data under study and allowing their visualization through maps and 3D scenes.

In emergency management, GIS can, among other things, provide secure access to up-to-date information necessary for accurate decision-making[7, 8]. GIS are used in practice to create, among other things, various types of hazard maps, which depict the geographic area covered by a hazard, taking into account various event scenarios; risk maps, also known as a risk matrix or risk model, which provide a description of the effects of a hazard on people, the environment, property and infrastructure.

Tasks of GIS in emergency management GIS provides considerable opportunities in managing, predicting and evaluating facts in emergency situations; they are useful for decision-making in all management functions (planning, organizing, leading, controlling). The application of GIS in emergency management can consist of the following tasks:

- managing information about actual and/or potential threats, identifying and assessing sources of threats, quick access to collected data, combining information layers,
- inventorying objects and events, integrating data obtained from various sources,
- performing in-depth spatial analyses, modeling and simulations, creating thematic maps,
- hazard maps, e.g. forecasting the impact zone of clouds of released toxic substances, flood hazard maps,
- analysis of land use, assessment of its exposure to potential hazards, and resources of services, inspections and guards that can take action,
- emergency risk analysis, modeling of emergency development, identification of disaster-prone areas,
- planning of rescue operations, determination of points of intersection of roads with the danger zone to determine the location of law enforcement patrols isolating

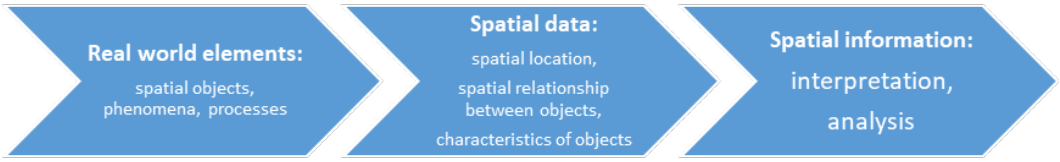

Fig. 1. The process of generating spatial information. Source: own elaboration
Rys. 1. Proces generowania informacji przestrzennej. Źródło: opracowanie własne

Fig. 2. Stages of GIS project. Source: own elaboration
Rys. 2. Etapy projektu GIS. Źródło: opracowanie własne

the danger zone, coordination of the activities of various services during rescue operations,
- identification of address points for which evacuation should be carried out, designation of places for evacuation of the population in case of emergency,
- estimating the number of people in the threatened area,
- studying the distribution of fires and other incidents,
- -analysis of floodplains during floods (flood risk maps),
- monitoring changes and determining the amount of damage,
- publishing maps and information on the Internet, and others. These tasks form the basis of the activities carried out by the services responsible for ensuring security. [9].

In this article, we will refer to the term critical infrastructure defined as real and cyber systems including: facilities, equipment or installations that are necessary for the minimum functioning of the economy and the state. Examples of critical infrastructure on a national and regional scale may include such systems as energy, water, food, energy resources and fuels supply, communications systems, ICT networks, financial systems, rescue and health systems, transportation systems, etc. Critical infrastructure plays a key role in the functioning of any state and is therefore subject to special oversight. As a result of events caused by, among other things, forces of nature or as a consequence of human actions, critical infrastructure may be destroyed, damaged, and its operation may be disrupted, so that the lives and property of citizens may be endangered. The cause of damage to critical infrastructure can be a disaster of various kinds, which is also interchangeably referred to as a crisis that causes destabilization and a sense of insecurity and can affect a community. Hence, the protection of critical infrastructure is one of the priorities facing government institutions of countries. The essence of the tasks related to critical infrastructure boils down not only to ensuring its protection from threats, but also to ensuring that any damage and disruptions to its functioning can be dealt with in the optimal time and do not cause additional losses to citizens and the economy. Hence, crisis management services are established in countries, ready to respond in case of emergency in areas affected by disaster or other random events. Emergency management services carry out activities in four main phases. In the first phase, the services always carry out activities aimed primarily at preventing undesirable events, and these activities are primarily related to actions to eliminate, reduce or limit the effects of possible hazards. The second phase concerns preparatory activities related to advance planning of undertakings in the event of a threat or disaster, and securing resources of forces and means to carry out rescue operations. The third phase of activities is response, the purpose of which is to halt the development of the emergency situation, provide direct assistance to the injured and limit losses and damage. The fourth stage of emergency management services is reconstruction, which is the type of action in the event of a disaster, which concerns material and moral undertakings aimed at restoring the previous state of affairs, before the emergency.

The purpose of the article is to characterize crisis management, including the main stages of the activities of anti-crisis headquarters. The paper presents extensive examples of critical infrastructure and develops sample maps in QGIS software, which can be important tools in conducting the activities of crisis management services. This paper presents A Free and Open Source Geographic Information System QGIS software for identifying selected critical infrastructure objects based on available GIS Open data from the Malaysian region and Poland. The analysis presents selected geoprocessing tools for generating areas with a set distance from identified critical infrastructure objects called buffers. Buffer layers are areas, visible on the generated maps, that can be used as a tool to visualize potential actions for emergency management services. Identifying these buffer zones makes it possible to build strategies for implementing adequate prevention or rescue actions during an emergency. The publication can provide a valuable example of the use of available information systems in crisis management.

2. THE FUNCTIONALITY OF QGIS SOFTWARE

A significant part of objects, phenomena and processes occurring in reality are spatial in nature, as they are defined by a specific place and time. All data on spatial objects, including phenomena and processes, located or occurring in space are called spatial data. This data, properly analyzed and interpreted, is a source of spatial information. Figure 1 shows the process of extracting from the complex real world selected elements, for example, selected critical infrastructure objects, with specific characteristics, which

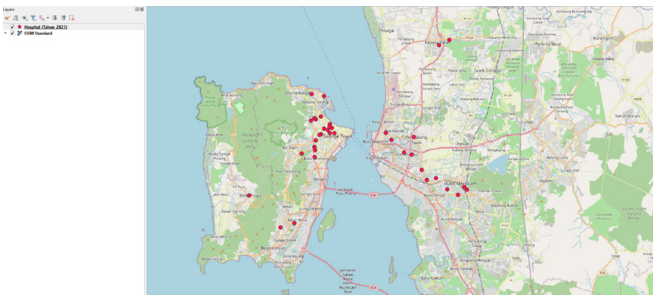

Fig. 3. Identification of critical infrastructure facilities in QGIS region Malaysia
Rys. 3. Identyfikacja obiektów infrastruktury krytycznej w regionie QGIS Malezja

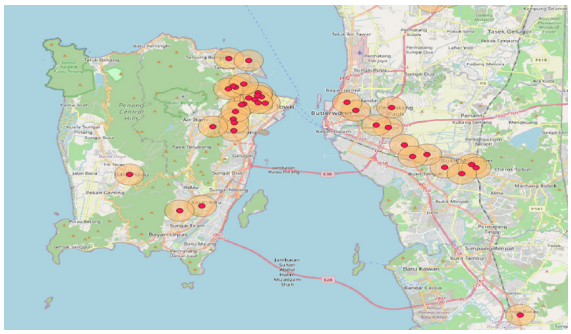

Fig. 4. Determination of buffer zones for surveyed critical infrastructure objects in QGIS Malaysia region
Rys. 4. Wyznaczenie stref buforowych dla badanych obiektów infrastruktury krytycznej w regionie QGIS Malaysia

after appropriate interpretation and analysis provide specific spatial information, otherwise known as geo-information.

GIS is an acronym for Geographic Information System and is usually defined as an organized set of computer hardware, software, spatially (or geographically) referenced data, and people (contractors and users), created to efficiently: storing/collecting, sharing, processing, analyzing, and visualizing spatial (geographic) data.

The development of GIS began less than fifty years ago, when Roger Tomlinson developed a model for collecting spatial data and created the world's first GIS system – the Geographic Information System of Canada. Its creation initiated the rapid development of GIS tools and analytical methods and techniques. In the early days of GIS implementation, they were mainly applied to professional projects for administration, management and planning, and scientific research.

This is because geographic data is understood to be that which is referenced to geographic coordinates, that is, it preserves spatial relationships corresponding to a specific cartographic mapping. Spatial data, on the other hand, can be mapped in any datum that uses rectangular coordinates (x, y), so also geographic reference, hence spatial data is considered to encompass a broader set, including geographic data. GIS data represent the results of measurements or otherwise acquired features that characterize the location, type and characteristics of an object, its size, composition, physical, chemical properties, legal status, etc. Data are represented by numbers, letters, symbols or in any other form suitable for entering into a computer and for further processing and visualization. They can appear in the form of so-called discrete or continuous data, which correspond to the two main types of layers, namely vector and raster data. Spatial information is supplemented by descriptive data, which as such is non-spatial data, but contains characteristics of the previous two types of data and is related to them.

3. METHODOLOGY AND DATA

This article presents the final GIS maps in which buffer zones were applied to vector layers representing critical infrastructure objects. The analysis was based on the four stages of GIS design presented in Figure 2, which are Identifying targets, collecting data, performing analysis, and generating maps with results.

The first stage of the research defined the purpose of the analysis, i.e. Identification of buffer zones for selected critical infrastructure facilities. In the second stage of the research, data for analysis was selected. Currently, there is a rapid development of open access databases for various types of GIS data. In this paper, open access data from the Malaysian territory GEO HUB was used. A set of files necessary for loading into QGIS was downloaded from the database, which contained information on hospital facilities located on Penang Malaysia island. Hospitals are critical infrastructure facilities, as they provide life and health protection for the population from the selected territory. The third stage of the study was analysis. The study uses selected analytical tools available in GIS systems. Typical GIS software systems have built-in analytical modules that are capable of performing all data processing functionalities. They are organized in the form of so-called toolboxes (literally translated as "toolbox") or grouped in the form of sets of so-called plugins or extensions. When a tool is selected, a dialog box appears, where the user defines the parameters necessary to perform the operation. Often a help window is also available, providing an explanation of how the tool works.

The third stage of the research identified zones called buffers, which is among the popular geoprocessing tools. We define buffering as the operation of delimiting zones from selected objects known as buffers. As a result of this operation, a polygon layer is created with areas that are no farther than a given criterion from the indicated objects. Many such polygons can be created, and each polygon can correspond to a different distance, for example.

Tab. 1. Risk matrix. Source: based on [9]

Tab. 1. Macierz ryzyka. Źródło: na podstawie [9]

PROBABILITY	1	HIGH			
	2	MEDIUM			
	3	LOW			
RISK VALUE			A	B	C
			LOW	MEDIUM	HIGH
			CONSEQUENCES		

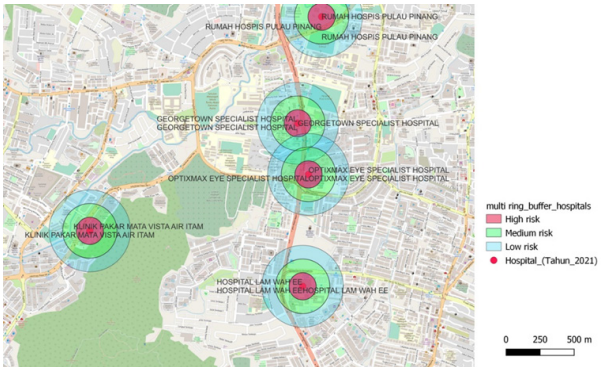

Fig. 5. Risk classification for buffer zones for the studied critical infrastructure facilities in QGIS area Malaysia. Source: own elaboration

Rys. 5. Klasyfikacja ryzyka dla stref buforowych dla badanych obiektów infrastruktury krytycznej w obszarze QGIS Malezja. Źródło: opracowanie własne

What's more, this distance can depend on the value indicated in the given object's attribute. The fourth stage of the research is the generation of the corresponding maps, which are a visualization of the effects of the analyses made.

4. RESULTS

4.1 Case study 1 Malaysia

The first step in analyzing the data in the software is to import the data and display it on a workspace. In the example studied, open-access data in the data geohub portal from Malaysia was used, with data on the location of hospitals on Penang Island, among others, as an example of critical infrastructure. The data was loaded as a vector layer as presented in Figure 3.

The second stage of the analysis was to use a standard geoprocessing tool to determine buffers for identified critical infrastructure facilities. Buffer areas in practice are an excellent tool for visualizing protection zones for selected objects located in the selected area as shown in Figure 4.

In the third stage of the analysis, risk classification was carried out for a selected number of buffer zones of the analyzed critical infrastructure objects. For this purpose, the multiring buffer tool was used in the software, which is presented in Figure 5.

The activities of emergency management services can be defined for the designated areas with a given buffer, and can also be differentiated for individual groups of risk, i.e. for several buffers categorized for the corresponding risk scale.

Risk, according to the Polish standard ISO 31000:2012, means the influence of internal and external factors on the uncertainty of achieving the set goals. In relation to emergencies, risk can be defined as an identified undesirable event that may occur with a certain probability. To quantify risk (the probability of a specific effect occurring at a specific time or in a specific situation) in crisis management, the formula is used [9]:

$$R = P \times S \quad (1)$$

where:

R – risk,

P – probability of occurrence of a crisis situation,

S – value of potential losses, estimated destruction after the occurrence of a crisis situation.

When assessing probability and impact, the Risk matrices, presented in Table 1, are applicable.

When using 3-point scales to assess the probability and impact of risks, the matrix allows you to identify three types of risk values (Table 1):

- small (blue color),
- medium (green color),
- large (red color).

If risk components are extracted, the values of these components (partial risks, depending on the type of emergency) should be defined, calculated and summed.

Categorization by distance makes it possible to create multiple security zones according to the identified threat level. In the figure, processing tools were used to determine three zones: high risk, medium risk and moderate risk for the analysed critical infrastructure in the Penang Malaysia island area.

As presented in the selected example, GIS software can be widely used to support and organize the work of emergency management services. Its rich tools and functionalities allow efficient visualization of various types of strategic plans and possible actions for selected areas of analysis.

4.2 Case study 2 Poland

As presented in the selected example, GIS software can be commonly used to support and organize the work of crisis management services. Its rich tools and functionalities enable efficient visualization of various types of strategic plans and possible actions for selected areas of analysis. The spatial geoinformation system is commonly used in crisis management. The article presents the area of Poland, the city of Cieszyn, where GIS was used to map flood hazards and landslide hazards, which was presen-

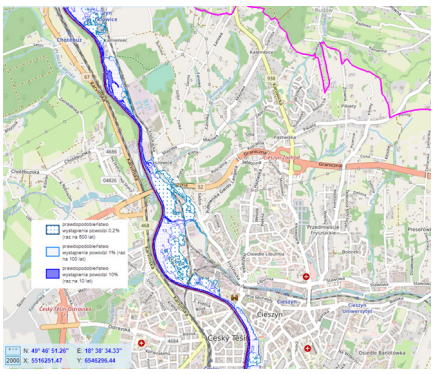

Fig. 6. Flood map according to GIS system. Source: own elaboration based on open data: geoportal of the city of Cieszyn
Rys. 6. Mapa powodziowa wg systemu GIS. Źródło: opracowanie własne na podstawie danych otwartych: geoportal miasta Cieszyna

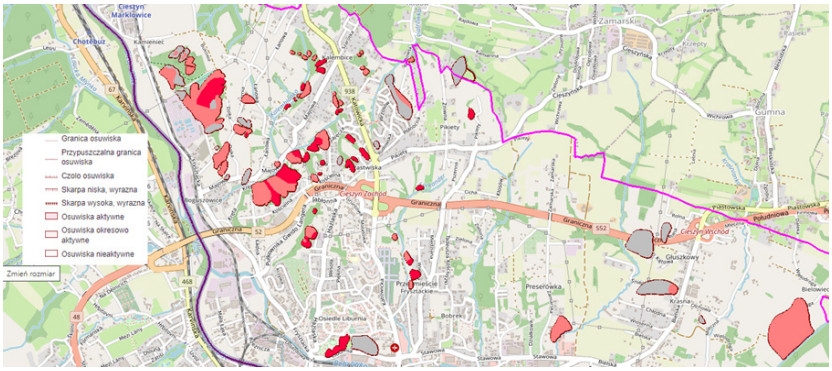

Fig. 7. Landslide map according to GIS system
Rys. 7. Mapa osuwisk wg systemu GIS

ted in the fig 6 and 7. Areas of particular flood risk have been classified into four categories: a) areas where the probability of flooding is average and amounts to once in 100 years, b) areas where the probability of flooding is high and amounts to once in 10 years, c) areas between the shoreline and the levee or natural high bank, in which the route of the flood embankment, as well as islands and sludge areas, were built, d) technical belt.

Areas of particular flood risk are identified through a series of analytical and research works leading to the creation of flood hazard maps and flood risk maps. On their basis, a flood risk management plan is created.

Among the many geological hazards in the city of Cieszyn, landslides occur in a significant number. In total, 82 landslides are registered in the Landslide Protection System of the Polish Geological Institute in the Cieszyn commune. Areas of active landslides cannot be developed. On the map, active landslides or periodically active landslides are marked in red, inactive landslides are marked in grey.

5. CONCLUSION

The purpose of the paper is to present the functionality of QGIS software for identifying critical infrastructure on a map and the use of selected geoprocessing tools for determining buffers, i.e. protective areas for selected critical infrastructure objects.

As demonstrated in the given study, QGIS software enables universal access to spatial information. Dynamic development means that we should expect rapid development of mobile-GIS, i.e. increasing access to GIS databases from mobile devices, using these devices for acquisition, management and automatic updating of spatial databases in near real time. The variety of technical and organizational solutions of GIS indicates the need to implement universally applicable, universal standards and norms in this area. This article demonstrates the application of GIS in security engineering, for example, for the purposes of decision support in public administration, or in authorities responsible for public security or emergency management. Properly selected GIS software on the basis of prepared data can help solve many security engineering problems by supporting the decision-making process. The study identifies potential critical infrastructure objects, locates them on a map, and generates so-called security buffers for these objects to which risk classification has been made. The tools presented can find application in decision-making for specific actions in case of crisis events such as pandemic and many others. Each zone with an appropriately assigned risk type can be associated with a specific range of anti-crisis actions and define specific actions of emergency management services such as access controls or disinfection. QGIS maps provide access to the operational picture and allow for a more efficient process of optimal decision-making.

6. ACKNOWLEDGEMENTS

This paper presents the results of Project Based Learning, Silesian University of Technology.

Literatura – References

1. Manowska A., Bluszcz A.: Forecasting crude oil consumption in Poland based on LSTM recurrent neural network, Energies, 2022, vol. 15, nr 13, 1-23, DOI:10.3390/en15134885
2. Bluszcz A.: Ecological growth boundaries, Management Systems in Production Engineering, 2017, vol. 25, nr 1, 55-59, DOI:10.1515/mspe-2017-0008
3. Grabowska S., Saniuk S., Gajdzik B.: Industry 5.0: improving humanization and sustainability of Industry 4.0, Scientometrics, vol. 127, nr 7, 2022, 1-28, DOI:10.1007/s11192-022-04370-1
4. Grabowska, S.: Key components of the business model in an Industry 5.0 environment, Scientific Papers of Silesian University of Technology – Organization & Management 2022, Series 158, 191-199, DOI:10.29119/1641-3466.2022.158.13
5. Saniuk S., Grabowska S., Straka M.: Identification of social and economic expectations: contextual reasons for the transformation process of Industry 4.0 into the Industry 5.0 concept, 2022, Sustainability, vol. 14, nr 3, 1391, 1-20, DOI:10.3390/su14031391
6. Kowal B., Świniarska O., Domaracká L.: Internal Communication Models Shaping Safe Behavior of Employees in the Raw Materials Sector During the Coronavirus Pandemic. Mineral Resource Management, 2022, Tom 1 Nr 2 (50).
7. Nur Suhaili Mansor, Helmi Zulhaidi Mohd Shafri, Shattri Mansor, Biswajeet Paradhan, The influence of urban development and social mobility on socioeconomic level: The application of GIS on urban ecosystems. IOP Conf. Series: Earth and Environmental Science 2014 ,20 ,012011 doi:10.1088/1755-1315/20/1/012011
8. Amirulikhsan Zolkafli, Nur Suhaili Mansor: Improving Public Participation for Land Use Planning in Malaysia: Can Participatory, GIS help? Journal of Governance and Development, 2018, Vol. 14. Issue Ładysz J., Gis technology in security engineering, Wrocław 2015. s.169

Wykorzystanie narzędzi geomatycznych w zarządzaniu infrastrukturą krytyczną

Celem artykułu jest scharakteryzowanie zarządzania kryzysowego, w tym głównych etapów działania sztabów antykryzysowych. W artykule przedstawiono obszerne przykłady infrastruktury krytycznej oraz opracowano przykładowe mapy w oprogramowaniu QGIS, które mogą być ważnymi narzędziami w prowadzeniu działań służb zarządzania kryzysowego. Przedstawiono oprogramowanie QGIS Free i OpenSource Geographic Information System do identyfikacji wybranych obiektów infrastruktury krytycznej na podstawie dostępnych danych GIS Open z regionu Malezji i Polski. W analizie przedstawiono wybrane narzędzia geoprzetwarzania służące do generowania obszarów o ustalonej odległości od zidentyfikowanych obiektów infrastruktury krytycznej zwanych buforami. Warstwy buforowe to obszary widoczne na generowanych mapach, które mogą posłużyć jako narzędzie do wizualizacji potencjalnych działań dla służb zarządzania kryzysowego. Zidentyfikowanie tych stref buforowych umożliwia budowanie strategii wdrażania adekwatnych działań zapobiegawczych lub ratowniczych w sytuacji zagrożenia. Przedstawiono klasyfikację ryzyka w poszczególnych strefach buforowych, która może posłużyć do optymalizacji działań podejmowanych przez służby zarządzania kryzysowego. Zademonstrowano szeroki zakres funkcjonalności systemów informacji przestrzennej geograficznej, który zwiększa efektywność działań i optymalizację podejmowania decyzji w zarządzaniu kryzysowym. Publikacja może stanowić cenny przykład wykorzystania dostępnych systemów informatycznych w zarządzaniu kryzysowym.

Słowa kluczowe: *geomatyka, zarządzanie kryzysowe, infrastruktura krytyczna*

Application of High–resolution Reflection Seismic Attributes for Researching 3D Shallow Marine Geology Structures

Cuong Van Anh LE[*1), 2)], *Man Ba DUONG*[3)], *Thuan Van NGUYEN*[1), 2)], *Truong Ngoc NGUYEN*[1),2)]

[1)] University of Science, Ho Chi Minh City, Vietnam; email: lvacuong@hcmus.edu.vn
[2)] Vietnam National University Ho Chi Minh city, Ho Chi Minh City, Vietnam
[3)] Ho Chi Minh City Institute of Resources Geography, VAST, Vietnam
* Corresponding author: lvacuong@hcmus.edu.vn

http://doi.org/10.29227/IM-2023-01-22

Submission date: 05-03-2023 | Review date: 24-03-2023

Abstract

In river sedimentology and bathymetry study, high–resolution seismic approach equipped with a sub–bottom profiler is necessary. Difference of acoustic impedances resulted by varies of sediment stratigraphy layers can be visualized through dynamic seismic vibration. In marine environments, detection of young sediment as sand dunes or mud, mixtures of sand and clay, and clay formations can help policy makers to launch policies or regulations in safety of water transportation as well as civil building infrastructure. We have measured, analyzed, and interpreted an enormous collection of 2D seismic sub-bottom profiles in Can Gio offshore, Ho Chi Minh City, Vietnam for understanding its shallow subsurface young deposits. Our approach is to combine three key seismic textural attributes (i.e., Correlation, Variance, and Homogeneity) in the representation of color-blended attribute for picking distinguished geological features. In our result, 2D seismic horizons representing boundaries of diverse types of sediments can provide a great input for modeling 3D seabed and distribution of sand, sand-clay mixture, and clay sediments within the interest area. The sand layer useful for mining in this area is strongly affected by channels stemming from Soai Rap river.

Keywords: *high-resolution seismic, textural attribute, bathymetry, color-blend*

1. Introduction

Reflection seismic method is useful in imaging geology boundaries when using exploiting interactions between seismic waves and difference of acoustic impedances (Ianniruberto et al., 2012, Bui Viet et al., 2013, Novak and Björck, 2002). Physics laws (i.e., Snell and Diffraction laws) can guide knowledge of seismic waves responding from the boundaries with underground structures. High resolution seismic reflection is especially compatible with research works for shallow marine sedimentology. Seismic waves emitted from a sub-bottom profiler can propagate downward to seabed, meet sediment formations, and bounce back to its fixed receiver. Smaller energy source comparing to the explosion seismic source, the high-resolution seismic method can only cover quite shallow depth investigations/ scale just around several tens of meters from the seabed.

The reflection signals reveal boundaries of sedimentary matters as mud, sand dunes, clay mixtures, Holocene structures, seabed, river channel sedimentation processes or even seagrass meadow distribution (Ianniruberto et al., 2012, Bui Viet et al., 2013, Le et al., 2020, Laws et al., 2019, Monnier et al., 2021). For improving the reflection seismic interpretation, computation of seismic attributes can be used for revealing many valuable structures or features hidden in abundant information raw seismic data. Overlay image of two attributes (i.e., seismic amplitude and its cosine of phase) can really help to interpret seismic horizons, faults, and channels (Le et al., 2016, Chopra and Marfurt, 2007, Zhao et al., 2015, Le et al., 2019).

We have applied seismic attributes to research sand dunes, young Holocene sediment and seabed by applying their different combinations. The interest area locates in Can Gio offshore, Ho Chi Minh City, Vietnam.

Research projects applied in Can Gio offshore, Ho Chi Minh City, Vietnam focus on seabed, young Holocene sediment and sand layers using high resolution seismic method (Le et al., 2020, Bui Viet et al., 2013, Le Ngoc Thanh et al., 2018). In our research, a workflow of processing seismic attributes from conventionally processed data is applied to 3D modelling sand dunes in Can Gio offshore, Ho Chi Minh City, Vietnam. Moreover, the attributes are color-blended to represent hidden features of each sediment features.

2. Study area

Can Gio District location is important in the socioeconomic development of Ho Chi Minh City because of its natural resources habitat (i.e., big rivers, mangrove Biosphere) (Bao Tuoi Tre, 2020). Can Gio as the southmost isolated island of Ho Chi Minh City has its area as 71,361 ha, containing one third of Ho Chi Minh City area and its 70% area is mangroves and rivers including Long Tau and Soai Rap ones and Its shoreline length is 20 km (People's Committee of District Can Gio Ho Chi Minh City, 2018). The data collection area is the extended southern area, in Can Gio district, Ho Chi Minh City, Vietnam (Fig. 1).

Late Cenozoic (KZ) sediments are widely distributed in Ho Chi Minh City. It is divided into strata, including Pliocene sediments, Early Pleistocene, Middle-Late Pleistocene, Late Pleistocene, and Holocene. The thickness of the late KZ deposits varies depending on the morphology of the rock foundation, ranging from a few tens to several hundred meters

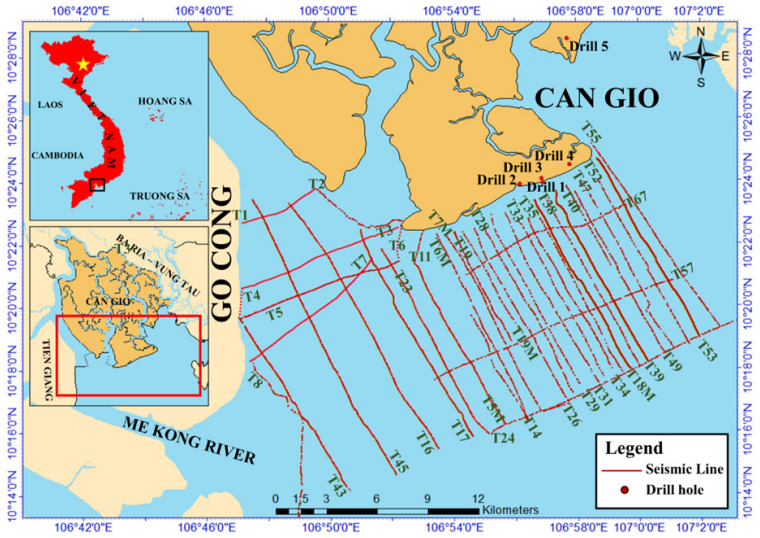

Fig. 1. Location of the survey area for research sediment structures in Can Gio, Ho Chi Minh City, Vietnam (Vietnam Department of Survey)

Rys. 1. Lokalizacja obszaru badawczego do badań struktur osadowych w Can Gio, Ho Chi Minh City, Wietnam (Wietnamski Departament Geodezyjny)

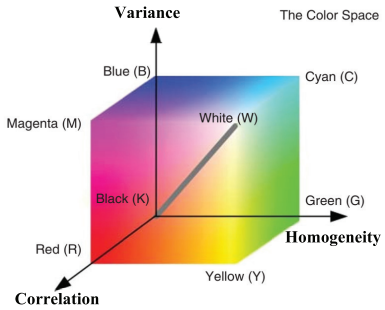

Fig. 2. A representation of three seismic texture attributes (Variance, Homogeneity, and Correlation) compatible with three axes (blue, green, red) of 3D subspace normalized color cube modified from the work of Al-Shuhail et al. (2017). The corners of the cube are shown as red, green, blue, cyan, magenta, yellow, black, and white

Rys. 2. Reprezentacja trzech atrybutów tekstury sejsmicznej (wariancja, jednorodność i korelacja) zgodnych z trzema osiami (niebieska, zielona, czerwona) trójwymiarowego znormalizowanego sześcianu kolorów podprzestrzeni zmodyfikowanego na podstawie prac Al-Shuhaila i in. (2017). Rogi sześcianu są pokazane jako czerwony, zielony, niebieski, cyjan, magenta, żółty, czarny i biały

(Nguyễn Xuân Bao et al., 1994, Hồ Chín et al., 2008, Le Ngoc Thanh et al., 2018, Kitazawa et al., 2006, Kitazawa, 2007).

In Can Gio, bedrock is characterized by old alluvium (Pleistocene sediments) (Nguyễn Xuân Bao et al., 1994, Hồ Chín et al., 2008, Le Ngoc Thanh et al., 2018, Kitazawa et al., 2006, Kitazawa, 2007). It has only a single outcrop at Giong Chua mountain, Thanh An commune. The ancient alluviums are not exposed to the surface, often locating at depths around tens of meters below the Holocene sediments. This ancient alluvial surface is basin-shaped having the great depth more than 40 m in the center of the district and shallower when moving to the sea (at the 30/4 Beach, its surface depth as about 18−20 m). Holocene sediments known as new alluvium are mostly dominant in the ground surface in Can Gio. The new Holocene alluvium includes middle Holocene marine sediments, intertidal sediments, wind-Giong sediments, marine-swamp sediments, river-sea sediments or tidal sediments (Le Ngoc Thanh et al., 2018).

Can Gio formation age is around 8000 to 7000 BP (David et al., 2018, Fujimoto et al., 2011) with the sediment supply of Saigon-Dong Nai River. Marine sediments in the study area were formed by the middle Holocene maximal transgression period (Le Ngoc Thanh et al., 2018). At that time, the sea covered most of the areas, except for the highlands of the ancient alluvium. The material left behind by the advancing sea is quite regular, continuous, and distributed under the receding marine sediments or younger sediments. Many shallow drillholes as the depth a few meters can meet the sediments. The marine sediments have layers of gray-green mud rich in biological remains.

Sand in Can Gio consists of two types, Giong sand and tidal sand (Le Ngoc Thanh et al., 2018). The Giong sand type includes continuous dunes located behind the shoreline. Material of the shore carried by the action of waves and other factors can form Giong sand type. Its heigh is ranging from 1 to 3 m over the surface. Giong sand can be active or inactive. The inactive ones are inland while the active one is set along the shoreline known as the new Giong field. New Giong runs from Dong Tranh cape to Ganh Rai cape and extends for more than 10 km, and its thickness is about 3.5−6.5 m. The other sand type is dependent on the tidal activity. The tidal beach with the lowest height includes sediment stripes around the fork, sea, especially bend of tide rivers. In the Can Gio shoreline, the tidal beach whose maximum thickness is around 3 m is upper soft clay zone (Le Ngoc Thanh et al., 2018).

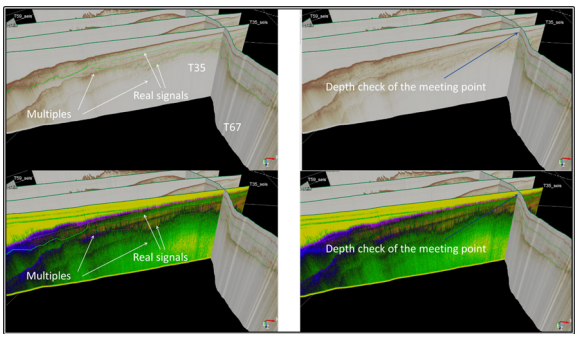

Fig. 3. Quality check of seismic data and 2D seismic interpretation. White arrows represent real signals that help formation of 2D horizons while similar depths are detected proving the excellent quality of the high-resolution seismic data

Rys. 3. Kontrola jakości danych sejsmicznych i interpretacji danych sejsmicznych 2D. Białe strzałki reprezentują rzeczywiste sygnały, które pomagają w tworzeniu horyzontów 2D, podczas gdy wykrywane są podobne głębokości, co dowodzi doskonałej jakości danych sejsmicznych o wysokiej rozdzielczości

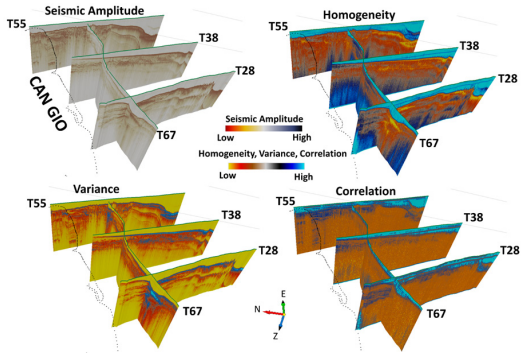

Fig. 4. Representation of 2D conventionally processed seismic amplitude and its seismic texture attributes as Homogeneity, Variance, and Correlation for the 2D seismic profiles T55, T38, T28, and T67

Rys. 4. Reprezentacja 2D konwencjonalnie przetworzonej amplitudy sejsmicznej i jej atrybutów tekstury sejsmicznej, takich jak jednorodność, wariancja i korelacja dla profili sejsmicznych 2D T55, T38, T28 i T67

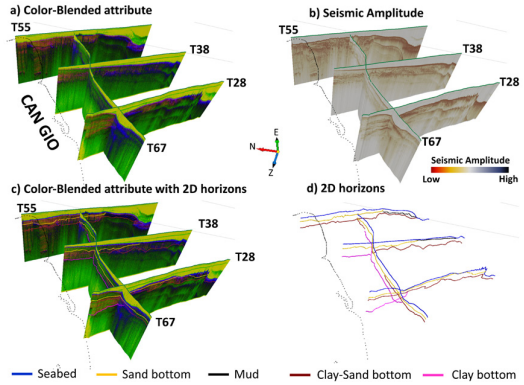

Fig. 5. Representation of 2D interpreted horizons overlaid with the color-blended representation of three seismic texture attributes as Homogeneity, Variance, and Correlation (a, c, d) and the conventionally processed seismic amplitude (b) for the 2D seismic profiles T55, T38, T28, and T67. Sand layer can be bounded by two 2D horizon top and bottom as seabed (blue) and sand bottom (yellow) lines

Rys. 5. Reprezentacja zinterpretowanych horyzontów 2D nałożona na mieszaną kolorystycznie reprezentację trzech atrybutów tekstury sejsmicznej, takich jak jednorodność, wariancja i korelacja (a, c, d) oraz konwencjonalnie przetworzonej amplitudy sejsmicznej (b) dla profili sejsmicznych 2D T55 , T38, T28 i T67. Warstwa piasku może być ograniczona przez dwie górne i dolne linie horyzontu 2D jako dno morskie (niebieskie) i dno piasku (żółte)

3. Methodology

Application of the high-resolution seismic method is well known for researching shallow subsurface marine structures (Bui Viet et al., 2013, Yutsis et al., 2014, Aiello et al., 2014, Le et al., 2020). Physics laws such as reflection, refraction, and diffraction have controlled the seismic wave propagation through the Earth environments.

For researching the shallow marine depth, the Sub-bottom profiler, namely SB-216 (EdgeTech, 2005) installed in a ship is used to measure the seismic vibration data. Data collection is conducted with 38 2D profiles covering the area up to 300 km square in 2017. The underground marine structures are imaged through researching characteristics of wavefield propagation (i.e., traveltime and amplitude) with the sources of frequency modulation having its length from 5 ms to 200 ms and frequency band from 2 to 16 kHz (EdgeTech, 2005). Going deep down to the earth, the seismic echoes from the reflectors are measured by specialized recording system (i.e., hydrophone) (Ianniruberto et al., 2012, Bui Viet et al., 2013, Novak and Björck, 2002).

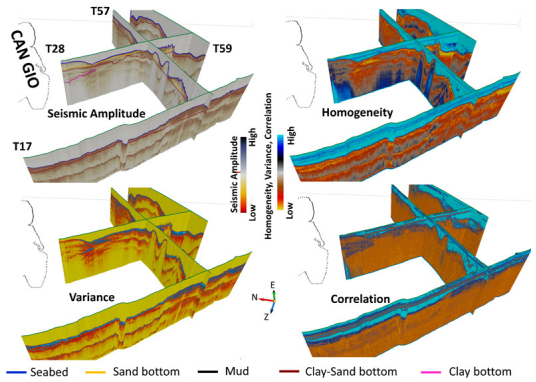

Fig. 6. Representation of 2D conventionally processed seismic amplitude and its seismic texture attributes as Homogeneity, Variance, and Correlation for the 2D seismic profiles T57, T59, T28, and T17

Rys. 6. Reprezentacja 2D konwencjonalnie przetworzonej amplitudy sejsmicznej i jej atrybutów tekstury sejsmicznej, takich jak jednorodność, wariancja i korelacja dla profili sejsmicznych 2D T57, T59, T28 i T17

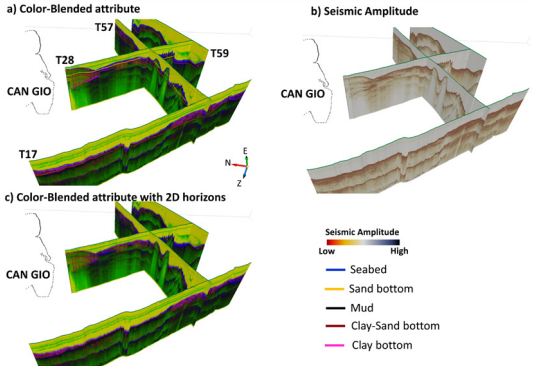

Fig. 7. Representation of 2D interpreted horizons overlaid with the color-blended representation of three seismic texture attributes as Homogeneity, Variance, and Correlation (a, c, d) and the conventionally processed seismic amplitude (b) for the 2D seismic profiles T57, T59, T28, and T17. Sand layer can be bounded by two 2D horizon top and bottom as seabed (blue) and sand bottom (yellow) lines

Rys. 7. Reprezentacja zinterpretowanych horyzontów 2D nałożona na mieszaną kolorystycznie reprezentację trzech atrybutów tekstury sejsmicznej, takich jak jednorodność, wariancja i korelacja (a, c, d) oraz konwencjonalnie przetworzonej amplitudy sejsmicznej (b) dla profili sejsmicznych 2D T57 , T59, T28 i T17. Warstwa piasku może być ograniczona przez dwie górne i dolne linie horyzontu 2D jako dno morskie (niebieskie) i dno piasku (żółte)

Prior data interpretation, two analysis stages are applied as processing and seismic attributes computing:

In data processing, transformation of raw data to interpretable data in 2D visualization is done with the help of the professional software packages, Reflexw (Sandmeier, 2020). Conventional routines such as Substract – DC – Shift and Divergent (div.) Compensation Gain are applied to all the 2D seismic profiles (Le et al., 2020, Sandmeier, 2020). The Compensation Gain filter helps to increase the weak amplitude of seismic signals in deeper part when the waves lose their energy because of spherical energy dissipation (Sandmeier, 2020).

OpendTect (dGB Earth Sciences, 2015) provides tools for computation of seismic attributes. The processed seismic data and its seismic attributes are mutual support for seismic horizons interpretation. In our research, representation of seismic textures attributes and their combination via color-blending are used to to reveal distinguished seismic patterns that reflect marine sediments (i.e., sand or mixtures of sand clay). The attributes are Variance, Homogeneity and Correlation.

3.1 Seismic Texture Attributes

2D horizons can be picked from strong seismic reflection amplitudes (Yilmaz, 2001, Le et al., 2020, Le et al., 2019, Le et al., 2016, Chopra and Marfurt, 2007). However, its seismic texture attributes play important roles in depicting many hidden geological features that the conventional seismic amplitude can miss. In our works, three texture attributes as Variance, Homogeneity, and Correlation (Le et al., 2019, Haralick et al., 1973, dGB Earth Sciences, 2015) are used for data interpretation. To process the texture attributes, two stages are following included:

(i) Calculation of the grey – level – occurrence Matrix (GLCM) (Hall-Beyer, 2007, Haralick et al., 1973, Wang, 2018). In this paper, the true seismic data (i.e., 2D matrix) can be rescaled into a new 32-bit integer data whose values range from 0 to (2^{32}-1). From equation 1, the new 32-bit data is namely matrix G(x,y) and GLCM matrix is $P_{i,j}$.

$$P_{i,j} = \sum_{x=0}^{N-1} \sum_{y=0}^{N-1} \begin{cases} 1, & G(x,y) = i \text{ and } G(x+\Delta x, y+\Delta y) = j, \\ 0, & \text{otherwise} \end{cases} \quad (1)$$

where x, y are spatial positions and Δx, Δy are offsets in x and y directions, respectively.

(ii) Specific equations for their texture definitions (Le et al., 2019, Haralick et al., 1973, dGB Earth Sciences, 2015):

$$\text{Variance} = \sum_{i=0}^{N-1} \sum_{j=0}^{N-1} (i-\mu_i)^2 P_{i,j} \quad (2)$$

$$\text{Homogeneity} = \sum_{i=0}^{N-1} \sum_{j=0}^{N-1} \frac{P_{i,j}}{1+|i-j|} \quad (3)$$

$$\text{Correlation} = \sum_{i=0}^{N-1} \sum_{j=0}^{N-1} \frac{ijP_{i,j}-\mu_x\mu_y}{\sigma_x\sigma_y} \quad (4),$$

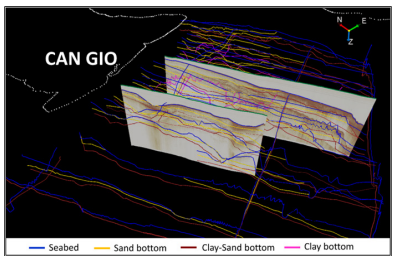

Fig. 8. Representation of 2D seismic horizons interpreted from the seismic sections. Blue lines represent seabed, yellow for bottom of sand layer, magenta for bottom of clay, and red for bottom of clay-sand mixture

Rys. 8. Reprezentacja poziomów sejsmicznych 2D zinterpretowanych na podstawie przekrojów sejsmicznych. Niebieskie linie reprezentują dno morskie, żółte dno warstwy piasku, karmazynowe dno gliny, a czerwone dno mieszanki gliny i piasku

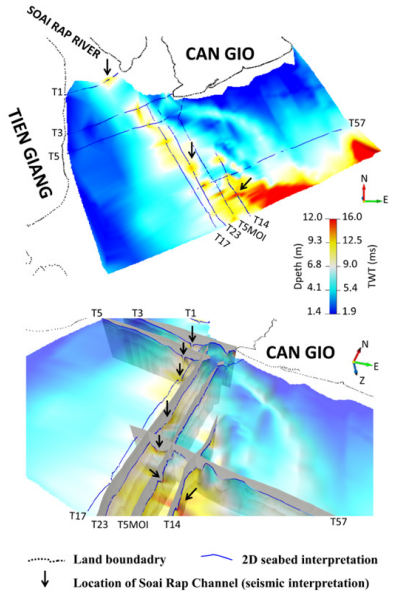

Fig. 9. 3D seabed represents geometry of Soai Rap channel (top and bottom images). The red color zones show its distinguished depth. For clarity, its positions can be detected through positions of black arrows

Rys. 9. Trójwymiarowe dno morskie przedstawia geometrię kanału Soai Rap (zdjęcia górne i dolne). Strefy koloru czerwonego pokazują jego wyróżniającą się głębię. Dla jasności jego pozycje można wykryć za pomocą pozycji czarnych strzałek

where $\mu_i = \sum_{i=0}^{N-1} \sum_{j=0}^{N-1} iP_{i,j}$; μ_x, μ_y, σ_x, and σ_y are the means and standard deviations for p_x and p_y (Haralick et al., 1973). p_x and p_y are sums of each row or column from the GLCM matrix $P_{i,j}$, respectively.

3.2 Color-blended Approach

The color-blended display technique is to form a color – blended representation that provides significantly clear detailed features (dGB Earth Sciences, 2015, Al-Shuhail et al., 2017, Chopra and Marfurt, 2007). Three seismic attributes as Variance, Homogeneity, and Correlation are rendered with specific color bands as red, green, and blue, respectively (Fig. 2).

The RGB model is commonly used on many visualization applications. The three attributes with each color are put into a RGB interface (Al-Shuhail et al., 2017). Each attribute is defined in the range of [0, 255] for 8-bit integer value. In other word, each RGB pixel have a scale of 24 bits. Then, each RGB value composed of three RGB elements can have $(2^8)^3$ = 16777216 colors that are shown in the Fig. 2.

3.3 Interpretation of 2D/3D Seismic Horizons

Interpretation of 2D seismic horizons for each type of sediment plays a key role in forming its 3D horizon. Understanding a sediment layer needs interpretation of its top and bottom 2D horizons.

A 2D seismic horizon is chosen from conformity of seismic waveforms in its seismic data or its similar seismic pattern (Le et al., 2016, Le et al., 2019, Yilmaz, 2001, Le et al., 2020). The similar seismic pattern can be extracted from the representation of seismic attributes as conventional seismic amplitude, texture attribute or even combination of two/three simultaneous attributes (i.e., color-blend attribute). Besides, multiple noises (i.e., Fig. 3) are cumbersome for interpreting seismic horizons, and they should be firstly detected before further interpretation.

The workflow for building a 3D surface consists of (i) a set-up of 2D interpreted seismic horizons and (ii) an interpolation algorithm. For the interpolation process, the Matlab built-in function, scatteredInterpolant.m (MathWorks, 2019) is used with linear approach. For converting two-way travel time (TWT) to depth domain, sound velocities are assumed to be 1500 m/s and 1550 m/s for sea water and shallow sediment environments, respectively (Le et al., 2020).

Data validity checking is important in deciding whether a 2D seismic line is good or not. For example, similar depths of two or three 2D seismic lines in their meeting points should be confirmed (Le et al., 2020) (see Fig. 3).

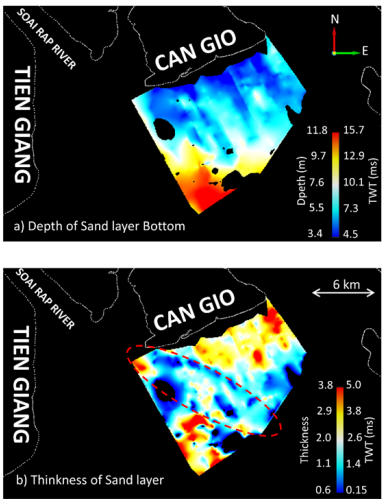

Fig. 10. Representation of the sand depth bottom (a) and its thickness (b). Note that existence of Soai Rap channel (stemming from Soai Rap river) can wipe out sand layer in the interest area. The red dashed ellipse refers to the sand zone with the smallest thickness

Rys. 10. Reprezentacja głębokości dna piasku (a) i jego miąższości (b). Należy zauważyć, że istnienie kanału Soai Rap (wynikającego z rzeki Soai Rap) może zniweczyć warstwę piasku w obszarze zainteresowania. Czerwona przerywana elipsa odnosi się do strefy piasku o najmniejszej miąższości

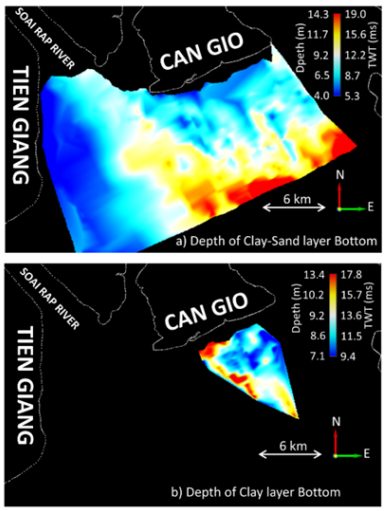

Fig. 11. 3D Horizons of the clay-sand mixture and clay bottom

Rys. 11. Horyzonty 3D mieszaniny iłowo-piaskowej i dna ilastego

4. Results and discussion

Seabed interface is the easiest to pick because of its visible reflection seismic amplitude. There does not need big effort to interpret the 2D horizons and 3D interpolation can be straightforward calculated from the 2D results. 2D horizons for seabed shown can represent boundaries of water volume and marine sediments. The seismic amplitude, its seismic attributes as textures or color blend can quickly show the 2D horizons for each seabed in any 2D seismic line (i.e., See Figs. 4 and 5). The water volume is visualized through the first prominent white zones from water level in seismic amplitude section, the cyan ones in Homogeneity and Correlation sections, the first yellow zone in Variance section and Color-blend sections (Figs. 4, 5 and 6).

For interpretation of other horizons relating to different sediments, we have calculated different seismic attributes. Figs. 5 to 8 are used to represent images of seismic amplitude input and the seismic textures as Homogeneity, Variance, and Correlation. The interpreted information are horizons of seabed, sand Bottom, clay-sand mixture (Mixture of Sand and Clay components), mud, and clay.

We have used different seismic attributes for specifying the bottom of each sediment type. Color-blended attribute and seismic amplitude are very useful in categorizing them. One example shown in Fig. 8 can show the different pattern of sand and clay type in both seismic and color blended images. Then, all 2D horizons of the sediments can be shown in Fig. 9, that would be input for 3D interpolation.

4.1 Seabed interpretation

3D interface interpolated from the 2D horizons (Fig. 9) can reflect bigger view of Soai Rap channel that was indicated in Thuan Nguyen et al 's work (2022). Overall, the sea depth looks gradually increasing from 2 m to 16 m when going far from the Can Gio shoreline although there're some channels wandering near the shoreline. According to the 3D seabed interpretation (see black arrows in Fig. 9), the direction of the Soai Rap channel is strongly influenced by the Soai Rap river.

4.2. Sand and other sediments' interpretation

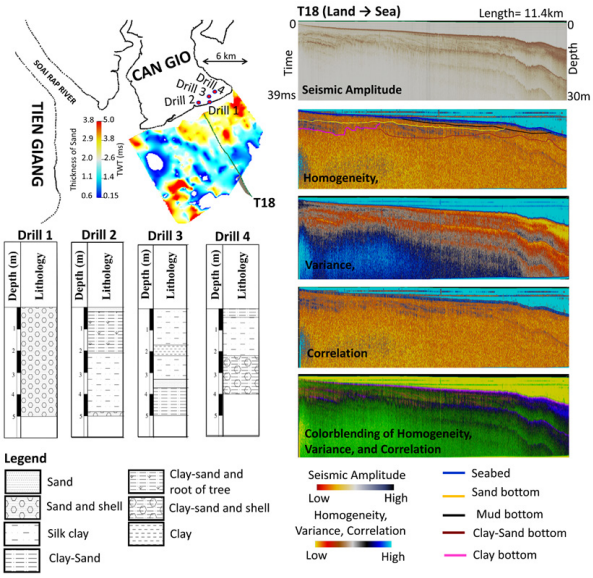

Fig. 12. Representation of 3D Horizons of the Sand thickness, the seismic data for the 2D profile T18, and information in the four drills (Drill 1, 2, 3, and 4). Note sediment types in Drills 1, 2, 3, and 4 are extracted from documents of Ho Chi Minh City Institute of Resources Geography, VAST, Vietnam (Le Ngoc Thanh et al., 2018)

Rys. 12. Reprezentacja horyzontów 3D miąższości piasku, dane sejsmiczne dla profilu 2D T18 oraz informacje z czterech odwiertów (wiertło 1, 2, 3 i 4). Uwaga typy osadów w wiertarkach 1, 2, 3 i 4 pochodzą z dokumentów Ho Chi Minh City Institute of Resource Geography, VAST, Wietnam (Le Ngoc Thanh et al., 2018)

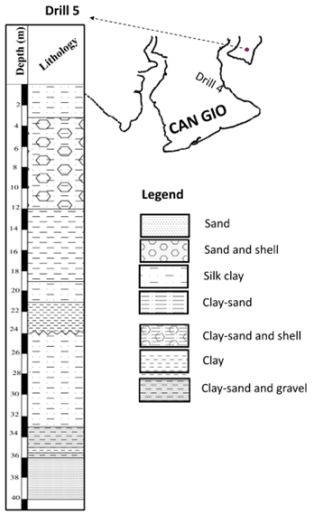

Fig. 13. Sediment information extracted from Drill 5. Note that information of sediment types are extracted from documents of Ho Chi Minh City Institute of Resources Geography, VAST, Vietnam (Le Ngoc Thanh et al., 2018)

Rys. 13. Informacje o osadach pobrane z wiertła 5. Należy zauważyć, że informacje o typach osadów pochodzą z dokumentów Instytutu Geografii Zasobów Miasta Ho Chi Minh, VAST, Wietnam (Le Ngoc Thanh i in., 2018)

We focused on sand, clay, clay-sand mixture signatures where we could build 3D horizons (Figs. 10 and 11). The sediment information for the seismic layer interpretation can be extracted from near drill holes in the shoreline (Le Ngoc Thanh et al., 2018) (Figs. 12 and 13).

From the interpretation of the drill holes (Figs. 12 and 13), clay layer is upper the Clay-sand Mixture layer. Imaging sand distribution is important because of its value. The near shoreline drill hole in Can Gio peninsula can confirm the sand existence in the shallow depth that is compatible with seismic data. For the deepest drill hole 5 with 40 m in Thanh An commune (Fig. 13), the sand, clay, clay-sand mixture are existed that can be used for interpreting the seismic data.

According to sediment interpretation from the color-blend attribute (i.e., Figs 3, 4, 5, and 12), sand looks like respond to green components, clay looks mix of all three colors (green, red, and blue), and clay-sand are seen mostly blue. Note that picking all horizons needs to visualize different pattern of seismic attributes including the conventionally processed seismic and seismic attributes.

For the sand distribution (Fig. 10), the sand erosions may exist because of the water flows of Soai Rap River and Soai Rap channel. That is, two different zones of sand are separated by the zone of the smaller thickness (See dashed red ellipse in Fig. 10) which shares the similar location of Soai Rap channel (See black arrows in Fig. 9).

The clay-sand mixture sediment has tendency to exist in the entire interest area while the clay layer just appears in the margin of Can Gio Peninsula (Fig. 11).

4. Conclusion

3D image of seabed and sand sedimentation in area of Can Gio district, Ho Chi Minh city, Vietnam can be presented using application of 2D high resolution seismic data. We have applied different seismic attributes for imaging sediment types, especially sand zone. 2D seismic horizons are the input for building 3D horizons. Distinguished Soai Rap channel can be further expressed in the bigger picture. We can notice that seismic interpretation of the sand, clay, and clay-sand mixture layers is compatible to information of drill holes in Can Gio.

5. Acknowledgments

This research is funded by University of Science, VNU-HCM under grant T2022-55. We would like to thank Dr. Le Ngoc Thanh and Mr. Nguyen Quang Dung for their helps. We are also grateful to dGB Earth Sciences and Curtin University for providing access to software tools.

6. Conflicts of Interest

The authors declare no conflict of interest.

Literatura – References

1. AIELLO, G., DI FIORE, V., MARSELLA, E. & PASSARO, S. 2014. High resolution seismic data coupled to Multibeam bathymetry of Stromboli island collected in the frame of the Stromboli geophysical experiment: implications with the marine geophysics and volcanology of the Aeolian Arc volcanic complex (Sicily, Southern Tyrrhenian sea, Italy). SpringerPlus, 3, 1-27.
2. AL-SHUHAIL, A. A., AL-DOSSARY, S. A. & MOUSA, W. A. 2017. Seismic data interpretation using digital image processing, John Wiley & Sons.
3. BAO TUOI TRE. 2020. Luồng Soài Rạp chính thức cho tàu biển 30.000 tấn về TP.HCM, Long An [Online]. Available: https://tuoitre.vn/luong-soai-rap-chinh-thuc-cho-tau-bien-30-000-tan-ve-tp-hcm-long-an-20200826115103097.htm [Accessed November 5th, 2021.
4. BUI VIET, D., STATTEGGER, K., UNVERRICHT, D., PHUNG VAN, P. & NGUYEN TRUNG, T. 2013. Late Pleistocene–Holocene seismic stratigraphy of the Southeast Vietnam Shelf. Global and Planetary Change, 110, 156-169.
5. CHOPRA, S. & MARFURT, K. J. 2007. Seismic attributes for prospect identification and reservoir characteriztion, United States of America, Tulsa, Okla. (8801 South Yale St., Tulsa OK 74137-3175) : Society of Exploration Geophysicists.
6. DAVID, F., MEZIANE, T., TRAN-THI, N.-T., VAN, V. T., THANH-NHO, N., TAILLARDAT, P. & MARCHAND, C. 2018. Carbon biogeochemistry and CO 2 emissions in a human impacted and mangrove dominated tropical estuary (Can Gio, Vietnam). Biogeochemistry, 138, 261-275.
7. DGB EARTH SCIENCES 2015. OpendTect dGB Plugins User Documentation version 4.6.
8. EDGETECH. 2005. Edgetect introduces new Portable Sub-Bottom Profiling System [Online]. Available: https://www.edgetech.com/edgetech-introduces-new-portable-sub-bottom-profiling-system/ [Accessed 15/04/2020.
9. FUJIMOTO, K., UMITSU, M., NGUYEN, V. L., TA, T. K. O., KAWASE, K., HUYNH, D. H. & NAKAMURA, T. 2011. Geomorphological evolution and mangrove habitat dynamics related to Holocene sea-level changes in the northern Mekong river delta and the Dong Nai river delta, southern Vietnam. In: PAUL E. SCHMIDT (ed.) River Deltas: Types, Structures and Ecology. Nova Science Publishers, Inc.
10. HALL-BEYER, M. 2007. GLCM Texture Tutorial [Online]. Available: http://www.fp.ucalgary.ca/mhallbey/tutorial.htm 03 May 2016].
11. HARALICK, R. M., SHANMUGAM, K. & DINSTEIN, I. 1973. Textural features for image classification. IEEE Transactions on systems, man, and cybernetics, 3, 610-621.
12. HỒ CHÍN ET AL. 2008. Mở rộng khảo sát địa chất trầm tích Đệ Tứ Cù lao Phú Lợi (Cần Giờ) phục vụ du lịch. Viện Địa lý tài nguyên TPHCM.
13. IANNIRUBERTO, M., CAMPOS, J. E. & ARAÚJO, V. 2012. Application of shallow seismic profiling to study riverbed architectural facies: A case study of the Tocantins river (Pará-Brazil). Anais da Academia Brasileira de Ciências, 84, 645-654.
14. KITAZAWA, T. 2007. Pleistocene macrotidal tide-dominated estuary–delta succession, along the Dong Nai River, southern Vietnam. Sedimentary Geology, 194, 115-140.
15. KITAZAWA, T., NAKAGAWA, T., HASHIMOTO, T. & TATEISHI, M. 2006. Stratigraphy and optically stimulated luminescence (OSL) dating of a Quaternary sequence along the Dong Nai River, southern Vietnam. Journal of Asian Earth Sciences, 27, 788-804.

16. LAWS, A. W., MALONEY, J. M., KLOTSKO, S., GUSICK, A. E., BRAJE, T. J. & BALL, D. 2019. Submerged paleoshoreline mapping using high-resolution Chirp sub-bottom data, Northern Channel Islands platform, California, USA. Quaternary Research, 93, 1-22.

17. LE, C. V. A., DUONG, M. B. & KIEU, T. D. 2020. High–Resolution Seismic Reflection Survey of Holocene Sediment Distribution at Thi Vai River, Ho Chi Minh City, Vietnam. Lecture Notes in Civil Engineering. Springer.

18. LE, C. V. A., HARRIS, B. D. & PETHICK, A. M. 2019. New perspectives on Solid Earth Geology from Seismic Texture to Cooperative Inversion. Scientific Reports, 9, 14737.

19. LE, C. V. A., HARRIS, B. D., PETHICK, A. M., TAKAM TAKOUGANG, E. M. & HOWE, B. 2016. Semiautomatic and Automatic Cooperative Inversion of Seismic and Magnetotelluric Data. Surveys in Geophysics, 37, 845-896.

20. LE NGOC THANH, NGUYEN SIEU NHAN, NGUYEN TIEN ANH MINH, NGUYEN QUANG DUNG, DUONG BA MAN & VO THI HONG QUYEN 2018. Research and assessment of the potential natural resources at Can Gio Offshore, Ho Chi Minh City and proposed solutions for suitable protection. Ho Chi Minh City Institute of Resources Geography, VAST, Vietnam.

21. MATHWORKS. 2019. Interpolate 2-D or 3-D scattered data [Online]. Available: https://www.mathworks.com/help/matlab/ref/scatteredinterpolant.html 2020].

22. MONNIER, B., PERGENT, G., MATEO, M. Á., CARBONELL, R., CLABAUT, P. & PERGENT-MARTINI, C. 2021. Sizing the carbon sink associated with Posidonia oceanica seagrass meadows using very high-resolution seismic reflection imaging. Marine Environmental Research, 170, 105415.

23. NGUYỄN XUÂN BAO ET AL. 1994. Địa chất và khoáng sản tờ Thành phố Hồ Chí Minh tỉ lệ 1:200.000. Liên đoàn Địa chất miền Nam.

24. NOVAK, B. & BJÖRCK, S. 2002. Late Pleistocene–early Holocene fluvial facies and depositional processes in the Fehmarn Belt, between Germany and Denmark, revealed by high-resolution seismic and lithofacies analysis. Sedimentology, 49, 451-465.

25. PEOPLE'S COMMITTEE OF DISTRICT CAN GIO HO CHI MINH CITY. 2018. Overview of Can Gio [Online]. Available: https://cangio.hochiminhcity.gov.vn/-/khai-quat-tinh-hinh-huyen-duyen-hai-can-gio-sau-ngay-chien-thang-30-4-1975?redirect=%2Fgioi-thieu%2Fgioi-thieu-chung [Accessed 9/9/2022 2022].

26. SANDMEIER, K.-J. 2020. Reflexw - GPR and seismic processing software [Online]. Available: https://www.sandmeier-geo.de/reflexw.html [Accessed July 7th, 2020.

27. VIETNAM DEPARTMENT OF SURVEY, A. M. A. G. I. Administrative Map of Socialist Republic of Vietnam [Online]. Available: https://www.bandovn.vn/vi/page/mau-ban-do-hanh-chinh-nuoc-cong-hoa-xa-hoi-chu-nghia-viet-nam-181 [Accessed August 11th, 2020.

28. WANG, Z. 2018. Computational seismic interpretation using geometric representation and tensor-based texture analysis. Georgia Institute of Technology.

29. YILMAZ, O. 2001. Seismic Data Analysis: Processing, Inversion, and Interpretation of Seismic Data, United States of America, Society of Exploration Geophysicists.

30. YUTSIS, V., KRIVOSHEYA, K., LEVCHENKO, O., LOWAG, J., DE LEÓN GÓMEZ, H. & PONCE, A. T. 2014. Bottom topography, recent sedimentation and water volume of the Cerro Prieto Dam, NE Mexico. Geofísica internacional, 53, 27-38.

31. ZHAO, T., JAYARAM, V., ROY, A. & MARFURT, K. J. 2015. A comparison of classification techniques for seismic facies recognition. Interpretation.

Zastosowanie atrybutów sejsmicznych odbić o wysokiej rozdzielczości do badania struktur 3D płytkiej geologii morskiej

W badaniach sedymentologicznych i batymetrycznych rzek konieczne jest podejście sejsmiczne o wysokiej rozdzielczości wyposażone w profiler poddenny. Różnicę impedancji akustycznych wynikającą ze zmienności warstw stratygraficznych osadów można zwizualizować za pomocą dynamicznych drgań sejsmicznych. W środowiskach morskich wykrywanie młodych osadów, takich jak wydmy lub błoto, mieszanki piasku i gliny oraz formacje gliny, może pomóc decydentom we wprowadzaniu polityk lub przepisów dotyczących bezpieczeństwa transportu wodnego, a także infrastruktury budynków cywilnych. Zmierzyliśmy, przeanalizowaliśmy i zinterpretowaliśmy ogromny zbiór profili sejsmicznych 2D pod dnem w Can Gio na morzu w mieście Ho Chi Minh w Wietnamie, aby zrozumieć jego płytkie, podpowierzchniowe młode złoża. Nasze podejście polega na połączeniu trzech kluczowych atrybutów tekstury sejsmicznej (tj. Korelacji, Wariancji i Jednorodności) w reprezentacji atrybutu mieszania kolorów w celu wybrania wyróżniających się cech geologicznych. W naszym wyniku, poziomy sejsmiczne 2D reprezentujące granice różnych typów osadów mogą stanowić doskonały materiał wejściowy do modelowania 3D dna morskiego i rozmieszczenia piasku, mieszanki piaskowo-gliniastej i osadów gliniastych w obszarze zainteresowania. Na warstwę piasku przydatnego do wydobycia na tym obszarze duży wpływ mają kanały wychodzące z rzeki Soai Rap..

Słowa kluczowe: *sejsmika wysokiej rozdzielczości, atrybut tekstury, batymetria, mieszanie kolorów*

Methodology for Determining Emissions of Pollutants into Atmospheric Air by Open-Pit Mining Works

Vadym SHCHOKIN[1)], Vladislav YEZHOV[2)], Olga SHCHOKINA[3)], Wiktoria SOBCZYK[4)]

[1)] Doctor tech. Sciences, Professor, Director of the Research Mining Institute of Kryvyi Rih National University; ORCID https://orcid.org/0000-0001-9709-1831; email: vadim.shchokin@gmail.com
[2)] PhD, Director of the Research Institute of Labor Safety and Ecology in the Mining and Metallurgical Industry of the Krivoy Rog National University; ORCID https://orcid.org/0009-0002-9638-1030
[3)] Senior Research Institute of Labor Safety and Ecology in the Mining and Metallurgical Industry of the Krivoy Rog National University; ORCID https://orcid.org/0000-0002-0275-8646
[4)] Prof. PhD, Eng. Faculty of Energy and Fuels, AGH University of Science & Technology, Krakow, Poland; ORCID https://orcid.org/0000-0003-2082-9644

http://doi.org/10.29227/IM-2023-01-23

Submission date: 15-03-2023 | Review date: 04-04-2023

Abstract

In recent years, significant changes have occurred in the mining industry in the qualitative and quantitative indicators of technical means and materials used during the open mining of iron ore. Technical parks of loading and unloading and transport equipment have been updated, new types of explosives have appeared. Currently, there are no methods for calculating emissions of pollutants into atmospheric air from modern mining equipment.

In 1989, the "Methodology for calculating emissions of harmful substances from quarries taking into account the non-stationarity of their technological processes" was developed, which today no longer takes into account the above-mentioned factors and needs revision and additions.

"Methodology for determining emissions of pollutants into atmospheric air by open-pit mining works" was created on the basis of "Methodology for calculating emissions of harmful substances from pits taking into account the non-stationary nature of their technological processes" of 1989, as well as the data from industrial research and instrumental measurements of atmospheric air pollution during various technological processes in pits at dumps and tailings storages, which have been carried out in recent years.

Thus, the developed "Methodology for determining emissions of pollutants into the air by open-pit mining works" includes the data from the methodology of 1989, which are still relevant today, the data on technical characteristics and parameters of the equipment presently used by open-pit mining works, as well as the results of scientific research conducted by the Research Institute of Labour Safety and Ecology in the Mining and Metallurgical Industry of Kryvyi Rih National University.

The basis for development of the "Methodology for determination of emissions of pollutants into the atmospheric air by open-pit mining works" is the need to determine the amount of emissions of pollutants into the atmospheric air from modern technological processes and equipment of open-pit mining operations.

Keywords: *opencast mining, methodology, emissions, non-stationarity, technological processes*

Mining of iron ores by an open method, depending on the accepted system of discovery and development of a deposit, is associated with certain technological processes: drilling and blasting of the mining massif, loading, moving and unloading of the mining mass, as well as technological processes during work on tailings and sludge storages and during dump formation. Special mining transport equipment is used to carry out technological processes in quarries, dumps, tailings and sludge storages.

Drilling of shafts is carried out mainly by drilling machines of mechanical impact on the bottom of shafts. Machine tools for drilling holes are used as machines for mechanical impact, which pass the shafts with 160–320 mm diameter down to the depth of 35 m, as well as drilling rigs of imported production, such as Atlas Copco are used, which drill the shafts with the diameter of 110–270 mm.

Explosive rocks in pits are carried out by separate blocks with single-row or multi-row arrangement of shafts using various types of explosives. The amount of explosives detonated simultaneously in one mass explosion reaches more than 1,000 tons. When mass explosions are carried out, a significant amount of dust and harmful gases are formed, which are carried out of the pit space in the form of a dust and gas cloud and dispersed over considerable distances. At the same time, a part of the harmful gases remains in the blasted mining mass, which is released into the atmosphere during its excavation.

Excavation of mining rocks and loading into vehicles is carried out by excavators of ECG type, with a bucket capacity of 4; 4.6; 8; 10; 12.5 and15 m^3, as well as excavators of imported production, for example, TEREX, CATERPILLAR, HITACHI and Komatsu.

The movement of the mining mass from the mines to the reception points and the delivery of auxiliary loads in the pit is carried out by mining transport. Cyclic transport is mainly used in pits. Cyclic types of transport include rail and road ones. Diesel-powered dump trucks with a carrying capacity of 27–230 tons are used as vehicles. Trains with 6–12 dump trucks with a carrying capacity of 90–140 tons each with a

capacity of up to 150 m^3. Electric, diesel and diesel-electric locomotives are used as traction [1, 2].

Overburden and substandard minerals, which are mined in the pit during the development of the deposit, are removed to dumps. The process of dump formation is determined by the type of mining transport equipment that moves the rock into the dump, and is divided into bulldozer, excavator and conveyor dump formation. The dusty surfaces of the formed dumps are also powerful sources of dust emission.

During washing of enrichment waste (tailings), as well as during the construction of dams from tailings, separate areas of up to 30–100 hectares or more are formed, which remain dehydrated for several months a year. Dry beaches of tailings are the intensive sources of dust emission. The fractional composition of the upper layer of the beaches of the tailings ponds has a slight difference. Therefore, the intensity of dust blowing from the surface of dry beaches will mainly depend on the wind speed and the humidity of the tails.

In iron ore pits, the sources of release of harmful substances are mainly unorganized. In addition, almost all production processes in pits are characterized by cyclicity, so the sources of allocation are non-stationary in time.

When calculating dust emissions from dusty surfaces of dumps and dry beaches of tailings, climatic conditions such as material freezing, snow cover, and seasonal precipitation should be taken into account.

Emissions of polluting substances into the atmosphere are determined based on the application of the following methods:

- instrumental ones, which use the results of direct measurements of the concentrations of harmful substances in emissions, as well as their parameters (speed of movement, consumption, etc.). These include the method of sampling various pollutants, the method of timing the working time and downtime of equipment, etc.;
- calculations using the results of analytical and instrumental methods. These include the method of calculating the intensity of emission of pollutants, determining the parameters of the dust and gas cloud, the method of approximating functions, etc.

Technical indicators of technological processes (equipment productivity, material consumption, parameters of emission sources, etc.), as well as specific emissions of pollutants per unit of process indicator, are determined by the indicated methods.

By summing up the value of pollutant release from the source over time, their annual indicators are determined for a certain equipment or technological process.

For a qualitative and quantitative assessment of the impact of technological processes and mining transport equipment on atmospheric air pollution of pits and the convenience of calculating this impact, a classification of pollutant emission sources is necessary.

The sources of emissions are determined by each technological process. Depending on the goal, the source of emissions can be:

- a separate unit of equipment;
- the sum of emissions from all technological equipment involved in this process. In this case, the emission source model will represent a stylized (equivalent) emission source with averaged parameters (height, area, coordinates, etc.) and the sum of emissions from all similar emission sources.

The linear dimensions of the emission sources are determined by the features of the technological process and the dimensions of the mining transport equipment and its quantity.

The height of the sources located in the pit is determined taking into account the minimum height of the ground sources of unorganized emissions, which is equal to 2 m [1] or the height of the discharge source (drawing height, body height, etc.), and the height of the vane, where the wind speed is determined (10 m).

For a single drilling rig, a model of a planar unorganized source and a height, that takes into account the minimum height of the ground source and the height of the weather vane, is adopted.

Due to the rapidity of the rock blasting process (fractions of a second), the maximum one-time emission of pollutants during mass explosions, as a rule (for example, when setting standards for pollutant emissions), is not determined. At the same time, the actual amount of emissions in g/s may not have a physical meaning if the emission itself will last less than 1 s. But in cases where it is necessary to determine the impact of mass explosions on the border of the sanitary protection zone or on the border of the residential zone, it is necessary to calculate the dispersion of polluting substances during the mass explosion. For this purpose, equivalent maximum single emissions of pollutants are defined, reduced to a twenty-minute time interval, which values can be used as the input data for the scattering calculation program. For each block that is blown up, the equivalent pollutant emission reduced to a 20-minute interval is taken from a plane source with sides equal to the length and width of the block and a height equal to the depth of the shaft on the block, taking into account the minimum height of the ground source.

For a single excavator slaughter a plane source with dimensions equal to the maximum scooping radius of the excavator is accepted taking into account the height of the vane.

The linear dimensions of the planar source of emissions during the movement of motor vehicles on quarry or dump roads are accepted depending on the dimensions of the dump truck body and the number of dump trucks that are simultaneously in the pit or on the dump. The height of the source is taken taking into account the height of the dump truck and the height of the vane.

For railway transport operating in a quarry or on a dump, a plane source with linear dimensions of the train (locomotive and wagons) and heights taking into account the height of the dump truck and the height of the vane is accepted.

For a bulldozer, given that the main place of its work in a pit is an excavator pit, a planar type of source is adopted with parameters similar to those of an excavator pit with a source height that takes into account the minimum height of the ground source and the height of the vane.

Depending on the type of landfill (excavator or bulldozer), the source of pollutant emissions will be planar. The cyclicity of dust generation will be determined by the cyclical operation of the technological equipment.

In addition, dust is also released from the folded surface during the formation of a dump. The rise of dust depends on the type of mining mass, its granulometric composition, meteorological conditions, etc. The process of lifting dust from the surface of the dump over time has a cyclical nature, which depends on the above mentioned factors. The characteristic dimensions of the planar source of emissions in this case will be determined by the area of the sawing surface of the operating dumps, with the exception of the part where the technological processes are carried out.

In addition to the fixed stationary sources in the pit, there will also be mobile sources (internal combustion engines of mining transport vehicles – dump trucks, diesel locomotives and bulldozers).Emissions from mobile sources should also be taken into account when assessing the object's impact on the air environment (calculation of dispersion). For this purpose, mobile sources are presented in the form of conventional unorganized sources with defined spatial coordinates. For the pit, these mobile sources have the same coordinates as the corresponding ("Auto dumpcar", "Dumpcar", "Bulldozer") unorganized sources.

Specific emissions of pollutants from mobile sources are determined according to [2, 3] or by the characteristics of the equipment.

The purpose of the developed "Methodology for determination of emissions of pollutants into the atmospheric air by open-pit mining works" is the qualitative and quantitative assessment of emissions of pollutants into the atmospheric air during the conduct of open-pit mining works on the basis of their specific emissions. The "Methodology..." determines the emissions of pollutants into the atmospheric air from unorganized sources of emissions, taking into account the non-stationarity of the operation of technological equipment and the conduct of technological processes by open-pit mining works. The "Methodology..." is intended as a normative document for calculations and evaluation of emissions of pollutants into atmospheric air in pits, dumps and tailings.

The obtained results of calculations of emissions of pollutants into atmospheric air according to the "Methodology..." can be used:

- for compilation of statistical reports and for development of permission documents, provided for by the legislation of Ukraine;
- for development of project and pre-project documentation for enterprises with open ore mining;
- for planning the amount of damage to the environment and the measures for its protection.

Literatura – References

1. OND-86 (1987). Methodology for calculating concentrations in atmospheric air of harmful substances contained in the emissions of enterprises. L.: Gidrometeoizdat, 92.
2. Methods of calculating emissions of pollutants by mobile sources (1999). Donetsk: UkrNTEK, 107.
3. Shchokin, V., Ezhov, V., Shchokina, O.& Chasova, E. (2021). Degasification and removal of dust at mass explosions in pits using a humate reagent in the internal and external storage. Ukrainian Journal of Ecology, 11(1), 132-138.
4. Gerasimchuk, O., Shchokin, V., Zamriy, S. & Ezhov, V. (2021). Degasation and dust control methods in major blasts in the open pit of inguletsky ore mining and processing complex (INGOK). Research and industrial tests results. Ukrainian journal of ecology 11(8), 99-105, doi: 10.1 5421/2021_275.
5. Shchokin, V. P., Kulish, S.A., Moshinskiy, V.I., Karapa, I.A. & Karnauh, A.V. (2022). Investigation into near-contour stresses in stoping with backfilling by the polarization-optical method. IOP Conference Series: Earth and Environmental Science 1049. 1: 012004. https://doi.org/10.1088/1755-1315/1049/1/012004
6. Pysmennyi, S., Chukharev, S., Kyelgyenbai, K., Mutambo, V. & Matsui, A. (2022). Iron ore underground mining under the internal overburden dump at the PJSC northern GZK. IOP Conference Series: Earth and Environmental Science, 1049(1), 012008 https://doi.org/10.1088/1755-1315/1049/1/012008

Metodyka wyznaczania emisji zanieczyszczeń do powietrza atmosferycznego z robót górnictwa odkrywkowego

W ostatnich latach w górnictwie zaszły istotne zmiany wskaźników jakościowych i ilościowych środków technicznych i materiałów stosowanych podczas odkrywkowego wydobycia rudy żelaza. Zaktualizowano parki techniczne załadunku i rozładunku oraz sprzętu transportowego, pojawiły się nowe rodzaje materiałów wybuchowych. Obecnie nie ma metod obliczania emisji zanieczyszczeń do powietrza atmosferycznego z nowoczesnych urządzeń górniczych. W 1989 r. opracowano „Metodykę obliczania emisji substancji szkodliwych z kamieniołomów z uwzględnieniem niestacjonarności ich procesów technologicznych", która obecnie nie uwzględnia już ww. czynników i wymaga rewizji i uzupełnień.

„Metodyka wyznaczania emisji zanieczyszczeń do powietrza atmosferycznego przez kopalnie odkrywkowe" powstała na podstawie „Metodyki obliczania emisji substancji szkodliwych z wyrobisk z uwzględnieniem niestacjonarności ich procesów technologicznych" z 1989 r. W ostatnich latach zostały przeprowadzone instrumentalne pomiary zanieczyszczeń powietrza atmosferycznego podczas różnych procesów technologicznych w wyrobiskach na hałdach i składowiskach odpadów. Opracowana „Metodyka wyznaczania emisji zanieczyszczeń do powietrza przez roboty odkrywkowe" zawiera aktualne do dziś dane z metodyki z 1989 roku, dane dotyczące charakterystyki technicznej i parametrów urządzeń stosowanych obecnie przez kopalnie odkrywkowe (z prac wydobywczych), a także wyniki badań naukowych prowadzonych przez Instytut Badawczy Bezpieczeństwa i Ekologii Pracy w Przemyśle Górniczo-Hutniczym Krzyworoskiego Uniwersytetu Narodowego. Podstawą opracowania „Metodyki wyznaczania emisji zanieczyszczeń do powietrza atmosferycznego przez zakłady odkrywkowe" jest potrzeba określenia wielkości emisji zanieczyszczeń do powietrza atmosferycznego z nowoczesnych procesów technologicznych i urządzeń kopalni odkrywkowej.

Słowa kluczowe: *górnictwo odkrywkowe, metodologia, emisje, niestacjonarność, procesy technologiczne*

Study of Valuable Impurities of Ore-Forming Titanium Minerals in the Ukraine

Olena REMEZOVA[1),5)], Mykola KOMSKY[2)], Olexandr KOMLIEV[3)], Serhii CHUKHAREV[4)], Svitlana VASYLENKO[1)]

[1)] Institute of Geological Sciences of the National Academy of Sciences of Ukraine; Olena REMEZOVA ORCID https://orcid.org/0000-0002-1955-1270; Svitlana VASYLENKO https://orcid.org/0000-0001-9327-5174; email: elena.titania2305@gmail.com
[2)] State research and production enterprise "State Information Geological Fund of Ukraine"; ORCID https://orcid.org/0009-0002-1487-8677
[3)] Taras Shevchenko National University of Kyiv; ORCID https://orcid.org/0000-0002-5081-7786
[4)] The National University of Water and Environmental Engineering; Department of Mineral Deposits and Mining Engineering, 11 Soborna Str., Rivne, 33028, Ukraine; ORCID https://orcid.org/0000-0002-4623-1598
[5)] Zhytomyr Polytechnic State University

http://doi.org/10.29227/IM-2023-01-24

Submission date: 21-03-2023 | Review date: 26-04-2023

Abstract

Titanium ore is a critical raw material for the EU. Ukraine has significant titanium ore reserves, which are represented by several genetic types and have a number of advantages: the possibility of extracting raw materials for various purposes; favorable mining and geological conditions for most placer and residual deposits; complexity of objects. Ilmenite is the most important titanium mineral, most typical for basic and ultrabasic rocks of the crystalline basement and sedimentary rocks. The value of titanium ores is enhanced by the presence of valuable impurities(V, Sc, Ta, Nb). The quality of titanium ores is related to their degree of alteration. The degree of alteration of ilmenite influences on the industry where the concentrates are used and the development of their processing technologies. The authors have developed approaches to assessing this parameter and have shown the dynamics of changes in the chemical composition of ilmenite in the weathered crust and sedimentary rocks. Based on the statistical processing of data from the chemical analysis of titanium ores, it is shown that Sc has the highest concentrations in the ilmenite of the Korosten complex compared to other geological bodies of the Ukrainian Shield, which provokes the need to improve the relevant technologies.

Keywords: *titanium ores, alteration of ilmenite, impurities, leucoxenization*

1. Introduction

1.1 Titanium deposits in the world and in the Ukraine

Titanium is one of the most important structural metals today. Its use is an indicator of the technical level of an industrially developed country in the world. Titanium deposits of Ukraine are represented by several genetic types and have a number of advantages: the possibility of extracting raw materials for various purposes; high potential of titanium resources and reserves; favorable mining and geological conditions for most placer and residual deposits; complexity of objects. Reserves of primary deposits of Ukraine constitute 53.6% of all reserves, coastal marine zircon-rutile-ilmenite placers – 27.2%, ilmenite alluvial placers – 8.9% and mantle of weathering – 10.3% (Galetskyi, 2009). Placers and partially residual deposits represent the basis of modern extraction of titanium-zirconium minerals in Ukraine. Today Mining is carried out directly from buried coastal and alluvial placers. Ilmenite is the most important titanium mineral of magmatic origin, most typical for basic and ultrabasic rocks of the crystalline foundation. Often, the development of continental ilmenite deposits occurs together with its ore-bearing weathering mantle.

The TiO_2 content of primary ores in Ukrainian deposits varies from 4–5% in poor ores to 34.2% in massive ores (Nosachivka deposit). Ilmenite in these ores is unaltered and is a high-quality raw material for both pigment production and metallurgy. Titanium-magnetite concentrate can also be used for metallurgy, which is likely to be extracted from some deposits (Kropyvenka, Davydky). Ores from magmatic deposits are complex and contain V_2O_5 up to 0.042% (Fedorivske deposit). The content of this component exceeds that of ores from the Bjorkreim-Sogndal massif (Norway) and even the Bushveld massif. V_2O_5 is also found in ores from the primary Stremihorod, Kropyvenka, Torchynske residual and other deposits.

The Ukrainian subprovince of titanium and titanium-zirconium placer deposits was actively studied after the Second World War. At that time, geologists of production organizations determined the chemical composition of ilmenite and other titanium minerals from these placers for the first time. In the works of E. Dudrovych (1977), M. Dyadchenko (1954, 1975), Komliev (2022), V. Ovcharenko (1977), G. Proskurin (1981), S. Tsymbal & Yu. Polkanov (1975) S. Shvaiberov (1989), substance composition, physical and chemical features of individual placer minerals, including impurities in titanium minerals. Impurities in titanium ores of Ukraine have not been sufficiently studied, yet. During the exploration of placers of the Volyn titanium district, the content of vanadium and scandium in ilmenite has been determined only selectively (60–80's of the 20th century).

1.2 The content of impurities in titanium minerals

Summary data on the content of impurities in titanium minerals in placers of the world are given by Elsner H. (2010). In this work, it is stated that the content of Nb_2O_5 in ilmenite concentrates can reach 0.2 wt.% (Capel, Western Australia) and 0.26 wt.% (Madagascar), V_2O_5 – at the level of 0.09 wt.% (Pulmoddai, Sri Lanka) to 0.25 wt.% (Egypt). In general, el-

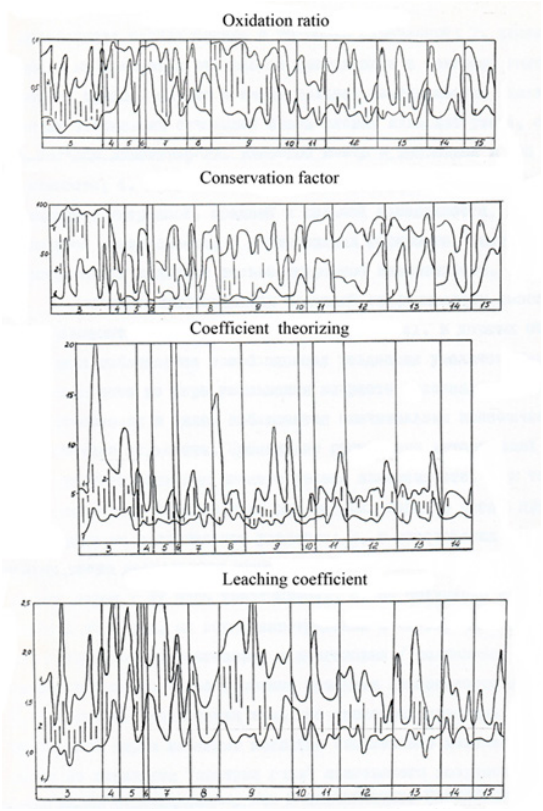

Fig. 1. Dynamics of changes in the chemical composition of ilmenite in sedimentary rocks of placer areas. 1 – intervals of values; 2 – prevailing values; 3– mantle of weathering; age of sedimentary rocks: 4 –J2; 5–K1 6 – K2 ; 7 – Pg2 ; 8 – Pg 2-3 ; 9 – Pg3-N1; 10 – N1-2 ;11 – aI; 12 – fII; 13 – gII; 14 – aIII-IV; 15 –dIV

Rys. 1. Dynamika zmian składu chemicznego ilmenitu w skałach osadowych w rejonie złóż 1 – przedziały wartości; 2 – dominujące wartości; 3- płaszcz wietrzenia; wiek skał osadowych: 4 –J2; 5–K1 6 – K2 ; 7 – Pg2 ; 8 – Pg 2-3 ; 9 – Pg3-N1; 10 – N1-2 ;11 – aI; 12 – fII; 13 – gII; 14 – aIII-IV; 15 –dIV

evated concentrations at the level of 0.1–0.2 wt.% V_2O_5 are characteristic of many alluvial-deluvial placers and residual deposits genetically related to weathering of the main rocks. Placers with this V_2O_5 content in titanomagnetites are known in the Philippines, New Zealand, and Japan, and some of them are being developed.

Currently, the demand for titanium minerals and valuable impurities in their composition is substantially increasing. The main reasons for the optimistic forecasts are that only Norway and Finland have their own sources of raw materials for titanium chemistry in Europe, the reserves of which are very limited and represented by primary deposits that require significantly greater capital investment in their development compared to placers. Unlike the chemistry of titanium, its metallurgy requires higher-quality ore raw materials, and with the exception of large deposits in Ukraine, there is no high-quality raw material base for titanium metallurgy in Europe at all. Therefore, there is a prospect of attracting investments of transnational companies to Ukraine.

It has to be mentioned that under current circumstances of the need to increase the defense capability of Ukraine and the transition to a new functional system of the Armed Forces of Ukraine in accordance with NATO standards (STANAG), there is an urgent need for strategic types of mineral raw materials, such as titanium and rare metals. Later, in the postwar recovery, Ukraine will need replenishment of the ore base of existing enterprises, which means development of new deposits. The value of Ti ores, however, increases even more due to the ability of titanium ore minerals to concentrate some extremely deficient metals as impurities. The latter primarily include Sc, Nb, Ta and V in ilmenite and leucoxene.

1.3 Methods

To estimate the levels of impurity elements in rocks and ores, the results of chemical analyzes of rocks and ores were statistically processed using Excel, MathCad. The study uses chemical analyzes of different years made in the laboratories of geological enterprises (Prockurin G.P.,1981; Schvaiberov S.K. 1989, 2002) and cited in numerous reports and papers (Kononov Yu.V.,1966; Korneliussen, A., 2000; Dushene J.-C.,1970; Jose C. Gespar ,1983; Valvasori, A.A.,2020; Vlad-Victor Ene,2014; Sílvio José Elias,2016). The method of processing analyzes of granulometry and chemical composition of ilmenite, calculation of quantitative indicators that parameterize the granulometric field and the field of variability of ilmenite, integrating the root rocks-weathering crust—mesozoic-cenozoic sedimentary deposits within the placers is used for plasers of Irshansk ore field (Komliev O., 2022). Interpretations of the obtained results were carried out on a broad paleogeographical basis, taking into account tectonics, paleorelief, and paleoclimates. This methods allow to estimate quality of ilmenite ores.

2. Characteristics of Ukrainian titanium ores

2.1. Ilmenite alteration

Titanium ores of Ukraine are noted for their quality and large reserves, so they represent considerable value. Today in

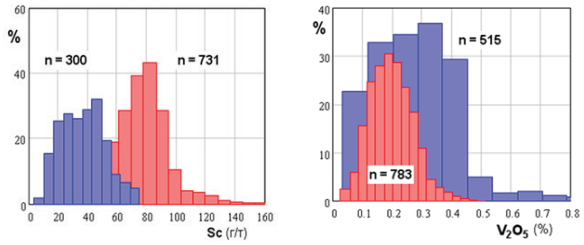

Fig. 2. Distributions of scandium and vanadium oxide in ilmenites and leucoxenes:
1) Korosten complex (Korosten and Korsun-Novomyrhorod plutons), in mantle of weathering and alluvium within the plutons – red histograms;
2) from other areas of the world (see Table 1) – blue histograms. Content of Sc is given in g/t

Rys. 2. Rozkłady tlenku skandu i wanadu w ilmenitach i leukoksenach:
1) Kompleks Korosteń (pluton Korosteń i Korsun-Nowomyrhorod), w strefie wietrzenia i aluwium w obrębie plutonów – histogramy czerwone;
2) z innych obszarów świata (patrz tabela 1) – histogramy niebieskie. Zawartość Sc podano w g/t

Tab. 1. Oxides of Ti, Fe, V in %; Sc, Nb, Ta in g/t. KST and KSN are Korosten and Korsun-Novomyrhorod plutons, respectively [* placers in the Middle Dnipro region: Samotkansky, Vovchansky, Krasnokutsky; ** – various coastal placers – Australia, Hindustan, Indochina, Africa, South and North America; GN, G, GA, A – gabbro-norites, gabbro, gabbro-anorthosites, anorthosites, respectively]

Tab. 1. Tlenki Ti, Fe, V w %; Sc, Nb, Ta w g/t. KST i KSN to odpowiednio plutony Korosteń i Korsun-Nowomyrhorod [* placery w regionie środkowego Dniepru: Samotkansky, Vovchansky, Krasnokutsky; ** – różne place przybrzeżne – Australia, Hindustan, Indochiny, Afryka, Ameryka Południowa i Północna; GN, G, GA, A – odpowiednio gabro-noryty, gabro, gabro-anortozyty, anortozyty]

Object (region, rocks, minerals)	TiO_2	Fe_2O_3	FeO	Sc	Nb	Ta	V_2O_5
KST– G,GA,A	49.21	3.36	43.18	81	109	22	0.206
KST – mantle of weathering	51.66	11.48	33.72	72	163	12	0.196
KST – placers	56.96	17.60	20.56	85	229	15	0.237
KSN – G,GA,A	50.71	3.41	42.99	69	373		0.181
KSN – mantle of weathering	52.40	8.42	36.72		455		0.138
KSN – placers	58.02	18.65	18.37	129	509		0.221
Bilokorovychi dyke (Ukraine)	50.67	2.95	44.04				0.30
Tarasivka placer (Kyiv region, Ukraine)	64.42			50		123	
Middle Dnipro * – placers	68.48	24.14	0.89		1245	558	0.141
Mokro-Yalynsky (Приазов'я) – placers	64.96	28.56	0.46		1679	1583	0.118
Water areas of the Black and Azov seas(Ukraine) (Укр.)	53.14	19.85	23.96			53	0.163
Norway. **Ilm,** G,GA,A	47.84	7.92	38.55				0.183
Norway. **Hemo-Ilm,** G,GA,A	32.84	33.37	26.56				0.407
Grenville (Canada) – **Hemo-Ilm,** G,GA,A	39.25	26.35	30.37	37	25	1	0.367
Labrador (Canada) – **Ilm,** G,GA,A	50.55	4.72	42.17	39			0.23
Kunene (Namibia) – G,GA	51.42	2.49	43.70	37	191	14	0.162
Mozambique – placers	48.80	25.02	15.78		662		0.11
Coastal sea placers **	79.34				2212	188	0.162
Panchzhihua (Southeast China) – G	52.63	3.71	38.40	43	79		0.156
South Africa – Ultramafic rocks	53.00	7.54	24.02	21	1312	124	0.186
Lyakhovych V.V., 1979. Gabbroids.					560	262	0.196
Lyakhovych V.V., 1979. Granitoids.					2214	820	
Industrial contents in ores					700–2800	200–800	≥ 0.2

the Ukraine, the placers of titanium minerals are exploited. They are also found in crystalline rocks – in gabbroids of the Korosten and Korsun-Novomyrhorod plutons, residual – in the weathering crusts of gabbroids. In alluvial placers, these ores are close to the sources of their formation and connected to the distant transportation. Useful ore mineralization is represented by pure ilmenite (in gabbroid ores), to which in weathering mantle and in the placers, especially abundantly in distant ones, are added leucoxenes and, in some places, rutile. There is currently quite a lot of interest in titanium in the world, and it will undoubtedly grow over time. At the same time, if you look closely at the compositions of ilmenites, the value of titanium ores begins to play out in a new, even brighter light.

The theoretical chemical composition of ilmenite is assumed to be TiO_2 (52.7%) and FeO (47.3%). On the earth's surface (in hypergenic conditions), the chemical composition of ilmenite changes due to the integrated action of tectonic, paleoclimatic, paleogeomorphological, and paleohydrological factors. They can create favorable conditions for weathering of crystalline rocks and their transformation into chemical weathering crust of kaolin type. Mantle of weathering formation is a necessary condition for the formation of alluvial ilmenite deposits. In the weathering mantle, chemically unchanged ilmenite is released from crystalline rocks and begins to undergo the stages of continental lithogenesis with the participation of the above factors. The "fresh" ilmenite brought to the level of denudation begins to change in the weathering crust and then continues continuously, accelerating with the activation of ancient exogenous processes, when complete or partial destruction of ilmenite placers occurs, slowing down

Tab. 2. Parameters of scandium distribution in the ilmenite deposits of the Korosten complex

Tab. 2. Parametry rozmieszczenia skandu w utworach ilmenitu kompleksu Korosteń

Deposit	Localization environment	N	mean	min	max	moda
Stremyhorod	G,GA,A	161	80	61	100	82
Stremyhorod	mantle of weathering	98	84	15	147	81
Fedorivka	G,GA,A	30	116	90	135	116
Torchyn	G,GA,A	33	66	50	90	60
Torchyn	mantle of weathering	167	64	30	100	70
Hatskivka area of Upper Irsha deposit	mantle of weathering	16	85	47	110	96
Hatskivka area of Upper Irsha deposit	placer	24	84	61	107	85
Valky-Hatskivka deposit	placer	25	62	30	110	50
Valky-Hatskivka deposit	placer	32	71	15	200	60
Trostyanytsya deposit	mantle of weathering	13	84	81	88	81
Trostyanytsya deposit	placer	18	93	88	103	88
Zlobychi deposit	mantle of weathering	29	66	24	94	67
Zlobychi deposit	placer	45	80	38	100	87
Paromivka deposit	mantle of weathering	16	85	62	116	98
Paromivka deposit	placer	14	94	65	134	80
Nosachivka deposit (KSN)	G,GA,A	6	69	48	98	
Southern part of KSN	placer	4	129	76	193	

when they become less active, and even stopping after they become buried. The chemical composition of ilmenite reflects the total result of exogenous processes and, in combination with other methods, provides important information about the paleogeographic development of territories. The main processes that change the chemical composition of ilmenite are oxidation and leaching. At the oxidation stage, unaltered ilmenite from igneous rocks begins to break down under the influence of mainly oxygen. It is oxidized, partially leached, the crystal lattice is destroyed, free titanium and iron oxides are formed, and the ilmenite phase is completely destroyed. The end product of the first stage of ilmenite alteration is leucoxenized ilmenite. At the second stage, the main process is iron leaching. At this stage, titanium hydroxides crystallize and end up forming leucoxene, and after complete iron leaching, pseudorutile is formed. Both processes occur simultaneously, but oxidation prevails at the first stage and leaching at the second. Changes in the chemical composition of ilmenite in the hypergene zone can be characterized by various coefficients, which we first proposed to solve various problems during paleogeographic and special paleogeomorphological works in areas promising for ilmenite placer deposits in the territory of the Ukrainian Shield. The results of chemical composition analyses of ilmenite monofractions taken from crystalline rocks of the basement, weathering crust, and Mesozoic and Cenozoic sediments were used. The coefficients were calculated using different methods. However, at the final stage, the oxidation coefficient (Fe^{3+}/FeS), leaching coefficient (FeS/TiO_2), and thiorization coefficient (TiO_2/Fe_2O_3) were used. The disadvantage of these coefficients is the inability to estimate the degree of alteration of ilmenite relative to its theoretical composition. Therefore, in addition to them, we also calculated the degree of preservation of ilmenite using the formula:

$$Cprs= 114.4\ FeO/TiO_2 \quad (1)$$

This indicator is recommended for the oxidation stage of ilmenite. Based on a large array of data on prospective sites, we studied the dependence of granulometric characteristics and chemical composition of ilmenite monofraction for various elements of the ancient relief of the Late Oligocene-Middle Miocene age. The empirical formula:

$$Md = - aK1+b/10/K2 - 1/x/ + c \quad (2)$$

was derived. Where: K1 – oxidation coefficient K2 – leaching coefficient, a, b, c – variable coefficients that vary depending on the initial conditions (composition of the source rock, paleorelief slopes, time spent in the hypergenesis zone). Fig. 1 shows the dynamics of changes in the chemical composition of ilmenite in the weathered crust and sedimentary rocks.

2.2. Impurities in titanium minerals from Ukrainian deposits

In Table 1 we provide the contents of some trace elements and mineral-forming oxides in ilmenites of a number of their accumulations in Ukraine and some other regions of the world. In many cases, these trace elements are present in ilmenite in such quantities that they definitely acquire industrial importance, especially if we take into account the large size and reserves of titanium deposits. Therefore, the accompanying extraction of trace elements during the processing of the mineral-bearer becomes economically profitable and provokes the need to improve the relevant technologies.

In this paper, which we hope will not be the last, we narrow our report to two rare metals: Sc and V in the ilmenite of numerous titanium deposits and occurrences of the Korosten complex – the Korosten and, to a lesser extent, the Korsun-Novomyrhorod plutons, due to lack of data. It is in the ilmenite of this complex that Sc shows the highest concentrations (at least twice), and this is reflected in Table 1 and the figure below. Moreover, the reserves of ilmenite ores on these plutons are huge.

As for vanadium, its impurities in the Korosten ilmenites are not significant (Table 1 and Figure2). Its highest concen-

Tab. 3. Parameters of vanadium pentoxide distribution in ilmenite deposits of the Korosten complex

Tab. 3. Parametry rozkładu pięciotlenku wanadu w złożach ilmenitu kompleksu Korosteń

Deposit	Localization environment	N	mean	min	max	moda
Stremyhorod	G,GA,A	56	0.184	0.060	0.370	0.200
Stremyhorod	mantle of weathering	149	0.168	0.050	0.320	0.140
Fedorivka	G,GA,A	39	0.214	0.024	0.425	0.303
Penyazevychi	G,GA,A	6	0.347	0.060	0.530	
Nosachivka deposit (KSN)	G,GA,A	14	0.215	0.110	0.430	0.200
Hatskivka area of Upper Irsha deposit	mantle of weathering	46	0.195	0.100	0.305	0.230
Valky-Hatskivka deposit	mantle of weathering	37	0.136	0.051	0.400	0.106
Hatskivka area of Upper Irsha deposit	placer	47	0.233	0.060	0.329	0.244
Trostyanytsya deposit	mantle of weathering	40	0.267	0.150	0.460	0.320
Trostyanytsya deposit	placer	67	0.246	0.112	0.355	0.235
Lemna deposit	mantle of weathering	52	0.220	0.140	0.380	0.190
Lemna deposit	placer	83	0.232	0.120	0.310	0.230
Southern part of KSN	mantle of weathering	107	0.138	0.060	0.310	0.160
Southern part of KSN	placer	15	0.221	0.120	0.400	0.190

trations are characteristic of hemi-ilmenites from deposits in Norway and Canada. Titanomagnetites contain even more vanadium, in particular, ores of the Suwalki massif (Poland) with vanadium pentoxide of 0.81% (maximum value 1.2%). Titanium-magnetite clusters are less typical for the Korosten pluton, although they are present in gabbroids at some deposits (Kropyvenka). In any case, we believe that the extraction of vanadium from ilmenite, along with titanium and scandium, is quite profitable.

As for vanadium, its impurities in the Korosten ilmenites are not significant (Table 1 and Figure 2). Its highest concentrations are characteristic of hemi-ilmenites from deposits in Norway and Canada. Titanomagnetites contain even more vanadium, in particular, ores of the Suwalki massif (Poland) with vanadium pentoxide of 0.81% (maximum value 1.2%). Titanium-magnetite clusters are less typical for the Korosten pluton, although they are present in gabbroids at some deposits (Kropyvenka). In any case, we believe that the extraction of vanadium from ilmenite, along with titanium and scandium, is quite profitable.

In Tables 2 and 3, we present statistical characteristics for Sc and V_2O_5 in some deposits mainly on the Korosten pluton(we have a small amount of such data for the Korsun-Novomyrhorod pluton).

The following is noteworthy:

1. In most cases, in the same deposits, ilmenite from placers is significantly richer in scandium than in the underlying residual environments (in mantle of weathering). The explanation for this is the greater stability of Sc compared to Fe in the process of leucoxenization. It is known that during weathering, the ferrous iron in ilmenite is gradually oxidized and leaves ilmenite in the form of Fe^{3+}. At least partially. Titanium and scandium remain on site and are enriched in leucoxene. Therefore, placers that have been exposed to weathering for a longer and/or more active period of time (for example, due to a longer transportation profile from the source of erosion) may be characterized by ilmenite richer in scandium. This may be the case with ilmenite in the southern Korsun-Novomyrhorod pluton placers, up to 190 g/t, for which we do not have sufficient data (on Sc).

2. Significantly elevated scandium contents were found in 30 analyzes of ilmenites from gabbroids of the Fedorivka deposit. We do not have an explanation for this.

3. As for vanadium, it seems that it is removed from ilmenite under the influence of weathering, but obviously weaker than iron.

3. Conclusion

Ukraine's titanium ores are distinguished by their quality and large reserves, which allows them to be used both to produce a range of chemical products and in metallurgy. Different applications require the ores of the appropriate quality. The main processes that change the chemical composition of ilmenite are oxidation and leaching. Changes in the chemical composition of ilmenite in the hypergene zone can be characterized by various coefficients, which we first proposed to solve various problems when conducting paleogeographic and special paleogeomorphological works in areas with prospects for ilmenite placer deposits in the Ukraine. The authors characterized ilmenites from different ages and conditions of placer formation. Based on these studies, it is possible to create models of ilmenite zonation in placers and further geometrization of deposits. An important problem is the content of useful impurities in ilmenites, in particular vanadium and scandium. In this case, placers that have been exposed to weathering for a longer and/or more active period of time (i.e., the above-mentioned processes of chemical composition changes) may be richer in scandium. Vanadium is removed from ilmenite by weathering, but this process is weaker than iron removal, and therefore may also be a valuable impurity, which should be taken into account when developing technologies for its extraction.

Literatura – References

1. Dudrovich, E. Ju., & Mukhin, Ju. M. (1977). Patterns of changes in the chemical composition of ilmeyine from placers in northern Ukraine. Ancient and buried placers of the USSR, Kyiv, Vol. 1, pp. 109–112, in Russian.
2. Dushene J.-C.(1970). MICROTEXTURES of Fe-Ti OXIDE MINERALS IN THE SOUTH-ROGALAND ANORTHOSITIC COMPLEX (NORWAY). Annales de la Societe Geologique de Belgique, Vol. 93, pp. 527-544.
3. Dyadchenko, M. G. & Hatunzeva A. J. (1954). New data on leucoxene. Geol. journal. Vol. 14. Issue 4. 75–78, in Ukrainian.
4. Elias Sílvio José (2016). MINERALOGY AND PROVENANCE OF THE TiO2 – ILMENITE HEAVY MINERAL SAND DEPOSIT OF NATAKA. Dissertation for the degree of Master of Science in Geology. University of Cape Town. 123p. https://open.uct.ac.za/bitstream/handle/11427/23762/thesis_sci_2016_elias_silvio_jose.pdf?isAllowed=y&sequence=1
5. Elsner, H. (2010). Heavy Minerals of Economic Importance. Assessment Manual Bundesanstalt für Geowissenschaften und Rohstoffe (BGR) (Federal Institute for Geosciences and Natural Resources), 218 p.
6. Ene Vlad-Victor (2014). Major and trace element geochemistry of ilmenite suites from the Kimberley diamond mines, South Africa. A thesis for the degree of Master of Applied Sciences, University Of Toronto, 97 p.
7. https://tspace.library.utoronto.ca/bitstream/1807/68029/1/Ene_Vlad_V_201411_MAS_thesis.pdf
8. Galetskyi, L.S. (2009). The state and prospects of titanium production in Ukraine [Report on research work]. Kyiv: Institute of Geological Sciences of the National Academy of Sciences of Ukraine.
9. Jose C. Gespar (1983). Ilmenite (high Mg,Mn,Nb) in the carbonatites from the Jacupiranga Complex, Brazil. American Mineralogist, Volume 68, p. 960-971
10. Komliev, O. O., & Zhylkin, S. V. (2022). Mesozoic-Cenozoic Morpholithogenesis of the Ukrainian Shield (Within the Irshansky Placer Field). Ukr. Geogr. Ž., 1, pp.27–35, in Ukrainian. DOI: https://doi.org/10.15407/ugz2022.01.027
11. Kononov Yu.V.(1966). Gabbro massifs of the Ukrainian Shield (central part). Kyiv, Naukova dumka Publishing, 99 pp., in Ukrainian.
12. Korneliussen, A., McEnroe, S. A., Nilsson, L.P (2000). An overview of titanium deposits in Norway NGU, Bull. 436, p. 28.
13. Lyakhovich V. V. (1979). Accessor minerals of rocks. Moscow, Nedra Publishing, 296 p., in Russian.
14. Ovcharenko, V. N. (1977). Typomographic features and physical properties of ilmenite from placers of northern Ukraine. Ancient and buried placers of the USSR. Kyiv, Vol. 1, pp. 113–115, in Russian.
15. Prockurin G.P.(1981). Stremihorod deposit of apatite-ilmenite ores. Exploration report. Kyiv, in Russian.
16. Schvaiberov S.K. (1989). Detailed exploration of Valky-Hatskivka alluvial deposit of ilmenite. Report. Kyiv, Vol.3, in Russian.
17. Schvaiberov S.K. (2002). Exploration of apatite-ilmenite ores of the Fedorovskoye deposit. Report.
18. Tsymbal, S. N., & Polkanov, Yu. A. (1975). Mineralogy of titanium-zirconium placers of Ukraine. Kyiv. Naukova dumka, 248 p., in Russian.
19. Valvasori, A.A., Hanchar, J.M., Piercey, S.J. et al. (2020). The origin and evolution of V-rich, magnetite dominated Fe-Ti oxide mineralization; Northwest River Anorthosite, south-central Labrador, Canada. Miner Deposita 55, pp. 555–575. https://doi.org/10.1007/s00126-019-00892-6.

Badanie cennych domieszek rudnych minerałów tytanu na Ukrainie

Ruda tytanu jest surowcem o krytycznym znaczeniu dla UE. Ukraina posiada znaczne zasoby rud tytanu, które są reprezentowane przez kilka typów genetycznych i mają szereg zalet: możliwość wydobywania surowców do różnych celów; korzystne warunki górniczo-geologiczne dla większości złóż rezydualnych. Ilmenit jest najważniejszym minerałem tytanu, najbardziej typowym dla skał zasadowych i ultrazasadowych podłoża krystalicznego oraz skał osadowych. Wartość rud tytanu podnosi obecność cennych domieszek (V, Sc, Ta, Nb). Jakość rud tytanu jest związana ze stopniem ich przeobrażenia. Stopień przemiany ilmenitu wpływa na przemysł, w którym stosowane są koncentraty oraz rozwój technologii ich przetwórstwa. Autorzy opracowali podejście do oceny tego parametru oraz pokazali dynamikę zmian składu chemicznego ilmenitu w zwietrzałej skorupie i skałach osadowych. Na podstawie statystycznego opracowania danych z analizy chemicznej rud tytanu wykazano, że Sc ma najwyższe stężenia w ilmenicie kompleksu Korosteń w porównaniu z innymi utworami geologicznymi Tarczy Ukraińskiej, co rodzi potrzebę udoskonalenia odpowiednich technologii.

Słowa kluczowe: *rudy tytanu, odmiany ilmenitu, domieszki, leukoksynizacja*

The Workflow of Ground Penetrating Radar Data Analysis Based on Maximum Energy Difference Steering

*Duy Hoang DANG[1), 2),3)], Cuong Van Anh LE[*1), 2)], Thuan Van NGUYEN[1), 2)], Long Quoc NGUYEN[4)], Nhan Thanh HUYNH[1),2)]*

[1)] University of Science, Ho Chi Minh City, Vietnam; email: lvacuong@hcmus.edu.vn
[2)] Vietnam National University Ho Chi Minh City, Vietnam
[3)] Loc Ninh Highschool, Binh Phuoc Province, Vietnam
[4)] Hanoi University of Mining and Geology, Vietnam
* Corresponding author: lvacuong@hcmus.edu.vn

http://doi.org/10.29227/IM-2023-01-25

Submission date: 20-05-2023 | Review date: 01-06-2023

Abstract

Ground Penetrating Radar is commonly used in civil engineering sectors. Underground anomalies (i.e., electric wires, water pipes or sinkholes) can be detected through representations of hyperbolae in the measured processed GPR image. Our work focuses on detecting the underground objects and understanding their metallic or nonmetallic characteristics. The max energy difference attribute is applied to illuminate their positions while phase analysis process can determine change of phase spectrum in the diffracted signals. For improving phase analysis, we applied a novel workflow combining conventional processed steps and a zooming step for preserving phase originality without disturbed by any unnecessary filters. We applied the workflow in model and real data for proving its effectiveness. Interpretation of two real datasets in Vietnam by our workflow can express existences of the artificial underground anomalies as well as their matter characteristics comparing to their surrounding environments.

Keywords: *ground penetrating radar, phase analysis, energy difference*

1. Introduction

Ground Penetrating Radar (GPR) plays a key role in detecting underground anomalies such as artificial objects or sinking holes. A conventional workflow (Le and Nguyen 2020a, Nguyen et al. 2017, Le and Nguyen 2020b, Zhao, Forte, and Pipan 2016) can convert the raw GPR data into the interpretable processed GPR data. The workflow often includes some key steps such as move-start time, background removal filter, frequency filters, gain function, velocity analysis, gain function, and migration. The processed steps can improve the ratio between signal over noise for the better recognition of underground objects, but they also can distort the original amplitudes and phases. The phase distortion will affect to analyzing metallic or unmetallic characteristics of the objects. Therefore, the original phase from the raw data needs to be kept for checking in phase or out of phase cases.

In seismic analysis, full waveform inversion is utilized to recover true acoustic impedance that answer many questions about the earth structures/ characteristics. Its input is the seismic data with preserved amplitude and phase originality (i.e., low frequency data domain) (Virieux and Operto 2009, Kumar, Ramrez, and Butt 2012). Applying the seismic spirit into GPR interpretation, we have focused on the workflow that can keep the GPR data originality and expressing the underground anomalies characteristics.

We have applied the new workflow to processing and interpreting the data. Modelling and real data are used for proving the efficiency of the workflow. The workflow focuses on two stages: (i) detecting the anomalies and (ii) analysis their phases for evaluating their matter characteristics comparing to surrounding environment.

2. Methodology

GPR data can reveal existences of different underground anomalies or ground structures by presenting their images through amplitude and phase vibrations. Raw data can be transformed into interpretable processed data by applying different filter and amplification techniques for enhancing reflection and diffraction signatures. Although diffracted hyperbolae ignited from underground objects like diffractors cannot show the true shapes of the anomalies, they can specially answer correct their positions in terms of their hyperbolae peaks (Le and Nguyen 2020a, Nguyen et al. 2017, Bitri and Grandjean 1998, Kang et al. 2019).

2.1 Conventional steps

For achieving an interpretable GPR processed data, we have applied some necessary traditional processing steps as (i) move start-time, (ii) background removal, (ii) frequency filters, and (iii) migration (Nguyen et al. 2017, Le and Nguyen 2020a, Le and Nguyen 2020b). Firstly, move start-time is so important in giving correct travel time of a real event by moving the start time of sources to zeroes. Background removal can delete background noises and frequency filters can focus on meaningful frequency band for enhancing the useful signal representation. Finally, the function of the migration step is to present the correct positions and shapes of anomalies. In our work, Kirchhoff migration is utilized (Nguyen et al. 2017, Le and Nguyen 2020a, Le and Nguyen 2020b).

For further interpretation, some GPR attribute processing steps could be applied (Fig. 1) (Nguyen et al. 2017, Le and Nguyen 2020b). For detecting anomalies, maximum energy difference can illuminate existence of anomalies and help to

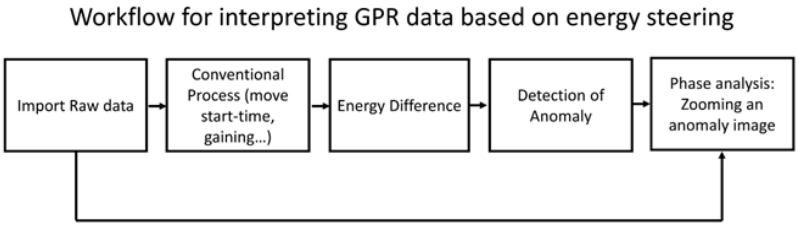

Fig. 1. The workflow of detecting metallic or unmetallic characteristics

Rys. 1. Proces wykrywania cech metalicznych lub niemetalicznych

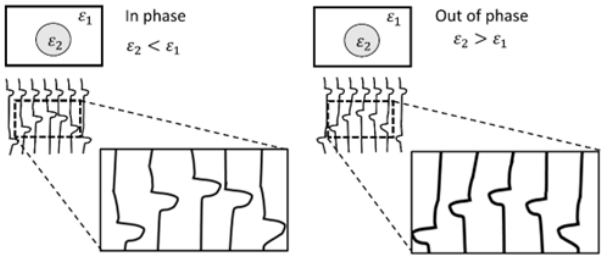

Fig. 2. In phase zooming and out of phase zooming

Rys. 2. Powiększanie w fazie i powiększanie poza fazą

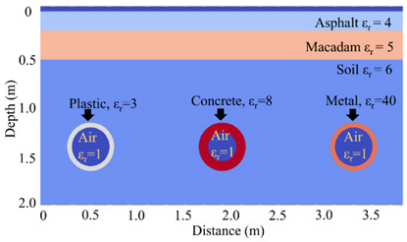

Fig. 3. Model representation

Rys. 3. Reprezentacja modelu

evaluate electromagnetic wave velocity within underground media (Nguyen et al. 2017).

Phase analysis aims to detect metal or unmetallic characteristics of an object. In phase or out of phase (Kang et al. 2019) come from phase variation of wave phase when the wave reflects from bigger to smaller electric permittivity zones and vice versa, respectively (Fig. 2).

2.2 The maximum energy difference steering workflow

In geophysical method areas like seismic and GPR, color is one kind of their special attributes (Chopra and Marfurt 2007, Le et al. 2016, Le, Harris, and Pethick 2019, Kang et al. 2020). In Kang et al. (2019) 's work, removal of the first wave can enhance the GPR data interpretation in defining in phase or out of phase cases. Our suggested workflow consists of two stages for examining an underground anomaly from the GPR data measurement: (i) Defining positions and true images of underground anomalies and (ii) analyzing phase shapes for determining the contrast of two media in which metallic or unmetallic matters are decided. Their positions can be located through their hyperbolae or visible strong GPR attributes after processing the raw data (Kang et al. 2019, Kang et al. 2020, Le and Nguyen 2020a, Le and Nguyen 2020b). Moreover, the processed phase can reveal the variation of environmental electric permittivity.

For preserving the phase information, only the move start-time step is applied. It does not harm the deeper original signals like other gain functions or many amplitude-distorted filters steps. The key thing is that recorded amplitude of first direct GPR wave is much stronger than any GPR waves travel down and bounce back from ground reflectors or diffractors. Therefore, a zooming image which shows only anomaly signals is much clearer when it does not include the first direct wave.

The conventional processing workflow is effective in detecting positions of anomalies (see Fig. 1) (Dang, Le, and Kieu 2020, Nguyen et al. 2017, Le and Nguyen 2020b). Firstly, the raw input data is processed through many conventional steps as move start-time, background filter, frequency filter, dewow, and gain function. Second, the processed are input for the maximum energy difference approach for object position estimation and velocity valuation (Nguyen et al. 2017). Third, positions and true shape of underground anomalies are achieved from Kirchhoff migration with the suitable velocity. Finally, hyperbolae phase signatures which are extracted from the processed and the first step (only move start-time) data are compared with the first direct wavelet for deciding in-phase or out of phase cases in explaining the characteristics of anomaly materials (Fig. 2).

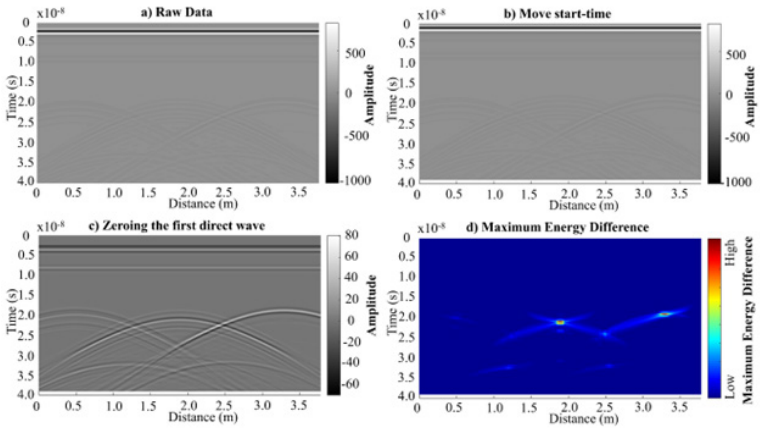

Fig. 4. Synthetic data and its processed data: a) Raw data is simulated from the model which show strongest amplitude of the first direct wave and weak hyperbolae signals. b) Move start time step is applied to raw data for representing correct wave travel time. c) The processed step is zeroing the first direct wave for illuminating the real signals of three circular objects. d) Maximum energy difference section which is computed can reveal strong values in time nearly 2.10^{-8} (s) or 20 ns for explaining their locations

Rys. 4. Dane syntetyczne i dane przetworzone: a) Surowe dane są symulowane z modelu, który pokazuje najsilniejszą amplitudę pierwszej fali bezpośredniej i słabe sygnały hiperboli. b) Krok czasu rozpoczęcia ruchu jest stosowany do surowych danych w celu przedstawienia prawidłowego czasu podróży fali. c) Przetworzony krok zeruje pierwszą falę bezpośrednią w celu oświetlenia rzeczywistych sygnałów trzech okrągłych obiektów. d) Maksymalna sekcja różnicy energii, która jest obliczana, może ujawnić silne wartości w czasie prawie $2{,}10^{-8}$ (s) lub 20 ns w celu wyjaśnienia ich lokalizacji

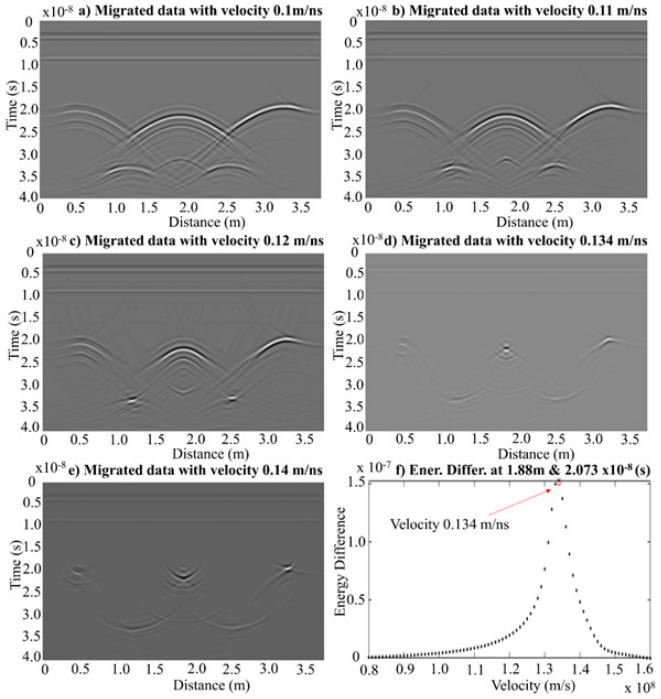

Fig. 5. Migration of Synthetic GPR data with different velocities and representation of energy difference versus velocity in the position 1.88 m and 2.073 x 10^{-8} (s)

Rys. 5. Migracja syntetycznych danych GPR z różnymi prędkościami i przedstawienie różnicy energii w funkcji prędkości w pozycji 1,88 m i 2,073 x 10^{-8} (s)

3. Results and Discussion

We applied our workflow for detecting the matter characteristics in the modelling data and real data.

3.1 Modelling data

We have used GPRMAX (Warren, Giannopoulos, and Giannakis 2016) for running synthetic data from the prior model (Fig. 3). The center frequency is 700 MHz. The model has three horizontal layers and three circular blocks (Fig.3). The three layers are asphalt, macadam, and clay with relative electric permittivity values as 4, 5, and 6, respectively. Besides, the three circular blocks which contain air inside are made up plastics, concrete, and metal with relative electric permittivity values as 3, 8, 40, respectively. Their outside radius values are 0.25 m while their inside radiuses are assigned 0.20 m, 0.15 m, and 0.20m for plastics, concrete, and metal, respectively.

In Fig. 4, the color representation is dependent on the minimum and maximum values of the direct waves. The extremes can prevent visualization of other deeper useful events such as three hyperbolae resulting from the three circular objects (Figs. 4a and 4b). This disadvantage inspires us to apply the removal technique of first direct wavelet. Therefore,

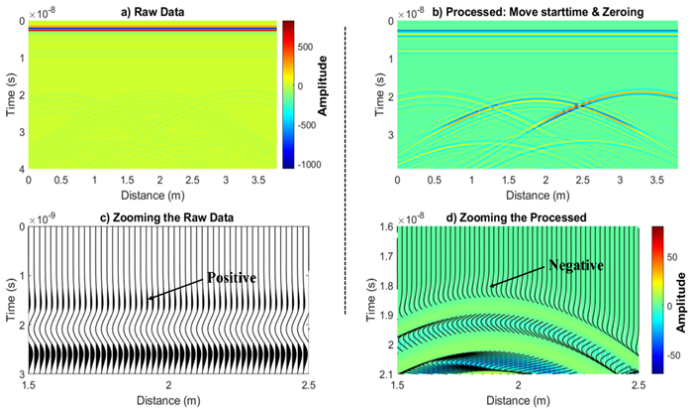

Fig. 6. Zooming image for analyzing phase

Rys. 6. Powiększenie obrazu do analizy fazy

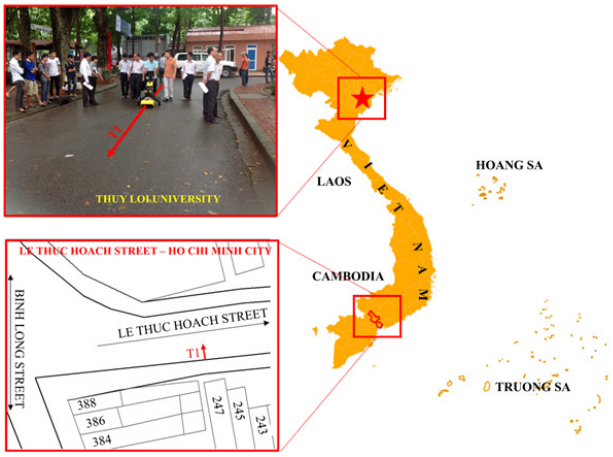

Fig. 7. Survey map for two locations (Ha Noi and Ho Chi Minh City) in Vietnam

Rys. 7. Mapa badania dla dwóch lokalizacji (Ha Noi i Ho Chi Minh City) w Wietnamie

zeroing the first direct wave is applied to this synthetic data (Fig. 4c).

For evaluation of wave propagation velocity, we tested many migrated sections (Fig. 5) with different velocities varying around the velocity picked by analysis of 1D maximum energy difference curve (Fig. 5f). Over-, focused and under- migration phenomena are easily seen in the sections with bigger values, correct value, and lower velocity values, respectively. The velocity 0.12 m/ns (meter per nano second) is chosen for calculating the circular anomalies 's depths for providing better depth value than the one 0.134 m/ns. The value 0.134 m/ns has an tendency gives the bigger depth because the Kirchhoff migration tries to compress the big circular shapes of the big anomalies (Le and Nguyen 2020a).

Besides, the processed zeroing data, migrated, and maximum energy difference sections can shed light on locations of the three circular anomalies in time nearly 2.10-8 (s).

The first and third objects at locations 0.56 m and 3.36 m can represent the phase types as in-phase and out of phase, respectively. However, the second object at x=1.88m needs more works to clarify its phase characteristics because of weak first break amplitudes. Therefore, Fig. 6 expresses two zooming images of the area containing the second object. It looks like that its first wavelet (Fig. 6c) is negative which is contrary to the positive wavelet of the first direct wave (Fig. 6d). Therefore, it is out of phase case compatible with the electric permittivity values of the second object and the surrounding background. Notice that the zooming image extracted from the zeroing first direct data (Fig. 4c) can show the hyperbolae so well.

3.2 Real data

Field data 1:

The electromagnetic method survey was conducted in Thuy Loi university, Ha Noi, Vietnam. We have used the GPR equipment branded IDS Duo Detector, 700 MHz, made in Italy (Fig. 7). The processed and maximum energy difference are computed from the raw data shown in Fig. 8. We can detect the position of a hyperbola = 3.424m and t=1.375x 10-8 (s) in the two processed attribute images (Figs. 8c and d). To analyze the position of artificial object at x= 3.424m and t=1.375x 10-8 (s), many migrated sections are analyzed (Fig. 9). The object is interpreted as the drainage pipe from the prior information. We can achieve the velocity of wave propagation at 0.074 m/ns to give its depth at 0.41m with the first wavelet time 1.1x 10-8 (s).

For phase analysis in zooming image (Fig. 10), first wave direct wave (Fig. 8a) and the first wavelet of its hyperbola are compared. In zooming images of Fig. 10, the trough shape (i.e., negative values) are seen in the processed and raw data.

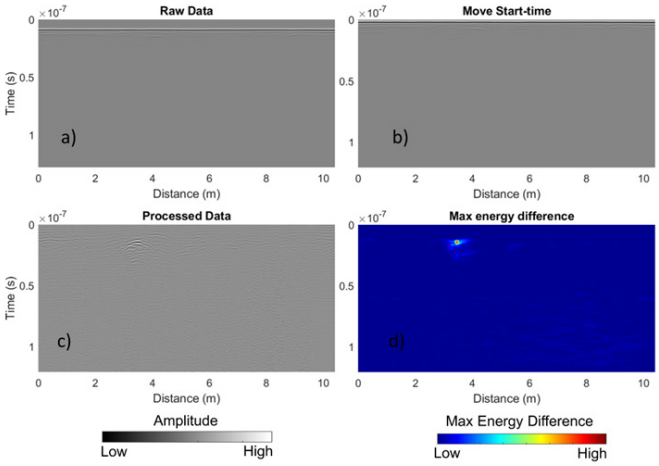

Fig. 8. The raw, move Start-time, processed data and its maximum energy difference attribute

Rys. 8. Nieprzetworzone, przesunięte w czasie, przetworzone dane i ich atrybut maksymalnej różnicy energii

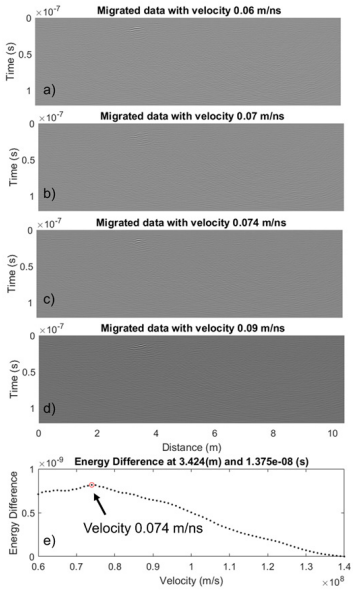

Fig. 9. Migration sections with different velocities and 1D Maximum energy difference curve versus velocities

Rys. 9. Odcinki migracji z różnymi prędkościami i krzywa maksymalnej różnicy energii 1D w funkcji prędkości

Notice that the first wavelet of the direct first wave is positive in the real data (Fig. 8a). This can explain that the electric permittivity of the object is more than the electric permittivity of the surrounding environment. In prior information seen in Fig. 7, the drainage pipe is made of concrete.

Field data 2:

We also conducted the GPR equipment as IDS Duo Detector, 700 MHz in Le Thuc Hoach street, Tan Phu District, Ho Chi Minh City, Vietnam. The raw data is processed the same workflow mentioned in the methodology (Fig. 11) (see Section 2.2). Its conventionally processed data shown in Fig. 11c and its maximum energy difference section in Fig. 11d can express location of one object. The object is known as a metal water supplying water. Its position has x=1.615 m and 2.3 x 10-8 (s). For computing its depth, we tested several migrated sections in Fig. 12. Under and over migration effects can be seen in Figs. 12a and b, and Fig. 12d, respectively. The chosen velocity, 0.087 m/ns, which is extracted from the 1D maximum energy difference curve (Fig. 12f), can estimate its depth at 0.94m with its first break 2.1 x 10-8 (s).

In the phase analysis stage, we represent two types of processed data and raw data in for zooming images (Fig. 13). Notice that the raw data does not receive any amplitude filter except move start-time step so it does keep its true amplitude. Negative effect is strongly seen in all the four zooming images. The out of phase case can expresses that the electromagnetic wave bounced at the anomaly having the electric permittivity bigger than the surrounding environment. The object interpretation is suitable the prior information that the supplying water pipe is metallic.

4. Conclusion

We have applied our workflow to investigate positions and characteristics of underground anomalies. The workflow focuses on detection of positions using maximum energy difference approach and phase analysis using in phase and out of phase cases. Besides, migration technique helps to estimate

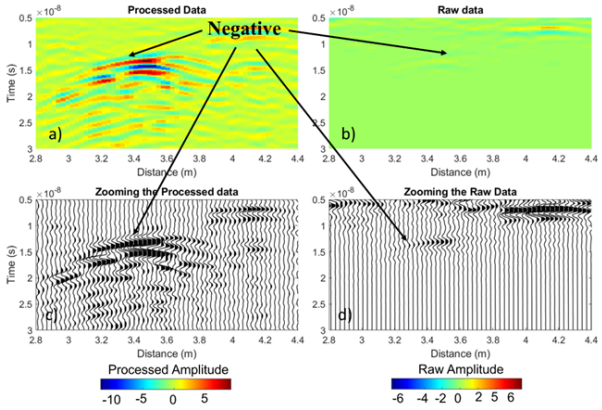

Fig. 10. zooming image for analyzing phase

Rys. 10. Powiększanie obrazu do analizy fazy

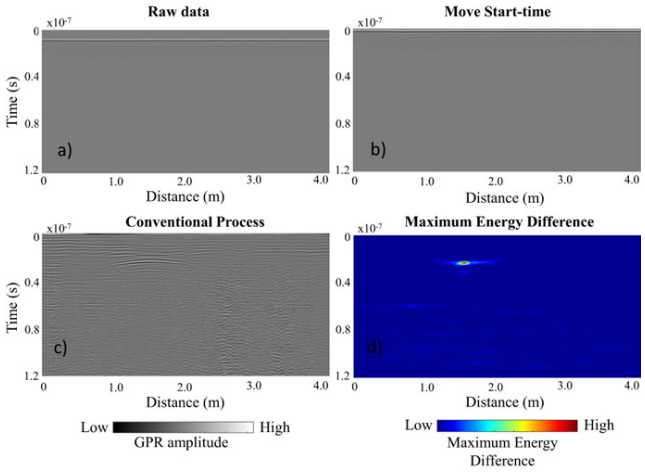

Fig. 11. The raw, Move Start-time, processed data and its maximum energy difference attribute in LeThuc Hoach street, Tan Phu district, Ho Chi Minh City, Vietnam

Rys. 11. Przetworzone dane surowe, czas rozpoczęcia ruchu i atrybut maksymalnej różnicy energii na ulicy LeThuc Hoach, dzielnica Tan Phu, miasto Ho Chi Minh, Wietnam

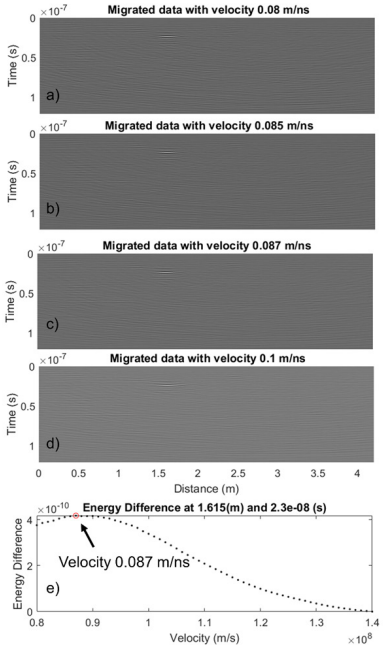

Fig. 12. Migration sections with different velocities and 1D Maximum energy difference curve versus velocities in Le Thuc Hoach street, Tan Phu district, Ho Chi Minh city, Vietnam

Rys. 12. Odcinki migracyjne o różnych prędkościach i krzywa maksymalnej różnicy energii 1D w zależności od prędkości na ulicy Le Thuc Hoach, dzielnica Tan Phu, miasto Ho Chi Minh, Wietnam

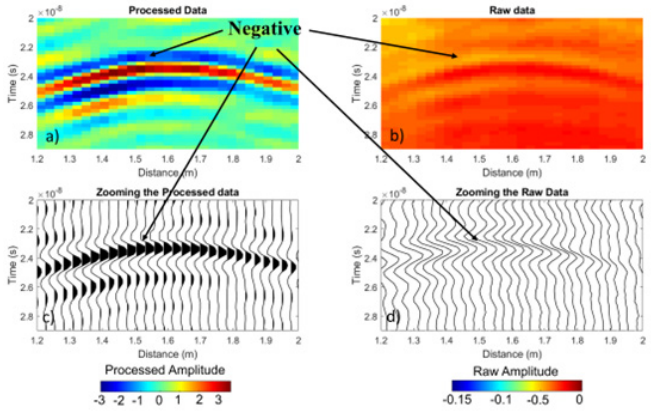

Fig. 13. Zooming image for analyzing phase of the processed and raw data in the interest zone containing a hyperbola

Rys. 13. Powiększanie obrazu do analizy fazy przetworzonych i nieprzetworzonych danych w strefie zainteresowania zawierającej hiperbolę

depths of the anomalies. For enhancing phase interpretation, we combine two zooming images of the raw and processed data for checking in-phase or out of phase cases in one modelling data and two real data. The originality of the raw data which can be seen in zooming image can be kept for checking the phase effects along with its processed data.

Acknowledgments

This research is funded by University of Science, VNUH-CM under grant number T2022-53.

Conflicts of Interest

The authors declare no conflict of interest.

Author Contribution

DHD run data modelling and data processing. CVAL wrote processing/ analysis Matlab codes for the GPR approach and interpreted GPR data. TVN measured real GPR data. LQN and NTH support data processing and manuscript writing. CVAL mainly write the manuscript.

Literatura – References

1. Bitri, A., and G. Grandjean. 1998, Frequency–wavenumber modelling and migration of 2D GPR data in moderately heterogeneous dispersive media. Geophysical Prospecting, 46, no. 3,287-301.
2. Chopra, S., and K. J. Marfurt. 2007, Seismic attributes for prospect identification and reservoir characteriztion. Edited by Stephen J. Hill, SEG Geophysical Development Series No. 11: Tulsa, Okla. (8801 South Yale St., Tulsa OK 74137-3175) : Society of Exploration Geophysicists.
3. Dang, D. H., C. V. A. Le, and T. D. Kieu. 2020, Ground Penetrating Radar attribute for analyzing underground anomaly. Paper read at EAGE 3rd Asia Pacific Meeting on Near Surface Geoscience & Engineering.
4. Kang, M.-S., N. Kim, S. B. Im, J.-J. Lee, and Y.-K. An. 2019, 3D GPR Image-based UcNet for Enhancing Underground Cavity Detectability. Remote Sensing, 11, no. 21,2545.
5. Kang, M.-S., N. Kim, J. J. Lee, and Y.-K. An. 2020, Deep learning-based automated underground cavity detection using three-dimensional ground penetrating radar. Structural Health Monitoring, 19, no. 1,173-185.
6. Kumar, J., A. C. Ramrez, and S. Butt. 2012, Preparing Data for Full Waveform Inversion: A Workflow for Free-surface Multiple Attenuation. Paper read at 74th EAGE Conference and Exhibition-Workshops.
7. Le, C. V. A., B. D. Harris, and A. M. Pethick. 2019, New perspectives on Solid Earth Geology from Seismic Texture to Cooperative Inversion. Scientific Reports, 9, no. 1,14737. doi: 10.1038/s41598-019-50109-z.
8. Le, C. V. A., B. D. Harris, A. M. Pethick, E. M. Takam Takougang, and B. Howe. 2016, Semiautomatic and Automatic Cooperative Inversion of Seismic and Magnetotelluric Data. Surveys in Geophysics, 37, no. 5,845-896. doi: 10.1007/s10712-016-9377-z.
9. Le, C. V. A., and T. V. Nguyen. 2020a, Detection of Underground Anomalies Using Analysis of Ground Penetrating Radar Attribute. Inżynieria Mineralna – Journal of the Polish Mineral Engineering Society, 1,23-34.
10. Le, C. V. A., and T. V. Nguyen. 2020b, Ground penetrating radar attributes analysis for detecting underground artificial structures in urban areas, Vietnam. Lowland Technology International, 22, no. 2,249-257.
11. Nguyen, T. V., C. V. A. Le, V. T. Nguyen, T. H. Dang, T. M. Vo, and L. N. L. Vo. 2017, Energy Analysis in Semiautomatic and Automatic Velocity Estimation for Ground Penetrating Radar Data in Urban Areas: Case Study in Ho Chi Minh City, Vietnam, International Conference on Geo-Spatial Technologies and Earth resources: Springer.
12. Virieux, J., and S. Operto. 2009, An overview of full-waveform inversion in exploration geophysics. Geophysics, 74, no. 6,WCC127–WCC152.
13. Warren, C., A. Giannopoulos, and I. Giannakis. 2016, gprMax: Open source software to simulate electromagnetic wave propagation for Ground Penetrating Radar. Computer Physics Communications, 209,163-170.
14. Zhao, W., E. Forte, and M. Pipan. 2016, Texture attribute analysis of GPR data for archaeological prospection. Pure and Applied Geophysics, 173, no. 8,2737-2751.

Przebieg pracy z danymi radarowymi penetrującymi ziemię. Analiza oparta na sterowaniu maksymalną różnicą energii

Ground Penetrating Radar jest powszechnie stosowany w inżynierii lądowej i wodnej. Podziemne anomalie (np. przewody elektryczne, rury wodociągowe lub zapadliska) można wykryć za pomocą reprezentacji hiperbol w zmierzonym przetworzonym obrazie GPR. Nasza praca koncentruje się na wykrywaniu podziemnych obiektów i zrozumieniu ich metalicznych lub niemetalicznych wła-ściwości. Atrybut maksymalnej różnicy energii jest stosowany do oświetlania ich pozycji, podczas gdy proces analizy fazowej może określić zmianę widma fazowego w dyfrakcyjnych sygnałach. Aby usprawnić analizę fazową, zastosowaliśmy nowatorski przepływ pracy łączący konwencjonalne kroki przetwarzania i krok powiększania w celu zachowania oryginalności fazy bez zakłócania przez niepotrzebne filtry. Zastosowaliśmy przepływ pracy w modelu i rzeczywistych danych, aby udowodnić jego skuteczność. Interpretacja dwóch rzeczywistych zbiorów danych w Wietnamie za pomocą naszego przepływu pracy może wyrazić istnienie sztucznych anomalii podziemnych, a także ich charakterystykę materii w porównaniu z otaczającym je środowiskiem.

Słowa kluczowe: *radar penetrujący podłoże, analiza fazowa, różnica energii*

Wycena wartości ekonomicznej zdecentralizowanego przedsiębiorstwa górniczego

Kacper GRZYWNOWICZ[1)], Arkadiusz KUSTRA[2)], Romuald OGRODNIK[3)]

[1)] Eng.; AGH University of Krakow, Faculty of Civil Engineering and Resource Management, Krakow, Poland; email: kacgrzy@gmail.com
[2)] Assoc. Prof. PhD. D.Sc. Eng.; AGH University of Krakow, Faculty of Civil Engineering and Resource Management; ORCID: 0000-0001-8416-4405
[3)] PhD. D.Sc. Eng.; AGH University of Krakow, Faculty of Civil Engineering and Resource Management

http://doi.org/10.29227/IM-2023-01-26

Submission date: 12-05-2023 | Review date: 23-06-2023

Abstrakt

W niniejszej pracy przeprowadzono badania literaturowe z zakresu wartości przedsiębiorstwa. Zaprezentowano podział wartości ze względu na metody ich kalkulacji wyróżniając metody majątkowe, rynkowe oraz ekonomiczne. Szczegółowo opisano metody szacowania wartości ekonomicznej, wyróżniając metody bazujące na przyszłych przepływach pieniężnych DCF oraz EVA, która oparta jest na kapitale zainwestowanym. Artykuł został uzupełniony o metodologię SOTP, która pomimo szerokiego zastosowania dzięki podziałowi wyceny na poszczególne segmenty działalności, dające szczegółowe informacje o generowaniu wartości. Zakończeniem pracy jest przeprowadzona wycena wartości ekonomicznej zdecentralizowanego przedsiębiorstwa górniczego. Wykazała ona, iż metody DCF oraz EVA są tożsame a także ukazała użyteczność metody SOTP w przedsiębiorstwach wielosegmentowych jako narzędzia wyceny.

Słowa kluczowe: *górnictwo przedsiębiorstwo zdecentralizowane, wartość ekonomiczna, zdyskontowane przepływy pieniężne DCF, ekonomiczna wartość dodana EVA, metoda sum częściowych SOTP*

1. Wstęp

W obliczu rozwoju technologii, ciągle postępującej globalizacji rynku oraz licznych zmian warunków geopolitycznych, przedsiębiorstwa i oddziałujące na nie grupy interesariuszy zmuszone są do ciągłego wzmacniania swojej pozycji zarówno krajowej jak i na arenie międzynarodowej. Wynika stąd konieczność wypracowania oraz zdefiniowania systemu stanowiącego podstawę budowania przedsiębiorstwa, który wspomoże realizację założonej misji opartej na wzroście wartości.

Opisane czynniki stanowią podstawę stworzenia systemu zarządzania wartością przedsiębiorstwa VBM (ang. Value Based Management). Koncepcja ta pomimo popularności – wciąż ma charakter elitarny. Wynika to głównie z faktu, iż od przedsiębiorstw stosujących VBM wymaga się określenia strategii, stosowania odpowiednich systemów ewidencjonowania oraz wykorzystania danych i mierników. Z tak skonstruowanego systemu korzystać powinny przedsiębiorstwa, które jednocześnie będą charakteryzowały się wysokim stopniem zorganizowania, ale też sformalizowania. Głównym założeniem VBM jest skupienie procesu decyzyjnego wokół znaczących czynników wpływających na wartość przedsiębiorstwa. Znaczącą rolą w całym procesie jest maksymalizowanie wartości dla akcjonariuszy, bowiem to właśnie oni dążą do takiego zarządzania przedsiębiorstwem, aby było ono zyskowne zarówno w kontekście krótko- jak i długoterminowym. Wzrost korzyści akcjonariuszy idzie w parze również ze wzrostem wszystkich związanych z przedsiębiorstwem podmiotów [3].

W rozwiniętych gospodarkach rynkowych, powszechny proces wyceny przedsiębiorstw odbywa się najczęściej bezpośrednio na rynkach kapitałowych, w toku masowo zawieranych transakcji. Bazując na tego rodzaju bezpośredniej wycenie rynkowej należy zauważyć, że można również dokonywać wyceny wartości przedsiębiorstwa bazując na innych kategoriach związanych z retrospektywnym ujęciem kosztów i nakładów poniesionych jak również prospektywnym podejściem związanym z szacowaniem korzyści z biznesu.

Celem niniejszego artykułu jest zdefiniowanie oraz prezentacja różnych podejść oraz metodyk wyceny przedsiębiorstwa, w ramach stałego procesu zarządzania wartością. Główny nacisk położono na metody wyceny wartości ekonomicznej, które z jednej strony są najbardziej metodologicznie poprawne w sensie kalkulacji a z drugiej strony odzwierciedlają prospektywną zdolność podmiotu do generowania korzyści z biznesu dysponującego kapitałem realnym i niematerialnym.

2. Wartość jako miernik

Wartość, zarówno w naukach ekonomicznych, jak i ogólne tego słowa znaczenie, nie posiada jednoznacznej definicji w literaturze naukowej, a także w praktyce gospodarczej. Różnorodność metod i technik wyceny wartości powoduje istnienie różnić wartości tego samego podmiotu w tym samym czasie. Określenie wartości w wielu sytuacjach, jest punktem wyjścia dla istotnych decyzji zarówno inwestycyjnych, operacyjnych jak i finansowych.

Według J. Duraj „wartość" można określić w trzech wymiarach znaczeniowych jako [4]:

- Dobro – wszystko co cenne i może stanowić cel ludzkich dążeń
- Odpowiedź na potrzebę – pozwala człowiekowi żyć, rozwijać się i doskonalić
- Idea ogólna – mająca doniosłe znaczenie dla człowieka i społeczeństwa

Wartość przedsiębiorstwa, jak można się dowiedzieć z różnych źródeł naukowych, jest oceniana z perspektywy

samych właścicieli. Zainwestowany przez nich kapitał oraz włożona praca skutkują oczekiwaniem określonego zwrotu. Upraszczając, całe to zjawisko można by przyrównać do wartości towaru na rynku – firma jest warta tyle, ile obecni właściciele otrzymaliby za posiadane udziały i akcje przy potencjalnej sprzedaży spółki. Jednakże na przestrzeni ostatnich lat samo pojęcie wartości ewoluowało powiększając swój zakres korzyści, nie tylko dla właścicieli, ale również dla wszystkich interesariuszy takich jak pracownicy czy dostawcy.

Brak zdefiniowania wartości przedsiębiorstwa uniemożliwia jego zarządzanie, co jest kluczowe przy podejmowaniu wszelakich decyzji. Definicja zarządzania wartością powinna determinować nośniki wartości, czyli obejmować czynniki zarówno strategiczne jak i operacyjne. Warto również zauważyć, że wartość przedsiębiorstwa w zależności od kategorii ujęcia, jest determinowana zdolnością do generowania korzyści w przyszłości, mierzonych przepływami (wartość ekonomiczna) oraz wartość posiadanych aktywów pomniejszonych o zobowiązania w ujęciu historycznym ich powstania (wartość majątkowa) lub też wartość rynkową kapitału własnego odzwierciedloną ceną akcji notowanych na rynku kapitałowym (wartość rynkowa).

Wyznaczają one podstawowe grupy metod wyceny przedsiębiorstwa:

- Metody majątkowe
- Metody mnożnikowe
- Metody dochodowe
- Metody mieszane

Sama wycena przedsiębiorstwa skupia się na przyszłości, to znaczy jakich korzyści się spodziewamy, dlatego też ma ona charakter szacunkowy. Dane historyczne nie są stosowane do wyceny przedsiębiorstwa, jednakże używa ich się w kontekście uwiarygodnienia prognoz, pod warunkiem braku całkowitej zmiany profilu czy sektora, w którym przedsiębiorstwo operuje. Oczywiście celem zarządzania jest maksymalizacja wartości, między innymi poprzez dążenie do takich celów operacyjnych jak [6]:

- uzyskanie określonego udziału w rynku
- osiągniecie przychodów ze sprzedaży
- ograniczenie kosztów działalności
- maksymalizacja wyników operacyjnych

Do głównych kategorii wartości przedsiębiorstwa zaliczyć można:

- Wartość majątkową
- Wartość rynkową
- Wartość ekonomiczną

3. Metody wyceny wartości majątkowej

Wartość majątkowa przedsiębiorstwa jest jedną z najbardziej podstawowych kategorii ekonomicznych. Przedstawia ona wartość bazującą na sumie wartości poszczególnych składnikach majątku.

Wyróżnia się cztery główne techniki wyceny przedsiębiorstwa metodą majątkową [7]:

- metoda księgowa – metoda opierająca się na sprawozdaniach finansowych firmy. Polega na wycenie przedsiębiorstwa na podstawie księgowej wartości majątku pomniejszonego o zobowiązania. Specyfiką tej metody są niskie koszty oraz prostota obliczeń.
- metoda likwidacyjna – metoda wycenia minimalną wartość podmiotu zatwierdzoną przez sprzedającego, a poniżej której, bardziej opłacalna jest likwidacja działalności, sprzedaż aktywów i spłata zobowiązań. Stosując tą metodę dodatkowo uwzględniania się koszty hipotetycznej likwidacji przedsiębiorstwa, ewentualne dyskonto z tytułu szybkiej sprzedaży składników majątkowych oraz koszty rozwiązania umów z pracownikami i kontraktów handlowych. Omawiana metoda jest stosowana przeważnie w sytuacjach, gdy przedsiębiorstwo znajduje się na schyłku swojej działalności gospodarczej.
- metoda odtworzeniowa – metoda uwzględniająca koszty zawiązania i organizacji spółki, obejmujące pozyskanie finansowania, zatrudnienia pracowników, zawarcia kluczowych dla jej przyszłej działalności kontraktów handlowych itp. Określa maksymalną wartość korzystną dla potencjalnego inwestora, powyżej której, bardziej rentowną decyzją jest zawiązanie i rozwój nowego podmiotu. Metoda odtworzeniowa jest charakterystyczna dla przedsiębiorstw będących we wczesnym etapie działalności.
- metoda skorygowanych aktywów netto (SAN) – metoda bazująca na metodzie księgowej, jednakże uwzględniająca swoiste korekty. Najczęściej korekty dotyczą nieruchomości, wartości niematerialnych i prawnych oraz udziałów w obcych jednostkach. Korekta zazwyczaj polega na sprowadzeniu wartości księgowej netto zarówno aktywów jak i zobowiązań do ich wartości rynkowej.

4. Metody wyceny wartości rynkowej

Definicja szacowania wartości rynkowej mówi, że jest to najniższa cena, na jaką może się zgodzić osoba sprzedająca oraz najwyższy koszt, jaki jest gotowy ponieść kupujący. Wartość rynkowa wykazuje charakter dynamiczny wynikający z dużej wrażliwości na zmienne preferencje kupującego, sytuacje polityczne, koniunkturę czy elastyczność sprzedającego.

Metody szacowania wartości rynkowej, zwane również mnożnikowymi, oparte są na założeniu, że to właśnie rynek finansowy dostarcza najlepszych informacji niezbędnych do wyceny. Są to metody wykorzystujące relacje ekonomiczne, które dotychczas ukształtowały się na rynku kapitałowym w związku z nieustannie dokonywanymi transakcjami sprzedaży – kupna zarówno akcji jak i przedsiębiorstw. Bazują one na swoistego rodzaju porównaniach z innymi, zbliżonymi podmiotami gospodarczymi. Proces przeprowadzania takich analiz polega na znalezieniu innej firmy bądź grupy firm o charakterze tożsamym np. z tej samej branży, ze zbliżoną wartością aktywów bądź z podobnymi produktami. Następnym kluczowym czynnikiem jest wybór pożądanego wskaźnika rynkowego (mnożnika) będącego trzonem całej wyceny. Najpopularniejszym wyborem jest między innymi wartość jednej akcji do wartości zysku netto na jedna akcję. W dalszej części analizy należy wyznaczyć wielkości będące podstawą wybranego wskaźnika dla wycenianej firmy np. zysk operacyjny lub przychód ze sprzedaży. Ostatnim krokiem jest ustalenie wartości przedsiębiorstwa poprzez pomnożenie wybranego mnożnika przez wybraną wielkość ekonomiczną.

5. Metody wyceny wartości ekonomicznej

Ostatnim – jednak równie ważnym rodzajem metod wyceny przedsiębiorstwa – są metody ekonomiczne zwane dochodowymi. Główne zasady funkcjonowania gospodarki rynkowej sprawiają, że podstawą oceny przedsiębiorstwa przez potencjalnych inwestorów bądź nabywców jest jego zdolność do generowania dochodów, a co za tym idzie przynoszenia wymiernych korzyści finansowych swoim właścicielom. Wysoka ranga metod dochodowych w procesie wyceny przedsiębiorstw wynika ponadto z cechy kapitału jako podstawy istnienia i funkcjonowania przedsiębiorstwa, którą jest zdolność do wzrostu, czyli pomnażania w rezultacie angażowanie go w działalność przedsiębiorstwa [1]. Z tego powodu ekonomiczne metody wyceny stanowią zasadniczą część niniejszego artykułu. Mnogość oraz zróżnicowanie metod dochodowych występujących w obecnej nauce uniemożliwia rzetelne oraz kompletne przedstawienie każdej z nich, w związku z czym wybrano następujące trzy metody, które zostały rozwinięte w tymże artykule.

5.1 Metoda DCF

Metoda zdyskontowanych przepływów pieniężnych DCF (z ang. Discounted Cash Flows) – jest to najbardziej znana oraz uznana metoda wyceny przedsiębiorstwa. W metodzie nie uwzględnia się majątku firmy na rzecz osiągalnych przepływów finansowych jakie w teraźniejszości bądź przyszłości przedsiębiorstwo będzie zdolne wygenerować. Warto zwrócić również uwagę na to, iż w metodach dochodowych wszelkiego rodzaje prognozy przepływów pieniężnych opierają się na jedynie na planach kształtowania się przyszłej wartości przychodów netto ze sprzedaży, stąd pozostałe pozycje wchodzące w skład wolnych przepływów pieniężnych są naliczane od zmiany wartości sprzedaży. Zaleca się uprzednio przeprowadzanie analizy fundamentalnej przedsiębiorstwa za co najmniej cztery ostanie lata działalności w celu oceny kondycji finansowej przedsiębiorstwa oraz zidentyfikowaniu potencjalnych zagrożeń, które mogłyby w znaczący sposób zaburzyć plan przyszłych przepływów. Przeprowadzenie poprawnej prognozy sprzedaży jest kluczowe dla całego procesu, dlatego wymaga kompleksowej znajomości wycenianego przedsiębiorstwa z wyszczególnieniem:

- Sektora, w którym firma funkcjonuje oraz zachodzących w nim zmian i trendów
- Charakteru związków z dostawcami i odbiorcami
- Posiadanych linii produktowych i oferowanych asortymentów produktów
- Siły i istoty konkurencji

Otrzymana prognoza przychodów ze sprzedaży powinna być również adekwatna do sytuacji wewnętrznej oraz zewnętrznej firmy oraz spójna z historycznymi rezultatami działalności poddawanego wycenie przedsiębiorstwa.

Wykorzystanie podejścia utraty wartości pieniądza, która opiera się na przekonaniu, że dana kwota dziś jest warta więcej aniżeli będzie na przestrzeni przyszłych lat, czyni omawianą metodę rzetelniejszą oraz bardziej dokładną.

Metoda DCF posiada kilka wariantów, które umożliwiają otrzymanie wyników z pożądanego zakresu. Poniżej przedstawiono niektóre z nich:

- Metoda przepływów pieniężnych dla właścicieli kapitałów z angielskiego Free Cash Flow to Equity (FCFE) – wolne przepływy pieniężne dla właścicieli kapitału własnego są to środki które stanowią nadwyżkę bądź niedobór środków pieniężnych wywodzących się z działalności dodatkowo pomniejszone o zobowiązania wobec inwestorów np. dywidendę. Wyniki otrzymane poprzez zastosowanie tej metody obrazują skuteczność decyzji podejmowanych przez właścicieli spółki. Omawiany wariant prezentuje podejście własnościowe, a więc dostarcza cennych informacji właścicielom kapitału.
- Metoda przepływów przedsiębiorstwa jako całości – z ang. free cash flows to firm (FCFF) – narzędzie umożliwiające określenie ilości gotówki generowanej przez przedsiębiorstwo z działalności operacyjnej oraz inwestycyjnej, po uregulowaniu wszystkich oczekiwań finansowych dawców kapitału. Tak samo jak FCFE, wykazuje większą dokładność względem np. zysku netto, ponieważ uwzględnia ona koszty, zmniejszające jego wartość, jednocześnie niebędące wydatkiem np. amortyzację. Przygotowane przez przedsiębiorstwo pomaga w ocenie efektywności podejmowanych decyzji. Metoda zakłada podejście podmiotowe.

Metoda zdyskontowanych przepływów pieniężnych stanowi najpowszechniej stosowany sposób przeprowadzania wycen przedsiębiorstw oraz jest nieodzowną częścią prowadzenia negocjacji biznesowych z inwestorami. Informuje inwestorów o najistotniejszych dla nich parametrach takich jak możliwe ryzyko oraz korzyści. Jednakże nie jest ona pozbawiona wad. Ogrom danych niezbędnych do przeprowadzenia kompleksowej analizy prowadzi do błędów wyliczeniowych co w rezultacie skutkuje fałszywą wyceną spółki. Ponadto trudność, a nawet w niektórych przypadkach, niemożliwość oszacowania przyszłych wyników przedsiębiorstwa powoduje, że ich poziom jest zależny od osoby prowadzącej wycenę. Sama metoda również nie da rzetelnych wyników dla małych i mikro przedsiębiorstw, których wyniki finansowe cechuje duża zmienność.

5.1 Metoda EVA

Ekonomiczna wartość dodana z – ang. Economical Value Added (EVA) – jest to metoda stworzona przez nowojorską firmę Stewart & Co., obrazująca efekt gospodarowania przedsiębiorstwa. Dzięki swojej uniwersalności oraz łatwości zrozumienia jest drugą, zaraz po DCF, najczęściej stosowną metodą wyceny przedsiębiorstw. Istotą EVA jest uwzględnienie w ocenie efektywności nie tylko wartości wypracowanych, skorygowanych zysków, ale również całkowitej wartości zaangażowanego kapitału wliczając to również kapitał własny [5]. Taka postać wskaźnika umożliwia kadrze zarządczej efektywniejsze kształtowanie wartości przedsiębiorstwa pod wpływem oczekiwanego przez inwestorów zwrotu oraz maksymalizację majątku akcjonariuszy. Sam twórca omawianej metody opisuje jej cztery główne filary znane jako 4M, czyli Measurement, Management System, Motivation, Mindset (Pomiar, System Zarządzania, Motywacja, Nastawienie). Prezentuje to, wyróżniające metodę EVA na tle innych, podejście do pracowników, któremu przyświeca przekonanie o tym, że nieopłacalna jest kontrola zatrudnionych, lecz budowanie re-

lacji opartej na wspólnym celu, którego osiągnięcie jest możliwe jedynie przez współpracę. Całą tą ideę uzupełnia budowa schematu planu wynagrodzeniowego opierającego się na wykreowanej wartości dodanej. Założenia metody wyraźnie precyzują sposoby powiększania wartości przedsiębiorstwa:

- Zwiększenie zwrotu z posiadanych aktywów,
- Uwolnienie zainwestowanego kapitału poprzez sprzedaż nierentownych aktywów,
- Wzrost efektywności wykorzystania kapitału poprzez zmianę wartości dźwigni finansowej
- Reinwestowanie kapitału oraz powiększanie wartości aktywów w momencie, gdy oczekiwany z nich zwrot przewyższa koszty kapitału zainwestowanego.

Pierwszym etapem metody EVA jest przełożenie wyniku księgowego na zysk ekonomiczny, poprzez zastosowanie swoistych korekt. W pierwotnej wersji opracowanej przez Stern Steward & Co było konieczne zastosowanie aż 164 różnych korekt, jednakże w przypadku wielu firm niemożliwe jest wprowadzeniu ich wszystkich z powodu braku niezbędnych do ich wykonania danych finansowych, w rezultacie wybierając jedynie kilka z nich w tym najistotniejszą, korektę podatku dochodowego. W drugim etapie dokonuje się zamiany z wartości księgowej na wartość ekonomiczną, poprzez zsumowanie kapitałów własnych podmiotu oraz zobowiązań odsetkowych jednocześnie pomniejszając je o koszty składające się ze średniej ważonej wyliczanej na podstawie kosztów kapitałów własnych firmy oraz zobowiązań odsetkowych.

Wzory na wyliczenie EVA zmieniały się na przestrzeni lat, jednakże bazując na oryginale opracowanym w 1989 roku. Przedstawiał on EVA w następujący sposób:

$$EVA=NOPAT-IC*WACC$$

Gdzie NOPAT (z ang. Net Operating Profit After Tax) oznacza zysk operacyjny netto po opodatkowaniu, a więc jest on równoznaczny z wartością EBIT pomniejszoną o podatek. IC jest wartością zainwestowanego kapitału w połączeniu z wartością oprocentowanego kapitału kredytodawców przedsiębiorstwa. Ostatnim elementem jest współczynnik WACC który został już omówiony w związku z metodą DCF.

Ekonomiczna wartość dodana umożliwia podejmowanie skuteczniejszych i efektywniejszych decyzji, dzięki dostarczaniu cennych informacji o całej firmie a również poprzez system motywacyjny wywiera pozytywny wpływ na wszystkich członków organizacji. Ponadto przystępność otrzymanych wyników daje możliwość poprawnej interpretacji zarówno laikom nauk ekonomicznych jak i profesjonalistom. Stosowanie EVA umożliwia przedsiębiorstwu odpowiednią alokację kapitału na wielu poziomach agregacji działalności. Wszystkie wyżej wymienione czynniki stanowią składowe popularności owej metody zarówno wśród analityków jak i właścicieli firm.

5.3 Metoda SOTP

W przypadku zdecentralizowanej struktury działalności przedsiębiorstwa możliwe jest oszacowanie DCF dla poszczególnych obszarów czy segmentów biznesowych których sumaryczna wartość może być odzwierciedlona poprze metodologię SOTP.

Wycena ta jest metodą szacowania wartości ekonomicznej sumy części poszczególnych obszarów działalności (segmentów biznesowych) z angielskiego Sum-Of-The-Parts (SOTP). Stanowi ona popularne podejście do wyceny wśród zaawansowanych praktyków i inwestorów, jednakże jest ona dość często pomijana przez badaczy i naukowców. Wycena opiera się na założeniu, że segmenty działalności firmy różnią się charakterystykami rentowności oraz wzrostu. W związku z tym uzasadniona jest oddzielna wycena każdego segmentu. Aby uzyskać szacunkową wartość całego przedsiębiorstwa, należy dodać oddzielne szacunki wartości poszczególnych segmentów [2]. Wycena sumy części jest inaczej nazywana analizą wartości podziału. SOTP informuje o wartości każdej części firmy, w porównaniu z wartością firmy jako całości. Umożliwia ona inwestorom i analitykom lepiej zrozumieć wartość firmy i zidentyfikować możliwości wzrostu lub oszczędności kosztów. Jeśli część firmy jest nabywana lub sprzedawana bez zastosowania owej metody, może to skutkować zaniżeniem rzeczywistej wartości danego segmentu co w rezultacie przyniesie znaczącą stratę zarówno dla właścicieli jak również dla inwestorów.

Identyfikacja nierentownych lub niedowartościowanych aktywów jest kluczowa z punktu widzenia zarządzania przedsiębiorstwem. Analiza SOTP wspomaga firmę w zidentyfikowaniu słabo działających lub niedowartościowanych aktywów, które mogą hamować ogólną wydajność firmy. Może to pomóc kierownictwu skupić się na poprawie tych aktywów lub rozważyć ich zbycie w celu odblokowania wartości dla akcjonariuszy. Oddzielając różne segmenty lub aktywa spółki, analiza SOTP wspomaga proces selekcji obszarów działalności, które mają duże perspektywy wzrostu. Dostarczanie kierownictwu informacji na temat danych sektorów, pozwala odpowiednio zarządzać zasobami, aby zmaksymalizować potencjalny wzrost i rentowność. Dzięki podziale kosztów i przychodów na wybrane segmenty analiza SOTP może pomóc spółce w lepszym komunikowaniu wartości inwestorom i analitykom. Może to poprawić przejrzystość i ułatwić interesariuszom zrozumienie ogólnej wartości firmy i perspektyw wzrostu. Omawiana metoda stanowi również narzędzie wspomagające kierownictwo w podejmowaniu strategicznych decyzji, takich jak fuzje i przejęcia, wspólne przedsięwzięcia i zbycia. Wyceniając aktywa spółki docelowej i porównując je z aktywami spółki przejmującej, zarząd może zdecydować, czy transakcja przyniesie spółce wzrost czy dewaloryzację.

Należy zauważyć, że metoda SOTP nie jest jedynym sposobem wyceny spółki, a jej wyniki powinny być rozpatrywane w kontekście innych metod wyceny i warunków rynkowych. Proces analizy obejmuje identyfikację segmentów biznesowych lub aktywów spółki, określenie wartości każdego segmentu lub aktywa przy użyciu metod takich jak analiza zdyskontowanych przepływów pieniężnych (DCF), analiza porównywalnych spółek lub analiza transakcji poprzedzających. Istotne jest również porównanie wartości SOTP z bieżącą kapitalizacją rynkową spółki i ciągłe monitorowanie wyników spółki.

SOTP jest powszechnie stosowany podczas modelowania lub wyceny spółki z różnymi liniami biznesowymi. Może to być duży konglomerat lub mniejsza firma, która ma kilka różnych ofert.

Metodologia SOTP nie ogranicza się do największych międzynarodowych konglomeratów (jak można by sądzić z dostępnych informacji). W rzeczywistości jest ona również niezwykle pomocna dla każdej firmy z różnymi działami lub

Tab. 1. Bilans całego przedsiębiorstwa. Źródło:Opracowanie własne

Tab. 1. Balance sheet of the entire enterprise. Source: Own study

	2023	2024	2025	2026	2027		2023	2024	2025	2026	2027
Aktywa trwałe	**344 923**	**939 915**	**817 361**	**1 310 204**	**838 548**	**Kapitał własny**	**663 768**	**492 592**	**1 952 352**	**2 232 000**	**1 912 413**
Rzeczowe aktywa trwałe	344 923	939 915	817 361	1 310 204	838 548	Kapitał podstawowy	460 000	460 000	1 721 176	1 725 068	1 725 068
						Kapitał zapasowy	115 808	3 732	28 556	43 780	32 703
						Wynik finansowy	87 960	28 860	202 620	463 152	154 642
Aktywa obrotowe	**1 124 130**	**1 926 932**	**2 682 112**	**2 867 032**	**2 616 831**	**Zobowiązania i rezerwy**	**805 285**	**2 374 255**	**1 547 121**	**1 945 236**	**1 542 966**
Zapasy	715 330	1 287 490	1 718 480	1 856 000	1 765 398	Zobowiązania długoterminowe	323 432	723 432	400 000	349 061	420 156
Należności	351 200	632 160	878 000	921 600	754 900	Kredyty bankowe krótk.	200 123	636 933	300 321	459 555	590 540
Inwestycje	57 600	7 282	85 632	89 432	96 533	Zobowiązania wobec dostwców	145 600	524 160	436 800	576 120	322 145
						Rozlicznia międzyokresowe krótkoterm	136 130	489 730	410 000	560 500	210 125
SUMA	**1 469 053**	**2 866 847**	**3 499 473**	**4 177 236**	**3 455 379**	**SUMA**	**1 469 053**	**2 866 847**	**3 499 473**	**4 177 236**	**3 455 379**

Tab. 2. Bilans segmentu A. Źródło: Opracowanie własne

Tab. 2. Segment A balance sheet. Source: Own study

	2023	2024	2025	2026	2027		2023	2024	2025	2026	2027
Aktywa trwałe	**310 431**	**845 924**	**735 625**	**1 179 184**	**754 693**	**Kapitał własny**	**423 604**	**334 319**	**1 297 431**	**1 601 286**	**1 076 410**
Rzeczowe aktywa trwałe	310 431	845 924	735 625	1 179 184	754 693	Kapitał podstawowy	226 426	314 000	1 107 333	1 152 561	985 894
						Kapitał zapasowy	31 066	2 612	19 989	30 646	22 892
						Wynik finansowy	166 113	17 706,40	170 108	418 079	67 624
Aktywa obrotowe	**504 638**	**840 807**	**1 178 830**	**1 268 362**	**1 202 302**	**Zobowiązania i rezerwy**	**391 464**	**1 352 412**	**617 025**	**846 260**	**880 585**
Zapasy	429 198	772 494	1 031 088	1 113 600	1 059 239	Zobowiązania długoterminowe	94 059	334 059	140 000	109 437	152 094
Należności	35 120	63 216	87 800	92 160	75 490	Kredyty bankowe krótk.	140 086	445 853	210 225	263 418	413 378
Inwestycje	40 320	5 097	59 942	62 602	67 573	Zobowiązania wobec dostwców	116 480	319 328	149 440	310 896	257 716
						Rozlicznia międzyokresowe krótkoterm	40 839	253 172	117 360	162 510	57 398
SUMA	**815 069**	**1 686 731**	**1 914 455**	**2 447 546**	**1 956 995**	**SUMA**	**815 069**	**1 686 731**	**1 914 455**	**2 447 546**	**1 956 995**

Tab. 3. Bilans segmentu B. Źródło: Opracowanie własne

Tab. 3. Segment B balance sheet. Source: Own study

	2023	2024	2025	2026	2027		2023	2024	2025	2026	2027
Aktywa trwałe	**34 492**	**93 992**	**81 736**	**131 020**	**83 855**	**Kapitał własny**	**240 164**	**158 273**	**654 921**	**630 714**	**836 003**
Rzeczowe aktywa trwałe	34 492	93 992	81 736	131 020	83 855	Kapitał podstawowy	233 574	146 000	613 843	572 507	739 174
						Kapitał zapasowy	84 742	1 120	8 567	13 134	9 811
						Wynik finansowy	-78 153	11 154	32 512	45 074	87 019
Aktywa obrotowe	**619 492**	**1 086 125**	**1 503 282**	**1 598 670**	**1 414 529**	**Zobowiązania i rezerwy**	**413 821**	**1 021 843**	**930 096**	**1 098 976**	**662 381**
Zapasy	286 132	514 996	687 392	742 400	706 159	Zobowiązania długoterminowe	229 373	389 373	260 000	239 624	268 062
Należności	316 080	568 944	790 200	829 440	679 410	Kredyty bankowe krótk.	60 037	191 080	90 096	196 138	177 162
Inwestycje	17 280	2 185	25 690	26 830	28 960	Zobowiązania wobec dostwców	29 120	204 832	287 360	265 224	64 429
						Rozlicznia międzyokresowe krótkoterm	95 291	236 558	292 640	397 990	152 728
SUMA	**653 984**	**1 180 116**	**1 585 018**	**1 729 690**	**1 498 384**	**SUMA**	**653 984**	**1 180 116**	**1 585 018**	**1 729 690**	**1 498 384**

Tab. 4. Rachunek zysków i strat całego przedsiębiorstwa. Źródło:Opracowanie własne

Tab. 4. Profit and loss account of the entire enterprise. Source: Own elaboration

	2023	2024	2025	2026	2027
Przychody ze sprzedaży	3 432 000	6 134 000	7 035 600	7 875 502	6 598 037
Koszty sprzedanych produktów	2 864 000	5 428 000	5 975 992	6 250 124	5 678 400
Koszty ogólnoadministracyjne	358 672	419 988	550 000	656 522	430 800
EBITDA	209 328	286 012	509 608	968 856	488 837
Amortyzacja	18 900	101 900	101 900	121 636	110 600
Wynik operacyjny (EBIT)	190 428	184 112	407 708	847 221	378 237
Koszty finansowe	43 828	136 012	70 008	75 300	120 500
Wynik brutto (EBT)	146 600	48 100	337 700	771 921	257 737
Podatek doch.	58 640	19 240	135 080	308 768	103 095
Wynik netto (EAT)	87 960	28 860	202 620	463 152	154 642

ofertami. Rozważmy przykład lokalnej firmy poligraficznej. Zajmuje się ona tylko dwiema rzeczami: drukowaniem dokumentów na miejscu w tradycyjnej drukarni oraz handlem elektronicznym. Model finansowy SOTP firmy zajmującej się drukowaniem dokumentów będzie wymagał analizy ilości wydruków, cen według rodzaju dokumentu, kosztów papieru, czynszu, pracowników sklepu itp. Z kolei model handlu elektronicznego będzie wymagał wglądu w liczbę sprzedanych drukarek, cenę drukarek, powierzchnię magazynową, wydatki na reklamę online itp. Najważniejszym punktem dla tego biznesu będzie różnica w wartości między tymi dwoma segmentami. Założono, że fizyczna działalność drukarska jest większa zarówno pod względem przychodów, jak i wartości EBITDA. W innej metodzie wpłynęłoby to proporcjonalnie na wartość firmy. Jednak inwestorzy i rynek są znacznie bardziej rozemocjonowani szybszym rozwojem oraz wyższą marżą działalności handlowej. Ta oferta jest nowsza i ma mniejsze przychody, ale będzie generować większą wartość w transakcjach.

Wycena SOTP, poprzez swoją specyfikę, nie zawsze znajduje zastosowanie we wszystkich rodzajach firm. Poniżej przedstawiono założenia, w których owa metodyka daje najlepsze rezultaty [8]:

- Firmy, które posiadają różne segmenty lub działy biznesowe
- Firmy holdingowe lub konglomeraty z wieloma różnymi firmami
- Spółki posiadające odrębne aktywa
- Sytuacje, które wymagają wysokiego stopnia szczegółowości
- Omawiany model nie sprawdza się w przypadku2:
- Spółki z pojedynczą linią biznesową
- Spółek, które nie ujawniają żadnych segmentów i w których nie można znaleźć tych informacji
- W przypadku gdy prosty, mniej szczegółowy model jest odpowiedni

6. Prezentacja zastosowania metod ekonomicznych wyceny przedsiębiorstwa na przykładzie fikcyjnej spółki

W celu zobrazowania dotychczasowych informacji, przedstawionych w niniejszym artykule, przeprowadzono wy-

Tab. 5. Rachunek zysków i strat segmentu A. Źródło: Opracowanie własne
Tab. 5. Segment A profit and loss account. Source: Own study

	2023	2024	2025	2026	2027
Przychody ze sprzedaży	2 402 400	3 680 400	4 924 920	5 512 851	4 618 626
Koszty sprzedanych produktów	2 004 800	3 311 080	4 183 194	4 062 581	3 974 880
Koszty ogólnoadministracyjne	146 530	171 607	356 726	678 199	342 186
EBITDA	251 070	197 713	385 000	772 071	301 560
Amortyzacja	13 230	71 330	71 330	85 145	77 420
Wynik operacyjny (EBIT)	237 840	126 383	313 670	686 926	224 140
Koszty finansowe	30 680	95 208	49 006	52 710	84 350
Wynik brutto (EBT)	207 161	31 174	264 664	634 216	139 790
Podatek doch.	41 048	13 468	94 556	216 138	72 166
Wynik netto (EAT)	166 113	17 706	170 108	418 079	67 624

Tab. 6. Rachunek zysków i strat segmentu B. Źródło: Opracowanie własne
Tab. 6. Segment B profit and loss account. Source: Own study

	2023	2024	2025	2026	2027
Przychody ze sprzedaży	1 029 600	2 453 600	2 110 680	2 362 651	1 979 411
Koszty sprzedanych produktów	859 200	2 116 920	1 792 798	2 187 543	1 703 520
Koszty ogólnoadministracyjne	212 142	248 381	193 274	-21 678	88 614
EBITDA	-41 742	88 299	124 608	196 785	187 277
Amortyzacja	5 670	30 570	30 570	36 491	33 180
Wynik operacyjny (EBIT)	-47 412	57 729	94 038	160 294	154 097
Koszty finansowe	13 148	40 804	21 002	22 590	36 150
Wynik brutto (EBT)	-60 561	16 926	73 036	137 704	117 947
Podatek doch.	17 592	5 772	40 524	92 630	30 928
Wynik netto (EAT)	-78 153	11 154	32 512	45 074	87 019

cenę fikcyjnego przedsiębiorstwa opartą o trzy metodologię: DCF, EVA oraz SOTP.

Na potrzeby wyceny wartości przedsiębiorstwa przyjęto następujące założenia:

- Przedsiębiorstwo z sektora wydobywczego
- W skład przedsiębiorstwa wchodzą dwie oddzielne kopalnie (segmenty): A i B
- Wysokość podatku wynosi 40%
- Wartość ważonego kosztu kapitału (WACC) jest równa 9%
- Okres: 5 lata
- Wartość firmy liczona dla roku 2023
- Wszystkie wartości podane w złotówkach

Poniższe tabele przedstawiają bilans finansowy oraz rachunek zysków i strat całej omawianej firmy w latach 2023–2027. Stanowią one bazę do podejmowanej wyceny.

Pierwszym a zarazem najważniejszym krokiem jest sporządzenie bilansu zarządczego dzielącego się na kapitał zainwestowany (IC) oraz kapitał zastosowany (EC). W skład kapitału zainwestowane wchodzą aktywa trwałe, zapotrzebowanie na kapitał obrotowy netto (ZKON) oraz Inwestycje. Zapotrzebowanie na kapitał obrotowy netto jest to suma zapasów oraz należności pomniejszona o zobowiązania oraz rozliczenia międzyokresowe krótkoterminowe. Natomiast kapitał zastosowany składa się z kapitału własnego, kapitału obcego oraz rezerw i rozliczeń, które nie występują w omawianym przykładzie. W poniższej tabeli zaprezentowano uzyskany bilans zarządczy.

6.1 Metoda DCF

Dzięki sporządzeniu owego bilansu możliwe jest rozpoczęcie głównej części wyceny. W pierwszej kolejności zastosowano metodę DCF, którą szczegółowo opisano w poprzednim rozdziale. Pierwszym krokiem jest stworzenie przepływów FCFF w omawianym przykładzie. Będą to przepływy dla lat 2024–2027, co wynika z zakresu posiadanych danych. FCFF jest sumą wyniku operacyjnego po opodatkowaniu (EBIT(1-T)), amortyzacji, zmiany na ZKON oraz zmiany na nakładach inwestycyjnych (CAPEX, ang. capital expenditures). Należy zwrócić uwagę, iż FCFF ukazuje przepływy pieniężne, dlatego też zmianę na zapotrzebowaniu na kapitał obrotowy netto interpretujemy w następujący sposób, przedsiębiorstwo dąży do minimalizacji zamrożonych środków pieniężnych w aktywach obrotowych, dlatego gdy jej wartość wzrasta różnica zostanie wykazana w przepływach jako wartość ujemna. Każdy nakład inwestycyjny jest jednoznaczny z kosztem dla przedsiębiorstwa z tego powodu wzrost wartości tej pozycji bilansu znajduje swoje odzwierciedlenie w przepływach również jako wartość ujemna. Aby wyliczyć DCF należy zsumować zdyskontowane przepływowy FCFF do wartości bieżącej (PV ang. Present Value). W celu obliczenia DCF stosuje się wzór:

$$DCF = \frac{FCFF_1}{(1+WACC)^1} + \frac{FCFF_2}{(1+WACC)^2} + \cdots + \frac{FCFF_n}{(1+WACC)^n}$$

W powyższym wzorze n wyraża rok, dla którego zostało obliczone FCFF. W przypadku niniejszego przykładu rok 2023 jest rokiem zerowym, 2024 jest pierwszym rokiem a 2025 drugim.

Ostatnim krokiem owej metody jest skorygowanie wskaźnika DCF o wartości inwestycji oraz kredytów bankowych dla roku zero. Takim oto sposobem uzyskano skorygowane DCF, które ukazuje bieżącą wartość przedsiębiorstwa. W poniższej tabeli przedstawiono proces wyliczeniowy omawianej metody wraz z wynikami:

6.2 Metoda EVA

Następną podejmowaną metodą wyceny jest metoda Economic Value Added (EVA). Jest to metoda bazująca na zmianach jakie wywiera na kapitał zainwestowany amortyzacja, zmiany na CAPEX oraz zmiany na ZKON. Na co warto zwrócić uwagę, w tej metodzie zmiana na CAPEX oraz ZKON idzie z odwrotnym aniżeli w przepływach FCFF. Powodem tego jest badanie ich wpływu na kapitał zainwestowany a co za tym idzie każdy wpływ powodujący jego wzrost będzie

Tab. 5. Rachunek zysków i strat segmentu A. Źródło: Opracowanie własne
Tab. 5. Segment A profit and loss account. Source: Own study

	2023	2024	2025	2026	2027		2023	2024	2025	2026	2027
Aktywa trwałe	344 923	939 915	817 361	1 310 204	838 548	Kapitał własny	663 768	492 592	1 952 352	2 232 000	1 912 413
ZKON	784 800	905 760	1 749 680	1 640 980	1 988 028	Rezerwy i Rozliczenia					
Inwestycje	57 600	7 282	85 632	89 432	96 533	Kapitał obcy	523 555	1 360 365	700 321	808 616	1 010 696
IC	**1 187 323**	**1 852 957**	**2 652 673**	**3 040 616**	**2 923 109**	**EC**	**1 187 323**	**1 852 957**	**2 652 673**	**3 040 616**	**2 923 109**

Tab. 8. Bilans zarządczy segmentu A. Źródło: Opracowanie własne
Tab. 8. Segment A management balance sheet. Source: Own study

	2023	2024	2025	2026	2027		2023	2024	2025	2026	2027
Aktywa trwałe	310 431	845 924	735 625	1 179 184	754 693	Kapitał własny	423 604	334 319	1 297 431	1 601 286	1 076 410
ZKON	306 999	263 210	852 088	732 354	819 615	Rezerwy i Rozliczenia					
Inwestycje	40 320	5 097	59 942	62 602	67 573	Kapitał obcy	234 145	779 912	350 225	372 854	565 472
IC	**657 750**	**1 114 231**	**1 647 655**	**1 974 140**	**1 641 882**	**EC**	**657 750**	**1 114 231**	**1 647 655**	**1 974 140**	**1 641 882**

Tab. 9. Bilans zarządczy segmentu B. Źródło: Opracowanie własne
Tab. 9. Segment B management balance sheet. Source: Own study

	2023	2024	2025	2026	2027		2023	2024	2025	2026	2027
Aktywa trwałe	34 492	93 992	81 736	131 020	83 855	Kapitał własny	240 164	158 273	654 921	630 714	836 003
ZKON	477 801	642 550	897 592	908 626	1 168 413	Rezerwy i Rozliczenia					
Inwestycje	17 280	2 185	25 690	26 830	28 960	Kapitał obcy	289 410	580 453	350 096	435 762	445 224
IC	**529 573**	**738 726**	**1 005 018**	**1 066 476**	**1 281 227**	**EC**	**529 573**	**738 726**	**1 005 018**	**1 066 476**	**1 281 228**

Tab. 10. Wyliczenia metodą DCF. Źródło: Opracowanie własne
Tab. 10. Calculations using the DCF method. Source: Own study

	2023	2024	2025	2026	2027
EBIT	190 428	184 112	407 708	847 221	378 237
Podatek		40%	40%	40%	40%
EBIT(1-T)		110 467	244 625	508 332	226 942
Amortyzacja		101 900	101 900	121 636	110 600
ΔCapex		-696 892	20 654	-614 479	361 056
ΔZKON		-120 960	-843 920	108 700	-347 048
FCFF		-605 485	-476 741	124 189	351 550
WACC		9%	9%	9%	9%
PV FCFF		-555 491	-401 264	95 897	249 047
DCF	-611 810				
Inwestycje	57 600				
Kredyty bankowe	523 555				
DCF Skoryg	**-1 077 765**				

widniał ze znakiem dodatnim. W konsekwencji, amortyzacja będzie pomniejszała kapitał początkowy (IC_0). Uwzględniając wszystkie czynniki wpływające uzyskano kapitał zainwestowany końcowy (IC_K), który jednocześnie jest kapitałem początkowym roku następnego. Wartość kapitału początkowego dla roku 2019 (bazowego/zero) jest sumą aktywów trwałych oraz ZKON z tego też roku. W poniższej tabeli przedstawiono owe wartości dla niniejszego przykładu:

Uzyskanie wartości ICK dla poszczególnych lat umożliwia wyliczenie EVA. Warto zwrócić uwagę na ICK w ostatnim roku, jest to wartość rezydualna z angielskiego Residual Value (RV). Na potrzeby tej metody przyjmuje się, że przedsiębiorstwo zostanie zlikwidowane z końcem ostatniego roku, dlatego w obliczeniach przyjmuje się tą wartość jako ujemną. Następnie należy zsumować zdyskontowane wartości EVA według poniższego wzoru w celu uzyskania zdyskontowanej ekonomicznej wartości dodanej (ang. Discounted Economic Value Added – DEVA):

$$DEVA = \frac{EVA_1}{(1+WACC)^1} + \frac{EVA_2}{(1+WACC)^2} + \cdots + \frac{EVA_n}{(1+WACC)^n} + \frac{RV_{EVA}}{(1+WACC)^n}$$

Ostatnim krokiem, podobnie jak w przypadku DCF, jest skorygowanie wartości poprzez dodanie do niej IC_K dla roku bieżącego oraz inwestycji, i jednoczesne pomniejszenie o kredyty bankowe. Tabela 12 ukazuje otrzymane rezultaty.

6.3 Metoda SOTP

Ostatnią metodą podjętą w niniejszym artykule jest metoda SOTP. Główne założenia owej metody zostały szczegółowo opisane we wcześniejszej części artykułu. W analizowanym przykładzie przedsiębiorstwo dzieli się na dwa segmenty A i B.

Do obliczeń wykorzystano metodę DCF dla poszczególnych segmentów. W poniższych tabelach zaprezentowano otrzymane wyniki wraz ze składowymi:

Ostatnim krokiem metody SOTP jest zsumowanie otrzymanych DCF skorygowanych poszczególnych segmentów co daje wynik -1 077 765 zł.

Wyniki uzyskane przy wykorzystaniu wszystkich omawianych metod pokazują taką samą wartość co wskazuję na poprawność wykonanych obliczeń. Analiza wskazuje wartość hipotetycznego przedsiębiorstwa na poziomie – 1 077 765 zł, co wskazuje na niezadawalającą sytuację finansową.

Tab. 11. Obliczenia kapitału końcowego. Źródło: Opracowanie własne
Tab. 11. Calculation of the final capital. Source: Own study

	2023	2024	2025	2026	2027
ICo		1 129 723	1 845 675	2 567 041	2 951 184
ΔCapex		696 892	-20 654	614 479	-361 056
Amortyzacja		-101 900	-101 900	-121 636	-110 600
ΔZKON		120 960	843 920	-108 700	347 048
ICk	1 129 723	1 845 675	2 567 041	2 951 184	2 826 576

Tab. 12. Obliczenia metodą EVA. Źródło: Opracowanie własne
Tab. 12. EVA calculations. Source: Own study

	2023	2024	2025	2026	2027	RV
EBIT (1-T)		110 467	244 625	508 332	226 942	
Ico		1 129 723	1 845 675	2 567 041	2 951 184	
WACC		9%	9%	9%	9%	
EVA		8 792	78 514	277 299	-38 664	-2 826 576
PV EVA		8 066	66 084	214 125	-27 391	-2 002 418
DEVA	-1 741 533					
ICk	1 129 723					
Inwestycje	57 600					
Kredyty bankowe	523 555					
DEVA skoryg	**-1 077 765**					

Tab. 13. Obliczenia metody SOTP – segment A. Źródło: Opracowanie własne
Tab. 13. Calculations of the SOTP method – segment A. Source: Own study

	2023	2024	2025	2026	2027
EBIT	237 840	126 383	313 670	686 926	224 140
Podatek		40%	40%	40%	40%
EBIT(1-T)		75 830	188 202	412 156	134 484
Amortyzacja		71 330	71 330	85 145	77 420
Capex		-606 823	38 969	-528 704	347 070
ZKON		43 789	-588 878	119 734	-87 261
FCFF		-415 874	-290 377	88 331	471 713
WACC		9%	9%	9%	9%
PV FCFF		-381 536	-244 405	68 208	334 173
DCF	-223 559				
Inwestycje	40 320				
Kredyty bankowe	234 145				
DCF Skoryg	**-417 385**				

Tab. 14. Obliczenia metody SOTP – segment B. Źródło: Opracowanie własne
Tab. 14. Calculations of the SOTP method – segment B. Source: Own study

	2023	2024	2025	2026	2027
EBIT	-47 412	57 729	94 038	160 294	154 097
Podatek		40%	40%	40%	40%
EBIT(1-T)		34 638	56 423	96 176	92 458
Amortyzacja		30 570	30 570	36 491	33 180
Capex		-90 069	-18 315	-85 775	13 986
ZKON		-164 749	-255 042	-11 034	-259 787
FCFF		-189 610	-186 364	35 858	-120 163
WACC		9%	9%	9%	9%
PV FCFF		-173 955	-156 859	27 689	-85 126
DCF	-388 251				
Inwestycje	17 280				
Kredyty bankowe	289 410				
DCF Skoryg	**-660 380**				

7. Podsumowanie

Przeprowadzony na potrzeby niniejszego artykułu przegląd literatury obrazuje klasyfikacje kategorii wartości na wartość majątkową, rynkową oraz ekonomiczną. Mnogość metod oraz różnice zakresów które badają pozwala potencjalnym właścicielom przedsiębiorstw na wybór odpowiadającej ich celom oraz wartościom, specyfiki branży bądź zakresu działalności.

Największe zainteresowanie zarówno środowiska akademickiego jak również świata biznesu w dalszym ciągu stanowią dochodowe metody wyceny wartości ekonomicznej. Samo zagadnienie wartości ekonomicznej swoją popularność zawdzięcza bazowaniu na przyszłych przepływach pieniężnych które w wymierny sposób obrazują zdolność przedsiębiorstwa do generowania potencjalnych przychodów, a co za tym idzie również zysku. W artykule szczegółowo przedstawiono meto-

dy wyceny DCF oraz EVA. Główną różnicą w przypadku tych metod jest prezentacja danych. Metoda DCF wyróżnia przyszłe przepływy pieniężne, które w znaczący sposób wpływają na bieżącą wartość ekonomiczną. Natomiast metoda EVA wyróżnia istotność kapitału zainwestowanego w przedsiębiorstwo prezentując czynniki wpływające na jego zmianę. Przeprowadzona wycena fikcyjnego przedsiębiorstwa wykazała takie same wartości w przypadku obu wyżej wymienionych metod co potwierdza, iż są one tożsame.

Niniejszy artykuł uzupełnia, wciąż ignorowana przez badaczy i naukowców, metoda SOTP. Metoda ta ma szczególne zastawanie w przypadku przedsiębiorstw o dekomponowanej strukturze, podzielonej na segmenty, produkty czy nawet obszary, na których są prowadzona jest działalność. Podział ten umożliwia precyzyjniejszą analizę generowanej wartości. Wszechstronność podziału sprawia, iż metoda może zostać zastosowana bez względu na rozmiar badanego przedsiębiorstwa. W badanym przedsiębiorstwie owa metoda wykazała wartość ekonomiczną analogiczną do metod DCF i EVA, jednocześnie dostarczając dokładniejsze informacje o segmentach A i B. Owe informacje pozwalają na ukierunkowanie potencjalnych decyzji inwestycyjnych na konkretne obszary działalności. Zawarcie metody SOTP miało również unaocznić jak wartościowym i istotnym elementem zarządzania jest szczegółowa wycena wartości przedsiębiorstwa i jak pomocnym jest narzędziem w tym zakresie.

Opisane powyżej metody zostały wybrane z chęci wskazania sposobów wyceny najbardziej precyzyjnych, miarodajnych oraz pożytecznych dla przedsiębiorstw. Dają one również wyniki które są czytelne dla interesariuszy. Zaprezentowane wady i zalety poszczególnych metod umożliwiają indywidualne dostosowanie sposobu wyceny przedsiębiorstwa. Nie bez znaczenia jest również, że pomimo znacznej złożoności oraz nie najniższych kosztów przeprowadzenia, w zestawieniu koszt – efekt, nie bez powodu nadal pozostają metodami najczęściej wykorzystywanymi.

Literatura – References

1. Borowiecki R. (red), 1993, Wycena przedsiębiorstw. Metody, procedury, przykłady, wyd. II, AE-TNOik, Warszawa-Kraków
2. Chlomou G., Demirakos E. (2019). How do financial analysts implement the Sum-of-the-Parts (SOTP) valuation framework? Athens University of Economics & Business, Greece.
3. Chrzanowski A., Głażewska I. (2010). Rola podejścia innowacyjnego w budowaniu wartości przedsiębiorstw, Zarządzanie Zmianami: zeszyty naukowe nr 3, 60-76.
4. Duraj J. (2004). Podstawy ekonomiki przedsiębiorstwa. Polskie Wydawnictwo Ekonomiczne S.A., Warszawa
5. Kochaniak K. (2010). Ekonomiczna wartość dodana (EBA) jako metoda oceny efektywności finansowej przedsiębiorstwa. Zeszyty naukowe nr 840, Uniwersytet Ekonomiczny w Krakowie.
6. https://analizafinansowa.pl/wycena-przedsiebiorstw/analiza-wartosci-przedsiebiorstwa-3162.html dostęp: 03.05.2023
7. https://financialcraft.pl/wycena-przedsiebiorstwa-metoda-majatkowa/; dostęp: 05.05.2023.
8. https://corporatefinanceinstitute.com/resources/valuation/sum-of-the-parts-sotp-valuation/l dostęp: 15.05.2023

Valuation of the Economic Value of a Decentralized Mining Company

In this paper, a literature survey was conducted in the field of enterprise value. A division of values by methods of their calculation was presented, distinguishing adjusted assets, market and economic methods. Methods of estimating economic value were described with details, distinguishing methods based on future cash flows DCF and EVA, which is based on invested capital. The article is supplemented by the SOTP methodology, which, despite its wide application thanks to the division of valuation into individual business segments, giving detailed information on value generation. The paper concludes with the conducted valuation of the economic value of a decentralized mining company. It showed that the DCF and EVA methods are the same and also demonstrated the usefulness of the SOTP method in multi-segment enterprises as a valuation tool.

Keywords: *mining, decentralized company, economic value, discounted casf flows DCF, economic value added EVA, sum of the parts SOTP*

The Impact of Methane Emitted from Coal Deposits on the State of the Atmosphere

Nikodem SZLĄZAK[1)], Justyna SWOLKIEŃ[2)]

[1)] Prof. dr hab. inż.; AGH University of Science and Technology, Faculty of Civil Engineering and Resource Management, al. Mickiewicza 30, 30-059 Kraków; email: szlazak@agh.edu.pl, ORCID: 0000-0001-8320-4751

[2)] Dr hab. prof. Uczelni; AGH University of Science and Technology, Faculty of Civil Engineering and Resource Management, al. Mickiewicza 30, 30-059 Kraków; email: swolkien@agh.edu.pl, ORCID: 0000-0003-4332-9415

http://doi.org/10.29227/IM-2023-01-27

Submission date: 23-05-2023 | Review date: 14-06-2023

Abstract

This article presents an analysis of methane emissions into the atmosphere, the amount of captured and utilized methane, as well as methane released from the methane drainage system. The results are then compared with data from the State Mining Authority (WUG) and the European Pollutant Release and Transfer Register (E-PRTR), which is maintained in Poland by the Chief Inspectorate for Environmental Protection. Additionally, based on greenhouse gas emissions data from UNFCCC and JSW S.A., the article determines the impact of methane emitted from its mines on the atmosphere at the European and global scale.

Keywords: *methane emissions, methane drainage efficiency, atmospheric protection*

1. Introduction

Methane (CH_4) and carbon dioxide (CO_2) have been recognized by the Intergovernmental Panel on Climate Change as the two most significant greenhouse gases [1]. These gases absorb infrared radiation, contributing to global warming. Over the years, their atmospheric concentrations have been heavily influenced by human activities. For example, methane concentration has increased by approximately 160% in the last 250 years [2]. Despite its significantly lower atmospheric abundance compared to carbon dioxide, methane has a 28-fold higher Global Warming Potential (GWP) over a 100-year timeframe [3]. Recent studies indicate that its GWP has actually increased to 32 [2], and considering the additional carbon footprint, it reaches 34 over a 100-year timeframe and 86 over a 20-year timeframe [4]. Furthermore, the radiative forcing attributed to methane emissions is approximately 0.97 Wm [2,3], and considering its relatively short lifespan (11.2 +/- 1.3 years), reducing methane emissions can have a short-term impact on associated radiative forcing [5]. This makes methane emissions observations an excellent source of information about climate change.

Methane is a gas primarily generated through anaerobic decomposition of organic matter in biological systems. However, according to IPCC data, currently half of its present-day atmospheric flux comes from anthropogenic sources, which are predominantly influenced by human activities [2]. Although global methane emissions account for about 4% of anthropogenic CO_2 emissions in mass flow units, it contributes to 20% of the accumulated enhanced greenhouse effect in the lower atmosphere since 1750 [3]. Another challenge lies in the fact that methane emission sources have not been fully characterized, and accurately estimating the quantities of emitted methane remains a significant challenge. According to UNFCCC, global methane emissions in 2022 were approximately 274.6 Mt, while IEA reported 356.2 Mt [6,7]. These emissions comprised around 40% from natural sources and the remaining 60% from anthropogenic sources. The largest methane-emitting sector is Agriculture, accounting for about a quarter of the total emissions, followed closely by the Energy sector, where significant methane is released from coal, oil, natural gas, and biofuels.

Methane is emitted from various sources, which are widely distributed and often geographically overlapping. Uncertainties in estimating methane quantities from Agriculture, Waste, and Fossil Fuels range from 20% to 30% [4,5]. Lack of accurate methane emission data mainly applies to regional scales (e.g., South America, China, India). Therefore, numerous efforts are being made to accurately determine greenhouse gas emissions, including methane, in order to mitigate their negative impact on climate change.

Poland has been a member of the United Nations Framework Convention on Climate Change (UNFCCC) since 1994 and the Kyoto Protocol (KP) since 2002, actively participating in actions to mitigate climate change [8]. Upon ratifying the Kyoto Protocol, Poland committed to reducing greenhouse gas emissions by 6% during the period of 2008-2012 compared to the base year emissions. In the second commitment period, from 2013 to 2020 (Doha Amendment), Poland committed to achieving average annual emissions at 80% of the sum of emissions from all countries (European Union and Iceland) during the base years [8].

Poland reports its national emissions in five source categories under the Common Reporting Format: Energy, Industrial Processes and Product Use, Agriculture, Land Use, Land-Use Change and Forestry (LULUCF), and Waste [6,8]. Greenhouse gas emissions are presented in CO_2 equivalents, using the GWP100 metric, which assigns a value of 25 for methane according to IPCC guidelines [2]. Using an increased GWP100 value would result in higher total annual greenhouse gas emissions due to the increased methane contribution (approximately 20%). However, this would not significantly affect long-term climate change trends [2]. The choice of metrics impacts the selection of policies and methods aimed at mitigating climate change, especially for high-emission sec-

Fig. 2.1 Comparison of the world's largest coal producers [7]
Rys. 2.1 Porównanie największych światowych producentów węgla [7]

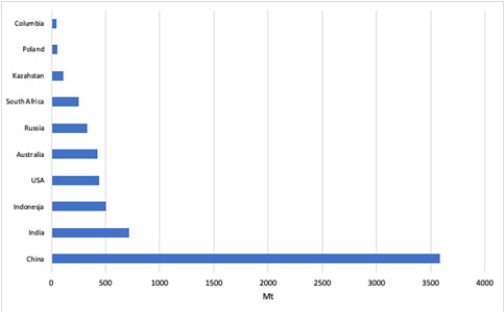

Fig. 2.2 Coal consumption in Poland by sectors [10]
Rys. 2.2 Zużycie węgla w Polsce według sektorów [10]

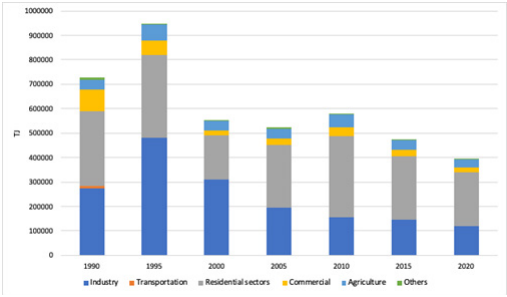

tors and countries other than CO_2. The detailed methodology for calculating emissions is described in the English version of the National Inventory Report for the period 1988–2020 [8].

From the perspective of the analyses conducted in this article, the most significant category is Energy, specifically the subcategory: Fugitive Emissions from Fuels, where emissions from underground mines have the largest share. The coal sector in Poland accounted for 38.7% of total methane emissions in 2020 [8].

The analyses presented in this article were conducted based on data available on the UNFCCC Greenhouse Gas Inventory Data website [6], which provides data on greenhouse gas emissions from all Annex I and non-Annex I countries.

2. Methane emissions from the mining sector in Poland

The global energy sector, including the coal sector, is responsible for emitting 133.4 million tons of methane [7]. China is the leading global coal producer, with a total production of 3,500 million tons (Figure 2.1). From the presented ranking in Figure 2.1, it is evident that Poland ranks ninth as a coal producer [7]. In 2020 and 2021, coal production in the country amounted to 54.5 million and 55.0 million tons, respectively [9].

Around 49.5% of Poland's energy sector relies on coal. Figure 2.2 presents the main sectors of the economy using coal as a raw material. Until 2000, the largest amount of coal was consumed by the industry and residential sectors as a fuel for heating buildings. After 1995, industrial coal consumption significantly decreased, reaching 120,247 TJ in 2020. From 2000 to 2020, the residential sector had the highest coal consumption, ranging from 330,255 TJ in 2010 to 217,719 TJ in 2020 [7].

Coal mining is accompanied by the emission of gases, primarily methane, carbon dioxide, higher hydrocarbons, nitrogen, and steam. Mine gas contains 86-99.6% methane [2], but its composition largely depends on the type of deposit and mining method and changes over time and with changing mining conditions.

According to the balance of mineral resources and underground waters in Poland in 2020, the presence of methane in coal deposits was documented mainly in the Upper Silesian Coal Basin [10]. The methane conditions of the Lower Silesian Coal Basin and the Lublin Coal Basin are poorly recognized, and the detected methane concentrations are significantly lower, making it difficult to assess their economic significance. The documented extractable resources in the Upper Silesian Coal Basin in 2021 amounted to 106,660.94 million m^3 and decreased by 568.32 million m^3 compared to 2020 [10].

In 2021, 815.3 million m^3 of methane was released from the rock mass affected by mining activities, which means that, on average, 1,551.17 m^3 was released per minute [9]. From 2015 to 2021, the relative methane emission in relation to the extracted coal (methane yield) ranged from 12.9 to 15 m^3.

In 2020, methane emissions in Poland amounted to 1,774.23 kt, which was 39.7% lower than the baseline year (1988) [8]. This value corresponds to 44.35 Mt of CO_2 equivalent assuming a GWP100 of 25. Using a GWP100 of 28 would result in a value that is 12% higher (49.68 Mt CO_2eq). Methane accounted for 11.8% of the total national greenhouse gas emissions in 2020. Three main sources of methane emissions belong to the categories: Fugitive Emissions from Fuels (38.5%), Agriculture (31.9%), and Waste (22%). The first category includes emissions from the combustion of solid fuels (including underground and surface mines) and the oil and natural gas and other emissions from energy production (combined approximately 6.0% of emissions). Figure 2.3 shows the percentage distribution of methane emissions from each category.

Fig. 2.3 Structure of methane emissions categories in Poland in 2020 [8]
Rys. 2.3 Struktura kategorii emisji metanu w Polsce w 2020 r. [8]

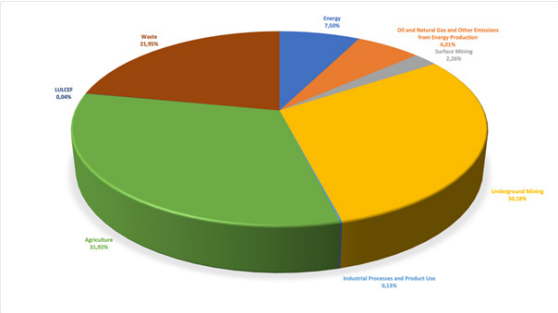

Fig. 2.4 Methane emissions status from Polish mines from 2015 to 2020 based on WUG data [9]
Rys. 2.4 Stan emisji metanu z polskich kopalń w latach 2015–2020 na podstawie danych WUG [9]

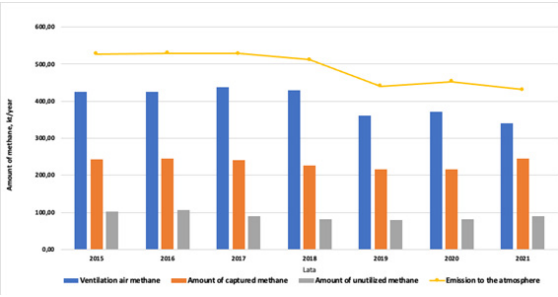

Fig. 2.5 Methane emissions status from Polish mines from 2015 to 2020 based on WUG and E-PRTR data [9, 12]
Rys. 2.5 Stan emisji metanu z polskich kopalń w latach 2015–2020 na podstawie danych WUG i E-PRTR [9, 12]

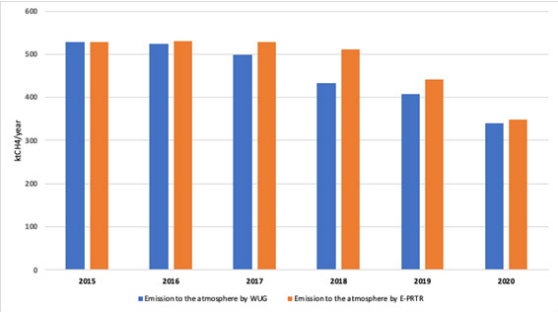

Fig. 2.6 Methane drainage status, methane utilization efficiency, and percentage of methane emissions into the atmosphere in Polish mines from 2015 to 2021 [9]
Rys. 2.6 Stan odmetanowania, efektywność wykorzystania metanu oraz procent emisji metanu do atmosfery w polskich kopalniach w latach 2015–2021 [9]

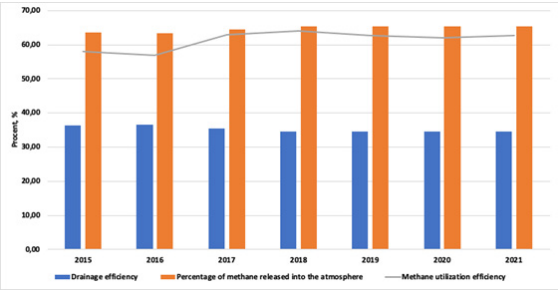

In the coming years, an increase in methane emissions from coal mines can be expected due to the increasing methane content with the depth of coal seams (in the last decade, methane emissions have increased by 60% per ton of coal extracted) [11]. Therefore, there should be a strong emphasis on its recovery and practical utilization.

The emission status of methane from the mining sector in Poland over the past five years is shown in Figure 2.4 [9]. Data analysis indicates that from 2015 to 2017, the total amount of methane released into the atmosphere remained around 530 kt (13.25 ktCO_2eq), and in the following five years, it decreased to 431 kt – 10.77 ktCO_2eq (yellow line in Figure 2.4). The results from the State Mining Authority (WUG) align with the data from the European Pollutant Release and Transfer Register (E-PRTR) shown in Figure 2.5 [12]. Minor discrepancies in the reported data mainly result from the different methodologies used in the emission registries. The WUG registry calculates the total methane emissions to the atmosphe-

Fig. 3.1 Indirect methane emissions from the global mining sector [7]
Rys. 3.1 Pośrednie emisje metanu z globalnego sektora wydobywczego [7]

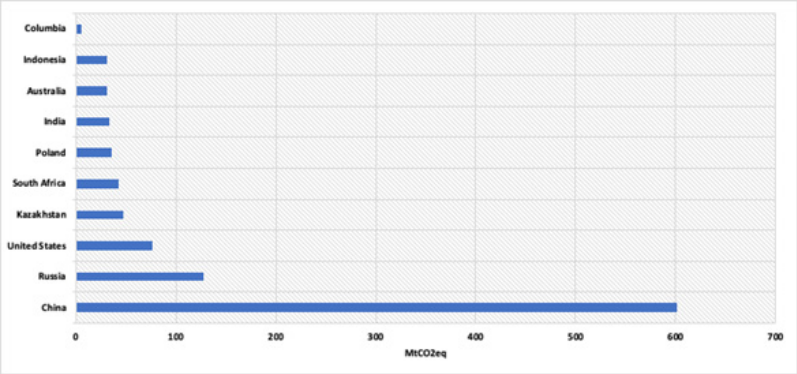

Fig. 3.2 Methane emissions from various sectors in Poland, other European Union countries, and other Annex I countries from 2015 to 2020 [6]
Rys. 3.2 Emisje metanu z różnych sektorów w Polsce, innych krajach Unii Europejskiej i innych krajach Załącznika I w latach 2015–2020 [6]

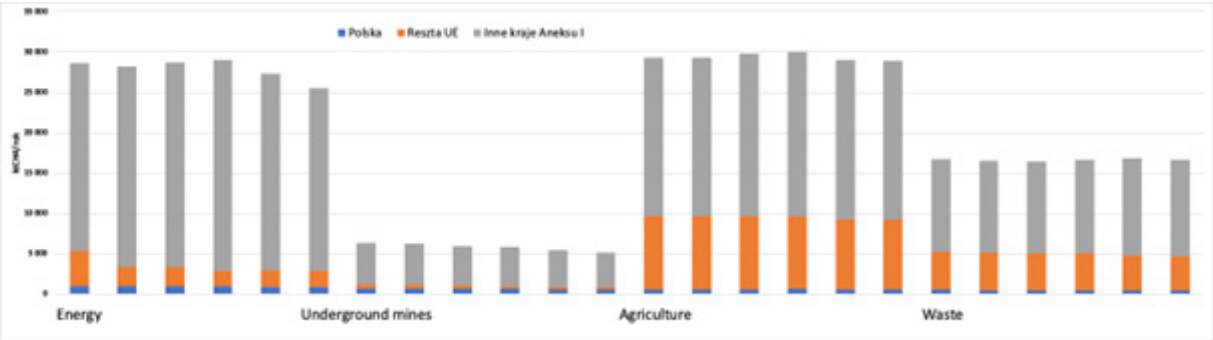

re based on the ventilation air methane from individual units and the total amount of unutilized methane. The E-PRTR database relies on data on the total methane emissions (ventilation air methane plus unutilized methane) directly from individual mines.

Considering that methane drainage in mines is mainly done for safety reasons, the overall efficiency for the years 2015–2021 ranged from 34.6% to 36.3% (Fig. 2.6). Analyzing the utilization level of the captured methane (gray line in Figure 2.6), it can be concluded that, compared to the entire underground mining industry, the efficiency remained at around 57% in 2017 and reached nearly 64% in 2018. However, its value slightly decreased from 2019 to 2021.

The data presented in Figure 2.6 regarding the percentage of methane released into the atmosphere is determined based on absolute methane emission, meaning they only include ventilation air methane values without considering unutilized methane. In this context, the percentage of methane released into the atmosphere during the studied period ranged from 63.7% in 2015 to over 65.40% in 2021. If the amount of unutilized methane were taken into account, this value would increase to 76%.

Currently, methane in active mines is only recovered through the methane drainage process carried out due to occupational safety regulations. Therefore, the technologies currently used result in approximately 30% of methane being captured through drainage and as much as 70% being removed through ventilation. Given the properties of methane as a greenhouse gas, it is crucial to reduce its emissions for atmospheric protection.

3. The impact of coal seam methane emissions on the atmosphere worldwide and in Europe

As a member of the United Nations Framework Convention on Climate Change (UNFCCC), Poland is obliged to report its national greenhouse gas emissions within the adopted reduction targets in five source categories using the format of the Common Reporting Tables [8]. The conducted analyses were based on data available on the UNFCCC Greenhouse Gas Inventory Data website [6], concerning greenhouse gas emissions from all countries belonging to the European Union, as well as those outside the EU but included in the Annex I. Like EU members, they are required to provide data on greenhouse gas emissions from all sectors of the economy. China, India, South Africa, Colombia, and Indonesia are not part of Annex I. While these countries are encouraged to submit reports, they are not obligated to do so. Therefore, data on methane emissions from the mining sectors of these countries are very limited, with the latest available data for China from 2014 and for India from 2016. Figure 3.1 presents the status of methane emissions from countries that are the largest coal producers based on data from the International Energy Agency [7]. According to this ranking, Poland ranks sixth in terms of methane emissions from the mining sector.

The data presented in this chapter will cover the analysis of methane emissions from European Union countries and Annex I countries from 2015 to 2020. However, it should be noted that China, currently the world's largest coal producer, has an annual production of approximately 3,580 million tons, and India of approximately 716 million tons [13]. Therefore, a comparison will be made between the available UNFCCC results from 2020 and the latest available emission data for China and India [6].

Fig. 3.3 Methane emissions from the energy sector in Annex I countries [6]
Rys. 3.3 Emisje metanu z sektora energetycznego w krajach Aneksu I [6]

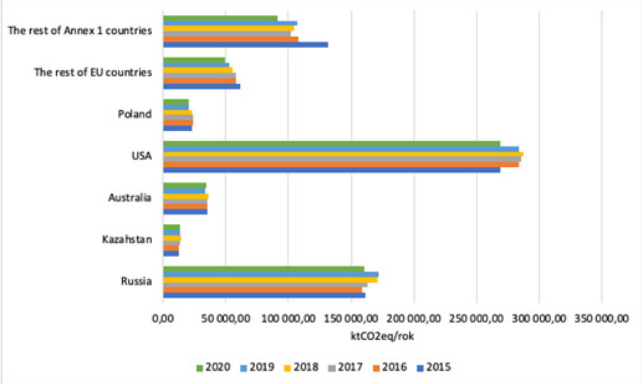

Fig. 3.4 Methane emissions from the energy sector in Europe [6]
Rys. 3.4 Emisja metanu z sektora energetycznego w Europie [6]

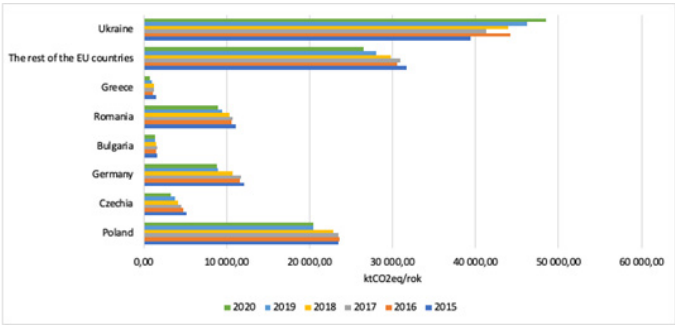

3.1. Methane emissions from various sectors of the economy in European and global countries

Methane is emitted from various sources, both of natural and anthropogenic origin, accounting for about 60% of its global emissions. Figure 3.2 shows the amounts of emitted methane from key sectors in Poland, other EU countries, and Annex I countries. Additionally, the chart illustrates the share of methane emissions from the mining sector in the energy sector.

The total methane emissions from the five main sectors of the economy in Annex I countries in 2020 amounted to 74.9 Mt (including the LULUCF category), which corresponds to 1872 $MtCO_2eq$ (GWP100=25). The main sectors of the economy that are sources of methane are Energy, Agriculture, and Waste. The data presented in the chart indicate that the Agriculture sector is the largest emitter of methane, with an average emission of 28.9 Mt during the study period, followed by the Energy sector with an average of 25.5 Mt of methane. The Waste sector ranks third with an average of 16.6 Mt of methane.

The data presented in Figure 3.2 also show that the global underground mining sector is a source of emissions, averaging 5.15 Mt of methane, of which Polish mines release 0.53 Mt. It should be noted that these data do not include emissions from China and India.

Taking into account the data available on the UNFCCC Greenhouse Gas Inventory Data website [6] regarding methane emissions from individual categories for China (last available data for 2014) and India (last available data for 2016), the total methane emissions for these two countries amount to approximately 75.0 Mt CH4 (1500 $MtCO_2eq$), which practically represents 100% of the methane emissions from Annex I countries.

Looking more closely at the energy sectors of individual countries, as shown in Figure 3.3, it is clear that the United States and Russia have the largest share of methane emissions, with average shares of 279.78 $MtCO_2eq$ and 164.46 $MtCO_2eq$, respectively. Poland's energy sector is responsible for an average emission of 22.37 $MtCO_2eq$.

The energy sector of the entire European Union accounts for about 11.55% of methane emissions compared to all Annex I countries, with Poland accounting for 3.3%.

Analyzing the state of methane emissions from the energy sector in European countries, as presented in Figure 3.4, it is evident that Ukraine releases the highest amounts, averaging 43.94 $MtCO_2eq$, which accounts for 35.5% of the total emissions in Europe. Poland's energy sector is responsible for 18.23% of methane emissions (averaging 22.36 $MtCO_2eq$), while Germany and Romania account for 8.8% and 8.4% of the total emissions in Europe, respectively. The remaining countries in Europe account for the remaining 29.07%.

3.2. Methane emissions from the underground mining sector in European and global countries

In the global energy sector, the share of methane emissions from underground mines averages 5.15 Mt of methane (Fig. 3.2), which corresponds to approximately 128.75 $MtCO_2eq$. Taking a closer look at the underground mining sectors of individual Annex I countries (Fig. 3.5), it is observed that the United States dominates with an average emission of 49.78 $MtCO_2eq$, accounting for 35.0% of the total methane emissions from this sector. The next countries in line are Russia

Fig. 3.5 Methane emissions from the underground mining sector, including JSW S.A., compared to Annex I countries [6]
Rys. 3.5 Emisje metanu z sektora górnictwa podziemnego, w tym JSW S.A. na tle krajów Aneksu I [6]

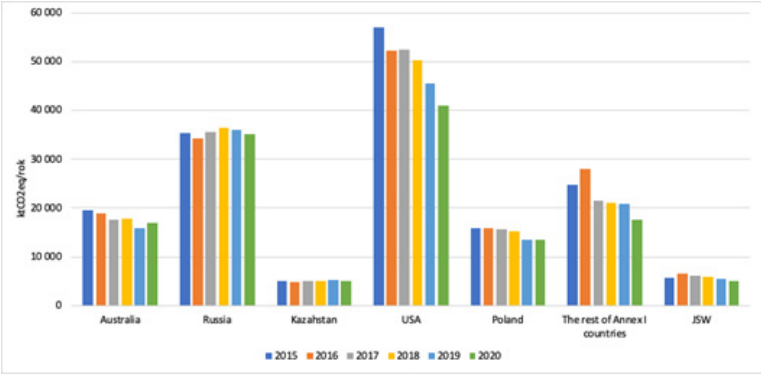

(35.49 $MtCO_2eq$ – 23.5%), followed by other Annex I countries, including Ukraine (15.4%), Australia (12.3%), Poland (14.84 $MtCO_2eq$ – 10.3%), and Kazakhstan (3.5%). The mines of the largest coal company in Poland, JSW S.A., are responsible for approximately 3.97% of the total methane emissions.

Considering the fact that China and India do not provide data on methane emissions from the mining sector, only approximate data can be provided for these two countries. The data from 2014 [13] indicate a total emission from the mining sector at around 441.31 $MtCO_2eq$. Available literature data [14] suggest emissions ranging from 350 to 700 $MtCO_2eq$. In the case of India [15], the emission value for 2015 is approximately 24.6 $MtCO_2eq$. Figure 3.6 presents methane emissions from the underground mining sector worldwide for the year 2020, including literature data for China (550 $MtCO_2eq$) and India (24.6 $MtCO_2eq$), as well as emissions attributed to JSW S.A. The data presented in the chart clearly show that emissions from Polish underground mining rank seventh, accounting for 1.9% of the total methane emissions worldwide in this category, while JSW S.A. is responsible for 0.7%.

Now, in Figure 3.7, the state of methane emissions from the entire mining sector (including underground and surface mines) in 2020 is presented. The emission values assigned to China and India are based on the UNFCCC registry [6]. Similar to above, Poland's mining sector ranks seventh in terms of methane emissions, accounting for 2.3% of the total emissions. The discrepancies in percentage results are due to adopting lower emission values for China and India.

In the European context, the largest emitters of methane from underground mines (Fig. 3.8) are Poland and Ukraine. They account for an average emission of 39.35% and 34.86%, respectively. The remaining 25.79% comprises other European countries, including Romania (5.42 $MtCO_2eq$), Germany (1.57 $MtCO_2eq$), and the Czech Republic (1.40 $MtCO_2eq$). JSW S.A. mines are responsible for approximately 15.28% of the total methane emissions.

4. Methane emissions from JSW S.A. mines in the context of Europe, the world, and the energy sector

In the period from 2015 to 2020, the Polish underground mining sector accounted for an average methane emission of 14.84 $MTCO_2eq$ worldwide. During this period, Polish mines released a total of 3,560.71 kt of methane into the air, equivalent to 89.02 $MtCO_2eq$. In this context, JSW S.A. mines were responsible for emitting 1,383.73 kt of methane, equivalent to 34.59 $MtCO_2eq$. Figures 4.1 and 4.2 show the share of methane emissions from JSW S.A. mines in relation to different sectors in European countries (Fig. 4.1) and Annex I countries (Fig. 4.2).

The data presented in Figure 4.1 shows that JSW S.A. mines were responsible for 1.27% of methane emissions on a European scale. Other underground mines in Poland accounted for 2.00% of emissions. The highest methane emissions were from the Agriculture sector at 52.30%, followed by Waste at 27.33% and Energy at 17.45%.

In the case of Annex I countries (Fig. 4.2), JSW S.A. mines accounted for 0.30% of methane emissions, while other Polish mines accounted for 0.47%. The dominant sectors were Agriculture at 38.13% and Energy at a combined 38.66%.

The emission of methane at the national level takes a different shape. From 2015 to 2020, JSW S.A. mines accounted for 9.88% of the total methane emissions, while other mines accounted for 15.48% (Fig. 4.3). Considering the entire analyzed period, the highest emissions in Poland were attributed to the Energy sector, approximately 38.08%, followed by Agriculture at 34.46% and Waste at 27.26%.

In Poland, the Energy sector is 49.5% reliant on hard coal, which is accompanied by methane emissions during its extraction. Table 4.1 presents the percentage contribution of methane emissions from Polish coal mines and JSW S.A.

The data clearly show that methane emissions from JSW S.A. mines accounted for 24% to nearly 27% of the energy sector's emissions in Poland. At the European Union level, this value decreases and ranges from 6.65% to 7.85%, while in Annex I countries, it only represents 0.79% to 0.94%.

5. Methane emissions from closed mines

Polish coal mining has undergone significant changes in the past five years. Thirteen mines were closed, and some were merged. In 2019, a total of five mines were in the process of closure [9], including two owned by JSW S.A.: KWK "Jas-Mos" (October 1, 2016) and KWK "Krupiński" (April 1, 2017). Both mines have active methane capture at levels of 99.43% and 86.91%, respectively.

In the Greenhouse Gas Inventory Data report sent to the UNFCCC registry [6], the emission factor for methane from abandoned mines is assumed to be 0.652 million m^3/mine. According to this factor, the average methane emissions from this activity amounted to 264.53 $ktCH_4$, which is equivalent to 6.61 $MtCO_2eq$ from 2015 to 2020. Figure 5.1 shows the methane emissions from

Fig. 3.6 Methane emissions from the underground mining sector worldwide for the year 2018 [6]
Rys. 3.6 Emisje metanu z górnictwa podziemnego na świecie w 2018 roku [6]

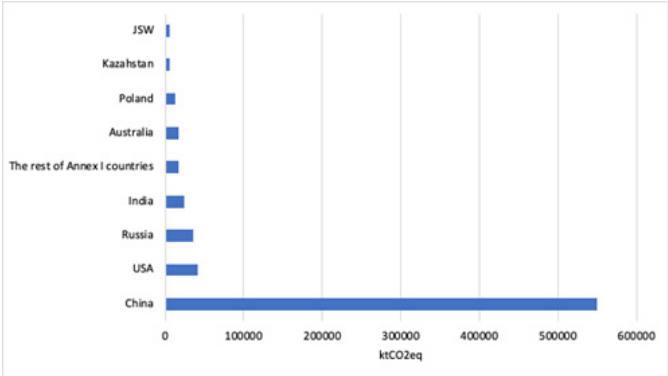

Fig. 3.7 Methane emissions from the mining sector (underground and open-pit mines) worldwide in 2020
Rys. 3.7 Emisje metanu z sektora wydobywczego (kopalnie podziemne i odkrywkowe) na świecie w 2020 r.

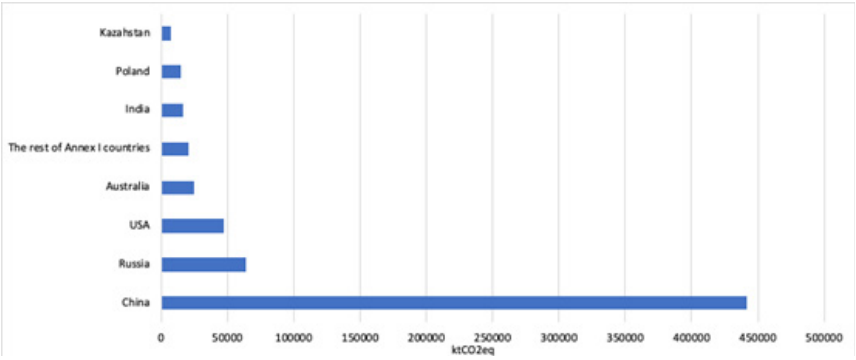

the underground mining category divided into mining activity, post-mining, and closed mines in comparison to Europe.

In Poland, the majority of methane emissions in the underground mining category came from mining activity (78% of total emissions), followed by post-mining activity (19%), and abandoned mines accounted for 3% of the emissions. In comparison to Europe, Poland was characterized by high emissions from mining activity (approximately 42% in this category in Europe) and post-mining activity (about 58%). Emissions from abandoned mines accounted for an average of 7% of the total methane emissions from abandoned mines in the sector. The highest emissions in this category were primarily attributed to Romanian mining, accounting for an average of 78%.

Considering the cumulative methane emissions from the underground mining category in Europe, emissions from abandoned mines in Poland accounted for approximately 1.16% of the total emissions, mining activity accounted for an average of 30% of the emissions, and post-mining activity accounted for 7%.

The methane emissions from the former JSW S.A. mines in 2019 amounted to 1.88 million m³, which corresponds to 1.35 ktCH_4 (0.03375 MtCO_2eq).

In comparison to Annex I countries, methane emissions in Poland in the mining activity category accounted for 10%, in the post-mining activity category 17%, and emissions from closed mines accounted for an average of 3% of the total methane emissions from closed mines in the sector (Fig. 5.2).

Polish coal mining is characterized by very low rock permeability. Methane emissions occur due to its expansion under the influence of mining activity. Increased methane release from the rock often occurs, and its capture becomes necessary. After mining operations are completed, the pressures in the rock equalize, resulting in increased stress and decreased permeability, ultimately leading to a decrease in methane emissions over time. Taking this into account, the release of methane from abandoned mines over a longer time period should not have a significant impact on the total methane emissions from the underground mining category.

6. Summary

Methane has been recognized by the Intergovernmental Panel on Climate Change (IPCC) as the second most significant greenhouse gas, contributing to global warming by absorbing infrared radiation. Methane emissions are associated with coal mining, and Poland is the ninth largest producer of coal. In the country, 88% of methane is released from underground mining activities, while only 12% comes from surface mines.

In Poland, the majority of methane emissions in the underground mining category come from mining activity (78% of total emissions), followed by post-mining activity (19%), and abandoned mines account for 3% of emissions.

In 2021, approximately 815.3 million m³ of methane was released from the rock affected by mining activities, which means that on average, 1551.17 m³ of methane was released per minute [9]. From 2015 to 2021, the relative methane emission rate, measured in cubic meters per ton of extracted coal, ranged from 12.9 to 15 m³.

The cumulative methane capture efficiency in Polish mines for the years 2015–2019 ranged from 34.6% to 36.3%, and the utilization rate remained at the level of 57% to almost 64%

Fig. 3.8 Methane emissions from underground mines in European countries

Rys. 3.8 Emisje metanu z podziemnych kopalń w krajach europejskich

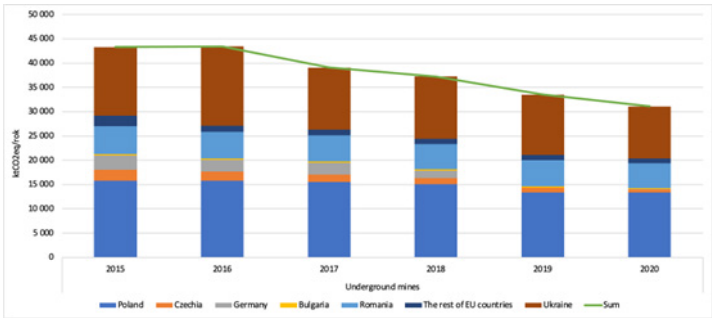

Fig. 4.1 Methane emissions from JSW S.A. mines in relation to different sectors in European countries from 2015 to 2020 [6]

Rys. 4.1 Emisje metanu z kopalń JSW S.A. na tle poszczególnych sektorów w krajach europejskich w latach 2015–2020 [6]

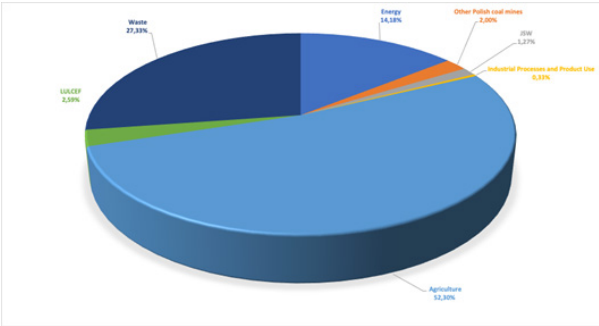

Fig. 4.2 The methane emissions from JSW S.A. mines in relation to different sectors in Annex I countries from 2015 to 2020 [6]

Rys. 4.2 Emisje metanu z kopalń JSW S.A. w odniesieniu do poszczególnych sektorów w krajach Załącznika I w latach 2015–2020 [6]

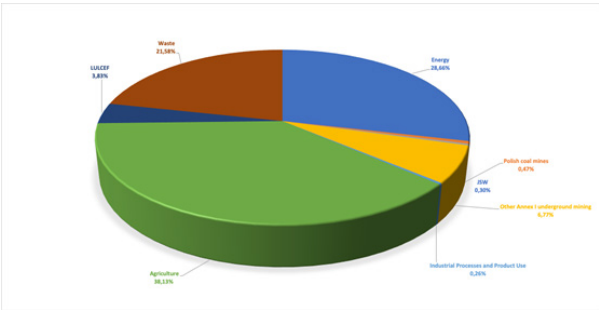

in 2018. However, from 2019 to 2021, these values slightly decreased. On the other hand, the percentage of methane released into the atmosphere during the examined period ranged from 63.7% to over 65.4% in 2021. It is important to note that these data are determined based on absolute methane content and only include ventilation air methane, excluding unutilized methane. If unutilized methane was taken into account, the percentage of methane released into the atmosphere would be around 76%.

In accordance with the obligations of the UNFCCC convention, Poland reports national emissions within the adopted reduction targets in five source categories using the Common Reporting Format [8]. Greenhouse gas emissions are presented in CO_2 equivalent, using the GWP100 metric, which, according to the IPCC guidelines, is 25 for methane [2]. Using an increased GWP100 value would result in higher total annual greenhouse gas emissions due to the increased contribution of methane (approximately 20%), but it would not significantly affect the long-term trend of changes [15]. However, the choice of other metrics, such as GWP20, could significantly increase the share of the mining sector in total methane emissions, which could influence the government's policy choices regarding climate change mitigation methods. This particularly applies to sectors and companies with high emissions levels other than CO_2, such as JSW S.A.

Compared to all Annex I countries, the Polish energy sector is responsible for approximately 3.3% of emitted methane, and on a European scale, it accounts for 18.23% of methane emissions (an average of 22.36 $MtCO_2eq$).

According to the ranking prepared by the International Energy Agency [7], Poland ranks sixth in terms of methane emissions from the mining sector. On a global scale (Annex I countries), the underground mining sector is a source of an average of 5.15 Mt of methane emissions, of which Polish mines release 0.53 Mt. It is important to note that these data do not include emissions from China and India.

Taking a closer look at the underground mining sectors of individual Annex I countries, it can be seen that

Fig. 4.3 Percentage of methane emissions from JSW S.A. mines in relation to other sectors in Poland from 2015 to 2020 [6]
Rys. 4.3 Udział procentowy emisji metanu z kopalń JSW S.A. w stosunku do innych sektorów w Polsce w latach 2015–2020 [6]

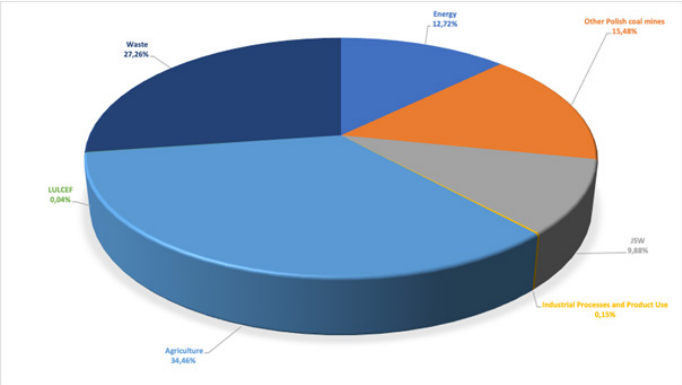

Tab. 4.1. Comparison of the percentage of methane emissions from Polish mines and JSW S.A. mines in relation to the energy sector in Poland, the European Union, and all Annex I countries [6]
Tab. 4.1. Porównanie udziału procentowego emisji metanu z polskich kopalń i kopalń JSW S.A. w odniesieniu do sektora energetycznego w Polsce, Unii Europejskiej i wszystkich krajach Aneksu I [6]

Percentage of methane emissions in the energy sector						
Lata	**2015**	**2016**	**2017**	2018	2019	2020
	Percentage of methane emissions in the energy sector in the European Union					
Percentage of methane emissions from Polish underground mines	18,52	18,78	18,48	19,24	18,34	19,16
Percentage of methane emissions from JSW S.A.	**6,65%**	**7,85%**	**7,17%**	**7,57%**	**7,37%**	**7,10%**
Percentage of methane emissions in the Polish energy sector						
Percentage of methane emissions from Polish underground mines	67,37%	66,76%	66,37%	65,93%	65,68	65,68
Percentage of methane emissions from JSW S.A.	**24,17%**	**27,90%**	**25,76%**	**25,95%**	**26,40%**	**24,33%**
Percentage of methane emissions in the energy sector of Annex I countries						
Percentage of methane emissions from Polish underground mines	1,42%	1,30%	1,33%	1,26%	1,17%	1,32%
Percentage of methane emissions from JSW S.A.	**0,79%**	**0,94%**	**0,84%**	**0,82%**	**0,79%**	**0,78%**

the United States is the dominant emitter, accounting for 35.0% of total methane emissions (in the underground mining sector). The next countries are Russia (35.49%), other Annex I countries including Ukraine (15.4%), Australia (12.3%), Poland (10.3%), and Kazakhstan (3.5%). In the case of Kazakhstan, the majority of methane emissions come from surface mining, accounting for 77.74%. The mines of JSW S.A. are responsible for approximately 3.97% of the total methane emissions from the underground mining sector.

When incorporating literature data on methane emissions from the mining sector for China (550 $MtCO_2eq$) and India (24.6 $MtCO_2eq$), two of the largest methane emitters, and adding JSW S.A., the Polish underground mining sector ranks sixth, accounting for 1.9% of the total global methane emissions from this sector, while emissions from JSW S.A. amount to 0.7%.

In the European context, Poland and Ukraine are the largest emitters of methane from underground mines, accounting for approximately 39.35% and 34.38% of emissions,

Fig. 5.1. The methane emissions from the underground mining category divided into mining activity, post-mining activity, and abandoned mines in Europe from 2015 to 2020 [6]

Rys. 5.1. Emisje metanu z kategorii górnictwo podziemne w podziale na działalność górniczą, działalność pogórniczą i kopalnie opuszczone w Europie w latach 2015–2020 [6]

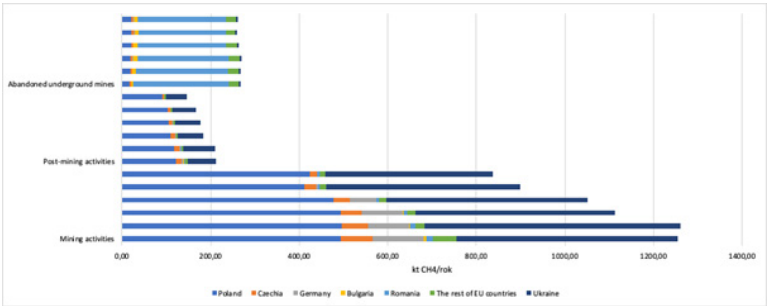

Fig. 5.2. The methane emissions from the underground mining category divided into mining activity, post-mining activity, and abandoned mines in Annex I countries from 2015 to 2020 [6]

Rys. 5.2 Emisje metanu z kategorii górnictwo podziemne z podziałem na działalność górniczą, działalność poeksploatacyjną i kopalnie opuszczone w krajach załącznika I w latach 2015–2020 [6]

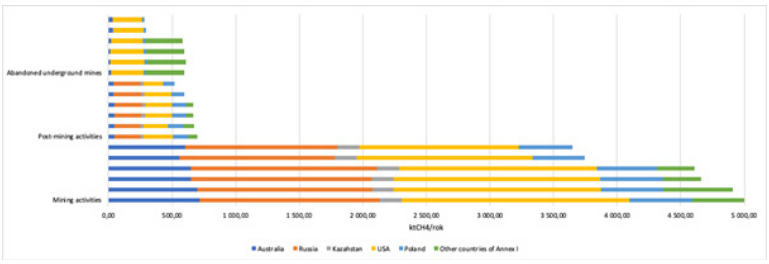

respectively. The remaining 27.79% of emissions come from other European countries, including Romania (5.42 $MtCO_2eq$), Germany (1.57 $MtCO_2eq$), and the Czech Republic (1.40 $MtCO_2eq$). The mines of JSW S.A. are responsible for approximately 15.28% of the total methane emissions.

In terms of total methane emissions in Europe, including the energy sector, the mines of JSW S.A. contributed only 1.27% of emissions from 2015 to 2020. Other underground mines in Poland accounted for 2.0%. The largest sources of methane release were the Agriculture sector (52.30%), followed by Waste (27.33%) and Energy (17.45%).

When compared to the Annex I countries, these values significantly decrease, with JSW S.A. accounting for 0.3% of methane emissions and other Polish mines accounting for 0.47%. The dominant sectors were Agriculture (38.13%) and Energy (38.66%) combined.

At the national level, the emissions of methane were distributed differently. From 2015 to 2020, the mines of JSW S.A. accounted for 9.88% of total methane emissions, while other mines accounted for 15.48% (Figure 4.3). Over the entire analyzed period, the largest emissions in Poland were attributed to the Energy sector (approximately 38.08%), followed by Agriculture (34.46%) and Waste (27.26%).

From the presented data, it is clear that methane emissions from JSW S.A. mines ranged from 24% to almost 27%. At the scale of the European Union, this value decreases to between 6.65% and 7.85%, and within the Annex I countries, it represents only 0.79% to 0.94%.

Given that methane emissions (as an associated gas) are inseparable from the activities of JSW S.A., the company strives to capture and utilize it to the greatest extent possible. However, due to safety reasons, it is not possible to completely avoid emissions with the ventilation air.

Including methane in the emissions trading system, with higher fees compared to carbon dioxide, would result in enormous costs for coal companies, ultimately leading them to bankruptcy. Therefore, the complete elimination of methane emissions from mines seems necessary, as proposed by the European Union regulations. However, the implementation of methane ventilation air management (VAM) would require significant financial investments to fully utilize it, which is not feasible. VAM methane utilization technology is costly and not adapted to the amount of airflow in the shafts.

The solution appears to be the funding of methane mitigation technology development and modernization, as well as the introduction of an obligation to apply it regardless of safety conditions (capturing from post-mining works). Legislative solutions are also necessary, such as treating methane captured through mitigation systems as a renewable energy source or a primary source for producing environmentally friendly electricity. The lack of such regulations significantly reduces the attractiveness of methane utilization in energy production since it does not allow for preferential pricing of the sold electricity. One possible solution could be treating investments in coal gas management as preferential due to environmental protection. However, this would require changes to Polish legislation that unequivocally include financial support for electricity and/or heat generated from coal gas processing on the same terms as support for renewable energy, regardless of the installed capacity in the source – granting it the status of environmentally friendly energy.

Due to the harmfulness of methane released into the atmosphere, any measure reducing its presence should be

unequivocally supported by legislation, promoted, and financially supported to the extent possible and in accordance with environmental regulations in the country. It is one of the ways to intensify the fight against harmful climate change caused by excessive emissions of this greenhouse gas into the atmosphere, while significantly increasing the safety of mining crews and reducing the costs of coal mining.

Considering the inclusion of electricity generated from coal gas as meeting the obligation to purchase energy from renewable sources would enable the intensification of investment processes in coal gas management by encouraging investors and significantly improving the safety of coal mining.

Literatura – References

1. IPCC, 2006: 2006 IPCC Guidelines for National Greenhouse Gas Inventories.
2. IPCC, 2014: Climate Change 2014: Synthesis Report. Contribution of Working Groups I, II and III to the Fifth Assessment Report of the Intergovernmental Panel on Climate Change [Core Writing Team, R.K. Pachauri and L.A. Meyer (eds.)]. IPCC, Geneva, Switzerland, 151 pp.
3. Myhre, G., D. Shindell, F.-M. Bréon, et al., 2013: Anthropogenic and Natural Radiative Forc- ing. In: Climate Change 2013: The Physical Science Basis. Contribution of Working Group I to the Fifth Assessment Report of the Intergovernmental Panel on Climate Change [Stocker, T.F., D. Qin, G.-K. Plattner, M. Tignor, S.K. Allen, J. Boschung, A. Nauels, Y. Xia, V. Bex and P.M. Midgley (eds.)]. Cambridge University Press, Cambridge, United Kingdom and New York, NY, USA.
4. Etminan, M., Myhre, G., Highwood, E.J., Shine, K.P., 2016: Radiative forcing of carbon dioxide, methane, and nitrous oxide: a significant revision of the methane radiative forcing. Geophys. Res. Lett. 43 (12), 623. https://doi.org/10.1002/2016GL071930. 614–12.
5. Saunois, M., Bousquet, P., Poulter, B., et al., 2016.: The global methane budget, 2000–2012. Earth Syst. Sci. Data 8, 697–751. https://doi.org/10.5194/essd-8-697- 2016.
6. UNFCCC Greenhouse Gas Inventory Data, https://di.unfccc.int/detailed_data_by_party
7. IEA World Energy Balances 2022 https://www.iea.org/subscribe-to-data-services/world-energy-balances-and-statistics
8. National Inventory Report, 2022. Inventory of Greenhouse Gases in Poland for the Years 1988–2020 A Synthesis Report. IEP-NRI, written in response to the requirements of the United Nations Framework Convention on Climate Change and the Kyoto Protocol, Warsaw.
9. WUG, 2022. Ocena stanu bezpieczeństwa pracy, ratownictwa górniczego oraz bezpieczeństwa powszechnego w związku z działalnością górniczo- geologiczną w 2021 roku. Wyższy Urząd Górniczy w Katowicach.
10. Bilans zasobów złóż kopalin w Polsce wg stanu na 31 XII 2021. Państwowy Instytut Geologiczny- PIB, Warszawa 2022, https://www.pgi.gov.pl/oferta-inst/wydawnictwa/serie-wydawnicze/bilans-zasobow-kopalin.html
11. Szlązak, N., Borowski, M., Obracaj, D., et al., 2014. Selected Issues Related to Methane Hazard in Hard Coal Mines. Wydawnictwa AGH, Kraków.
12. European Pollutant Release and Transfer Register (E-PRTR): https://prtr.eea.europa.eu/#/home
13. Statista: Leading hard coal producing countries worldwide in 2018: https://www.statista.com/statistics/264775/top-10-countries-based-on-hard-coal-production/
14. Sheng J., Song, Sh., Zhang Y., Prinn,R.G., Janssens-Maenhou G., 2019:Bottom-Up Estimates of Coal Mine Methane Emissions in China: A Gridded Inventory, Emission Factors, and Trends Environ. Sci. Technol. Lett. 2019, 6, 8, 473–478 Publication Date:May 31, 2019 https://doi.org/10.1021/acs.estlett.9b00294
15. India Coal Mine Methane Market Study EPA Publication No: 456R19001 May 2019 https://www.epa.gov/sites/production/files/2019-05/documents/india_cmm_market_study_may2019.pdf

Wpływ metanu emitowanego ze złóż węgla na stan atmosfery

W artykule przedstawiono analizę emisji metanu do atmosfery, ilości metanu wychwyconego i wykorzystanego, a także metanu uwolnionego z systemu odmetanowania. Wyniki są następnie porównywane z danymi pochodzącymi z Wyższego Urzędu Górniczego (WUG) oraz Europejskiego Rejestru Uwalniania i Transferu Zanieczyszczeń (E-PRTR), który w Polsce prowadzony jest przez Główny Inspektorat Ochrony Środowiska. Dodatkowo, na podstawie danych o emisji gazów cieplarnianych z UNFCCC i JSW S.A., w artykule określono wpływ metanu emitowanego z jej kopalń na atmosferę w skali europejskiej i światowej.

Słowa kluczowe: *emisje metanu, efektywność odmetanowania, ochrona atmosfery*

Wykorzystanie wody dołowej w odbiorze i wykorzystaniu ciepła skraplania z podziemnych układów klimatyzacji w kopalniach

Nikodem SZLĄZAK[1)], Dariusz OBRACAJ[2)], Marek KORZEC[3)]

[1)] prof. dr hab. inż.; AGH w Krakowie, Wydział Inżynierii Lądowej i Gospodarki Zasobami, Kraków, Polska; email: szlazak@agh.edu.pl, ORCID: 0000-0001-8320-4751 orcid iD

[2)] dr hab. inż., prof. AGH; AGH w Krakowie, Wydział Inżynierii Lądowej i Gospodarki Zasobami, Kraków, Polska; email: obracaj@agh.edu.pl, ORCID: 0000-0001-5987-6718

[3)] dr inż.; AGH w Krakowie, Wydział Inżynierii Lądowej i Gospodarki Zasobami, Kraków, Polska; email: mkorzec@agh.edu.pl, ORCID: 0000-0001-5958-3157

http://doi.org/10.29227/IM-2023-01-28

Submission date: 17-05-2023 | Review date: 06-06-2023

Abstrakt

Stosowanie różnych systemów chłodzenia powietrza w kopalniach podziemnych wynika z trudnych warunków klimatycznych panujących na stanowiskach pracy. Podziemne instalacje chłodnicze z agregatami sprężarkowymi są szeroko stosowane w systemach chłodzenia powietrza. Sprawne działanie agregatów chłodniczych zależy od właściwego odprowadzania ciepła skraplania. Moc chłodnicza i lokalizacja instalacji chłodniczej mają największy wpływ na podjęcie decyzji o odprowadzeniu ciepła skraplania do powietrza lub wody. W artykule skoncentrowano się na zastosowaniu urządzeń chłodniczych zabudowanych w wyrobiskach podziemnych. Przedstawiono rozważania dotyczące ograniczeń przekazywania ciepła skraplania do powietrza kopalnianego oraz warunki sprzyjające wykorzystaniu wody dołowej w odbiorze ciepła skraplania z układów klimatyzacji. Omówiono uwarunkowania i możliwości wykorzystania ciepła odpadowego zawartego w pompowanej na powierzchnię wodzie dołowej.

Słowa kluczowe: *zagrożenie klimatyczne, klimatyzacja kopalń, agregaty chłodnicze, ciepło skraplania, wykorzystanie ciepła odpadowego*

1. Wprowadzenie

Eksploatacja w kopalniach podziemnych wiąże się z występowaniem wielu zagrożeń naturalnych. W kopalniach głębokich jednym z dominujących zagrożeń jest zagrożenie klimatyczne. Jego skala zależy od wielu czynników, które zostały przedstawione między innymi w pracach (Maurya T. i in. 2015; Szlazak i in. 2018a; Li i in. 2021, Szlązak i in. 2021). Podstawowym z nich jest temperatura pierwotna górotworu. Temperatury pierwotne górotworu zależą od głębokości i stopnia geotermicznego, który może osiągać różne wartości w zależności od lokalizacji kopalni (McPherson 2012; Doležal i in. 2013, Hemp 2014; Kamyar 2016).

Na stan zagrożenia klimatycznego wpływa także właściwe planowanie wykonywania wyrobisk podziemnych, racjonalna wentylacja wyrobisk oraz organizacja procesu technologicznego, a przede wszystkim transportu materiałów, odstawy urobku i lokalizacji urządzeń elektrycznych. Wymienione czynniki determinują stosowanie różnych rozwiązań klimatyzacji.

W zależności od miejsca lokalizacji urządzeń chłodniczych w kopalniach można wyróżnić trzy rodzaje układów klimatyzacyjnych. Ich podział został przedstawiony na rysunku 1. O wyborze rozwiązania klimatyzacji decyduje przede wszystkim występujące zapotrzebowanie na moc chłodniczą w rejonach prowadzonych robót górniczych. Istotnym czynnikiem jest także rodzaj zastosowanych urządzeń chłodniczych, zwanych agregatami chłodniczymi, oraz możliwości odprowadzania ciepła skraplania. Opis działań związanych z projektowaniem klimatyzacji w kopalniach przedstawiono między innymi w publikacjach (Szlązak i in. 2017; Szlązak i in. 2018b).

Niezależnie od zastosowanego rozwiązania klimatyzacji istotna jest kwestia odbioru ciepła skraplania czynnika chłodniczego w sprężarkowych urządzeniach chłodniczych. Odbiór ciepła skraplania może być realizowany następująco:

- W układach klimatyzacji lokalnej ciepło skraplania ze skraplaczy indywidualnych urządzeń chłodniczych pośredniego lub bezpośredniego działania oddawane jest do powietrza za pośrednictwem wody schładzanej w wyparnych chłodnicach wody (rys. 2a), wody technologicznej (np. z rurociągów p.poż. – rys. 2b) lub do wody dołowej w systemie odwadniania kopalni (rys. 2c). Bezwarunkowo woda ta musi być w sposób kontrolowany ujmowana i odpompowywana poza rejon, w którym pracują urządzenia chłodnicze.
- W układach klimatyzacji grupowej ciepło skraplania czynnika chłodniczego oddawane może być również do powietrza za pośrednictwem wody schładzanej w zgrupowanych wyparnych chłodnicach wody, najczęściej przy szybie wentylacyjnym (rys. 2a). Ciepło może być również przekazywane do wody dołowej pompowanej systemami odwadniania na powierzchnię (rys. 2c). Znane jest również rozwiązanie schładzania skraplaczy dołowych agregatów chłodniczych klimatyzacji grupowej za pomocą wody lodowej powrotną z układu klimatyzacji centralnej (Szlązak i in. 2010b).
- W klimatyzacji centralnej ciepło skraplania ze skraplaczy tych urządzeń oddawane jest na powierzchni do powietrza atmosferycznego lub do wody.

Rys. 1. Klasyfikacja rozwiązań klimatyzacji kopalń
Fig. 1. Mine cooling systems clasification

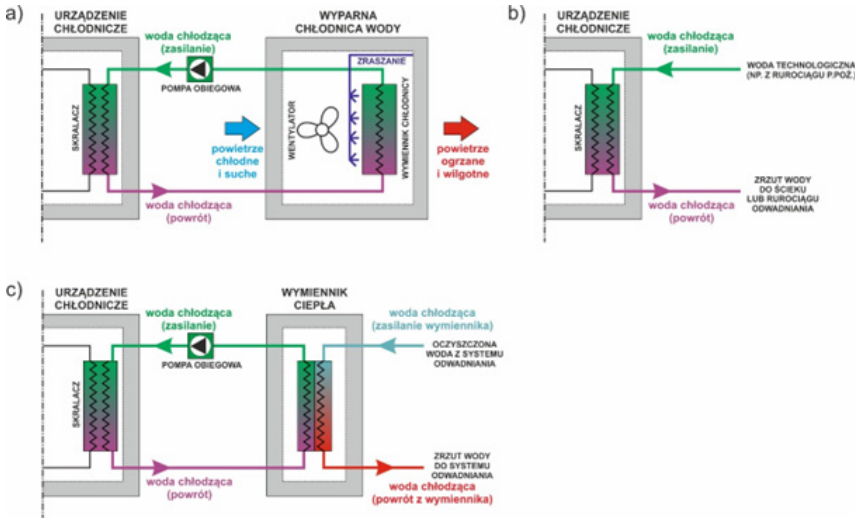

Rys. 2. Sposoby odprowadzenia ciepła skraplania z urządzeń chłodniczych zabudowanych w wyrobiskach dołowych: a) odprowadzenie do powietrza w wyparnych chłodnicach wody, b) odprowadzenie do wody technologicznej, c) odprowadzenie do wody dołowej za pośrednictwem wymiennika ciepła
Fig. 2. Ways of removing condensation heat from underground refrigeration plants: a) removing to the air using evaporative water coolers, b) removing to the service water, c) removing to the dewatering system in heat exchangers

Wykorzystanie wody dołowej do chłodzenia skraplaczy urządzeń chłodniczych rozważa się najczęściej w kontekście zastosowania układów klimatyzacji lokalnej i grupowej. Do tej pory w Polsce stosowano podziemne instalacje wyposażone w sprężarkowe urządzenia chłodnicze lokalizowane w wyrobiskach kopalni, o ile zapotrzebowanie na moc chłodniczą zwykle nie przekraczało 2,0–3,0 MW (Szlązak i in. 2019b). Podziemnych stacji klimatyzacji z wyższą mocą chłodniczą nie budowano, ponieważ praktycznie niemożliwe było odprowadzenie większej ilości ciepła skraplania czynnika chłodniczego.

W jednej z podziemnych kopalń zbudowano system klimatyzacji z odprowadzeniem ciepła skraplania z podziemnych urządzeń chłodniczych na powierzchnię za pomocą rurociągów w szybie wdechowym. Jednak koszty eksploatacyjne spowodowały, że taki system nie został szerzej rozpowszechniony (Szlązak i in. 2018). Dlatego przy zapotrzebowaniu dużych mocy chłodniczych (powyżej 3,0 MW) zwykle rozpatruje się budowę klimatyzacji centralnej z powierzchniowymi stacjami urządzeń chłodniczych. W takich układach klimatyzacyjnych niezbędne jest zastosowanie rozwiązań obniżających ciśnienie hydrostatyczne słupa wody pomiędzy rurociągiem pionowym w szybie, a rurociągami na poziomie głębokościowym kopalni.

Nie mniej jednak można rozważać budowę podziemnej stacji urządzeń chłodniczych z większą mocą chłodniczą. Aktualnie w jednej z kopalń budowany jest układ klimatyzacji o mocy 4,0 MW, z planem rozbudowy do 6,0 MW, w którym ciepło skraplania z urządzeń chłodniczych odprowadzane będzie do systemu odwadniania kopalni (Projekt dla CFT). Takie rozwiązanie musi spełniać kilka kluczowych warunków, aby w sposób skuteczny i ekonomiczny eksploatować układ klimatyzacyjny w kopalni.

2. Ograniczenia dotychczasowych sposobów przekazywania ciepła skraplania z podziemnych urządzeń chłodniczych

W układach klimatyzacji z urządzeniami chłodniczymi zabudowanymi w wyrobiskach podziemnych możliwości oddawania ciepła skraplania do powierza wentylacyjnego są ograniczone. Wynika to z parametrów termodynamicznych powietrza przepływającego wyrobiskami górniczymi.

Z dotychczasowych doświadczeń związanych ze stosowaniem podziemnych urządzeń chłodniczych i oddawaniem ciepła do powietrza wynika, że:

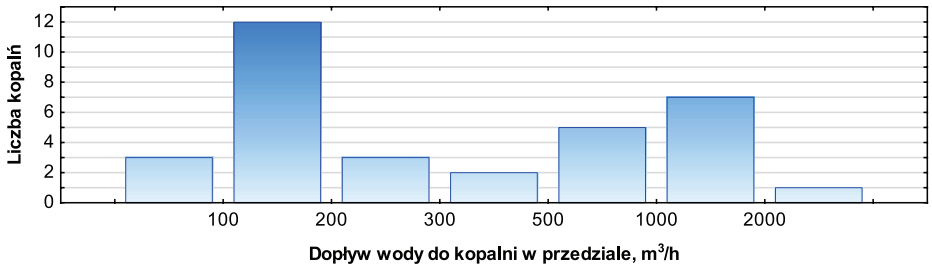

Rys. 3. Rozkład dopływu wody do polskich kopalń podziemnych
Fig. 3. Distribution of water inflow in Polish underground mines

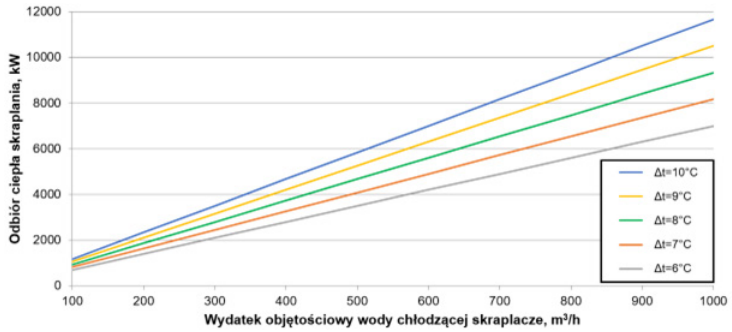

Rys. 4. Możliwości odbioru ciepła skraplania w zależności od wydatku wody i różnicy temperatur wody chłodzącej
Fig. 4. Possibilities of recovering condensation heat depending on the water flow rate and the temperature difference of the cooling water

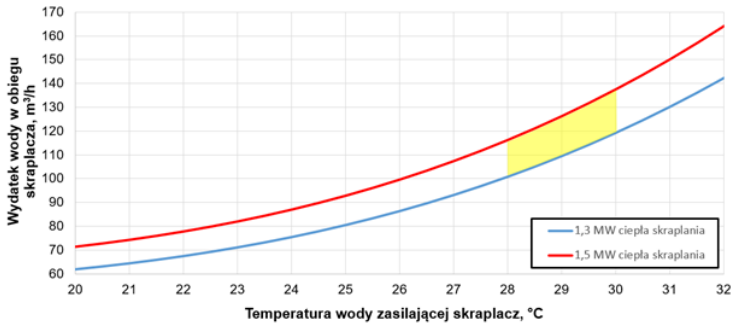

Rys. 5. Wymagany wydatek wody chłodzącej skraplacze w zależności od temperatury wody zasilającej
Fig. 5. Required cooling water flow for condensers depending on the water temperature

- Odbiór ciepła skraplania jest kluczowy dla uzyskiwania w urządzeniach chłodniczych pełnej mocy chłodniczej, a tym samym poprawnej pracy całego układu klimatyzacyjnego;
- Przekazywanie ciepła skraplania do powietrza wiąże się bardzo często z koniecznością zabudowy chłodnic wyparnych w znacznej odległości od urządzeń chłodniczych, a tym samym zabudową długich rurociągów i pomp obiegowych dla pokonania oporów przepływu wody;
- Wyparne chłodnice wody muszą być wyposażane w wentylatory przetłaczające powietrze wentylacyjne przez wymienniki ciepła, co zwiększa energochłonność układu klimatyzacyjnego;
- Temperatura powietrza wentylacyjnego nie powinna przekraczać 27°C a wilgotność względna 75%;
- Strumień objętości powietrza dostosowany musi być do wielkości przekazywanego do powietrza strumienia ciepła.

Takie wymagania na drogach powietrza odprowadzanego do szybów wentylacyjnych ograniczają możliwości lokalizacji wyparnych chłodnic wody o dużych mocach chłodniczych. Nie zawsze jest więc możliwe schłodzenie wody do wymaganej temperatury na wlocie skraplacza urządzenia chłodniczego.

Kopalnie w schładzaniu skraplaczy bardzo często wspomagają się wodą technologiczną (z rurociągów p.poż.). Jednakże jest to rozwiązanie nieuzasadnione ekonomicznie i przyczynia się do zwieszania zużycia wody. Dodatkowo, znaczne zwiększenie zużycia wody może być realizowane jeśli system odwadniania kopalni posiada rezerwy zwiększenia wydajności.

3. Czynniki warunkujące wykorzystanie systemu odwadniania kopalni w układach klimatyzacyjnych

W kopalniach występują dwa główne źródła wody dołowej. Całkowity dopływ wody do wyrobisk związany jest z dopływem wody pochodzenia naturalnego jak i z dopływem wody technologicznej. W polskich kopalniach zużycie wody technologicznej jest stosunkowo niewielkie w stosunku do całkowitej ilości wody odpompowywanej na powierzchnię.

Głównym zadaniem całego systemu odwadniania kopalni jest ujęcie dopływów wody możliwie blisko ich powstawania

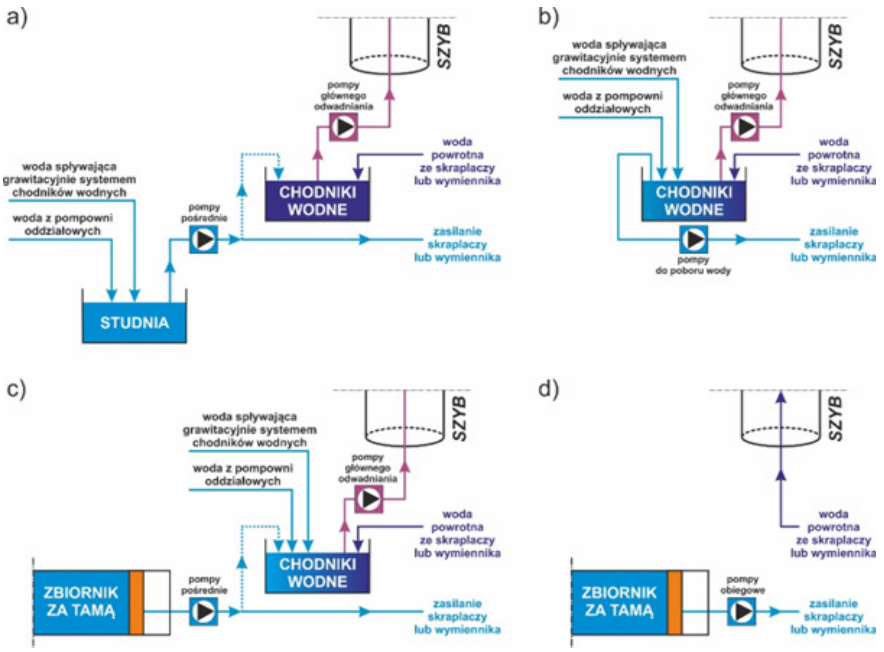

Rys. 6. Rozwiązania poboru wody do chłodzenia skraplaczy urządzeń chłodniczych z systemu odwadniania: a) rozwiązanie z układem pośrednim, b) układ bezpośredni, c) rozwiązanie poboru wody zza tamy z układem pośrednim, d) rozwiązanie poboru wody zza tamy z bezpośredniego pompowania wody na powierzchnię

Fig. 6. Solutions of intake water for cooling condensers from the dewatering system: a) indirect system, b) direct system, c) water intake from behind the dam with indirect system, d) water intake from behind the dam with direct pumping of water to the surface

i odprowadzanie na powierzchnię kopalni. W kopalniach większość wody spływa grawitacyjnie z miejsc prowadzenia eksploatacji do centralnej komory pomp odwadniania. Pozostała część wody jest przepompowywana. Kluczową rolę w całym systemie odwadniania stanowią chodniki wodne i komory głównego odwadniania.

Woda z wyrobisk gromadzących wodę może być przetłaczana na powierzchnię pośrednio (dwu lub wielostopniowo) lub bezpośrednio. Sposób odpompowywania wody w kopalni zależy od jej dopływu oraz liczby czynnych poziomów wydobywczych. W warunkach polskich kopalń przy dużych dopływach wody stosuje się przede wszystkim system bezpośredniego odprowadzania wody na powierzchnię (Praca zbiorowa 1975). W systemie odwaniania pośredniego woda przekazywana jest między poziomami głębokościowymi, a następnie na powierzchnię. Komory głównego odwadniania w takiej sytuacji lokalizuje się na poziomie o największym dopływie wody. Pomiędzy poziomami woda może spływać grawitacyjnie lub być przepompowywana.

Możliwości odprowadzenia ciepła skraplania w układach odwadniania kopalń ogranicza ilość wody w systemie odwadniania kopalni. Polskie kopalnie podziemne należą generalnie do kopalń o małym dopływie wody. Charakteryzują się także zróżnicowaną ilością wody w systemie odwadniania. W roku 2022 w Polsce eksploatacja prowadzona była w 20 kopalniach węgla kamiennego, w 30 ruchach oraz z 3 kopalniach rud miedzi. Dopływy wody w tych kopalniach zmieniają się w szerokich granicach, od około 10 m^3/h do ponad 3500 m^3/h (Sas 2022). Średni dopływ wynosi około 600 m^3/h. Struktura dopływu wody jest jednak różna, co wpływa na to, że bardzo często woda odpompowywana jest z różnych rejonów kopalni oraz różnych poziomów co uniemożliwia jej całkowite wykorzystanie w układach klimatyzacji. Na rysunku 3 przedstawiono histogram liczby kopalń z różnymi dopływami wody. W przypadku kopalń wieloruchowych, uwzględniono dopływy do poszczególnych ruchów.

W kopalniach o dużym dopływie wód dołowych można zwrócić uwagę na możliwość ich wykorzystania w odbiorze ciepła skraplania z dołowych urządzeń chłodniczych. Przy rozpatrywaniu takiego sposobu należy jednak rozważyć dostępny strumień wody kopalnianej oraz jej jakość i czystość.

W kontekście wykorzystania wody dołowej w układach klimatyzacji, najważniejszymi czynnikami są:

- ciągłość pompowania wody na powierzchnię,
- maksymalny dopływ wody i jego zmienność w czasie,
- lokalizacja chodników wodnych i komór głównego odwadniania względem planowanej lokalizacji urządzeń chłodniczych,
- skład chemiczny wody i poziom jej zanieczyszczenia częściami stałymi,
- struktura rozpływu wody w systemie odwadniania rozumiana jako:
  – liczba miejsc pompowania wody – komora głównego odwadniania i lokalne przepompownie wody,
  – sposób pompowania wody na powierzchnię – bezpośredni, pośredni,
- możliwość poboru wody poza miejscem jej odpompowywania na powierzchnię (występowanie zbiorników pośrednich).
- temperatura wody i jej zmienność w czasie.

Biorąc pod uwagę powyższe czynniki należy mieć na uwadze, że nie każda kopalnia ma warunki do wykorzystywania wody dołowej jako medium chłodzącego skraplacze urządzeń chłodniczych. Tylko szczegółowa analiza powyższych czynników pozwala określić potencjał takiego rozwiązania.

Na rysunku 4 przedstawiono wielkości strumieni ciepła jakie można oddać do wody w zależności od jej wydatku ob-

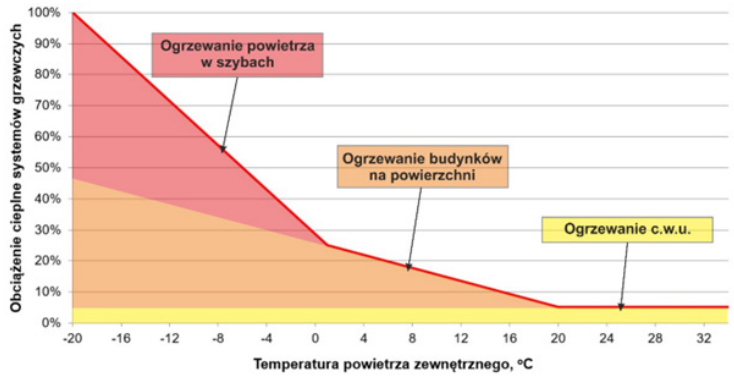

Rys. 7. Zmiana obciążenia cieplnego systemów grzewczych w kopalni w zależności od temperatury powietrza zewnętrznego
Fig. 7. Changes of heat requirements of the heating systems in the mine depending on the outside air temperature

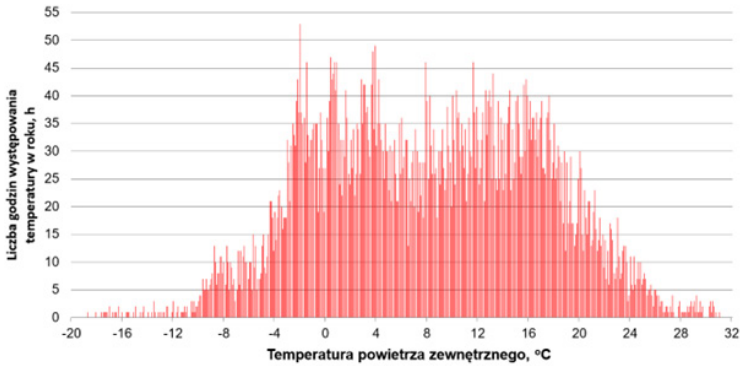

Rys. 8. Częstość występowania temperatur dla miejscowości Katowice
Fig. 8. Frequency of outside air temperatures in Katowice

jętościowego oraz różnicy temperatur przy przepływie przez skraplacze. Z przedstawionego wykresu wynika, że dla odbioru ciepła z układów o większej mocy niezbędne jest zapewnienie dużego wydatku wody chłodzącej w miejscu lokalizacji urządzeń, co w warunkach kopalń podziemnych często nie jest zapewnione. Z przedstawionego na rysunku 4 wykresu wynika, że dla odebrania większych ilości ciepła skraplania (w domyśle z układów większej mocy) wody musi być dużo lub trzeba zakładać dużą różnicę temperatur Δt wody zasilającej i powrotnej na skraplaczach. W większości dostępnych na rynku urządzeń chłodniczych woda zasilająca skraplacz powinna mieć od 28-30°C, a w czasie przepływu przez skraplacz ogrzewa się ona o 8-10°C. Takie założenia wskazują, że dla odbiorów dużych ilości ciepła skraplania wymagany jest duży wydatek wody.

Woda w systemie odwaniania bardzo często zawiera zanieczyszczenia i najczęściej nie może być w sposób bezpośredni wykorzystana do chłodzenia skraplaczy, gdyż spowodowałaby ich szybkie zanieczyszczenie. Woda taka może być zastosowana z wykorzystaniem wymienników ciepła wody dołowej pośredniczących w wymianie ciepła. Kolejnym czynnikiem, który może ograniczać potencjał wody dołowej jest jej temperatura zależna od głębokości, na której zlokalizowane są chodniki wodne i występująca tam temperatura górotworu. Wahania temperatury wody mogą być związane także ze zmiennością temperatury powietrza w ciągu roku. W przypadku, gdy temperatura wody będzie zbyt wysoka, to nie zapewni ona odbioru wymaganej ilości ciepła skraplania przy ustalonym przepływie. Na rysunku 5 przedstawiono wykres obrazujący zmiany wymaganego wydatku wody do chłodzenia skraplaczy wraz ze zmianą temperatury wody zasilającej skraplacz. Wykres opracowano na podstawie wyników pomiarów w różnych urządzeń sprężarkowych o mocach skraplaczy w zakresie od 1,3 MW do 1,5 MW. Obszar żółty oznacza zakres wydatku wody niezbędny do chłodzenia skraplaczy dla popularnych w kopalniach urządzeń chłodniczych z typowymi czynnikami chłodniczymi. Na wykresie można zauważyć, że przy wzroście temperatury wody chłodzącej, dla zachowania pełnej wydajności chłodniczej urządzenia należy zapewnić zdecydowanie wyższy wydatek wody.

Skład wody i jej zanieczyszczenie są równie istotne jak temperatura w jej wykorzystywaniu do celów chłodniczych (Szlązak i in. 2010a).

Woda może być kierowana na różnego rodzaju wymienniki ciepła pośredniczące w wymianie ciepła pomiędzy wodą dołową, a układem skraplacza urządzenia chłodniczego. Woda może być kierowana bezpośrednio na skraplacz. Kwestia konieczności zastosowania wymiennika ciepła będzie zależeć przede wszystkim od składu chemicznego wody oraz zawartości części stałych i/lub zawiesin. W instalacji poboru wody dołowej należy dobrać odpowiednie urządzenia filtrujące i/lub uzdatniające wodę.

Istotnym aspektem analizy wykorzystania wody dołowej jest obliczenie jej temperatury przy odpompowaniu na powierzchnię (aspekty prawne związane ze zrzutem wód do ścieków). W przypadku zabudowy rurociągów odwadniających w szybach wdechowych może dochodzić do ogrzewania powietrza doprowadzanego do wyrobisk. Istotne są również warunki środowiskowe zrzutu ciepłych wód. Odzysk ciepła z ciepłej wody powinien być wzięty pod uwagę podczas ana-

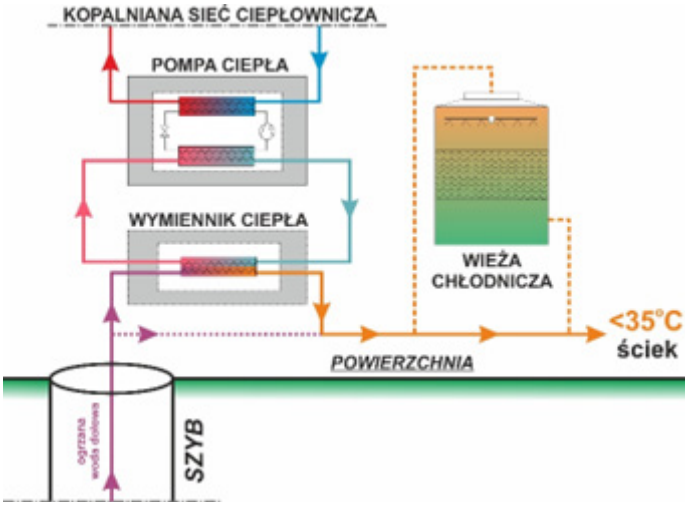

Rys. 9. Idea pozyskiwania ciepła odpadowego z wody pompowanej systemem odwadniania na powierzchni
Fig. 9. Idea of waste heat recovery from water pumped to the surface by the dewatering system

lizy rozpatrywania wykorzystywania wody dołowej do celów chłodniczych.

4. Przykłady rozwiązań wykorzystania wody dołowej w chłodzeniu skraplaczy układów klimatyzacji

Istotnym czynnikiem warunkującym możliwości wykorzystania wody dołowej do chłodzenia skraplaczy maszyn chłodniczych jest rozwiązanie systemu odwadniania. Na rysunku 6 przedstawiono przykłady rozwiązań wykorzystywania wody dołowej:

W rozwiązaniu przedstawionym na rysunku 6a woda z rejonów gromadzona jest w zbiorniku (np. studni), z którego jest przepompowywana do chodników wodnych. Pobór wody do chłodzenia agregatów realizowany jest z obiegu pomiędzy zbiornikiem, a chodnikami wodnymi. Woda ogrzana kierowana jest do chodników wodnych. Pompy głównego odwadniania pobierają wodę z chodników wodnych i odprowadzają na powierzchnię.

W rozwiązaniu przedstawionym na rysunku 6b woda kierowana jest z rejonów bezpośrednio do chodników wodnych. Pobór wody do chłodzenia agregatów realizowany jest z najczęściej z jednego z chodników, a ogrzana woda jest kierowana do drugiego chodnika. Pompy głównego odwadniania pobierają wodę z chodników wodnych i odprowadzają na powierzchnię. Strumień wody pobieranej do chłodzenia skraplaczy i przekazywanej z powrotem do chodników wodnych powinien być mniejszy od strumienia wody dopływającej do systemu odwadniania kopalni.

W rozwiązaniu przedstawionym na rysunku 6c wykorzystuje się wodę z otamowanych zbiorników wodnych w kopalni. Pobór wody do chłodzenia agregatów realizowany jest zza tamy wodnej, a ogrzana woda kierowana jest do chodników wodnych. Pompy głównego odwadniania pobierają wodę z chodników wodnych i odprowadzają na powierzchnię.

W rozwiązaniu przedstawionym na rysunku 6d woda z rejonów gromadzona jest w otamowanym wyrobisku. Pobór wody do chłodzenia agregatów realizowany jest zza tamy wodnej, a ogrzana woda jest kierowana bezpośrednio na powierzchnię.

W perspektywie wykorzystania wody do chłodzenia skraplaczy najlepsze jest rozwiązanie z układem pośrednim (rys. 6a). W takim rozwiązaniu woda pobierana do chłodzenia skraplaczy i oddawana po ogrzaniu do chodników wodnych nie miesza się z wodą spływającą z rejonów. W przypadku układu bezpośredniego (rys. 6b) woda pobierana jest z chodników wodnych i po ogrzaniu w skraplaczach kierowana również do chodników wodnych. Nawet jeżeli są to dwa równoległe chodniki będzie dochodziło do jej mieszania i wzrostu temperatury wody w chodnikach. Warunki odbioru ciepła w skraplaczach będą się pogarszać w czasie utrudniając uzyskanie przez urządzenia chłodnicze pełnej wydajności. Dobrym rozwiązaniem jest także pobór wody zza tam wodnych w wyrobiskach. W zależności od warunków woda pobrana zza tam, po ogrzaniu w agregatach może być kierowana do chodników wodnych (rys. 6c) lub pompowana bezpośrednio na powierzchnię (rys. 6d).

5. Parametry wody na powierzchni

Zgodnie z polskim ustawodawstwem pod pojęciem ścieków rozumie się między innymi wprowadzane do wód lub do ziemi wody pochodzące z odwodnienia zakładów górniczych, z wyjątkiem wód wtłaczanych do górotworu (Ustawa... 2017). Podmiot korzystający z usług wodnych wprowadzający ścieki do wód lub do ziemi w ramach usług wodnych jest obowiązany do stosowania przyrządów pomiarowych lub systemów pomiarowych umożliwiających pomiar ilości i temperatury wprowadzonych ścieków, jeżeli wprowadza do wód lub do ziemi ścieki w ilości średniej dobowej powyżej 0,01 m^3/s.

Ścieki zbliżone składem do ścieków przemysłowych, powstające w wyniku działalności innej niż działalność handlowa, przemysłowa, składowa, transportowa lub usługowa albo ścieki przemysłowe będące mieszaniną ścieków bytowych, wód z odwodnienia zakładów górniczych, wód chłodniczych, lub ścieków pochodzących ze stacji uzdatniania wody, a także wód opadowych i roztopowych mogą być wprowadzane do ziemi jedynie w sytuacjach, gdy zastosowanie dostępnych technik w zakresie wprowadzania ścieków do wód jest niemożliwe lub ekonomicznie nieuzasadnione, pod warunkiem że temperatura wód chłodniczych przed zmieszaniem ze ściekami bytowymi, wodami z odwodnienia zakładów górniczych, wodami opadowymi lub roztopowymi lub ściekami pochodzącymi ze stacji uzdatniania wody nie jest wyższa niż 35°C (Rozporządzenie... 2019).

Temperatura wody odpompowanej na powierzchnię kopalni będzie zależna od temperatury powietrza wprowadzanego do szybu oraz od temperatury wody pompowanej na powierzchnię.

Woda opuszczająca skraplacze agregatów chłodniczych, w zależności od typu zastosowanego agregatu może osiągać nawet powyżej 40°C. Woda o takich parametrach może więc być pompowana na powierzchnię. Wynika z tego, że okresowo temperatura wody pompowanej na powierzchni może przekraczać 35°C (Szlązak, Swolkień 2019; Szlązak i in. 2022), co będzie skutkować tym, że będzie musiała być chłodzona przed zrzutem do ścieku. Stwarza to korzystne warunki do zagospodarowania ciepła w niej zawartego na powierzchni. Zamiast ochładzać wodę w zbiornikach, czy też chłodniach wentylatorowych można ja wykorzystać dla potrzeb energetycznych zakładu poprzez układy do odzysku ciepła niskotemperaturowego.

6. Wykorzystanie ciepła zawartego w wodzie dołowej

Oddawanie ciepła skraplania do systemu odwadniania kopalni daje możliwość jego wykorzystania na powierzchni. Oddawanie ciepła skraplania do wody pompowanej na powierzchnię powoduje podwyższenie jej temperatury, co z kolei podnosi jej potencjał energetyczny i pozwala na jej energetyczne wykorzystanie, np. do celów grzewczych w kopalni (ogrzewanie cwu, ogrzewanie budynków, ogrzewania powietrza wlotowego w szybach wdechowych). Ciepło to może zostać wykorzystane bezpośrednio lub poprzez zastosowanie układów z pompami ciepła lub wykorzystanie układów ORC. Należy też podkreślić, że okresowo woda posiadać może zbyt wysoką temperaturę, aby mogła być zrzucana do ścieku, więc tym bardziej zasadne jest wykorzystanie ciepła w niej zawartego.

Zakłady górnicze cechują się dużym zapotrzebowaniem na energię cieplną, zarówno w wyrobiskach dołowych, jak również na powierzchni. Istnieje wiele możliwości wykorzystania ciepła odpadowego celem pokrycia tych potrzeb. Bardzo często w kopalniach rozważa się wykorzystanie ciepła odpadowego z różnych procesów. Trudności polegają jednak na skorelowaniu ilości i ciągłości parametrów ciepła odpadowego z potrzebami energetycznymi zakładu.

Kierunki wykorzystania ciepła odpadowego na powierzchni zakładu mogą być różne. Najbardziej możliwie jest zagospodarowanie ciepła do celów:

- Ogrzewania ciepłej wody użytkowej – zapotrzebowanie stałe w ciągu roku, a wymagana temperatura wody powinna wynosić minimum 55°C;
- Ogrzewania powietrza w szybach wdechowych – zapotrzebowanie zmienne w ciągu roku, występuje kiedy temperatura powietrza zewnętrznego spada poniżej 1°C, a wymagana temperatura czynnika grzewczego zależna jest od konstrukcji układu nagrzewnic;
- Ogrzewania budynków na powierzchni – zapotrzebowanie tylko sezonie grzewczym i zależy od temperatur powietrza zewnętrznego, a wymagana temperatura czynnika grzewczego zależna od typu systemu ogrzewania.

Instalacja cwu zapewnia potrzeby bytowe i technologiczne użytkowników obiektów powierzchniowych. Największe zużycie cwu dotyczy łaźni pracowniczych, warsztatów działowych oraz potrzeb bytowych obiektów biurowych. W kopalni można przyjąć, że obciążenie cieplne układu cwu jest stałe w ciągu roku.

Zapotrzebowanie na ciepło do ogrzewania powietrza w szybie zależy od temperatury powietrza zewnętrznego i wydatku powietrza nim doprowadzanego do kopalni. Powietrze powinno być ogrzewane do wymaganej przepisami temperatury 1°C (Rozporządzenie... 2017). Zmiana temperatury powietrza zewnętrznego zmienia się w ciągu roku wpływając na obciążenie cieplne wymagane w układzie ogrzewania powietrza w szybach.

W przypadku budynków na powierzchni obciążenie cieplne jest również zależne od zmian temperatury zewnętrznej.

Szczytowe obciążenie cieplne występuje przy najniższych temperaturach powietrza występujących w danym rejonie i jest krótkotrwałe w ciągu roku. Wraz ze wzrostem temperatury powietrza zewnętrznego obciążenie cieplne maleje, co przedstawiono na rysunku 7.

Przedstawiony na rysunku 7 wykres nie obrazuje jednak zapotrzebowania na ciepło, a jedynie zmienność obciążenia cieplnego. Dlatego dla dokładniejszej analizy należy uwzględniać zmienność temperatur w ciągu roku. Na rysunku 8 przedstawiono wykres częstości występowania temperatur powietrza zewnętrznego wg danych statystycznych dla stacji metrologicznej w Katowicach (Serwis Rzeczypospolitej Polskiej 2017). Z przedstawionego wykresu wynika, że bardzo niskie temperatury powietrza występują stosunkowo rzadko, a wtedy obciążenia cieplne systemów grzewczych są największe.

Wymagania powierzchniowych instalacji grzewczych powodują, że temperatura wody pompowanej systemem odwadniania na powierzchnię jest zbyt niska i nie pozwala na jej bezpośrednie wykorzystanie nawet po przekazaniu do niej ciepła z agregatów chłodniczych. Dlatego też dla wykorzystania ciepła odpadowego w niej zawartego można rozważyć zastosowanie pomp ciepła typu woda/woda. W przypadku układów z pompami ciepła należy szczególnie mieć na uwadze wymagania temperatury górnego źródła ciepła, czyli zasilania sieci ciepłowniczych. Generalnie im niższa wymagana temperatura tym wyższa ich efektywność. W rozwiązaniach przemysłowych znane są jednak rozwiązania wysokotemperaturowych pomp ciepła, które pozwalają uzyskać temperatury powyżej 60°C (Wang i in. 2019). Z uwagi na możliwe zanieczyszczenia wody, a tym samym ochrony parowników pomp ciepła zaleca się stosować wymienniki pośredniczące w wymianie ciepła. Znane są rozwiązania odzysku ciepła z wody kopalnianej za pomocą pomp ciepła w kopalniach, między innymi w Tauron Wydobycie czy KGHM S.A. (Sas 2022). Na wypadek braku odbioru ciepła z systemu odwadniania za pomocą pomp ciepła należy przewidzieć konieczność ochłodzenia wody przed zrzutem do ścieku. Schemat ideowy rozwiązania pozyskiwania ciepła odpadowego z wody kopalnianej za pomocą pomp ciepła na powierzchni przedstawiono na rysunku 9.

Inną możliwością wykorzystania niskotemperaturowego ciepła odpadowego z wody kopalnianej jest zastosowanie układów ORC, w których źródła ciepła niskotemperaturowego są wykorzystywane są w celu wytworzenia energii elektrycznej, lub do wytwarzana zarówno energii elektrycznej, jak

i czynnika grzewczego (CHP) w procesach przemysłowych (Ryms 2011; Kajurek, Rusowicz 2017; Głodek-Bucyk 2021). Dysponując pełną i dokładną inwentaryzacją gospodarki energii w danej kopalni z uwzględnieniem zidentyfikowanych strat energetycznych, można rozważać lokalne wykorzystanie ORC do odzysku ciepła z wody kopalnianej.

Wykorzystanie ciepła odpadowego z podgrzanej wody systemu głównego odwadniania kopalni poprzedzone musi być analizą techniczno-ekonomiczna z uwzględnieniem możliwości finansowania inwestycji ze źródeł zewnętrznych.

7. Podsumowanie

Wykorzystanie wody kopalnianej w podziemnych urządzeniach chłodniczych małej mocy jest znane. Przedstawione rozwiązania pozwalają na większy zakres odprowadzania ciepła skraplania w układach klimatyzacji grupowej do wody kopalnianej. Korzystne warunki do wykorzystania wody dołowej w układzie klimatyzacji to:

- Lokalizacja urządzeń chłodniczych w sąsiedztwie wyrobisk głównego systemu odwadniania kopalni.
- Temperatura wody nie przekraczająca 32°C przy wydatku określonym odbiorem wymaganego strumienia ciepła skraplania z agregatów chłodniczych.
- Możliwość poboru wody w miejscu innym niż późniejszy jej zrzut w systemie głównego odwadniania kopalni, tak aby nie dochodziło do jej mieszania.
- Możliwość odzysku ciepła z ogrzanej wody kopalnej na powierzchni kopalni.

Oddanie ciepła skraplania z urządzeń chłodniczych do głównego odwadniania kopalni będzie prowadzić do podwyższenia temperatury wody odpompowywanej na powierzchnię. Bezpośredni zrzut wody do cieków powierzchniowych może być utrudniony z uwagi na jej zbyt wysoką temperaturę. Stwarza to jednak korzystne warunki dla zastosowania rozwiązań odzysku niskotemperaturowego ciepła odpadowego z wykorzystaniem wysokotemperaturowych pomp ciepła lub konwersji energii za pomocą układów ORC. Potencjał energetyczny ciepła odpadowego z wody dołowej pozwoliłby na pokrycie części potrzeb energetycznych zakładu na powierzchni.

Projekt badawczy finansowany ze środków programu „Inicjatywa Doskonałości – Uczelnia Badawcza" w AGH oraz subwencji nr 16.16.100.215

Literatura – References

1. Doležal L., Knechtel J., Taufer A., Trávníček L. 2013 – Primary Rock Temperature Fields in Czech and Polish Part of the Upper of the Upper Silesian Coal Basin. Archives of Mining Sciences, vol. 58, no. 1, s. 55–72
2. Głodek-Bucyk E. 2021 – Możliwość wykorzystania ciepła odpadowego w przemyśle mineralnym. Szkło i Ceramika, r. 72, nr 1, s. 25–27
3. Hemp R. 2014 – Sources of Heat in Mines, in Ventilation and Occupational Environment Engineering in Mines (third edition, chapter 32). Editor DU PLESSIS J. J. L., Mine Ventilation Society of South Africa: Johannesburg, s. 406–440
4. Kajurek J., Rusowicz A. 2017 – Zastosowanie organicznego obiegu Rankine'a (ORC) zasilanego niskotemperaturowymi źródłami ciepła do produkcji energii elektrycznej. Aparatura Badawcza i Dydaktyczna, t. 22, nr 3, s. 159–173
5. Kamyar A., Aminossadati S.M., Leonardi C., Sasmito A. 2019 – Current Developments and Challenges of Underground Mine Ventilation and Cooling Methods. Proceedings of the 2016 Coal Operators' Conference, Mining Engineering, University of Wollongong, Australia, 18–20 February 2019
6. Li Z., Xu Y.U., Li R., Jia M., Wang Q., Chen Y., Cai R., Han, Z. 2021 – Impact of the water evaporation on the heat and moisture transfer in a high-temperature underground roadway. Case Studies in Thermal Engineering, vol. 28, 101551
7. Maurya T., Kailash K., Vardhan H., Aruna M., Raj G.M. 2015 – Potential Sources of Heat in Underground Mines – A Review. Procedia Earth and Planetary Science, vol. 11, s. 463–468
8. McPherson M.J., 2012 – Subsurface ventilation and environmental engineering (Chapter 17). Springer Science & Business Media, New Delhi
9. Obracaj D., Szlązak N., Korzec M. 2022 – Using a mine dewatering system to increase cooling capacity and energy recovery of underground refrigeration plant: a case study. Energies, vol. 15, iss. 24, art. no. 9481, s. 1–15
10. Praca zbiorowa, 1975 – Poradnik Górnika, tom II. Wydawnictwo Górniczo-Hutnicze
11. Praca zespołowa pod kierunkiem prof. Nikodema Szlązaka, 2019 – Projekt klimatyzacji grupowej o mocy chłodniczej 6,0 MW dla Oddziału KWK Ruda Ruch Halemba (niepublikowana)
12. Rozporządzenie Ministra Gospodarki Morskiej i Żeglugi Śródlądowej z dnia 12 lipca 2019 r. w sprawie substancji szczególnie szkodliwych dla środowiska wodnego oraz warunków, jakie należy spełnić przy wprowadzaniu do wód lub do ziemi ścieków, a także przy odprowadzaniu wód opadowych lub roztopowych do wód lub do urządzeń wodnych (Dz.U. 2019 poz. 1311 wraz z późniejszymi zmianami)
13. Rozporządzenie Ministra Energii z dnia 23 listopada 2016 r. w sprawie szczegółowych wymagań dotyczących prowadzenia ruchu podziemnych zakładów górniczych (Dz.U. 2017, poz. 1118 wraz z późniejszymi zmianami)
14. Ryms M. 2011 – Konwersja średnio- i niskotemperaturowego ciepła odpadowego w energię elektryczną w instalacjach przemysłowych. Ropzrawa doktorska, Politechnika Gdańska
15. Sas S., 2022 – Ocena możliwości obniżenia zużycia energii pierwotnej w ogrzewaniu powietrza wlotowego do kopalni. Rozprawa doktorska, Akademia Górniczo-Hutnicza w Krakowie
16. Serwis Rzeczypospolitej Polskiej 2023 – Typowe lata meteorologiczne i statystyczne dane klimatyczne do obliczeń energetycznych budynków, dostęp on line (10.02.2023): https://www.gov.pl/web/archiwum-inwestycje-rozwoj/dane-do-obliczen-energetycznych-budynkow
17. Szlązak N., Obracaj D., Swolkień J. 2010a – Parametry wody i ich szkodliwy wpływ na instalacje klimatyzacyjne. Prace Naukowe GIG, Górnictwo i Środowisko, Główny Instytut Górnictwa, nr 1/1, s. 264–278
18. Szlązak N., Obracaj D., Borowski M. 2010b – Możliwości rozbudowy klimatyzacji grupowej w kopalni podziemnej. Wiadomości Górnicze, 61, nr 9, s. 536–543
19. Szlązak N., Obracaj D., Korzec M., Swolkień J. 2017 – Wspomaganie projektowania klimatyzacji z wykorzystaniem programu KlimaSystem. Aktualny stan zagrożeń aerologicznych w polskich kopalniach, pod red. Nikodema Szlązaka, Agencja Wydawniczo-Poligraficzna ART-TEKST, s. 119–138, ISBN: 978-83-7783-176-2
20. Szlązak N., Obracaj D., Swolkień J. 2018a – Ocena i możliwości poprawy stanu zagrożenia klimatycznego w polskich kopalniach podziemnych. Agencja Wydawniczo-Poligraficzna ART-TEKST, ISBN: 978-83-7783-198-4
21. Szlązak N., Obracaj D., Korzec M., Swolkień J. 2018b – Projektowanie systemów klimatyzacji kopalń przy zastosowaniu programu KlimaSystem. Systemy Wspomagania w Inżynierii Produkcji, vol. 7, iss. 1, s. 377–393
22. Szlązak N., Swolkień J. 2019a – Możliwości wykorzystania wody dołowej do odprowadzenia ciepła odebranego od powietrza kopalnianego. Wybrane zagrożenia aerologiczne w polskich kopalniach, pod red. nauk. Wacława Dziurzyńskiego, 10. Szkoła Aerologii Górniczej, 16–19 września 2019, Stryszawa, s. 95–104, ISBN: 978-83-953913-2-3

23. Szlązak N., Obracaj D., Swolkień J. 2019b – Systemy klimatyzacji wyrobisk górniczych w polskich kopalniach. Przegląd Górniczy, t. 75, nr 11, s. 23–33
24. Szlązak N., Obracaj D., Swolkień J. 2021 – Termoizolacja a warunki klimatyczne w wyrobiskach kopalń podziemnych. Pod red. Nikodema Szlązaka, Wydawnictwa AGH, ISBN: 978-83-66727-12-0
25. Ustawa z dnia 20 lipca 2017 r. Prawo wodne
26. Wang R.Z., Xu Z.Y., Hu B., Du S., Pan Q.W., Jiang L., Wang L.W. 2019 – Heat Pumps for Efficient Low Grade Heat Uses: From Concept to Application. Thermal Science and Engineering, 27, no.1, s. 1–15

Using Underground Water for Condensation Heat Rejection and Recovery in Underground Refrigeration Plants of Mines

Using various air cooling systems in underground mines results from harsh climatic conditions at workplaces. Underground refrigeration plants with compressor chillers are widely used in air cooling systems. The efficient operation of refrigeration units depends on the proper condensation heat rejection. Cooling capacity and localization of a refrigeration plant have the most significant influence on deciding of rejecting condensation heat to air or water. The limitation of the heat rejection capacity of return air streams in a typical mine and conditions facilitative to using underground water from an underground mine dewatering system is presented. Determinants and opportunities for heat recovery from water discharged to the surface are also discussed.

Keywords: *harsh climate conditions, mine cooling systems, mine refrigerant plant, condensation heat, waste heat recovery*

Analiza zużycia energii pierwotnej na świecie w kontekście przemian energetycznych

Robert RANOSZ[1)], Joanna JAKÓBCZYK[2)], Klaudia PALMOWSKA[1)]

[1)] AGH University in Krakow, Faculty of Civil Engineering and Resource Management, Krakow, Poland; email: rranosz@agh.edu.pl, ORCID: 0000-0001-7478-9129

2) AGH University in Krakow, Faculty of Civil Engineering and Resource Management, Krakow, Poland; ORCID: 0000-0001-5030-9637

3) AGH University in Krakow, Faculty of Civil Engineering and Resource Management, Krakow, Poland

http://doi.org/10.29227/IM-2023-01-29

Submission date: 12-05-2023 | Review date: 06-06-2023

Abstrakt

Celem niniejszego artykułu jest zbadanie konsumpcji energii w podziale na konsumpcję bazującą na źródłach nieodnawialnych, takich jak: węgiel, ropa naftowa, gaz ziemny i energia nuklearna, oraz konsumpcję bazującą na odnawialnych źródłach energii, takich jak: energia słoneczna, wiatrowa, wodna, geotermalna i z biomasy. Przeprowadzone badania wykazały, że zużycie energii pierwotnej stale rośnie, podczas gdy rozwój energetyki odnawialnej wciąż nie nadąża za tempem tego wzrostu (mimo, iż z roku na rok jej udział w całkowitym mikście energetycznym rośnie). Przyczyną tej sytuacji jest w głównej mierze fakt, iż w wielu krajach gospodarka nadal oparta jest na konwencjonalnych źródłach energii, a w niektórych z nich konsumpcja energii pierwotnej ulega wręcz znacznemu wzrostowi (jak ma to miejsce np. w Chinach). Z tego też powodu, sensownym wydaje się być podejmowanie różnego rodzaju przedsięwzięć zmierzających w kierunku obniżenia przez poszczególne kraje zużycia energii pierwotnej, co jak wykazał rok 2019, jest jak najbardziej możliwe.

Słowa kluczowe: *energia, energia pierwotna, źródła energii konsumpcja energii, PKB*

1. Wstęp

Wytwarzanie oraz konsumpcja energii należą do podstawowych procesów zachodzących na Ziemi. To właśnie energia stanowi jedną z najważniejszych materialnych potrzeb ludzkości, zaraz obok żywności i tlenu, a także zapewnia nieustanny rozwój świata. Użytkowanie energii przez człowieka umożliwiło szeroki postęp cywilizacyjny, kulturowy oraz gospodarczy [1, 2].

Światowa Rada Energetyczna klasyfikuje zasoby energetyczne na dwie kategorie [1]:

- źródła nieodnawialne (węgiel kamienny, węgiel brunatny, ropa naftowa, gaz ziemny),
- źródła odnawialne (energia wodna, energia słoneczna, energia wiatrowa, energia geotermalna i biomasa, drewno).

Źródła nieodnawialne można określić jako zasoby (resources) lub rezerwy (reserves). Zasoby to całkowita możliwa do eksploatacji ilość surowca energetycznego. Natomiast rezerwy to część zasobów, którą nadająca się do wydobycia przy aktualnych możliwościach technologicznych oraz ekonomicznych [1, 3].

Człowiek wykorzystywał energię już od czasów starożytnych, pozyskując ciepło ze spalania drewna czy też suchych roślin. Wtedy energia służyła głównie do ogrzania się oraz do podgrzewania posiłków. Dodatkowo za pomocą łuczywa lub pochodni wytwarzano energię świetlą. Pojawiły się także pierwsze metody odciążenia pracy ludzkich mięśni poprzez wykorzystanie pracy zwierząt. Około 3 tys. lat p.n.e. ludzkość nauczyła się pozyskiwać energię z wiatru, służącą do napędzania statków, a pod koniec epoki energię wodną stosowaną przy kołach wodnych [2, 3, 4].

Szczególnie istotne zmiany w energetyce miały miejsce w czasach nowożytnych, gdy w XVIII wieku wynaleziono maszynę parową. Wynalazek ten okazał się przełomem dla przemysłu na całym świecie, a także wpłynął na szybszy rozwój społeczeństwa oraz poprawę jakości życia. Praca parowozu zastąpiła czynności niegdyś wykonywane ręcznie, co przyczyniło się do zwiększenia efektywności procesu oraz skrócenia czasu jego trwania. Do napędzania maszyny parowej wykorzystywano węgiel, który w wieku XIX stanowił główne źródło energii [2, 3, 4].

W energetyce XIX i XX można wyszczególnić 3 kamienie milowe mające wpływ na rozwój sektora paliwowego. Pierwszym z nich było wynalezienie silnika spalinowego, następnie wykorzystanie ropy naftowej na skalę globalną oraz zwiększone wydobycie gazu ziemnego. Gwałtowny wzrost zużycia energii nastąpił po zakończeniu II wojny światowej, spowodowany był rozwojem motoryzacji, lotnictwa oraz potrzebą odbudowy globalnej gospodarki. Zaczęto odchodzić od węgla, jako głównego surowca energetycznego i zastępować go ropą oraz gazem. Funkcjonująca wtedy gospodarka przybrała model, który był uzależniony od tzw. czarnego złota [1, 5].

Zużycie energii dynamicznie rosło, ze względu na zwiększającą się liczbę ludności oraz szybki wzrost gospodarczy świata. Niestety takie działanie miało negatywny wpływ na środowisko, zmiany klimatyczne, a także na eskalację skutków globalnego ocieplenia. To jak ważna stała się energia dla gospodarki okazało się w latach siedemdziesiątych XX wieku, kiedy doszło do pierwszego kryzysu energetycznego. Został on wywołany zwiększonym embargiem krajów wschodnich na dostawy ropy do państw zachodu. Doprowadziło to do znacznych podwyżek cen czarnego złota na rynku światowym. Już początku lat osiemdziesiątych nastąpił drugi kryzys energetyczny. Wysokie ceny ropy oraz nieregularne dostawy osłabiły globalną gospodarkę i przemysł wytwórczy, a także dalszy rozwój społeczny świata. Zrozumiano wtedy, że ilość surowców w skorupie ziemskiej jest ograniczona, a rozsądne

gospodarowanie zasobami jest podstawą dalszego rozwoju. Zaczęto w większej mierze wykorzystywać gaz ziemny, węgiel i energię jądrową. Istotną rolę zaczęły również odgrywać odnawialne źródła energii (OZE), ponieważ świat, a głównie Europa podjęła kroki ograniczające negatywny wpływ sektora energetycznego na środowisko naturalne [1].

Światowa Rada Energetyczna (WEC) została utworzona w 1923 roku przez Daniel Dunlop'a. Jest to bezstronna, pozarządowa oraz niekomercyjna organizacja z siedzibą w Londynie, która zjednoczyła już ponad 3000 członków z prawie 100 krajów. Główną misją Rady jest: „Promowanie zrównoważonych dostaw i wykorzystywania energii z największą korzyścią dla ludzi" [6]. Rada prowadzi swoje działania zgodnie z przyjętą przez siebie definicją zrównoważonej energii, która opiera się na trzech podstawowych filarach [7]:

- Bezpieczeństwo energetyczne,
- Równość energetyczna,
- Zrównoważenie środowiskowe systemów energetycznych.

Rada odpowiedzialna jest także za organizowanie Światowych Kongresów Energetycznych, które są najważniejszymi spotkaniami w tym sektorze na świecie [7]. Do tej pory Kongres odbył się 24 razy, w tym ostatni miał miejsce w roku 2019 w Abu Dhabi. Na tych wydarzeniach przedstawiane są najnowsze wyzwania dla energetyki, ale i nowe technologie, które umożliwiają dalszy rozwój sektora [8].

Dodatkowo Rada co rok publikuje ranking World Energy Trilemma Index, który ocenia wydajność energetyczną państw i pomaga dostosować systemy energetyczne do aktualnej sytuacji politycznej. Wyniki Indeksu publikowane są w odniesieniu do bezpieczeństwa i równości energetycznej oraz zrównoważenia środowiskowego. Ranking przedstawia wyzwania danego kraju w równoważeniu Trilemma Energetycznego oraz prezentuje możliwości poprawy w osiąganiu aktualnych i przyszłych celów energetycznych. Indeks dostarcza także niezbędne informacje dla decydentów oraz liderów sektora energetycznego, finansowego i inwestycyjnego. W latach 2020 i 2021 państwami, które znalazły się w czołówce rankingu była: Szwecja, Szwajcaria oraz Dania. Natomiast kraje, które od roku 2000 odnotowały największy postęp energetyczny to: Kambodża, Birma i Republika Dominikany [9, 10].

Jeszcze przed pandemią światowi eksperci dyskutowali na temat nowej ery energetyki na świecie. W roku 2020 opublikowano pierwszy Indeks od czasu epidemii Covid-19 [7]. Został tam zaprezentowany kierunek sektora energetyki, w którym systemy energetyczne będą zorientowane na klienta, a nie na podaż jak w latach ubiegłych.

Przedstawiono także nowy model Energetyki 4D składający się z 4 głównych trendów dla tego sektora [7]:

- Dekarbonizacja (decarbonisation),
- Decentralizacja (decentralisation),
- Cyfryzacja (digitalisation),
- Zakłócenia (Distruption-as-usual).

Dekarbonizacja jest to proces systematycznego ograniczania emisji gazów cieplarnianych do atmosfery, dążący do całkowitego zaprzestania wydziałania dwutlenku węgla. Dekarbonizacja odpowiada za zredukowanie ilości wydzielanych gazów na rzecz ochrony środowiska i przeciwdziałaniu globalnemu ociepleniu. Jest to szereg działań zmieniających zachowania społeczne oraz gospodarcze, poprzez wykorzystywanie nowych technologii i bezemisyjnych źródeł energii. Plan działania globalnego sektora energii zakłada zerową emisję netto do 2050 roku [11, 12].

Proces decentralizacji opiera się na wytwarzaniu energii z lokalnych źródeł. W tym modelu dużą rolę odgrywają konsumenci, którzy powinni stosować zamknięty obieg gospodarki. Dodatkowo powinni oni inwestować w niewielkie źródła produkujące energie na własny użytek, rezygnując z importu energii w dużych ilościach [13].

Postęp technologiczny i szeroko rozumiana cyfryzacja nie ominęła również sektora energetycznego na świecie. Zastosowanie nowoczesnych rozwiązań pozwoli zwiększyć wydajność i niezawodność istniejących systemów energetycznych oraz sprawi, że będą one inteligentne i zrównoważone. Istotną kwestią cyfryzacji jest bezpieczeństwo cybernetyczne, które jest niezbędnym elementem przy rozwoju rozwiązań cyfrowych. Może również pomóc w zintegrowaniu rosnącego udziału energii odnawialnej poprzez dostarczanie elastycznych systemów elektroenergetycznych, które zapewniają rozwiązania po stronie popytu i magazynowanie energii, w tym dla sektorów, które są trudne do dekarbonizacji [14].

Światowa Rada Energetyczna ułatwiała wymianę wpływów, działań i prognoz przez cały czas dla swojej światowej społeczności, aby wydobyć nowe lekcje z pandemii w odniesieniu do energii. Rada opracowała także nową wizję sektora energetycznego 2025 opierającego się na humanizacji energii. World Energy Trilemma ma zapewnić nowe narzędzia, które zostaną wykorzystane do poprawy jakości projektowania polityki społecznej oraz globalnej energii [7, 9].

Już od wieków można zauważyć głębokie zmiany występujące w tym sektorze. W dzisiejszych czasach dotyczą one głównie odchodzenia od konwencjonalnych źródeł energii na rzecz energetyki odnawialnej. Taką tendencję w szczególności można zaobserwować w Europie. Dodatkowo energetyka centralnie planowana zastępowana jest rozproszonymi źródłami energii [15]. W artykule tym autorzy starają się odpowiedzieć między innymi na pytanie, czy podejmowane działania są wystarczające w kontekście ciągle rosnącego zapotrzebowania na energię pierwotną.

2. Metodologia – źródła danych

Analiza sektora energetycznego została oparta na danych zawartych w dokumencie Statistical Review of World Energy 2021 BP [16] Obejmowała ona dane za lata 2000–2021 dla dziewięciu podstawowych źródeł energii: energii pierwotnej, ropy, gazu ziemnego, węgla, energii nuklearnej, energii wodnej, energii słonecznej, energii wiatrowej, energii geotermalnej oraz z biomasy.

W ramach artykułu autorzy wsparli się również danymi pochodzącymi z World Bank Open Data [17] – w tym przypadku wykorzystano dane dotyczące wielkości Produktów Krajowych Brutto poszczególnych krajów świata. Analiza w głównej mierze oparta jest o badania ilościowe.

3. Analiza konsumpcji energii pierwotnej

Do funkcjonowania oraz rozwoju gospodarek świata, jak i gospodarstw domowych niezbędna jest energia. Analizując jej zużycie w XXI wieku z łatwością można zauważyć, iż z roku na rok jej zużycie rośnie. Na początku tego stulecia konsumpcja energii pierwotnej wyniosła 396,43 EJ (w przeliczeniu na

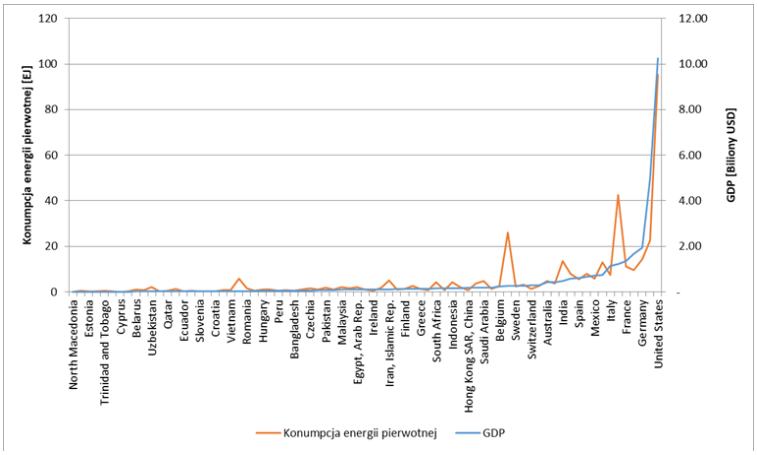

Rys. 1. Zależność pomiędzy PKB a konsumpcją energii pierwotnej dla roku 2000. Opracowanie własne na podstawie [16,17]
Fig. 1. Relationship between GDP and primary energy consumption for the year 2000. Own elaboration based on [16, 17]

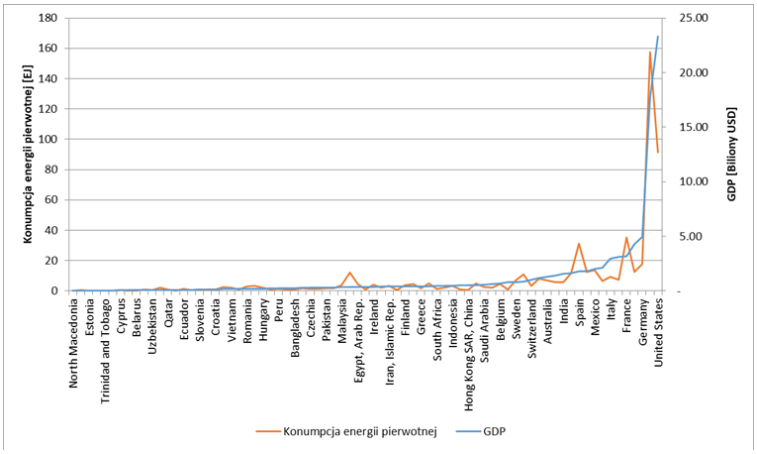

Rys. 2. Zależność pomiędzy PKB a konsumpcją energii pierwotnej dla roku 2021. Opracowanie własne na podstawie [16,17]
Fig. 2. Relationship between GDP and primary energy consumption for 2021. Own elaboration based on [16,17]

jedną osobę 64,69 EJ), a w roku 2021 całkowita konsumpcja wynosiła już 591,05 EJ (w przeliczeniu na jedną osobę 96,14 EJ). Tak więc w analizowanym okresie całkowita konsumpcja oraz w przeliczeniu na jedną osobę wzrosła o 49%.

W roku 2000 największy udział w konsumpcji energii miały takie kontynenty jak: Ameryka Północna (28,9%), Azja i Pacyfik (28,5%) oraz Europa (22,2%), zaś najmniejsze Afryka (2,9%). W ramach Ameryki Północnej największa konsumpcja wystąpiła w Stanach Zjednoczonych (24,1% całkowitej światowej konsumpcji), w Azji i Pacyfiku Chiny (10,7% całkowitej konsumpcji światowej), a w Europie liderem pod tym względem były Niemcy (3,6% całkowitej konsumpcji światowej).

Niemniej jednak, jeżeli analizie poddamy te same dane w przeliczeniu na jedną osobę, wówczas klasyfikacja ta będzie się przedstawiała inaczej. Liderem w tej klasyfikacji jest Ameryka Północna ze zużyciem energii pierwotnej na jedną osobę w wysokości 277,9 GJ/osobę, a krajem liderującym w tej części świata pod tym kątem jest Kanada (427,74 GJ/osobę), kontynentem na drugim miejscu w roku 2000 pod kątem zużycia energii pierwotnej na jedną osobę było total CIS ze zużyciem 140,75 GJ/osobę, a liderem była Rosja (177,47 GJ/osobę). Europa pod tym względem nie dużo ustępowała z zużyciem na poziomie 139,04 GJ/osobę, zaś liderem była Norwegia (465,02 GJ/osobę) oraz Islandia (426,57 GJ/osobę). Azja Pacyficzna w okresie tym zużywała jedynie 32,52 GJ/osobę, a liderem była Australia ze zużyciem 246,56 GJ/osobę. Liderem pod kątem zużycia energii pierwotnej na jedną osobę w roku 2000 był Katar (815,43 GJ/osobę), zaś regionem, który najmniej zużywał energii pierwotnej w przeliczeniu na mieszkańca była środkowa Afryka (3,55 GJ/osobę)

W roku 2021 również wcześniej wymienione kontynenty były liderami pod kątem zużycia energii, niemniej jednak ich udziały uległy znacznym zmianom i tak na pierwszym miejscu uplasowała się Azja pacyficzna (46% całkowitego zużycia energii pierwotnej), drugie miejsce to Ameryka Północna (19%), a na trzecim miejscu znalazła się Europa (13,8%). W ramach Azji Pacyficznej liderem były Chiny (26,7% całkowitego zużycia energii pierwotnej), Stany Zjednoczone (15,5%) były liderem w Ameryce Północnej, a w Europie pod tym kątem wyróżniały się Niemcy (2,1%).

Biorąc pod uwagę zużycie energii pierwotnej na jedna osobę, podobnie jak to miało miejsce w roku 2000, tak też w roku 2021 sytuacja wygląda inaczej. Nadal liderem wśród kontynentów pozostała Ameryka Północna ze zużyciem 223,85 GJ/osobę, a Kanada liderem w ramach kontynentu (362,11 GJ/osobę) – w tym przypadku zarówno Stany Zjednoczone, jak i Kanada w tym okresie zmniejszyły zużycie energii na jedną osobę. Meksyk utrzymuje zużycie na podobnym poziomie w analizowanym okresie (między 50 a 60 GJ/

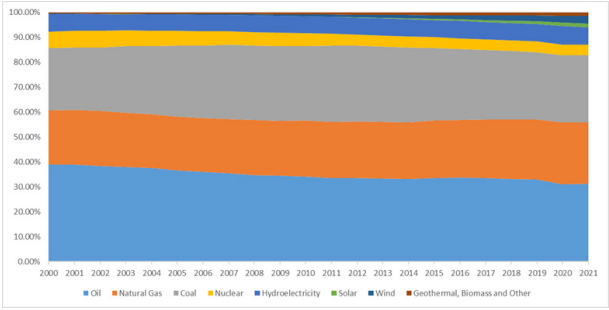

Rys. 3. Procentowy udział poszczególnych źródeł energii w całkowitej konsumpcji energii pierwotnej. Opracowanie własne na podstawie [16]

Fig. 3. Percentage share of individual energy sources in total primary energy consumption. Own elaboration based on [16]

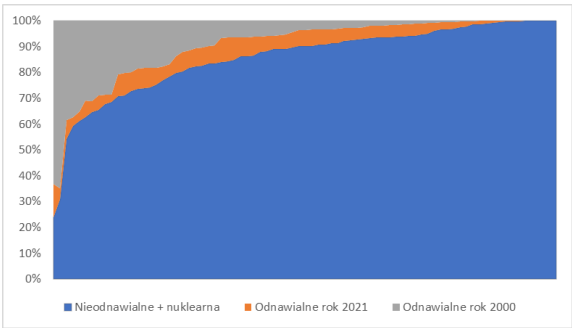

Rys. 4. Udział energii odnawialnej oraz nieodnawialnej (wraz z energią nuklearną) w całkowitym zużyciu energii pierwotnej dla roku 2000 oraz 2021. Opracowanie własne na podstawie [16]

Fig. 4. Share of renewable and non-renewable energy (including nuclear energy) in total primary energy consumption for 2000 and 2021. Own study based on [16]

osobę). Na drugim miejscu podobnie jak w roku 2000 znalazły się kraje CIS, niemniej jednak w odróżnieniu od Ameryki Północnej zużycie energii pierwotnej na jedną osobę wzrosło i wyniosło 162,96 GJ/osobę, a liderem pozostała Rosja (214,46 GJ/osobę). W odróżnieniu od roku 2000 w roku 2021 na trzecim miejscu uplasował się Środkowy Wschód ze zużyciem energii pierwotnej 143,01 GJ/osobę, a liderem w tym regionie oraz na całym świecie jest Katar (686,21 GJ/osobę). W roku 2021 regionem, który zużywał najmniej energii pierwotnej na jedną osobę była Eastern Africca (4,67 GJ/osobę).

W miejscu tym należy nadmienić, iż rok 2019 w skali całego świata był rokiem wyjątkowym ze względu na pojawienie się pandemii Covid-19, a co za tym idzie, wprowadzenie nowych dla obecnie funkcjonujących w społeczeństwie rozwiązań – np. takich jak powszechna praca zdalna – jak wykazują dane, w roku tym można było zaobserwować znaczący spadek konsumpcji energii pierwotnej.

W badaniu zużycia energii pierwotnej postanowiono również nałożyć na nią wielkość wytworzonego produktu krajowego brutto (PKB) przez poszczególne kraje. Wielkości zużycia energii pierwotnej oraz PKB dla poszczególnych krajów zostały zaprezentowane na rysunku 1 (rok 2000) oraz na rysunku 2 (rok 2021).

Jak wynika z powyższych rysunków, istnieje bardzo duża zależność pomiędzy PKB a zużyciem energii pierwotnej (w jednym i drugim przypadku korelacja to 90%). Zatem zużycie energii pierwotnej wpływa na rozwój gospodarczy danych krajów, tak więc aby dany kraj czy też region mogły się rozwijać, muszą konsumować coraz to większe ilości energii pierwotnej.

W tym miejscu należy jednak zwrócić uwagę na źródła, z których korzysta się, aby osiągnąć wzrost gospodarczy na wysokim poziomie. Na rysunku 3 zaprezentowano jak to wygląda dla całego świata.

Jak wynika z rysunku 3 świat w ponad 80% konsumuje energię nieodnawialną (pochodzącą z: ropy naftowej, węgla oraz gazu ziemnego). W roku 2000 udział tych trzech paliw w ogólnej konsumpcji energii pierwotnej to 85,64%, natomiast w roku 2021 udział ten uległ niewielkiemu spadkowi i wyniósł 82,85%. W przypadku odnawialnych źródeł energii, do których zaliczono: energię wiatrową, słoneczną, wodną, geotermalna i biomasę, udział w całości konsumpcji energii pierwotnej w roku 2000 to 7,71%, natomiast w roku 2021 udział ten wzrósł do 12,87 %. Najbardziej dynamiczny wzrost udziału odnotowano w przypadku energii wiatrowej oraz słonecznej. Niemniej jednak rozpatrując tylko te dwa źródła energii, to ich udział w całości konsumpcji energii pierwotnej nadal jest na bardzo niskim poziomie i w roku 2021 wyniósł on 4,61%.

W miejscu tym warto zwrócić uwagę na wykorzystanie poszczególnych źródeł energii w poszczególnych regionach oraz krajach. Na rysunku 4 przedstawiono wykorzystanie źródeł odnawialnych oraz nieodnawialnych (poszerzonych o energię nuklearną) w roku 2000 oraz 2021.

Jak wynika z powyższego rysunku, na przestrzeni ostatnich 21 lat nastąpiła niewielka poprawa, jeżeli chodzi o wykorzystanie źródeł odnawialnych w całości konsumpcji energii pierwotnej. Krajami liderującymi w tej klasyfikacji jest Islandia oraz Norwegia – w krajach tych wykorzystanie energii odnawialnej to odpowiednio 87% i 72%.Należy jednak podkreślić, iż zdecydowana większość to energia wodna oraz z geotermii i biomasy, wykorzystanie energii wiatrowej i słonecznej w tych krajach to odpowiednio 0% i 6%. Poza tymi dwoma krajami reszta z analizowanych państw wykorzystuje energię nieodnawialną

Tab. 1. Udział w konsumpcji energii pierwotnej dla krajów, które stanowią ponad 80% konsumpcji całego świata. Opracowanie własne na podstawie [16]
Tab. 1. Share in primary energy consumption for countries that account for over 80% of the world's consumption. Own elaboration based on [16]

Kraj	Rok 2000			Rok 2021			
	Nieodnawialne*	Odnawialne	Słońce i wiatr	Nieodnawialne*	Odnawialne	Słońce i wiatr	Udział % w konsupcji
China	94.3%	5.7%	0.0%	85.1%	14.9%	5.9%	26.7%
US	96.1%	3.9%	0.1%	90.8%	9.2%	5.7%	15.5%
India	93.6%	6.4%	0.1%	90.9%	9.1%	3.6%	6.0%
Russian Federation	93.3%	6.7%	0.0%	93.4%	6.6%	0.1%	5.3%
Japan	95.2%	4.8%	0.0%	88.6%	11.4%	5.0%	3.0%
Canada	70.3%	29.7%	0.0%	70.6%	29.4%	2.7%	2.3%
South Korea	99.5%	0.5%	0.0%	96.5%	3.5%	1.9%	2.1%
Germany	97.2%	2.8%	0.7%	81.3%	18.7%	12.5%	2.1%
Iran	99.2%	0.8%	0.0%	98.7%	1.3%	0.1%	2.1%
Brazil	58.4%	41.6%	0.0%	58.0%	42.0%	7.2%	2.0%
Saudi Arabia	100.0%	0.0%	0.0%	99.9%	0.1%	0.1%	1.8%
France	93.4%	6.6%	0.0%	87.5%	12.5%	5.2%	1.6%
Indonesia	96.3%	3.7%	0.0%	93.1%	6.9%	0.1%	1.4%
United Kingdom	98.9%	1.1%	0.1%	82.7%	17.3%	10.2%	1.2%
Turkey	89.3%	10.7%	0.0%	83.5%	16.5%	6.1%	1.2%
Mexico	92.9%	7.1%	0.0%	89.6%	10.4%	4.6%	1.1%
Italy	92.8%	7.2%	0.1%	82.3%	17.7%	6.8%	1.1%
Australia	96.0%	4.0%	0.0%	87.1%	12.9%	9.6%	1.0%
Spain	93.0%	7.0%	0.9%	78.4%	21.6%	15.2%	0.9%
Thailand	97.4%	2.6%	0.0%	94.5%	5.5%	1.7%	0.8%
Taiwan	98.4%	1.6%	0.0%	97.0%	3.0%	1.9%	0.8%
South Africa	99.6%	0.4%	0.0%	96.6%	3.4%	3.0%	0.8%
Argentina	87.7%	12.3%	0.0%	89.7%	10.3%	4.2%	0.6%
Średnia ważona	**93.5%**	**6.5%**	**0.1%**	**87.6%**	**12.4%**	**5.0%**	

*wraz z energią nuklearną

Tab. 2. Konsumpcja energii pierwotnej dla krajów, które stanowią ponad 80% konsumpcji całego świata. Opracowanie własne na podstawie [16]
Tab. 2. Primary energy consumption for countries that account for over 80% of the world's consumption. Own elaboration based on [16]

Kraj	Rok 2000			Rok 2021			
	Nieodnawialne*	Odnawialne	Słońce i wiatr	Nieodnawialne*	Odnawialne	Słońce i wiatr	Udział % w konsupcji
China	40.1	2.4	0.0	134.1	23.5	9.3	26.7%
US	91.7	3.7	0.1	83.1	8.4	5.2	15.5%
India	12.6	0.9	0.0	32.1	3.2	1.3	6.0%
Russian Federation	24.2	1.7	0.0	29.2	2.1	0.0	5.3%
Japan	21.4	1.1	0.0	15.7	2.0	0.9	3.0%
Canada	9.2	3.9	0.0	9.8	4.1	0.4	2.3%
South Korea	8.0	0.0	0.0	12.1	0.4	0.2	2.1%
Germany	13.9	0.4	0.1	10.2	2.3	1.6	2.1%
Iran	5.0	0.0	0.0	12.0	0.2	0.0	2.1%
Brazil	4.7	3.3	0.0	6.8	4.9	0.8	2.0%
Saudi Arabia	4.8	0.0	0.0	10.8	0.0	0.0	1.8%
France	10.4	0.7	0.0	8.1	1.2	0.5	1.6%
Indonesia	4.0	0.2	0.0	7.4	0.6	0.0	1.4%
United Kingdom	9.5	0.1	0.0	5.9	1.2	0.7	1.2%
Turkey	2.8	0.3	0.0	5.7	1.1	0.4	1.2%
Mexico	5.5	0.4	0.0	6.1	0.7	0.3	1.1%
Italy	7.0	0.5	0.0	5.2	1.1	0.4	1.1%
Australia	4.5	0.2	0.0	5.0	0.7	0.5	1.0%
Spain	5.1	0.4	0.1	4.3	1.2	0.8	0.9%
Thailand	2.6	0.1	0.0	4.7	0.3	0.1	0.8%
Taiwan	3.6	0.1	0.0	4.8	0.2	0.1	0.8%
South Africa	4.3	0.0	0.0	4.8	0.2	0.2	0.8%
Argentina	2.2	0.3	0.0	3.0	0.4	0.1	0.6%
Suma	297.2	20.9	0.3	421.0	59.9	23.9	0.8

*wraz z energią nuklearną

w 50% i powyżej. Należy również zwrócić uwagę na taki kraj jak Dania, który na przestrzeni analizowanego okresu znacząco zwiększył udział energii pochodzącej ze słońca oraz wiatru i w tym przypadku wartość ta wynosi 25%.

W przypadku krajów, które zużywają największą ilość energii pierwotnej udział procentowy w roku 2021 kształtuje się następująco: Stany Zjednoczone w roku 2021 bazują w 91% na energii nieodnawialnej oraz nuklearnej, Chiny w 85% korzystają ze źródeł nieodnawialnych oraz energii nuklearnej, Niemcy w 81% a Rosja w 93% używa energii nieodnawialnej wraz z energią jądrową. W tabeli 1 zestawiono 23 kraje, które konsumują energię pierwotną w ponad 80% całości.

Jak wynika z tabeli powyżej, wszystkie kraje obniżyły swój udział nieodnawialnych źródeł energii, jednak nie były to spadki znaczące i w roku 2021 nadal ponad 80% energii pozyskiwano z nieodnawialnych źródeł energii. Na wyróżnienie zasługują takie państwa jak Niemcy, Wielka Brytania oraz Hiszpania, których udział energii pozyskiwany z wiatru oraz słońca przekracza 10% w całości zużycia energii pierwotnej. Można na ten problem spojrzeć jednak jeszcze z innej strony – czy jeżeli obniżony został udział źródeł nieodnawialnych to znaczy, że mniej produkujemy energii z tych źródeł? Odpowiedzią na to pytanie jest zestawienie tych samych krajów, jednak nie z udziałem procentowym, a konsumpcją z poszczególnych źródeł w ujęciu nominalnym (taela 2).

Jak wynika z tabeli 2, tylko 7 państw obniżyło konsumpcję z nieodnawialnych źródeł energii i są to: Stany Zjednoczone, Japonia, Niemcy, Francja, Wielka Brytania, Włochy oraz Hiszpania – łącznie obniżono konsumpcję z nieodnawialnych źródeł energii o 26,61 EJ – nie jest to wartość imponująca,

szczególnie biorąc pod uwagę, iż same Chiny w tym czasie zwiększyły konsumpcję z nieodnawialnych źródeł energii o 94,01 EJ, czyli o tyle ile z tych źródeł w roku 2021 konsumują łącznie takie kraje jak: Iran, Brazylia, Arabia Saudyjska, Francja, Indonezja, Wielka Brytania, Turcja, Meksyk, Włochy, Australia, Hiszpania, Tajlandia, Taiwan, Afryka południowa oraz Argentyna.

Podsumowanie

Mimo, iż udział odnawialnych źródeł energii w ogólnym mikście energetycznym rośnie z roku na rok, to i tak zwiększone zapotrzebowanie na energie pierwotną powoduje, iż globalnie zwiększamy konsumpcję z nieodnawialnych źródeł energii. W analizowanym okresie produkcja z nieodnawialnych źródeł energii dla 23 państw, które stanowią ponad 80% konsumpcji energii pierwotnej na całym świecie wzrosła o ponad 123 EJ czyli na przestrzeni 21 lat jest to wzrost o 42% – sytuacja ta pokazuje, iż jeżeli chcemy obniżyć zużycie tych źródeł energii to tempo wzrostu energetyki odnawialnej musi rosnąc w znacznie wyższym tempie. Ewentualnie muszą zostać wprowadzone skuteczne rozwiązania powodujące obniżenie konsumpcji energii pierwotnej – w szczególności z uwagi na fakt, iż pandemia COVID-19 (rok 2019) wykazała, iż możliwym jest obniżenie zużycia energii w skali globalnej przez poszczególne kraje. Jak wykazano w artykule wzrost zużycia energii pierwotnej nie jest związany tylko i wyłączenie z faktem, iż na ziemi jest coraz więcej ludzi, ale z faktem, iż ludzie zużywają coraz więcej energii.

Literatura – References

1. Soliński J., Kluczowe elementy rozwoju światowego i polskiego sektora energii. Zakład Wydawniczy Energetyka 2004
2. Kopecki K.: Człowiek w świecie energii. Książka i Wiedza, Warszawa 1979
3. Soliński J., Gawlik L.: Rys historyczny, rozwój i stan obecny światowego i polskiego sektora energii. Zakład Wydawniczy Energetyka, Katowice 2012, s. 142-149
4. Mejro C.: Podstawy gospodarki energetycznej. Wydawnictwo Naukowo–Techniczne, Warszawa 1980.
5. World Energy Supplies 1954-1974. UN, New York 1976
6. World Energy Council https://www.worldenergy.org/about-us
7. World Energy Trilemma Index 2020, World Energy Council, Londyn 2020
8. Światowa Rada Energetyczna https://en.wikipedia.org/wiki/World_Energy_Council
9. World Energy Trilemma Index 2021, World Energy Council, Londyn 2021
10. World Energy Trilemma Index https://www.worldenergy.org/transition-toolkit/world-energy-trilemma-index
11. Dekarbonizacja https://mfiles.pl/pl/index.php/Dekarbonizacja
12. International Energy Agency: Zerowe emisje netto do 2050 r. Plan działania dla globalnego sektora energii. IEA Publications, Francja 2022
13. Strategie energetyczne https://wysokienapiecie.pl/24254-nagle-rozmnozenie-rzadowych-strategii-energetycznych-czy-ilosc-przejdzie-w-jakosc/
14. Cyfryzacja energetyki https://energy.ec.europa.eu/topics/energy-systems-integration/digitalisation-energy-sector_en
15. Olkuski T., Stala-Szlugaj K.: Tendencje zmian występujące w światowej energetyce. Zeszyty naukowe Instytutu Gospodarki Surowcami Mineralnymi i Energią Polskiej Akademii Nauk nr. 98, Kraków 2017
16. Statistical Review of World Energy – BP https://www.bp.com/en/global/corporate/energy-economics/statistical-review-of-world-energy.html
17. World Bank Data https://www.data.worldbank.org

Analysis of Primary Energy Consumption in the World in the Context of Energy Transformations

The purpose of this article is to examine energy consumption broken down into consumption based on non-renewable sources, such as: coal, oil, natural gas and nuclear energy, and consumption based on renewable energy sources, such as: solar, wind, hydro, geothermal and biomass. The conducted research has shown that the consumption of primary energy is constantly growing, while the development of renewable energy still lags behind the pace of this growth (although its share in the total energy mix is growing year by year). The reason for this situation is mainly the fact that in many countries the economy is still based on conventional energy sources, and in some of them the consumption of primary energy is even significantly increasing (as is the case, for example, in China). For this reason, it seems reasonable to undertake various types of projects aimed at reducing the consumption of primary energy by individual countries, which, as 2019 showed, is absolutely possible.

Keywords: *energy, primary energy, energy sources, energy consumption, GDP*

Occupational Risk Management Method for Quarry Blasting Operations Based on Modified FMECA Algorithm

Michał DWORZAK[1)]

[1)] AGH University of Krakow; Faculty of Civil Engineering and Resource Management, Mickiewicza 30 av., Krakow, Poland; email: dworzak@agh.edu.pl, ORCID: https://orcid.org/0000-0002-6356-3228

http://doi.org/10.29227/IM-2023-01-30

Submission date: 15-05-2023 | Review date: 03-06-2023

Abstract

Occupational risk assessment is one of the most crucial legal obligation for employers and the basis of accident prevention. In the case of highly repetitive work operations and an almost constant work environment, performing a preliminary risk analysis and checking risk levels periodically may be sufficient. In the case of blasting operations in quarries: the mining and geological conditions, technology, blasting methods, explosives, and initiating agents are variables that affect occupational safety. Moreover they make occupational risk assessment difficult to apply on the operational level. Therefore, occupational risk management followed by a deep analysis of hazards and their associated risks may allow to design and manage blasting works with regard to occupational risk. The paper presents the method for the support of occupational risk management in quarry blasting operations based on a modified FMECA algorithm. The designed method provides a systematic approach to risk identification, and allows to indication of the main occupational hazards that should be prioritized for preventive action. The preventive action which could be implied in the design stage by changes in technology or work organization based on options available for a particular quarry.

Keywords: *occupational risk, risk management, safety, blasting, quarry*

1. INTRODUCTION

The application of explosives in open-pit mining is usually the basic stage of the production process. Explosives are commonly used in quarrying to break a mineral-bearing material. This can be explained by the fact that drilling and blasting operations are the most effective methods of extracting natural aggregates in hard rock quarries. Furthermore it is the cheapest and fastest method to produce a large volume of rock. Despite its benefits, the use of explosives in mining poses several potential hazards to personnel, the natural environment, and the surrounding structures.

Current research on quarry blasting safety focuses mainly on the environmental impact of explosives detonation on the mine surroundings and its mitigation.The occupational health and safety (OHS) of employees who performs blasting works is not a commonly addressed area in research papers. This reflection in lack of research interest may result from the detailed blasting safety procedures in national legislation, and the need to meet rigorous safety requirements when handling explosives, and that does not give much space for innovation.

One of the main tools to evaluate and improve employee safety during work is the occupational risk assessment [1,2,3]. In Poland, like in other European Union countries, occupational risk assessment is mandatory [4,5,6]. Framework Directive 89/391/EEC requires employers to carry out risk assessments as part of the protective measures to improve the safety and health of workers [6]. This fact makes an occupational risk assessment a legally required document for any worker undertaking work in the European Union. The key components of a risk assessment are: the identification of hazards and associated risks, estimation of the risk level, determination of risk acceptance, and implementation of preventive or corrective actions where necessary [7,8]. Awareness of risks and their levels can provide the basis for managing operational activity focused on improving employee safety, which lays the foundation for occupational risk management.

Occupational risk assessment for blasting operations can be both complex and require particular expertise in explosive handling, quarry operations, and workplace safety. Due to varying mining and geological conditions, available methods of blasting works, types of explosives and initiating systems, and the relationship between used technology and materials, occupational risk assessment for quarry blasting operations shouldn't be considered as a single activity, but as a dynamic process of assessing risks for each particular blast. This approach allows to optimization of the process in terms of work safety through the application of risk assessments in existing conditions. Moreover, it includes the assessment results, to select technology or resources that should reduce the level of occupational risk.

This paper presents an engineering approach to the occupational risk management framework for quarry blasting works based on a modified Failure Mode, Effects & Criticality Analysis (FMECA) method. The presented method aims to provide an intuitive, time-efficient way of managing occupational risks during the design and execution of blasting operations, identifying key safety issues, and helping to prevent negative impacts on the health and safety of workers.

2. QUARRY BLASTING SAFETY

The safety of quarry blasting operations is generally considered in two main areas: the environmental impact of blasting, and occupational health and safety. Both of these aspects are regulated in Poland by legislation.

Polish regulations recognize the following environmental impacts of blasting operations: blast-induced ground vibra-

Fig. 1. Quarry blasting process stages for typical crushed aggregates production blasting (long boreholes blasting method up to 6 m length)
Rys. 1. Proces realizacji robot strzałowych dla typowych strzelań produkcyjnych w górnictwie skalnym (strzelanie długimi otworami strzałowymi powyżej 6 m)

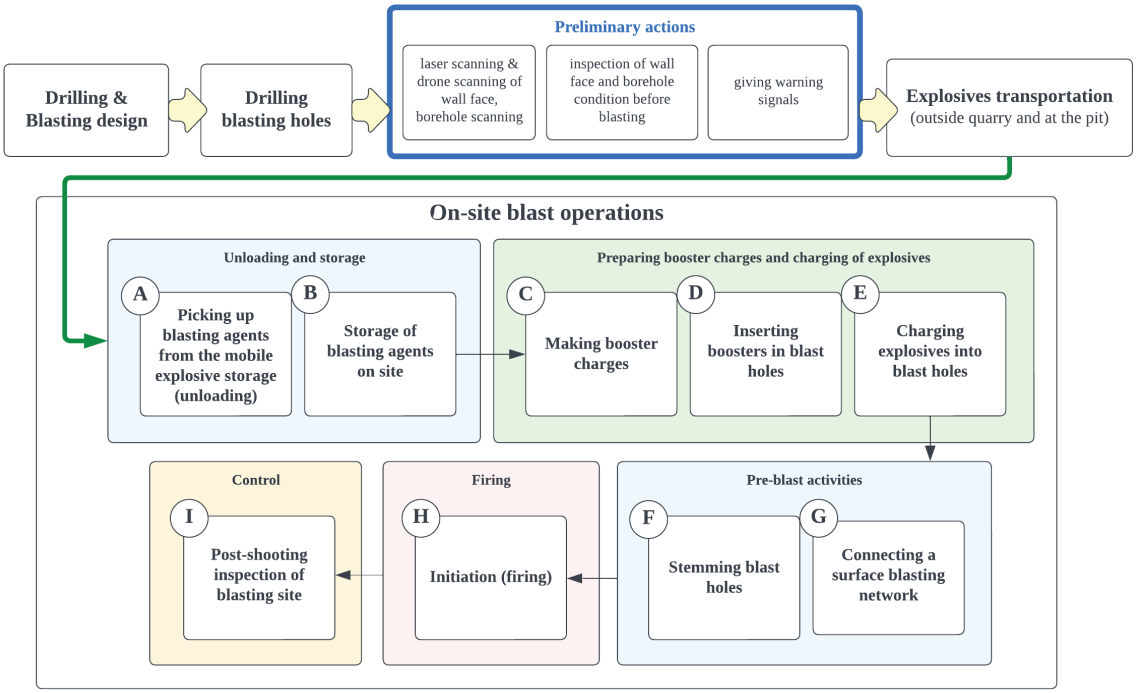

tions, air blast, and flyrock. Their prevention is also considered by establishing safety zones for each selected hazard [9].

Current research work on blasting safety mainly focuses on the environmental impact of blasting. In the case of blast-induced ground vibrations research was done on prediction of intensity and modeling of ground-borne vibration phenomena [10,11,12,13,14,15], the effect of blast-induced vibrations on buildings and structures [16,17,18], and the influence of blasting technology on the seismic effect [19,20,21]. Considering airblast and flyrock, research was mostly made in prediction models of its intensity [22,23,24,25,26]. Blasting operation former studies were also presented by Kiani et al. [27].

Environmental impacts generally affect the mine's surroundings and external people. Given Polish legal obligations, these impacts can have only a minor influence on the safety of the workers carrying out the blasting works because of the necessary safety precautions [9]. The only real hazard that could be identified is the possibility of injury to personnel securing access routes to the flyrock safety area. Other quarry employees are obliged to stay in the blasting shelters until the signal declaring the end of blasting works is given [9]. Therefore, the proposed approach to occupational risk management does not take into account the environmental hazards resulting from the detonation of an explosive as they are unlikely to affect workers.

In the case of Polish OHS regulations, when performing blasting work in quarries, we can distinguish between general regulations based on the Labour Code [4,5], regulations on safety at work in mines and on the handling of explosives [9,28,29,30], and detailed OHS requirements related to work environment factors and work performance [31,32]. These regulations provide detailed guidelines on how to perform the work safely.

Recent research in quarry safety has focused mainly on measuring, simulating, and reducing selected hazards in mines [33,34,35], safety management & occupational risk assessment [34,36,37,38], and preventive measures [39,40]. In the case of occupational risk assessment in quarry blasting operations research was done by Kiani et al., Seccatore et al., and Ke et al. [27,41,42], suggesting various approaches to risk assessment dedicated to quarry blasting. Kiani et al. identified blasting operations risks and used the Fuzzy Analytical Hierarchy Process (FAHP) to compare and rank them [27]. Seccatore et al. studied the applicability of the HAZOP (Hazard and Operability Study) method to assess occupational risks level in rock blasting [41], and Ke et al. adopt Social Network Analysis (SNA) to find relationships between safety risk factors and occupational accidents [42].

An analysis of the available literature shows that current research on quarry occupational safety focuses mainly on general mine hazards, with blasting as one of the sources of hazards that can affect workers. New occupational risk assessment methods have been proposed for blasting operations, however this subject is not commonly addressed in current research studies.

3. OCCUPATIONAL HAZARDS AND RISKS IN QUARRY BLASTING OPERATIONS

Blasting operations expose workers to several hazards which can have different sources. The root causes of occupational hazards can be divided into four categories: how the work is carried out, work environment and conditions, materials used to perform the work & used equipment.

Due to the specifics of the quarry blasting works operations, the hazards in each category may differ for each blasting even in the same mine. This is due to variable blasting locations, used methods of blasting, geological conditions, types of explosives and initiating agents, and changing weather conditions. Additionally, each stage of blasting operations exposes workers to a different range of hazards. It is therefore

Tab. 1. Quarry blasting occupational hazards and risks [*W - the way in which work is carried out; EC - work environment and conditions; M - materials used to perform work; E - used equipment.]

Tab. 1. Zagrożenia I ryzyka zawodowe w robotach strzałowych w odkrywkowym górnictwie skalnym [*W - sposób wykonywania pracy; WE – środowisko i warunki pracy; M - materiały użyte do wykonania pracy; E - sprzęt używany.]

Blasting operations stages	Root cause of hazards*	Occupational hazards	Occupational risks	Technological, organizational and environmental variables	
Unloading and storage on site	W	Manipulation of heavy & fragile objects	Static and dynamic load during lifting & manual transportation, tripping, stress due to time pressure	Type and packaging of used explosives (bulk, cartridges), type of mobile explosive storage unit	
	EC	Dust, noise, weather conditions (hot, cold, rainy), sun exposure	Exposure to negative work environment factors, sunstroke, dehydration, exposure of the skin and eyes to UV radiation	Location of machines in operation, weather & wind	Staff awareness and experience, safety culture level of the company
	M	Explosives, boosters, initiating agents	Uncontrolled detonation, damage to the initiating agent (detonation or misfire), exposure to chemical agents (explosives)	Type of used explosives, boosters and initiating agents	
	E	Mobile explosives storage car	Hit or run over, hitting on vehicle parts	Type of mobile explosive storage unit, organization of safe unloading	
Preparing boosters and charging of explosives	W	Forced body position, bending torso, precision manipulation of objects, manipulation of heavy & fragile objects, operational errors	Static and dynamic load, overloading of the musculoskeletal system, tripping, falling from the working bench, loss of the blasting line to the detonator, faulty detonator connection, stress due to time pressure	Type and packaging of used explosives, type of initiating agents, number of blasting holes & type of surface network connection, organization of safe work on blasting site & concentration during work	
	EC	Dust, noise, weather conditions (hot, cold, rainy), sun exposure, upper and working bench face	Exposure to negative work environment factors, sunstroke, dehydration, exposure of the skin and eyes to UV radiation, impact from a falling overhanging rock, falling from a working bench	Location of machines in operation, weather & wind, proximity of upper and working bench face, organization of safe work on blasting-site	
	M	Explosives, boosters, initiating agents	Uncontrolled detonation, damage to the initiating agent (detonation or misfire), exposure to chemical agents (explosives)	Type of used explosives, boosters and initiating agents, type and complexity of surface network connection, number of boreholes	
	E	Operating MEMU (bulk explosives production units), use of hand tools	Impacts, vibrations, splashing with explosives (eyes contamination), exposure to exhausts, lifting explosives charging pipe	Type of MEMU device & charged explosives, types of used hand tools (authorization to operate with explosives)	
Pre-blast activities	W	Work with hand tools (shovel), Forced body position, bending torso, precision manipulation of objects, operational errors	Overloading of the musculoskeletal system, tripping, falling from working bench, loss of the blasting line to the detonator, faulty detonator connection, stress due to time pressure	Type of initiating agents, number of blasting holes & type of surface network connection, organization of safe work on blasting-site & concentration during work	
	EC	Dust (from quarry), weather conditions (hot, cold, rainy), sun exposure, upper and working bench face	Exposure to negative work environment factors, impact from a falling overhanging rock, falling from working bench, exposure of the skin and eyes to UV radiation	Weather & wind, proximity of upper and working bench face, organization of safe work on blasting-site	
	M	Dust from stemming material, initiating agents in explosive column	Exposure to dust containing crystalline silica, faulty detonator connection, accidental initiation of an explosive charge, stress due to time pressure	Type of initiating agents, number of blasting holes & type of surface network connection, organization of safe work on blasting site & concentration during work	
	E	Use of hand tools and initiating system devices (i.e. logger)	Injury due to tool failure or uncontrolled detonation by an equipment malfunction	Type of used tools and devices	
Initiation (firing) and post-blasting control	W	Entering the blasting shelter	Hit against blasting shelter elements, scuffs and scratches	Condition of blasting shelters, time pressure	
	EC	Detonation effect, dust and post-blast fumes, unstable ground, weather conditions, sun exposure, upper and working bench face	Hearing damage (noise), inhalation of post-blast fumes with carbon and nitrogen oxides, tripping, falling from unstable working bench, exposure of the skin and eyes to UV radiation	Explosives volume, wind, time between blasting and control, blasting technology & output	
	M	Explosives and detonators	Uncontrolled detonation of misfires	Type and quality of used explosives & detonators, quality of blasting operations	
	E	-	-	-	

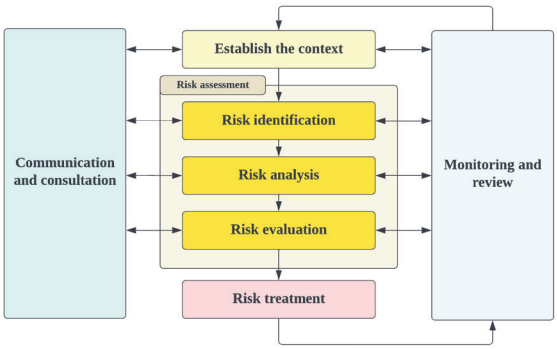

Fig. 2. Risk management process [45]
Rys. 2. Proces zarządzania ryzykiem [45]

necessary to identify the hazards not only in terms of root cause but also considering the potential variable conditions and technologies, for each stage of the blasting work. For hazard identification, the quarry blasting process for typical crushed aggregates production blasting (for blastholes longer than 6 m) was mapped as shown in Figure 1.

Through a systematic approach to hazard identification based on quarry site investigations and literature review, hazards & occupational risks have been identified for each stage of the blasting process, in each hazard root cause category, and by pointing the variable factors that affect the nature and level of hazard for typical production blasting in Polish quarries. For this paper's purpose, the results are presented in condensed form in Table 1 for aggregated blasting operations.

Concluding upon the identified hazards and risks (tab. 1), it can be pointed out that blasting workers in quarries are exposed to wide range of hazards including safety hazards (tripping, falls, impacts), physical hazards (explosion, noise, vibration, UV radiation), chemical hazards (explosives, dust), psychosocial hazards (working under time pressure, the stress of working with hazardous materials) and they are strongly affected by many ergonomic risk factors (heavy lifting and manual handling, static and dynamic loads, forced body position). Due to the changeable on-site and geological conditions, various available methods to execute blasting works, as well as different materials and initiating agents that can be applied, only periodically revised occupational risk assessment may not be sufficient to keep workers safe. A risk assessment based on all detected occupational risks is formally acceptable [5], but does not allow to manage work safety at an operational level. Therefore, the use of an occupational risk management tool can improve safety and help to make technological choices with a focus on employees' safety.

4. OCCUPATIONAL RISK ASSESSMENT AND MANAGEMENT

Risk assessment is an essential part of the risk management process. It consists of three steps: risk identification (finding, recognizing, and describing risks), risk analysis (comprehending the nature of risk and determining its level), and risk evaluation (comparing assessed risk levels with risk criteria to determine whether the risk is acceptable or not) [43]. Legal obligations [4,5] as well as the requirements of the health and safety management system [44] imply the need to assess occupational risks. ISO 45001 standard also includes risk-based approach, which lay the foundation for occupational risk management [44]. Through the outcomes of the risk assessment, it is possible to manage the work process concerning existing risks using risk management methodology. Figure 2 shows the concept of the risk management process based on [45] and the role of risk assessment in managing the risk. The relevant publications detail the stages and requirements of risk management [45,46,47].

Risk assessment could be conducted using various qualitative, quantitative, and semi-quantitative methods, and regarding occupational safety, there are also recognized dedicated methods for specific types of hazards [48]. Good practice and legal requirements [5] indicate, that the choice of assessment method should be tailored to the type of analyzed hazard. Also, different methods may be used for each step of the risk assessment, depending on their applicability [8].

Risk management is a set of coordinated activities to direct and control an organization with regard to risk [45]. According to the definition, risk management in occupational safety could be the basic tool to improve safety as risk is the fundamental concern of OHS. Risk evaluation can indicate the necessity of risk mitigation, which is one of the available options at the risk treatment stage.

Evaluation and dealing with risk is the most common way to conduct legal-based occupational risk assessment in the practice of industrial companies. Ways of meeting the need for communication and consultation, as well as monitoring and review are also implemented in the Polish regulations, although they do not provide any specific guidance beyond the general requirements of involving employees in the risk assessment process, communicating risks to workers and periodically reviewing the validity of the occupational risk assessment [5].

Despite the availability of numerous algorithms enabling a detailed and quite objective assessment of occupational risks, there is a lack of methods to minimize the risk by deliberate choice of safer operations. In the case of blasting operations with different available technologies, materials, and equipment, such a tool can improve safety not only by implementing protective and corrective measures but also by selecting the work technology and its organization from a safety point of view at the design stage.

5. FMEA METHOD

Failure Modes and Effects Analysis (FMEA) was first applied in 1949 by US Army to study the risks of malfunction of

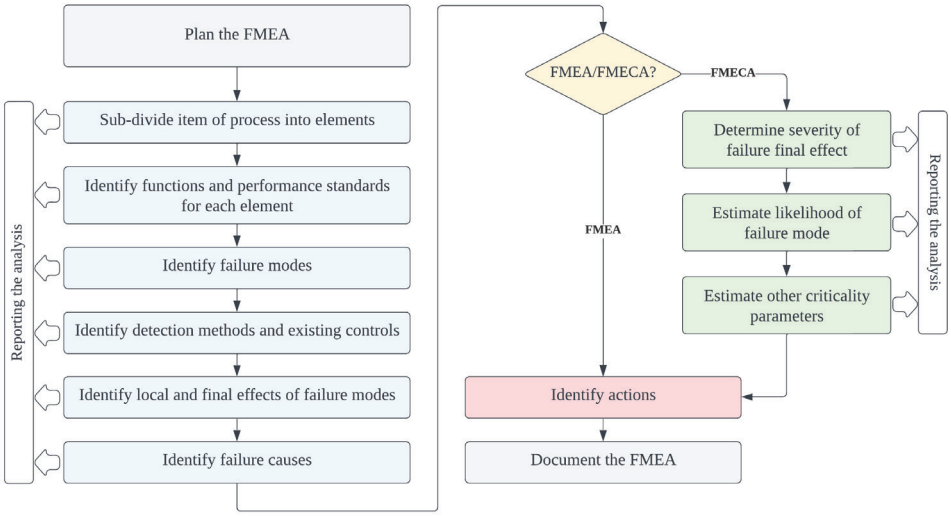

Fig. 3. FMEA/FMECA analysis steps [50]
Rys. 3. Etapy analizy FMEA/FMECA [50]

the military systems [49]. This method is widely used in various industries to evaluate how products or processes might fail, providing a systematic approach for identifying modes of failure, and possible effects and could include identification of the causes of failure modes. FMECA (Failure Modes, Effects and Criticality Analysis) as an extension of this method provide moreover ranking of the failure modes in terms of criticality [50]. The general steps of FMEA/FMECA method are shown in Figure 3, and the full description of the method was described in [50].

One of the advantages of this method is its process-based approach, which is essential in today's management systems based on ISO standards. The requirements of the FMEA method are not dogmatic, therefore this analytical approach can be tailored, adapted to different scopes, and applied in different ways. It can therefore be used as a framework for managing occupational risks to which blasting staff is exposed.

6. METHODOLOGY

The proposed method for the support of occupational risk management in quarry blasting operations is based on the general concept of FMECA analysis. A detailed investigation of the particular steps and requirements of the method was carried out. To adapt this framework to the problem of occupational risk management in quarry blasting, necessary changes have been made. They considered:

- the state of the art in occupational health and safety,
- a set of legal requirements related to the safety of blasting operations,
- the various nature of occupational hazards arising at blasting operations,
- different types of occupational risk assessment techniques.

The suggested method of risk management does not intend to estimate risks according to a single unified method. Good practice strongly recommends that occupational risks should be estimated using the method most appropriate to the risk in question. For the risk assessment stage the FMECA suggests a qualitative or semi-quantitative parametric method, in which the severity is determined, and likelihood is estimated along with selected criticality parameters (like detectability) [50]. Not all occupational risks can be accurately assessed using parametric methods, for instance, ergonomic hazards for which dedicated risk assessment methods exist. Therefore, the presented approach does not guide the selection of the risk estimation method but indicates the possible types of methods and the formulation of their results in the occupational risk management procedure. The methodology allows using most suitable method of estimating risk level based on accuracy, available data, and resources, as well as experience and knowledge of the personnel.

To make fully informed decisions about blasting operations in terms of health and safety, the method provides a ranking of the identified risks using the Pareto principle. It can be used to identify the main occupational hazards that should be prioritized for preventive action which could be implied in the design stage by changes in technology or work organization based on options available for a particular quarry. Therefore the main aim of the presented tool is to combine the process of occupational risk assessment and its outputs with the design stage and quarry blasting at the operational level.

7. RISK MANAGEMENT FOR QUARRY BLASTING OPERATIONS

The main purpose of the presented method is to provide a precise design toolkit which will improve decision making process on technology, work organization, or resource changes to minimize occupational risk on the employee. A diagram of the risk management method was presented in the figure 4. The method involves five main stages:

a. hazards and risks identification stage,
b. selection of risk assessment techniques for each identified risk,
c. estimation of risk level and its standardization,
d. ranking the risks depending on risk level,
e. analyzing risks for scenarios including change of technology or resources.

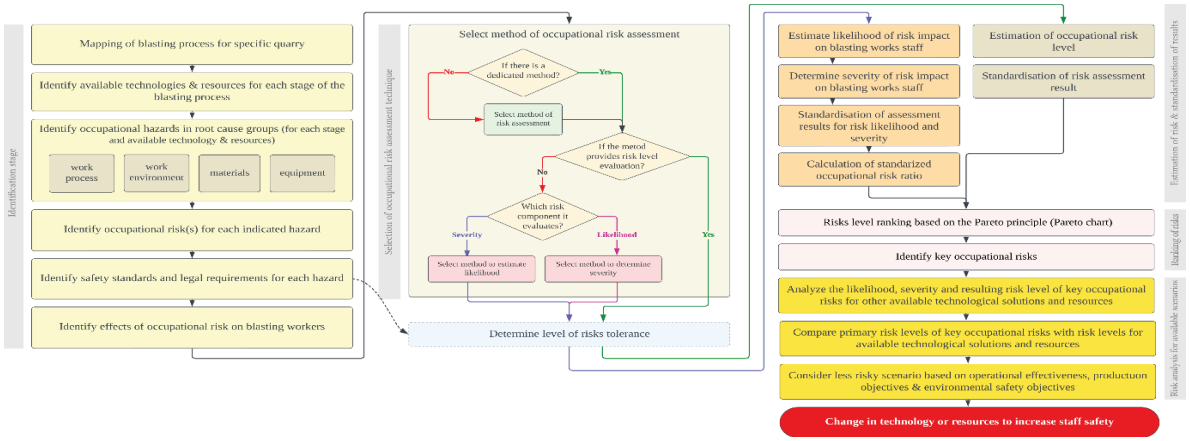

Fig. 4. Occupational risk management method for quarry blasting operations

Rys. 4. Metoda zarządzania ryzykiem zawodowym dla prac strzałowych w odkrywkowym górnictwie skalnym

The first stage starts by detecting all operations for quarry blasting depending on the specifics of the analyzed quarry. For each operation it should be identified all available methods, technologies, equipment, materials and work performance options that could be used. This stage allows to identify all available alternatives, the application of which may improve safety. Then the occupational hazards are identified in four categories, depending on their origin: the way work is executed, work environment (natural and quarry environment), used materials & equipment. This approach allows to make systematic identification of safety hazards depending on the sources identified in the next step risks. For each identified risk analysis of standards and legal requirements should be made, to comply with limit values if they are relevant. If a legal limit exists, it can be used to determine the acceptable level of risk. To understand the possible impact of risk on the employee's health or life, an analysis of risk scenarios should be made. Its results can provide useful insight into the severity of the risk.

For each identified risk it should be considered if there is any dedicated technique to assess risk level, or which method will provide the most accurate estimation result. Selection of the method could be based on [8], and can be proceeded by assessing risk level or each of its components separately. In this method, the classic definition of risk was used, where risk is a function of the likelihood and severity of consequences. Therefore these two risk parameters could be assessed individually and with different methods, to obtain more accurate estimation results. Determining the level of risk acceptance could be applied to combine this methodology with occupational risk assessment in legal terms.

The estimation of the occupational risk level could be carried out depending on whether the technique used makes it possible to assess the risk level or whether separate methods are used to estimate the likelihood and severity. Results at different scales are obtained by different risk assessment methods. To compare and rank risk levels, it is necessary to standardize the results of risk assessment. It has been suggested that simple outcome scales should be used: 0 – 100 for both likeliness and severity, and 0 – 10000 for risk level (equivalent to the result of the multiplication of risk components ratios). Standardization of results can be made by comparing two scales and determining the level in the proposed scale through the use of aspect ratios.

To determine which assessed occupational risks should be prioritized for preventive action, the Pareto principle was used. It implies, that 80% of consequences come from 20% of causes, and is commonly used in occupational safety issues to hazard prioritization [51]. Prioritization can be made according to the operations of the blasting process, root cause groups for hazards, or all risks in a process. Various approaches to prioritization allow to identification of critical areas for which the level of risk can significantly affect employees' safety.

For identified key risks or critical safety areas should be considered the change of technology, materials, tools, or work methods. The available resources, technologies, and materials identified in the first step should be considered by analyzing the level of risk as they are been used. Comparing the obtained risk level with the risk level for selected key occupational risks allows for a selection of available modifications in blasting operations which should have a positive impact on worker safety. It should be also considered if applied changes do not negatively affect the operational effectiveness, production objectives, and environmental safety objectives. If the modification of the blasting process does not affect the production or the environment, the results based on the presented methodology should make it possible to control the occupational risks at the stage of the blasting works design and to take preventive measures through a conscious choice of technology, materials, and work equipment.

8. CONCLUSION

Risk assessment is one of the fundamental legal obligations of the employer. By carrying out an occupational risk assessment for a particular position and regularly monitoring the level of risk, this requirement can be met. However, this approach does not allow the use of occupational risks analysis at the design stage of blasting operations daily. Quarry blasting is often carried out under varying mining and geological conditions, using a range of blasting methods, explosives, and initiating agents, and can be organized differently in the same quarry. To benefit from the awareness of recognized occupational risks, they should be considered about the conditions of the blasting operation for a particular blast.

The application of risk management methodology can allow to apply a piece of information about occupational risk levels to make informed technological and organizational de-

cisions at the design phase of blasting in the quarry. A methodology based on the assumptions of the FMECA algorithm has been proposed for the management of occupational risks in quarry blasting operations. The algorithm itself has been extended to include the option of adopting various methods of evaluation of occupational risk level, taking into account the variable nature of occupational hazards in blasting operations. A risk ranking method based on the Pareto principle has been proposed to enable the selection of critical stages, work activities, resources, or hazards regarding to employees' safety. The application of the proposed procedure requires both time and a detailed analysis of the blasting process and the factors affecting workers directly and indirectly.

To verify the potential to improve workers' safety by applying the occupational risk management method to blasting work operations in quarries, a pilot study on a quarry with its own blasting works staff and for the contracted blasting company is planned. The results of the forthcoming analyses, combined with a study of the organization's safety level, will further elaborate on the subject discussed in this paper.

Literatura – References

1. MOREL, G.; PILLAY, M. The occupational risk assessment method: a tool to improve organizational resilience in the context of occupational health and safety management. In Advances in Safety Management and Human Factors, 2020, p. 367-376.
2. FASORANTI, A.J. Occupational risk assessment as a tool for minimizing workplace accidents in Nigeria industries. In International Journal of Education and Research, vol. 3, no. 5, 2015, p. 143-156.
3. BĂBUȚ, G.B.; MORARU, R.I. Occupational risk assessment: imperatives for process improvement. In Quality – Access to Success, vol. 19, issue 166, 2018, p. 133-144.
4. Labour Code of 26 June 1974 (Journal of Laws 1974 no. 24 item 141 as amended).
5. Decree of the Minister of Labour and Social Policy of 26 September 1997 on general regulations of safety and hygiene at work (Journal of Laws 2003 no. 169 item 1650 as amended).
6. Council Directive 89/391/EEC of 12 June 1989 on the introduction of measures to encourage improvements in the safety and health of workers at work.
7. PN-N-18002:2011 - Occupational health and safety management systems - General guidelines for risk assessment.
8. IEC 31010:2019 - Risk management - Risk assessment techniques.
9. Decree of the Minister of Energy of 9 November 2016 on the particular requirements for the storage and use of blasting agents and equipment in the mining plant's operation (Journal of Laws 2016 item 321).
10. YAN, Y.; HOU, X.; FEI, H. Review of predicting the blast-induced ground vibrations to reduce impacts on ambient urban communities. In Journal of Cleaner Production, vol. 260, 2020.
11. DING, X.; HASANIPANAH, M.; RAD, H.N.; ZHOU, W. Predicting the blast-induced vibration velocity using a bagged support vector regression optimized with firefly algorithm. In Engineering with computers, vol. 37, 2021, p. 2273-2284.
12. CHOI, Y.; LEE, S.S. Predictive modelling for blasting-induced vibrations from open-pit excavations. In Applied Sciences, no. 11, vol. 16, 2021.
13. MATIDZA, M.I.; JIANHUA, Z.; GANG, H.; MWANGI, A.D. Assessment of blast-induced ground vibration at Jinduicheng molybdenum open pit mine. In Natural Resources Research, vol. 29, 2020, p. 831-841.
14. AKYILDIZ, O.; HUDAVERDI, T. ANFIS modelling for blast fragmentation and blast-induced vibrations considering stiffness ratio. In Arabian Journal of Geosciences, vol. 13, 2020.
15. GORAI, A.K.; HIMANSHU, V.K.; SANTI, C. Development of ANN-based universal predictor for prediction of blast-induced vibration indicators and its performance comparison with existing empirical models. In Mining, Metallurgy & Exploration, vol. 38, 2021, p. 2021-2036.
16. KANGDA, M.Z.; BAKRE, S. Dynamic analysis of base isolated connected buildings subjected to seismic and blast induced vibrations. In Soil Mechanics and Foundation Engineering, vol. 58, 2021, p. 416-424.
17. KANGDA, M.; BAKRE, S. Performance of linear and nonlinear damper connected buildings under blast and seismic excitations. In Innovative Infrastructure Solutions, vol. 6, 2021.
18. KANGDA, M,Z.; BAKRE, S. Performance evaluation of moment-resisting steel frame buildings under seismic and blast-induced vibrations. In Journal of Vibration Engineering & Technologies, vol. 8, 2020, p. 1-26.

19. WANG, P.; MA, Y.; ZHU, Y.; ZHU, J. Experimental study of blast-induced vibration characteristics based on the delay-time errors of detonator. In Advances in Civil Engineering, vol. 2020, 2020.

20. ROY, M.P.; MISHRA, A.K.; AGRAWAL, H.; SINGH, C.P. Blast vibration dependence on total explosives weight in open-pit blasting. In Arabian Journal of Geosciences, vol. 13, 2020.

21. SINGH, C.P.; AGRAWAL, H.; MISHRA, A.K. Frequency channeling: a concept to increase the frequency and control the PPV of blast-induced ground vibration waves in multi-hole blast in surface mine. In Bulletin of Engineering Geology and the Environment, vol. 80, 2021, p. 8009-8019.

22. HASANIPANAH, M.; AMNIEH, H.B. A fuzzy rule-based approach to address uncertainty in risk assessment and prediction of blast-induced flyrock in a quarry. In Natural Resources Research, vol. 29, 2020, p. 669-689.

23. NGUYEN, H.; BUI, X-N.; BUI, H-B.; MAI, N-L. A comparative study of artificial neural networks in predicting blast-induced air-blast overpressure at Deo Nai open-pit coal mine, Vietnam. In Neural Computing and Applications, vol. 32, 2020, p. 3939-3955.

24. ZHOU, X.; ARMAGHANI, D.J.; YE, J.; KHARI, M.; MOTAHARI, M.R. Hybridization of parametric and non-parametric techniques to predict air over-pressure induced by quarry blasting. In Natural Resources Research, vol. 30, 2021, p. 209-224.

25. FANG, Q.; NGUYEN, H.; BUI, X-N.; TRAN, Q-H. Estimation of blast-induced air overpressure in quarry mines using cubist-based genetic algorithm. In Natural Resources Research, vol. 29, 2020, p. 593-607.

26. HAN H.; ARMAGHANI, D.J.; TARINEJAD, R.; ZHOU, J.; TAHIR, M.M. Random forest and Bayesian network techniques for probabilistic prediction of flyrock induced by blasting in quarry sites. In Natural Resources Research, vol. 29, 2020, p. 655-667.

27. KIANI M., HOSSEINI, S.H., TAJI, M.; GHOLINEJAD, M. Risk assessment of blasting operations in open pit mines using FAHP method. In Mining of Mineral Deposits, vol. 13, issue 3, 2019, p. 76-86.

28. Act of 21 June 2002 on explosives for civil use (Journal of Laws 2002 no. 117 item 1007).

29. Decree of the Minister of Economy of 8 April 2013 on detailed requirements for the operation of an opencast mine (Journal of Laws 2013 item 1008).

30. Decree of the Minister of Economy of 18 February 2011 on how to perform work with explosives for civil use and when clearing areas (Journal of Laws 2011 no. 42 item 216).

31. Decree of the Minister of Labour and Social Policy of 14 March 2000 on health and safety at work in manual handling activities (Journal of Laws 2000 no. 26 item 313).

32. Decree of the Minister of Health of 2 February 2011 on the analysis and measurement of factors hazardous to health in the working environment (Journal of Laws 2011 no. 33 item 166).

33. ZHENG, X.; YANG, Q.; JIN, L.; ZHENG, Y.; LUO, H.; MA, G. Numerical simulation on spatio-temporal distribution regularities of blasting dust mass concentration in open quarry. In China Safety Science Journal, vol. 30, issue 10, 2020, p. 55-62.

34. DEGAN, A.G.; LIPIELLO, D.; PINZARI, M. Occupational hazard prevention and control in a quarry environment: exposure to airborne dust. In WIT Transactions on the Built Environment, vol. 151, 2015, p. 27-38.

35. CARBONE, S.; DE BRITO, V. A simulation approach to predict workers' exposure to respirable dust in a quarry site: a case study. In International Multidisciplinary Scientific GeoConference SGEM 2, 2016, p. 25-32.

36. EKONG, A.E.; EZEOKORO C.; NWAICHI, E.O.; OBELE, R.E. Occupational health and safety management in selected stone quarries in Akamkpa, Cross River State, Nigeria. In Current Journal of Applied Science and Technology, vol. 39, issue 34, 2020, p. 107-122.

37. TIMOFEEVA, S.S.; DROZDOVA, I.V.; BOBOEV, A.A. Assessment of occupational risks of employees engaged in open pit mining. In E3S Web of Conferences - XVIII Scientific Forum "Ural Mining Decade", vol. 177, 2020.

38. [KOVACS, A.; BORDOS, S.; GARALIU-BUSOI, B.; MIRON, C.; STANILA, S. The analysis of the technological and professional danger factors specific to the works of exploitation of useful rocks from quarries, which can generate risk of accident and/or technological breakdown. In MATEC Web of Conferences - 9th International Symposium on Occupational Health and Safety SESAM 2019, vol. 305, 2020.

39. MELIKA, F.F.; AMER, F.G.M. Proposal guideline for preventive measures toward occupational health hazards for quarries workers. In Egyptian Journal of Health Care, vol. 11, no. 4, 2020, p. 1260-1274.

40. ERSOY, M. The role of occupational safety measures on reducing accidents in marble quarries of Iscehisar region. In Safety Science, vol. 57, 2013, p. 293-302.

41. SECCATORE, J.; ORIGLIASSO, C.; DE TOMI, G. Assessing a risk analysis methodology for rock blasting operations. In Blasting in Mining – New Trends, 2012.

42. KE, L.; CHEN, K.; HU, N.; TAN, M.; ZHANG, G.; MENG, H. Safety risk assessment of blasting in open-pit mine based on SNA. In China Safety Science Journal, vol. 32, issue 10, 2022, p. 48-56.
43. ISO 31073:2022 - Risk management – Vocabulary.
44. ISO 45001:2018 - Occupational health and safety management systems - Requirements with guidance for use.
45. ISO 31000:2018 - Risk management – Guidelines.
46. LALONDE C.; BOURAL, O. Managing risks through ISO 31000: A critical analysis. In Risk Management, vol. 14, 2012, p. 272-300.
47. BJORNSDOTTIR, S.H.; JENSSON, P.; THORSTEINSSON, S.E.; DOKAS, I.M.; DE BOER, R.J. Benchmarking ISO risk management systems to assess efficacy and help identify hidden organizational risk. In Sustainability, vol. 12, issue 9, 2022.
48. KRAUSE M. Praktyczne aspekty doboru metod oceny ryzyka zawodowego. In Zeszyty Naukowe Politechniki Śląskiej, Seria: Organizacja i Zarządzanie, z. 59, 2011, p. 173-190.
49. SPREAFICO, C.; RUSSO, D.; RIZZI, C. A state-of-the-art review of FMEA/FMECA including patents. In Computer Science Review, vol. 25, 2017, p. 19-28.
50. EN IEC 60812:2018 - Failure modes and effects analysis (FMEA and FMECA).
51. WOODCOCK, K. Safety Evaluation Techniques, Ryerson University, Toronto.

Metoda zarządzania ryzykiem zawodowym dla robót strzałowych w odkrywkowym górnictwie skalnym w oparciu o zmodyfikowany algorytm FMECA

Ocena ryzyka zawodowego stanowi jedno z podstawowych wymagań prawnych stawianych pracodawcy oraz fundament prewencji wypadkowej. W przypadku prac charakteryzujących się powtarzalnymi czynnościami i niewielką zmiennością środowiska pracy, wykonanie oceny ryzyka zawodowego wraz z okresową kontrolą poziomu ryzyka wydaje się wystarczające i spełnia wymaganie stawiane przez prawo. Rozważając prace strzałowe w kamieniołomach, warunki górnicze i geologiczne, stosowana technologia i metody strzelania, środki strzałowe i inicjujące są zmiennymi, które mogą wpływać na poziom bezpieczeństwa pracy. Ponadto zmienne występujące w trakcie robót strzałowych powodują, że ocena ryzyka zawodowego i jej wyniki są trudne do wdrożenia na poziomie operacyjnym. Rozwiązaniem tego problemu może być zarządzanie ryzykiem zawodowym poprzedzone szczegółową analizą zagrożeń i towarzyszących im ryzyk, które może pozwolić na projektowanie i zarządzanie robotami strzałowymi z uwzględnieniem ryzyka zawodowego pracowników.

Artykuł prezentuje metodę wspierającą zarządzanie ryzykiem zawodowym w robotach strzałowych w odkrywkowym górnictwie skalnym opartą na zmodyfikowanym algorytmie FMECA. Zaproponowana metoda pozwala na systematyczne podejście do identyfikowania ryzyk zawodowych i wskazuje na kluczowe zagrożenia zawodowe, dla których powinny zostać w szczególności zastosowane działania profilaktyczne. Ograniczenie ryzyka zawodowego może być osiągnięte na etapie projektowania robót strzałowych poprzez zmianę technologii lub organizacji pracy w oparciu o dostępne możliwości dla danego zakładu górniczego, a wybór charakteru rodzaju zmian jest wspierany przez zaproponowany w niniejszym artykule algorytm.

Słowa kluczowe: *ryzyko zawodowe, zarządzanie ryzykiem, bezpieczeństwo pracy, roboty strzałowe, kamieniołomy*

Ocena stanu bezpieczeństwa pracy w oparciu o analizę wypadkowości w górnictwie

Romuald OGRODNIK[1)], Marek KĘSEK[2)]

[1)] Ph.D. Eng.; AGH University of Science and Technology, Cracow, Poland; email: rogrod@agh.edu.pl
[2)] Ph.D., DSc, Eng.; AGH University of Science and Technology, Cracow, Poland; email: kesek@agh.edu.pl

http://doi.org/10.29227/IM-2023-01-31

Submission date: 18-05-2023 | Review date: 07-06-2023

Abstrakt

Głównym celem pracy jest przedstawienie poziomu wypadkowości w polskim górnictwie oraz uzyskanie odpowiedzi m.in. na następujące pytania: jak przedstawiają się w ostatniej dekadzie wskaźniki wypadkowości oraz w jakich rodzajach górnictwa występuje najwięcej wypadków przy pracy? Chcąc zrealizować cele pracy, dokonano analizy danych statystycznych z lat 2013-2022 pochodzących z Wyższego Urzędu Górniczego oraz Głównego Urzędu Statystycznego. Analizę danych przeprowadzono dla całego górnictwa jak również dla poszczególnych jego rodzajów tj. górnictwa podziemnego, odkrywkowego i otworowego. Oprócz analizy wypadkowości bezwzględnej, wykorzystano również analizę wskaźnikową ze szczególnym uwzględnieniem wskaźników częstości wypadków przy pracy: ogółem, ciężkich i śmiertelnych. W pracy zdefiniowano również podstawowe pojęcia dotyczące wypadków przy pracy.

Słowa kluczowe: *wypadkowość, wskaźniki wypadkowości, górnictwo, przedsiębiorstwa górnicze*

1. WPROWADZENIE

Górnictwo to specyficzny rodzaj działalności związany z niespotykanymi w innych gałęziach przemysłu zagrożeniami, które mogą powodować szkody i straty, a w szczególności wypadki, urazy i choroby pracowników. Występowanie poszczególnych zagrożeń naturalnych uzależnione jest między innymi od sposobów eksploatacji złóż. W górnictwie odkrywkowym występują zagrożenia naturalne o zupełnie innym charakterze niż w górnictwie podziemnym czy górnictwie otworowym. Zagrożenia techniczne mogą być uwarunkowane rodzajami maszyn i urządzeń wykorzystywanych przy danym sposobie eksploatacji oraz uzależnione od konieczności wykorzystania materiałów wybuchowych [1]. Analizy dotyczące wpływu zagrożeń na wypadkowość w przemyśle wydobywczym można znaleźć w licznych pozycjach w literaturze [2-4].

Priorytetowym zadaniem przedsiębiorstw górniczych jest ograniczenie wypadkowości i poprawa warunków BHP w swoich zakładach. Do podejmowania skutecznych i mądrych decyzji potrzebne są odpowiednie informacje, w tym dane i wnioski pochodzące z analiz wypadkowości. Analiza wypadkowości to nie tylko narzędzie, na podstawie którego przekazuje się informacje dotyczące liczby i skutków wypadków, ale przede wszystkim narzędzie, które może być wykorzystane do podejmowania działań korygujących i zapobiegawczych ograniczających i eliminujących przyczyny wypadków [5]. Przy badaniu poziomu wypadkowości często szuka się zależności z innymi czynnikami np. z poziomem zatrudnienia, wydajnością itp. [6]. Na potrzeby pracy dokonano identyfikacji wybranych danych pochodzących z corocznych raportów dotyczących stanu bezpieczeństwa pracy, ratownictwa górniczego oraz bezpieczeństwa powszechnego w związku z działalnością górniczo-geologiczną oraz raportów dotyczących stanu bezpieczeństwa i higieny pracy w górnictwie, publikowanych przez Wyższy Urząd Górniczy (WUG). Wykorzystane dane dotyczyły m.in. liczby i rodzaju wypadków, kształtowania się wskaźników częstotliwości i ciężkości wypadków, przyczyn, które doprowadziły do powstania wypadków oraz stanu zatrudnienia w górnictwie. Analizie poddano dane pochodzące z ostatnich dziesięciu lat tj. 2013-2022.

Przedstawiony podział górnictwa na: górnictwo podziemne (górnictwo węgla kamiennego, kopalnie rud miedzi, pozostałe górnictwo podziemne), górnictwo odkrywkowe (kopalnie węgla brunatnego, pozostałe górnictwo odkrywkowe), górnictwo otworowe oraz roboty przygotowawcze jest podziałem stosowanym przez WUG, z którego sprawozdań pochodzą dane wykorzystane w pracy.

WYPADKI I WYPADKOWOŚĆ

W ustawie z dnia 30 października 2002 r. o ubezpieczeniu społecznym z tytułu wypadków przy pracy i chorób zawodowych zawarto definicje: wypadku przy pracy, wypadku ciężkiego i śmiertelnego [7].

Za wypadek przy pracy uważa się [7]:

- nagłe zdarzenie;
- wywołane przyczyną zewnętrzną;
- powodujące uraz lub śmierć;

które nastąpiło w związku z pracą:

– podczas lub w związku z wykonywaniem przez pracownika zwykłych czynności lub poleceń przełożonych,

– podczas lub w związku z wykonywaniem przez pracownika czynności na rzecz pracodawcy, nawet bez polecenia,

– w czasie pozostawienia pracownika w dyspozycji pracodawcy w drodze między siedzibą pracodawcy a miejscem wykonywania obowiązku wynikającego ze stosunku pracy.

Dane zdarzenie może zostać uznane za wypadek tylko w przypadku, gdy wszystkie powyższe cztery elementy wystąpią łącznie. W przypadku braku wystąpienia jednego z wymienionych elementów, zdarzenie nie zostanie uznane za wypadek

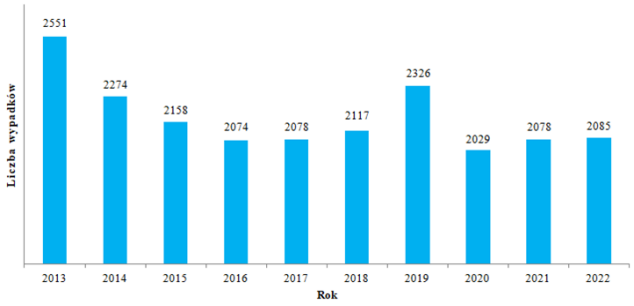

Rys.1. Liczba wypadków w polskim górnictwie w latach 2013-2022. Źródło: opracowanie własne na podstawie [9-11]
Fig. 1. Number of accidents in the Polish mining industry in the years 2013-2022. Source: [9-11]

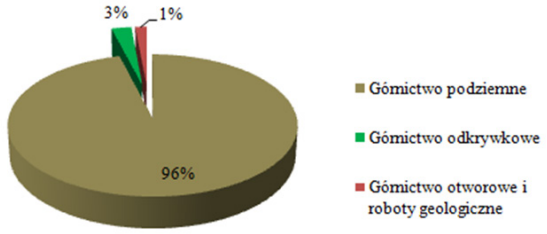

Rys. 2. Udział wypadków w głównych rodzajach górnictwa w latach 2013-2022. Źródło: opracowanie własne na podstawie [9-11]
Fig. 2. Share of accidents in the main types of mining in the years 2013-2022. Source: [9-11]

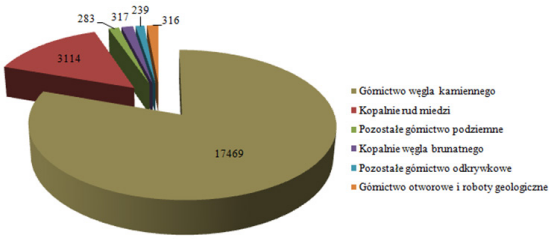

Rys. 3. Liczba wypadków w poszczególnych rodzajach górnictwa w latach 2013-2022. Źródło: opracowanie własne na podstawie [9-11]
Fig. 3. Number of accidents in the particular types of mining in the years 2013-2022. Source: [9-11]

przy pracy. Bardzo często dzięki uwadze pracowników, ich doświadczeniu lub za sprawą innych okoliczności nie dochodzi do urazów. Takie zdarzenia nazywane są wówczas zdarzeniami wypadkowymi. Dokładne określenie wszystkich składników powyższej definicji jest niezbędne dla prawidłowego kwalifikowania zdarzenia jako wypadku przy pracy [5].

Za śmiertelny wypadek przy pracy uważa się wypadek, w wyniku którego nastąpiła śmierć w okresie nieprzekraczającym 6 miesięcy od dnia wypadku [7].

Za ciężki wypadek przy pracy uważa się wypadek, w wyniku którego nastąpiło ciężkie uszkodzenie ciała, takie jak: utrata wzroku, słuchu, mowy, zdolności rozrodczej lub inne uszkodzenie ciała albo rozstrój zdrowia, naruszające podstawowe funkcje organizmu, a także choroba nieuleczalna lub zagrażająca życiu, trwała choroba psychiczna, całkowita lub częściowa niezdolność do pracy w zawodzie albo trwałe, istotne zeszpecenie lub zniekształcenie ciała [7].

Wypadkowość to obliczona statystycznie liczba wypadków [12]. Pojęcie wypadkowości wykorzystywane jest w analizach i prezentacjach danych dotyczących wypadków przy pracy.

Wypadki przy pracy przedstawiane są bardzo często ze względu na takie zmienne jak [8]: rodzaj działalności, zawód wykonywany przez poszkodowanego, skutki wypadku, liczba dni niezdolności do pracy, miejsce powstania wypadku, proces pracy, czynność wykonywana przez poszkodowanego w chwili wypadku, wydarzenia powodujące uraz, przyczyna wypadku.

Ponieważ porównywanie danych liczbowych o różnej wielkości nie przedstawia rzeczywistej skali danego zjawiska, do opisu sytuacji i analiz w zakresie wypadkowości stosuje się różne wskaźniki wypadków.

W pracy wykorzystano wskaźnik częstości wypadków, które bazuje na liczbie wypadków (poszkodowanych). Aby wskaźnik mógł być porównywalny w różnych grup zbiorowości konieczna jest standaryzacja wskaźnika poprzez podzielenie przez właściwą jednostkę. Najczęściej tą jednostką jest liczba pracowników (np. na 1000 pracujących). Wskaźnik częstości wypadków zdefiniowany jest wzorem:

$$W_1 = \frac{Liczba\ wypadków\ (poszkodowanych)}{Liczba\ pracujących} \times 1000 \qquad (1)$$

W górnictwie stosowany jest jeszcze wskaźnik w oparciu o ilość wydobytej kopaliny. Wskaźnik ten określa jaka liczba wypadków przy pracy przypada na milion ton wydobytej kopaliny.

$$W_2 = \frac{Liczba\ wypadków\ (poszkodowanych)}{Liczba\ wydobytych\ ton\ kopaliny} \times 1\,000\,000 \qquad (2)$$

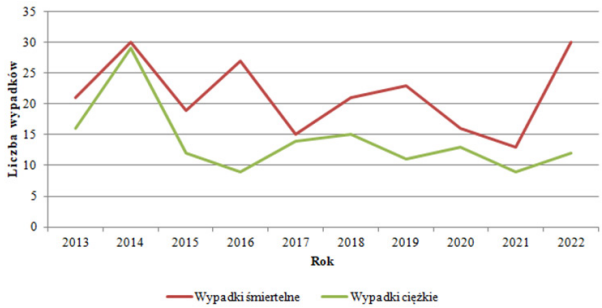

Rys. 4. Liczba wypadków śmiertelnych i ciężkich w latach 2013-2022. Źródło: opracowanie własne na podstawie [9-11]
Fig. 4. Number of fatal accidents and severe accidents in the years 2013-2022. Source: [9-11]

Tab. 1. Liczba wypadków śmiertelnych. Źródło: opracowanie własne na podstawie [9-11]
Tab. 1. Number of fatal accidents. Source: [9-11]

Rodzaj górnictwa	2013	2014	2015	2016	2017	2018	2019	2020	2021	2022
Górnictwo węgla kamiennego	14	20	12	10	10	15	16	9	9	22
Kopalnie rud miedzi	3	5	2	17	2	1	5	3	2	2
Pozostałe górnictwo podziemne	0	0	0	0	1	0	0	0	0	1
Kopalnie węgla brunatnego	1	0	1	0	0	0	0	1	0	0
Pozostałe górnictwo odkrywkowe	3	4	3	0	2	5	2	3	2	5
Górnictwo otworowe i roboty geologiczne	0	1	1	0	0	0	0	0	0	0

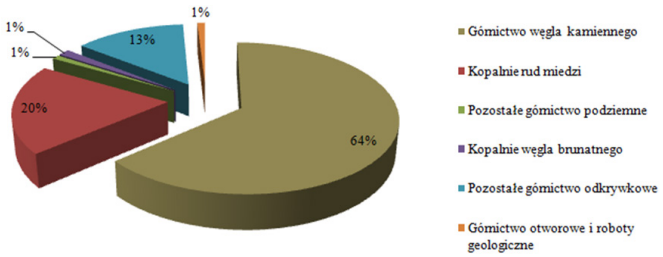

Rys. 5. Udział wypadków śmiertelnych w poszczególnych rodzajach górnictwa w latach 2013-2022. Źródło: opracowanie własne na podstawie [9-11]
Fig. 5. Share of accidents in the particular types of mining in the years 2013-2022. Source: [9-11]

3. ANALIZA BEZWZGLĘDNA

Liczba poszkodowanych w wypadkach przy pracy w polskim górnictwie w latach 2013-2022 została przedstawiona na wykresie – rysunek 1.

Liczba poszkodowanych w wypadkach przy pracy w analizowanym okresie uległa zmniejszeniu z 2551 do 2085 osób, co stanowi spadek o ponad 18%. W tym czasie zmniejszyło się zatrudnienie w górnictwie o 37,5 tysiące pracowników. Łącznie w omawianym okresie wypadkom uległo 21,7 tysiące pracowników.

W latach 2013-2022 najwięcej wypadków miało miejsce w górnictwie podziemnym – 96%. Wypadkom w tej branży uległo blisko 21 tysięcy osób. Wypadki w górnictwie odkrywkowym stanowiły 3 procentowy udział w wypadkach w polskim górnictwie, natomiast dla górnictwa otworowego i robót geologicznych udział ten stanowił 1%. Udział wypadków w głównych rodzajach górnictwa w latach 2013-2022 przedstawiono na rysunku 2.

Rysunek 3 przedstawia liczbę poszkodowanych w wypadkach przy pracy w poszczególnych rodzajach górnictwa w latach 2013-2022. W badanym okresie najwięcej poszkodowanych w wypadkach przy pracy zatrudnionych w górnictwie pracowało w kopalniach węgla kamiennego – 17469 osób oraz w kopalniach rud miedzi – 3114 osób. W kopalniach węgla brunatnego uległo wypadkom 317 osób, podobnie jak w kopalniach otworowych 316 osób.

Na rysunku 4 przedstawiono liczbę wypadków śmiertelnych i ciężkich w latach 2013-2022 w polskim górnictwie. W omawianym okresie zginęło przy pracy 215 osób, natomiast 140 osoby doznały urazów ciężkich. Niestety w badanym okresie nastąpił wzrost liczby wypadków śmiertelnych z 21 w roku 2013 do 30 w roku 2022.

Najwięcej wypadków śmiertelnych w omawianym okresie wystąpiło w kopalniach węgla kamiennego – 137, w kopalniach rud miedzi – 42 oraz głównie w kopalniach żwiru i piasku – 29. W tabeli 1 zaprezentowano szczegółowe dane dotyczące wypadków śmiertelnych w latach 2013-2022.

Porównując udział wypadków śmiertelnych w poszczególnych rodzajach górnictwa można stwierdzić, iż najniebezpieczniejsza praca ma miejsce w kopalniach podziemnych, głownie w kopalniach węgla kamiennego i rud miedzi – rysunek 5.

4. ANALIZA WSKAŹNIKOWA

Porównywanie jednostek mających różną ilość zatrudnionych pracowników za pomocą prostych wskaźników wypadkowości nie daje rzeczywistego odzwierciedlenia istniejącej sytuacji. Wynika to z faktu, iż w jednostkach, w których za-

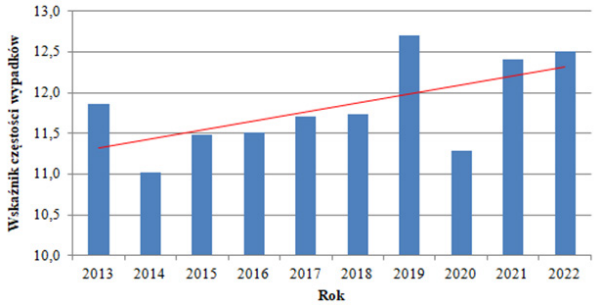

Rys. 6. Wskaźnik częstości wypadków w przeliczeniu na 1000 pracowników w latach 2013-2022. Źródło: opracowanie własne na podstawie [9-11]
Fig. 6. Accident frequency rate per 1000 employees in the years 2013-2022. Source: [9-11]

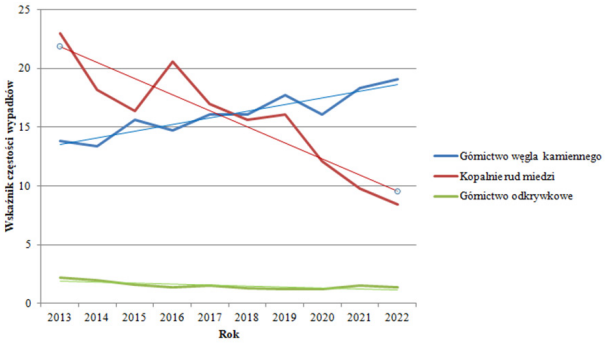

Rys. 7. Wskaźnik częstości wypadków w przeliczeniu na 1000 pracowników dla wybranych rodzajów górnictwa w latach 2013-2022. Źródło: opracowanie własne na podstawie [9-11]
Fig. 7. Accident frequency rate per 1000 employees for selected types of mining in the years 2013-2022. Source: [9-11]

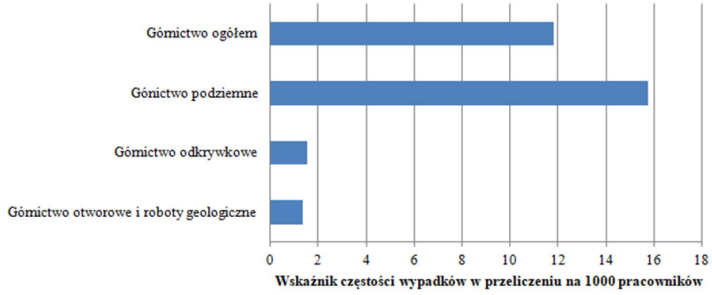

Rys. 8. Średnioroczny wskaźnik częstości wypadków w przeliczeniu na 1000 pracowników dla wybranych rodzajów górnictwa. Źródło: opracowanie własne na podstawie [9-11]
Fig. 8. Average annual accident frequency rate per 1000 employees for selected types of mining. Source: [9-11]

trudnionych jest więcej pracowników, prawdopodobieństwo powstania zdarzenia wypadkowego jest większe niż w jednostkach zatrudniających mniejszą ilość pracowników. To samo dotyczy porównywania branży, spółek czy zakładów w określonym horyzoncie czasu, w którym wystąpiła znacząca zmiana zatrudnienia. Aby zniwelować wpływ zróżnicowania porównywanych grup, liczbę wypadków należy podzielić przez odpowiednią jednostkę. Najczęściej stosuje się wskaźnik częstości wypadków w odniesieniu do 1000 zatrudnionych [5]. W górnictwie stosowany jest jeszcze dodatkowy wskaźnik w oparciu o ilość wydobytej kopaliny – liczba wypadków przy pracy przypadająca na 1 mln ton wydobytej kopaliny.

Na rysunku 6 można zauważyć trend rosnący wskaźnika częstości wypadków w przeliczeniu na 1000 zatrudnionych. W 2014 roku zaistniały 11 wypadki na 1000 pracowników, a w roku 2022 statystycznie wypadków było już 12,5. W analizowanym okresie omawiany wskaźnik maksymalną swoją wartość osiągnął w 2019 roku, gdzie statystycznie wystąpiły 12,7 wypadki na 1000 pracowników.

Rysunek 7 przedstawia wskaźniki częstości wypadków w przeliczeniu na 1000 pracowników w wybranych rodzajach górnictwa. W latach 2013-2022 największe wartości wskaźnika częstości wypadków odnotowano w górnictwie podziemnym. W kopalniach rud miedzi omawiany wskaźnik ma tendencje spadkową. Maksymalną swoją wartość osiągnął w roku 2013, gdzie wystąpiły blisko 23 wypadki na 1000 zatrudnionych pracowników, natomiast w 2022 roku osiągnął swój minimalny poziom, przy którym zanotowano ponad 8 wypadków. Odmiennie kształtuje się wskaźnik dla górnictwa węgla kamiennego, który ma wyraźną tendencje wzrostową. W 2013 roku odnotowano prawie 14 wypadków pracowników zatrudnionych w kopalniach węgla kamiennego, natomiast w 2022 roku omawiany wskaźnik wynosił już ponad 19. W porównaniu z górnictwem podziemnym, na stosunkowo niskim poziomie kształtuje się wskaźnik częstości wypadków dla górnictwa odkrywkowego. W analizowanym okresie ma delikatny trend malejący. Na początku odnotowano ponad 2 wypadki na 1000 pracowników zatrudnionych w kopalniach

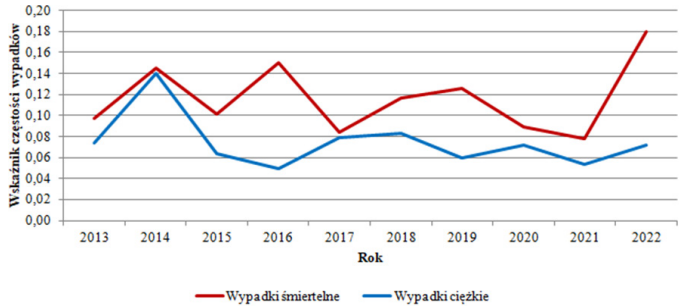

Rys. 9. Wskaźnik częstości wypadków w przeliczeniu na 1000 osób pracujących w górnictwie. Źródło: opracowanie własne na podstawie [9-11]
Fig. 9. Accident frequency rate per 1000 people working in the mining industry. Source: [9-11]

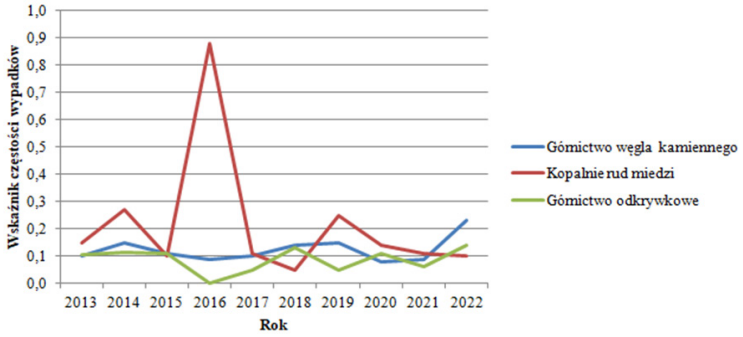

Rys. 10. Wskaźnik częstości wypadków śmiertelnych w przeliczeniu na 1000 pracowników dla wybranych rodzajów górnictwa. Źródło: opracowanie własne na podstawie [9-11]
Fig. 10. Fatal accident rate per 1000 employees for selected types of mining. Source: [9-11]

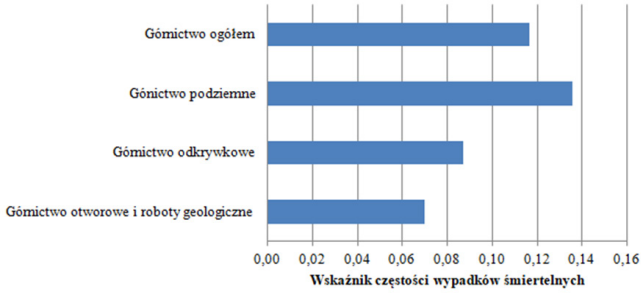

Rys. 11. Średnioroczny wskaźnik częstości wypadków śmiertelnych w przeliczeniu na 1000 pracowników dla wybranych rodzajów górnictwa. Źródło: opracowanie własne na podstawie [9-11]
Fig. 11. Average annual fatal accident rate per 1000 employees for selected types of mining

odkrywkowych, natomiast na koniec analizowanego okresu wskaźnik spadł do wartości 1,4.

Na rysunku 8 przedstawiono średnioroczny wskaźnik częstości wypadków w przeliczeniu na 1000 pracowników w wybranych rodzajach górnictwa. W analizowanym okresie średnioroczny wskaźnik dla całego górnictwa wyniósł 11,8, przy czym dla górnictwa podziemnego wyniósł 15,7 a dla górnictwa odkrywkowego i otworowego, odpowiednio 1,5 i 1,3.

Rysunek 9 przedstawia wskaźniki częstości wypadków w polskim górnictwie dla wypadków śmiertelnych i ciężkich. Wskaźnik dla wypadków ciężkich ma tendencję malejącą, natomiast wskaźnik dla wypadków śmiertelnych z uwagi na wyjątkowo dużą liczbę wypadków śmiertelnych w roku 2022, tendencje rosnącą. W 2013 roku zanotowano 21 wypadków śmiertelnych i 16 ciężkich W 2022 roku tych wypadków było odpowiednio 30 i 12.

Wskaźniki częstości wypadków śmiertelnych dla górnictwa węgla kamiennego i górnictwa odkrywkowego kształtują się podobnie – rysunek 10. W 2013 roku wyniósł on 0,1, co oznacza 1 wypadek śmiertelny na 10 tys. pracowników. W 2022 roku wskaźnik wyniósł odpowiednio 0,23 i 0,14. Od powyższych trendów znacząco odbiega wykres wskaźnika częstotliwości wypadków śmiertelnych występujący w kopalniach rud miedzi. W 2016 roku osiągnął on w analizowanym okresie rekordową wartość wynoszącą 0,88, oznaczając blisko 1 wypadek śmiertelny na 1000 osób zatrudnionych. Spowodowane to było kilkoma zdarzeniami, do których doszło w kopalniach rud miedzi m.in. takich jak: dynamiczne oddziaływanie wstrząsu górotworu (tąpnięcia) – 9 wypadków śmiertelnych, oberwanie się skał ze stropu i ociosów – 4 wypadki śmiertelne, uderzenie przez urządzenia transportu poziomego – 2 wypadki śmiertelne. W tym tragicznym roku w kopalniach rud miedzi zginęło 17 górników.

W ostatniej dekadzie najbardziej niebezpieczną pracą pod względem wypadków śmiertelnych jest praca w podziemnych zakładach górniczych – średniorocznie blisko 14 wypadków śmiertelnych na 100 tyś zatrudnionych – rysunek 11. W kopalniach rud miedzi wskaźnik częstości wypadków śmi-

ertelnych wyniósł ok. 0,22, a w kopalniach węgla kamiennego 0,12, oznaczając statystycznie 2,2 i 1,2 wypadki na 10 tysięcy pracowników. Najmniej wypadków odnotowano w górnictwie otworowym i odkrywkowym – poniżej 1 wypadku na 10 tysięcy zatrudnionych.

Innym wskaźnikiem często stosowanym w górnictwie jest wskaźnik „wydajności", określa on jaka liczba wypadków przypada na milion ton wydobytej kopaliny. W badanym okresie, średniorocznie zanotowano w górnictwie węgla kamiennego 28 wypadków na milion ton wydobytego węgla, natomiast w kopalniach rud miedzi – blisko 10 wypadków na milion ton wydobytej rudy. Stosunkowo niski wskaźnik występuje w kopalniach węgla brunatnego – 5 wypadków na 10 milionów ton wydobytego węgla, wynika on jednak z zupełnie innego rodzaju zagrożeń i specyfiki pracy występującym w kopalniach odkrywkowych.

Podsumowanie

W ostatniej dekadzie nastąpiła poprawa sytuacji gospodarczej kraju, na co wskazują pozytywnie kształtujące się wskaźniki makroekonomiczne. Pomimo okresowego spowolnienia gospodarczego wynikające z pandemii Covid-19 w analizowanym okresie nastąpiło zwiększenie liczby miejsc pracy oraz spadek bezrobocia. W 2022 roku w polskim górnictwie zatrudnionych było łącznie 167 tysięcy osób, które były narażone na liczne zagrożenia, mogące powodować wypadki, urazy i choroby. Na podstawie przeprowadzonej analizy danych pochodzących z Wyższego Urzędu Górniczego jak również z Głównego Urzędu Statystycznego dotyczącego wypadkowości w polskim górnictwie można wysunąć następujące wnioski:

1. W latach 2013-2022 w górnictwie nastąpił 18% spadek liczby poszkodowanych w wypadkach przy pracy, przy jednoczesnej redukcji zatrudnienia o 48 tysięcy osób. W przeliczeniu na 1000 zatrudnionych, wskaźnik częstości wypadków wzrósł w analizowanym okresie o 0,63, co oznacza, że pomimo zmniejszenia liczby całkowitej liczby wypadków, bezpieczeństwo w górnictwie nie uległo poprawie. Łącznie w badanym okresie wypadkom uległo 21,7 tys. osób.
2. W analizowanym okresie wskaźnik częstości wypadków ciężkich jest na podobnym poziomie, natomiast niepokojący jest trend rosnący wskaźnika częstości wypadków śmiertelnych – wzrost o 0,08, co oznacza statystycznie 8 wypadków śmiertelnych więcej na 100 tysięcy zatrudnionych, w porównaniu z początkiem badanego okresu.
3. Najbardziej niebezpieczną pracą pod względem wypadków przy pracy jest praca w podziemnych zakładach górniczych. W omawianym okresie średnioroczny wskaźnik częstości wypadków wyniósł tam 15,7, natomiast wskaźnik częstości wypadków śmiertelnych 0,14, który był dwukrotnie wyższy niż wyliczony wskaźnik dla górnictwa otworowego i robót geologicznych.
4. Pracownicy górnictwa węgla kamiennego stanowią największą grupę osób zatrudnionych w górnictwie, w 2022 roku zatrudnionych było ponad 93 tyś. osób, w tym 68 tyś. to załoga własna. Wskaźnik częstości wypadków ogółem w analizowanym okresie ma wyraźny trend rosnący. W 2022 roku wystąpiło ponad 5 wypadków więcej na 1000 zatrudnionych, niż w roku 2013. Zwiększył się również wskaźnik częstości wypadków śmiertelnych z 0,1 do 0,23, co oznacza, iż w ostatnim analizowanym roku wystąpiło ponad dwukrotnie więcej wypadków śmiertelnych na 1000 zatrudnionych niż w na początku badanego okresu.
5. Statystycznie najbardziej niebezpieczna dla życia pracownika jest praca w kopalniach rud miedzi. Średnioroczny wskaźnik częstości wypadków śmiertelnych w tych kopalniach wyniósł 0,22 i jest najwyższy w całym górnictwie. Przyczyniły się do tego tragiczne zdarzenia mające miejsce w 2016 roku, w którym zginęło 17 górników. Odmiennie kształtuje się za to wskaźnik częstości wypadków ogółem, który w przypadku kopalń rud miedzi ma wyraźną tendencje spadkową. Z 22,9 w 2013 roku, spadł do 8,4 w roku 2022. Oznacza to blisko 15 wypadków mniej na 1000 zatrudnionych.
6. Najmniejsza wypadkowość występuje w górnictwie otworowym i robotach geologicznych. Wskaźnik częstości wypadków ogółem jest 10 krotnie mniejszy niż w całym górnictwie i średniorocznie dla analizowanego okresu wyniósł 1,36. Drugim rodzajem górnictwa, w którym występuje najmniej wypadków jest górnictwo odkrywkowe – wskaźnik częstości wypadków ogółem wyniósł 1,53. Pomimo stosunkowo niskiej wypadkowości w górnictwie odkrywkowym występują tam liczne wypadki ciężkie i śmiertelne. W 2022 roku wskaźnik częstości wypadków śmiertelnych był wyższy niż w kopalniach rud miedzi i wyniósł 0,14.
7. Warunki pracy dla górnictwa podziemnego są odmienne od prac prowadzonych na powierzchni. Występują inne zagrożenia i niebezpieczeństwa, mogące powodować wypadki, urazy i choroby. Przedstawiona analiza wskaźnikowa wypadkowości w górnictwie wydaje się potwierdzać te różnice.

Literatura – References

1. Ogrodnik R.; Burtan Z.; Kapusta M. Natural and technical hazards affecting the status of safety in the polish open-pit mines, Modern Menagement Review. 2016, 24, 99-115. http://doi.prz.edu.pl/pl/pdf/zim/288
2. Burtan Z.; Kapusta M.; Ogrodnik R. Natural hazards affecting the status of safety in the Polish coal mining. Zagrożenia na stanowiskach pracy : wybrane zagadnienia, Oficyna Wydawnicza Politechniki Rzeszowskiej, Rzeszów 2017.
3. Saleh J.; Cummings E. Safety in the mining industry and the unfinished legacy of mining accidents: Safety levers and defense-in-depth for addressing mining hazards, Safety Science. 2011, 49, 764-777; https://doi.org/10.1016/j.ssci.2011.02.017.
4. Liu Q.; Meng X.; Hassall M.; Li X. Accident-causing mechanism in coal mines based on hazards and polarized management. Safety Science. 2016, 85, 276-281; https://doi.org/10.1016/j.ssci.2016.01.012.
5. Ogrodnik R.; Kapusta M. Analysis of the level and structure of accidents in Polish industry. Bezpieczeństwo pracy - edukacja i dobre praktyki, ART-TEKST, Kraków 2019.
6. Wyganowska M.; Tobór-Osadnik M. Analysis of mining accident levels against the employment in the hard coal mining industry, Journal of the Polish Mineral Engineering Society. 2022, 49,117–121; https://doi.org/10.29227/IM-2022-01-14.
7. Ustawa z dnia 30 października 2002 r. o ubezpieczeniu społecznym z tytułu wypadków przy pracy i chorób zawodowych. Tekst jednolity. Dz. U. 2022 poz. 2189
8. Dudka, J.; Bojanowski, J. Metodyka statystycznych analiz wypadków przy pracy. Centralny Instytut Ochrony Pracy - Państwowy Instytut Badawczy, Warszawa 2007.
9. Statistical data GUS. Rocznik Statystyczny Przemysłu. Główny Urząd Statystyczny, Warszawa.
10. Statistical data WUG. Stan bezpieczeństwa i higieny pracy w górnictwie. Wyższy Urząd Górniczy. Katowice.
11. Statistical data WUG. Ocena stanu bezpieczeństwa pracy, ratownictwa górniczego oraz bezpieczeństwa powszechnego w związku z działalnością górniczo-geologiczną, Wyższy Urząd Górniczy. Katowice.
12. Słownik Języka Polskiego. Wydawnictwo Naukowe PWN. Warszawa 2015.

Assessment of Occupational Safety Based on the Analysis of Accidents in the Mining Industry

The main purpose of the work is to present the level of accidents in the Polish mining industry and to obtain answers, among others, to the following questions: what are the accident rates in the last decade and in which types of mining do the most accidents at work occur? In order to achieve the objectives of the work, statistical data from the years 2013-2022 from the State Mining Authority and the Central Statistical Office were analyzed. The data analysis was carried out for the entire mining industry as well as for its individual types, i.e. underground, open pit and borehole mining. In addition to the absolute accident rate analysis, an indicator analysis was also used, with particular emphasis on the frequency rates of accidents at work: total, severe and fatal. The work also defines the basic concepts of accidents at work.

Keywords: *accidents, accident rate, mining, mining companies*

Analiza efektywności finansowej przedsiębiorstw sektora paliwowego w dobie przemian energetycznych

Robert RANOSZ[1)], Joanna JAKÓBCZYK[2)], Klaudia PALMOWSKA[3)]

[1)] AGH University in Krakow, Faculty of Civil Engineering and Resource Management, Krakow, Poland; email: rranosz@agh.edu.pl, ORCID: 0000-0001-7478-9129

[2)] AGH University in Krakow, Faculty of Civil Engineering and Resource Management, Krakow, Poland; ORCID: 0000-0001-5030-9637

[3)] AGH University in Krakow, Faculty of Civil Engineering and Resource Management, Krakow, Poland

http://doi.org/10.29227/IM-2023-01-32

Submission date: 21-05-2023 | Review date: 12-06-2023

Abstrakt

Celem niniejszego artykułu jest zbadanie podstawowych wielkości finansowych dla przedsiębiorstw sektorów produkujących energię elektryczną z następujących źródeł: z paliw kopalnych, nuklearnej, wodnej, słonecznej, wiatrowej oraz geotermalnej i biomasy. Badane wielkości finansowe to: zysk netto, poziom aktywów oraz kapitału własnego. Na podstawie tych wielkości dokonano obliczenia podstawowych wskaźników rentowności tj.: ROA i ROE. Wyniki badań jednoznacznie wskazują, iż przedsiębiorstwa z sektora bazującego na produkcji energii z paliw kopalnych osiągają najgorsze wyniki zarówno rentowności, jak i nominalnego wyniku netto. Jednocześnie są spółkami, które posiadają największy poziom aktywów. Z drugiej strony przedsiębiorstwa z sektora energii wiatrowej okazały się być najbardziej efektywnymi zarówno pod kątem rentowności kapitału własnego, jak i aktywów przy jednoczesnym najniższym poziomie aktywów.

Słowa kluczowe: *energia, wyniki finansowe, źródła energii, surowce, zysk netto, aktywa, kapitał własny, ROA, ROE*

1. Wprowadzenie

Wytwarzanie oraz konsumpcja energii należą do podstawowych procesów zachodzących na Ziemi. Na przestrzeni wieków można zauważyć głębokie zmiany występujące w tym sektorze. W dzisiejszych czasach dotyczą one głównie odchodzenia od konwencjonalnych źródeł energii na rzecz energetyki odnawialnej. Taką tendencję w szczególności można zaobserwować w Europie [1,2,3,4,5]. Dodatkowo energetyka centralnie planowana zastępowana jest rozproszonymi źródłami energii [6].

Zmiany dotyczące struktury energetyki przekładają się także na sytuację finansową przedsiębiorstw z tego sektora. Jedynie firmy, które umieją dostosowywać się do obecnych uwarunkowań odniosą sukces na rynku, a co za tym idzie, ich kondycja finansowa ulegnie poprawie. Problemy oceny efektywności funkcjonowania przedsiębiorstw branży energetycznej w Polsce, a także sytuacja i wyniki finansowe, zdeterminowane w dużym stopniu przez zmienność cen węgla, były przedmiotem publikacji [7,8,9].

Istotny wpływ na sektor energetyczny mają również występujące kryzysy gospodarcze, które przynoszą często trudne do naprawy skutki. Za ostatni taki kryzys uznaje się pandemię COVID-19 [10,11,12], oraz wojnę w Ukrainie, które to zdarzenia spowodowały wiele zakłóceń w światowej energetyce [13,14]. Dlatego tak istotna jest odpowiednia ocena stanu jednostki gospodarczej oraz umiejętne dostosowywanie decyzji do panujących warunków [15].

Sukces przedsiębiorstwa zależny jest m.in. od poziomu rozwoju danej jednostki, osiąganiu założonych celów, a także od wzrostu jej stanu majątkowo-kapitałowego czy umiejętności zmniejszenia zagrożeń, które potencjalnie mogą pojawić się w przyszłości [15,16,17,18,19]. Jednym z głównych aspektów, na których koncentrują się podmioty z branży energetycznej to wzrost efektywności [4]. Niezbędne jest zatem zbadanie sytuacji przedsiębiorstwa w przeszłości, tak aby dopasować je do obecnych warunków gospodarczych i zapewnić lepszą przyszłość, poprzez podejmowanie odpowiednich decyzji. Analiza finansowa poprzez wykorzystanie swoich narzędzi umożliwia określenie aktualnej sytuacji finansowej firm oraz stanowi źródło informacji odnośnie funkcjonowania przedsiębiorstw w przyszłości [20].

2. Istota analizy finansowej w przedsiębiorstwie

Źródła energii (zarówno te odnawialne, jak i konwencjonalne), są jednym z głównych czynników kształtujących sytuację ekonomiczną wielu krajów, a w konsekwencji poszczególnych przedsiębiorstw w nich funkcjonujących. Energia jest potrzebna nie tylko do komfortowego funkcjonowania poszczególnych gospodarstw domowych, ale także dla przedsiębiorstw funkcjonujących na wolnym rynku. Ponieważ celem każdego przedsiębiorstwa jest efektywność finansowa mająca przynosić określone efekty ekonomiczne, niezbędne jest stałe badanie jego sytuacji finansowej by odpowiednio reagować na dokonujące się zmiany w strukturze energetyki i występujące kryzysy gospodarcze.

Przedmiotem badań analizy finansowej są wielkości ekonomiczne takie jak [21, 22]:

- Stan majątkowo-finansowy przedsiębiorstwa,
- Wynik finansowy,
- Płynność finansowa firmy.

Analiza finansowa to instrument zarządzania finansami, którego główną istotą jest obserwacja poszczególnych danych ekonomicznych oraz wyciąganie wniosków, które pozwolą określić aktualną kondycję przedsiębiorstwa. Celem analizy jest zebranie informacji, które umożliwiają osiągnięcie od-

powiedniej struktury majątku oraz racjonalne zarządzanie strumieniami pieniężnymi. Analiza finansowa gwarantuje stałą kontrolę kosztów, przychodów oraz wyniku finansowego. Dodatkowo ułatwia ocenę efektywności finansowej przedsiębiorstwa oraz umożliwia podejmowanie decyzji w zakresie dalszego rozwoju firmy i inwestycji [21, 23].

Podstawowym źródłem danych niezbędnym do przeprowadzenia analizy finansowej jest sprawozdanie finansowe. Sprawozdanie finansowe zawiera wszystkie niezbędne informacje na temat rocznej działalności finansowej przedsiębiorstwa i sporządzane jest na dzień zamknięcia ksiąg rachunkowych [24].

Wyróżnia się dwa podstawowe etapy analizy finansowej [25]:

- Wstępną analizę sprawozdań finansowych,
- Analizę wskaźnikową.

Wstępna analiza sprawozdań finansowych umożliwia pozyskanie podstawowych informacji na temat struktury majątkowo-kapitałowej oraz dynamiki finansowej przedsiębiorstwa. W skład analizy finansowej wchodzi analiza pionowa oraz pozioma [21,25].

Drugi etap stanowi analiza wskaźnikowa, której głównym celem jest rozwinięcie uzyskanych wyników ze wstępnej analizy. Analiza wskaźnikowa umożliwia ocenę sytuacji finansowej w firmie oraz badanie zachodzących trendów.

3. Metodologia

Analiza finansowa przedsiębiorstw z sektora energetycznego została przeprowadzona na podstawie danych z Serwisu Ekonomicznego EMIS dla lat 2018–2021. Analizie poddano 9500 (dane surowe) przedsiębiorstw z poszczególnych kontynentów. Z uwagi na fakt, iż serwis EMIS nie ma dostępu do wszystkich przedsiębiorstw z każdego państwa na świecie, dane swoim zasięgiem obejmują następujące kontynenty oraz państwa:

- Afryka (South Africa, Kenya, Zambia, Mauritius, Nambia, Maroco, Algeria, Ghana, Nigeria, Ivory Coast, Mozambique, Egypt)
- Ameryka południowa (Chile, Brazil, Uruguay, Colombia, Peru, Argentina, Ecuador, Panama, Bolivia, Venezuela)
- Ameryka Północna (Mexico)
- Azja (South Korea, China, Thailand, Malaysia, Hong Kong SAR, China, United Arab Emirates, Russia, India, Turkey, Indonesia, Pakistan, Vietnam, Qatar, Iran, Jordan, Oman, Taiwan, Kazakhstan, Bangladesh, Singapore, Palestine, Sir Lanka, Moldavia, Azerbaijan, Laos, Uzbekistan, Armenia, Saudi Arabia, Kuwait, Philippines)
- Europa (Poland, Ukraine, Slovakia, Seribia, Hungary, Croatia, Romania, Bosnia and Herzegovina, Lithuania, Bulgaria, Czech Republic, Estonia, Latvia, Slovenia, Montenegro, North Macedonia, Moldavia)

Analizie poddano następujące dane finansowe: zysk netto, aktywa ogółem, kapitał własny, wskaźniki rentowności. Wskaźniki rentowności dostarczają informacji odnośnie zyskowności przedsiębiorstwa. Analiza rentowności przedsiębiorstwa najczęściej stosowana jest w trzech głównych obszarach działalności [25]:

- Sprzedaży – Rentowność sprzedaży (Return on Sales),
- Aktywów – Rentowność aktywów (Return on Assets),
- Kapitału – Rentowność kapitału własnego (Return on Equity).

Do analizy finansowej przedsiębiorstw z sektora energetycznego wykorzystano dwa główne wskaźniki rentowności: wskaźnik rentowności aktywów, wskaźnik rentowności kapitału własnego.

Wskaźnik rentowności aktywów wyrażony jest za pomocą wzoru numer 1 [26].

$$ROA = (\text{zysk netto}) / (\text{aktywa ogółem}) \quad (1)$$

Wskaźnik rentowności kapitału własnego wyrażony jest za pomocą wzoru numer 2 [9].

$$ROE = (\text{zysk netto}) / (\text{kapitał własny}) \quad (2)$$

4. Analiza finansowa przedsiębiorstw z sektora energetycznego

4.1 Zysk netto

Jako pierwszy został poddany analizie zysk netto przedsiębiorstw produkujących energię z poszczególnych źródeł. Średnie zyski netto dla poszczególnych sektorów zostały przedstawione w tabeli 1.

Przedsiębiorstwa z sektora energetycznego, w analizowanych latach i poszczególnych segmentach, generowały dodatnie wyniki finansowe. Wyjątkiem są tutaj dwa segmenty, a mianowicie: segment bazujący na produkcji energii z paliw kopalnych (lata 2019 oraz 2020) oraz segment bazujący na produkcji energii słonecznej (rok 2020).

W ramach segmentu bazującego na produkcji energii z paliw kopalnych, wynik finansowy w roku 2019 był spowodowany w głównej mierze przez afrykańskie przedsiębiorstwo Eskom Holdings Soc Limited oraz w Europie, które były wywołane przez polską firmę PGE S.A.

W roku 2021 zysk netto przekroczył poziom 5 mln USD. Najistotniejszy wpływ na ten wynik miał wzrost średniego zysku operacyjnego firm mających swoje siedziby Ameryce Południowej, Azji i w Europie oraz zmniejszenie straty w Eskom Holdings Soc Limited w Afryce. Natomiast w Azji największe zyski przynosiły firmy z siedzibą w Chinach takie jak: China Shenhua Energy Company Limited, Yankuang Energy Group Company Limited oraz Sdic Power Holdings Co., Ltd, a także Abu Dhabi National Energy Company Pjsc z siedzibą w Zjednoczonych Emiratach Arabskich.

W roku 2018 średni zysk netto generowany przez przedsiębiorstwa bazujące na energii nuklearnej wynosił 797,09 mln USD. Największy wpływ na ten wynik miała Ameryka Południowa oraz Azja. Spadek zysku netto w roku 2019 spowodowany był stratami występującymi w amerykańskiej firmie produkującej energię nuklearną. Wartość zysku netto w Azji w roku 2020 to głownie zasługa eliminacji strat w rosyjskim przedsiębiorstwie Rusatom Service+ AO. Największy średni zysk netto wynoszący 904,56 mln USD odnotowano w roku 2021, na co główny wpływ miały cztery azjatyckie przedsiębiorstwa: Cgn Power Co., Ltd oraz China National Nuclear Power Co., Ltd z siedzibą w Chinach, indyjska firma Nuclear Power Corporation Of India Limited, a także CGN Power Company Limited z siedzibą w Hong Kongu.

Tab. 1. Średni zysk netto wygenerowany przez przedsiębiorstwa w poszczególnych segmentach w mln USD. Opracowanie własne na podstawie [27]
Tab. 1. Average net profit generated by enterprises in individual segments in USD million. Own elaboration based on [27]

Źródło energii	2018	2019	2020	2021
Energia z paliw kopalnianych	$ 107,37	$ -150,74	$ -144,31	$ 5,31
Energia nuklearna	$ 797,09	$ 71,03	$ 138,46	$ 904,56
Energia wodna	$ 46,95	$ 56,81	$ 78,77	$ 55,23
Energia słoneczna	$ 4,35	$ 3,47	$ -7,29	$ 17,94
Energia wiatrowa	$ 88,86	$ 120,72	$ 86,97	$ 201,79
Energia geotermalna i z biomasy	$ 29,03	$ 17,13	$ 24,25	$ 26,30

Tab. 2. Średnia wartość aktywów firm, których główną działalnością jest produkcja energii z paliw kopalnianych wyrażona w mln USD. Opracowanie własne na podstawie [27]
Tab. 2. Average value of assets of companies whose main activity is the production of energy from fossil fuels, expressed in USD million. Own elaboration based on [27]

Źródło energii	2018	2019	2020	2021
Energia z paliw kopalnianych	$ 15 617,73	$ 13 607,01	$ 12 589,35	$ 15 496,60
Energia nuklearna	$ 5 909,40	$ 5 432,06	$ 5 854,05	$ 27 396,07
Energia wodna	$ 1 718,74	$ 1 811,36	$ 1 802,34	$ 1 891,55
Energia słoneczna	$ 634,43	$ 745,49	$ 798,03	$ 1 230,75
Energia wiatrowa	$ 2 048,16	$ 2 211,05	$ 2 105,45	$ 3 768,28
Energia geotermalna i z biomasy	$ 953,91	$ 965,44	$ 994,08	$ 633,62

Średni zysk netto dla przedsiębiorstw, których główną działalnością jest produkcja energii wodnej, w roku 2018 wynosił 46,95 mln USD, a wpływ na taki wynik miała Ameryka Południowa, Azja oraz jedyna afrykańska firma Kenya Electricity Generating Company Plc. W roku 2019 nastąpił wzrost średniego zysku o prawie 10 mld USD głownie dzięki amerykańskim i azjatyckim koncernom.

W roku 2018 wartość średniego zysku netto dla firm produkujących energię słoneczną wynosiła nieco ponad 4 mln USD, a największy wpływ na ten wynik miały cztery azjatyckie przedsiębiorstwa: Hanergy Thin Film Power Group Limite i GCL New Energy Holdings Limited z Hong Kongu, Qatar Electricity & Water Company Q.P.S.C. oraz Banpu Power Pcl z Tajlandi. W roku 2018, 2020 i 2021 odnotowano straty w afrykańskim przedsiębiorstwie Azure Power Global Limited zajmującym się produkcją energii słonecznej na Mauritiusie. Spowodowało to ujemny światowy zysk netto w roku 2020. Najwyższy średni zysk netto równy 17,94 mln USD odnotowano już rok później, a istotny wpływ na ten wynik miało pojawienie się danych finansowych przedsiębiorstwa z Ameryki Południowej

Średni zysk netto dla przedsiębiorstw bazujących na energii wiatrowej w roku 2018 wynosił 88,86 mln USD, a największy wpływ na ten wynik miały azjatyckie przedsiębiorstwa z siedzibą w Hong Kongu oraz Ameryka Południowa, gdzie zdecydowanym liderem była firma ENEL Generacion Chile S.A. i brazylijskie koncerny energetyczne. W roku 2019 nastąpił wzrost średniego zysku netto o ponad 30 mln USD. Główne zmiany zaszły w Europie, ponieważ PGE Energia Odnawialna S.A. i Enel Green Power Romania SRL przyniosły znaczące zyski. W roku 2020 odnotowano spadek zysków spowodowany głownie przez rumuńską firmę. Znaczny wzrost miał miejsce w roku 2021, wpływ na to miała amerykańska firma ENEL Generacion Chile S.A., która przestała odnotowywać straty, oraz azjatyckie przedsiębiorstwa z Chin i Hong Kongu, które zwiększyły swoje zyski netto.

W roku 2018 średni zysk netto dla firm, których główną działalnością jest produkcja energii geotermalnej i energii z biomasy, wynosił 29,03 mln USD. Największy wpływ na ten wynik miały dwa brazylijskie przedsiębiorstwa produkujące energię z biomasy: Sao Martinho S.A. oraz Companhia Agricola e Pecuaria Lincoln Junqueira, a także azjatyckie firma Energy Absolute Pcl z siedzibą w Tajlandii. Istotną rolę odegrały także wysokie średnie zyski netto firm, które zajmują się produkcją energii geotermalnej, głównie Paju Energy Service Co.,Ltd. z Korei Południowej oraz Societatea Nationala z Rumuni. W roku 2019 odnotowano spadek średniego zysku netto na świecie, który był wywołany niskimi zyskami w Ameryce Południowej. Dodatkowo brazylijskie firmy Guarani S.A. oraz Usina Eldorado S.A-em Recuperacao Judicial zaraportowały straty w tym okresie. Sytuacja w Ameryce Południowej znacząco polepszyła się w roku 2020, gdy średni zysk netto na tym kontynencie wzrósł o ponad 20 mln USD. W tym okresie znacząco obniżyły się zyski w Azji. W roku 2021 wzrosły wyniki firm z Ameryki Południowej oraz Azji.

4.2. Aktywa ogółem

Jako drugi został poddany analizie poziom aktywów przedsiębiorstw produkujących energię z poszczególnych źródeł. Średni poziom aktywów dla poszczególnych sektorów zostały przedstawione w tabeli 2.

Średnia wartość aktywów dla firm produkujących energię z paliw kopalnych na świecie w latach 2018-2021 mieściła się w zakresie od około 12 mld USD do około 15,5 mld USD. Corocznie niekwestionowanym liderem w średniej wartości aktywów było przedsiębiorstwo Eskom Holdings Soc Limited z siedzibą w Republice Południowej Afryki. Średnie aktywa Ameryki Południowej utrzymywały się na poziomie ponad 3 mld USD, a dopiero w ostatnim okresie raportowania zwiększyły się aż do blisko 5,5 mld USD. Na ten wynik wpłynęły głównie dwa przedsiębiorstwa: ENEL Americas S.A. z Chile oraz Neoenergia S.A. z siedzibą w Brazylii. W Ameryce Północnej średnie wartości aktywów stale rosły za zasługą dwóch meksykańskich firm: Infraestructura Energetica Nova, S.A.B. de C.V. oraz Naturgy Mexico, S.A. de C.V. Na średnią wartość aktywów w Azji główny wpływ miały przedsiębiorstwa z Chin oraz z Hong Kongu.

W przypadku przedsiębiorstw produkujących energię nuklearną na świecie średnia wartość aktywów osiągnęła swój najwyższy wynik w roku 2021 równy 27 396,07 mln USD. Szczególnie istotną rolę na wzrost tej danej miała Azja, której średnia aktywów w roku 2021 znacząco przewyższała średnią

Tab. 3. Średnia wartość kapitału własnego firm, których główną działalnością jest produkcja energii z paliw kopalnianych wyrażona w mln USD. Opracowanie własne na podstawie [27]

Tab. 3. Average value of equity of companies whose main activity is the production of energy from fossil fuels, expressed in USD million. Own elaboration based on [27]

Źródło energii	2018	2019	2020	2021
Energia z paliw kopalnianych	$ 4 400,65	$ 3 656,71	$ 3 697,22	$ 5 322,23
Energia nuklearna	$ 1 747,11	$ 1 927,07	$ 2 240,94	$ 9 356,33
Energia wodna	$ 846,35	$ 883,06	$ 904,35	$ 950,94
Energia słoneczna	$ 164,17	$ 209,23	$ 208,33	$ 358,08
Energia wiatrowa	$ 896,68	$ 1 002,39	$ 894,08	$ 1 501,66
Energia geotermalna i z biomasy	$ 401,16	$ 375,71	$ 371,12	$ 238,62

Tab. 4. Finansowanie kapitałem własnym dla przedsiębiorstw z poszczególnych sektorów. Opracowanie własne

Tab. 4. Equity financing for enterprises from individual sectors. Own study

Źródło energii	2018	2019	2020	2021
Energia z paliw kopalnianych	28.18%	26.87%	29.37%	34.34%
Energia nuklearna	29.56%	35.48%	38.28%	34.15%
Energia wodna	49.24%	48.75%	50.18%	50.27%
Energia słoneczna	25.88%	28.07%	26.11%	29.09%
Energia wiatrowa	43.78%	45.34%	42.47%	39.85%
Energia geotermalna i z biomasy	42.05%	38.92%	37.33%	37.66%

światową. Tak wysoki wynik ustanowiły cztery dominujące firmy w sektorze energetyki nuklearnej w Azji: Cgn Power Co., Ltd oraz China National Nuclear Power Co., Ltd. z siedzibą w Chinach, CGN Power Company Limited z Hong Kongu oraz Nuclear Power Corporation Of India Limited.

Średnie wartości aktywów dla przedsiębiorstw bazujących na produkcji energii wodnej stale rosły od wartości 1 718,74 mln USD w roku 2018 do 1 891,55 mln USD w 2021. Największy wpływ na ten wynik miała Afryka, a dokładniej przedsiębiorstwo Kenya Electricity Generating Company Plc. Aktywa w Ameryce Południowej również ciągle zwiększały swoją wartość, głownie dzięki firmie Minera Valparaiso S.A. z Chile oraz brazylijskim przedsiębiorstwom. Najmniejsza średnia wartość aktywów wystąpiła w Europie, ponieważ była ona na poziomie około 500 mln USD.

Z kolei średnia wartość aktywów dla przedsiębiorstw produkujących energię słoneczną firm na świecie w roku 2018 wynosiła 634,43 mln USD i co rok rosła, aż do roku 2021, w którym odnotowano szczytową wartość równą 732,09 mln USD. Największą wartość aktywów wśród firm produkujących energię ze słońca zaobserwowano w Afryce, a dokładniej w koncernie Azure Power Global Limited z siedzibą na Mauritiusie. Azjatyckie firmy o największych aktywach znajdują się w Hong Kongu, w Katarze oraz w Tajlandii.

Natomiast dla przedsiębiorstw produkujących energię wiatrową średnia wartość aktywów w 2018 wynosiła 2048,16 mln USD i rosła, aż do 3 768,28 mln USD w 2021 roku. W roku 2010 odnotowano spadki wartości aktywów w Ameryce Południowej oraz w Europie. Spadek w Ameryce spowodowany był zmniejszeniem się ilości aktywów trzech głównych przedsiębiorstw zajmujących się produkcją energii wiatrowej tj. Companhia Paranaense de Energia - Copel oraz Edp - Energias do Brasil S.A. z siedzibą w Brazylii, a także ENEL Generacion Chile S.A. z Chile. Natomiast na obniżkę wartości aktywów wpłynęła sytuacja finansowa polskiej firmy PGE Energia Odnawialna S.A. Średnia Aktywów w Azji z roku na rok wciąż rosła, głownie dzięki chińskiej firmie China Three Gorges Renewables (Group) Co.,Ltd oraz trzem przedsiębiorstwom z Hong Kongu: China Longyuan Power Group Corporation Limited, Beijing Jingneng Clean Energy Company Limited, China Suntien Green Energy Corporation Limited.

W latach 2018-2020 średnia wartość aktywów dla firm produkujących energię geotermalną i energię z biomasy stale rosła osiągając najwyższy poziom w roku 2020 równy 994,08 mln USD. W roku 2021 nastąpił spadek do 633,62 mln USD, wywołany głównie obniżką wartości aktywów w Azji i w Europie.

4.3. Kapitał własny

Jako trzeci został poddany analizie poziom kapitałów własnych przedsiębiorstw produkujących energię z poszczególnych źródeł. Średni poziom kapitałów własnych dla poszczególnych sektorów zostały przedstawione w tabeli 3.

Średnia wartość kapitału własnego dla firm, których główną działalnością jest produkcja energii z paliw kopalnych, mieściła się w przedziale od 3 656,71 mln USD w roku 2019 do 5 322,23 mln USD w 2021. W tym okresie największy kapitał własny wśród firm zajmujących się produkcją energii z paliw kopalnych zgromadziło przedsiębiorstwo Eskom Holdings Soc Limited w Republice Południowej Afryki. Średni kapitał własny w Ameryce Południowej wynosił ponad 1 500 mln USD w latach 2018 i 2002. W roku 2019 wzrósł on o około 200 mln USD, natomiast w roku 2021 wynosił blisko 2 500 mln USD. Najistotniejszy wpływ na takie wyniki miało przedsiębiorstwo ENEL Americas S.A.z siedzibą w Chile. Kapitał własny w Ameryce Północnej osiągnął wartość ponad 2 600 mln USD w roku 2018 i ciągle rósł, aż do ponad 3 mld USD w ostatnim okresie raportowania. Na ten wynik główny wpływ miało meksykańskie przedsiębiorstwo Infraestructura Energetica Nova, S.A.B. de C.V. Zbliżone wartości odnotowano w Azji, z tą różnicą, że w roku 2019 zaobserwowano delikatny spadek wartości kapitału własnego. Głównym liderem w Azji było przedsiębiorstwo China Shenhua Energy Company Limited. Średni kapitał własny Europy w latach 2018-2020 był zbliżony do poziomu 1 mld USD. Wysoki wzrost tej wartości miał miejsce w roku 2021.

Przedsiębiorstwa, których główną działalnością jest produkcja energii nuklearnej, w 2018 roku osiągnęły średnią wartość kapitału własnego na poziomie 1 747,11 mln USD i wartość ta ciągle rosła, a swój szczytowy wynik równy 9 356,33 mln USD osiągnęła w roku 2021. Największe średnie kapitały własne zaobserwowano w Azji. W latach 2018–2020

Tab. 5. Poziom wskaźnika ROA dla poszczególnych sektorów. Opracowanie własne.
Tab. 5. ROA level for individual sectors. Own study.

Źródło energii	2018	2019	2020	2021
Energia z paliw kopalnianych	0.69%	-1.11%	-1.15%	0.03%
Energia nuklearna	13.49%	1.31%	2.37%	3.30%
Energia wodna	2.73%	3.14%	4.37%	2.92%
Energia słoneczna	0.69%	0.47%	-0.91%	1.46%
Energia wiatrowa	4.34%	5.46%	4.13%	5.35%
Energia geotermalna i z biomasy	3.04%	1.77%	2.44%	4.15%

Tab. 6. Poziom wskaźnika ROE dla poszczególnych sektorów. Opracowanie własne
Tab. 6. ROE level for individual sectors. Own study

Źródło energii	2018	2019	2020	2021
Energia z paliw kopalnianych	2.44%	-4.12%	-3.90%	0.10%
Energia nuklearna	45.62%	3.69%	6.18%	9.67%
Energia wodna	5.55%	6.43%	8.71%	5.81%
Energia słoneczna	2.65%	1.66%	-3.50%	5.01%
Energia wiatrowa	9.91%	12.04%	9.73%	13.44%
Energia geotermalna i z biomasy	7.24%	4.56%	6.53%	11.02%

mieściły się one w przedziale od około 3,4 do 4,6 mld USD. Najwyższy wynik wynoszący ponad 18 mld USD odnotowano w 2021, na który najistotniejszy wpływ miały 2 przedsiębiorstwa z Chin oraz CGN Power Company Limited z Hong Kongu. Średnia wartość kapitału własnego przedsiębiorstw produkujących energię nuklearną w Europie mieściła się na poziomie powyżej 1 mld USD. Liderami w tej kategorii była słowacka firma Slovenske Elektrarne,a.s. oraz przedsiębiorstwo Kozloduy NPP EAD z Bułgarii. Najniższy średni kapitał własny odnotowano w Ameryce Południowej w brazylijskim koncernie Eletrobras Termonuclear S.A.

Z kolei średnia wartość kapitału własnego dla firm, których główną działalnością jest produkcja energii wodnej na świecie, ciągle rosła, osiągając najwyższy poziom 950,94 mln USD w roku 2021. Zdecydowanym liderem okazała się być Afryka, a dokładniej firma Kenya Electricity Generating Company Plc. Z roku na rok zwiększały się także średnie kapitały własne w Azji, które mieściły się w przedziale od około 580 do 770 mln USD oraz w Europie, które osiągały wartości między 300 a 414 mln USD. W Azji zdecydowanymi liderami były dwa chińskie przedsiębiorstwa China Yangtze Power Co., Ltd oraz Huaneng Lancang River Hydropower In. W Europie firma o najwyższej średniej wartości kapitału własnego to Ukrhydroenergo PrA z siedzibą na Ukrainie. Jedyny spadek średniego kapitału własnego został odnotowany w Ameryce Południowej w roku 2020 i wynikał z obniżenia wartości kapitału w brazylijskich przedsiębiorstwach Centrais Eletricas Norte Brasil S.A. oraz Cesp - Cia Energetica de Sao Paulo, a także w firmie Minera Valparaiso S.A. z Chile.

Firmy, których główną działalnością jest produkcja energii słonecznej, w roku 2018 osiągnęły średnią wartość kapitału własnego równą 164,17 mln USD, w latach kolejnych wzrosła ona o około 20 mln USD. Najwyższą wartość średniego kapitału na świecie odnotowano w roku 2021, na którą wpływ miała głównie Ameryka Południowa. Na wynik Ameryki najistotniejszy wpływ miały dwa przedsiębiorstwa: Compania Nacional de Fuerza Electrica S.A. z Chile oraz Omega Energia S.A. z siedzibą w Brazylii. Najwyższą średnią wartość kapitału własnego w Afryce równą 367,16 mln USD odnotowano w roku 2019, a za ten wynik odpowiedzialna była firma Azure Power Global Limited z siedzibą na Mauritiusie. Wartość kapitałów w Azji sukcesywnie rosła osiągając najwyższy wynik w 2021 wynoszący 304,35 mln USD. Największy kapitał zgromadziło przedsiębiorstwo Qatar Electricity & Water Company Q.P.S.C, a istotny wpływ miały również firmy z Hong Kongu i z Tajlandii. Wśród europejskich koncernów zajmujących się produkcją energii słonecznej największą wartość kapitału została osiągnięta w roku 2020 głownie dzięki dwóm przedsiębiorstwom ze Słowenii: Teb D.o.o. oraz Interenergo D.o.o..

Natomiast średnia wartość kapitału własnego dla firm, których główną działalnością jest produkcja energii wiatrowej, w 2018 wynosiła 896,68 mln USD, w roku następnym odnotowano wzrost tej wartości do około 1 mld USD, a w okresie kolejnym niewielki spadek. Najwyższą wartość wynoszącą 1 501,66 mln USD zaobserwowano w roku 2021. Regionami, które miały najistotniejszy wpływ ta ten wynik była Ameryka Południowa oraz Azja. Wartość średniego zgromadzonego kapitału w Ameryce w latach 2018–2019 mieściła się na poziomie około 1,3 mld USD, w 2020 odnotowano spadek o ponad 150 mln USD, natomiast już w roku 2021 wartość ta przekroczyła 1,6 mld USD. Na ten wynik przełożyły się głównie kapitały brazylijskich firm tj: Companhia Paranaense de Energia – Copel i Edp – Energias do Brasil S.A. oraz przedsiębiorstwa ENEL Generacion Chile S.A. W Azji średni kapitał własny ciągle rósł, osiągając najwyższą wartość w roku 2021 wynoszącą ponad 1,3 mld USD. Wśród azjatyckich firm występowało dwóch liderów, którzy mieli zgromadzony największy kapitał własny – pierwszy z nich to chińska firma China Three Gorges Renewables (Group) Co.,Ltd., zaś drugi to China Longyuan Power Group Corporation Limited z Honk Kongu. Europa najwyższą średnią kapitału własnego odnotowała w roku 2019 równą 703,01 mln USD, a rok później nastąpił spadek o około 30%. Sytuacja ta była głównie spowodowana spadkiem kapitałów w polskiej firmie PGE Energia Odnawialna S.A. Przedsiębiorstwa z Europy w roku 2021 nie zamieściły danych finansowych.

W latach 2019–2020 średnia wartość kapitału własnego dla firm, których główną działalnością jest produkcja energii geotermalnej i energii z biomasy, wynosiła nieco ponad 370 mln USD, a swoją najwyższą wartość równą 401,16 mln USD osiągnęła w roku 2018. W Ameryce Południowej największą wartość średniego kapitału własnego zaobserwowano w roku 2018, głównie dzięki 3 przedsiębiorstwom z Brazylii: Sao Martinho S.A., Guarani S.A. (Olimpia) oraz Companhia

Agricola e Pecuaria Lincoln Junqueira. Firmy te zajmowały się produkcją energii z biomasy. Niestety w następnych okresach wartości te zaczęły znacząco maleć, a niewielki wzrost miał miejsce dopiero w 2021 roku. W Azji natomiast w latach 2018–2020 zgromadzony kapitał stale rósł, osiągając swoją szczytową wartość równą 545,11 mln USD. W Azji z roku na rok zwiększały się wartości kapitałów własnych 2 głównych liderów produkujących energię z biomasy: Dynagreen Environmental Protection Group Company Limited z siedzibą w Hong Kongu oraz Energy Absolute Pcl z Tajlandii, a także chińskiej firmy Wuxi Huaguang Environment& Energy Group Co.,Ltd. produkującej energię geotermalną. Europa największą wartość średnią kapitałów własnych wynoszącą 235,19 mln USD zgromadziła w 2020. Największy wpływ na ten wynik miała firma Societatea Nationala z Rumuni, która produkuje energię geotermalną.

4.4. Podstawowe wskaźniki

Na podstawie wyżej przedstawionych i opisanych wyników finansowych oraz stanu aktywów i kapitału własnego, w ramach artykułu dokonano analizy podstawowych wskaźników finansowych dla poszczególnych źródeł energii. w pierwszej kolejności policzono, w jakim stopniu przedsiębiorstwa średnio z poszczególnych źródeł finansują się kapitałem własnym – wyniki obliczeń zostały przedstawione w tabeli 4.

Na podstawie otrzymanych wyników można stwierdzić, iż wszystkie przedsiębiorstwa nie przekraczają finansowania kapitałem własnym w 50% – zatem zdecydowana większość finansuje swoje aktywa kapitałem obcym (kredyty oraz kredyty kupieckie) – liderem w tym obszarze są przedsiębiorstwa z segmentu bazującego na paliwach kopalnych oraz z segmentu bazującego na energii jądrowej. W analizowanych latach finansowanie kapitałem obcym dla tych segmentów wacha się w granicach 70%. W najmniejszym stopniu z kapitału obcego korzystają przedsiębiorstwa z segmentu produkującego energię na bazie energii wodnej – w tym przypadku w połowie aktywa są finansowane kapitałem obcym.

Ważnym aspektem, z finansowego punktu widzenia, jest stopień wykorzystania posiadanych aktywów do generowania zysków. Wyniki tych obliczeń zostały zaprezentowane w tabelach 5.

Jak przedstawiono w tabeli 2 najwyższy poziom aktywów posiadany jest przez segment paliw kopalnych oraz energii nuklearnej (jest to ponad 80% aktywów z wszystkich analizowanych segmentów). Niemniej jednak, jak wynika z tabeli 5, segmenty te nie posiadają najwyższych stóp zwrotu z zaangażowanych aktywów – co więcej, przedsiębiorstwa z segmentu paliw kopalnych prezentują się najgorzej na tle pozostałych segmentów. Najwyższy wskaźnik ROA, na przestrzeni analizowanych lat, osiągnięto w segmencie energii wiatrowej oraz energii z biomasy. O ile bardzo dobry wynik przedsiębiorstw z segmentu energii z biomasy można wytłumaczyć stosunkowo niskim poziomem stanu aktywów, o tyle już w przypadku segmentu energii wiatrowej poziom aktywów to trzeci co do wielkości. Na tej podstawie można wysnuć wniosek, iż aktywa w segmencie energii wiatrowej są najlepiej wykorzystywane (w stosunku do posiadanych aktywów przynoszą najwyższe zyski), a najgorzej na tym tle wypadają przedsiębiorstwa z segmentu energii z paliw kopalnych. W podobny sposób dokonano analizy rentowności kapitału własnego, a wyniki zostały zaprezentowane w tabeli 6.

Do niemalże identycznych wniosków można dojść w przypadku analizy wskaźnika ROE. W tym przypadku zdecydowanie najgorszy zwrot z zainwestowanego kapitału własnego posiadają przedsiębiorstwa z segmentu paliw kopalnych, a najlepszym wykorzystaniem kapitału zainwestowanego przez właścicieli mogą się pochwalić przedsiębiorstwa produkujące energię wiatrową.

Wnioski

Wytwarzanie oraz konsumpcja energii to podstawowe procesy zachodzące na Ziemi. Od momentu, gdy człowiek po raz pierwszy nauczył się pozyskiwać energię, aż po dziś dzień w strukturze energetycznej odnotowano szereg transformacji. Zmiany te nie tylko spowodowały poprawę jakości życia, zwiększyły wydajność procesów oraz zminimalizowały negatywny wpływ energetyki na środowisko, ale także przełożyły się na sytuację finansową przedsiębiorstw z tego sektora.

W dzisiejszych czasach obserwuje się odejście od konwencjonalnych źródeł energii na rzecz wykorzystania energii odnawialnej. Tylko przedsiębiorstwa, które umieją dopasować się do aktualnie panujących uwarunkowań odniosą sukces na rynku, który przełoży się na poprawę kondycji finansowej firmy. Zastosowanie analizy finansowej w obszarze rentowności pozwoliło wyszczególnić przedsiębiorstwa, których sytuacja finansowa w latach 2018-2021 była najlepsza. Najwyższe średnie wskaźniki rentowności aktywów oraz kapitałów własnych odnotowano w firmach, których główną działalnością jest produkcja energii wiatrowej, zaś najniższe w przedsiębiorstwach wytwarzających energię na bazie paliw kopalnych. W tym okresie czasu najwyższe średnie wartości wskaźnika ROE i ROA zaobserwowano w Ameryce Północnej i w Azji, zaś najniższe przede wszystkim w Afryce.

Literatura – References

1. Bluszcz, A.; Manowska, A. Research on the differentiation of the level of sustainable development of energy markets. Energies 2020, 13(18), 4882. DOI: 10.3390/en13184882
2. Bluszcz, A.; Manowska, A. The use of hierarchical agglomeration methods in assessing the Polish energy market. Energies 2021, 14(13). DOI: 10.3390/en14133958
3. Bluszcz, A.; Ranosz, R. The use of multidimensional exploration techniques to assess the similarity level of development of energy markets. Journal of the Polish Mineral Engineering Society 2020, r.21, nr. 1, p. 199-204. DOI: 10.29227/IM-2020-01-74
4. Ranosz, R.; Bluszcz, A.; Kowal D. Conditions for the innovation activities of energy sector enterprises shown on the example of mining companies. Journal of the Polish Mineral Engineering Society 2020, r.21, nr.1, p.249-256. DOI: 10.29227/IM-2020-01-82
5. Manowska, A. Analysis and Forecasting of the Primary Energy Consumption in Poland Using Deep Learning. Journal of the Polish Mineral Engineering Society 2020, 1(1), p. 217–222. https://doi.org/10.29227/IM-2020-01-77
6. Olkuski T., Stala-Szlugaj K.: Tendencje zmian występujące w światowej energetyce. Zeszyty naukowe Instytutu Gospodarki Surowcami Mineralnymi i Energią Polskiej Akademii Nauk nr. 98, Kraków 2017
7. Pepłowska, M.; Gawlik, L. Financial Liabilities of the Hard Coal Mining Sector in Poland. Journal of the Polish Mineral Engineering Society 2019, No.2, p. 293-299. DOI: 10.29227/IM-2019-02-47
8. Ranosz, R.; Kowal, B. How Selected Energy Commodity Prices Volatility Impacts Gross Domestic Product (GDP) Fluctuation with Respect to Selected European Countries. Journal of the Polish Mineral Engineering Society 2020, R. 22, nr 1, p. 93–98. DOI: 10.29227/IM-2020-01-15
9. Gołębiowski, G.; Królikowska, E. Wskaźniki rentowności jako miary efektywności gospodarowania w spółkach węglowych w latach 2014–2018. Journal of the Polish Mineral Engineering Society 2020, no. 1, vol.1. http://doi.org/10.29227/IM-2020-01-16
10. Kowal, B.; Świniarska, O.; Domaracká, L. Internal communication models shaping safe behavior of employees in the raw materials sector during the coronavirus pandemic. Journal of the Polish Mineral Engineering Society 2022, no. 2, p. 31–38. DOI: 10.29227/IM-2022-02-04
11. Sukiennik, M.; Kowal, B. Analysis and Verification of Space for New Businesses in Raw Material Market—A Case Study of Poland. Energies 2022, 15, 3042. https://doi.org/10.3390/en15093042
12. Kowal, B.; Ranosz, R.; Herezy, Ł.; Cichy, W.; Świniarska, O.; L. Domaracka, L. Overview of Taken Initiatives and Adaptation Measures in Polish Mining Companies during a Pandemic. Energies 2022, 15, 6403. https://doi.org/10.3390/en15176403
13. Lewicka, E.D.; Burkowicz, A.; Czerw, H.; Figarska-Warchoł, B.; Galos, K.; Gałaś, A.; Guzik, K.; Kamyk, J.; Kot-Niewiadomska, A.; Szlugaj, J. The Russian-Ukrainian war versus the mineral security of Poland. Mineral Resources Management 2022, Vol. 38, Iss. 3, p. 5–30. DOI: 10.24425/gsm.2022.142792
14. Stala-Szlugaj, K.; Grudziński, Z. Alternative directions of coal supply to Poland as a result of the Russian-Ukrainian war. Mineral Resources Management 2022, Vol. 38, Iss. 3, p. 31–47. DOI: 10.24425/gsm.2022.142790
15. Kustra, A.; Ranosz, R.; Kowal, B. Model of the process of preparing annual technical and economic plans in the public sector. Journal of the Polish Mineral Engineering Society 2020, R. 22, nr 1, p. 211–215. DOI: 10.29227/IM-2020-01-76
16. Kowal, B.; Ranosz, R.; Karkula, M.; Kowal, D. Process Management in Hard Coal Mining Companies. Journal of the Polish Mineral Engineering Society 2018, iss. 2 (42), 111-116. DOI: 10.29227/IM-2018-02-14
17. Sierpińska, M.; Jachna, T. Methods of making financial decisions - analysis of examples and cases, Scientific Publisher PWN, Warszawa 2007. [in Polish]
18. Groeneveld, B.; Topal, E.; Leenders, B. Robust, flexible and operational mine design strategies. Min. Technol. 2012, 121, p. 20-28, DOI: 10.1179/1743286311Y.0000000018.
19. Bluszcz, A.; Kijewska, A.; Sojda, A. Economic Value Added in metallurgy and mining sector in Poland. Metalurgija 2015, 54, iss. 2, p. 437-440.
20. Grad P.: Analiza-prognoza finansowa. Rzeszów 2020
21. Stępień K., Kasperowicz Stępień A.: Analiza finansowa jako narzędzie wykorzystanie do badania sytuacji finansowej jednostki gospodarczej. Zeszyty Naukowe Akademii Ekonomicznej w Krakowie nr 750, Kraków 2007
22. Bednarski L.: Analiza finansowa w przedsiębiorstwie. Polskie Wydawnictwo Ekonomiczne, Warszawa 2007
23. Analiza finansowa https://inewi.pl/Blog/analiza-finansowa-przedsiebiorstwa-na-czym-polega-i-jak-sie-do-niej-przygotowac, 1 marzec 2023

24. Sprawozdanie finansowe https://www.biznes.gov.pl/pl/portal/00245, 1 marzec 2023
25. Gad J.: Analiza i ocena sytuacji finansowej przedsiębiorstwa. Uniwersytet Łódzki – Wydział Zarządzania, Łódź 2015
26. Kątnik J.: Analiza i ocena wskaźników pomiaru rentowności przedsiębiorstwa jako instrument rozwoju. Zeszyty Naukowe Akademii Ekonomicznej w Krakowie nr 863, Kraków 2011, Energy Council, Londyn 2021
27. EMIS, 1 marzec 2023

The Analysis of the Financial Efficiency of Enterprises from the Fuel Sector in the Era of Energy Transformations

The aim of this article is to examine the basic financial figures for companies in the sectors producing electricity from the following sources: fossil fuels, nuclear, hydro, solar, wind, geothermal and biomass. The financial values examined are: net profit, the level of assets and equity. On the basis of these figures, the basic profitability ratios were calculated, ie: ROA and ROE. The research results clearly show that companies from the sector based on the production of energy from fossil fuels achieve the worst results, both in terms of profitability and the nominal net result. At the same time, they are companies that have the largest level of assets. On the other hand, companies from the wind energy sector turned out to be the most effective in terms of both return on equity and assets with the lowest level of assets.

Keywords: *energy, financial results, energy sources, raw materials, net profit, assets, equity, ROA, ROE*

The Method for Assessing the Impact of Variable Coal Demand on the Efficiency of Mine Operations

Dariusz FUKSA[1)]

[1)] AGH University of Science and Technology, Mickiewicza 30, 30-059 Kraków, Poland; email: fuksa@agh.edu.pl, ORCID: 0000-0001-5519-5923

http://doi.org/10.29227/IM-2023-01-33

Submission date: 19-05-2023 | Review date: 08-06-2023

Abstract

The method presented in the article is based on Monte Carlo simulation and involves studying the impact of random demand fluctuations on the efficiency of mines and mine groups (companies). For random demand fluctuations, a normal distribution is assumed, and the analysis variants present-ed include:

- *Adopting the mean and variance values based on retrospective data,*
- *Considering the most probable forecast error resulting from predictive formulas,*
- *Taking into account correlated changes in demand.*

The results obtained are presented in the form of histograms of the degree of operational lever-age. These histograms allow for predicting how the degree of operational leverage of mines will de-velop, as well as estimating the direction and probability of these changes. The developed and veri-fied sensitivity analysis using real examples constitutes a useful element in rationalizing decision-making processes.

Keywords: *sensitivity analysis, degree of operating leverage, the SIMPLEX algorithm, the Monte Carlo method*

1. INTRODUCTION

Changes in the level of coal requirement have a significant effect on the financial situations of both individual mines and groups. Therefore, in market conditions it is essential to carry out multivar-iant analyses to assess the sensitivity of coal production and sales plans, as well as other economic and technical quantities on changes in requirements.

The present author's research [5, 6, 7] on the options for sensitivity analysis of coal production and sales plans, the product structure, reserves, capacity and so on to changes in demand have re-vealed the significant suitability of the Monte Carlo method in the unbalanced Polish coal market [3, 4, 12, 14].

The sensitivity analysis using the Monte Carlo method presented in this paper covers research on the effect of random fluctuations in demand on the profit and the degree of operating leverage on the basis of a real coal mines.

2. THE ESSENCE OF OPERATING LEVERAGE

Leverage (in terms of finance) is used when changing the values of certain economic quantities causes more than proportionate change in other economic quantities.

Any increase (decrease) in gross receipts from sales will bring the company a more than pro-portional increase (decrease) in gross profit on sales (percentage-wise) - assuming constancy in other factors which affect its level. This is called operating leverage. In order to determine what change in profit will be accompanied by a specific gain in sales, the degree of operating leverage (DOL) is cal-culated [13]:

$$DOL = \frac{\%\Delta EBIT}{\%\Delta S} \tag{1}$$

or

$$DOL = \frac{S_o - Kz_o}{EBIT_o} \tag{2}$$

where:

%ΔEBIT – Percentage increase in profit before interest and taxes,

%ΔS – Percentage growth in net sales,

S_o – The value of net sales as of the base, (PLN),

Kz_o – The level of variable costs as of the base, (PLN),

$EBIT_o$ – The level of profit before interest and taxes as of the base, (PLN).

The operating leverage mechanism is a useful tool in the ongoing management of a company. With it, the rate of change in profit can be determined, for example: with an increase (decrease) sales, for example, of 10%, the profit made by the company will increase (decrease) by 10% × DOL. The degree of operating leverage (DOL) will depend on the profitability of sales and the cost structure taking into account their variability. Its size varies depending on the level of sales, which is the basis for the calculations. Hence, the operating leverage is used, inter alia, for predicting a company's fu-ture economic performance [13].

3. CHARACTERISTICS OF THE PROPOSED METHOD

The basis for an analysis of profit sensitivity and the degree of operating leverage to changes in demand is the set of optimal solutions for optimising production and coal sales for the mining com-pany. The Monte Carlo method is used for this. The set of optimal solutions for optimisation is creat--ed by repeated calculation of an optimal programme for the production and sale of coal with a given, random, demand scenario. The optimal solution, however, is obtained using the SIMPLEX algorithm.

The analysis is conducted for a set of 1 000 random demand sets. The demand vector drawn is the subvector of the right sides of the 4 optimisation model equation [7]:

Tab. 1. Technical and economic coefficients for mines „B" and „D". Source: Own preparation
Tab. 1. Wskaźniki techniczno-ekonomiczne kopalń „B" i „D". Źródło: przygotowanie własne

Specification	Unit	Mine „B"	Mine „D"
Average Extraction	ton/day	11,800	12,000
Max. Extraction	netto ton	2,700,000	4,600,000
Unit cost	PLN/t	159.02	115.87
Fixed cost	%	86.96	86.98

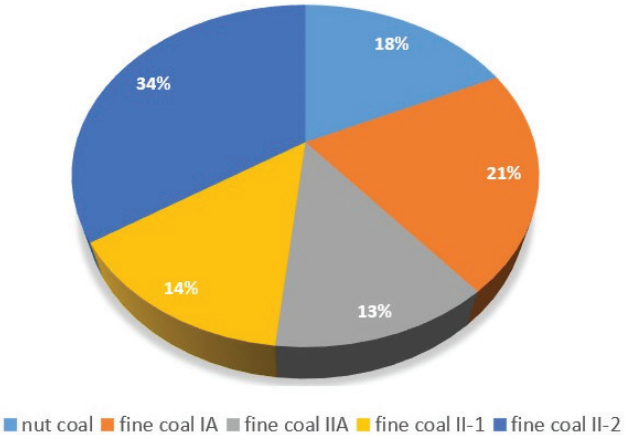

Fig. 1. Assortment structure of production for mine „B". Source: Own preparation
Rys. 1. Struktura asortymentowa produkcji kopalni „B"

Objective function:

$$\sum_{j=1}^{p}\sum_{i=1}^{r_j}\sum_{k=1}^{m_{ij}}(c_{ijk}-kz_{ijk})\cdot x_{ijk}-\sum_{j=1}^{p}Ks_j \rightarrow \max \qquad (3)$$

Sales restrictions:

$$\sum_{j=1}^{p}\sum_{i=1}^{r_j}\sum_{k=1}^{m_{ij}}x_{ijk}\le Z_k \qquad \text{for all k} \qquad (4)$$

where:
x_{ijk} – net amount of extracted coal of *ij* type accepted by consumers in group *k*, (netto tone),
c_{ijk} – price of *ij* type of coal,
kz_{ijk} – variable cost for mine *j*,
Ks_j – fixed cost for mine *j*,
Z_k – consumer demand for group *k*,
i – index of coal type, $i = 1, 2, 3, \ldots r_j$,
j – index of mine, $j = 1,2,3,\ldots p$,
k_n – index of consumer groups, $k = 1,2,3,\ldots, m_{ij}$, where m_{ij} marks numerousness miscellany k_n for coal of *ij* type.

The remaining restrictions in the model relate to the structure of production and the capacity of individual mines [7]. The reality of the solutions obtained is assured by allowing the possibility of storing coal.

Each of the randomly selected demand elements is a random variable with normal distribution. The projected volume of demand is adopted as the expected value (nominal), and the most likely forecast error resulting from the predictive formulae is adopted as the dispersion (standard devia-tion).

As a result of the test, new optimal solutions are obtained when considering different demands (new values for the objective function). This makes it possible to present the results of the analysis in the form of a histogram of profit and other economic and technical quantities for both the entire com-pany and individual mines, as well as determining the likelihood of obtaining the assumed level for the analyzed quantities for the company and the mines comprising it.

4. EXAMPLE OF CALCULATIONS AND EVALUATION OF RESULTS

Calculations are performed for a selected mine „D", which is part of a coal company compris-ing seven mines with different production characteristics. In Table 1, the production capacity of the analyzed „B" and „D" mines is shown, together with technical and economic indicators, and their the product structure is illustrated in Figures 1 and 2.

In the first stage of the analysis, the magnitude of demand for each group of consumers was randomly generated according to a normal distribution with the expected value (nominal) equal to the planned demand (sales). For retrospective data, the best model for each group of consumers was fit-ted using regression analysis, and based on this, the forecasted demand for the planned forecast year was determined. The adopted dispersion value (σ_r) represents the standard error of estimation of the regression function, which is a measure indicating the average deviations of actual values of the de-pendent variable (coal demand of consumers) from the theoretical values of this variable calculated from the regression function. It is one of the parameters of the random component distribution that allows us to infer the goodness of fit of the model to the available empirical data. It is calculated using the formula [1, 2, 8, 9, 10, 11]:

$$\sigma_r^2=\frac{\sum_{n=1}^{N}\left(y_n-y_{\text{mod}}\right)^2}{N-K}, \qquad (5)$$

Table 2 compares the annual nominal values and dispersions in demand for individual groups of customers. Table 3, meanwhile, presents the optimal production and sales plan for „B" and „D" mines.

For various coal products, the following sales prices were chosen:

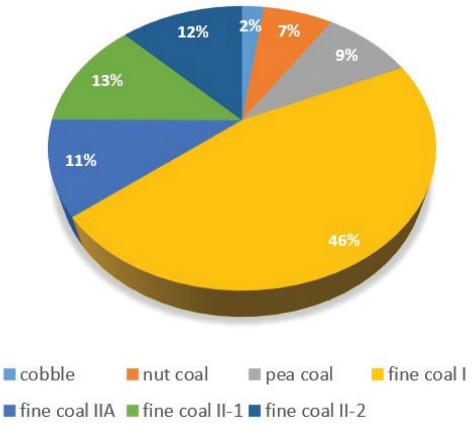

Fig. 2. Assortment structure of production for mine „D". Source: Own preparation
Rys. 2. Struktura asortymentowa produkcji kopalni „D"

Tab. 2. Nominal value and dispersion σ_{yprog} for every group of consumers]. Source: Own preparation
Tab. 2. Zestawienie wartości nominalnej zapotrzebowania oraz dyspersji σ_r dla poszczególnych grup odbiorców. Źródło: przygotowanie własne

Name of consumer group	Nominal prognosis values (t)	Dispersion σ_r (t)
Export 8	300,857	95,728
Export 9	419,447	133,461
Indv. consumers 1	336,060	13,035
Indv. consumers 3	5,475,600	212,387
Indv. consumers 4	1,391,200	53,962
Dust kettles	2,385,300	92,521
Grates 2	265,940	10,315
Grates 3	1,095,000	42,472
Grates 4	567,619	22,017
Chamber grates 1	425,765	16,514

- cobble – 450 PLN/t,
- nut coal – 381 PLN/t,
- pea coal – 365 PLN/t,
- fine coal I – 324 PLN/t,
- fine coal IA – 321 PLN/t,
- fine coal IIA – 310 PLN/t,
- fine coal II – 300 PLN/t.

The variable unit cost was estimated at 40 PLN/t.

The use of the Monte Carlo method for sensitivity analysis of coal production and sales plans to changes in demand involves multiple iterations to determine the optimal production and sales pro-gram for mines under assumed random demand scenarios.The selected number of 1 000 draws ena-bles an adequate set of production tasks and corresponding financial results for the various mines to be obtained, as well as the calculation of the degree of operating leverage.

The obtained results are presented in Table 6 and illustrated in Figures 3-10. The vertical black line represents the value of the operational leverage resulting from the optimal plan for each mine.

In the second stage, an analysis of the effects of random changes in demand was conducted based on the most probable forecast error. To estimate the forecast error of demand for each consum-er, the following formula was used [1, 2, 8, 9, 10, 11]:

$$\sigma_{yprog} = \sqrt{\sigma_r^2 + \sigma_{\hat{y}}^2} \tag{6}$$

where:
σ^2_r – variation in the remainder factor, defining according to the following formula:

$$\sigma_r^2 = \frac{\sum_{n=1}^{N} (y_n - y_{\mathrm{mod}})^2}{N - K}, \tag{7}$$

where:
y_n – actual value of endogenous factor,
y_{mod} – model-based value of endogenous factor,
N – number of observations,
K – number of estimating parameters for model structure.
$\sigma^2_{\hat{y}}$ – Estimation of variance in prognosis model:

$$\sigma_{\hat{y}}^2 = \begin{bmatrix} 1 & x_{N+2} \end{bmatrix} \cdot \left[X^T \cdot X \right]^{-1} \cdot \begin{bmatrix} 1 & x_{N+2} \end{bmatrix}^T \cdot \sigma_r^2, \tag{8}$$

where:
x_{N+2} – time, during which prognosis is prepared.
also

$$X = \begin{bmatrix} 1 & x_1 \\ 1 & x_2 \\ 1 & x_3 \\ \vdots & \vdots \\ 1 & x_N \end{bmatrix}, \qquad X^T X = \begin{bmatrix} N & \sum_{n=1}^{N} x_n \\ \sum_{n=1}^{N} x_n & \sum_{n=1}^{N} x_n^2 \end{bmatrix} \tag{9}$$

The nominal values and dispersions of consumer demand used in this stage of the analysis are presented in Table 4. The obtained results are shown in Table 6 and illustrated in Figures 3-10.

In the third stage, the impact of correlated fluctuations in demand on the operational leverage of individual mines was examined. To do this, the nominal value of the demand forecast for each consumer was decreased (P1) by the value of the model error in one case and increased (P2) by the value of the model error in another case (Formula 6). The data is

Tab. 3. The optimal plans of production and sales for "B" and „D" mines. Source: Own preparation
Tab. 3. Optymalny plan produkcji i sprzedaży węgla dla kopalń „B" i „D". Źródło: przygotowanie własne

Mine "B"		
Offer: 2,700,000 t Sold: 1,776,600 t	Gross profits: 62,938,398 PLN Mine reserves: 0 t	
Consumers	**Coal assortment**	**Quantity (t)**
Indv. consumers 4	nut coal	328,143
Export 8	nut coal	14,857
Indv. Consumers 1	nut coal	143,000
Indv. consumers 3	fine coal IA	237,000
Dust kettles	fine coal IA	330,000
Dust kettles	fine coal II	380,700
Export 9	fine coal II	342,900
Coal dump	fine coal II	923,400
Mine "D"		
Offer: 4,600,000 t Sold: 4,022,220 t	Gross profits: 371,140,074 PLN Mine reserves: 0 t	
Consumers	**Coal assortment**	**Quantity (t)**
Indv. consumers 4	cobble	101,200
Indv. consumers 4	nut coal	322,000
Indv. consumers 4	pea coal	414,000
Indv. consumers 3	fine coal I	2,120,600
Grates 4	fine coal II	567,620
Indv. consumers 3	fine coal IIA	496,800
Coal dump	fine coal II	7,380
Coal dump	fine coal II	570,400

Tab. 4. Nominal value and dispersion σ_{yprog} for every group of consumers [t]. Source: Own preparation
Tab. 4. Zestawienie wartości nominalnej zapotrzebowania oraz dyspersji σ_{yprog} dla poszczególnych grup odbiorców. Źródło: przygotowanie własne

Name of consumer group	Nominal prognosis values (t)	Dispersion σ_{yprog} (t)
Export 8	300,857	70,205.89
Export 9	419,447	116,913.60
Indv. consumers 1	336,060	10,565.02
Indv. consumers 3	5,475,600	140,552.80
Indv. consumers 4	1,391,200	35,710,60
Dust kettles	2,385,300	61,228.09
Grates 2	265,940	6,826.40
Grates 3	1,095,000	28,107.22
Grates 4	567,619	14,570.20
Chamber grates 1	425,765	10,928,80

Tab. 5. The compilation of the nominal forecast values P1 and P2, as well as the dispersions σ_{yprog} for each con-sumer group. Source: Own preparation
Tab. 5. Zestawienie wartości nominalnej prognoz P1 i P2 oraz dyspersji σ_{yprog} dla poszczególnych grup odbiorców. Źródło: przygotowanie własne

Name of consumer group	Nominal prognosis values P_1 (t)	Nominal prognosis values P_2 (t)	Dispersion σ_{yprog} (t)
Export 8	230,651.11	371,062.89	70,205.89
Export 9	302,533.40	536,360.60	116,913.60
Indv. consumers 1	325,494.98	346,625.02	10,565.02
Indv. consumers 3	5,335,046.20	5,616,151.80	140,552.80
Indv. consumers 4	1,355,489.40	1,426,910.60	35,710.60
Dust kettles	2,324,071.91	2,446,528.10	61,228.09
Grates 2	259,113.60	272,766.40	6,826.40
Grates 3	1,066,892.78	1,123,107.20	28,107.22
Grates 4	553,048.80	582,189.20	14,570.20
Chamber grates 1	414,836.20	436,693.80	10,928.80

presented in Table 5, and the ob-tained results are shown in Table 6 and illustrated in Figures 3-10

Analyzing the presented histograms (Figures 3-10) of the achieved operational leverage degree for mines "B" and "D," their distortion can be observed. This distortion results from the mismatch between the production structure of the analyzed mines and the demand from consumers, as con-firmed in previous studies [1].

The nominal value of the operational leverage degree for mine "B" is 6.52 (represented by the black vertical line). This means that a decrease in sales, for example, by 10%, will result in a profit decrease of 65.2%, and vice versa. The probability of maintaining such a leverage degree is 0.80 and 0.90, respectively, for σ_r and σ_{yprog} (Figures 3 and 4). With a decrease in demand to the P_1 level, the probability of achieving the nominal leverage value will be approximately 50% (Figure 5), while in the case of an increase in consumer demand to the P_2 level, it will be only 13% (Figure 6). In each analyzed case, there is a higher probability of a favorable situation for the mine, namely a decrease in the degree to the mean value. For σ_r, the DOL will be 6.28 (89% chance), for σ_{yprog}, the DOL will be 6.41 (92% chance), and for P_1 and P_2, respectively, the DOL will be 6.19 (70% chance) and 6.29 (90% chance). Other values of the leverage degree may occur, but with a very low probability ranging from 0.001 to 0.129 (Table 6).

For mine "D," the probability of achieving the nominal level of the leverage degree (represent-ed by the black vertical line) is almost equal to 1 in each analyzed case, corresponding to a level of 2.16 (Figures 7-10). There are only 3 chances out of 1000 for the value 2.27 to occur (for σ_r and P_1) (Figure 2, Table 4).

5. CONCLUSION

The magnitude of the demand from potential and existing customers has a decisive impact on the mine's production volume, and thus the effectiveness of the company. The presented method of analysis provides a useful tool in assisting decision making, particularly in the area of reasonable volumes for production and sale of coal and also when conducting specific strategies regarding the mine's (company's) continued operation. It also provides the basis for action to

Tab. 6. The compilation of nominal, minimum, maximum, and mean values of the predicted operational lever-age, as well as the probability of achieving these values for the nominal values P1 and P2, and dispersions σ_r and σ_{yprog}. Source: Own preparation

Tab. 6. Zestawienie wartości nominalnej, minimalnej, maksymalnej i średniej przewidywanego stopnia dźwigni operacyjnej oraz prawdopodobieństwa jego osiągnięcia dla wartości nominalnych P1 i P2 oraz dyspersji σ_r, σ_{yprog}. Źródło: przygotowanie własne

	Degree of operating leverage (-)				Likelihood of attaining (-)			
	Nominal value	Minimum value	Maximum value	Average value	Minimum value	Maximum value	Nominal value	Average value
Mine „B"								
σ_r	6.52	2.19	7.53	6.28	0.001	0.008	0.805	0.886
σ_{yprog}	6.52	3.73	6.53	6.41	0.003	0.003	0.902	0.917
P_1	6.52	3.58	6.91	6.19	0.003	0.054	0.523	0.696
P_2	6.52	2.80	6.52	6.29	0.003	0.129	0.129	0.900
Mine „D"								
σ_r	2.164	2.16	2.26	2.169	0.115	0.003	0.885	0.454
σ_{yprog}	2.164	2.16	2.18	2.166	0.003	0.003	0.586	0.437
P_1	2.164	2.16	2.27	2.17	0.006	0.003	0.892	0.514
P_2	2.164	2.16	2.18	2.162	0.446	0.003	0.156	0.994

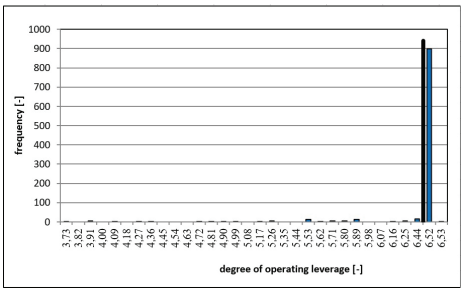

Fig. 3. Histogram showing frequencies of achieving given degree of operating leverage for mine „B" with dispersion σr . Source: Own preparation

Rys. 3. Histogram częstości uzyskiwanych stopni dźwigni operacyjnej dla kopalni „B" przy dyspersji σr. Źródło: przygotowanie własne

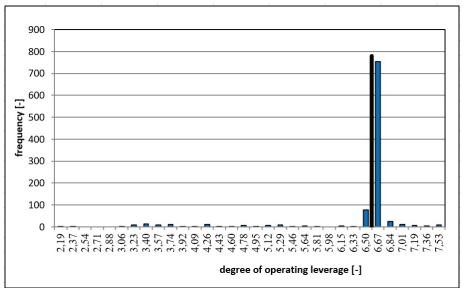

Fig. 4. Histogram showing frequencies of achieving given degree of operating leverage for mine „B" with dispersion σ_{yprog}. Source: Own preparation

Rys. 4. Histogram częstości uzyskiwanych stopni dźwigni operacyjnej dla kopalni „B" przy dyspersji σ_{yprog}. Źródło: przygotowanie własne

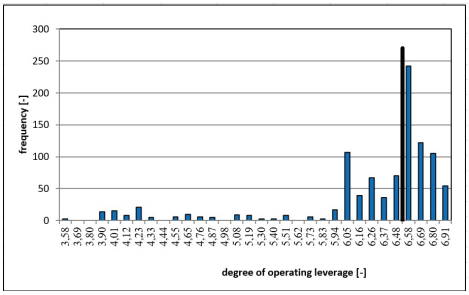

Fig. 5. Histogram of the frequency of obtained operational leverage degrees for mine "B" with the nominal value P1 and dispersion σ_{yprog}

Rys. 5. Histogram częstości uzyskiwanych stopni dźwigni operacyjnej dla kopalni „B" przy wartości nominalnej P1 i dyspersji σ_{yprog}. Źródło: przygotowanie własne

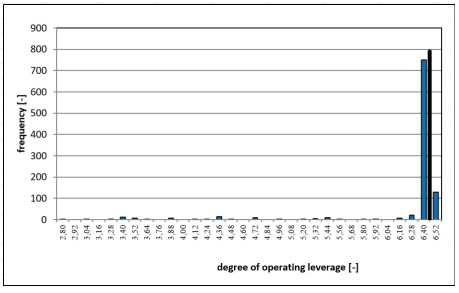

Fig. 6. Histogram of the frequency of obtained operational leverage degrees for mine "B" with the nominal value P_2 and dispersion σ_{yprog}

Rys. 6. Histogram częstości uzyskiwanych stopni dźwigni operacyjnej dla kopalni „B" przy wartości nominalnej P_2 i dyspersji σ_{yprog}

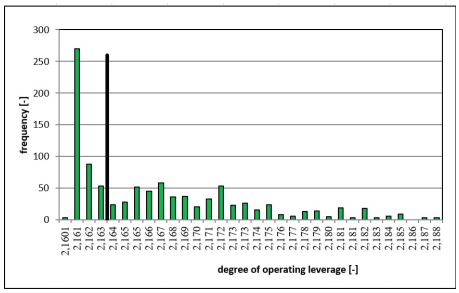

Fig. 7. Histogram showing frequencies of achieving given degree of operating leverage for mine „D" with dispersion σ_r. Source: Own preparation

Rys. 7. Histogram częstości uzyskiwanych stopni dźwigni operacyjnej dla kopalni „D" przy dyspersji σ_r. Źródło: przygotowanie własne

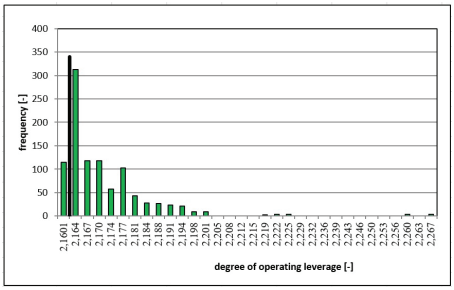

Fig. 8. Histogram showing frequencies of achieving given degree of operating leverage for mine „D" with dispersion σ_{yprog}. Source: Own preparation

Rys. 8. Histogram częstości uzyskiwanych stopni dźwigni operacyjnej dla kopalni „D" przy dyspersji σ_{yprog}. Źródło: przygotowanie własne

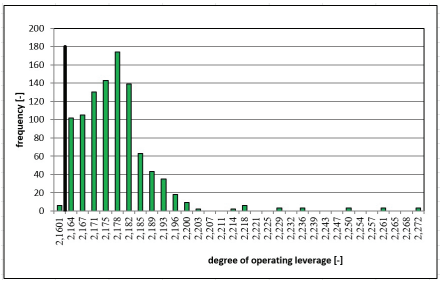

Fig. 9. Histogram of the frequency of obtained operational leverage degrees for mine "D" with the nominal value P1 and dispersion σ_{yprog}

Rys. 9. Histogram częstości uzyskiwanych stopni dźwigni operacyjnej dla kopalni „D" przy wartości nominalnej P1 i dyspersji σ_{yprog}

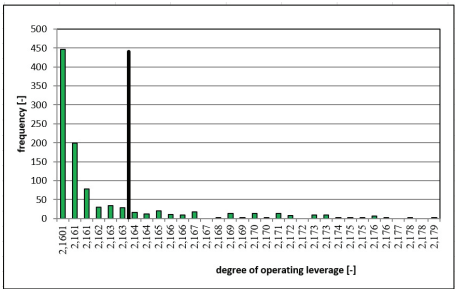

Fig. 10. Histogram of the frequency of obtained operational leverage degrees for mine "B" with the nominal value P2 and dispersion σ_{yprog}

Rys. 10. Histogram częstości uzyskiwanych stopni dźwigni operacyjnej dla kopalni „D" przy wartości nominalnej P2 i dyspersji σ_{yprog}

adapt the production structure, both in terms of quantity and quality, to customer requirements.

This method of analysis is likely to reflect real situations that might occur. The results obtained for the multi-variant change in demand enable a direct indication of what values the volumes ana-lysed can achieve (for example: profit or the degree of operating leverage), and with what probability.

This research was prepared as part of a scientific subsidy from the AGH University of Science and Technology in Poland under number 16.16.100.215.

Literatura – References

1. Barnett V. (1982) Elementy pobierania prób. PWN, Warszawa, Poland.
2. Bobrowski D. (1986) Probabilistyka w zastosowaniach technicznych. WNT, Warszawa, Poland.
3. Brandt S. (1998) Analiza danych. Metody statystyczne i obliczeniowe. PWN, Warszawa, Poland.
4. Buslenko N. (1967) Metoda Monte Carlo. PWN, Warszawa, Poland.
5. Fuksa D. (2005) Utilization of the Monte Carlo method to analysis the influence of demand on changes in profitability of mines, Information systems and computational methods in manage-ment, Kraków, Poland, 202–211.
6. Fuksa D. (2006) Utilization of the Monte Carlo Method to analyze sensitivity of assortment struc-ture of mines production on changes in demand, Mine Planning and Equipment Selection 2006: MPES, Torino, Italy, 419–424.
7. Fuksa D. (2012) Metoda oceny wpływu zmiennego zapotrzebowania odbiorców węgla kamiennego na efektywność funkcjonowania wielozakładowego przedsiębiorstwa górniczego. Wydawnictwo AGH, Kraków, Poland.
8. Gnot S. (1991) Estymacja komponentów wariancyjnych w modelach liniowych, WNT, Warszawa, Poland.
9. Goryl A., Jędrzejczyk Z. (1996) Wprowadzenie do ekonometrii w przykładach i zadaniach, PWN, Warszawa, Poland.
10. Grabiński T., Wydymus S., Zaliaś A. (1982) Metody doboru zmiennych w modelach ekonometrycznych. PWN, Warszawa, Poland.
11. Rocki M. (2002) Ekonometria praktyczna, SGH, Warszawa, Poland.
12. Sadowski W. (1976) Teoria podejmowania decyzji, PWE, Warszawa, Poland.
13. Sierpińska M., Wędzki D. (1999) Zarządzanie płynnością finansową w przedsiębiorstwie. PWN, Warszawa, Poland.
14. Zieliński R. (1974) Metody Monte Carlo. WNT, Warszawa, Poland.

Metoda oceny wpływu zmiennego zapotrzebowania odbiorców węgla na efektywność funkcjonowania kopalń

Zaprezentowana w artykule metoda oparta jest na symulacji Monte Carlo i obejmuje badanie wpływu wahań losowych zapotrzebowania na efektywność kopalń oraz ich grup (spółek). Dla losowych wahań zapotrzebowania przyjęto rozkład normalny, a przedstawione warianty analizy uwzględniają:

- *przyjęcie wartości oczekiwanej i dyspersji według danych retrospektywnych;*
- *przyjęcie najbardziej prawdopodobnego błędu prognozy wynikającego z formuł predykcyjnych;*
- *uwzględnienie skorelowanych zmian zapotrzebowania.*

Uzyskane wyniki przedstawiono w postaci histogramów stopnia dźwigni operacyjnej. Pozwalają one przewidywać, jak będzie kształtował się stopień dźwigni operacyjnej kopalń, jak również umożliwia oszacować, w którym kierunku zmiany te będą postępować i z jakim prawdopodobieństwem. Opracowana i zweryfikowana na realnych przykładach analiza wrażliwości stanowi przydatny element racjonalizacji procesów decyzyjnych.

Słowa kluczowe: *analiza wrażliwości, dźwignia operacyjna, algorytm SIMPLEX, metoda Monte Carlo*

Niebezpieczne odpady wtórne z instalacji termicznego przekształcania odpadów komunalnych

Wacław ANDRUSIKIEWICZ[1)]

[1)] dr hab. inż., prof. AGH; Department of Mining Engineering and Occupational Safety, Faculty of Civil Engineering and Resources Management, AGH University of Krakow; email: andus@agh.edu.pl, ORCID: 0000-0002-4845-1404

http://doi.org/10.29227/IM-2023-01-34

Submission date: 22-05-2023 | Review date: 11-06-2023

Abstrakt

Odpady towarzyszą człowiekowi od zawsze. W miarę postępu ewolucyjnego człowieka zmieniała się nie tylko jakość odpadów, ale także ich ilość. Już w starożytności podejmowano próby uporządkowania kwestii odpadów, co poprzez stulecia skutkowało różnymi regulacjami prawnymi.

Ostatnie 150 lat to gwałtowny rozwój technik i technologii mających na celu rozwiązania problemów związanych z odpadami, w tym także komunalnymi. Wymusiły to m. in. rewolucja przemysłowa, której towarzyszył gwałtowny rozwój miast związany ze wzrostem liczby mieszkańców, a w konsekwencji wzrosła ilość wytwarzanych odpadów.

Aktualne działania, szczególnie w Unii Europejskiej, zmierzają w kierunku maksymalnego wykorzystania odpadów, ograniczając ich składowanie na wysypiskach na rzecz ponownego zagospodarowania. Jednym z elementów w tym łańcuchu działań jest spalanie odpadów komunalnych, które pozwala na istotne ograniczenie ilości odpadów kierowanych na wysypiska. Problemem są jednak odpady wtórne, będące produktami spalania, które są klasyfikowane jako odpady niebezpieczne. Po poddaniu ich odpowiedniej obróbce docelowo trafiają na składowiska odpadów niebezpiecznych, które mimo stosowania zaawansowanych zabezpieczeń stanowią potencjalne zagrożenie dla środowiska.

Słowa kluczowe: *odpady komunalne, spalanie odpadów, odpady wtórne*

Wprowadzenie

Jednym z elementów towarzyszącym człowiekowi od zarania dziejów są odpady. Sięgając czasów prehistorycznych takimi odpadami były np. niejadalne resztki pożywienia, odpady z obróbki skór upolowanych zwierząt, odpady z obróbki drewna, kamienia itp. Nie stanowiły one wówczas i przez kolejne tysiąclecia istotnego problemu, gdyż były to odpady w pełni biodegradowalne bądź neutralne dla środowiska, a do tego powstające w stosunkowo niewielkich ilościach.

Wraz z rozwojem cywilizacyjnym wzrastał wolumen wytwarzanych przez człowieka odpadów, zmieniała się również ich jakość. Mówiąc współczesnym językiem można stwierdzić, że odpady „nadążały" za rozwojem technologicznym.

Problem odpadów dostrzeżono już w starożytnej Grecji w V w. p.n.e. organizując pierwsze wysypiska odpadów, a w 320 r p.n.e. w Atenach ustanowiono pierwsze regulacje prawne dotyczące odpadów [2]. Pierwsze służby komunalne odpowiedzialne za oczyszczanie miasta powołali Rzymianie w III w. p.n.e.

W 1373 r. w Krakowie wydano jedną z pierwszych w Europie ustawę (tzw. wilkierz) dotyczącą zachowania czystości i porządku w mieście. Mieszkańcy gospodarstw domowych zostali zobowiązani do zbierania nieczystości ze swojego terenu oraz z połowy ulicy. Dopiero ponad 150 lat później podobne ustawy pojawiły się w Paryżu oraz w Wiedniu [2].

XVIII wiek rozpoczyna gwałtowny rozwój przemysłu. Wraz z nim powstają nowe miasta, a istniejące się powiększają. To z kolei napędza konsumpcjonizm, efektem czego jest coraz większe zróżnicowanie odpadów trafiających na wysypiska oraz ich wolumen. Dopiero wiek XIX wraz z rewolucją przemysłową rozpoczął nową erę odpadów: spalanie (o czym dalej), recykling i selektywną ich zbiórkę. Jednak należy zauważyć, że już w XI w. w Japonii przerabiano zużyty papier do ponownego wykorzystania, co niewątpliwie należy uznać za formę recyklingu.

Dostrzeżono, że z odpadów można wyselekcjonować pewną ich część do powtórnego wykorzystania. Pierwszy zakład zajmujący się recyklingiem odpadów powstał w Nowym Jorku w 1898 r. [1], to jednak dopiero w 2 poł. XX w. rozpoczęto na szeroką skalę wykorzystywać odpady i surowce wtórne.

Coraz większe ilości odpadów i ich duże zróżnicowanie to efekt z jednej strony zwiększającej się liczby ludności, z drugiej zaś skutek rozwoju gospodarczego. Aby można było racjonalnie postępować z odpadami, koniecznym było stworzenie usystematyzowanego katalogu odpadów, co w przypadku Polski znalazło swoje odzwierciedlenie w obowiązującym prawie [11]. Odpady podzielono na 20 grup w zależności od źródła ich powstawania. Te z kolei podzielono na podgrupy i rodzaje, wskazując równocześnie odpady niebezpieczne. W sumie katalog zawiera ok. 950 rodzajów odpadów.

Przyjmując za kryterium miejsce powstawania odpadów rozróżnia się [10]:

- odpady przemysłowe, związane z działalnością gospodarczą – wg katalogu [11] są to grupy 1-19;
- odpady komunalne, powstające na terenach zamieszkałych i związanych z bytowaniem ludzi – wg katalogu [11] są to odpady o kodzie 20 03 xx (inne odpady komunalne), a także odpady o kodzie 15 01 xx z sektora komunalnego (odpady opakowaniowe, włącznie z selektywnie gromadzonymi komunalnymi odpadami opakowaniowymi) oraz o kodzie 19 12 xx – odpady z mechanicznej obróbki odpadów (np. obróbki ręcznej, sortowania, zgniatania, granulowania) nie ujęte w innych grupach.

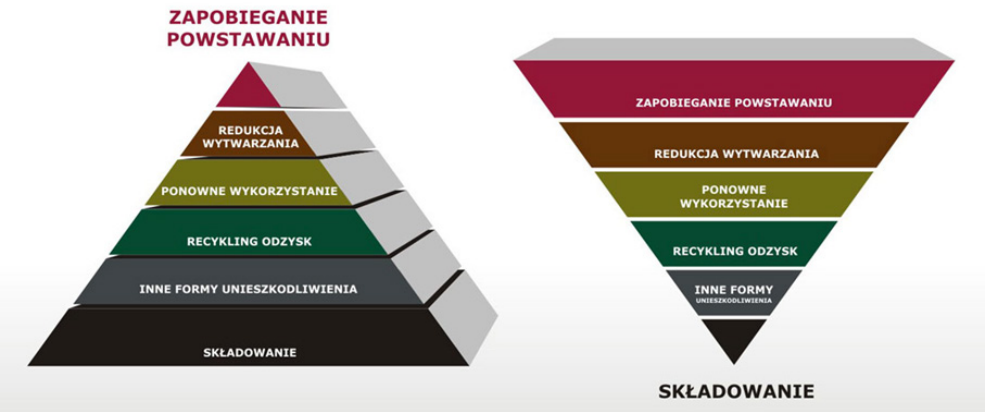

Rys. 1. Hierarchia postępowania z odpadami. Po lewej stronie stan obecny, po prawej – stan docelowy. Źródło: [3]
Fig. 1. Waste management hierarchy. On the left, the current state, on the right - the target state. Source: [3]

Tab. 1. Zebrane odpady komunalne w latach 2013–2022. Źródło: opracowanie własne na podstawie danych GUS
Tab. 1. Municipal waste collected in 2013–2022. Source: own elaboration based on Central Statistical Office data

Rok	Ilość zebranych odpadów	Zmiana rok do roku	Zmiana w stosunku do roku bazowego (2013)	w tym zebrane selektywnie:			
				ilość	udział w całym strumieniu odpadów	zmiana rok do roku	zmiana w stosunku do roku bazowego (2013)
	tys. Mg	%	%	tys. Mg	%	%	%
2013	**9 474**	**0,0**	**0,0**	**1 275**	**13,5**	**0,0**	**0,0**
2014	10 330	9,0	9,0	2 050	19,8	47,4	47,4
2015	10 864	5,1	14,7	2 537	23,4	17,7	73,5
2016	11 654	7,3	23,0	2 942	25,2	8,1	87,6
2017	11 969	2,7	26,3	3 239	27,1	7,2	101,1
2018	12 485	4,3	31,8	3 608	28,9	6,8	114,7
2019	12 753	2,1	34,6	3 977	31,2	7,9	131,7
2020	13 117	2,9	38,5	4 975	37,9	21,6	181,8
2021	13 674	4,2	44,3	5 440	39,8	4,9	195,6
2022	13 420	**-1,9**	41,7	5 361	39,9	0,4	196,8

Szeroko rozumiana gospodarka odpadami ma głównie na celu zapobieganie powstawaniu odpadów poprzez rozwiązywanie problemu odpadów „u źródła", a następnie odzyskiwanie surowców i ponowne wykorzystanie odpadów. W przypadku odpadów niewykorzystanych, celem jest bezpieczne dla środowiska końcowe ich unieszkodliwianie, zaś forma ostateczną jest ich składowanie (Rys. 1).

Przedstawiona procedura dotyczy wszystkich wytwarzanych odpadów. W odniesieniu do odpadów przemysłowych istnieją rozwiązania techniczno-technologiczne, których ciągły rozwój pozwala na coraz efektywniejsze wpisywanie się w poszczególne etapy hierarchii postępowania z odpadami. Problemem są odpady komunalne, gdyż przez długie dziesięciolecia były one składowane na wysypiskach, natomiast nowe regulacje prawne, w tym unijne, dążą do zmiany społecznego myślenia o tych odpadach, a w konsekwencji ograniczania liczby i powierzchni wysypisk oraz poddawania ich procesom związanym z odzyskiem.

Nowe myślenie i postępowanie z odpadami komunalnymi

Szeroka akcja edukacyjno-społeczna na temat odpadów komunalnych prowadzona od kilku lat zdaje się przynosić oczekiwane skutki. Efektem tego jest ustabilizowanie się ilości zebranych odpadów, która w ciągu ostatnich 2 lat oscyluje w okolicy 13,4 – 13,7 mln Mg. Z drugiej strony, w okresie ostatnich 10 lat przyrost zebranych odpadów komunalnych przekroczył 40%. Mimo tego obserwuje się inne pozytywne zjawisko – wzrasta ilość odpadów zbieranych selektywnie. Poziom segregacji wynosi niemal 40% wszystkich zebranych odpadów, a na przestrzeni minionej dekady jest to wzrost blisko 200% – Tab. 1.

Zebrane odpady komunalne zmieszane (a więc te, które nie podlegały zbiórce selektywnej) kierowane są do procesów:

- odzysku, w tym:
  - – przekształcania termicznego z odzyskiem energii;
  - – przetwarzania biologicznego (kompostowanie lub fermentacja);
  - – recyklingu;
- unieszkodliwiania, w tym:
  - – przekształcania termicznego bez odzysku energii;
  - – składowania.

Analizując minioną dekadę wyraźnie widać zmiany in plus, które w tym czasie nastąpiły – Tab. 2.

Analizując dane przedstawione w Tab. 1 i 2 oraz inne statystyki podane przez GUS można wyciągnąć kilka istotnych wniosków:

- ilość zbieranych odpadów komunalnych ma tendencję rosnącą, choć w 2022 r. obserwuje się niewielkie przełamanie tego trendu;
- w wydzielonym strumieniu odpadów zebranych selektywnie obserwuje się istotny wzrost ilości tak zebranych odpadów, jednak w okresie ostatnich 3 lat sytuacja uległa pewnej stabilizacji. Prawdopodobnie można to zjawisko powiązać z liczbą Punktów Selektywnego Zbierania Odpadów Komunalnych (tzw. PSZOKów). Jak podaje GUS, w 2022 r. w Polsce było 2301 PSZOKów, wobec 2477 gmin. Wynika z tego, że statystycznie blisko 10% gmin nie posiada w swoich granicach takich punktów. Z kolei w przypadku dużych aglomeracji miejskich takich punktów powin-

Tab. 2. Sposób zagospodarowania zebranych odpadów komunalnych w latach 2013-2022. Źródło: opracowanie własne na podstawie danych GUS
Tab. 2. Method of managing collected municipal waste in 2013-2022. Source: own elaboration based on Central Statistical Office data

Rok	Ilość zebranych odpadów	w tym przeznaczone do:			
		przekształcenia termicznego	przetwarzania biologicznego	recyklingu	składowania
	tys. Mg				
2013	9 474	766	1 230	b.d.	5 979
2014	10 330	1 560	1 154	2 180	5 437
2015	10 864	1 439	1 750	2 867	4 808
2016	11 654	2 266	1 890	3 244	4 255
2017	11 969	2 724 [a] 198 [b]	848	3 199	5 000
2018	12 485	2 822 [a] 191 [b]	1 012	3 269	5 191
2019	12 753	2 742 [a] 179 [b]	1 153	3 192	5 487
2020	13 117	2 656 [a] 166 [b]	1 578	3 499	5 218
2021	13 674	2 702 [a] 171 [b]	1 824	3 681	5 296
2022	13 420	2 741 [a] 113 [b]	1 899	3 585	5 108

a) z odzyskiem energii, b) bez odzysku energii

Fot. 1. Paleniska w spalarni „Descructor". Źródło: [8]
Photo. 1. Hearths in the "Descructor" incinerator. Source: [8]

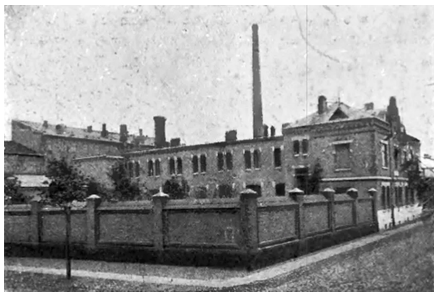

Fot. 2. Miejskie Zakłady Sanitarne w Warszawie wraz ze spalarnią odpadów komunalnych. Źródło: [15]
Photo. 2. Municipal Sanitary Works in Warsaw with a municipal waste incineration plant. Source: [15]

no być co najmniej kilka. W związku z tym poprawy w zakresie ilości odpadów zebranych selektywnie należy upatrywać w zwiększeniu liczby PSZOKów;

- ilość odpadów poddawana przekształcaniu termicznemu wynika z możliwości (wydajności) istniejących zakładów. Niewątpliwie budowa kolejnych jest w stanie zwiększyć wolumen odpadów przeznaczonych do tej formy utylizacji, dodatkowo generując odzysk energii;
- ilość odpadów przeznaczonych do przetwarzania biologicznego (kompostowanie i fermentacja) również uległa stabilizacji ilościowej, natomiast od strony procentowej udziału w całym strumieniu odpadów obserwuje się nieznaczny wzrost tej formy odzysku odpadów;
- podobną stabilizację ilościową można zauważyć w odpadach poddanych procesom recyklingu, jednak procentowo można odnotować spadek;
- za mniej więcej stabilną można uznać ilość odpadów kierowaną na składowiska, przy równoczesnym spadku liczby tych obiektów z 431 o powierzchni 1944, 3 ha w 2013 r. do 259 o powierzchni 1624 ha w 2022 r. Porównując rok 2013 z rokiem 2022 można stwierdzić spadek powierzchni składowisk o ok. 15%, co jest wprost proporcjonalne do ilości umieszczanych na tych składowiskach odpadów – ich ilość również spadła o ok. 15%;
- ilość odpadów lokowanych na składowiskach w odniesieniu do całego strumienia odpadów komunalnych ma trend malejący. W 2013 r. odpady na składowiskach stanowiły ok. 63% wszystkich odpadów komunalnych, gdy w 2022 r. było to już 38%;
- ponadto 92% składowisk jest wyposażonych w instalacje służące do odgazowywania, w wyniku czego w 2022 r. poprzez spalanie ujętego gazu odzyskano ok. 30,9 GWht (energia cieplna) oraz ok. 102,5 GWhe (energia elektryczna).

Szacuje się, że w ciągu kolejnych 10 lat ilość wytwarzanych odpadów komunalnych osiągnie poziom ok. 15,5 mln Mg [14].

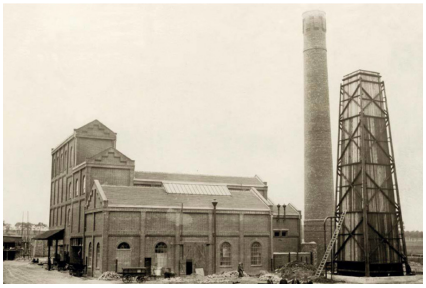

Fot. 3. Spalarnia odpadów w Poznaniu uruchomiona w 1927 r. Źródło: [15]
Photo. 3. Waste incineration plant in Poznań launched in 1927. Source: [15]

Fot. 4. Elektrociepłownia Zabrze z kotłem wielopaliwowym. Źródło: [15]
Photo. 4. Zabrze Heat and Power Plant with a multi-fuel boiler. Source: [15]

Z kolei oczekuje się, że poziom przygotowania do ponownego użycia i recyklingu odpadów komunalnych wyniesie 55% w roku 2025, 60% w roku 2030 oraz 65% w roku 2035. Równocześnie zakłada się, że na składowiska odpadów komunalnych trafi 30% wytworzonych odpadów w 2025 r., 20% w 2030 r. i 10% w 2035 r. W związku z tym w perspektywie do roku 2034 zakłada się budowę 814 nowych PSZOKów oraz modernizację ok. 30% obecnie funkcjonujących. Oceniono, że w dużych miastach (aglomeracjach miejskich) powinien funkcjonować 1 PSZOK na 50 tys. mieszkańców. W przypadku małych miast (poniżej 50 tys. mieszkańców) – 1 PSZOK, podobnie w gminach wiejskich. Łącznie w skali kraju występuje zapotrzebowanie na poziomie ok. 2 714 PSZOKów [12].

Tymczasem obecnie poziom przygotowania do ponownego użycia i recyklingu odpadów komunalnych wynosi ok. 40%, a na składowiska trafia ok. 38% odpadów komunalnych.

Aby sprostać tym wyzwaniom jednym z kierunków działania powinno być zwiększenie potencjału instalacji do termicznego przekształcania odpadów komunalnych.

Termiczne przekształcanie odpadów komunalnych szansą na poprawę obecnej sytuacji?

Z dużą dozą prawdopodobieństwa można domniemywać, że proceder spalania odpadów towarzyszy człowiekowi od chwili opanowania przez niego ognia. I trwa po dzień dzisiejszy, choć w różnych formach. Najbardziej pożądaną to sposób kontrolowanego spalania w dostosowanych do tego urządzeniach, najlepiej z odzyskiem energii. Inną formą jest spalanie odpadów w paleniskach domowych, aktualnie w Polsce zakazaną z uwagi na znaczny stopień szkodliwości, co nie oznacza, że niepraktykowaną. Na szczęście wzrasta poziom świadomości społecznej w tym zakresie, co jest niewątpliwie skutkiem kampanii edukacyjnych.

Pierwsze próby spalania odpadów na większa skalę podjęto w 2 poł. XIX w. w Wielkiej Brytanii. W 1870 r. uruchomiono w Paddington pod Londynem pierwszą spalarnię, jednak w krótkim czasie została ona zamknięta z uwagi na niską efektywność. Kolejną, tym razem udaną, próbę podjęto w Nottingham w 1874 r. Powstała spalarnia „Destructor" (Fot. 1) pracowała 24 godz./dobę, a jej roczna wydajność wynosiła ok. 24 tys. Mg spalanych odpadów.

Projekt ten można określić mianem sukcesu, gdyż w do 1890 r. na terenie Wielkiej Brytanii pracowało 39 takich instalacji. W tym czasie instalacja pierwotna była udoskonalana, czego efektem było odzyskiwanie ciepła i produkcja pary do napędu generatorów elektrycznych [8].

Technologia ta zyskała na tyle dużą popularność, że w latach 1876–1908 w Europie wybudowano ponad 210 instalacji do spalania odpadów, i ponad 180 w Stanach Zjednoczonych [15].

Pierwsza spalarnia w Polsce powstała w 1912 r. w Warszawie przy ul. Spokojnej 15 (Fot. 2). Działała do 1944 r., zniszczona w trakcie Powstania Warszawskiego.

Kolejna, jedna z najnowocześniejszych w owym czasie, powstała w 1927 r. w Poznaniu (Fot. 3) i pracowała przez kolejnych 30 lat.

Z początkiem lat 50. XX w. spalarnie uznano za obiekty zbyt kosztowne wobec składowisk odpadów. Było to przyczyną regresu w budowie nowych obiektów termicznego unieszkodliwiania odpadów, który trwał do lat 70. Wówczas zaczęły powstawać instalacje kolejnej generacji, których zadaniem było wytworzenie energii elektrycznej i cieplnej, ale równocześnie ograniczenie nadmiernej emisji odprowadzanych do atmosfery zanieczyszczeń pyłowych i gazowych [2].

Aktualnie w Europie działa blisko 500 instalacji termicznego przekształcania odpadów, z czego 8 w Polsce – Tab. 3.

Łącznie aktualnie pracujące instalacje są w stanie przetworzyć 1114 tys. Mg odpadów komunalnych. Po zakończeniu rozbudowy instalacji w Warszawie i Rzeszowie zdolności przerobowe osiągną wartość 1459 tys. Mg.

Tab. 3. Instalacje termicznego przekształcania odpadów w Polsce. Źródło: opracowanie własne

Tab. 3. Waste thermal treatment installations in Poland. Source: own study

Nazwa	Lokalizacja	Rok uruchomienia	Wydajność tys. Mg/rok	Zdolność odzysku energii
Zakład Unieszkodliwiania Stałych Odpadów Komunalnych	Warszawa	2001 po rozbudowie 2024	40 po rozbudowie 305	10,5 GWh_e 67 GWh_t po rozbudowie 100 GWh_e 200 GWh_t
Zakład Termicznego Unieszkodliwiania Odpadów Komunalnych	Konin	2015	94	47 GWh_e 33 GWh_t
Zakład Unieszkodliwiania Odpadów Komunalnych	Białystok	2016	120	43 GWh_e 100 GWh_t
Zakład Termicznego Przekształcania Odpadów w Krakowie (Ekospalarnia)	Kraków	2016	220	65 GWh_e 280 GWh_t
Instalacja Termicznego Przekształcania Odpadów Komunalnych	Poznań	2016	210	130 GWh_e 83 GWh_t *108 GWh_e* [a] *146 GWh_t* [a]
Zakład Termicznego Przekształcania Odpadów Komunalnych	Bydgoszcz	2017	180	88,5 GWh_e 180 GWh_t
Zakład Unieszkodliwiania Odpadów	Szczecin	2017	150	88 GWh_e 256 GWh_t *88,5 GWh_e* [a] [b] *202 GWh_t* [a] [b]
Instalacja Termicznego Przetwarzania z Odzyskiem Energii	Rzeszów	2018 po rozbudowie 2024	100 po rozbudowie 180	37 GWh_e 123 GWh_t

[a] dane za 2022 r., [b] produkcja brutto bez uwzględnienia potrzeb zakładu

Tab. 4. Cementownie posiadające instalacje do termicznego przekształcania odpadów. Źródło: opracowanie własne na podstawie [6, 14]

Tab. 4. Cement plants with installations for thermal waste treatment. Source: own study based on [6, 14]

Cementownia	Właściciel	Lokalizacja (województwo)	Moce przerobowe [tys. Mg/rok]	Moce wykorzystane [a] [%]	Odzysk energii [a] [GWh_t]
Karsy	Cement Ożarów S.A.	świętokrzyskie	1 000	30,9	1 718
Chełm	Cemex Polska sp. z o.o.	lubelskie	934	33,8	1 674
Rudniki		śląskie	201		387
Bielawy	Lafarge Cement S.A.	kujawsko-pomorskie	430	32,5	1 155
Małogoszcz		świętokrzyskie	634		1 018
Górażdże	Górażdże Cement S.A.	opolskie	580	80,2	2 874
Nowiny	Dyckerhoff Polska sp. z o.o.	świętokrzyskie	510	27,7	848
Trębaczew	Warta S.A.	łódzkie	260	55,3	0,3
Opole	Odra S.A.	opolskie	85	36,4	229

[a] dane za rok 2020, za [14]

Tab. 5. Planowane budowy instalacji termicznego przekształcania odpadów. Źródło: opracowanie własne na podstawie [7]

Tab. 5. Planned construction of thermal waste treatment installations. Source: own study based on [7]

Lokalizacja	Wydajność [tys. Mg/rok]	Uwagi
Łódź	150	
Łódź	200	
Bełchatów	180	
Ruda Śląska	80–120	
Bielsko-Biała	100	min. wartość opałowa odpadów 12 MJ/kg
Będzin	200	
Chorzów	100	
Oświęcim	130 + 20 [a]	[a] odpady komunalne + osady ściekowe
Inowrocław	310	głównie odpady komunalne z niewielkim strumieniem odpadów przemysłowych
Gliwice	46	w tym 6 tys. Mg podsuszonych osadów ściekowych
Tychy	25	spalanie RDFu Refuse Derived Fuel – paliwa obejmujące szeroką gamę odpadów, które zostały przetworzone w celu osiągnięcia wysokiej wartości opałowej. RDF, najczęściej stosowany jest w odniesieniu do frakcji kalorycznej odpadów o dużej wartości opałowej (zwykle około 18 MJ na kilogram masy).
Rzeszów	50–100	druga spalarnia w mieście
Chrzanów	23,6	spalanie RDFu w ciepłowni
Andrychów	30	
Krosno	22	
Starachowice	30	

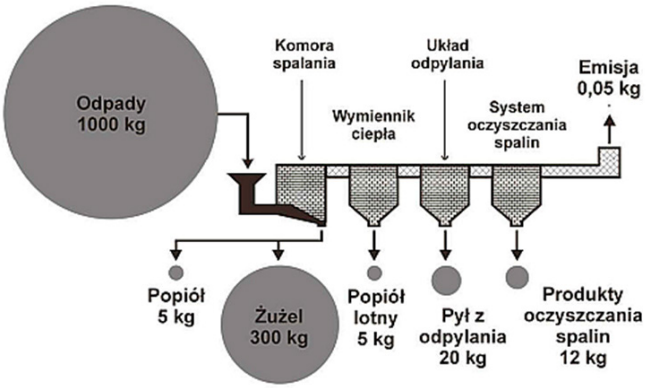

Rys. 2. Przykładowy bilans masy spalarni odpadów komunalnych. Źródło: [4]
Fig. 2. An example of a mass balance of a municipal waste incineration plant. Source: [4]

W trakcie budowy są instalacje w Gdańsku i Olsztynie, których realizacja powinna być zakończona w 2023 r. Ich uruchomienie to szansa na przetworzenie kolejnych 260 tys. Mg odpadów.

Prócz typowych instalacji do termicznego przekształcania odpadów komunalnych z odzyskiem energii (Tab. 3) istnieją współspalarnie odpadów w cementowniach oraz w zakładzie energetycznym. Należy jednak zauważyć różnicę pomiędzy spalarnią a współspalarnią. Ta pierwsza ma za zadanie przekształcanie odpadów, natomiast uzykana energia jest niejako efektem ubocznym. W przypadku współspalarni spalane odpady wraz z innymi paliwami mają na celu wytworzenie energii, która jest wykorzystywana w procesach podstawowych danego zakładu (produkcja cementu i klinkieru, wytwarzanie energii elektrycznej i cieplnej) [13].

Współspalanie odpadów w cementowniach jest możliwe dzięki specjalnie dedykowanym instalacjom do termicznego przekształcania odpadów, których w Polsce jest 9 – Tab. 4.

Wskazane w Tab. 4 cementownie mają łączny potencjał przerobowy na poziomie ok. 4,6 mln Mg odpadów rocznie. W 2020 r. wykorzystane zostało tylko 39,3% mocy przerobowych, tj. przekształceniu poddano 1819,9 tys. Mg odpadów odzyskując przy tym energię w ilości 9,9 TWht. Należy zaznaczyć, że ponad 87% spalonych odpadów to odpady o kodzie 19 12 10, natomiast nie spalano odpadów z grupy 20, tj. odpadów komunalnych [14]. Na uwagę zwraca również fakt, że sukcesywnie w cementowniach węgiel zastępowany jest paliwami alternatywnymi (tu: odpadami). W 2019 r. w ogólnym wolumenie paliwa do zasilania procesów produkcyjnych udział odpadów stanowił 75% [5].

Współspalarnia w zakładzie energetycznym została zrealizowana w Elektrociepłowni Zabrze (Fot. 4) w zakładzie energetycznego spalania paliw. Zgodnie z posiadanym pozwoleniem, Elektrociepłownia może poddawać termicznemu przekształceniu 450 tys. Mg odpadów rocznie, w tym 250 tys. Mg odpadów komunalnych oraz pochodzących z przetworzenia odpadów komunalnych. W 2020 r. instalacja odzyskała 396 GWht spalając 101,7 tys. Mg odpadów o kodzie 19 12 10, z czego 81,1 tys. Mg stanowiły odpady komunalne [14].

Obecnie w Polsce istnieje kilkadziesiąt projektów, które rozważają na przestrzenie najbliższych kilku – kilkunastu lat możliwość budowy instalacji termicznego przekształcania odpadów. Stopień zaawansowania tych projektów jest mocno zróżnicowany i obejmuje instalacje o wydajności od 22 do 310 tys. Mg/rok – Tab. 5. Jest również wskazanych kilkanaście innych lokalizacji (np. Katowice, Wodzisław Śląski), jednak w chwili obecnej brak jest jakichkolwiek danych na temat ewentualnych instalacji.

Aktualnie przepustowość czynnych instalacji przekształcania odpadów jest niewystarczająca w stosunku do potrzeb, co może skutkować tym, że zabraknie wolnej pojemności na składowiskach [1]. Wobec powyższego, budowa kolejnych instalacji wydaje się być koniecznością. Jednak dążąc w kierunku gospodarki o obiegu zamkniętym należy dążyć w kierunku maksymalnego wykorzystania surowców. Przekształceniu termicznemu powinny być poddawane przede wszystkim odpady nienadające się do recyklingu.

Odpady generują nowe odpady

Na skutek termicznego przekształcania odpadów komunalnych powstaje szereg produktów, będących efektem spalania. Ich rodzaj oraz ilość w głównej mierze zależy od struktury spalanych odpadów komunalnych (należy zauważyć, że struktura ta charakteryzuje się pewną zmiennością w czasie – sezonowością, co jest związane z porami roku, w których powstają spalane odpady komunalne), ale także od technologii spalania odpadów oraz technologii oczyszczania spalin.

Efektem termicznego przekształcania odpadów komunalnych (w procesie spalania) jest powstawanie stałej pozostałości w postaci żużli i popiołów paleniskowych. Do tego dochodzą jeszcze tzw. popioły lotne. Powstają one na skutek przepływu powietrza przez strefę spalania, które „porywa" drobne cząsteczki ciał stałych tworząc emisje pyłu z procesu spalania. Wraz ze wzrostem prędkości przepływu powietrza i w związku z tym lepszym natlenianiem strefy spalania emisja pyłów jest większa. Wielkość emisji pyłów jest uzależniona od wielu czynników, m. in. technologii spalania odpadów, ale też od zawartości substancji niepalnych w paliwie (odpadach komunalnych). Głównym składnikiem pyłów są związki krzemu, glinokrzemiany, tlenki żelaza, ale też związki alkaliczne, w szczególności tlenki siarki. Z uwagi na ochronę środowiska niezbędne jest oczyszczanie spalin – reguluje to dyrektywa unijna 2010/75/WE. System oczyszczania spalin jest dość skomplikowany i składa się z kilku elementów:

- odpylania gazów spalinowych;
- usuwania gazów kwaśnych;
- usuwania tlenków azotu;

Tab. 6. Klasyfikacja produktów termicznego przekształcania odpadów komunalnych wg [11]. Źródło: opracowanie własne
Tab. 6. Classification of municipal waste thermal treatment products according to [11]. Source: own study

Miejsce powstania odpadów	Nazwa odpadu wg Rys. 2	Kod odpadu	Grupy, podgrupy i rodzaje odpadów wg katalogu odpadów
Komora spalania	Żużel, popiół paleniskowy	19 01 11*	Żużle i popioły paleniskowe zawierające substancje niebezpieczne
		19 01 12	Żużle i popioły paleniskowe inne niż wymienione w 19 01 11
Wymiennik ciepła	Popiół lotny	19 01 13*	Popioły lotne zawierające substancje niebezpieczne
		19 01 14	Popioły lotne inne niż wymienione w 19 01 13
Układ odpylania	Pył z odpylania	19 01 15*	Pyły z kotłów zawierające substancje niebezpieczne
		19 01 16	Pyły z kotłów inne niż wymienione w 19 01 15
System oczyszczania spalin	Produkty oczyszczania spalin	19 01 05*	Osady filtracyjne (np. placek filtracyjny) z oczyszczania gazów odlotowych
		19 01 06*	Szlamy i inne odpady uwodnione z oczyszczania gazów odlotowych
		19 01 07*	Odpady stałe z oczyszczania gazów odlotowych
	Zużyte sorbenty (węgiel aktywny)	19 01 10*	Zużyty węgiel aktywny z oczyszczania gazów odlotowych

Odpady oznaczone * (gwiazdką) oznaczają odpady niebezpieczne

Tab. 7. Gospodarcze wykorzystanie żużli i popiołów paleniskowych w niektórych państwach UE. Źródło: opracowanie własne na podstawie [16]
Tab. 7. Commercial use of slags and bottom ashes in some EU countries. Source: own study based on [16]

Państwo	Stopień wykorzystania gospodarczego [%]	Sposób wykorzystania gospodarczego
Austria	0	kierowane na składowiska
Belgia	100	materiały budowlane
Czechy	0	kierowane na składowiska
Dania	98	budownictwo drogowe
Francja	30	materiały budowlane
Hiszpania	0	kierowane na składowiska
Holandia	75	budownictwo drogowe
Niemcy	85	budownictwo drogowe
Portugalia	0	kierowane na składowiska
Szwecja	85	budownictwo drogowe
Wielka Brytania	40	budownictwo drogowe
Włochy	20	budownictwo drogowe

- usuwania metali ciężkich;
- usuwania związków organicznych.

Niewątpliwą zaletą termicznego przekształcania odpadów jest redukcja objętości odpadów na wejściu do instalacji w porównaniu z objętością na wyjściu z instalacji i kształtuje się na poziomie 80–95%. Z kolei redukcja masy wynosi od 60 do 70% [9].

Na Rys. 2 pokazano przykładowy bilans masy spalarni odpadów komunalnych. Pokazane wartości wychodu poszczególnych frakcji należy traktować orientacyjnie.

Prócz produktów spalania pokazanych na Rys. 2 występują również jako odpady wszelkiego rodzaju sorbenty wykorzystane w procesie oczyszczania spalin, albo w postaci ciał stałych (np. węgiel aktywny w przypadku metody „suchej") bądź szlamów (w przypadku technologii „mokrej"). Wysuszone szlamy określane są jako tzw. placki filtracyjne.

Każdy produkt spalania (tu: odpad wtórny) podlega zaklasyfikowaniu do właściwej grupy odpadów zgodnie z katalogiem odpadów [11]. Klasyfikację tę w odniesieniu do odpadów zidentyfikowanych na Rys. 2 przedstawiono w Tab. 6.

Jak wynika z Tab. 6, część odpadów jest kwalifikowana jako niebezpieczne z uwagi na zawartość w nich substancji niebezpiecznych. W zdecydowanej większości żużle i popioły paleniskowe nie są kwalifikowane jako odpady niebezpieczne, dzięki czemu mogą być wykorzystane gospodarczo. Niemniej jednak przed skierowaniem ich do ponownego wykorzystania poddaje się je wstępnej obróbce, której celem jest separacja frakcji metalicznej (odzyskanie złomu metali). Docelowo materiał ten najczęściej wykorzystywany jest w budownictwie drogowym (Polska), bądź do produkcji prefabrykatów budowlanych.

Mimo możliwości wykorzystania żużli i popiołów paleniskowych w budownictwie, w niektórych krajach Unii Europejskiej odpady te kierowane są na składowiska – Tab. 7. Najprawdopodobniej jest to konsekwencja bardziej restrykcyjnych przepisów krajowych w stosunku do Dyrektywy Unijnej.

O wiele poważniejszy problem stanowią odpady z oczyszczania gazów spalinowych (popioły lotne, pyły z oczyszczania gazów odlotowych), które zawierają znaczne ilości metali ciężkich oraz produkty niepełnego spalania (dioksyny, bifenyle, wielopierścieniowe węglowodory aromatyczne itp.). Ponieważ są to odpady zaliczane do grupy odpadów niebezpiecznych, w Polsce odpady te kierowane są – po wcześniejszej dodatkowej obróbce (immobilizacji) – na specjalnie przygotowane powierzchniowe składowiska odpadów niebezpiecznych. W Tab. 8 zestawiono ilości popiołów i pyłów zakwalifikowanych jako niebezpieczne (odpady „z gwiazdką"), wytwarzanych przez spalarnie odpadów komunalnych.

W przypadku odpadów stanowiących mieszankę odpadów oznaczonych odpowiednimi kodami, mieszanka może być przyporządkowana tylko do jednego kodu odpadów. Wówczas pod tym kodem próbka odpadów przechodzi przez cały proces zarządzania odpadami dla potrzeb odzysku lub unieszkodliwiania.

Odpady wskazane w Tab. 8 stanowią niespełna 4% masy przekształcanych termicznie odpadów komunalnych. Wydaje się to być sukcesem, ale tylko pozornie. Trzeba pamiętać, że ta

Tab. 8. Roczny wolumen wtórnych odpadów niebezpiecznych (frakcja sucha) wytworzonych w 2019 r. przez krajowe instalacje termicznego przekształcania odpadów komunalnych. Źródło: opracowanie własne

Tab. 8. Annual volume of secondary hazardous waste (dry fraction) generated in 2019 by domestic installations for the thermal treatment of municipal waste. Source: own study

Nazwa instalacji, lokalizacja	Ilość wytwarzanych odpadów o określonych kodach [Mg/rok]			
	19 01 07*	19 01 11*	19 01 13*	19 01 15*
Zakład Unieszkodliwiania Stałych Odpadów Komunalnych, Warszawa	952,52		196,08	
Zakład Termicznego Unieszkodliwiania Odpadów Komunalnych, Konin	2 533,36 [a)]		[a)]	698,72
Instalacja Termicznego Przekształcania Odpadów Komunalnych, Poznań	7 487,34 [b)]	[b)]		b.d.
Zakład Unieszkodliwiania Odpadów Komunalnych, Białystok	3 024,91 [c)]			[c)]
Zakład Termicznego Przekształcania Odpadów, Kraków	2 211,76		6 051,78	
Zakład Termicznego Przekształcania Odpadów Komunalnych, Bydgoszcz	5 069,00		900,00	
Zakład Unieszkodliwiania Odpadów, Szczecin			300,00 [d)]	7 000,00 [e)]
Instalacja Termicznego Przetwarzania z Odzyskiem Energii, Rzeszów	2 000,00		2 000,00	
R A Z E M	**23 278,89**		**9 447,86**	**7 698,72**
S U M A	**40 425,47**			

[a)] mieszanka 19 01 07* i 19 01 13*, odpady zbierane we wspólnym silosie, kod 19 01 07* dominujący
[b)] mieszanka 19 01 07* i 19 01 11*, odpady zbierane we wspólnym silosie, kod 19 01 07* dominujący
[c)] mieszanka 19 01 07* i 19 01 15*, odpady zbierane we wspólnym silosie, kod 19 01 07* dominujący
[d)] mieszanka dodatku i sorbentu
[e)] ciężka frakcja pyłu kotłowego i lekka frakcja z filtra elektrostatycznego łącznie
W przypadku odpadów stanowiących mieszankę odpadów oznaczonych odpowiednimi kodami, mieszanka może być przyporządkowana tylko do jednego kodu odpadów. Wówczas pod tym kodem próbka odpadów przechodzi przez cały proces zarządzania odpadami dla potrzeb odzysku lub unieszkodliwiania.

ilość odpadów po odpowiedniej obróbce trafi na składowisko odpadów niebezpiecznych.

Podsumowanie

Instalacje do termicznego przekształcania odpadów komunalnych cieszą się dużą popularnością na całym świecie, a w szczególności w krajach o wysokim stopniu rozwoju. Wymusza to niewątpliwie rozwój cywilizacyjny w poszczególnych krajach. Polska stara się nadążyć za tym trendem, o czym świadczą działające już spalarnie, oraz te, które zostaną uruchomione w najbliższej przyszłości. I choć budzą wiele kontrowersji, to niewątpliwie mają duży wpływ na rozwiązania związane ze składowaniem odpadów. Nie podlega dyskusji uzyskany efekt energetyczny.

Jakikolwiek proces spalania pozostawia po sobie spalania. Podobnie jest w spalarniach odpadów komunalnych. Sporą część produktów spalania – odpadów wtórnych – można wykorzystać gospodarczo. Jednak pozostają niewielkie ilości odpadów („z gwiazdką"), które ze względu na swoją specyfikę nie mogą być wykorzystane gospodarczo i w związku z tym trafiają na składowiska odpadów niebezpiecznych. Działanie to nie jest korzystne od strony finansowej, niesie ze sobą także potencjalnie niekorzystne oddziaływanie na środowisko. W związku z tym koniecznym staje się poszukiwanie innych rozwiązań, które pozwolą na ograniczenie ilości odpadów trafiających na składowiska odpadów niebezpiecznych.

Literatura – References

1. Hryb W., Ceglarz K. Odpady komunalne w aspekcie gospodarki o obiegu zamkniętym. Wydawnictwo Politechniki Śląskiej. Gliwice 2021.
2. http://www.forum-dyrektorow.pl/cms/artykuly/cykl-artykulow-autor-wojciech-janka#historia-gospodarki-odpadami (dostęp 12.06.2023).
3. http://www.kampania-ekon.pl/pl/odpady (dostęp: 12.06.2023).
4. https://docplayer.pl/21778633-Wtorne-odpady-ze-spalania-odpadow-komunalnych-bariery-i-perspektywy-ich-wykorzystania.html (dostęp 13.06.2023).
5. https://www.polskicement.pl/2022-informator-spc-przemysl-cementowy-w-liczbach/ (dostęp 13.06.2023).
6. https://przemyslisrodowisko.pl/cementownie-i-zaklady-energetycznego-spalania-paliw-ich-udzial-w-termicznym-przeksztalcaniu-odpadow-w-polsce/ (dostęp 13.06.2023).
7. Kozioł M. Możliwość substytucji węgla paliwami z odpadów w warunkach polskich. Rynek Energii nr 3, 2022.
8. Lewis H. Centenary History of Waste and Waste Managers in London and South East England. The Chartered Institution of Wastes Management. 2007.
9. Mokrosz W. Ekologiczne aspekty oczyszczania spalin ze spalarni odpadów komunalnych i przemysłowych. https://docplayer.pl/6677159-Ekologiczne-aspekty-oczyszczania-spalin-ze-spalarni-odpadow-komunalnych-i-przemyslowych.html (dostęp 13.06.2023).
10. Ochrona środowiska 2022. Główny Urząd Statystyczny. Warszawa 2022.
11. Rozporządzenie Ministra Klimatu z dnia 2 stycznia 2020 r. w sprawie katalogu odpadów. Dz. U. 2020 r., poz. 10.
12. Uchwała Rady Ministrów z dnia 12 czerwca 2023 r. w sprawie Krajowego planu gospodarki odpadami 2028. Monitor Polski z 2023 r. poz. 702.
13. Ustawa z dnia 14 grudnia 2012 r. o odpadach. Dziennik Ustaw 2013, poz. 21.
14. Waszczyłko-Miłkowska B., Kamińska-Borak J. Raport Termiczne przekształcanie odpadów komunalnych w Polsce w roku 2020 – dane BDO. Instytut Ochrony Środowiska, Państwowy Instytut Badawczy. Warszawa 2021.
15. Wielgosiński G. Termiczne przekształcanie odpadów. Wydawnictwo Nowa Energia, Racibórz 2020.
16. Vehlow J., Bergfeldt B., Wilen C., Ranta J., Schwaiger H., Visser H J.M., Gu S., Gyftopoulou E., Brammer J. Management of Solid Residues In Waste-to-Energy and Biomass Systems. Forschungszentrum Karlsruhe (FZKA 7347). Karlsruhe 2007.

Hazardous Secondary Waste from Municipal Waste Incineration Installations

Waste has always accompanied man. As human evolution progressed, not only the quality of waste changed, but also its quantity. Already in antiquity, attempts were made to organize the issue of waste, which over the centuries resulted in various legal regulations. The last 150 years have seen a rapid development of techniques and technologies aimed at solving problems related to waste, including municipal waste. This was forced, among others, by the industrial revolution, which was accompanied by the rapid development of cities associated with the increase in the number of inhabitants, and as a consequence, the amount of generated waste increased. Current activities, especially in the European Union, are aimed at the maximum use of waste, limiting its storage in landfills for re-use. One of the elements in this chain of activities is the incineration of municipal waste, which significantly reduces the amount of waste sent to landfills. However, the problem is secondary waste, which is the product of combustion and is classified as hazardous waste. After being properly treated, they end up in hazardous waste landfills, which, despite the use of advanced security measures, pose a potential threat to the environment.

Keywords: *municipal waste, waste incineration, secondary waste*

Przyjazna dla środowiska przeróbka surowców mineralnych – przegląd referatów zaprezentowanych podczas konferencji naukowo-technicznej KOMEKO 2023

Małgorzata MALEC[1)], Lilianna STAŃCZAK[1)]

[1)] Instytut Techniki Górniczej KOMAG

http://doi.org/10.29227/IM-2023-01-35

Submission date: 19-05-2023 | Review date: 09-06-2023

Abstrakt

Artykuł stanowi przegląd wybranych referatów zaprezentowanych podczas konferencji KOMEKO 2023, zorganizowanej w Szczyrku przez Instytut Techniki Górniczej KOMAG w dniach od 27 do 29 marca br. Ich tematyka dotyczyła m.in. innowacyjnych rozwiązań technicznych i technologicznych
w zakresie przeróbki mechanicznej surowców mineralnych, racjonalnego gospodarowania odpadami zgodnie z wymaganiami Zielonego Ładu, wytwarzania wodoru i kompozytów geopolimerowych z odpadów pogórniczych, wzbogacanie odpadów oraz kruszyw zawierających pierwiastki ziem rzadkich czy też recyklingu odpadów zawierających lit. Dużym zainteresowaniem uczestników konferencji KOMEKO 2023 cieszył się panel dyskusyjny poświęcony zautomatyzowanemu, zeroodpadowemu zakładowi przeróbczemu. Szczególną uwagę zwrócono na temat zagospodarowania odpadów wydobywczych w Polsce w świetle wyzwań europejskiej gospodarki o obiegu zamkniętym oraz na temat bezpieczeństwa eksploatacji maszyn i urządzeń przeróbczych w aspekcie wdrażania innowacyjnych rozwiązań. Konferencja naukowo-techniczna KOMEKO 2023 stanowiła forum interesującej wymiany wiedzy i doświadczeń zawodowych między naukowcami, producentami maszyn i urządzeń przeróbczych, a ich użytkownikami reprezentującymi sektor producentów surowców mineralnych. O sukcesie konferencji świadczą ożywione i owocne dyskusje między wszystkimi interesariuszami procesu przeróbki surowców mineralnych.

Słowa kluczowe: *przeróbka surowców mineralnych, gospodarowanie odpadami, recykling odpadów, odpady pogórnicze, maszyny i urządzenia przeróbcze*

1. Wprowadzenie

Konferencja naukowo-techniczna KOMEKO 2023 została zorganizowana przez Instytut Techniki Górniczej KOMAG w okresie od 27 do 29 marca br. Na miejsce konferencji wybrano hotel "Klimczok" w Szczyrku, gdzie uczestnicy mogli w komfortowych warunkach brać udział w sesjach, dyskusjach oraz wydarzeniach towarzyszących. Honorowy patronat objęło Ministerstwo Aktywów Państwowych, natomiast partnerami konferencji byli: Jastrzębska Spółka Węglowa S.A., Polska Grupa Górnicza S.A. oraz HALDEX S.A., partnerami merytorycznymi zostali: Instytut Gospodarki Surowcami Mineralnymi i Energią Polskiej Akademii Nauk oraz Polskie Towarzystwo Przeróbki Kopalin. Patronat medialny sprawowały czasopisma: "Inżynieria Mineralna" oraz "Mining Machines". Tematykę pięciu sesji konferencyjnych ukierunkowano na przemysł przyjazny dla środowiska. Program obejmował prezentację 25 referatów przygotowanych przez naukowców, producentów maszyn i urządzeń przeróbczych oraz ich użytkowników reprezentujących kopalnie surowców mineralnych. Konferencja KOMEKO 2023 stanowiła forum wymiany wiedzy i doświadczeń między interesariuszami procesów przeróbki surowców mineralnych. Na podkreślenie zasługuje fakt, że w wielu referatach zaprezentowano innowacyjne rozwiązania techniczne i technologiczne w zakresie przeróbki surowców mineralnych, racjonalnego gospodarowania odpadami, wytwarzania wodoru i kompozytów geopolimerowych z odpadów pogórniczych, wzbogacania odpadów oraz kruszyw zawierających pierwiastki ziem rzadkich, rekuperacji ciepła z istniejących składowisk odpadów pogórniczych, czy recyklingu odpadów zawierających lit. Konferencję rozpoczął panel dyskusyjny, którego tematyka była ukierunkowana na w pełni zautomatyzowany, zeroodpadowy zakład przeróbczy w aspekcie racjonalnego gospodarowania odpadami. W dyskusji uczestniczyli przedstawiciele następujących instytucji: KGHM Cuprum – Centrum Badawczo-Rozwojowe, Instytut Techniki Górniczej KOMAG, Instytut Gospodarki Surowcami Mineralnymi i Energią Polskiej Akademii Nauk oraz Politechnika Krakowska. Z dużym zainteresowaniem uczestnicy konferencji KOMEKO 2023 wysłuchali referatu przedstawiciela Wyższego Urzędu Górniczego na temat bezpieczeństwa eksploatacji maszyn i urządzeń w odkrywkowym zakładzie górniczym. Tematyka poszczególnych sesji przedstawiała się następująco:

Sesja I – Zeroodpadowy zakład przeróbczy

Tematyka referatów dotyczyła zagospodarowania odpadów wydobywczych w Polsce w świetle wyzwań europejskiej gospodarki o obiegu zamkniętym, modernizacji zakładu przeróbczego w kierunku niskiej emisji i automatyzacji procesów, nowych sposobów zagospodarowania produktów procesu przeróbczego w polskim górnictwie oraz ekonomicznej oceny koncepcji budowy w pełni zautomatyzowanego, niskoemisyjnego zakładu przeróbczego w warunkach polskich.

Sesja II – Gospodarowanie odpadami

Tematyka referatów była ukierunkowana na odzysk litu z odpadów, nową technologię wytwarzania wodoru i kompozytów geopolimerowych z odpadów pogórniczych, potencjał

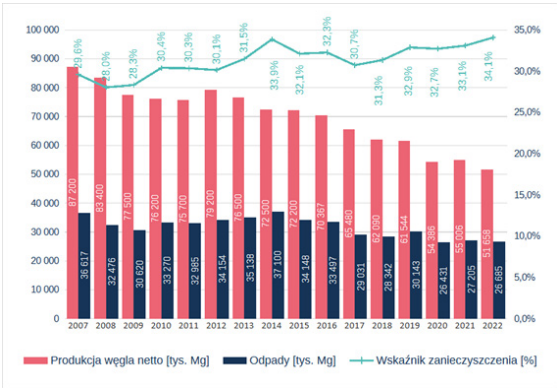

Rys. 1. Węgiel kamienny a środowisko – odpady wydobywcze
Fig. 1. Hard coal and the environment – mining waste

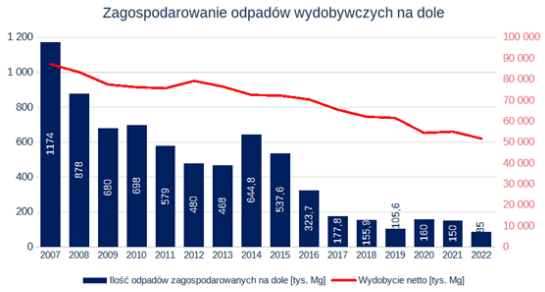

Rys. 2. Odpady w produkcji węgla kamiennego
Fig. 2. Waste in hard coal production

finansowy i technologiczny recyklingu zużytych sprzętów elektrycznych i elektronicznych oraz na koncepcję przyjaznej dla środowiska technologii odzysku metali z zużytych płyt obwodów drukowanych.

Sesja III – Wykorzystanie odpadów

Zagadnienia, przedstawione w referatach wygłoszonych w tej sesji, były związane z ochroną powierzchni terenu przed szkodami górniczymi, wykorzystaniem kopaliny towarzyszącej wydobyciu węgla do produkcji kruszyw, efektywnym wykorzystaniem drobnoziarnistych surowców węglowych w procesach kompaktowania, prototypem dezintegratora, rozwojem technologii wychwytu CO2 oraz rekuperacją ciepła z istniejących i budowanych składowisk odpadów pogórniczych.

Sesja IV – Zakład przeróbczy przyszłości

Referaty prezentowały kierunki działań modernizacyjnych w zakładach przeróbki mechanicznej, a także innowacyjną metodę wymiany taśmy w przenośniku taśmowym, informacje o komponentach ze stali trudnościeralnej stosowanych w zakładach przeróbczych, na temat nowoczesnych rozwiązań przeróbki mechanicznej węgla, poprawy własności użytkowych węgli oraz konsekwencji dla zakładów przeróbczych wynikających ze zmiany wymogów dla silników elektrycznych.

Sesja V – Innowacyjne rozwiązania

W ostatniej sesji konferencyjnej przedstawiono wyniki badań systemu do zabezpieczania kolejowych transportów węgla przed pyleniem wtórnym oraz działaniem czynników atmosferycznych, informacje na temat wzbogacenia odpadów oraz kruszyw naturalnych zawierających pierwiastki ziem rzadkich, wyniki badań wpływu zakresu uziarnienia węgla koksowego na efektywność procesu flotacji pianowej oraz drogi rozwoju od maszyny do systemu mechatronicznego na przykładzie flotacji mułów węglowych.

Uczestnicy konferencji zwracali uwagę na aktualność jej tematyki, zwłaszcza w aspekcie Sprawiedliwej Transformacji Rejonów Pogórniczych, Gospodarki o Obiegu Zamkniętym oraz Zielonego Ładu. Podkreślali celowość organizacji tego typu wydarzeń, sprzyjających nie tylko wymianie doświadczeń naukowych, badawczych i technicznych, ale również integracji środowiska interesariuszy procesów przeróbki surowców mineralnych.

2. Przegląd literatury

Problematyka konferencji jest opisana w wielu dostępnych publikacjach zarówno krajowych, jak i zagranicznych. Jej aktualność oraz interdyscyplinarny charakter potwierdzają przeanalizowane artykuły, zawierające wyniki badań i analiz, w szczególności dotyczy to metod zarządzania środowiskiem na terenach pogórniczych i transformacji terenów składowisk odpadów górniczych i przeróbczych na terenie Zagłębia Górnośląskiego, co było przedmiotem analiz, których wyniki opisano w [1]. Analizy dotyczyły składowisk różnej wielkości, tworzonych w różnych okresach czasu na przestrzeni wielu lat. Były tu składowiska o różnym kształcie i różnej szacie roślinnej na ich powierzchni. Zidentyfikowano obszary nagrzewania się składowisk. Palące się składowiska stanowią poważne zagrożenie dla środowiska, więc ich monitoring odgrywa bardzo ważną rolę, umożliwiając

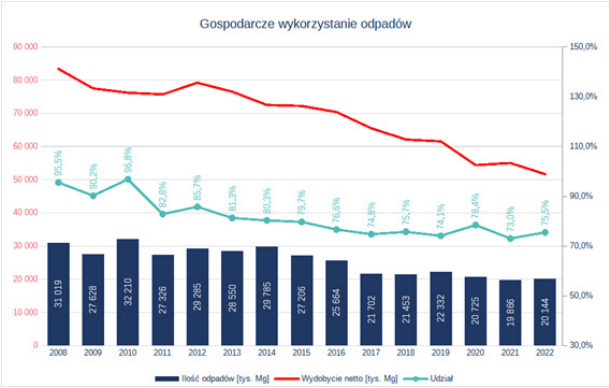

Rys. 4. Gospodarcze wykorzystanie odpadów
Fig. 4. Economic use of waste

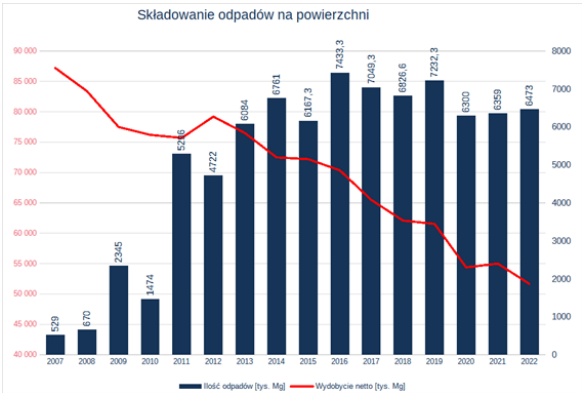

Rys. 3. Składowanie odpadów na powierzchni
Fig. 3. Storage of waste on the surface

optymalne zarządzanie składowiskami odpadów z punktu widzenia ochrony środowiska. Innowacyjną metodę monitorowania neutralizacji odpadów pochodzących z procesów przeróbczych przedstawiono w [2]. Wykorzystano w niej zależność między wapniem i siarką występującymi w odpadach. Metoda ta pozwala skutecznie wyeliminować tworzenie się kwasów w odpadach powstałych w wyniku przeróbki węgla. W literaturze można znaleźć interesujące publikacje dotyczące rekultywacji terenów zajmowanych przez składowiska odpadów pogórniczych w aspekcie wtórnego wykorzystania minerałów odzyskanych ze składowisk oraz tworzenia nowych ekosystemów na rekultywowanych terenach [3]. Wpływ odpadów górniczych i energetycznych na jakość gleby zaprezentowano w [4]. Analizowano zawartość metali ciężkich (Cd, Co, Cr, Cu, Ni, Pb, Zn) z zastosowaniem metody spektrometrii emisyjnej (ICP-AES) oraz dyfrakcji z zastosowaniem promieni Roentgena (XRD). Materiały odzyskane ze składowisk mogą stanowić cenny surowiec dla budownictwa, w wielu przypadkach zastępujący cement [5]. Geomateriały pochodzące ze składowisk są wykorzystywane jako kruszywa. W [6] przedstawiono wyniki badań ukierunkowanych na określenie przydatności odpadów górniczych i przeróbczych do produkcji cegieł, stwierdzając, że może to być surowiec alternatywny. W [7] podano przykłady wykorzystania odpadów węglowych, pochodzących z recyklingu, jako materiału do budowy dróg. W procesie wzbogacania minerałów stosowane są różne technologie m.in. klasyfikatory z autogenicznym łożem zawiesinowym [8] czy osadzarki do wzbogacania węgla koksowego [9]. Aspekt ochrony środowiska analizowano w przypadku wód odprowadzanych z nieczynnej kopalni w Północnej Portugalii [10]. Badano 46 parametrów jakościowych wody pochodzącej z wyrobisk, stwierdzając, że zarówno pod względem chemicznym, jak i fizycznym, woda ta nie stanowi zagrożenia dla środowiska. Jedną z metod wykorzystania drobnych sortymentów węgla oraz popiołów lotnych jest ich granulowanie i brykietowanie [11]. Jak już wcześniej wspomniano [1], palące się składowiska odpadów górniczych na górnym Śląsku są przedmiotem badań oraz działań zaradczych, realizowanych od wielu lat różnymi metodami, których skuteczność nie jest satysfakcjonująca. Zmiany w glebie wywołane przez palące składowiska przeanalizowano w [12]. Zarządzanie składowiskami odpadów wymaga współpracy między przedstawicielami przemysłu, urzędnikami na szczeblu państwowym, regionalnym i lokalnym, a także naukowcami i interesariuszami procesu zagospodarowania składowisk, którzy reprezentują różne grupy społeczne [13]. System ten efektywnie funkcjonuje w Australii. Wyniki wielu projektów naukowo-badawczych w zakresie mechanicznej przeróbki surowców mineralnych, innowacyjnych rozwiązań maszyn i urządzeń, gospodarowania odpadami w aspekcie ich ponownego wykorzystania zgodnie z wymaganiami gospodarki o obiegu zamkniętym przedstawiono w [14]. Przegląd literatury stanowił dla Autorek istotną wskazówkę ułatwiającą wybór referatów przedstawionych podczas konferencji KOMEKO 2023 do zaprezentowania w niniejszym artykule.

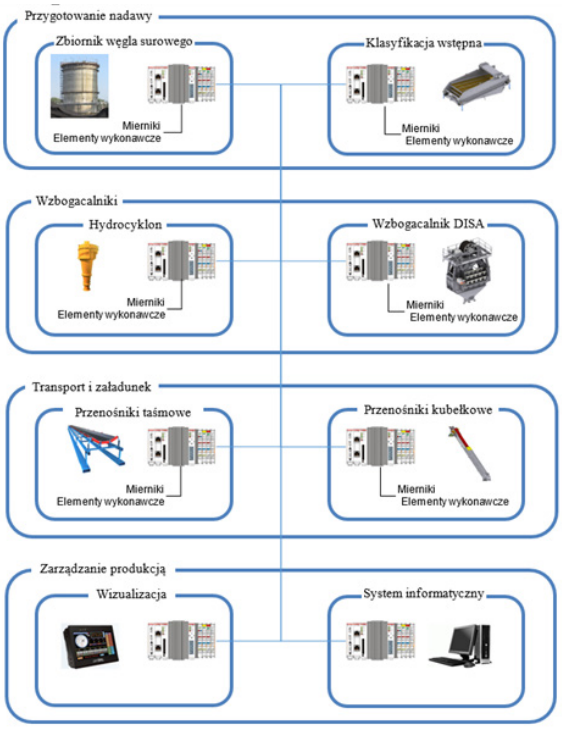

Rys. 5. Porównanie istniejącego i planowanego układu wzbogacania
Fig. 5. Comparison of the existing and planned enrichment system

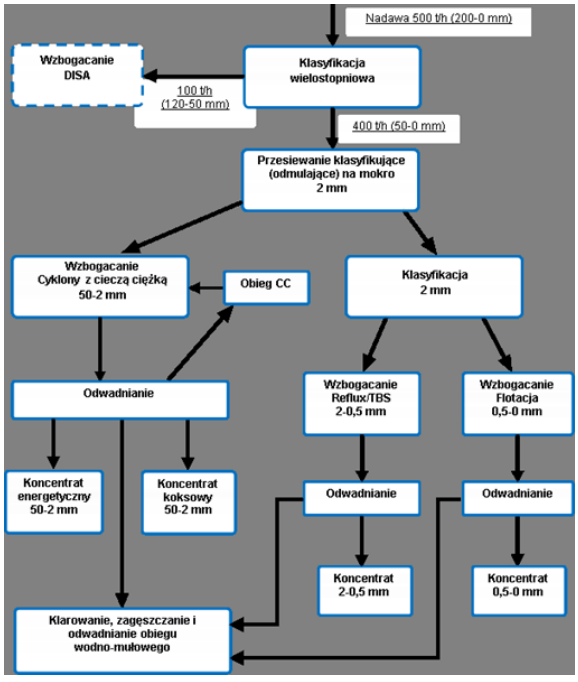

Rys. 6. Uproszczony schemat technologiczny nowego zakładu przeróbczego
Fig. 6. Simplified technological scheme of the new processing plant

3. Przegląd wybranych referatów

Autorki publikacji postanowiły dokonać wyboru sześciu referatów, które ich zdaniem przedstawiały problematykę przeróbki surowców mineralnych w sposób interdyscyplinarny oraz miały charakter rozwiązań innowacyjnych, a także dotyczyły zagadnień gospodarki o obiegu zamkniętym, Sprawiedliwej Transformacji Rejonów Pogórniczych oraz Zielonego Ładu.

- ***Gospodarka o obiegu zamkniętym - unijne wymagania w odniesieniu do odpadów wydobywczych [15]***

W Unii Europejskiej obowiązują trzy dyrektywy dotyczące zagospodarowania odpadów wydobywczych w kontekście gospodarki o obiegu zamkniętym:

– Dyrektywa 2006/21/WE określa zasady postępowania z odpadami wydobywczymi oraz wymagania w zakresie ochrony środowiska i zdrowia człowieka,

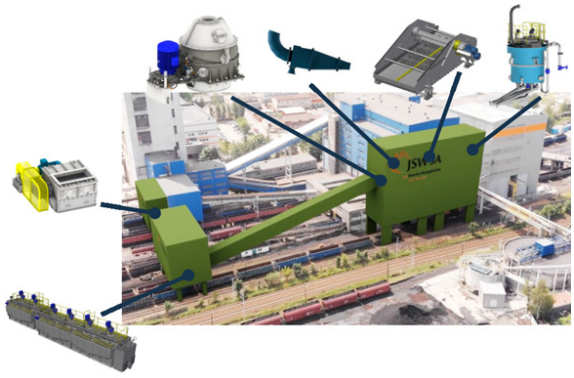

Rys. 7. Proponowana lokalizacja nowego Zakładu Przeróbczego
Fig. 7. Proposed location of the new Processing Plant

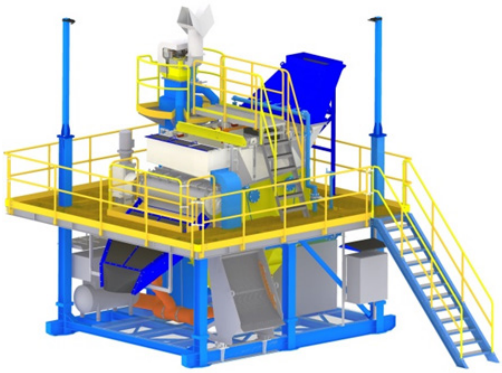

Rys. 8. Mobilny system wzbogacania odpadów
Fig. 8. Mobile waste enrichment system

– Dyrektywa 2008/98/WE promuje gospodarkę o obiegu zamkniętym poprzez minimalizowanie ilości odpadów, maksymalizowanie odzysku surowców oraz zmniejszanie emisji gazów cieplarnianych i zanieczyszczeń.
– Dyrektywa Parlamentu Europejskiego i Rady 2018/851 z 30 maja 2018 roku zmieniająca dyrektywę 2008/98/WE w sprawie odpadów.

Dyrektywa Rady Europy 2006/21/WE określa szczegółowe wymagania dotyczące gospodarowania odpadami wydobywczymi oraz ustanawia zasady ich przemieszczania i unieszkodliwiania w sposób bezpieczny dla środowiska. Jej założenia obejmują m.in. minimalizację ilości odpadów poprzez wykorzystanie najlepszych dostępnych technologii i procesów produkcji, selekcję odpadów, które mogą być poddane odzyskowi surowców wtórnych lub wykorzystaniu w inny sposób, oraz wprowadzenie procedur postępowania z odpadami, określenie wymagań dotyczących planowania, projektowania, budowy i eksploatacji składowisk odpadów, zwiększenie odpowiedzialności producentów za odpady, m.in. poprzez wprowadzenie obowiązku dostarczania informacji na temat właściwości odpadów, sposobów ich przechowywania i transportu. Wprowadza wymaganie wdrożenia systemu monitorowania emisji i działań na rzecz ochrony środowiska, a także wspierania innowacji i rozwoju technologii, które pozwolą na lepsze wykorzystanie surowców wtórnych. Na rys. 1-4 przedstawiono informacje na temat odpadów pochodzących z górnictwa węgla kamiennego.

W Polsce zdefiniowano gospodarkę o obiegu zamkniętym w "Mapie drogowej transformacji w kierunku gospodarki o obiegu zamkniętym" w 2019 roku. Odpady, powstające przy wydobyciu węgla kamiennego, w 2022 roku wyniosły 20,14mln ton, z czego 75% zostało gospodarczo wykorzystanych na powierzchni. W przypadku górnictwa węglowego około 5 milionów ton składowanych odpadów wydobywczych może być wykorzystanych do produkcji metakaolinitu, zeolitu, geopolimerów oraz kruszyw lekkich.

• ***Modernizacja zakładu przeróbczego w kierunku niskiej emisji i automatyzacji procesów – innowacyjność przeróbki przyszłości [16].***

Istotnym ogniwem w ciągu technologicznym produkcji węgla, jako produktu handlowego, są zakłady mechanicznej przeróbki węgla, których kluczowym zadaniem jest wytworzenie produktu zgodnego ze zróżnicowanym zapotrzebowaniem poszczególnych segmentów rynkowych. Produkcja węgla kamiennego o wysokich parametrach jakościowych wymaga automatyzacji procesów przeróbczych, innowacyjnych rozwiązań urządzeń oraz technologii wzbogacania. Obecnie wzbogacanie węgla kamiennego w polskich zakładach przeróbczych opiera się na technologii cieczy ciężkiej zawiesinowej dla ziaren > 20 (30) mm, osadzarkach pulsacyjnych dla ziaren < 20(30)mm oraz na zastosowaniu flotacji dla ziaren < 0,5 mm w przypadku wzbogacania węgli koksowych.

Za granicą proces wzbogacania odbywa się wyłącznie w cieczy ciężkiej zawiesinowej. Zawężanie klas ziarnowych, kierowanych do wzbogacania, zwłaszcza w przypadku ziaren drobnych, ma istotny wpływ na skuteczność procesu wzbogacania, toteż celowe jest zastosowanie wzbogacalnika z au-

Rys. 9. Kostki wykonane z geopolimerów
Fig. 9. Cubes made of geopolymers

Rys. 10. Przykładowe zastosowanie geopolimerów: a) poziomowanie b) wypełnianie kawern c) wsparcie strukturalne
Fig. 10. Example application of geopolymers: a) leveling b) cavities filling c) structural support

togenicznym łożem zawiesinowym do wzbogacania ziaren 2-0,5mm.

Automatyzacja procesów przeróbczych obejmuje całokształt zagadnień związanych z automatyzacją kierowania nadawy i zasilania poszczególnych urządzeń, a także ich sterowanie i blokady. Obejmuje również sterowanie i zarządzanie dyspozytorskie, automatykę obiegu cieczy ciężkiej, regulację i sterowanie procesami technologicznymi. Nowy paradygmat rozwoju społeczno-gospodarczego, jakim jest zasobooszczędność i gospodarka o obiegu zamkniętym uwzględnia fakt, że odpady górnicze i odpady przeróbcze, poza substancją węglową, zawierają wiele surowców i pierwiastków, które mogą zostać wykorzystane na skalę przemysłową. Są to przede wszystkim piaskowce, mułowce, iłowce i łupki węglowe, które mogą być wykorzystane w budownictwie. Na rys.5-7 pokazano informacje na temat układu wzbogacania oraz nowego zakładu przeróbczego.

Zastosowanie nowoczesnych rozwiązań techniczno-technologicznych w postaci cyklonów z cieczą ciężką oraz wzbogacalników zawiesinowych umożliwi zwiększenie efektywności procesów wzbogacania węgla koksowego i w efekcie zwiększoną produkcję koncentratu koksowego dla założonej zawartości popiołu oraz uzyskanie korzystniejszych parametrów jakościowych produktu odpadowego, co zostało potwierdzone wynikami badań laboratoryjnych zrealizowanych w ITG KOMAG. System rozproszonego sterowania zwiększy zakres automatyzacji, zapewniając optymalizację produkcji i zużycia energii, a także niezawodność i bezpieczeństwo procesu wzbogacania.

• Nowa technologia wytwarzania wodoru i kompozytów geopolimerowych z odpadów pogórniczych [17]

W referacie przedstawiono główne cele projektu europejskiego koordynowanego przez ITG KOMAG, realizowanego w ramach Funduszu Badawczego Węgla i Stali. Celem projektu jest opracowanie nowej technologii przetwarzania odpadów mineralnych i popiołów lotnych z wykorzystaniem CO2 do produkcji kompozytów geopolimerowych. Projekt określi kierunki zagospodarowania frakcji energetycznej wydzielonej z odpadów. Zaplanowane badania będą ukierunkowane na opracowanie efektywnej metody produkcji wodoru z gazu syntezowego otrzymywanego w procesie zgazowania frakcji węglowych. W celu uzyskania wysokiej jakości materiałów z odpadów wydobywczych zostanie opracowana koncepcja i dokumentacja mobilnego systemu wzbogacania odpadów kopalnianych, który będzie wyposażony w innowacyjny system sterowania umożliwiający efektywną separację odpadów. Technologie przetwarzania odpadów pogórniczych, opracowane w ramach projektu pozwolą na likwidację hałd, co jest spójne z wizją gospodarki o obiegu zamkniętym, w której odpady powstałe na etapie produkcji mogą zostać poddane recyklingowi i stać się zasobem. Na rys.8 pokazano mobilny system wzbogacania odpadów, który zostanie zbudowany w ramach projektu.

Składowiska odpadów kopalnianych, powstałe głównie w wyniku mechanicznej przeróbki węgla kamiennego, degradują środowisko i stwarzają wiele zagrożeń, do których należy zaliczyć pożary i związane z nimi wydzielanie gazów zanieczyszczających atmosferę, a także zanieczyszczanie wód powierzchniowych i gruntowych poprzez wymywanie ze składowisk chlorków i siarczanów. Składowiska zajmują znaczne powierzchnie gruntu, który staje się nieużytkiem. Wykorzystanie odpadów, zalegających na składowiskach, wpisuje się w politykę zrównoważonego rozwoju, gdyż przyczynia się do zmniejszenia ilości składowanych odpadów oraz uzyskania oszczędności w nieodnawialnych zasobach surowców naturalnych. Po odpowiedniej przeróbce odpady kopalniane można wykorzystać jako:

- mieszanki kruszyw wzbogacanych innymi mrozoodpornymi kruszywami,
- materiały do budownictwa hydrotechnicznego,
- składnik do produkcji materiałów budowlanych,
- składnik do podbudów zasadniczych i pomocniczych,
- materiał podsadzkowy do podsadzania wyrobisk podziemnych,
- materiał podsypkowy do zimowego utrzymania dróg oraz stabilizacji i wypełniania gruntów.

Z analizy literatury wynika, że zawartość węgla w odpadach wydobywczych może sięgać nawet 30%. Frakcje mine-

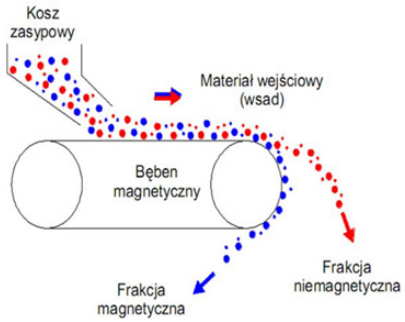

Rys. 11. Separator magnetyczny – zasada działania
Fig. 11. Magnetic separator – principle of operation

Rys. 12. Separator magnetyczny – podajnik wibracyjny materiału
Fig. 12. Magnetic separator – material vibrating feeder

Rys. 13 Separator magnetyczny – odbiór materiału diamagnetycznego
Fig. 13 Magnetic separator – collection of diamagnetic material

ralne i energetyczne, odzyskane w wyniku procesu wzbogacania w osadzarkach, mogą stanowić surowiec do dalszego przetwarzania z wykorzystaniem innych materiałów odpadowych. Jednym z kierunków jest możliwość wytworzenia geopolimerów, które znalazły szerokie zastosowanie w transporcie, metalurgii, materiałach filtracyjnych i utylizacji odpadów jądrowych. Na rys. 9 pokazano kostki wykonane z geopolimerów.

Do zalet geopolimerów należy zaliczyć doskonałe właściwości mechaniczne oraz odporność na działanie wysokich temperatur i kwasów, natomiast ich wadą jest wyższa temperatura utwardzania, gdyż temperatura otoczenia nie jest wystarczająca, krótki czas wiązania oraz stosunkowo wysoka cena. W przypadku utwardzania w temperaturze otoczenia geopolimery mają niższą wytrzymałość i twardość. Na rys. 10 przedstawiono przykładowe zastosowanie geopolimerów.

Należy podkreślić fakt, że w ramach projektu zostanie przeprowadzona inwentaryzacja czynnych i rekultywowanych składowisk odpadów kopalnianych w wybranych krajach Europy, będą przeprowadzone badania fizykochemicznych i mechanicznych właściwości odpadów wydobywczych oraz zostanie opracowana baza danych. Realizacja projektu przyczyni się do osiągnięcia następujących celów:

– środowiskowe: lepsza efektywność wykorzystania zasobów i zredukowany wpływ na środowisko, zmniejszenie ilości odpadów zalegających na hałdach kopalnianych,
ekonomiczne: pozyskanie inwestycji, wdrożenie innowacyjnych rozwiązań i stworzenie nowych miejsc pracy, odzysk i recykling materiałów z odpadów kopalnianych,
– społeczne: opracowanie modelu przekształcenia terenów pogórniczych, utworzenie nowych miejsc pracy,
– techniczne/ technologiczne: wdrożenie nowych produktów i usług,
– naukowe: wzmocnienie Europejskiej Przestrzeni Badawczej i promocja europejskiego przywództwa w dziedzinie innowacji środowiskowych.

Podsumowując można stwierdzić, że projekt wprowadzi nowe praktyki w zakresie przetwarzania odpadów górniczych ze składowisk. Zostanie stworzona baza danych zwałowisk odpadów górniczych w wybranych krajach europejskich, będzie określona charakterystyka zdeponowanych odpadów i opracowany system wzbogacania odpadów kopalnianych oraz zostanie określona możliwość wykorzystania odpadów mineralnych do produkcji kompozytów geopolimerowych. Dla opracowanego systemu zostaną wykonane analizy ekonomiczne, środowiskowe, społeczne i prawne.

• Wzbogacanie odpadów oraz kruszyw naturalnych zawierających pierwiastki ziem rzadkich [18].

Prezentacja dotyczyła ilościowej analizy zawartości pierwiastków ziem rzadkich (REE) w następujących materiałach: muły węglowe, odpady energetyczne, kruszywo bazaltowe oraz kruszywa naturalne. Wykorzystano technikę spektrometrii mas plazmowych dla materiału, który poddano klasyfikacji granulometrycznej oraz separacji magnetycznej. Pierwiastki ziem rzadkich dzielą się na dwie grupy: lantanowce i skandowce. Do potencjalnych źródeł pierwiastków ziem rzadkich należą: węgiel kamienny, popiół węgla kamiennego, odpad energetyczny, złoża piasków i żwirów, zużyty sprzęt elektroniczny, a także odpad fosfogipsowo-apartytowy.

Tab. 1. Zestawienie produktów rozkładu masowego separacji magnetycznej

Tab. 1. List of mass decomposition products of magnetic separation

Lp.	Identyfikacja próbki	Natężenie pola mag. [V]	Masa próbki [g]	Oznaczenie próbki, masa produktu paramagnetycznego mocniejszego [g]	Oznaczenie próbki, masa paramagnetycznego słabszego [g]
1	Kruszywo 2-0	25	90	189/21/P1 1,06	-
2	Muły węglowe	25	90	173/21/P10 0,46	173/21/P11 1,41
3	Kruszywo bazaltowe	25	90	180/21/P16 2,84	189/21/P11 5,04
4	Kruszywo bazaltowe 0,125-0	25	90	180/21/P13 3,05	180/21/P14 2,91
5	Kruszywo bazaltowe 0,5-0,125	25	90	180/21/P9 2,06	180/21/P10 4,19
6	Odpad energetyczny Kraków	25	90	189/21/P3 24,06	189/21/P6 7,92
7	Odpad energetyczny Kraków 0,125-0	25	90	189/21/P2 4,0	189/21/P5 1,82
8	Odpad energetyczny Kraków 0,5-0,125	25	90	189/21/P7 4,04	189/21/P4 8,25

Tab. 2. Total content of rare earth elements in magnetic separation products

Tab. 2. Sumaryczne zawartości pierwiastków ziem rzadkich w produktach separacji magnetycznej

Lp	Identyfikacja próbki	Surowy materiał	Produkt paramagnetyczny mocniejszy		Produkt paramagnetyczny słabszy	
		Zawartość pierwiastków ziem rzadkich [ppm]	Numer próbki	Zawartość pierwiastków ziem rzadkich [ppm]	Numer próbki	Zawartość pierwiastków ziem rzadkich [ppm]
1	Kruszywo 2-0	252,85	189/21/P1	96,06	brak produktu	
2	Muły węglowe	263,8	173/21/P10	40,45	173/21/P11	36,29
3	Kruszywo bazaltowe	190,0	180/21/P16	26,35	189/21/P11	212,87
4	Kruszywo bazaltowe 0,125-0 mm	190,0	180/21/P13	151,54	180/21/P14	150,5
5	Kruszywo bazaltowe 0,5-0,125 mm	190,0	180/21/P9	250,22	180/21/P10	229,54
6	Odpad energetyczny Kraków	261,5	189/21/P3	177,44	189/21/P6	66,16
7	Odpad energetyczny Kraków 0,125-0	261,5	189/21/P2	206,14	189/21/P5	179,12
8	Odpad energetyczny Kraków 0,5-0,125	261,5	189/21/P7	200,06	189/21/P4	109,56

Badaniom poddano muły węglowe pochodzenia górniczego pozyskane ze składowiska w okolicach Nowej Rudy, odpad energetyczny był mieszaniną żużli oraz popiołów lotnych pozyskanych ze składowiska zlokalizowanego w Krakowie, kruszywo bazaltowe pochodziło z kopalni bazaltu znajdującej się w południowo-zachodniej Polsce, a kruszywo 2-0 mm było odpadem uzyskanym z wzbogacalników strumieniowo-zwojowych pracujących w jednej z górnośląskich kopalń węgla kamiennego. Na rys.11-13 przedstawiono realizację badań intensyfikacji REE w klasach ziarnowych 0-0,125 oraz 0,125 - 0,5 mm z wykorzystaniem separatora magnetycznego.

Zestawienie produktów rozkładu masowego separacji magnetycznej przedstawia Tabela 1.

Badania zawartości pierwiastków ziem rzadkich w próbkach materiałów przeprowadzono w Laboratorium Inżynierii Materiałowej i Środowiska ITG KOMAG. Wykorzystano metody spektrometrii mas z jonizacją w plazmie indukcyjnie sprzężonej (ICP-MS). Metoda polega na pomiarze intensywności jonów powstałych w strumieniu plazmy. Rys.14 przedstawia spektrometr ICP-MS wykorzystany w badaniach ze względu na drobne uziarnienie materiału oraz zróżnicowany skład chemiczny próbek.

W Tabeli 2 przedstawiono sumaryczne zawartości pierwiastków ziem rzadkich w produktach separacji magnetycznej.

Brak wzrostu lub niewielki wzrost zawartości pierwiastków ziem rzadkich w produktach poddanych procesowi separacji magnetycznej może wskazywać na zbyt niskie natężenie zastosowanego pola magnetycznego. Dalszy etap prac badawczych powinien uwzględniać wielowariantowe badania natężenia pola magnetycznego lub zastosowanie innej metody wzbogacania np. separacja magnetyczna w ośrodku wodnym.

• Recykling odpadów zawierających lit z rejonu Krušné Hory w Czechach [19]

Rys. 14. Spektrometr ICP-MS
Fig. 14. ICP-MS spectrometer

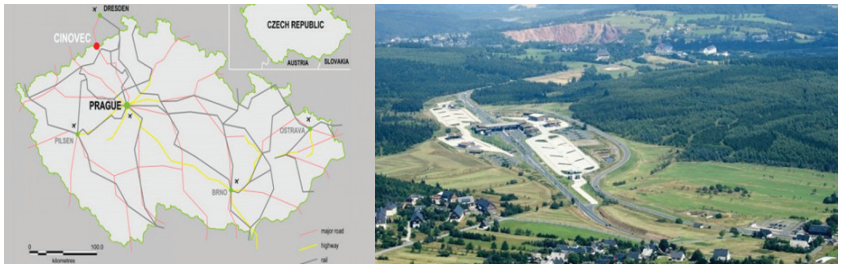

Rys. 15. Lokalizacja kopalni Cinovec
Fig. 15. Location of the Cinovec mine

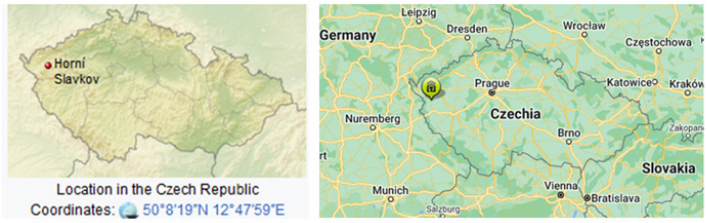

Rys. 16. Lokalizacja kopalni Horni Slavkov
Fig. 16. Location of the Horni Slavkov mine

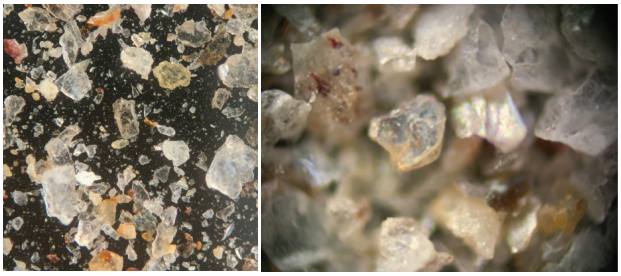

Rys. 17. Ziarna zinnwaldytu
Fig. 17. Zinnwaldite grains

Zasoby litu na świecie wynoszą około 22 mln ton, natomiast produkcja światowa dochodzi do 82tys. ton/rok. Biorąc pod uwagę fakt, że w 2022 roku cena LiCO3 wynosiła 81 130 USD/tonę, to wartość rocznej produkcji dochodzi do około 6 mld 653 mln USD. Polska jest piątym na świecie dostawcą litowo-jonowych akumulatorów samochodowych lub ich komponentów, natomiast w Europie jest na pierwszym miejscu. W 2021 r. nasz kraj zaspokajał około 60% europejskiego popytu na akumulatory do pojazdów elektrycznych. Na rys.15 pokazano lokalizację kopalni Cinovec w Czechach, gdzie prowadzono badania.

Kopalnia Cinovec posiada 3,5 mln ton odpadów, w których zawartość litu wynosi 0,2%. Stosuje się wzbogacanie grawitacyjne magnetyczne oraz flotację. Rys.16 przedstawia lokalizację kopalni Horni Slavkov w Czechach.

Do wzbogacania zaproponowano separację magnetyczną na makro o dużym natężeniu pola (WHIMS) celem oddzielenia miki zawierającej lit (zinnwaldyt) i uzyskania produktu magnetycznego - koncentratu miki. Separacja magnetyczna jest właściwa w tym przypadku, ponieważ zinnwaldyt zawiera w sieci żelazo i jest paramagnetyczny. Na rys.17 przedstawiono ziarna zinnwaldytu.

Schemat procesu wzbogacania przedstawiono na rys.18

Lit znajduje obecnie szerokie zastosowanie w napędach elektrycznych samochodów, samolotów, pociągów, autobusów, e-rowerów, ciężarówek oraz hulajnóg. W 2010 roku w USA lit wykorzystywano do produkcji szkła i ceramiki (29%), baterii i akumulatorów (27%), smarów (12%), odlewania ciągłego (5%), oczyszczania powietrza (4%), produkcji polimerów (3%), produkcji aluminium (2%), produkcji farmaceutyków (2%) oraz innych wyrobów (16%).

• Innowacyjne i nowoczesne rozwiązania współczesnej przeróbki mechanicznej węgla na przykładzie LW "Bogdanka" S.A. [20]

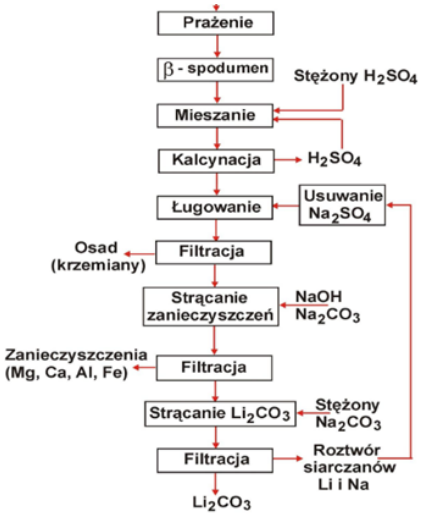

Rys. 18. Schemat procesu wzbogacania
Fig. 18. Scheme of the enrichment process

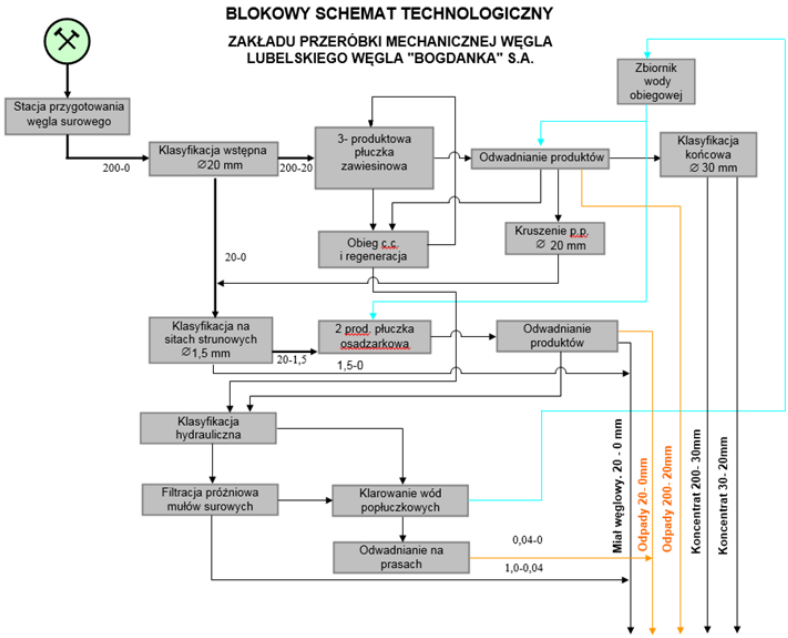

Rys. 19. Blokowy schemat technologiczny Zakładu Przeróbki w LW "Bogdanka" (ZPMW)
Fig. 19. Block diagram of the Processing Plant at LW "Bogdanka" (ZPMW)

Historia Zakładu Przeróbki Mechanicznej Węgla w LW "Bogdanka" S.A. sięga 1987 roku, gdy oddano do eksploatacji pierwsze obiekty budowlane, maszyny i urządzenia związane z placem składowania węgla, klasyfikacją grubych sortymentów i załadunkiem surowego miału do wagonów. W 1992 roku zakończono budowę zakładu, oddając do ruchu płuczkę miałową. W 2009 roku przystąpiono do rozbudowy celem zwiększenia wydajności z 1200 Mg/h do 2400Mg/h. Rozbudowę zakończono w 2014 roku. Technologia Zakładu Przeróbczego składa się z następujących elementów:

- Przygotowanie i klasyfikacja węgla surowego.
- Wzbogacanie węgla surowego 200 - 20 mm w separatorach cieczy ciężkiej.
- Wzbogacanie węgla surowego 20 - 1,5 (0) mm w osadzarkach wodnych.
- Klasyfikacja i filtracja mułów.
- Odstawa, załadunek i magazynowanie produktów wzbogacania.

Blokowy schemat technologiczny Zakładu Przeróbki Mechanicznej Lubelskiego Węgla "Bogdanka" przedstawiono na rys. 19.

Maszyny i urządzenia w ZPMW pracują w bardzo trudnych warunkach. Są narażone na korozję i erozję. Do najważniejszych rozwiązań technologicznych należą półki przesypowe, blachy napawane, kompozyty polimerowe, rury polietylenowe oraz zdzieraki z węglikiem napawanym zabudowane w miejscach transportu urobku z dużą prędkością, przy znacznej różnicy wysokości. Dzięki wdrożonym rozwiązaniom półek przesypowych wyeliminowano problem zużywających się blach wkładkowych większości przesypów, a także uszkodzeń taśm przenośników. Blachy napawane są stosowane w miejscach transportu urobku z dużą prędkością,

Rys. 20. System monitoringu ciągłego Zakładu Przeróbki Mechanicznej Węgla
Fig. 20. Continuous monitoring system of the Mechanical Coal Processing Plant

Rys. 21. Instalacja zraszająca przeciwpożarowa
Fig. 21. Fire sprinkler system

gdy nie ma możliwości stosowania półek przesypowych. Blachy te mają dużą twardość (ok. 63 HB) oraz wysoką odporność na ścieranie. Kompozyty polimerowe są wykorzystywane do napraw, regeneracji i zabezpieczeń, do których należy zaliczyć wyklejanie magnesów na wale rekuperatora, naprawy ubytków pras filtrujących i wykładzin trudnościeralnych wirówek sedymentacyjno-sitowych. Dzięki zastosowanym rozwiązaniom wydłużono okresy międzyremontowe eksploatowanych maszyn i urządzeń, zwiększono trwałość i ulepszono parametry pracy zespołów pompowych. Natomiast rury polietylenowe są stosowane do transportu wszystkich mediów (wody płuczkowe zawierające ziarna ilaste, jak i ciężkie ciecze magnetytowe). Wykazują dużą odporność na ścieranie, nie korodują i są łatwe w montażu. Dzięki temu wdrożeniu wyeliminowano problem eksploatacji rurociągów. Zdzieraki z węglikiem spiekanym służą do czyszczenia taśm przenośnikowych podczas transportu materiałów lepkich, zabłoconych i trudnych do usunięcia. Zdzieraki skutecznie czyszczą taśmy przenośnikowe. Najnowsze działania modernizacyjne w Zakładzie Przeróbki Mechanicznej Węgla obejmują instalację centralnego odkurzania, podglądy na pracę węzła hydroklasyfikacji, system wspomagający produkcję, dyspozytornię, zwałowarki gąsienicowo-obrotowo-taśmowe, instalację zraszającą przeciwpożarową, wykorzystanie sit strunowych do "odmulania na sucho" oraz mobilne urządzenie dźwigowe do opuszczania i podnoszenia ludzi. Technologie usprawniające i modernizujące pracę ZPMW wprowadzono w celu optymalizacji i unowocześnienia procesu wzbogacania, szybszego reagowania na usterki i awarie układu technologicznego, wdrożenia programu Solaris Helios do systemów predykcyjnych monitorujących pracę maszyn, szybszego przepływu informacji między pracownikami węzła produkcyjnego oraz zwiększenia kontroli podczas etapów wzbogacania. Na rys.20 przedstawiono system ciągłego monitoringu ZPMW zawierający w systemie dyspozytorskim 50 kamer i w systemie stanowiskowym 42 kamery.

Do najnowszych modernizacji należy zaliczyć instalację zraszającą przeciwpożarową. Kurtyny wodne wyposażono w tryskacze z ampułkami, które pękają powyżej 57°C, po czym następuje wypływ wody. Jednocześnie zostaje zatrzymany ruch przenośnika, co przedstawiono na rys.21.

Należy również wspomnieć o wielu projektach racjonalizatorskich ukierunkowanych m.in. na zautomatyzowanie pomiaru jakości węgla podawanego do osadzarek, zastosowanie automatycznych szufladowych próbobierników w przesypach z przenośników taśmowych, zabudowę siłowników hydraulicznych do przestawiania klap przesypowych na zwałowiskach odpadów pogórniczych oraz zastosowanie elastomerów jako wykładki zsuwni nadawczych do wzbogacalników DISA.

4. Podsumowanie

- Uczestnicy konferencji KOMEKO 2023 zwracali uwagę na aktualność jej tematyki, zwłaszcza w aspekcie Sprawiedliwej Transformacji Rejonów Pogórniczych, wyzwań europejskiej gospodarki o obiegu zamkniętym oraz Zielonego Ładu.
- Dużym zainteresowaniem cieszyła się prezentacja, dotycząca zagospodarowania odpadów wydobywczych w kontekście gospodarki o obiegu zamknię-

tym, w której określono zasady postępowania z odpadami wydobywczymi oraz wymagania w zakresie ochrony środowiska i zdrowia człowieka. Istota działań polega na minimalizowaniu ilości odpadów, maksymalizowaniu odzysku surowców oraz zmniejszeniu emisji gazów cieplarnianych i zanieczyszczeń.

- W Polsce zdefiniowano gospodarkę o obiegu zamkniętym w "Mapie drogowej transformacji w kierunku gospodarki o obiegu zamkniętym" w 2019. W 2022 r. ilość odpadów powstających przy wydobyciu węgla kamiennego, wyniosła 20,14 mln ton, z czego 75% zostało gospodarczo wykorzystanych na powierzchni.
- Nowy paradygmat rozwoju społeczno-gospodarczego, jakim jest zasobooszczędność i gospodarka o obiegu zamkniętym uwzględnia fakt, że odpady górnicze i odpady przeróbcze, poza substancją węglową, zawierają wiele surowców i pierwiastków, które mogą zostać wykorzystane na skalę przemysłową. Są to przede wszystkim piaskowce, mułowce, iłowce i łupki węglowe, które mogą być wykorzystane w budownictwie.
- Wykorzystanie odpadów, zalegających na składowiskach, wpisuje się w politykę zrównoważonego rozwoju, gdyż przyczynia się do zmniejszenia ilości składowanych odpadów oraz uzyskania oszczędności w nieodnawialnych zasobach surowców naturalnych.

Literatura – References

1. Abramowicz, A., Rahmonov, O., & Chybiorz, R. (2020). Environmental management and landscape transformation on self-heating coal-waste dumps in the Upper Silesian Coal Basin. Land, 10(1), 23.
2. de Jesús López-Saucedo, F., Batista-Rodríguez, J. A., Carrillo-Pedroza, F. R., Díaz-Martínez, R., & Ramos-Méndez, K. L. (2023). Demonstration of a methodology for measuring the neutralization potential in coal waste. International Journal of Coal Preparation and Utilization, 43(4), 666-676.
3. Pawul, M., Kępys, W., & Śliwka, M. (2022). The Role of Natural Succession in the Reclamation of Mining Waste Disposal Facilities. Inżynieria Mineralna – Journal of the Polish Mineral Engineering Society (2), str.159-165
4. Marcisz, M., Adamczyk, Z., Gawor, Ł., & Nowińska, K. (2021). The impact of depositing waste from coal mining and power engineering on soils on the example of a central mining waste dump. gospodarka surowcami mineralnymi, 37(2).
5. Vo, T. L., Nash, W., Del Galdo, M., Rezania, M., Crane, R., Nezhad, M. M., & Ferrara, L. (2022). Coal mining wastes valorization as raw geomaterials in construction: A review with new perspectives. Journal of Cleaner Production, 336, 130213.
6. Binal, G., & Bacaksizoglu, A. (2023). Brick production and characterization containing coal mining waste. International Journal of Coal Preparation and Utilization, 43(1), 135-147.
7. Kien, T. T., & Lanh, P. T. V. (2021). UTILIZATION OF RECYCLED COAL MINING WASTE FOR ROAD FOUNDATION LAYERS IN VIETNAM. GEOMATE Journal, 21(87), 11-18.
8. Kowol, D., & Kurama, H. (2020). Recovery of fine coal grains from post-mining wastes with use of autogenous suspending bed technology. Management Systems in Production Engineering, 28(4), 220-227.
9. Matusiak, P., & Kowol, D. (2020). Use of state-of-the-art jigs of KOMAG type for a beneficiation of coking coal. Mining Machines.
10. Mansilha, C., Melo, A., Flores, D., Ribeiro, J., Rocha, J. R., Martins, V., ... & Espinha Marques, J. (2021). Irrigation with coal mining effluents: Sustainability and water quality considerations (São Pedro da Cova, North Portugal). Water, 13(16), 2157.
11. Borowski, G., Alsaqoor, S., & Alahmer, A. (2021). Using Agglomeration Techniques for Coal and Ash Waste Management in the Circular Economy. Advances in Science and Technology. Research Journal, 15(3).
12. Kruszewski, Ł., Kisiel, M., & Cegiełka, M. (2021). Soil development in a coal-burning environment: The Upper Silesian waste heaps of Poland. Geological Quarterly, 65.
13. Ofori, P., Hodgkinson, J., Khanal, M., Hapugoda, P., & Yin, J. (2022). Potential resources from coal mining and combustion waste: Australian perspective. Environment, Development and Sustainability, 1-18.
14. Lutyński, A. (2021). KOMAG activities in the domestic and international research areas. Mining Machines, (4).
15. Kulpa J., Jarosz J. (2023): Charakterystyka zagospodarowania odpadów wydobywczych w Polsce w świetle wyzwań europejskiej gospodarki o obiegu zamkniętym. Prezentacja podczas konferencji KOMEKO 2023, Szczyrk, 27-29 marca 2023 r. - niepublikowana

16. Matusiak P., Kowol D. (2023): Modernizacja zakładu przeróbczego w kierunku niskiej emisji i automatyzacji procesów - innowacyjność przeróbki przyszłości. Prezentacja podczas konferencji KOMEKO 2023, Szczyrk, 27-29 marca 2023 r. - niepublikowana
17. Matusiak P., Kowol D. (2023): Nowa technologia wytwarzania wodoru i kompozytów geopolimerowych z odpadów pogórniczych. Prezentacja podczas konferencji KOMEKO 2023, Szczyrk, 27-29 marca 2023 r. - niepublikowana
18. Lutyński M., Baron R. (2023): Wzbogacanie odpadów oraz kruszyw naturalnych zawierających pierwiastki ziem rzadkich z zastosowaniem separacji magnetycznej. Prezentacja podczas konferencji KOMEKO 2023, Szczyrk, 27-29 marca 2023 r. - niepublikowana
19. Tora B., Olkuski T. et al. (2023): Recykling odpadów zawierających lit z rejonu Krusne Hory w Czechach. Prezentacja podczas konferencji KOMEKO 2023, Szczyrk, 27-29 marca 2023 r. - niepublikowana
20. Świercz M., Sołtys K. (2023): Innowacyjność i nowoczesne rozwiązania współczesnej przeróbki mechanicznej węgla na przykładzie LW "Bogdanka" S.A. Prezentacja podczas konferencji KOMEKO 2023, Szczyrk, 27-29 marca 2023 r. - niepublikowana

Environmentally Friendly Processing of Mineral Resources - Review of Papers Presented during the KOMEKO 2023 Scientific and Technical Conference

The article is an overview of selected papers presented during the KOMEKO 2023 conference, organized in Szczyrk by the KOMAG Institute of Mining Technology from 27 to 29 March this year. Their topics included innovative technical and technological solutions in the field of mechanical processing of mineral raw materials, rational waste management in accordance with the requirements of the Green Deal, production of hydrogen and geopolymer composites from post-mining waste, enrichment of waste and aggregates containing rare earth elements or recycling of waste containing lithium. Participants of the KOMEKO 2023 conference were very interested in the discussion panel devoted to the automated, zero-waste processing plant. Particular attention was paid to the management of mining waste in Poland in the light of the challenges of the European circular economy and the safety of operation of processing machines and devices in the aspect of implementing innovative solutions. The KOMEKO 2023 scientific and technical conference was a forum for an interesting exchange of knowledge and professional experience between scientists, manufacturers of machinery and processing equipment, and their users representing the sector of mineral raw material producers. The success of the conference is evidenced by lively and fruitful discussions between all stakeholders in the mineral processing process.

Keywords: *processing of mineral resources, waste management, waste recycling, post-mining waste, machinery and processing equipment*

Monitoring of the Extent of Surface Waters of an Inactive Post-Flotation Reservoir as an Element of its Safety Assessment

Wojciech JAŚKOWSKI[1)]

[1)] AGH University of Science and Technology, Faculty of Geo-data Science, Geodesy and Environmental Engineering; email: jaskow@agh.edu.pl, ORCID: 0000-0002-5771-5790

http://doi.org/10.29227/IM-2023-01-36

Submission date: 22-05-2023 | Review date: 05-06-2023

Abstract

The post-flotation tailings yard is one of the important elements in the copper production process. An inseparable element of the operation of the landfill is closely related to it, systematically conducted research and control observations. These are mainly geodetic measurements of the embankment deformation and the surface of the land in the foreground of the landfill, hydrological observations of water levels in the embankment body and its close foreground. The article presents the methods and results of geodetic monitoring of the now closed "Gilów" mining waste dump and the technologies used in monitoring the extent of the overlying floodplain.

Keywords: *geodetic monitoring, measurements of the extent of the floodplain, facilities for the disposal of mining waste, mining waste*

1. Introduction

Hydrotechnical objects are an interesting field of experiments for surveyors. Predicting the influence of various factors on the behavior of dams, accompanying objects, ground and near foreground helps to develop the necessary and economic justification of the scope of geodetic observations [5]. Due to the variety of objects being the subject of research, it is necessary to use various geodetic technologies. In addition to careful and quick measurements of the deformation of the object, care should be taken to prepare appropriate numerical and graphic material that will suggestively show specialists from other fields what is happening with objects observed using geodetic methods. This material is also intended to indicate the benefits of modern geodetic technologies as well as the scope of their use in solving, for example, safety problems of hydrotechnical facilities, especially those located in mining areas [6].

2. Tailings and their disposal

Copper ore supplied from the mines of KGHM Polska Miedź SA is enriched in the flotation process at the installations of the Ore Enrichment Plant Branch located in the Lubin, Polkowice and Rudna regions. The level of mineralization of Polish copper ores, which does not exceed 2%, means that in the processes of their enrichment, about 94% of the extracted mass is separated as waste. This means that with the current extraction of approximately 32 million Mg/year, up to 30 million Mg of flotation waste is generated.

The tailings from the flotation process are finely ground gangue containing trace amounts of ore-bearing minerals. The basic components of the waste are quartz, dolomite, calcite and kaolinite. The waste from the Polkowice mine is dominated by carbonate rocks (mainly dolomite), and the waste from the Lubin and Rudna mines is dominated by sandstone. Differences in the composition of flotation tailings from individual enrichment plants result from different proportions of these minerals in the processed ore. In addition to the basic components, the waste contains small amounts of metal compounds and organic carbon in the form of bituminous compounds in mineralized shale rocks. Metals in flotation tailings occur in the form of compounds that are sparingly soluble in water, generally in the form of sulphides, sulphur salts, arsenides, and noble metals, partly also in native form.

A characteristic feature of the ores extracted and processed in the LGOM enrichment plants is the alkaline nature of the gangue, resulting from the presence of dolomite and calcite. The presence of carbonate minerals prevents the acidification of the environment and the oxidation of sulfides, and thus prevents the leaching of metals from waste both during ore processing and during transport. The specific nature of the LGOM deposit means that in the case of flotation tailings produced here, there is no risk of generating acid effluents, which are the main nuisance in the management of tailings from the enrichment of sulphide ores from other deposits. Due to the method of enrichment, the waste is in the form of a passable sludge, in which the bulk of the mass is a fraction with a grain diameter below 0.75 mm, and the size of the solid particles generally does not exceed 2 mm. [1]

3. Description of the Gilów tailings storage facility

The "Gilów" landfill put into operation in 1968 was located in the vicinity of the mining area of the Lubin Mine, on the slope of flat hills. It is limited by an embankment with a length of 6.76 km (Fig. 1). The body of the embankment (Fig. 2), which reached the elevation of 179 m above sea level, forms an arch line running from east to west, with its convexity facing south. The maximum height of the embankment is 22 m, the width in the crest is 4 m, and the maximum width in the base is 97 m.

The internal slope has a slope of 1:2 and is covered with concrete slabs 15 cm thick, and the external slope has a slope of 1:2 to 1:2.25 and is covered with grass. The drainage system of the embankment is a triangular gravel heap near the escarpment.

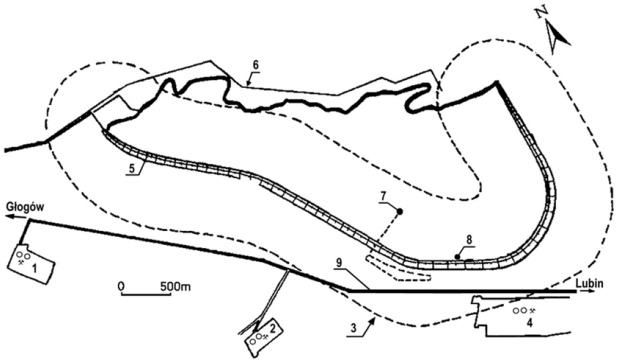

Fig. 1. A situational sketch of the "Gilów" landfill: 1. shaft PW; 2. shaft LZ; 3. boundary of the embankment of the protective pillar; 4. shaft LG; 5. pipeline distributing waste along the embankment; 6. pipeline distributing waste along the flood axis; 7. overflow tower No. 2; 8. overflow tower No. 1; 9. return water pipeline[2]

Rys. 1. Szkic sytuacyjny składowiska „Gilów": 1. szyb PW; 2. szyb LZ; 3. granica obwałowania filara ochronnego; 4. szyb LG; 5. rurociąg rozprowadzający odpad y wzdłuż obwałowania; 6. rurociąg rozprowadzający odpad y wzdłuż osi zalewu; 7. wieża przelewowa nr 2; 8. wieża przelewowa nr 1; 9. rurociąg wody zwrotnej[2]

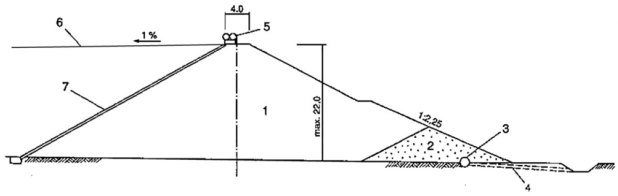

Fig. 2. Section of the embankment of the "Gilów" landfill: 1. mechanically compacted medium and fine sands; 2. partnership; 3. drainage; 4. concrete pipes; 5. distribution pipelines; 6. beach; 7. concrete slabs 6 x 6 m x 15 cm on lean concrete [2]

Rys. 2. Przekrój obwałowania składowiska „Gilów": 1.piaski średnie i drobne zagęszczone mechanicznie; 2. pospółka; 3. drenaż; 4. rury betonowe; 5. rurociągi rozprowadzające; 6. plaża; 7. płyty betonowe 6 x 6 m; gr. 15 cm na chudym betonie [2]

The body of the embankment was built of medium and coarse sand transported from the deposit. Its total cubic capacity is approximately 3.7 million m^3. The area of the floodplain assuming the height of waste depositing is 176 m above sea level. was 5.4 km^2. In this case, the target capacity of the landfill was 51.7 million m^3.

The bedrock of the landfill is made up of fluvioglacial sediments in the form of sands, gravels and clays of varying thickness from 30 to 50 m, resting on a layer of several dozen meters of Pliocene clays, which is the top of the Tertiary. Generally, the thickness of the Quaternary and Tertiary formations is about 300 m. Beneath it, there are Variegated Sandstones and Zechstein formations. Groundwater of the Quaternary level, fed by precipitation and infiltration from the landfill, has a runoff direction perpendicular to the embankment.

The reservoir is bounded by the ridge of the Trzebnica Hills from the north, and by an earth dam from the other sides. An earth dam (crown elevation +179.0 m above sea level) with a length of about 6.7 km and a maximum height of 22 m, it is shaped in the form of a strongly bent arch with its convex side facing south. The dam consists of two wings, the eastern one with the N-S course, approximately 2 km long and the western one with the SE-NW course, approximately 5 km long. The width of the crown, which also serves as a road to service the tank, is 4 m, and the width of the shelf is 2 m (Fig. 1). The dam is equipped with a drainage system. Through this system, water from the dam is discharged into the ring ditch. The overflow tower, located in the central part of the reservoir, rises to a height of +185m above sea level. The pipes that discharge water from the spillway tower are protected by a channel called a gallery. This channel has a segmental structure.

In order to deliver the waste to the landfill and to drain the supernatant water, the following devices were built (Fig. 1):

1. steel pipelines with a diameter of 500 mm, one running along the embankment crest and the other running along the flood line, for the discharge of waste,'
2. steel pipelines with a diameter of 1000 mm, running from the overflow tower No. 1 and No. 2 to the pumping station within the tunnel landfill, used for the discharge of supernatant water,
3. reinforced concrete overflow towers, one of which is located by the embankment in its southern part, and the other is located in the central part of the landfill, 500 m from the embankment.

In the first phase of operation of the landfill, the discharge of all waste produced in mining plants was carried out by the method of horizontal spreading from special open channels, arranged diagonally with an appropriate slope on the inner slope of the embankment. The channels were equipped with outlets that opened as the sediment level rose. A layer of water was kept above the settlements, the maximum depth of which was limited to 2.0 m.[2]

In the light of the consequences of the "Iwiny" landfill disaster, it was decided to ensure greater safety of the "Gilów" landfill. For this purpose, the method of waste storage was changed, consisting in moving the overlying water away from the embankment. This effect was achieved by discharge of waste onto the inner embankment with the use of terminals installed at 20 m intervals in the distribution pipeline running along the top of the embankment. This way of distributing the waste led to the deposition of coarser fractions at the embankment and finer fractions as they moved away from the discharge points.

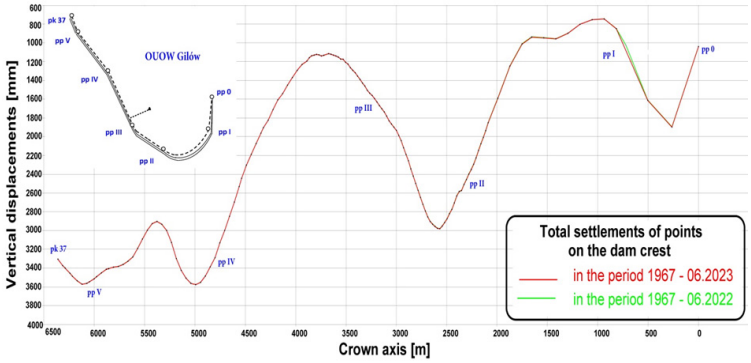

Fig. 3. Total settlements of points on the dam crest
Rys. 3. Całkowite osiadania punktów kontrolnych na koronie zapory

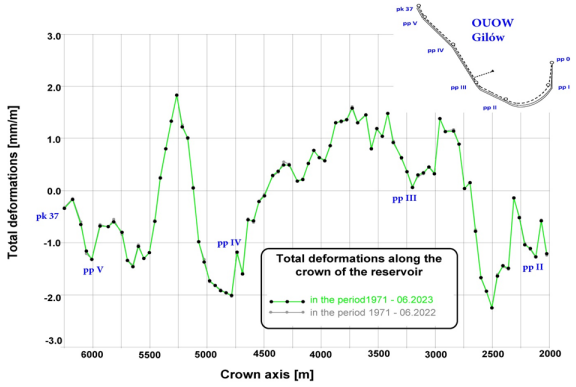

Fig. 4. Total deformations along the crown of the reservoir
Rys. 4. Całkowite odkształcenia poziome wzdłuż korony zapory zbiornika

The introduction of these changes was preceded by an attempt at the so-called "Mały Gilów", an experimental landfill built at that time in the eastern part of the "Gilów" landfill, [3]. As a result of these studies, data were obtained on the process of precipitation segregation depending on the different location of the overlying water discharge sites, as well as data on the possibility of sealing the bottom of the landfill with waste. It should be noted that the originally used waste discharge system caused flooding of the areas on the outside of the embankment, reaching the Lubin - Zielona Góra provincial road. This problem was eliminated after changing the waste discharge system by sealing the bottom of the landfill. Practically, the groundwater has decreased to its original state before the construction of the landfill.

Due to the production of two types of waste, i.e. sandstone and carbonate, significantly different in grain size composition, the next step towards ensuring greater safety of the landfill was their independent depositing. Sandstone waste, characterized by a coarser grain size and a greater degree of different grain size, was dumped from the embankment. On the other hand, carbonate waste, characterized by a finer grain size and a lower degree of heterogeneity, was discharged from the landfill flooding line (Fig. 1). In this way, it was beneficial from the point of view of maximum filling of the landfill and its safety, closing in the so-called ring.

The overlying water was continuously brought to the ore enrichment plants, and its periodic excess was temporarily discharged into the Oder River. Both overflow towers and pipelines, which ran in tunnels within the landfill, were used for this purpose. Tower No. 1 was operated only in the period when the discharge of waste was carried out from open channels, i.e. when water retention occurred at the embankment. When the method of discharge was changed, which resulted in the removal of the overlying basin, the collection of water was carried out with tower no. 2.

Another operational condition was the introduction of the principle of permanent maintenance of the sediment beach at the embankment with a width equal to or greater than 100 m [5].

4. Mining exploitation in the protection pillar of the Gilów tailings storage facility

The condition of maintaining the appropriate width of the sediment beach was related to the permit issued in 1975 for the mining of copper ore with roof caving directly under the landfill and in the embankment protective pillar, which has been carried out until now. It should be emphasized that this was possible thanks to the changes introduced in the method of depositing waste.

Despite the continuous exploitation of the deposit in the protective pillar, the height of depositing waste in the "Gilów" landfill was increased twice, up to the height of the embankment crown with the permissible ordinate of damming up the supernatant water at 177.5 m above sea level. As a result, approximately 68 million m^3 of waste was eventually deposited in the landfill on an area of 5.7 km^2.

The "Gilów" landfill, after reaching the permissible water damming level in June 1980, served only as an emergency retention reservoir for the discharge of excess water from the neighboring, active "Żelazny Most" landfill and water intake for

Fig. 5. Map of the location of floodplains above the post-flotation sediments
Rys. 5. Mapa lokalizacji terenów zalewowych nad osadami poflotacyjnymi

mechanical processing of the ore. The water level has been systematically lowered since 1980. The depth and size of the basin made it possible to keep the overflow tower in continuous operational efficiency. The observed phenomenon of meandering of the overlying basin was mainly related to surface depressions as a result of the exploitation of the protective pillar. The width of the beach along the entire embankment was always greater than the minimum allowable width of 100 m.

Due to the significant reduction of the basin, from mid-1989, overflow tower no. 2 ceased to operate automatically. If the basin periodically came closer than 100 m to the embankment, water was pumped out to the overflow tower, draining the water outside the landfill by gravity by means of a return water pipeline.

5. Geodetic monitoring of the Gilów tailings storage facility.

An inseparable element of the operation of the landfill was closely related to it, systematically conducted research and control observations. These were mainly geodetic measurements of the deformation of the embankment and the surface of the land in the foreground of the landfill, hydrogeological observations of water levels in the embankment body and its close foreground, and water flows in the ditch, as well as groundwater chemistry. Photogrammetric measurements of the landfill and meteorological observations were also carried out. Field geotechnical laboratory tests of sediments within the beach area were carried out on an ad hoc basis.

Geodetic stability studies of the over 6 km long dam limiting the reservoir from the south and east, as well as its close foreground and engineering facilities in its vicinity, were based on a geodetic monitoring project developed in the 1970s, consisting of the following control measurements: [4]

- the basic horizontal control network (currently determined by the GNNS satellite technology) consisting of 9 points (of which 6 are located on the dam crest),
- detailed control network in the form of polygon sequences developed between the points of the basic control network on the crown,
- high-altitude network, including benchmarks located on the dam crest, on the ledge, at the foot of the dam and in the close foreground, as well as benchmarks located on the "Gilów" supernatant water pumping station,
- deformations on selected sections along the crown and in cross-sections extending to its close foreground,
- a line of technical leveling with increased accuracy between benchmarks stabilized in the gallery to the overflow tower.

The lowering of the dam of the "Gilów" sedimentary pond in LGOM is an example of the overlapping of various factors influencing the lowering of the mining area [6]. These are:

- compression of the dam body due to compaction of the fill material, from which the dam is built;
- subsidence of the dam base due to the weight of the dam body;
- subsidence of the pond base together with the dam due to the pressure of deposited exploitation waste;
- large-area depressions caused by dehydration of the rock mass caused by underground exploitation;
- direct impact of the deposit exploitation on the dam and the pond.

On this object, in order to obtain parameters describing the deformations of the dam, observations are made all the time in annual intervals, including: GPS measurements, field measurements with the use of high-precision electronic total stations, leveling measurements of the crown, shelves and foot of the dam, and deformation measurements.

On the basis of the test results and control observations, periodic assessments of the embankment condition and assessment of the safety margin from the point of view of slip stability of external slopes are made. This procedure became necessary when the exploitation of the copper ore deposit in the embankment's protective pillar was introduced. Additionally, the so-called periodical confrontation of space-time forecasts of embankment deformations with the results of observations of actual deformations [2]. The forecast of deformations is updated each time, as the directions and locations of the current exploitation of the copper ore deposit change.

The surface of the landfill sediment beach was recultivated by afforestation of a large area. At the same time, all devices related to the hydrotransport of waste were liquidated.

The measurements from June 2023 show that the crown of the embankment has been lowered, reaching ordinates from 178.0 to 175.3 m above sea level. compared to the original elevation of 179 m a.s.l. (Fig.3)

Fig. 6. Photo of the disused overflow tower No. 2
Rys. 6. Zdjęcie nieczynnej wieży przelewowej nr 2

Fig. 7. Photo of the floodplain in the sediments of the Gilów mining waste disposal facility
Rys. 7. Zdjęcie powierzchni zalewowej w osadach obiektu unieszkodliwiania odpadów wydobywczych Gilów

Fig. 8. Photo of the shoreline of the floodplain in the settlements of the Gilów mining waste disposal facility
Rys. 8. Zdjęcie linii brzegowej zalewiska osadnika w obiekcie unieszkodliwiania odpadów wydobywczych Gilów

The horizontal deformations of the control sections, which are located on the section of the dam from 2500 m to its end, have been determined since 1973. They range between -2.25 mm/m in the vicinity of 2500 m (and this is the highest value of compressive deformations along the dam crest, slightly higher than the value found in previous observation periods) and +1.59 mm/m on the section of 3800 m (Fig.4) and do not pose any threat to this type of engineering structure what is an earth dam.

6. Studies of the extent of surface waters

Indirect impacts of mining exploitation are a wide group of often very complex geomechanical and hydrological phenomena occurring both in the rock mass and on the surface of the terrain. They can occur under the influence of: dewatering of the rock mass, transformations of the relief resulting from direct influences, mining seismic tremors [7]. Among the more important indirect effects of underground mining, the following should be mentioned:

1. Disturbance of water balance and loss of groundwater resources and degradation of drinking water quality.
2. Deformations of the land surface as a result of mining drainage. Among them, there are continuous deformations, resulting from the consolidation of the drained soil, and discontinuous deformations, related to the development of the suffosion process (suffosion funnels).
3. Degradation of agricultural and forest land as a result of lowering the groundwater table.
4. Flooding and swamps of the area and the formation of permanent or temporary floodplains.

They may form within the subsidence basin as a result of the relative lifting of the groundwater table, as a result of the formation of cesspools and a change in the direction of surface runoff, or as a result of deformation of watercourses, which prevents the gravitational discharge of their waters. In this way, agricultural and forest land is lost or the conditions for plant vegetation deteriorate. In addition, the geological and engineering properties of construction soils undergo negative changes [8].

In the case of post-flotation tanks, there is an additional concern that under the influence of mining activities, sediments may liquefy within the beach area.

Land flooding and the formation of permanent or temporary floodplains can also be caused by precipitation, especially in the situation of impermeable ground and lack of outflow.

Monitoring of the range of floodplains can be carried out using classic geodetic techniques, such as tacheometric me-

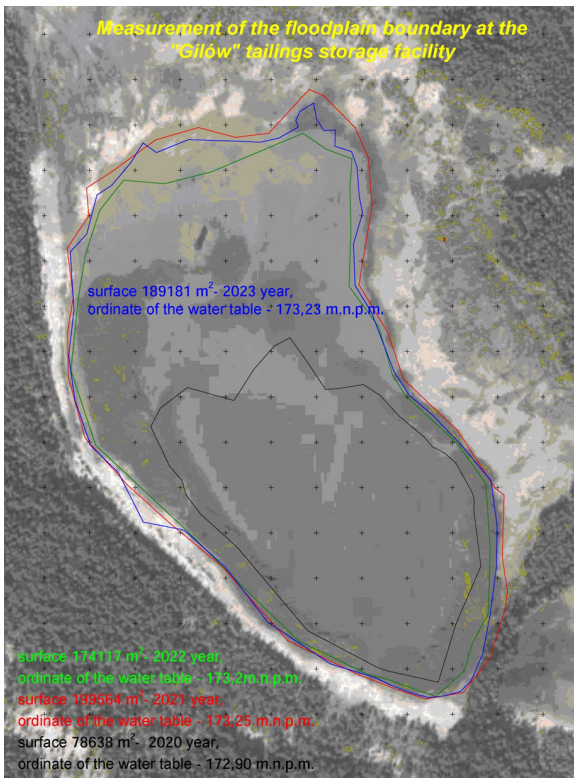

Fig. 9. Measurement of the floodplain boundary at the "Gilów" tailings storage facility

Rys. 9. Pomiar granicy powierzchni zalewowej na terenie składowiska odpadów wydobywczych „Gilów"

asurements (determination of coordinates of selected points based on the measurement of the angle and length) or satellite RTN (Real Time Network). The RTN method is one of the real-time satellite measurement methods. It uses surface corrections calculated on the basis of a network of physical reference stations (Continuously Operating Reference Stations – CORS) and virtual reference stations (VRS) generated by the computational algorithm.[12] It is also possible to use photogrammetric or remote sensing methods for monitoring floodplains using UAS - Unmanned Aircraft Systems. These are modern technologies effectively used in the preparation of maps, research of engineering structures or land surfaces, [13]. Unmanned ships serve as carriers for scanning devices, cameras and video cameras. They are an important element of aerial photogrammetry – methods of data acquisition using photographic equipment to generate orthophotos, topographic maps or 3D terrain models [14]. The effectiveness of the use of unmanned systems has significantly increased by equipping them with navigation technologies – a global navigation satellite system (GNSS) or an inertial navigation system (INS).

One of the elements of the deformation study of the Gilów tailings storage facility are site and height measurements to determine the extent of the floodplain around the inactive tower No. 2 (Fig. 5 and Fig. 6). From the methods of measuring the floodplain presented above, the RTN satellite technology was selected using the Topcon Hiper V receiver. Photos of the floodplain were also taken using a camera placed on an unmanned aerial vehicle - a multirotor (fig. 6, 7, 8) for documentation purposes.

Based on the measurements, the range of the floodplain and the average height of the water table were determined. Figure 9 summarizes the results from June 2020 to June 2023 (Fig. 9).

The average height of the water table reached its highest height in June 2021 and amounted to 173.25 m. In June 2023 it slightly decreased to 173.23 m (Fig.9). The lowest value was recorded during measurements in June 2020 and it was 172.90 m. Along with the increase in the height of the water table, the area of the floodplain increases from 78 thousand. m² in 2020 to 199,000 m² in 2021. In June 2023, the area of the floodplain is approximately 189,000 m². Analyzing changes in the area of the floodplain in comparison with the data of the Polish Institute of Meteorology and Water Management – National Research Institute, one can see correlations between the annual sums of precipitation in the vicinity of Lubin and the size of the floodplain. In 2019, the sum of precipitation was about 500 mm and in the following year, 2020, it was over 600 mm. The greatest rainfall was recorded in 2021, about 750 mm, which in the following year, 2022, amounted to 650 mm. In the vicinity of the Gilów. Reservoir, the highest rainfall occurs in June-July and on average it is about 80 mm/month.

7. Summary

During the entire period of mining exploitation, no threat to the embankment stability was observed in the embankment protective pillar, both in the phase of waste depositing, retention of mine water and landfill reclamation, despite the recorded lowering of the embankment crown of 3.58 m and the continuous movement of stretching zones in the embankment body along with the change of deposit exploitation fronts [3]. Moreover, the locally increasing intensity of paraseismic vibrations did not cause any traces of sediment liquefaction within the beach.

The currently used technology of testing the deformation of the dam and its foreground, based on the use of the most modern equipment, guarantees proper accuracy and unambiguous interpretation of the results. The basic network is still made up of points determined by GPS technology, although access to locations with a horizon suitable for satellite measurement is becoming more and more difficult.

The influence of the impacts caused by the drainage of the tertiary strata of the orogen by the Lubin O/ZG on the dam and its foreground remains at the level of the previous observation periods. Currently, periodic depressions caused by this phenomenon for the dam area are in the range of 4 to 6 millimeters. Changes caused by seasonality and, in particular, different amounts of precipitation in the pre-measurement period should be added to the picture of changes found annually.

The changes (total values of deformation indexes) found so far, which the dam has experienced against the background of the mining exploitation in its protective pillar, should be assessed as correct, and their course so far as regular and consistent with the results of the preliminary forecasts that have been carried out (within the accuracy limits of these forecasts).

Monitoring the extent of the floodplain and its impact on sediment liquefaction requires correlation of the measurements made with meteorological data for this region, which allows for rationally conducting safety analyzes of the sediment liquefaction status.

Literatura – References

1. Izabela Kotarska Odpady wydobywcze z górnictwa miedzi w Polsce – bilans, stan zagospodarowania i aspekty środowiskowe Cuprum nr4 (65) 2012, Wrocław 2012,
2. Józef Lewiński, Wojciech Wolski Monografia KGHM Polska Miedź S.A. część V Składowiska odpadów. CBPM Cuprum, Lubin 1996,
3. Werno M., Januskiewicz-Bednarczyk B., Dembiński B. Zachowanie się zapory składowiska odpadów poflotacyjnych Gilów w warunkach eksploatacji złoża w filarze ochronnym. Materiały Seminarium Geotechniczne Aspekty Składowania Odpadów, Gdańsk 1994.
4. Baran L., Downorowicz S., Najder J., Werno M. Zbiornik Doświadczalny „Gilów II"- poligon badań hydrotechnicznych w zakresie nowych technologii składowania odpadów poflotacyjnych. Materiały Sympozium Problemy Projektowania, Budowy i Eksploatacji Zbiorników Odpadów Poflotacyjnych w Górnictwie Rud Miedzi, Lubin 1974.
5. Milewski M.: Stan deformacji zapory zbiornika Gilów w świetle wyników obserwacji geodezyjnych. Geodezja nr 107, Kraków 1990.
6. Molisz R., Werno M., Baran L. Hydrotechniczna ocena stateczności zapory zbiornika osadowego „Gilów" w warunkach eksploatacji górniczej, Ochrona Terenów Górniczych WUG nr 45, Katowice 1978.
7. Pielok J. Badania deformacji powierzchni terenu i górotworu wywołanych eksploatacją górniczą. Wydawnictwo AGH Kraków 2002
8. Mzyk T. , Czajkowska A. , Gorol M. Adhibition of GNSS receiver for the impact of mining activities on the land surface monitoring. Systemy Wspomagania w Inżynierii Produkcji 2016 z. 5 (17): 176-191
9. Frohn RC, Reif M, Lane CR i Autrey B : Satellite remote sensing of isolated wetlands using object-oriented classification of Landsat-7 data. Wetlands 29 (2009): 931-941
10. Tate EC, Maidment DR, Olivera F i Anderson DJ. Create a terrain model for floodplain mapping. Journal of Hydrologic Engineering 72, 2002: 100–108
11. Davidovic, Marina & Kuzmić, Tatjana.. Application of geodetic technologies in water management. Nowy Sad 2018.
12. Kudas D., Szylar M., Cegielska K. Daily measurement of point coordinates using RTN GPS method. Episteme 30/2016, t. IIs. 511-524
13. Bliš'an, P., Bliš'anová, M., Pukanská, K., Kovanič, Ľ., Gil, M., Frąckiewicz, P., Patera, M. Bezzałogowe systemy latające UAS jako narzędzie mapowania zagrożeń naturalnych. „Nowoczesne systemy pomiarowe w geomatyce i inżynierii środowiska", red. Wolski B., Wydawnictwo Politechniki Świętokrzyskiej, Kielce, 2018, s. 11-19
14. Stumpf A., Malet J.P., Kerle N., Niethammer U., Rothmund S., Image-based mapping of surface fissures for the investigation of landslide dynamics, "Geomorphology" 2013, Vol. 186, s. 12–27

Monitoring zasięgu wód powierzchniowych nieczynnego zbiornika poflotacyjnego jako element oceny jego bezpieczeństwa

Składowisko odpadów poflotacyjnych stanowi jeden z ważnych elementów w procesie produkcji miedzi. Nieodłącznym elementem eksploatacji składowiska jest ściśle z nią związane, prowadzone systematycznie badania i obserwacje kontrolne. Głównie są to geodezyjne pomiary deformacji obwałowań i powierzchni terenu na przedpolu składowiska, hydrologiczne obserwacje stanów wód w korpusie obwałowania i bliskim jego przedpolu. W artykule przedstawiono metody i wyniki monitoringu geodezyjnego nieczynnego już składowiska odpadów wydobywczych Gilów oraz technologie stosowane w monitorowaniu zasięgu zalewiska nadosadowego.

Słowa kluczowe: *monitoring geodezyjny, pomiary zasięgu zalewiska, obiekty unieszkodliwiania odpadów wydobywczych, odpady wydobywcze*

The Use of Stochastic Modeling and Simulation to Optimize the Mining Processes

Ryszard SNOPKOWSKI[1)], Marta SUKIENNIK[2)], Aneta NAPIERAJ[3)]

[1)] prof. dr hab. inż., AGH University of Krakow; email: snopkows@agh.edu.pl, ORCID 0000-0002-1584-4842
[2)] dr hab. inż., prof. AGH, AGH University of Krakow; email: marta.sukiennik@agh.edu.pl, ORCID 0000-0002-1882-1064
[3)] dr inż., AGH University of Krakow; email: aneta.napieraj@agh.edu.pl, ORCID 0000-0002-0437-7273

http://doi.org/10.29227/IM-2023-01-37

Submission date: 24-05-2023 | Review date: 20-06-2023

Abstract

The article aims to study the possibilities and benefits of using the stochastic modeling and simulation method in the optimization of production processes. The article presents general characteristics of modelling and simulation and presents examples of stochastic models of selected production processes implemented in hard coal mines in Poland. The presented analysis led to the conclusion that the method of stochastic modelling and simulation is one of the methods worth using as a tool supporting process optimization. Its most important feature is enabling process analysis, which, regardless of the time range, can be verified within a few minutes. As a consequence, many variants of action can be analysed before their actual implementation in real conditions.

Keywords: *stochastic modelling and simulation, production process, mining process, optimization*

1. Introduction

There is no need to convince anyone about the need to optimize production processes. Over the years, we have learned a lot as scientists and practitioners about process optimization methods. We use methods and tools aimed at improving the functioning of enterprises of all types, improving processes to the optimal level, i.e. the one that is most beneficial for us given certain operating criteria.

There are many modeling and simulation methods that are implemented in various computer programs, which were mentioned in Chapter 2. However, this article is devoted to stochastic modeling and simulation, which, according to the authors, are useful in optimizing production processes, including mining processes. In addition to general information characterizing stochastic modeling and simulation, examples of their use are presented.

2. General characteristics of modeling and simulation

Modeling means "the act of matching the original with an acceptable substitute called a model, i.e. it is an approximate reproduction of the most important properties of the original" (Gościński 1982). In other words, it is building a model that „is a representation of the most important features of the tested or designed object from the point of view of the task it serves in a specific reality or abstraction" (Durlik 2000).

The literature talks about various models of the production process (Zdanowicz 2007; Wieczorek 2008; Matuszek, Kurczyk 2013). The most universal and used at all management levels are schematic models (block diagrams, business process maps in various notations, e.g. IDEF, BPMN, UML, etc.). These are the methods of notation used primarily to prepare process maps.

Their role is mainly to statically analyze the problem. They reflect the production process, its structure, elements and relationships between them and the way the production system functions, but they do not allow to determine the effects of the decisions made. Computer simulation models are used for this purpose (Vasudevan, Devikar 2011; Burduk 2013). They belong to the group of symbolic models in which reality is reflected using symbols and mathematical relations.

The computer simulation model captures the logic of behavior and mutual relations between the individual elements of the production process being tested, as well as the data that represent the characteristics of these elements. The course of the process can be presented graphically through animation, and after a simulation experiment, results are obtained in the form of charts, reports or a set of statistics describing specific elements of the process, with both the content and the form of presenting the results largely dependent on the approach used simulation (Maciąg in. 2013). The results of the experiments can be the basis for making decisions regarding the changes that should be made in the existing process (e.g. in terms of the number of machines, assembly stations, type of assortment, warehouse capacity, etc.) to achieve the assumed goal (e.g. increase in production efficiency, reduction of production costs or shortening the production cycle).

Modeling and simulation of the production process is carried out according to the general procedure presented in Figure 1.

Delving into this scheme, it can be said that the modeling and simulation procedure begins with formulating the problem and defining the research goal. Then, the simulation model is created in two steps: (1) determining its structure by deciding which elements and features of the process are important in the context of the defined problem and research goal; (2) collecting the data needed to determine the parameters of the model. The next step is to program the model using the selected simulation approach and an IT tool. The results obtained after the implementation of the initial simulation experiments on the software model are used to validate and approve the model. Validation consists in checking whether the model reflects the real production process with appropriate convergence and whether it can be used, with full confidence, to support decisions regarding the real process. The ap-

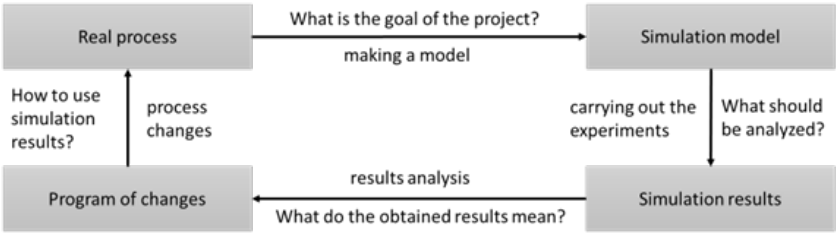

Fig. 1. Modeling and simulation of production processes. Source: (Maciąg i in. 2013)
Rys. 1. Modelowanie i symulacja procesów produkcyjnych. Źródło: (Maciąg i in. 2013)

proval of the model is usually carried out by people from the enterprise where the project is carried out. This stage forces many times to revise the previous assumptions and repeat the previous activities. The next phases of the discussed procedure consist in designing experiment scenarios that meet the research objective, conducting experiments and interpreting their results. The analysis of the results can be the basis for defining a program of changes to improve the examined process. This procedure can be continuous (Gordon 1974; Gregor i in. 1998; Burduk 2013). The main problem areas in which modeling and simulation of the production process are used are: (Łatuszyńska, 2015):

- forecasting the financial result,
- forecasting and planning material needs,
- planning the execution of production orders,
- designing production systems,
- comparing alternative manufacturing processes,
- production scheduling,
- analysis and comparison of different manufacturing strategies,
- analysis of the use of production resources (e.g. identification of bottlenecks),
- improving production systems and eliminating waste,
- visualization of the effects of activities related to production management,
- conducting presentations and trainings for staff.

3. Stochastic simulation

The stochastic simulation method is used for computer modeling of any processes (physical, economic, technological, etc.) or their fragments, the characteristic feature of which is the presence of at least one random variable in their description. The method was first used during the Manhattan Project research to build the American atomic bomb. The stochastic model developed at that time concerned the analysis of neutron propagation in a nuclear reactor. It was developed jointly by John von Neumann and the Polish mathematician Adam Ulman. The stochastic simulation method is also successfully used nowadays. The ability to create complex stochastic models, their recording in the form of a computer program in a language focused on solving such problems, as well as ever-faster computers - all this determines the frequent choice of stochastic simulation as a method of solving problems described by indeterminate models (Snopkowski 2005). Taking into account the nature of mining processes, as well as the participation of many undetermined factors in their course, it is justified to use this method also in mining.

The basis of stochastic simulation is the concept of a random number. According to what Knuth writes about it: "In a sense, there is no such thing as a random number; for example, is 2 a random number? On the other hand, we can talk about a sequence of independent random variables with a definite distribution, which means, roughly speaking, that each of the numbers was chosen completely randomly, with no connection to the selection of the other numbers in the sequence, and that each number falls into any fixed range. range of values with a certain probability" (Knuth 2002; Rolski 2013). Thus, a numerical value resulting from an experiment (e.g. the number of dice rolled) can vary from case to case, hence it is a variable. Since the outcome is decided by chance, so this variable is random.

The optimization methodology is based on a detailed analysis of the process (e.g. procurement, manufacturing, order fulfillment, etc.), or the production system (e.g. stations, cells, or production line) and visualization using one of the selected (depending on the needs and expected results) methods/tools, such as: Gantt chart (schedule), network of activities, modeling and simulation, virtualization – 3D scanning, process mapping, etc.

The next step is to optimize the analyzed process and evaluate the proposed solutions to improve its implementation.

From a practical point of view, the following facts speak for the use of stochastic simulation: it is a simple way to study random phenomena; closely related to stochastic simulations are computational methods called "Monte Carlo" (MC), which rely on the use of "artificially generated" randomness to solve deterministic tasks; moreover, it is available to everyone, in particular, the R "environment", which is a really powerful tool, is distributed for free.

4. Application examples

This chapter presents two methods, the construction of which is based on stochastic modeling and simulation. Possibilities of their application in mining practice were also indicated.

4.1 The method of probabilistic modeling of the duration of the production cycle activities carried out in longwall faces of hard coal mines

The production process carried out in longwall faces of hard coal mines is characterized by the influence of many factors that do not occur in other production processes. These factors are related to technical and organizational as well as geological and mining conditions. The production cycle performed in the longwall face of a hard coal mine is defined as a set of operations repeated in a specific order and time, necessary to advance the face of the longwall face to the distance of one (Kozdrój M., Kozdrój-Weigel M. 1993). After completing

the cycle, the crew repeats the set of operations, i.e. performs the next cycle.

The implementation of the production cycle includes the performance of a number of activities directly related to the mining of the coal body, as well as the development of the face space, with the proper maintenance of intersections of the longwall with the longwall gallery and the longwall gallery, etc. All works are necessary due to the implemented technology, but not all of them affect the directly for the duration of the production cycle. In the discussed methodology, first, the selection of those activities that have a direct impact on the duration of the production cycle was made, the factors affecting the instability of the duration of the activities were defined, and a set of density functions was established that will best describe the selected activities of the production cycle.

Scheme of modeling and stochastic simulation of the duration of the production cycle activities carried out in the longwall face consists of the following stages:

1. Defining the density function of the duration of the production cycle activities in the conditions of a given longwall face
2. Generation of production cycle activity durations based on defined probability density functions
3. Determining the duration of the production cycle based on the generated values
4. Determination of shift mining from the longwall face
5. Checking the fulfillment of the probabilistic modeling termination condition (if the condition is not met, return to step 2)
6. Analysis of the results from the stochastic simulation of the duration of the production cycle activities.

A detailed description of the procedure is presented in (Napieraj, Snopkowski 2012). The practical benefit of the discussed model is the possibility to determine shift extraction, and to be precise, determination:

- the probability that production from a selected longwall will exceed a predetermined level W_0 during a work shift,
- the probability that the output from the selected longwall will vary from W_1 to W_2,
- the level of shift extraction W_3, which is equally likely to be exceeded and not exceeded and amounts to 0.5.

4.2 The method of longwall face crew selection with respect to stochastic character of the production process

Organizing work in a hard coal mine is a difficult task due to the high unpredictability of mining conditions. Geological studies of the deposit allow for estimation of production parameters, but these approximations may not always be the basis for precise calculations at the stage of production organization. The occurrence of inhomogeneities in the geological structure of the deposit, natural hazards or machine failures are just some of the factors that may cause the stochastic nature of the production process carried out in mines. One of the most important aspects of organizing work is staffing. The efficiency of production and its effectiveness depend to a large extent on the rational allocation of employees to positions. Very high costs of purchase of machinery and equipment installed in the mining face, as well as energy and labor, mean that any downtime generates significant economic losses. There may be downtimes resulting from random events, such as machine failures, and only preventive measures related to their repairs and maintenance can be applied here. However, downtime resulting from poor work organization should be definitely eliminated. One of the main reasons for this type of downtime can be the wrong selection of the number of employees for the activities performed. The use of an appropriate mathematical apparatus, combined with data obtained as a result of repeated observations of actual times of performing activities, allows for identifying the nature of random phenomena and determining the staffing of positions, taking into account the stochastic nature of the production process. The methodology for determining the longwall face stock in hard coal mines, which takes into account the stochastic nature of the analyzed production process, consists of the following stages:

1. Identification of key activities in the production process
2. Division of the production process into characteristic modules, due to the simultaneity of the activities
3. Identification of the density function of activity durations in separate modules,
4. Adoption of initial cast variants for individual modules,
5. Optimization of staffing in modules by taking into account the probabilities of performing activities with the assumed staffing, taking into account the characteristics of the modules.

A detailed description of the procedure is included in the following works (Snopkowski, Sukiennik 2012; Snopkowski, Sukiennik 2013)

5. Discussion

The production process, carried out in the longwall face of hard coal mines, takes place underground, in specific geological and mining as well as technical and organizational conditions, which determine its specificity. The analysis of this process, in order to, for example, determine the level of achievable shift mining, can be carried out using determinate or stochastic models. The beginnings of the creation of determinate models date back to the 1960s and have been constantly developed since then. The disadvantage of these models is determinism, understood in such a way that for a specific set of data, the desired characteristic (e.g. extraction) is obtained in the form of points. However, the practice of longwall faces operation shows that the obtained extraction is not always constant - it may be subject to certain fluctuations. Therefore, it is worth using stochastic models in this case.

A similar situation accompanies the determination of the longwall face staffing, which is to ensure the continuity of the production process in this longwall face with the smallest number of employees needed. Each of the activities included in the production process is assigned an optimal staffing, and the staffing of the entire production process is determined by assigning specific employees to individual activities, taking into account the fact that some activities can be performed by the same employees. It can also be assumed that some modules can be implemented by the same staff, if there is no time conflict between these modules.

6. Conclusions

The considerations that accompanied the development of the method of probabilistic modeling of the duration of the production cycle activities and the method of longwall face crew selection make it possible to formulate the following conclusions:

- modeling the duration of the production cycle activities in the form of a probability density function makes it possible to take into account the influence of many factors on the course of these activities, and this influence results in variable time of their implementation in the conditions of a specific longwall face,
- analysis of the production cycle using the probability density function of the duration of activities allows to obtain the value of the duration of the production cycle in the modeling in the functional form,
- each production process can be divided into a finite number of modules differing in the simultaneity of the activities, which simplifies the analysis of the production process and, as a result, facilitates the selection of crew,
- the use of stochastic modeling and simulation in the described examples leads to the formulation of an objective assessment of the longwall face's production capacity level and the size of longwall face crew.

Literatura – References

1. Burduk A. (2013), Modelowanie systemów narzędziem oceny stabilności procesów produkcyjnych, Oficyna Wydawnicza Politechniki Wrocławskiej, Wrocław
2. Durlik I. (2000), Inżynieria zarządzania, część I, Agencja Wydawnicza PLACET, Warszawa
3. Gordon G. (1974), Symulacja systemów, Wydawnictwa Na-ukowo-Techniczne, Warszawa
4. Gościński J. (1982), Sterowanie i planowanie. Ujęcie systemowe, PWE, Warszawa
5. Gregor M., Haluskova M., Hromada J., Kosturiak J., Matuszek J. (1998), Simulation of Manufacturing System, Wydawnictwo Politechniki Łódzkiej – Filii w Bielsku-Białej, Bielsko-Biała Available from: https://www.researchgate.net/publication/338246081_ MODELOWANIE_I_SYMULACJA_W_ZARZADZANIU_PRODUKCJA [accessed Jul 27 2023].
6. Knuth D. (2002) Sztuka programowania – Algorytmy seminumeryczne, vol. II. WNT, Warszawa
7. Kozdrój M., Kozdrój-Weigel M. (1993) Teoria i praktyka organizowania produkcji górniczej, Wydawnictwo Politechniki Śląskiej, Gliwice
8. Maciąg A., Pietroń R., Kukla S. (2013), Prognozowanie i symulacja w przedsiębiorstwie, PWE, Warszawa
9. Matuszek J., Kurczyk D. (2013), Tendencje rozwoju w projektowaniu i zarządzaniu procesami produkcyjnymi, Innowacje w zarządzaniu i inżynierii produkcji, Oficyna Wydawnicza Polskiego Towarzystwa Zarządzania Produkcją, Opole, Available from: https://www.researchgate.net/publication/338246081_MODELOWANIE_I_SYMULACJA_W_ZARZADZANIU_PRODUKCJA [accessed Jul 27 2023].
10. Napieraj A. Snopkowski R. (2012) Method of the production cycle duration time modeling within hard coal longwall faces / Metoda probabilistycznego modelowania czasu trwania czynności cyklu produkcyjnego realizowanego w przodkach ścianowych kopalń węgla kamiennego, Archives of Mining Sciences, No 1, DOI: 10.2478/v10267-012-0009-2
11. Niemiro W. (2010) Symulacje stochastyczne i metody Monte Carlo, Wydział Matematyki, Informatyki i Mechaniki UW, Available from: https://mst.mimuw.edu.pl/lecture.php?lecture= sst&part=Ch1 [accessed Jul 27 2023].
12. Rolski T. (2013) Symulacje stochastyczne i teoria Monte Carlo, Available from: http://www.math.uni.wroc.pl/~rolski/Downloads/sym.pdf [accessed Jul 27 2023]
13. Snopkowski R. (2005) Funkcje zmiennych losowych – możliwości redukcji modeli stochastycznych, Górnictwo i Geoinżynieria, Rok 29, Zeszyt 2
14. Snopkowski R., Sukiennik M. (2012) Selection of the Longwall Face Crew with Respect to Stochastic Character of the Production Process – Part 1 – Procedural Description / Wyznaczanie Obsady Przodka Ścianowego Z Uwzględnieniem Stochastycznego Charakteru Procesu Produkcyjnego. Cz. 1 – Opis Metody, Archives of Mining Sciences, No 4, DOI: 10.2478/v10267-012-0071-9
15. Snopkowski R., Sukiennik M. (2013) Longwall Face Crew Selection With Respect to Stochastic Character of the Production Process – Part 2 – Calculation Example / Wyznaczanie obsady przodka ścianowego z uwzględnieniem stochastycznego charakteru procesu produkcyjnego cz. 2 – przykład obliczeniowy, Archives of Mining Sciences 2013, No 1, DOI: 10.2478/amsc-2013-0016
16. Wieczorek T. (2008), Neuronowe modele procesów techno-logicznych, Wydawnictwo Politechniki Śląskiej, Gliwice
17. Vasudevan K., Devikar A. (2011), Selecting SimulationAbstraction Levels in Simulation Models of Complex Ma-nufacturing Systems, [in:] S. Jain, R. Creasey, J. Himmel-spach (eds.), Proceedings of the 2011 Winter SimulationConference WSC'11, Michigan, Available from: https://www.researchgate.net/publication/338246081_MODELOWANIE_I_SYMULACJA_W_ZARZADZANIU_PRODUKCJA [accessed Jul 27 2023].
18. Zdanowicz R. (2007), Modelowanie i symulacja proce -sów wytwarzania, Wydawnictwo Politechniki Śląskiej, Gliwice

Wykorzystanie modelowania i symulacji stochastycznej do optymalizacji procesów wydobywczych

Celem artykułu jest analiza możliwości i korzyści, jakie daje użycie metody modelowania i symulacji stochastycznej w optymalizacji procesów produkcyjnych. W artykule przedstawiono ogólną charakterystykę modelowania i symulacji oraz zaprezentowano przykłady modeli stochastycznych wybranych procesów produkcyjnych realizowanych w kopalniach węgla kamiennego w Polsce. Przedstawiona analiza pozwoliła na sformułowanie wniosku, że metoda modelowania i symulacji stochastycznej jest jedną z metod, którą warto stosować jako narzędzie wspomagające optymalizację procesów. Jej najważniejszą cechą jest umożliwianie analizy procesu, które bez względu na zakres czasowy trwania, mogą być weryfikowane w ciągu kilku minut. W konsekwencji można przeanalizować wiele wariantów działania przed właściwym wprowadzeniem ich do realizacji w warunkach rzeczywistych.

Słowa kluczowe: *modelowanie i symulacja stochastyczna, proces produkcyjny, proces wydobywczy, optymalizacja*

Bursztyn z Polski – żywiczny skarb i kopalina przyszłości – przegląd wiedzy o zasobach surowca

Anna MŁYNARCZYKOWSKA[1)]

[1)] PhD AGH University of Science and Technology, Kraków, Poland; email: mindziu@agh.edu.pl, ORCID ID 0000-0001-8072-5113

http://doi.org/10.29227/IM-2023-01-38

Submission date: 14-05-2023 | Review date: 02-06-2023

Abstrakt

Artykuł stanowi omówienie zmieniającego się znaczenia kulturowo-gospodarczego bursztynu bałtyckiego oraz opracowanie ilościowej oceny wykazów zasobów złóż bursztynonośnych za lata 2012–2023 w oparciu rozpoznanie geologiczne i opracowania naukowe. Autorka przedstawia wybrane aktualne aspekty formalno-prawne w odniesieniu do złoża strategicznego jakim stać się bursztyn.

Słowa kluczowe: *bursztyn, złoża bursztynu, surowiec, Morze Bałtyckie*

Wprowadzenie historyczne

Lądowy szlak handlowy, nazwany bursztynowym, rozpoczynający się u ujścia Wisły a kierujący się w kierunku jej górnego biegu, następnie poprzez Wartę, Prosnę i Odrę i lądem od Kotliny Kłodzkiej przez Wrota Morawskie, przełęcze alpejskie oraz karpackie aż do Grecji i Włoch połączył przed wiekami rejony śródziemnomorskie z polskimi terenami nad Bałtykiem (Bień, 2018). Jak wskazują źródła historyczne już w okresie między 2500–1800 r. p.n. e. Niektórzy mieszkańcy rejonów nad Zatoką Pucką oraz Gdańską podejmowali handel wymienny zboża, miedzi czy przedmiotów użytku domowego w zamian za polski bursztyn (złoto Bałtyku). Rzemieślnicy oraz ludność zamieszkująca ówczesne tereny Żuław oraz delty Wisły zajmowała się obróbką bursztynu określanego również jako tzw. złoto Bałtyku. Rozwój handlu bursztynem między datuje się na około 400 r. p.n.e. kiedy to prawdopodobnie cesarz Neron zorganizował pierwsza wyprawę po bałtycki bursztyn, co zapoczątkowało rozkwit wymiany handlowej trwającej do III w.n.e. Wówczas z powodu osłabienia Italii znaczenie szlaku uległo istotnemu zmniejszeniu. Z pełną historią rozwoju bursztyniarstwa nad Bałtykiem można zapoznać się odwiedzając na przykład Muzeum Bursztyn zlokalizowane w Starym Młynie w Gdańsku, gdzie znajduje się niebywały okaz, czyli największa na świecie bryła bursztyny sumatrzańskiego sprzed około. 23 mln. lat (okres neogenu) i ważąca 68,20 kg.

Swoiste odrodzenie bursztynowego szlaku nastąpiło w 1997 roku, kiedy to na Konferencji Bałtyckiej Komisji Turystyki w Gdańsku, postawiono wniosek o wpisanie Szlaku Bursztynowego na listę tzw. Europejskich Szlaków Kulturowych, co w 2008 roku po podpisano listu intencyjnego opisującego promocyjne działania turystyczne doprowadziło ostatecznie do pozyskania stosownego certyfikatu oraz wpisania Szlaku na listę Europejskich Szlaków Kulturowych. Kolejnym krokiem było powstanie autostrady Amber One (autostrada bursztynowa), łączącą drogą lądową tereny nad Morzem Bałtyckim oraz Morzem Adriatyckim (Pałkiewicz, 2017; Suchodolska & Studzieniecki, 2013).

Formy występowania bursztynu w Polsce

Uważa się powszechnie, że złoża bursztynu powstały wskutek zastygnięcia żywicy drzew iglastych tworzących lasy bursztynowe, które porastały współczesną Skandynawię (wówczas był to jednolity ląd nazwany Fenno-samacją) i Morze Bałtyckie. Istnieją dwie hipotezy mające wyjaśnić masowa produkcji żywicy przez rośliny iglaste ponad 40 mln temu. Pierwsza to, pojawienie się nowego, nieznanego szkodnika przed którym drzewa usiłowały się bronić. Druga zaś przyjmuje założenie pojawienia się w bezpośrednim sąsiedztwie lasów silnej aktywności wulkanicznej powodując intensywny opad pyły pokrywający liście i doprowadzający do ograniczenia wymiany gazowej powodując produkcję żywicy. W eocenie (56-34 mln lat temu), Europe stanowiły liczne wyspy tworzące archipelag od południa otoczony Morzem Tetydy, a od północy Morzem Eoceńskim. Fenno-samację przecinała rzeka Eridan o silnie rozbudowanej zlewni z licznymi dopływami, która płynąc z północy na południe znajdowała ujście na obszarze dzisiejszej Zatoki Gdańskiej. Delta Eridanu stanowiła w okresie wysokich temperatur otoczenia idealne środowisko do generowania się żywic spływających do ówczesnego Morza Eoceńskiego. Stad też nagromadzenie bursztynów występujących in situ, w Polsce związane jest z utworami paleogeńskimi kenozoiku zlokalizowanych na obszarach przybrzeżnych właśnie tego prehistorycznego morza Pierwotne formy bursztynu zostały zachowane w okolicach Chłapowa , w tzw. delcie chłapowsko-sambijskiej osady bursztynonośne występują na głębokości między 60–130 m. oraz w okolicach Jantarnego (stąd inna nazwa bursztynu-jantar) na półwyspie Sambijskim w Rosji. Koncentracje wtórne do dziś ujawniane na plażach wzdłuż wybrzeża Bałtyku, począwszy od Kołobrzegu aż do Mierzei Wiślanej, pochodzą z okresu czwartorzędu. Są to nagromadzenia bardzo drobnych bursztynów przyniesionych przez lodowiec i rzeki polodowcowe z plejstoceńskich utworów trzeciorzędowych (2,6 mln–11,7 tys. lat temu). Wędrujący lądolód bowiem znacząco zniszczył pierwotne złoża bursztynu u ujścia Eridanu, a rozdrobnione żywice rozproszył na obecnych obszarach ich występowania. Na przykład złoże udokumentowane w Kątach Rybackich posiada bursztyn występujący tam w formie gniazd lub wydłużonych soczew w holoceńskich, płytkowodnych, morskich osadach piaszczysto-mułkowych na głębokości około 8–37 m. Podobnie jak złoże Rybakówka na Wyspie Sobieszewskiej (granice Gdańska), które składa się z nagromadzeń gniazdowo-soczewko-

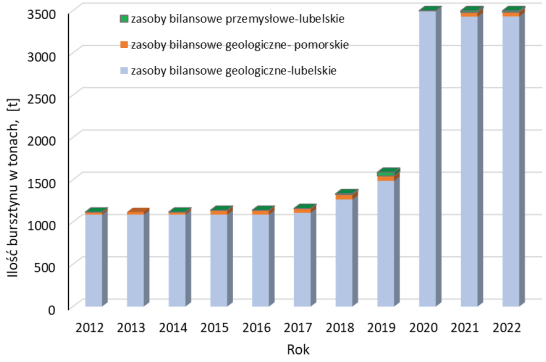

Rys. 1. Wykaz zmian złóż bursztynu w Polsce za lata 2012–2022 (opracowano na podstawie raportów bilansu złóż PIG-PIB)
Fig. 1. List of changes in amber deposits in Poland for the years 2012–2022 (prepared on the basis of PGI-NRI deposit balance reports)

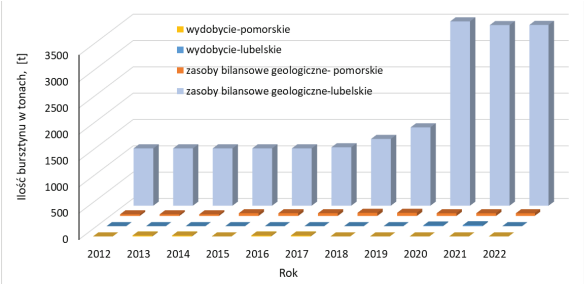

Rys. 2. Zestawienie struktury wydobycia z bilansem geologicznym złóż bursztynu w Polsce za lata 2012–2022 (opracowano na podstawie raportów bilansu złóż PIG-PIB)
Fig. 2. Comparison of the mining structure with the geological balance of amber deposits in Poland for the years 2012–2022 (prepared on the basis of PGI-NRI deposit balance reports)

we typu przybrzeżno-morskiego, a czysty bursztyn występuje w piaszczystych utworach plażowych lub dennych z roztartą martwą materią roślinną, do głębokości 7–8 m przy miąższości 30 centymetrów.

Natomiast w tzw. delcie Parczewskiej, czyli strefie południowej (rejonie Parczewa) dominują trzeciorzędowe osady bursztynonośne znajdują się na głębokości do 20–30 m. Przykładem takiego złoża jest Górka Lubartowska (delta Parczewa), która tworzą bursztynonośne mułkowo-piaszczyste osady deltowe górnego eocenu, gdzie bursztyn jest kopalina towarzyszącą. Koncentracje bursztynu występują akcesorycznie w eoceńskiej serii glaukonitowej o barwie szarozielonej, tzw. formacji z Siemienia (Pałasz, 2017), natomiast bursztynonośna warstwa zlokalizowana jest poniżej złoża piasków budowlanych o średniej miąższości około 4–12 m na głębokościach około 8–22 metrów. Pozyskany surowiec ze złoża Górka Lubartowska IX z uwagi na swoją jakość, w około 81% wag. może mieć zastosowanie w jubilerstwie, a pozostałe 19% wag. – w medycynie, przemyśle kosmetycznym lub chemicznym. Pozyskany surowiec może mieć zastosowanie w przemyśle jubilerskim (jako kamień ozdobny), chemicznym, farmaceutycznym i kosmetycznym. Należy znaczyć, że największe i jednocześnie pierwsze w pełni udokumentowane złoże eoceńskich piasków kwarcowo-glaukonitowych w Polsce znajduję się w rejonie Niedźwiada Kolonia I, II zalegających bezpośrednio na zwietrzelinie węglanowych utworów kredy górnej oraz Brzeźnicy Leśnej w województwie lubelskim. Jest ono eksploatowane metodą odkrywkową.

Jako osady trzeciorzędowy bursztyny występują również w rejonie Możdżanowa w piaskach i żwirkach górno-eoceńskich, tworzących kuliste (gniazdowe) nagromadzenia wśród osadów czwartorzędowych. Seria bursztynonośna występuje na głębokości ok. 11 m.

Udokumentowane zasoby bursztynu

Na świecie bursztyn jest zdeponowany w dnie Morza Bałtyckiego i linii wzdłuż brzegów w krajach bałtyckich, Polsce, Niemczech, Danii, Szwecji i na Białorusi. Do niedawna największe było złoże Prymorskie w obwodzie kaliningradzkim (Rosja) Według sprawdzonych zasobów bursztynu, Ukraina zajmuje trzecie miejsce na świecie po Polsce (700 000 ton) i Rosji (160 000 ton).

Informacje o bilansie zasobów złóż kopalin, a w tym konkretnym przypadku bursztynów zaklasyfikowanych do grupy innych surowców i lokalizowanych początkowo głównie jako kopaliny pomorskie, są publikowane jako coroczne raporty zasobów, udokumentowanych złóż i wysokości eksploatacji przez Państwowy Instytut Geologiczny – Państwowy Instytuty Badawczy (PIG-PIB) i ogólnodostępne od roku 2012. Dla potrzeb tego opracowania, bardziej szczegółowe informacje zostały zawężone do okresu 2018–2023 ze stanem wiedzy na dzień 31 grudnia 2022 roku. Wcześniejszy okres został ujęty bilansowo w celu wskazania zmian w tym obszarze górnictwa i przeróbki omawianego surowca. Rysunek 1 przedstawia zmiany wykazu złóż bursztynu w Polsce od roku 2012 z uwzględnieniem podziału na zasoby bilansowe geologiczne i przemysłowe oraz wydobycie realizowane najczęściej podczas robót rozpoznawczych. Rysunek 2 przedstawia zestawienia zmian struktury bilansowych złóż względem wydobycia za lata 2012–2022. Wynika z nich w sposób wyraźny, że na znaczeniu w kontekście prowadzonej już eksploatacji bądź pełnego rozpoznania złóż, zyskują zasoby zlokalizowane

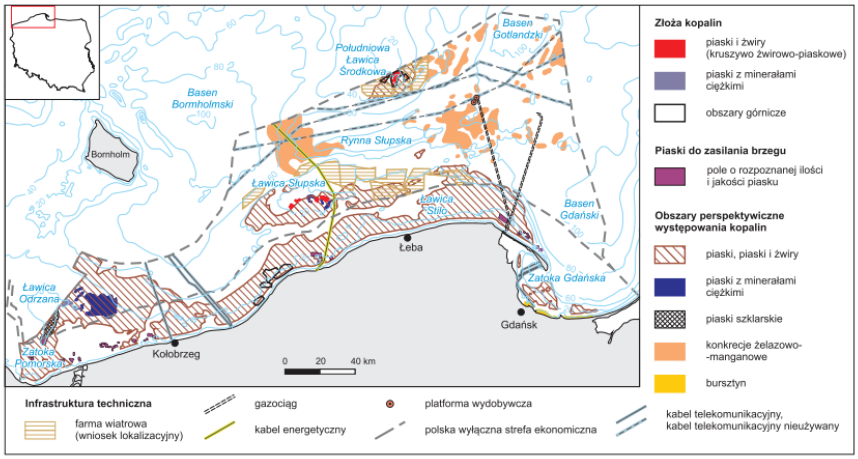

Rys. 3. Mapa występowania na dnie Bałtyku złóż i obszarów perspektywicznych kopalin na tle wybranych elementów infrastruktury (Szamałek i inni, 2020)
Fig. 3. Map of the deposits occurrence and prospective areas of minerals on the bottom of the Baltic against the background of selected infrastructure elements (Szamałek et all., 2020)

w województwie lubelskim, gdzie bursztyn jest głównie kopaliną towarzyszącą zasadniczym zasobom piasków, żwirów czy minerałów ilastych.

W ciągu dziesięciu lat nastąpiło zwiększenie rozpoznanych geologicznie zasobów o 2373,58 ton, natomiast zasobów przemysłowych o 2057,32 ton. Przełomowym wydaje się być rok 2014 i 2015 kiedy to całkowite wydobycie bursztynu w trakcie wykonywania prac poszukiwawczych wyniosło 1033.3 kg, a liczba złóż kategorii D (rozpoznanie wstępne) i C1 (rozpoznanie szczegółowe) z początkowej liczby trzech w województwie pomorskim (Możdżanowo, Przeróbka SL i Wiślinka I), zwiększyła się do siedmiu (Smołdzino, Stegnę I Sztutowo I i II). Podczas gdy w województwie lubelskim (Górka Lubartowska) eksploatowane było w tym czasie jedno złóż. Takie zmiany niewątpliwie były następstwem silnego zainteresowania inwestorów albowiem zatwierdzono 32 projekty robót geologicznych poszukiwawczo- rozpoznawczych (28 woj. pomorskie, 4 woj. Lubelskie). Ponadto zostały zatwierdzone dwa projekty robót geologicznych dla w rejonu Rawina i Stawna (woj. zachodniopomorskie) i sześć dla województwa lubelskiego (rejon Leszkowic, Niedźwiad, Brzeźnicy Leśnej i Brzeźnicy Książęcej a w województwie lubelskim).Natomiast w 2017 roku zatwierdzono 5 nowych projektów dla woj. zachodniopomorskiego, rejonów Babigoszczy, Budzieszewic, Rarwina, Szumiącej oraz 20 w woj. pomorskim dla okolic: Bogatki, Gdańska, Gołębiewski, Lublewa, Łebienia, Możdżanowa, Przejazdowa, Roszczyc, Skowarcz, Stegny, Sztutowa (dotychczas eksploatacja okresowa), Trzcinisk, Wiślinki (gdzie nie prowadzono eksploatacji) oraz Wytowna.

W kolejnych latach udokumentowano złoża bursztynu jako kopaliny towarzyszącej eoceńskim pokładom szarozielonych piasków kwarcowo-glaukonitowym dla znajdujących się w powiecie lubartowskim: Górki Lubartowska-Niedźwiada (98.00 ton) i Leszkowic 1 (4.40 ton), których miąższość wynosi około 5–7 m i głębokości około 11–21 m. Jednak odkrywkowa eksploatacja złoża objęła koncesją kopalinę główną, czyli kruszywo naturalne (piasek) oraz piaski szklarskie dla złoża Leszkowice 1.

Kolejny przełom w bilansie zasobów bursztynu zarejestrowano w roku 2020 (rys.1 i 2), kiedy to odnotowano przyrost ilości złóż o 131.5% względem roku poprzedniego. Było to efektem udokumentowania nowych zasobów bursztynu w złożu Niedźwiada II (zwiększenie o 2 032.80 ton) oraz poszerzeniem granic złoża Górka Lubartowska-Leszkowice (zwiększenie o 14.32 ton). Oprócz osadów glaukonitonośne, zidentyfikowano jako kopaliny towarzyszące, bursztyn, konkrecje fosforytowe i surowce szklarskie w postaci piasków i pyłów kwarcowych oraz iłami polimineralnymi. Przeciętna zawartość bursztynu w złożu wynosi 1 062.5 g/m^3, a zasobność złoża szacowana jest na 7 850.7 g/m^2 (Natkaniec-Nowak i inni, 2019).

Rozpoznawane sukcesywnie przez firmę Stallarium Sp.zo.o. z Niedźwiada-Kolonii, jak dotychczas największe złoża eoceńskich piasków kwarcowo-glaukonitowych zostały eksploatacyjnie udostępnione w czerwca 2020 roku (www.stellariu.com.pl) i zwiększyły się o kolejne bilansowe 5.68 ton bursztynu oraz pozabilansowe – 1.16 tony w złożu Niedźwiada III. Tutaj bursztyn występuje na głębokości od 11.9 do 19.2 m p.p.t. przy średniej jego zawartości wynoszącej 9.24 g/m^3 i szacowanej zasobności na 38.3 g/m^2. Należy dodać, iż w złożu Niedźwiada Kolonia II (zasoby 3. 33 tony) przeciętna zawartość bursztynu oszacowana jest na 0.02%, przy średniej zasobności na poziomie 82.25 g/m^2 (Natkaniec-Nowak i inni, 2019).

Wspólne wydobycie bursztynu wraz ze złożem kruszywa dotyczyło także obszaru Zatoki Koszalińskiej w omawianym okresie i pozyskania około 200 kg żywicy.

Opisane aktywności eksploracyjne inwestorów potwierdzają potencjał złóż bursztynonośnych w Polsce, co za skutkowało również zwiększeniem ogólnej liczby udokumentowanych złóż do sześciu na Lubelszczyźnie i kolejnych dwóch na wybrzeżu w kątach Rybackich i Rybakówce (razem 9), dając łączną liczbę 15 złóż bursztynu w roku 2018. Zainteresowania tego nie zmniejszył nawet ujemny bilans rozliczenia złoża Przeróbka – SL, uszczuplający ogólne zasoby bursztynu (125.68 ton) spowodowany zaprzestaniem eksploatacji z powodów ekonomicznych.

Jak podaje raport bilansu perspektywicznego PIG-PIB (Szamałek i inni, 2020) surowców ze stanem wiedzy na koniec roku 2018, zasoby bursztynu na Pomorzu sukcesywnie od lat 90-tych XX wieku były rozpoznawane i dokumentowane, chociaż znaczne trudności w realizacji robót geologicznych nastręczają warunki techniczne panujące szczególnie w strefie

Tab. 1. Stan rozpoznania i zagospodarowania polskich złóż bursztynonośnych w tonach (Szuflicki i inni, 2023)
Tab. 1. State of recognition and development of Polish amber-bearing deposits in tonnes (Szuflicki et al., 2023)

Wyszczególnienie	Ilość złóż	Zasoby geologiczne				Zasoby przemysłowe
		bilansowe			pozabilansowe	
		Razem	A+B+C_1	C_2+D		
ZASOBY OGÓŁEM	**20**	**3 491.58**	**2 130.91**	**1 360.67**	**25.84**	**2 057.32**
w tym - zasoby złóż zagospodarowanych						
Złoża eksploatowane okresowo	2	123.62	45.83	77.79	3.57	39.40
w tym - zasoby złóż niezagospodarowanych						
Razem -	16	3 348.21	2 065.33	1 282.88	22.27	2 017.92
1. Złoża rozpoznane szczegółowo	5	2 065.33	2 065.33	-	0.57	1 982.27
2. Złoża rozpoznane wstępnie	11	1 282.88	0.00	1 282.88	21.70	35.65
w tym - złoża, których eksploatacji zaniechano						
Eksploatacja zaniechana	2	19.75	19.75	-	-	-

morskiej sięgającej nawet do 2,5 km od linii brzegowej. Ma to miejsce w przypadku złóż na dnie Zatoki Gdańskiej w pasie przybrzeżnym od Gdańska-Brzeźna do Kątów Rybackich. Potwierdzono również występowanie nagromadzenia okruchów bursztynu pomiędzy zachodnim krańcem Wyspy Sobieszewskiej a wschodnią stroną ujścia Wisły Przekop oraz na Mierzei Wiślanej (obszar eksploracji: 3–8m głębokości i 100 m w głąb wód morskich (Kramarska, 2002; Szamałek, 2003, Jurys i in., 2008, za Szamałek i inni, 2020).

Dokładną lokalizację obszarów perspektywicznych dla występowania bursztynu przedstawia Rys. 3. ze wskazaniem na Zatokę Gdańską, eksploatowalną część delty Wisły oraz Mierzeje Wiślana na wysokości Gdańska-Stegny opracowany wg Kramarskiej i Szarafina (Szamałek i inni,2020) na podstawie Mapy geośrodowiskowej polskich obszarów morskich (Kramarska i in., 2019)

Tabela 1 przedstawia stan rozpoznania zasobów bursztynu i stopień ich zagospodarowania złóż bursztynu z uwzględnienie zasobów bilansowych geologicznie i przemysłowo oraz ilości kopalin pozabilansowych według stanu na dzień 31 grudnia 2022 roku. Z zawartym tam danych wynika, że obecnie udokumentowanych w Polsce jest 20 złóż, w tym 5 szczegółowo, 11 wstępnie, 2 złoża są eksploatowane okresowo a w dwóch zaniechano wydobycia. Złoża o zasobach rozpoznanych wstępnie (w kat. C2+D) opiewają na 1360.67 ton, zaś zasoby złóż rozpoznanych szczegółowo (w kat. A+B+C1) są oceniane na 2131.91 ton. Względem roku poprzedniego zwiększyła się liczba udokumentowanych złóż w województwie lubelskim o jeden obszar – Niedźwiada Kolonia II z zasobami geologicznie bilansowymi surowców w ilości 3.33 tony.

Bursztyn jako surowiec o znaczeniu strategicznym

Bursztyn jest nie tylko cennym surowcem jubilerskim, bo z tego zastosowania jest najbardziej znany. Wybrane okazy, szczególnie te nietypowe, np. zawierające zatopione w żywicy owady czy drobne kręgowce, są niezwykle cennym nabytkiem kolekcjonerskim. Ponadto ilości pozyskiwanego bursztynu na drodze zbieractwa na plażach wynosi rok do roku kilka ton. Jak podają raporty surowcowe PiG-PIB , skarb państwa traci w ten sposób średnio rocznie 5–6 ton bursztynu, co w okresie ostatniej dekady daje 50–60 ton. Oczywiście jest do głównie drobny materiał wyrzucony przez morskie fale z głębin Morza Bałtyckiego, które mogą pochodzić nie tylko z polskich zasobów tego surowca. Dokładne obliczenie ilości tak traconej kopaliny jest niezwykle trudne o ile w obecnym stanie prawnym, w ogóle możliwe.

Dokładniejsze informacje o ubytku z runku polskiego bursztynu można pozyskać z Departamentu Ceł Ministerstwa Finansów od Służby Celno-Skarbowej, która konfiskuje bursztyn podczas prób przemytu na granicach zewnętrznych Polski (przejścia drogowe, morskie i lotnicze). Surowiec jest następnie sprzedawany na licytacjach organizowanych przez Izbę Administracji Skarbowej. Tabela 3 przedstawia zestawienia ilościowe zarekwirowanego i zlicytowanego bursztynu w latach 2015–2022, które opracowano na postawie danych udostępnionych w raportach bilansu surowców PIG-PIB. Największy przemyt obserwowano w latach 2015–2017, natomiast najniższy w latach 2020–2021 co czego powodem zapewne było ograniczenie podróżowania w wyniku pandemii Covid-19. Zaskakująca jest sumaryczna ilość zarekwirowanego bursztynu (brak jest szczegółowych danych czy był on w postaci czystego surowca czy też wyrobów jubilerskich), która wyniosła 19.5 tony przez siedem lat. Jednak gdy zestawimy dan z tab.1, z wartościami szacowanych oraz już udokumentowanych złóż bursztynonośnych to wyraźnie widać, że każdego roku właściwie odzyskiwane jest jedno znacząco zasobne złoże czystego bursztynu. Cena bursztynu rośnie ostatnio w tempie 5–10 procent rocznie. Ceny bursztynu kolekcjonerskiego zależą od wagi okazu, np. bryłki o ciężarze 2,5–5,0 g osiągają ostatnio cenę 960 zł/kg; 5–10 g – 2200 zł/kg; 10–20 g – 3900 zł/kg; 20–50 g – 5900 zł/kg. Za największe okazy, które mają masę 1–1,5 kg można otrzymać nawet 100–150 tysięcy złotych. Przyjmując minimalną cenę bursztynu na poziomie 100 zł/1g, to zbycie całego zarekwirowanego przez polskie służby celne bursztynu dałoby zysk w kwocie 1 mln 950 tys. 306 zł.

Natomiast jak podaje Smakowski i in. (2015), do jubilerskiego wykorzystania w Polsce w latach 2009–2013 wykorzystywano 60–70 ton bursztynu rocznie

Mając zatem na uwadze przedstawione dotychczas informacje ilościowe oraz pamiętając również o wielowiekowym związaniu polskiej kultury ale przede wszystkim niegdysiejszego szybkiego rozwoju gospodarczego w zakresie handlu i unikatowego rzemiosła bursztynników, Szamałek (2016) podał za raportem Głównego Urzędu Statystycznego z 20015 roku, że ogólną liczbę związanych z przemysłem bursztynniczym w Polsce, poza klientami, można oszacować na poziomie ok. 100–120 tys. co zatem jest porównywalne do ówczesnego poziomu zatrudnienia w sektorze górnictwa innego aniżeli skalne. Jak wskazuje autor utrzymanie możliwości wydobycia bursztynu musi być strategicznym celem działania dla instytucji rządowych, podkreślając iż niezwykle ważne historycznie i kulturowo obiekty powstały właśnie w Polsce

Tab. 2. Wykaz złóż bursztynu w Polsce w tonach, na 31.XII.2022 r. (Szuflicki i inni, 2023)
Tab. 2. Inventory of amber deposits in Poland in tonnes, 31.XII.2022 (Szuflicki et al., 2023)

Lp.	Nazwa złoża	Stan zag. złoża	Zasoby		Wydobycie	Powiat
			geologiczne bilansowe	przemysłowe		
ZŁOŻA UDOKUMENTOWANE złóż: 20; OGÓŁEM			**3 491.58**	**2 057.32**	**-**	
woj. lubelskie złóż: 11			**3 432.70**	**2 057.32**	**-**	
1	Brzeźnica Leśna	P	298.02	-	-	lubartowski
2	Górka Lubartowska	P	895.38	-	-	lubartowski
3	Górka Lubartowska IX	P	47.97	26.30	-	lubartowski
4	Górka Lubartowska VIII	R	7.54	7.27	-	lubartowski
5	Górka Lubartowska-Leszkowice	T	45.83	25.83	-	lubartowski
6	Górka Lubartowska-Niedźwiada	T	77.79	13.57	-	lubartowski
7	Leszkowice 1	P	4.40	3.67	-	lubartowski
8	Niedźwiada II	R	2 032.80	1 975.00	-	lubartowski
9	Niedźwiada III	P	5.68	5.68	-	lubartowski
10	Niedźwiada Kolonia I	R	13.96	-	-	lubartowski
11	Niedźwiada Kolonia II	P	3.33	-	-	lubartowski
woj. pomorskie złóż: 9			**58.88**	**-**	**-**	
1	Kąty Rybackie	P	6.90	-	-	nowodworski
2	Możdżanowo	R	10.00	-	-	słupski
3	Przeróbka - SL	Z	17.05	-	-	m.Gdańsk
4	Rybakówka	R	1.03	-	-	m.Gdańsk
5	Smołdzino	P	0.60	-	-	słupski
6	Stegna	P	1.40	-	-	nowodworski
7	Sztutowo-p.I	P	10.30	-	-	nowodworski
8	Sztutowo-p.II	P	8.90	-	-	nowodworski
9	Wiślinka I	Z	2.70	-	-	gdański

gdzie skróty literowe stanu zagospodarowania zasobów w wykazach złóż oznaczają:
B – dla kopalin stałych – kopalnia w budowie, a dla ropy i gazu – przygotowane do wydobycia lub eksploatacja próbna
E – złoże eksploatowane
G – podziemny magazyn gazu (PMG)
M – złoże skreślone z bilansu zasobów w roku sprawozdawczym
P – złoże o zasobach rozpoznanych wstępnie (w kat. C2+D, a dla ropy i gazu – w kat. C)
R – złoże o zasobach rozpoznanych szczegółowo (w kat. A+B+C1, a dla ropy i gazu – w kat. A+B)
Z – złoże, z którego wydobycie zostało zaniechane
T – złoże zagospodarowane, eksploatowane okresowo
K – zmiana rodzaju kopaliny w złożu

(m.in., bursztynowa komnata, przedmioty liturgiczne, ołtarz w Kościele św, Brygidy w Gdańsku, unikatowa biżuteria), zaś zawód bursztynnika jest powszechnie dziedziczony w kolejnych pokoleniach. Autor wskazuje również, że ochroną zasobów bursztynu przemawia nielegalna eksploatacja (zwłaszcza w rejonie pomorskim) mająca swoją historię równie długa jak historia przeciwdziałania takiemu procederowi. Nieoficjalne pozyskiwanie bursztynu może mieć miejsce przy okazji na przykład budowy stawów rybnych, oczek wodnych, wykonywania studni kopanych czy głębinowych oraz podczas wydobywania kruszyw na własne potrzeby. Szamałek w tym opracowaniu postuluje: efektywniejsze działanie służb geologicznych, górniczych i porządkowych dążąc do wyeliminowania nielegalnego wydobycia bursztynu; rozwoju metodyk dokumentowania złóż bursztynu, działań administracyjnych w zakresie legislacji z jednej strony chroniącej zasoby bursztynu nie ograniczając możliwości rozwój jego wydobycia.

Odpowiedzią na powyższe postulaty jest uchwalenie planów zagospodarowania obszarów morskich poprzez Rozporządzenie Rady Ministrów z dnia 14 kwietnia 2021 r. w sprawie przyjęcia planu zagospodarowania przestrzennego morskich wód wewnętrznych, morza terytorialnego i wyłącznej strefy ekonomicznej w skali 1:200 000 (Dz.U. z 2021, poz.935), które zaczęło obowiązywać od 22 maja 2021 roku. Ten akt prawny zawiera ustalenia ogólnych zasad rozstrzygania w zakresie rozmieszczania inwestycji celu publicznego, kierunków rozwoju transportu i infrastruktury technicznej dla obszarów nadbrzeżnych oraz „ rozstrzygnięć dotyczących poszczególnych akwenów lub ich wydzielonych części oraz informacji o szczególnie istotnych uwarunkowaniach mających wpływ na przyszłe użytkowanie poszczególnych akwenów".

Podobnie, zmianie w roku 2022 uległy przepisy w zakresie kar za nielegalne korzystanie ze środowiska czy niszczenie środowiska (Dz.U. 2022 poz. 1576). Natomiast aktualnie w obiegu legislacyjnym jest projekt ustawy o zmianie ustawy – Prawo geologiczne i górnicze oraz niektórych innych ustaw (skierowany do Sejmu 5 maja 2023 r). Kontrowersje wzbudzają zapisy projektu dotyczące inwestycji strategicznych , które wedle przepisów będą mogły być realizowane nawet wbrew przepisom ochrony środowiska, czy protestom społeczny czy w bez konsultacyjnym w trybie pozwoleń dla inwestycji "strategicznych" albo wbrew woli gminy i wbrew istniejącym miejscowym planom zagospodarowania przestrzennego. Analitycy prawni specjalizujący się w przepisach ochrony środowiska wskazują zagrożenia jakie może wywołać przyjęcie wzmiankowanych przepisów w postaci m.in.:

- realności wywłaszczania obywateli bez odszkodowań,
- radykalnego działania w postaci objęcia znaczących obszarów Polski strategiczną ochroną zasobów surowcowych i zablokowanie na czas nieokreślony na ich terenie wszelkich inwestycji zarówno prywatnych jak i inwestorskich,
- umożliwienia globalnym podmiotom na eksploatację strategicznych zasobów wody pitnej znajdujących się pod ziemią czyniąc ją tym samy kosztownym dobrem,
- pozbawienia samorządów prawa rozwoju terenów własnych wskutek możliwości wprowadzenia całkowitego zakazu zabudowy nad złożami strategicznymi,
- wyłączenia samorządów z procesu wydawania koncesji na wydobycie,
- dopuszczalności kar dla władz samorządowych za nieujawnienie złóż w studiach i planach miejscowych,

Tab. 3. Zestawienie ilości bursztynu konfiskowanego i sprzedawanego przez służby celne w Polsce w latach 2015–2022
Tab. 3. Summary of the amount of amber confiscated and sold by customs services in Poland in 2015–2022

ROK	ZAREKWIROWANY BURSZTYNU, KG	ZLICYTOWANY BURSZTYN, KG
2015	1664.9	373.2
2016	7484.9	73.2
2017	6245.9	689.1
2018	1236.0	808.0
2019	1049.0	548.0
2020	249.0	11.7
2021	140.0	711.0
2022	1433.4	166.0
razem	**19503.1**	**3380.1**

- obawy, że koncesja stanie się ostatecznym aktem prawnym niepodlegającym zaskarżeniu, np. przez właścicieli nieruchomości lub władze samorządowe.

Wnioski

Rozpatrując definicje surowca strategicznego czy krytycznego, w pierwszej kolejności łączy się to pojęcie z bezpieczeństwem militarnym kraju, Europy, świata. Należy tutaj wskazać jednak na bezpieczeństwo surowcowe stanowiące jeden z priorytetów polityki Unii Europejskiej (UE), co nabrało jeszcze większego znaczenia po kłopotach wywołanych zerwaniem łańcuchów dostaw surowców w okresie pandemii Covid-19. Zdaniem Szałamka, (2016), za każdy surowiec niezwykle ważny, określany kluczowym dla wybranej branży, który równocześnie cechuje się unikalnymi właściwościami, przez co nie może zostać zastąpiony przez inny materiał (substytut), należy nazwać surowcem strategicznym. Zdaniem autora, właśnie bursztyn z polskich złóż wypełnia wszystkie wymienione kryteria/warunki. Autorka tego opracowania podziela zacytowane opinie, wskazując jednak na konieczność rozważnego kształtowania uwarunkowań formalno-prawnych w zakresie ochrony złóż na terenie Polski, mając szczególnie na uwadze bezpieczeństwo surowcowe kraju przy równoczesnym nie zaniedbaniu zasad zrównoważonego gospodarowania zasobami.

Finansowanie

Praca zrealizowana w ramach programu badań Akademii Górniczo-Hutniczej w Krakowie, Nr No.16.16.100.215

Literatura – References

1. Bień E., (2018), Szlak bursztynowy - historia i jego przebieg, "Bursztyn – Wczoraj.Dziś.Jutro", Region, s. 144-14
2. Jurys L., Kramarska R., Oller M., Cylkowska H. (2008). O metodyce dokumentowania i eksploatacji holoceńskich złóż bursztynu w delcie Wisły. Górn. Odkryw, 50 (2/3), 111–118
3. Kramarska R. (2002). Pakiet informacyjny dla potencjalnie bursztynonośnych obszarów Zatoki Gdańskiej. Zatoka Gdańska – rejon 2. Nar. Arch. Geol. PIG-PIB, Oddz. Geol. Morza, Gdańsk [nr kat. 614].
4. Kramarska R., Szarafin T., Pączek U. (2019). Mapa geośrodowiskowa polskich obszarów morskich w skali 1:250 000. PIG-PIB, Warszawa
5. Kramarska R., Kasiński J.R., Słodkowska B., 2020 - Bursztyn, sukcynit (amber, succinite). W: Bilans perspektywicznych zasobów kopalin Polski wg stanu na 31.12.2018 r. (red. Szamałek K., Szuflicki M., Mizerski W.): 371-377. PIG-PIB, Warszawa.
6. Malanchuk Y., Viktor Moshynskyi V., Korniienko V., & Malanchuk Z. (2018). Modeling the process of hydromechanical amber extraction. E3S Web of Conferences 60, 00005 (2018) https://doi.org/10.1051/e3sconf/20186000005
7. Natkaniec-Nowak L, Piestrzyński A., Wagner M., Hefli k W., Naglik B., Paluch J., Pałasz K, Milovská S. & Stach P. (2019). Złoże „Górka Lubartowska-Niedźwiada" (E Polska) jako potencjalne źródło surowca glaukonitowego. Gospodarka Surowcami Mineralnymi – Mineral Resources Management. 35(2), 5–30
8. Pałasz, K. (2017). Charakterystyka mineralogiczna glaukonitu z okolic Niedźwiady (woj. lubelskie). Kraków: Archiwum KMPiG WGGiOŚ AGH, 42
9. Pałkiewicz J. (2017), Powrót na Bursztynowy Szlak, "Rzeczpospolita', s. 24-25.
10. Rozporządzenie Rady Ministrów z dnia 14 kwietnia 2021 r. w sprawie przyjęcia planu zagospodarowania przestrzennego morskich wód wewnętrznych, morza terytorialnego i wyłącznej strefy ekonomicznej w skali 1:200 000 (Dz.U. z 2021,poz.935),
11. Smakowski T., Galos K., Lewicka E. (2015). Bilans gospodarki surowcami mineralnymi Polski i świata 2013. PIG-PIB, GSMiE PAN, Kraków.
12. Szamałek K. (2003). Koncesje na poszukiwanie bursztynu. Prz. Geol., 51 (11), 906 -916
13. Szamałek K. (2016) Bursztyn jako surowiec strategiczny. Biul. Państw.. Inst. Geolog. 466: 291–296. doi: 10.5604/01.3001.0009.4326
14. Szamałek K., Szuflicki M., Mizerski W. (2020). Bilans perspektywicznych zasobów kopalin Polski wg stanu na 31.12.2018 r. PIG-PIB, Warszawa 2020. ISBN 978-83-66509-92-4
15. Szuflicki M., Malon A., Tymiński M. (2023) Bilans Zasobów złóż w Polsce wg stanu na 31 XII 2022 r., PIG-PIB, Warszawa 2023. ISSN 2299-4459
16. Suchodolska T., Studzieniecki T. (2013). Potencjał i produkty turystyczne szlaku bursztynowego, "Szlaki kulturowe: organizacja, promocja, zarządzanie", Bernardinum, s. 112-125.
17. www.stellariu.com.pl (dostęp 30.07.2023 r.)
18. Ustawa z dnia 7 lipca 2022 r. o zmianie ustawy - Prawo ochrony środowiska oraz niektórych innych ustaw, (Dz.U. 2022 poz. 1576)

Amber from Poland – a Resin Treasure and Mineral of the Future – a Review of Knowledge about the Resources of this Raw Material

The article is a discussion of the changing cultural and economic importance of Baltic amber and the development of a quantitative assessment of amber-bearing deposits for the years 2012–2023 based on geological exploration and scientific studies. The author presents selected current formal and legal aspects in relation to the strategic deposit of amber.

Keywords: *mber, amber deposits, raw material, Batlic Sea*

Marketing cyfrowy w branży surowcowej – Case Study

Barbara KOWAL[1)], Iga ŚWIĄTEK[2)]

[1)] Ph.D., DSc, Eng.; AGH University of Science and Technology, Cracow, Poland; email: bkowal@agh.edu.pl, ORCID: 0000-0003-4643-1140
[2)] student; AGH University of Science and Technology, Cracow, Poland, email: igaswiatek@student.agh.edu.pl

http://doi.org/10.29227/IM-2023-01-39

Submission date: 15-05-2023 | Review date: 06-06-2023

Abstrakt

Działania podejmowane przez obecnie działające przedsiębiorstwa w ramach marketingu cyfrowego stają się coraz bardziej ich codziennością. Od czasu pandemii stanowią główną formę kontaktu z klientem, dlatego są tak niezmiernie ważne w działalności każdego przedsiębiorstwa. Niniejszy artykuł przedstawia przeprowadzoną analizę działań marketingowych prowadzonych przez wybrane pięć przedsiębiorstw surowcowych w zakresie marketingu cyfrowego. Badania objęły strony internetowe oraz aktywności analizowanych przedsiębiorstw w mediach społecznościowych. Pokazały jakie działania są podejmowane przez przedsiębiorstwa, czy osiągają one wysoki poziom zaangażowania odbiorców na portalach, na których istnieją oraz co należałoby zrobić, aby wykorzystanie marketingu cyfrowego było skuteczniejsze.

Słowa kluczowe: *rynek surowcowy, marketing cyfrowy, media społecznościowe, komunikacja marketingowa*

1. Wstęp

Działania marketingowe są w obecnych czasach niezmiernie ważne w działalności każdego przedsiębiorstwa, gdyż stanowią główną formę kontaktu z klientem. Taki rodzaj komunikacji, komunikacji cyfrowej, zyskał na znaczeniu w ostatnich latach. Szczególnie okres pojawienia się COVID-19 pokazał jak ważny dla społeczeństwa jest dostęp do internetu i rozwój cyfryzacji. Bezpośredni kontakt z klientem zamienił się na kontakt w formie online. Ze względu na fakt, iż dostęp do Internetu ma aż 61.8% społeczeństwa na świecie [1] działania marketingowe w sieci docierają do szerokiej publiczności, a firmy mają szanse na zdobycie wielu klientów z różnych krajów. Ostatnie dwa, trzy lata spowodowały zmianę na rynku surowców mineralnych. Okres pandemii i kolejne lockdowny zakłóciły łańcuchy dostaw, ograniczył się też popyt na surowce, a jedyną formą kontaktu czy komunikacji przez pewien okres był internet. Dodatkowo działania wojenne na Ukrainie przyczyniły się do kryzysu energetycznego oraz światowego kryzysu gospodarczego [2, 3, 4], który spowodował wzrost zapotrzebowania UE na surowce mineralne (głównie surowce krytyczne).

W kontekście obecnej sytuacji globalnej Polska posiada zróżnicowaną bazę zasobową surowców mineralnych [2, 5, 6], a wszystkie kluczowe kopaliny uzyskały status o dużym znaczeniu gospodarczym [7]. Powoduje to, że Polska staje się ważnym dostawcą wielu surowców mineralnych do krajów UE [8]. A przy obecnie posiadanych zasobach utrzymanie produkcji surowców mineralnych na znaczącym poziomie będzie możliwe najmniej przez 30 lat [9]. Dokumentami, który regulują funkcjonowanie branży surowcowej w Polsce jest „Prawo geologiczne i górnicze" z 9 czerwca 2011 roku określające „zasady i warunki podejmowania, wykonywania oraz zakończenia działalności w zakresie wydobywania kopalin ze złóż" [10] oraz „Polityka Surowcowa Państwa" (nazywana również PSP2050), która została przyjęta przez Radę Ministrów 1 marca 2022 r. PSP2050 ma być „filarem bezpieczeństwa i efektywnego gospodarowania zasobami wszystkich dostępnych w Polsce kopalin i surowców mineralnych łańcucha wartości" [11]. Jednym z jej celów szczegółowych jest „zapewnienie sprzyjających warunków prawnych dla obecnych i przyszłych inwestorów oraz rozwój i unowocześnienie branży geologiczno-górniczej" [12]. Realizacja tych celów mogłaby być łatwiejsza przy wykorzystaniu marketingu cyfrowego i prowadzeniu szeroko pojętych działań marketingowych.

Celem niniejszej publikacji jest analiza działań w zakresie marketingu cyfrowego pięciu przedsiębiorstw działających na rynku surowcowym i porównanie uzyskiwanych wyników zaangażowania ich odbiorców na poszczególnych portalach społecznościowych.

2. Digital marketing

Digital marketing określany jest „najszybciej rozwijającym się obszarem marketingu w historii tej dziedziny" [13]. Określany jest jako e-marketing lub marketing cyfrowy. To jeden z elementów stosowanego w pozyskiwaniu klientów marketingu 4.0, gdzie „klienci mają bardziej bezpośredni wpływ na kierunek marki, dzięki bardziej intymnej relacji za pośrednictwem technologii cyfrowej" [14]. W literaturze przedmiotu znaleźć można różniące się definicje e-marketingu, przedstawiające go jako:

- działania przedsiębiorstwa prowadzone za pośrednictwem Internetu zmierzające do promowania oraz sprzedawania produktów i usług, a także do budowania relacji z klientem [15],
- całościowy proces planowania i organizowania, a także realizacji działań marketingowych w Internecie ukierunkowanych równocześnie na zaspokajanie potrzeb klientów oraz osiąganiu celów organizacji [16],
- centrum cyfrowego biznesu, polegającego na zbliżaniu się do klientów w celu ich lepszego zrozumienia, a także poszerzanie kanałów dystrybucji i zwiększanie sprzedaży poprzez prowadzenie kampanii marketingu cyfrowego z wykorzystaniem jego kanałów [17],

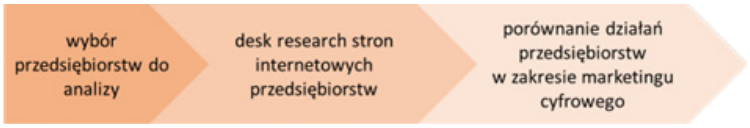

Rys. 1. Schemat przeprowadzonych badań. Source: own study
Fig. 1. Research scheme. Źródło: opracowanie własne

- metoda promocji wykorzystująca cyfrowe środki przekazu jako jej kanały komunikacji z potencjalnym nabywcą danych dóbr [18].

Reasumując marketing cyfrowy to zbiór działań w celach promocyjnych, których zadaniem jest dotarcie do potencjalnych klientów, szukających produktów lub usług danej firmy [19].

Istnieje wiele rodzajów oraz kanałów marketingu cyfrowego [20]. Do głównych działań marketingowych zalicza się:

- Influencer Marketing – to działania skierowane na osoby znane i wpływowe w obrębie grupy docelowej [16],
- Content Marketing – tzw. marketing treści, opiera się na przygotowaniu istotnych i wartościowych dla klienta materiałów w odpowiedniej formie graficznej i tekstowej [16],
- Search Engine Marketing (SEM) – tzw. marketing w wyszukiwarkach, obejmuje działania promocyjne w celu podniesienia pozycji danego serwisu w wynikach wyszukiwania (głównie poprzez odpowiednie frazy lub słowa kluczowe) [21],
- Video Marketing – tworzenie i publikowanie materiałów wideo oraz zarządzanie nimi po udostępnieniu [22, 23],
- Social Media Marketing – działania skierowane na wzrost rozpoznawalności marki, budowanie pozytywnego wizerunku, nawiązywanie relacji z klientami mające na celu osiągnięcie wyższych wyników sprzedażowych [24, 25],
- E-mail Marketing – tzw. marketing bezpośredni, narzędzie komunikacji wykorzystujące pocztę elektroniczną [16, 26],
- Display Marketing – graficzna reklama internetowa przekierowująca do docelowej strony internetowej [20, 27].

Zadaniem każdego kanału jest przyciągnięcie jak największej liczby klientów, a także zapewnienie skutecznej reklamy dla firmy. W marketingu cyfrowym wykorzystywane są narzędzia umożliwiające analizę stosowanych przez firmę działań, jak i tworzenie wszelakich treści. Do najpopularniejszych należą m.in: Brand24, Google Analytics, Google Ads, BuzzSumo, Senuto i inne [szerzej w: 28].

3. Metodologia badań

Celem przeprowadzonych badań była analiza działań przedsiębiorstw surowcowych w zakresie marketingu cyfrowego. Wybrano pięć przedsiębiorstw z branży surowcowej, w tym: KGHM Polska Miedź, Grupa LOTOS, PKN ORLEN, Lubelski Węgiel „Bogdanka" SA oraz PGNiG SA. Wszystkie przedsiębiorstwa posiadają strony internetowe i są aktywne w mediach społecznościowych. Jedynie Lubelski Węgiel „Bogdanka" S.A. nie miała Twittera i Instagrama.

Badania przeprowadzono według schematu przedstawionego na rysunku 1.

Po wyborze przedsiębiorstw surowcowych przeprowadzono desk research ich stron internetowych, a następnie dokonano porównania działań tych przedsiębiorstw pod kątem wykorzystywanych przez nie kanałów oraz sposobów ich użycia wraz z osiągniętymi efektami.

W szczególności badania polegały na sprawdzeniu stron internetowych oraz mediów społecznościowych analizowanych pięciu przedsiębiorstw. Analiza porównawcza obejmowała:

- wykorzystywane kanały marketingu cyfrowego,
- pozycjonowanie stron internetowych przedsiębiorstw (wykorzystano SEO oraz aplikację Senuto),
- obliczenie wskaźnika zaangażowania odbiorców na profilach we wszystkich używanych przez przedsiębiorstwa mediach społecznościowych (Engagement Rate, ER, wzór 1) [29].

$$ER = \frac{wszystkie\ interakcje}{liczba\ obserwujących}\ x\ 100\% \qquad \text{(wzór 1)}$$

Przy czym interakcje obejmowały liczbę polubień, komentarzy oraz ilości udostępnień stworzonych przez firmę treści w serwisie.

4. Analiza stron internetowych i mediów społecznościowych – wyniki

4.1 Kanały marketingu cyfrowego

Wstępna analiza stron internetowych oraz mediów społecznościowych każdego z analizowanych przedsiębiorstw z branży surowcowej pokazała, że Grupa LOTOS, PKN ORLEN i PGNiG SA wykorzystują wszystkie kanały marketingu cyfrowego jakie zostały przedstawione w rozdziale 2. KGHM Polska Miedź nie wykorzystuje takich kanałów jak: Influencer Marketing oraz Display Marketing. Natomiast Lubelski Węgiel „Bogdanka" SA – Influencer Marketing, E-mail Marketing oraz Display Marketing.

4.2 Pozycjonowanie stron internetowych w wyszukiwarkach

W aplikacji Senuto utworzono analizę widoczności dla stron internetowych wybranych wcześniej przedsiębiorstw poprzez wpisanie adresów każdej z domen. Otrzymane wyniki pokazały, że:

- największą liczbę słów na jakich domena wyświetla się w wynikach TOP3 w wyszukiwarce posiada przedsiębiorstwo PGNiG SA,
- najmniejszą wartość słów kluczowych dla wyników firmy w TOP 3 ma LW „Bogdanka" SA, jest on ponad dziesięciokrotnie niższy niż w przypadku PGNiG SA,
- przedsiębiorstwa zajmują stałe miejsca w „rankingu" tworzonym podczas analizy,
- najwyższe wartości zarówno dla szacowanego ruchu, jak i reszty danych występują dla PGNiG SA, które zajmuje 78. miejsce w rankingu kategorii biznes. Kolejny jest ORLEN (149. miejsce w rankingu o tej samej tematyce, co PGNiG). Trzecie w kolej-

a) Facebook

b) LinkedIn

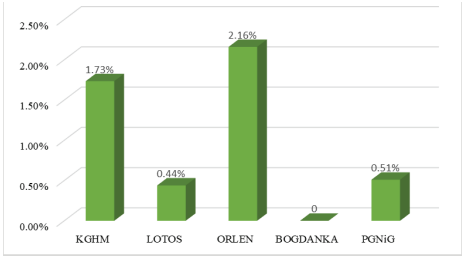

c) Twitter

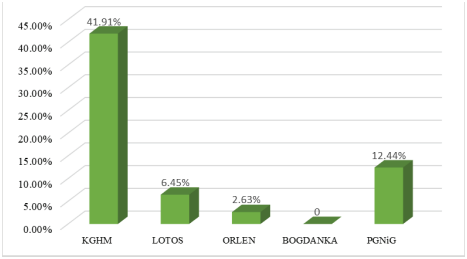

d) Instagram

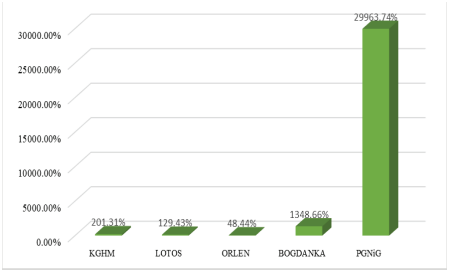

e) YouTube

Rys. 2. Wartości wskaźnika zaangażowania odbiorców (ER) analizowanych przedsiębiorstw na poszczególnych portalach. Source: own study
Fig. 2. Values of Engagement Rate of the analyzed enterprises on individual portals. Źródło: opracowanie własne

ności jest przedsiębiorstwo LOTOS zajmujące 405. miejsce w rankingu. Następny jest KGHM, a za nim „Bogdanka".

4.3 Wskaźnik zaangażowania odbiorców na profilach

W celu obliczenia skuteczności zarządzania profilami w mediach społecznościowych przez poddane analizie przedsiębiorstwa, obliczono (wg wzoru 1) wskaźnik zaangażowania odbiorców tzw. Engagement Rate (ER) dla każdego z nich na poszczególnych portalach. Wskaźnik ten pokazuje aktywność obserwatorów pod udostępnianymi treściami. Analiza dotyczyła pięciu najnowszych wpisów, postów oraz filmów udostępnionych przez przedsiębiorstwa w poszczególnych mediach społecznościowych. Wartości wskaźnika zaangażowania odbiorców ER dla poszczególnych portali analizowanych przedsiębiorstw przedstawiono na rysunku 2.

Wyniki przedstawione na rysunku 2a) pokazują, że największą wartość wskaźnika ER na portalu Facebook ma profil przedsiębiorstwa LW „Bogdanka" SA, który nie posiada tak pokaźnej liczby obserwatorów (776 obserwatorów), jak większość firm poddanych analizie. Jak widać liczba obserwatorów nie koniecznie idzie w parze z zaangażowaniem odbiorców. Druga co do wielkości wartość wskaźnika ER przypadła PGNiG SA z liczbą obserwatorów wynoszącą 20079. Obserwacje tych przedsiębiorstw są niższe od pozostałych (KGHM Polska Miedź - 20457, Grupa LOTOS – 24839, PKN ORLEN – 59256). Przedsiębiorstwo Lubelski Węgiel „Bogdanka" SA może również pochwalić się największą liczbą udostępnień stworzonych treści wśród pięciu analizowanych firm, bo aż 66. Najniższy wskaźnik ER występuje w przedsiębiorstwie ORLEN, gdzie liczba obserwatorów, polubień oraz komentarzy jest najwyższa.

Najwyższy wskaźnik zaangażowania odbiorców na portalu LinkedIn, podobnie jak w przypadku serwisu społecznościowego Facebook, posiada Lubelski Węgiel „Bogdanka" SA i wynosi on 30,80%. Jest on ponad 80 razy wyższy od najmniejszego wskaźnika zaangażowania występującego na profilu firmy ORLEN. Powodem jest ogromna różnica w liczbie obserwatorów obydwu firm licząca ponad 58 tysięcy. Mimo niewielu, w porównaniu z resztą przedsiębiorstw, użytkowników obserwujących konto „Bogdanki", bo jest ich zaledwie 776, ilość interakcji jest bardzo duża, co świadczy o dobrej relacji firmy z odbiorcami. Wyniki analizy wskaźników przedsiębiorstw na portalu LinkedIn przedstawiono w formie graficznej na rysunku 2b).

Przy obliczaniu wskaźników zaangażowania odbiorców na portalu Twitter (rys. 2c), z wyjątkiem przedsiębiorstwa LW „Bogdanka" S.A., które nie korzysta z niego wcale, wymagało jedynie zamiany sumy komentarzy w liczniku na sumę odpowiedzi. W tym przypadku najwyższą wartość wskaźnika ER, który wyniósł 2,16%, osiągnął PKN ORLEN. Widać, że duża liczba obserwatorów (30001) na tym portalu przekłada się na większy ruch na profilu przedsiębiorstwa. Zarówno polubienia (431), jak i odpowiedzi (65) oraz udostępnienia (152) są

znaczne wyższe niż w pozostałych firmach. W zestawieniu czterech firm, najgorzej wypadła Grupa LOTOS, która mając drugie miejsce pod względem ilości obserwatorów (10709), osiąga jedne z najniższych wyników w zakresie interakcji odbiorców na publikowane treści, bo tylko 2 komentarze.

Porównanie graficzne wskaźników ER dla portalu Instagram przedstawiono na rysunku 2d). W przypadku obliczeń wskaźników zaangażowania dla tego portalu pod uwagę brano jedynie sumę polubień oraz komentarzy do podsumowania interakcji, ponieważ serwis społecznościowy Instagram w Polsce nie ma możliwości bezpośredniego udostępniania treści w formie postu na swój profil. W przypadku tego portalu LW „Bogdanka" SA również nie posiada konta. Najlepszy wynik wskaźnika wystąpił na profilu KGHM Polska Miedź. Wyniósł on aż 41,91%, co jest wartością powyżej średniej. Sumy polubień oraz komenatrzy w przypadku firmy KGHM oraz Grupy LOTOS były niemal identyczne (polubienia odpowiednio 199 i 200; komentarze 3 i 4), jednakże liczba obserwatorów profilu LOTOS jest ponad 6-krotnie wyższa i wynosi 3162, co przełożyło się na niższą wartością wskaźnika ER wynoszącą 6,45%. Na drugim miejscu znalazło się przedsiębiorstwo PGNiG SA, które osiągnęło wysoki wynik ER wynoszący 12,44% pomimo małej ilości polubień (75) oraz komentarzy (3).

Do obliczeń wskaźniki zaangażowania ER na kanałach analizowanych przedsiębiorstw w serwisie YouTube wzięto pod uwagę jedynie sumę polubień oraz komentarzy, które podzielono przez liczbę subskrybentów kanału. Poziom wskaźnika na kanale PGNiG SA znacznie przewyższył wyniki pozostałych przedsiębiorstw mimo niskiej liczby polubień (28) oraz wyłączonej możliwości komentowania pod swoimi filmami. Na drugim miejscu, ze znacznie mniejszą wartością wskaźnika, znajduje się LW „Bogdanka" SA, która również wyłączyła możliwość komentowania filmów. Najniższy wynik osiągnęło przedsiębiorstwo ORLEN, które posiada największą liczbę subskrybentów, bo 10000 oraz sumę komentarzy pod pięcioma ostatnimi filmami (10). Zestawienie graficzne analizy przedstawiono na rysunku 2e).

5. Wnioski

Oceniając działania marketingowe analizowanych przedsiębiorstw surowcowych nasuwają się następujące wnioski dla:

- KGHM Polska Miedź – lepsze wyniki osiąga w mediach społecznościowych niż na stronie internetowej firmy; powinna zostać podjęta współpraca z influencerem, który wygeneruje ruch na stronie internetowej firmy i sprawi, że jej pozycja w rankingach wzrośnie wraz z pozycją w wynikach wyszukiwania; potrzebna jest analiza wyboru słów kluczowych oraz dodanie nowych, bardziej ogólnych, dzięki którym odbiorcy znajdą stronę KGHM; w przypadku mediów społecznościowych, przedsiębiorstwo powinno starannie dobierać treści, a także zachęcać (odbiorców, pracowników) do ich udostępniania, aby zaangażowanie odbiorców pod postami było jak największe;
- Grupa LOTOS – więcej działań wymaga usprawnień; strona internetowa powinna być częściej uaktualniana oraz zostać przeprojektowana, aby była łatwiejsza w nawigacji, a jej zawartość lepiej widoczna; zbiór słów kluczowych powinien zostać poszerzony; powinien powstać harmonogramu postów, aby treści były regularnie publikowane, co zwiększyłoby ich widoczność; odpowiednie dobranie treści pod odbiorców i przeprowadzenie badania rynku, które umożliwi zwiększenie interakcji pod postami;
- PKN ORLEN – osiąga dobre wyniki w przypadku swojej strony internetowej, natomiast jej działania w mediach społecznościowych wymagają poprawy; potrzeba regularności w dodawaniu treści na profile, a także zachęcenia odbiorców do interakcji; modyfikacji wymaga również video marketing, gdyż filmy w serwisie YouTube publikowane są zbyt rzadko;
- Lubelski Węgiel „Bogdanka" SA – nie korzysta z wielu działań w cyfrowego marketingu, co powinno ulec zmianie; strona internetowa powinna zostać całkowicie zmodyfikowana; uruchomienie newslettera dla klientów; reklamy graficzne w formie banerów przekierowujących do docelowej strony internetowej pomogłyby zwiększyć ruch na stronie internetowej; słowa kluczowe wymagają aktualizacji, aby jej pozycjonowanie w wynikach wyszukiwania się polepszyło; w mediach społecznościowych, na których działa LW „Bogdanka" SA osiąga znakomite wyniki, aczkolwiek nie korzysta wcale z dwóch kluczowych serwisów społecznościowych, których używa konkurencja; założenie kont na portalu Twitter oraz Instagram pomogłoby w powiększeniu grupy odbiorców i promowaniu swojej strony internetowej; włączenie możliwości komentowania pod filmami na portalu YouTube;
- PGNiG SA – jej działania są na bardzo wysokim poziomie, zwłaszcza jeśli chodzi o stronę internetową, więc nie wymagają usprawnień; jednak na profilach w mediach społecznościowych odzew zwrotny ze strony odbiorców jest bardzo mały w przypadku komentarzy – treści powinny zostać zmodyfikowane tak, aby zachęcały do interakcji, co pozwoli zwiększyć zasięgi postów; regularność publikowania na każdym z portali społecznościowych (zwiększenie aktywności na koncie w serwisie LinkedIn); umożliwienie zostawiania komentarzy pod filmami na portalu YouTube.

6. Podsumowanie

Główną rolą marketingu cyfrowego w działalności przedsiębiorstwa jest promocja oraz budowanie świadomości marki. Sprzyjają temu wszystkie dostępne narzędzia marketingu cyfrowego. Przeprowadzona analiza porównawcza pozycjonowania stron internetowych pokazała, że wszystkie przedsiębiorstwa korzystają z tzw. content marketingu oraz marketingu w mediach społecznościowych. W zakresie stron internetowych firmą, która osiągnęła najlepsze wyniki jest PGNiG SA ze względu na najlepsze pozycjonowanie w wynikach wyszukiwania. Z kolei najgorzej wypadła LW Bogdanka SA, czego powodem była najsłabiej dopracowana strona internetowa. Dodatkowo obliczony wskaźnik zaangażowania odbiorców ER na poszczególnych profilach analizowanych przedsiębiorstw we wszystkich używanych przez nie mediach społecznościowych wskazał na braki efektów w działaniach większości z nich.

Mamy nadzieję, że niniejszy artykuł przyczyni się do pozytywnych i skutecznych zmian w działaniach marketingowych przedsiębiorstw surowcowych, które znalazły się w ostatnim czasie w trudnej sytuacji. Poprzez publikację treści i umiejętne zarządzanie mediami społecznościowymi będą mogły one zbudować bliższe relacje z klientami, a przede wszystkim polepszyć swój wizerunek.

This paper was supported by the AGH University of Science and Technology [No. 16.16.100.215]

Literatura – References

1. DIGITAL 2021: GLOBAL OVERVIEW REPORT. Available online: https://datareportal.com/reports/digital-2021-global-overview-report , 27.07.2023.
2. Sukiennik, M.; Kowal, B. Analysis and Verification of Space for New Businesses in Raw Material Market—A Case Study of Poland. Energies 2022, 15, 3042; https://doi.org/10.3390/en15093042.
3. Kowal, B.; Świniarska, O.; Domaracká, L. Internal communication models shaping safe behavior of employees in the raw materials sector during the coronavirus pandemic. Journal of the Polish Mineral Engineering Society 2022, no. 2, p. 31–38. https://doi.org/10.29227/IM-2022-02-04.
4. Kowal, B.; Ranosz, R.; Herezy, Ł.; Cichy, W.; Świniarska, O.; Domaracka, L. Overview of Taken Initiatives and Adaptation Measures in Polish Mining Companies during a Pandemic. Energies 2022, 15, 6403. https://doi.org/10.3390/en15176403.
5. Raw materials market report 2020: entrepreneurial opportunities in the raw materials sector in Hungary, the Czech Republic, Poland and the Slovak Republic, ed. by Lucia Domaracká; [aut.] Patrycja BĄK, [et al.], Barbara Kowal, [et al.], Marta Sukiennik, [et al.]. Hungary: University of Miskolc, cop. 2020.
6. Sukiennik, M.; Kowal, B.; Bąk, P. Identification of Market Gap as a Chance for Enterprise Development—Example of Polish Raw Materials Industry. Energies 2021, 14, 4678. https://doi.org/10.3390/en14154678.
7. Galos, K.; Lewicka, E.; Burkowicz, A.; Guzik, K.; Kamyk, J.; Kot-Niewiadomska, A.; Szlugaj J. Nowa metodyka wyznaczania surowców kluczowych, strategicznych i krytycznych dla polskiej gospodarki. Przegląd Geologiczny 2021, vol. 69, nr 10. Available online: https://yadda.icm.edu.pl/baztech/element/bwmeta1.element.baztech-c198bb7f-942e-47ca-a318-10bd716122c7 (accessed on 25 July 2023). [in Polish]
8. Galos, K.; Kot-Niewiadomska, A.; Kamyk, J. The Role of Poland in the European Union Supply Chain of Raw Materials, Including Critical Raw Materials. Mater. Proc. 2021, 5, 14. https://doi.org/10.3390/materproc2021005014.
9. Kot-Niewiadomska, A.; Galos, K.; Kamyk, J. Safeguarding of Key Minerals Deposits as a Basis of Sustainable Development of Polish Economy. Resources 2021, 10, 48. https://doi.org/10.3390/resources10050048.
10. Prawo geologiczne i górnicze. Available online: https://sip.lex.pl/akty-prawne/dzu-dziennik-ustaw/prawo-geologiczne-i-gornicze-17724218/art-1 (accessed on 15 July 2023)
11. Zamorowska, K. Projekt Polityki Surowcowej Państwa już w konsultacjach. Available online: https://www.teraz-srodowisko.pl/aktualnosci/polityka-surowcowa-panstwa-konsultacje-10585.html (accessed on 29 June 2023)
12. Polityka Surowcowa Państwa. Available online: https://www.gov.pl/web/klimat/polityka-surowcowa-panstwa. (accessed on 27 July 2023)
13. Ryan D., Jones C. Najlepsze kampanie marketingu cyfrowego. Wyd. 1, Wolters Kluwer Polska, Warszawa 2011. [in Polish]
14. Wróblewski, P. Marketing 4.0 – w pogoni za nowoczesną technologią. Available online: https://www.seomanagment.com/marketing-4-0-w-pogoni-za-nowoczesna-technologia. (accessed on 15 July 2023) [in Polish]
15. Armstrong G., Kotler P.: Marketing. Wprowadzenie. Wyd. 1, Wolters Kluwer Polska, Warszawa 2012. [in Polish]
16. Mazurek G.: E-Marketing. Planowanie. Narzędzia. Praktyka. Wyd. 1, Poltext, Warszawa 2018. [in Polish]
17. Chaffey D., Smith P.R.: Digital Marketing Excellence: Planning, Optimizing and Integrating Online Marketing. Wyd. 5, Routledge, Abingdon, Londyn 2017.
18. Digital marketing to dziś być albo nie być na rynku. Nie możesz z niego rezygnować! Available online: https://afterweb.pl/linki-sponsorowane/digital-marketing-to-dzis-byc-albo-nie-byc-na-rynku-nie-mozesz-z-niego-rezygnowac. (accessed on 21 July 2023)
19. Storm M.: The Role of Digital Marketing (And How It Helps Your Business). Available online: https://www.webfx.com/blog/marketing/the-role-of-digital-marketing. (accessed on 13 July 2023)

20. Budziak W.: Co to jest marketing internetowy – Definicja. Available online: https://ks.pl/slownik/co-to-jest-marketing-internetowy. (accessed on 13 July 2023)
21. Byczek A.: SEO, SEM – co to jest i czym się różni? Available online: https://greenparrot.pl/blog/seo-sem-co-to-jest. (accessed on 17 July 2023)
22. Gregor B., Kaczorowska-Spychalska D.: Marketing w erze technologii cyfrowych: Nowoczesne koncepcje i wyzwania. Wyd. 1, Wydawn. Nauk. PWN, Warszawa 2018. [in Polish]
23. Surówka A.: Co to jest i czym charakteryzuje się skuteczny video marketing? Available online: https://harbingers.io/blog/video-marketing. (accessed on 1 July 2023)
24. Mazurek G.: Transformacja cyfrowa - perspektywa marketingu. Wyd. 1, Wydawn. Nauk. PWN, Warszawa 2019. [in Polish]
25. Social Media Marketing – wszystko, co musisz o nim wiedzieć. Available online: https://dais.pl/social-media-marketing-wszystko-co-musisz-o-nim-wiedziec. (accessed on 1 July 2023)
26. Email marketing - jak skutecznie trafić do klientów i promować firmę? Available online: https://poradnikprzedsiebiorcy.pl/-email-marketing-na-czym-polega. (accessed on 10 June 2023)
27. https://flowagency.pl/co-to-sa-reklamy-display. (accessed on 8 June 2023)
28. Wałczyk P.: #TOPOWA 7 – Najlepsze narzędzia do analizy działań marketingowych. Available online: https://brand24.pl/blog/analiza-dzialan-marketingowych-narzedzia. (accessed on 12 June 2023)
29. Franczuk M.: Jak mierzyć zaangażowanie społeczności na Instagramie? Available online: https://miarabiznesu.pl/jak-mierzyc-zaangazowanie-spolecznosci-na-instagramie/. (accessed on 2 June 2023)

Digital Marketing in the Raw Materials Industry – Case Study

Activities undertaken by currently operating enterprises as part of digital marketing are becoming more and more their daily routine. Since the pandemic, they have been the main form of contact with the client, which is why they are so important in the operation of every company. This article presents an analysis of marketing activities carried out by five selected raw materials companies in the field of digital marketing. The research covered websites and activities of the analyzed enterprises in social media. They showed what actions are taken by enterprises, whether they achieve a high level of audience involvement on the portals where they exist and what should be done to make the use of digital marketing more effective.

Keywords: *raw materials market, digital marketing, social media, marketing communication*

Machine Activity Recognition Using Clustering Method

Marek KĘSEK[1)], Romuald OGRODNIK[2)], Marta PODOBIŃSKA-STANIEC[3)]

[1)] Ph.D., DSc, Eng.; AGH University of Science and Technology, Cracow, Poland; ORCID: 0000-0001-6217-8435
2) Ph.D. Eng.; AGH University of Science and Technology, Cracow, Poland; ORCID: 0000-0003-4025-9191
3) Ph.D. Eng.; AGH University of Science and Technology, Cracow, Poland; ORCID: 0000-0002-3250-0646

http://doi.org/10.29227/IM-2023-01-40

Submission date: 18-05-2023 | Review date: 16-06-2023

Abstract

Machine activity recognition is important for benchmarking and analysing the performance of individual machine, machine maintenance needs and automated monitoring of work progress. Additionally, it can be the basis for optimizing manufacturing processes. This article presents an attempt to use object clustering algorithms for recognizing the type of activity in the production complex. For this purpose, data from the production process and the k-means algorithm were used. The most common object clustering algorithms were also discussed. The results and the presented analysis approach demonstrate that this method can be successfully utilized in practice.

Keywords: *Machine Activity Recognition, clustering, process mining, performance of individual machines, operational efficiency*

1. INTRODUCTION

In mining production, significant financial and human resources are involved. How these resources are utilized in the actual production process often determines the profitability of production. Data from the production process, collected through sensors installed in machines, allows for monitoring the performance of production systems. This enables calculating the utilization of machines and tracking the progress in line with the adopted schedule. Proper data analysis can also lead to the optimization of the production process, which is often far from the ideal model due to real-world conditions.

Such analyses are conducted within the framework of a process known as Process Mining, whose aim is to identify potential issues occurring in the production process and find areas for improvement. In the current context of process automation, achieving this goal requires having an appropriate set of data. In addition to data from automatic measurement systems, information about the type of machine activity (e.g., transit, operation, downtime) is essential. Such information is not measurable and is not part of the sensor data stream recorded in the database. Comparing the actual sequence of activities performed in the production process with the adopted model process allows for identifying bottlenecks, identifying unnecessary repetitions of activities, and determining the causes of downtime and failures. If you do not have the appropriate event log, then the solution is MAR (Machine Activity Recognition). Methods of this kind involve recognizing the activities performed by machines based on the analysis of multiple parameters of their operation recorded at the same time. In the literature, there is a growing number of examples of such approaches, mainly in the construction industry. It most commonly concerns excavators [4, 10, 11, 12], loaders [5, 12, 13], or compactors [8]. In the mining industry, such analyses primarily pertain to the operation of loaders (open-pit mining) or shearers [6, 16].

Most commonly, machine activity recognition is accomplished using supervised machine learning methods based on labelling, where observed machine states are assigned to recorded machine operation parameters. In the majority of cases described in the literature, this involves observing video recordings of machine activities along with timestamps of their start and end times. For this purpose, supervised classification methods are employed, with neural networks being the most commonly used. However, conditions suitable for video camera operation are not always present, and the nature of activities may not be identifiable through this approach. In such situations, unsupervised classification methods become the solution. In the following part of the study, an example of activity recognition in a mining complex will be presented, based on the recorded current intensities flowing through motors driving its elements.

2. METODY GRUPOWANIA OBIEKTÓW

Object clustering methods, often referred to as clustering or cluster analysis, aim to identify groups/clusters of objects that are similar to each other within the group but dissimilar to objects in other groups. The most popular methods include:

K-means algorithm – is one of the simplest and most popular clustering algorithms. This algorithm involves dividing the dataset into k clusters, where k is a predetermined number. Each cluster is represented by its mean values, called centroids. In each step of the algorithm, each object is assigned to the class whose centroid is the closest. Then, new centroids for each class are calculated as the average value of all objects in that class. This process is repeated iteratively until the objects achieve a stable assignment to the clusters or a stopping condition is met. [3]

K-medoids algorithm – is similar to k-means, but instead of using mean values as cluster representatives, it selects one of the objects from the cluster, which is called a medoid. A medoid is a point that is closest to the other objects in the cluster. The main advantage of k-medoids is its greater robustness to outliers, as the medoid is not sensitive to extreme values in the cluster. The k-medoids algorithm is iterative and

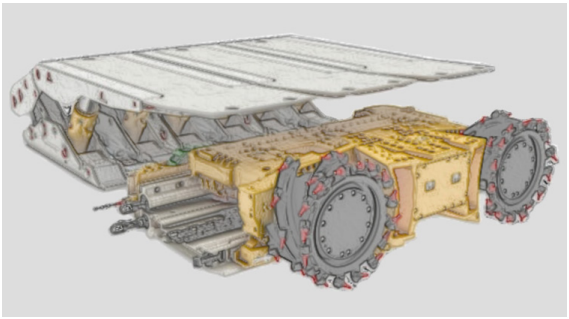

Fig. 1. "Mikrus" longwall system [17]
Rys. 1. System ścianowy "Mikrus"

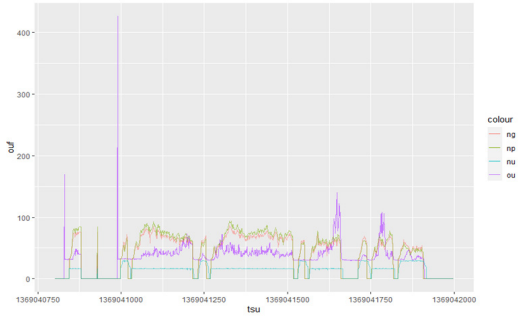

Fig. 2. A plot of the variation of recorded current intensities as a function of time. Source: own study
Rys. 2. Wyres przebiegu zmienności rejestrowanych natężeń prądów w funkcji czasu

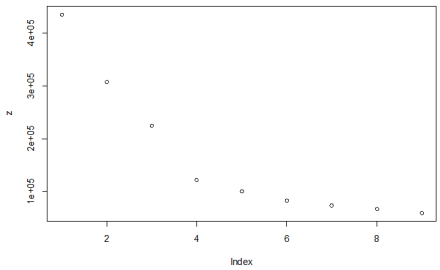

Fig. 3. Elbow rule plot. Source: own study
Rys. 3. Wykres reguły "łokcia"

relies on assigning objects to the nearest medoid and updating the medoids in each iteration. The iterative process is repeated until the objects achieve a stable assignment to the clusters, and the difference between the medoids in consecutive iterations is small .[7]

Hierarchical Clustering – is a family of clustering methods that create a hierarchical tree or dendrogram of objects, where each level of the tree represents a different level of grouping. It can be categorized into two main types: agglomerative (starting with individual objects and merging the most similar clusters) and divisive (starting with a single large cluster and recursively dividing it into smaller ones). The hierarchical clustering process continues until all objects are assigned to their individual clusters or until a stopping criterion is met. This method is useful for exploring the structure of the data at different scales, as it provides a visual representation of the nested relationships between clusters. [14]

DBSCAN – is a density-based clustering method that groups together objects based on their spatial density. It classifies objects into three categories: core points, border points, and noise points. Core points are densely surrounded by other points within a specified radius (epsilon) and are used as seeds to form clusters. Border points are within the epsilon neighborhood of a core point but are not core points themselves, and noise points have no core points within their epsilon neighborhood. DBSCAN efficiently discovers clusters of arbitrary shapes and is robust to outliers, as they are treated as noise points. The algorithm starts with an arbitrary point, finds its epsilon neighborhood, and recursively expands the cluster by adding reachable core and border points. The process continues until all points are assigned to clusters or marked as noise. [7]

The Expectation-Maximization (EM) algorithm – is a probabilistic clustering method that assumes data are generated by an underlying statistical model with latent (unobserved) variables. EM is an iterative process that alternates between two steps: the E-step (Expectation step) and the M-step (Maximization step). In the E-step, it estimates the probabilities of the latent variables given the observed data and the current model parameters. In the M-step, it updates the model parameters by maximizing the expected log-likelihood of the complete data. The EM algorithm converges to a

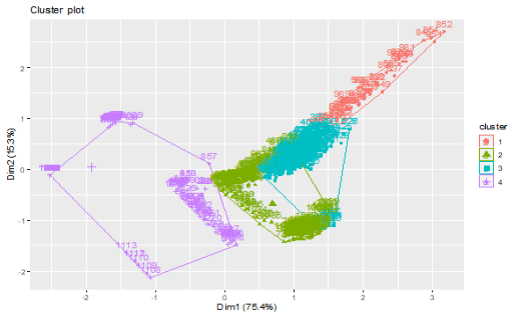

Fig. 4. Cluster plot. Source: own study
Rys. 4. Wykres grupowania

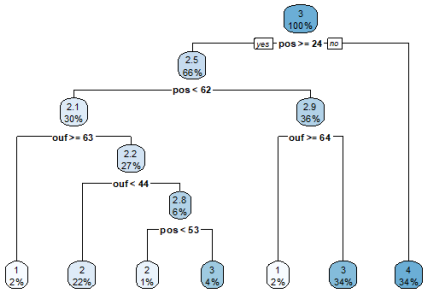

Fig. 5. Decision tree obtained after clustering process. Source: own study
Rys. 5. Drzewo decyzyjne pogrupowanych danych

local maximum of the likelihood function and is often used to find maximum likelihood estimates for models with missing data or unobserved variables. It has wide applications in various fields, including data clustering, image processing, and statistical modeling. [1]

The Fuzzy C-Means (FCM) algorithm – is a variation of the traditional k-means clustering method that allows objects to be assigned to multiple clusters with different degrees of membership. In FCM, each object is characterized by a set of membership values, indicating the likelihood of belonging to each cluster. Unlike k-means, where an object is rigidly assigned to the nearest cluster, FCM softens the assignment by using fuzzy logic. The algorithm iteratively updates the membership values and the cluster centers until a certain convergence criterion is met. FCM is particularly useful when an object can belong to more than one group simultaneously or when there is ambiguity in assigning objects to distinct clusters. It has applications in various fields, including image segmentation, pattern recognition, and decision-making systems. [2]

In the example presented below, the k-means algorithm was used due to its fast convergence, scalability, simplicity, and efficiency.

3. PRACTICAL EXAMPLE

The results presented below concern the "Mikrus" longwall complex, during the period when the complex was tested under real conditions. The "Mikrus" longwall complex is designed for extracting thin coal seams with a thickness of 1.1–1.5 meters. It is equipped with the GUŁ-500 cutting-loading head, which is moved along the coal face by a longwall conveyor. The movement of the head is carried out using a traction system of cutting elements beneath mechanized housing sections (Fig. 1). The exploitation of this complex is associated with an innovative mining technology using perpendicular caving, enabling the completion of a full shearing cycle in approximately 1 minute. [https://famur.com/urzadzenia-dla-gornictwa-podziemnego/kompleks-mikrus/]

The control of the complex is carried out by an operator utilizing a central control panel located in the goaf. The traction system of cutting elements is powered by electric motors supplied from frequency converters placed in the drivages. [17].

The original data format contained information about changes in current intensities, the time of their occurrence, and the engine code to which the change pertained. The investigated dataset contained columns with the following parameters:

tsu – time of observation (unix timestamp),
ouf – current intensity of the cutting element motor [A],
ngf – current intensity of the main drive motor [A],
npf – current intensity of the auxiliary drive motor [A],
nuf – current intensity of the cable layer motor [A].

The decision to register changes in current intensity effectively reduced the amount of transmitted and stored data, but for their analysis, it was necessary to reconstruct their original arrangement. This was achieved by using appropriate functions in the R programming language. This has been further elaborated in the work [9].

The operation of the main drive and auxiliary motors did not differ significantly. The values of the currents they consumed varied within a small range. This is illustrated in Figure 2, which shows a section of the recorded data.

In Figure 2, both the working and idle periods of the harvester can be observed. The current intensity values of the cutting element motor (ouf) are represented in the violet co-

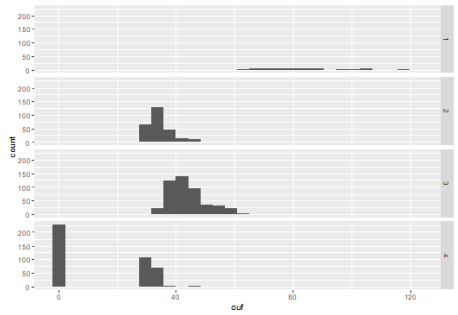

Fig. 6. Histogram of cutting head drive motor current with division into determined groups. Source: own study
Rys. 6. Histogramy natężeń prądów głowicy urabiającej z podziałem na wyodrębnione grupy

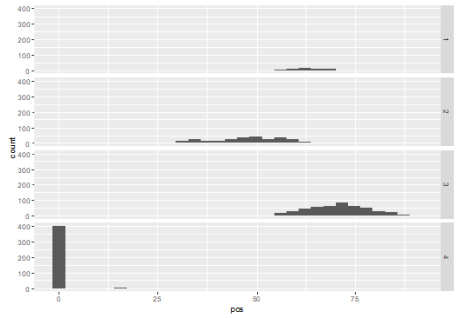

Fig. 7. Histogram of feed drive motor current with division into determined groups. Source: own study
Rys. 7. Histogramy natężeń prądów silników posuwu z podziałem na wyodrębnione grupy

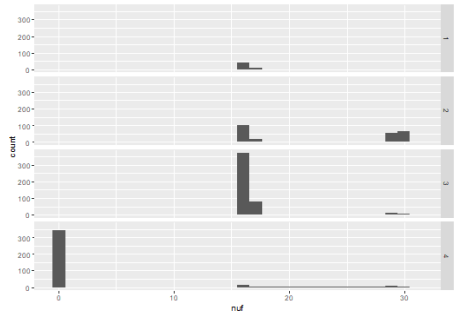

Fig. 8. Histogram of cable laying drive motor current with division into determined groups. Source: own study
Rys. 8. Histogramy natężeń prądów silnika układaka z podziałem na wyodrębnione grupy

lour. During the depicted time period, a peak reaching values exceeding 400 [A] is visible, associated with the start-up of this motor. This is confirmed by simultaneous increases in the current values flowing through the other motors. This figure well illustrates the mutual similarity of the current intensity values in both advancing drive motors and the relatively constant current intensity values in the conveyor drive motor. Due to the similar values of both advancing drive motors, which would result in repetitive information, the average of their values was used in the further analysis.

In the next stage, outliers were removed from the dataset, which, like the aforementioned peak, could disrupt the clustering process. To determine the boundaries beyond which outliers lie, a method based on the interquartile range was adopted The IQR * 1.5 rule, also known as the Tukey rule [15], is a statistical technique used for detecting and handling outliers in data. It involves calculating the interquartile range (IQR), which is the range between the 75th percentile (Q3) and the 25th percentile (Q1) of the data. The IQR represents the spread of the middle 50% of the data. According to the rule, data points that fall below Q1 - (IQR * 1.5) or above Q3 + (IQR * 1.5) are considered outliers and can be potentially removed or treated separately. This rule is especially useful in robust statistics, where it helps in identifying and dealing with extreme values that could adversely affect the results of statistical analysis.

The next step in the conducted analysis was to determine the number of clusters to which the observations could be assigned. The elbow rule was used for this purpose.

The Elbow Rule is a heuristic method used to determine the optimal number of clusters in a clustering algorithm, such as k-means. It involves plotting the variance explained (or another clustering performance metric) against the number of clusters, and looking for an 'elbow point' in the graph. The elbow point is the value of k at which the explained variance starts to level off significantly. The idea is that the optimal number of clusters is often located at this point, as adding more clusters beyond the elbow may not lead to significant improvement in the clustering quality. The Elbow Rule is a useful visual aid for selecting an appropriate number of clus-

Tab. 1. Activity identification. Source: own study

Tab. 1. Identyfikacja czynności

Group	Activity	Premise
1	maneuvering	occasional high values of feeding motor current, occasional high values of cutting element motor current
2	engaging	occasional high values of feeding motor current, high values of cutting element motor current
3	cutting	high values of feeding motor current, the highest values of cutting element motor current
4	idle	zero values of feeding motors current, zero values of cutting element motor current

ters when conducting clustering analysis. In this way, the graph presented in Figure 3 was obtained.

Based on the graph in Figure 3, it was determined that the optimal number of clusters is four. The clustering process was carried out using the k-means function available in the R language after loading the stats library. As a result, a list is generated, containing the cluster numbers to which the consecutive observations in the analysed data were assigned. Figure 4 presents the observations assigned to clusters in a coordinate system reduced to two principal components.

The clustering process conducted, however, does not provide answers to the fundamental question: what characterizes the separated groups of observations, or in other words, which machine operating states have been assigned to the resulting clusters? The answer to this question can be obtained by using a decision tree method, which generates decision rules. Figure 5 presents the decision tree generated using the rpart function available in R. It operates based on the CART (Classification and Regression Trees) algorithm, which involves recursively partitioning the dataset into subsets, based on feature analysis aimed at minimizing the entropy in the partition nodes.

The decision tree from Figure 5 displays the boundary values of the parameters ouf and pos in its nodes, which are used to assign measurements to the corresponding groups. The decision rules generated based on the tree are presented below:

```
cluster
 1 when pos is 24 to 62 & ouf >= 63
 1 when pos >= 62 & ouf >= 64
 2 when pos is 24 to 53 & ouf is 44 to 63
 2 when pos is 24 to 62 & ouf < 44
 3 when pos is 53 to 62 & ouf is 44 to 63
 3 when pos >= 62 & ouf < 64
 4 when pos < 24
```

As can be observed, the parameter associated with the conveyor drive does not have an impact on the assignment to the resulting groups. Based on the generated decision rules, the current operation of the harvester can be attributed to the identified clusters. These groups correspond to specific machine activities, and the analysis of the obtained rules often allows for the identification of these activities. Additional assistance in this identification can be provided by histograms of the analysed parameters with division into groups. They are presented in figures 6, 7, and 8.

Simultaneous interpretation of decision rules and histograms allows for the following group assignments:

The extracted activities and rules for assigning observations of machine operating parameters can be used to determine the current machine's activities, but they can also be utilized for analyzing historical data stored in databases.

4. CONCLUSION

The presented method can be applied to a wide range of machines and devices. The widespread use of various sensors enables detailed control over the executed production processes. The results presented in this article are of an indicative nature, but conducting a similar analysis on a larger dataset would significantly enhance their credibility. Utilizing a larger amount of data would likely allow for the identification of a greater number of machine activities/states.

A significant advantage of the presented approach is the absence of the need for event logs, from which information about the occurrence times of specific activities could be obtained. However, if such event logs were available, neural networks could be successfully employed for activity recognition. The conducted analysis allows for the assignment of activities performed by the machine based on measured parameters of its operation. Further work should be conducted to verify the correctness of the recognized sequence of activities to detect deviations from the model sequence of activities envisaged for this production process.

Rozpoznawanie czynności maszyn z użyciem metody grupowania

Rozpoznawanie czynności realizowanych przez maszyny jest bardzo istotne dla porównywania i analizy wydajności poszczególnych maszyn, potrzeb konserwacji maszyn oraz automatycznego monitorowania postępu prac. Dodatkowo, może być ono podstawą do optymalizacji realizowanych procesów produkcyjnych. W niniejszym artykule przedstawiono próbę wykorzystania algorytmów grupowania obiektów do rozpoznawania rodzaju aktywności kompleksu urabiającego. Do tego celu użyto danych pochodzących z procesu produkcyjnego oraz algorytmu k-means. Przybliżono także najpowszechniejsze algorytmy grupowania obiektów. Wyniki oraz zaprezentowany sposób przeprowazania analizy pokazują, że taki sposób postępowania może być z powodzeniem wykorzystywany w praktyce.

Słowa kluczowe: *rozpoznawanie czynności maszyn, grupowanie, process mining, stopień wykorzystania maszyn, wydajność operacyjna*

Literatura – References

1. Bishop, C. M. (2006) Pattern Recognition and Machine Learning. Springer, 2006
2. Bezdek, J. C., Ehrlich, R., & Full, W. (1984) FCM: The fuzzy c-means clustering algorithm. Computers & Geosciences, 1984. Volume 10, Issue 2-3.
3. Błażewicz J., Formanowicz P., Jarosz K., Kalinowski A., Klimek M., Kołaczkowski P., Kwiecień R., Michalak K., Traczyk T. (2006) Rozpoznawanie wzorców. Metody i zastosowania. Wydawnictwo Naukowe PWN.
4. Chen C., Zhu Z., Hammad A. (2020) Automated excavators activity recognition and productivity analysis from construction site surveillance videos, Automation in Construction, Volume 110.
5. Cheng C.-F.; Rashidi A.; Davenport M.A.; Anderson D. (2019) Evaluation of Software and Hardware Settings for Audio-Based Analysis of Construction Operations. International Journal of Civil Engineering.
6. Gackowiec, P.; Brzychczy, E.; Kęsek, M. (2021) Enhancement of Machinery Activity Recognition in a Mining Environment with GPS Data. Energies 2021.
7. Han J., Kamber M., Pei J. (2011) Data Mining: Concepts and Techniques. Morgan Kaufmann, 3rd Edition, 2011.
8. Jeong G.; Ahn C.R.; Park M. (2022) Constructing an Audio Dataset of Construction Equipment from Online Sources for Audio-Based Recognition, Conference paper, Proceedings - Winter Simulation Conference, 2022-December
9. Kęsek M., Ogrodnik R. (2021) Method for determining the utilization rate of thin-deck shearers based on recorded electromotor loads. Energies 2021 vol. 14 iss. 13 art. no. 4059, s. 1–14.
10. Kim, I.-S.; Latif, K.; Kim, J.; Sharafat, A.; Lee, D.-E.; Seo, J. (2023) Vision-Based Activity Classification of Excavators by Bidirectional LSTM. Appl. Sci. 2023, 13, 272.
11. Mahamedi E., Rogage K., Doukari O., Kassem M. (2021) Automating excavator productivity measurement using deep learning, Proceedings of the Institution of Civil Engineers - Smart Infrastructure and Construction, 2021, p. 121-133.
12. Rashid K.M., Louis J. (2020) Automated Activity Identification for Construction Equipment Using Motion Data From Articulated Members, Frontiers in Built Environment, Vol.5, 2020.
13. Sherafat B.; Rashidi A.; Asgari S. (2022) Sound-based multiple-equipment activity recognition using convolutional neural networks, Automation in Construction, Volume 135, 2022.
14. Tan, P.-N., Steinbach, M., & Kumar, V. (2006) Introduction to Data Mining. Addison-Wesley.
15. Tukey, J. W. (1977) Exploratory Data Analysis. Addison-Wesley.
16. Xu, J.; Wang, Z.; Tan, C.; Liu, X. A (2016) State Recognition Approach for Complex Equipment Based on a Fuzzy Probabilistic Neural Network. Algorithms 2016.
17. https://famur.com/urzadzenia-dla-gornictwa-podziemnego/kompleks-mikrus